



Australian Government
Geoscience Australia

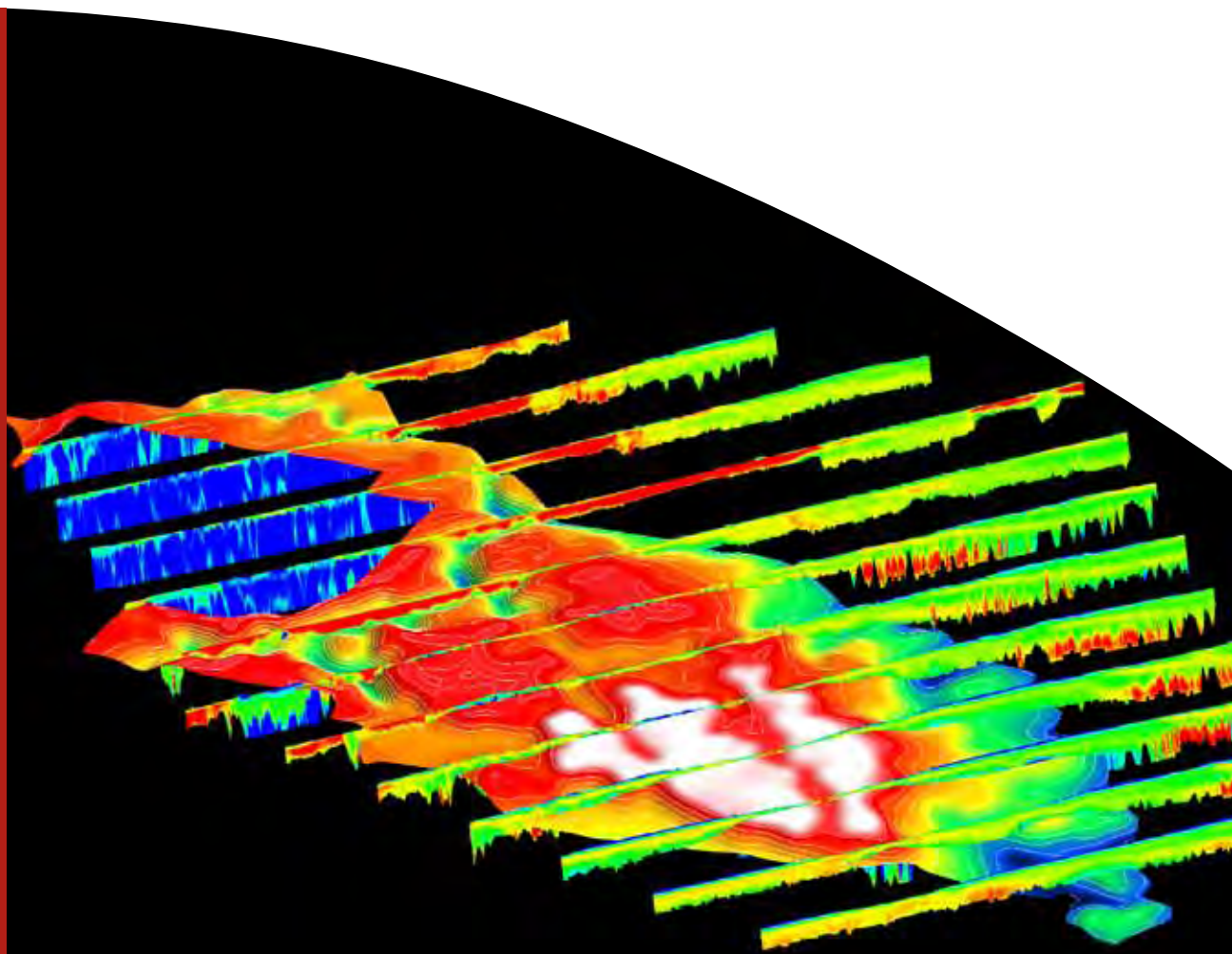
Geological and energy implications of the Paterson Province airborne electromagnetic (AEM) survey, Western Australia

I. C. Roach (editor)

Record

2010/12

GeoCat #
70302



Geological and energy implications of the Paterson Province airborne electromagnetic (AEM) survey, Western Australia

GEOSCIENCE AUSTRALIA
RECORD 2010/12

By

I. C. Roach (editor)

With contributions from:

K. F. Cassidy¹, M. T. Costelloe², K. Czarnota³, P. Duerden⁴, D. K. Hutchinson², D. Huston³, S. Jaireth⁵, S. F. Liu², D. Maidment^{6,7}, D. Miggins⁸, I. C. Roach², C. Sorensen⁹, A. J. Whitaker⁵, J. R. Wilford¹⁰ and N. C. Williams²

-
1. Bare Rock Geological Services, PO Box 1633, Fremantle WA 6959
 2. Airborne EM Project, Onshore Energy and Minerals Division, Geoscience Australia, GPO Box 387, Canberra ACT 2601 Australia
 3. Onshore Energy Geodynamic Framework Project, Onshore Energy and Minerals Division, Geoscience Australia, GPO Box 387, Canberra ACT 2601 Australia
 4. Alkane Resources Ltd., 19 Kenna St., Orange NSW 2800
 5. National Projects, Resources and Advice, Onshore Energy and Minerals Division, Geoscience Australia, GPO Box 387, Canberra ACT 2601 Australia
 6. Formerly Onshore Energy Geodynamic Framework Project, Onshore Energy and Minerals Division, Geoscience Australia, GPO Box 387, Canberra ACT 2601 Australia
 7. Present address: Mawarid Mining, PO Box 476, Sohar, Postal Code 321, Sultanate of Oman.
 8. US Geological Survey, Denver Federal Center, Box 25046, MS 963, Denver CO 80225.
 9. Formerly Geophysics Group, Onshore Energy and Minerals Division, Geoscience Australia, GPO Box 387, Canberra ACT 2601 Australia
 10. Geophysics Group, Onshore Energy and Minerals Division, Geoscience Australia, GPO Box 387, Canberra ACT 2601 Australia.

Department of Resources, Energy and Tourism

Minister for Resources and Energy: The Hon. Martin Ferguson, AM MP
Secretary: Mr Drew Clarke, PSM

Geoscience Australia

Chief Executive Officer: Dr Chris Pigram



© Commonwealth of Australia, 2010

This work is copyright. Apart from any fair dealings for the purpose of study, research, criticism, or review, as permitted under the *Copyright Act 1968*, no part may be reproduced by any process without written permission. Copyright is the responsibility of the Chief Executive Officer, Geoscience Australia. Requests and enquiries should be directed to the **Chief Executive Officer, Geoscience Australia, GPO Box 378 Canberra ACT 2601**.

Geoscience Australia has tried to make the information in this product as accurate as possible. However, it does not guarantee that the information is totally accurate or complete. Therefore, you should not solely rely on this information when making a commercial decision.

ISSN 1448-2177

ISBN 978-1-921672-80-4 print

ISBN 978-1-921672-79-8 web

GeoCat # 70302

Bibliographic reference: Roach, I. C. ed. 2010. *Geological and energy implications of the Paterson Province airborne electromagnetic (AEM) survey, Western Australia*. Geoscience Australia **Record 2010/12**, 318 pp.

Example chapter reference: Huston, D. L., Czarnota, K., Jaireth, S., Williams, N.C., Maidment, D., Cassidy, K. F., Duerden, P. and Miggins, D. 2010. Minerals systems of the Paterson region. In: Roach, I. C. ed. *Geological and Energy implications of the Paterson airborne electromagnetic (AEM) survey, Western Australia*. Geoscience Australia **Record 2010/12**, pp. 155-218.

Contents

Executive Summary.....	1
1 Introduction (I. C. Roach and M. T. Costelloe)	3
1.1 Survey characteristics	3
1.2 Survey location	3
1.3 Survey purpose.....	4
1.3.1 Uranium systems.....	4
1.3.2 Other mineral systems.....	6
1.3.3 Groundwater systems.....	7
1.4 Survey economic framework.....	8
1.5 Survey design considerations.....	9
1.5.1 Climate	9
1.5.2 Terrain (Drape)	11
1.5.3 Aircraft access.....	12
1.5.4 Forward modelling.....	12
1.5.5 Native Title and Land Access issues.....	13
1.5.6 Other no fly zones	13
1.5.7 Communication strategy	14
1.5.8 Final survey design	14
1.6 Survey partners, contributors and cost.....	16
1.7 Climate.....	18
1.8 Vegetation.....	20
1.9 Geomorphology	22
1.10 References.....	26
2 Previous and concurrent work (I. C. Roach and M. T. Costelloe)	29
2.1 Geological mapping	29
2.2 Geophysics.....	29
2.3 Drilling data compilation	35
2.4 Rock properties	40
2.5 Summary of hydrogeological investigations.....	42
2.5.1 Surface water.....	42
2.5.2 Groundwater.....	43
2.5.3 Palaeovalleys.....	44
2.6 References.....	46
3 Geology (A. J. Whitaker, I. C. Roach, S. F. Liu and J. R. Wilford).....	49
3.1 Introduction.....	49
3.2 Bedrock geology	49
3.2.1 Introduction	49
3.2.2 The Precambrian rocks.....	51
3.2.4 Canning Basin	66
3.3 Regolith geology	71
3.3.1 Introduction	71
3.3.2 Previous work	72
3.3.3 Regolith map development	75
3.3.4 Regolith mapping scheme	76
3.3.5 Regolith units (RUs)	78
3.4 References.....	82

4 AEM Geophysics (M. T. Costeloe, D. K. Hutchinson and I. C. Roach).....	87
4.1 Introduction	87
4.2 Previously released data	87
4.3 The TEMPEST™ AEM system	88
4.4 Background on the GA-LEI inversion	89
4.5 GA-LEI Inversions.....	90
4.5.1 Description	90
4.6 Reference Model	92
4.7 Geo-electrical models.....	93
4.8 GA-LEI inversion products.....	93
4.8.1 Depth of Investigation.....	93
4.8.2 Grids.....	94
4.8.3 Gridding parameters.....	95
4.8.4 AEM Go Map.....	95
4.8.5 Depth Slices	96
4.8.6 Elevation slices	97
4.9 Sections	98
4.9.1 Georeferenced JPEGs.....	99
4.9.2 GA-LEI multiplots	100
4.10 Comparison with conductivity logs.....	102
4.10.1 Conductivity Logging	102
4.11 References.....	105
5 Interpretations of AEM data (I. C. Roach, M. T. Costeloe and D. K. Hutchinson)	107
5.1 Introduction	107
5.2 Determine “fit-for-purpose”	107
5.2.1 Quality control and quality assurance of the contractor supplied data	107
5.2.2 Depth of Investigation grid	113
5.3 Methods used to define correlations.....	114
5.4 Geological validation of the AEM data.....	115
5.5 Broad geological correlations.....	119
5.5.1 Pinjyan Chert Member and Jeerinah Formation	119
5.5.2 Rudall Complex	121
5.5.3 Broadhurst Formation	121
5.5.4 Tarcunyah Group	124
5.5.5 Permian-Mesozoic strata.....	125
5.5.6 Waukarlycarly Embayment.....	127
5.5.7 Anketell Shelf	128
5.5.8 Throssell Shelf	132
5.6 Unconformities.....	133
5.7 Palaeovalleys.....	139
5.8 Groundwater.....	142
5.9 Known mineral deposits.....	148
5.9.1 Nifty	148
5.9.2 Telfer	149
5.9.3 Kintyre	149
5.9.4 Woodie Woodie	150
5.10 Discrete Anomalies	151
5.11 References.....	153

6 Mineral systems of the Paterson region (D. L. Huston, K. Czarnota, S. Jaireth, N. C. Williams, D. Maidment, K. F. Cassidy, P. Duerden and D. Miggins)	155
6.1 Introduction	155
6.2 Mineral systems associated with the Miles Orogeny	155
6.2.1 Uranium-bearing deposits associated with the Coolbro Sandstone and Rudall Complex	155
6.2.2 Sediment-hosted copper deposits.....	165
6.2.3 Other zinc-lead deposits	175
6.2.4 Model for mineral systems associated with inversion of the Yeneena Basin	177
6.3 Mineral systems associated with the O'Callaghans tectonothermal event	189
6.3.1 Granite-related gold-copper and tungsten-copper-zinc-lead deposits.....	189
6.3.2 Model for mineral systems associated with the O'Callaghans tectonothermal event.....	201
6.4 Calcrete-Hosted Uranium Systems	209
6.4.1 Types of calcrete-hosted uranium deposits.....	209
6.4.2 Source of uranium, vanadium and potassium	209
6.4.3 Drainage system.....	210
6.4.4 Geochemical factors controlling precipitation of carnotite in calcrete-hosted uranium deposits.....	210
6.4.5 Lamil Hills Prospect	211
6.5 References	214
7 Implications for uranium mineral systems (S. F. Liu and S. Jaireth)	219
7.1 Overview of uranium mineral systems and implications of AEM data in the Paterson area	219
7.2 Concentration of uranium in rocks and uranium anomalies in the Paterson area.....	220
7.2.1 Radiometric data.....	221
7.2.2 Geochemical analyses.....	224
7.2.3 Uranium/thorium ratios	224
7.3 Diagenetic fluid-related uranium mineral systems.....	229
7.3.1 Unconformity-related uranium mineral systems	229
7.3.2 Stratabound uranium-copper mineral systems associated with the Broadhurst-Coolbro contact	244
7.4 Sandstone-hosted uranium mineral systems.....	249
7.4.1 AEM responses of Permian and younger sediments	252
7.4.2 Potential for sandstone-hosted uranium mineral systems	254
7.5 Calcrete-hosted uranium mineral systems.....	259
7.5.1 Prospective for calcrete-hosted uranium mineral systems.....	261
7.5.2 Lake Waukarlycarly.....	261
7.5.3 Lake Disappointment west.....	262
7.5.4 Lake Disappointment southeast	269
7.5.5 Lake Winifred.....	270
7.5.6 Lake Auld and Percival Lakes-Tobin Lake	270
7.5.7 Lake Dora and Lake Blanche.....	272
7.6 Conclusions	272
7.7 References	273

8 Summary and conclusions (I. C. Roach, D. K. Hutchinson, A. J. Whitaker, M. T. Costelloe, D. Huston, S. F. Liu and S. Jaireth)	277
8.1 Implications for Uranium mineral systems	277
8.2 Implications for other mineral systems	279
8.3 Implications for regional geology	280
8.4 Utility of regional AEM for mineral exploration	282
8.5 Implications for groundwater	283
8.6 The future	283
9 Acknowledgements	285
Appendix 1 Fugro Airborne Surveys Flight Duration considerations	287
Appendix 2 Additional climate data	293
Appendix 3 Inversion data	295
A3.1 GA Phase 2 data release products	295
A3.2 GA-LEI inversion of TEMPEST™ data	297
A3.2.1 Introduction	297
A3.2.2 Formulation	297
A3.2.3 Objective function	301
A3.2.4 Minimisation scheme	304
A3.3 Conductivity data header information	307
A3.4 Technical specifications of map projections	308
A3.5 Induction conductivity logging	309
A3.5.1 Method	309
A3.5.2 Results	310
A3.6 Comparison between bore hole conductivity logs and GA LEI	314
A3.7 References	316

Figures

Figure 1.1: Survey location.....	4
Figure 1.2: Regional survey line spacing.....	5
Figure 1.3: Major commodity deposits and prospects within the Paterson region	7
Figure 1.4: Basement versus cover relationships for the Paterson AEM survey area.....	9
Figure 1.5: Distribution of drill holes in the Paterson AEM survey area.....	10
Figure 1.6: Tenement holdings before and after the Paterson AEM survey	11
Figure 1.7: Tenement purpose	12
Figure 1.8: Drape analysis results for the Paterson AEM survey	13
Figure 1.9: Native Title Application and Determination Areas for the Paterson survey area.....	15
Figure 1.10: Final survey design with infill areas for the Paterson AEM survey	17
Figure 1.11: Cartoon of flight line planning including overfly areas.....	17
Figure 1.12: Temperature and rainfall averages for Telfer Airport	19
Figure 1.13: Telfer Airport 9 am and 3 pm average wind speed and direction data	19
Figure 1.14: Examples of vegetation types in the Paterson region	21
Figure 1.15: SRTM DEM of the Paterson region	23
Figure 1.16: Soil-landscape polygons intersecting the Paterson AEM survey area.....	24
Figure 1.17: Multiresolution Valley Bottom Flatness (MRVBF) image of the Paterson area.....	26
Figure 2.1: Available 1:100 000 and 1:250 000 geological maps in the Paterson region	30
Figure 2.2: Publicly-available industry-generated airborne magnetic, radiometric and digital elevation model surveys in the Paterson region	33
Figure 2.3: Publicly-available industry-generated AEM surveys in the Paterson region	34
Figure 2.4: Regional geophysical data sets available for the Paterson AEM survey area	35
Figure 2.5: Seismic lines in and around the Paterson AEM survey area	36
Figure 2.6: Hunt Oil Company 1996 seismic survey interpreted sections across the Waukarlycarly Embayment.....	37
Figure 2.7: Distribution of public-domain drill holes used in the interpretation project	38
Figure 2.8: Drill hole frequency versus depth range.....	39
Figure 2.9: Locations of GA conductivity-logged drill holes in the Paterson survey area	42
Figure 2.10: Phanerozoic aquifers of the Canning Basin.....	44
Figure 2.11: Interpreted palaeovalley traces in the Paterson AEM survey area	45
Figure 3.1: Simplified province map of the Paterson Project	50
Figure 3.2: Gradient-enhanced Bouguer anomaly gravity image	53
Figure 3.3: Total magnetic intensity image	54
Figure 3.4: First vertical derivative of total magnetic intensity image	55
Figure 3.5: Generalised stratigraphy of the Throssell Range Group and Isdell Formation	58
Figure 3.6: Stratigraphic correlations of formations in the Tarcunyah and Disappointment Groups in the northwest Officer Basin.....	64
Figure 3.7: Permian solid geology with glacial flow directions in the Paterson area	68
Figure 3.8: Mesozoic solid geology and major drainage systems in the Paterson area	71
Figure 3.9: Regolith map of the Paterson area	79
Figure 4.1: Schematic diagram of 1D vertically smooth layered earth model used in the GA-LEI	91
Figure 4.2: An example of a forward model from the Paterson AEM Survey.....	93
Figure 4.3: Sample conductivity depth sections	95
Figure 4.4: The DOI grid	96
Figure 4.5: A selection of depth slice	97
Figure 4.6: Selection of elevation slice	98

Figure 4.7: Georeferenced JPEG for line 10000.....	99
Figure 4.8: Colour scale bar for georeferenced JPEGs	100
Figure 4.9: GA-LEI multiplot for line 10000	101
Figure 4.10: The location of logged boreholes plotted over conductance from 0-200 m	103
Figure 4.11: Conductivity logs compared to GA-LEI results	104
Figure 5.1: An example of a multiplot from the Paterson survey	111
Figure 5.2: Subsection of multiplot for line 42321	112
Figure 5.3: Subsection of multiplot for line 43530	113
Figure 5.4: 0-5 m GA-LEI conductivity depth slice	116
Figure 5.5: GA-LEI 400 m log10 conductance image compared to solid geology.....	117
Figure 5.6: GA-LEI conductivity sections for line 30211 with drill hole graphic logs	118
Figure 5.7: GA-LEI conductivity sections for line 30570 with drill hole graphic log.....	119
Figure 5.8: Conductive Jeerinah Formation and Pinjian Chert Member highlighted in the 0-400 m GA-LEI conductance image	120
Figure 5.9: GA-LEI conductivity depth slices of the Rudall Complex.....	122
Figure 5.10: GA-LEI 200-250 m conductivity depth slice and 1st vertical derivative magnetics (grey scale) of the Rudall Complex	123
Figure 5.11: 0-400 m GA-LEI conductance image of the Paterson North AEM data set.....	123
Figure 5.12: Conductive Karara Formation, Tarcunyah Group, in Paterson South.....	124
Figure 5.13: Conductive Tarcunyah Group faulted against Jeerinah Formation in Paterson North.....	125
Figure 5.14: Stacked GA-LEI conductivity sections showing Permian and Mesozoic strata lapping onto the eastern side of the Anketell Shelf	126
Figure 5.15: Perspective view of the Paterson South survey area showing a shaded relief model of the interpreted Permian-Neoproterozoic unconformity surface and GA-LEI conductivity sections.....	127
Figure 5.16: Stacked GA-LEI conductivity sections through the Waukarlycarly Embayment	128
Figure 5.17: GA-LEI 0-400 m conductance image and conductivity sections showing the extent of the Waukarlycarly Embayment in the central Paterson North survey area.....	129
Figure 5.18: The Anketell Shelf depicted using the GA-LEI 0-400 m conductance image (background) and stacked GA-LEI conductivity sections.....	130
Figure 5.19: Conductivity anomaly contours approximating the Permian-Neoproterozoic unconformity over the Anketell Shelf.....	131
Figure 5.20: Perspective views of the Proterozoic-Paleozoic unconformity over the Anketell Shelf and Throssell Shelf interpreted from conductivity anomaly contours.	132
Figure 5.21: Shaded relief model of the Throssell Shelf (left)	133
Figure 5.22: Stacked GA-LEI conductivity sections of the eastern edge of the Anketell Shelf showing Mesozoic sediments unconformably overlying Permian sediments.....	135
Figure 5.23: An interpreted scour by Anketell Sandstone into Frezier Sandstone	136
Figure 5.24: Graphic log for drill hole 91WYRC003	136
Figure 5.25: Stacked conductivity sections showing the Coolbro-Rudall unconformity.....	137
Figure 5.26: Stacked GA-LEI conductivity sections showing conductivity anomalies near the Coolbro-Rudall unconformity in the Paterson South survey area	138
Figure 5.27: Multi resolution valley bottom flatness (MRVBF) images of the Paterson AEM survey area	140
Figure 5.28: (Top) 20 m interval conductivity anomaly contours associated with the conductive Permian palaeovalleys in the Kintyre area	143
Figure 5.29: Shaded relief model of the interpreted Permian palaeovalley systems in the Throssell Shelf area with interpreted ice flow directions	144
Figure 5.30: Shaded relief model of the Canning Palaeovalley	145
Figure 5.31: Shaded relief model of the Disappointment Palaeovalley	146
Figure 5.32: The Wallal Palaeovalley and tributaries	147

Figure 5.33: GA-LEI 40-60 m depth slice of AEM data in the Kintyre area.....	148
Figure 5.34: Subsection of conductivity section of line 30860 over the Nifty copper mine.....	149
Figure 5.35: GA-LEI subsection of line 30890 over Telfer.....	149
Figure 5.36: GA-LEI Line 41920 over Kintyre	150
Figure 5.37: GA-LEI conductivity sections of lines 30850 (north of) and 30860 (south of) Woodie Woodie.....	150
Figure 5.38: EM Flow multiplot created by FAS for line 20641	151
Figure 5.39: Sub-sections of the multiplot for line 20641	152
Figure 5.40: A comparison between EM Flow and GA-LEI for line 2064.....	152
 Figure 6.1: Simplified event history of the Paterson region	156
Figure 6.2: Simplified solid geology of the Paterson region	157
Figure 6.3: Geological cross section of the Kintyre ore lens, Kintyre uranium deposit	160
Figure 6.4: Geophysical signature of the area surrounding the Kintyre uranium deposit.....	161
Figure 6.5: Geophysical signature of the area surrounding the Sunday Creek, Mt Sears and Maroochydore prospects	165
Figure 6.6: Geological plan and cross section of the Nifty deposit	168
Figure 6.7: Geophysical signature of the area surrounding the Nifty copper deposit	171
Figure 6.8: Portion of a layered earth inversion conductivity section across the Nifty deposit	172
Figure 6.9: Geological cross section of the Maroochydore deposit.....	172
Figure 6.10: Portion of a layered earth inversion conductivity section across the Maroochydore deposit.....	174
Figure 6.11: Geological map of the Warrabarty deposit.....	176
Figure 6.12: Geological cross section of the Dromedary prospect	178
Figure 6.13: Mineral system model for the Miles mineral system.....	179
Figure 6.14: Image of the Cottesloe Syncline area showing variations in the Al-OH absorption feature of white mica, as determined from ASTER data and PIMA analyses	186
Figure 6.15: Diagrams showing solubility of uranium, copper, lead and zinc in a 5 wt. % NaCl fluid.....	188
Figure 6.16: Geology of the northern part of the Paterson region	190
Figure 6.17: Geological map of the Telfer Dome	192
Figure 6.18: Schematic cross section showing the geology of the Telfer	193
Figure 6.19: Geophysical signature of the Telfer area	196
Figure 6.20: A portion of a layered earth inversion conductivity section across the Telfer deposit	198
Figure 6.21: Geological section through the Magnum prospect	198
Figure 6.22: Photographs of core from the Magnum prospect	200
Figure 6.23: ^{40}Ar - ^{39}Ar age spectra of biotite and muscovite from the Magnum deposit	201
Figure 6.24: Plan and schematic cross section of the O'Callaghans tungsten-zinc-lead- copper skarn	202
Figure 6.25: Mineral system model for the O'Callaghans mineral system	203
Figure 6.26: Rb/Sr versus Fe_2O_3 -FeO diagram showing the composition of granites from the Paterson region	206
Figure 6.27: Model depicting the formation of calcrete-hosted uranium deposits	213
 Figure 7.1: Scheme of three families of uranium mineralising systems	220
Figure 7.2: Ternary diagram of radiometric data in the Paterson region	222
Figure 7.3: Uranium anomalies from radiometric data in the Paterson region	223
Figure 7.4: Uranium and vanadium abundances in the Rudall 1:250 000 map sheet area.....	225
Figure 7.5: Thorium anomalies from radiometric data in the Paterson region	226
Figure 7.6: Image of U^2/Th ratio anomalies in the Paterson region.....	227
Figure 7.7: Normalised U^2/Th ratio anomalies in the Paterson region	228

Figure 7.8: Conceptual model for diagenetic fluid-related uranium mineral systems	230
Figure 7.9: Neoproterozoic unconformities in the Paterson region.	235
Figure 7.10: Conductivity sections over pre-Permian solid geology of the Warroo Hill-Mt Gregory area	234
Figure 7.11: The Coolbro-Rudall unconformity depicted in a Geoscience Australia layered earth inversion (GA-LEI) AEM conductivity section	239
Figure 7.12: Potential trap rocks in the Rudall Complex and Coolbro Sandstone in the Kintyre-Rudall area.....	242
Figure 7.13: Conductivity sections over pre-Permian solid geology in the Paterson South survey area	247
Figure 7.14: Selected AEM conductivity sections over pre-Permian solid geology in the Paterson area	248
Figure 7.15: GA-LEI conductivity depth slice at 150 m for the Paterson North survey area	250
Figure 7.16: Conceptual models of sandstone-hosted uranium mineral systems.....	251
Figure 7.17: Palaeovalley-palaeochannel type sandstone-hosted uranium deposit at Beverley, South Australia	252
Figure 7.18: Inferred top surface of Proterozoic in 3D from AEM data in the Paterson South survey area	255
Figure 7.19: The Rudall River-Lake Dora area	260
Figure 7.20: Major current drainage and palaeo-drainage systems in the Paterson area	262
Figure 7.21: Distribution of key components of calcrete-hosted uranium systems in the Paterson area	265
Figure 7.22: Mapped calcrete and lakes over GA-LEI 200-250 m conductivity depth slice of the Paterson South survey area	266
Figure 7.23: Prospectivity map for calcrete-hosted uranium mineral systems in the Paterson area	267
Figure 7.24: The Lake Waukarlycarly area	268
Figure 7.25: Lake Disappointment West area.....	269
Figure 7.26: Lake Disappointment Southeast area	270
Figure 7.27: Percival Lakes – Lake Auld area.....	271
 Figure A1.1: Average annual thunder days for Australia	293
Figure A1.2: Average annual total lightning flash density for Australia.....	293
Figure A3.1: Schematic representation of the framework for GA-LEI inversion of TEMPEST AEM data	298
Figure A3.2: The principle of operation of inductive conductivity borehole logging tool	309
Figure A3.3: Comparison of logs from the repeat hole, from the beginning and end of field trip.....	311
Figure A3.4: An example of repeat conductivity logs for hole HB326	312
Figure A3.5: Conductivity logs compared to GA-LEI results	314
Figure A3.5: Conductivity logs compared to GA-LEI results (continued).....	315
Figure A3.5: Conductivity logs compared to GA-LEI results (continued).....	316

Tables

Table 1.1: Paterson AEM survey in-fill companies	18
Table 1.2: Atlas of Australian Soils landform attributes for polygons	25
Table 2.1: Available geological maps in the Paterson AEM area.....	31
Table 2.2: Compilation of seismic surveys within or intersecting the Paterson survey area	34
Table 2.3: Drill hole depth frequency for the public domain drill hole database.....	39
Table 2.4: Rock properties important for geophysical surveying	41
Table 2.5: Electrical properties of selected geological materials in the Paterson survey area	41
Table 3.1: Fortescue Group stratigraphy.....	52
Table 3.2: Talbot Terrane metasedimentary stratigraphy	56
Table 3.3: Throssell Range Group stratigraphy, Paterson North	58
Table 3.4: Lamil Group stratigraphy.....	59
Table 3.5: Tarcunyah Group - Paterson north stratigraphy.....	65
Table 3.6: Other Tarcunyah Group units	65
Table 3.7 Permian sediments in the Paterson area	67
Table 3.8: Mesozoic sedimentary sequences in the Paterson area.....	70
Table 3.9: Data sets and rules used to develop the Paterson regolith map.....	77
Table 3.10: Regolith unit code explanations.....	78
Table 4.1: TEMPEST™ AEM system specifications	89
Table 4.2: GA-LEI model layer thicknesses and depths from surface.....	92
Table 4.3: Conductivities used in the forward modelling	93
Table 4.4: JPEG world file contents for line 10000	99
Table 4.5: Panel descriptions for GA-LEI multiplots	100
Table 4.6: Coordinates (MGA94 Zone 51) and depths of the 19 conductivity-logged boreholes	102
Table 5.1: Quality control and quality assurance steps.....	108
Table 5.2a: X component additive noise (standard deviation of high altitude data) for the Paterson Survey.....	109
Table 5.2b: Z component additive noise (standard deviation of high altitude data) for the Paterson Survey.....	109
Table 5.3: Panel descriptions for sample multiplot in Figure 5.1	110
Table 5.4: XYZ resolutions of AEM raster data sets used for validation and correlation	114
Table 6.1: Features and mappable characteristics of the Miles mineral system	180
Table 6.1: Features and mappable characteristics of the Miles mineral system (continued)	181
Table 6.2: Features and mappable characteristics of the O'Callaghans mineral system	204
Table 6.3: Features and mappable characteristics of calcrete-hosted uranium systems.....	212
Table 7.1: Key assessment criteria for potential of uranium mineral systems and implication of AEM data in the Paterson area.....	221
Table 7.2: U/Th ratios of analysed samples from Western Australia	224
Table 7.3: U ² /Th ratios of analysed samples from Western Australia	225
Table 7.4: Key mappable criteria for assessing potential of unconformity-related uranium mineral systems in the Paterson area.....	230
Table 7.5: Key components of mineral systems and potential of unconformity-related uranium mineral systems.....	233
Table 7.6: Tarcunyah Group stratigraphy	231
Table 7.7: Hardey Formation (Fortescue Group) stratigraphy.....	236

Table 7.8: Throssell Range Group stratigraphy	238
Table 7.9: Key mappable criteria for assessing potential of stratabound uranium-copper associated with the Broadhurst-Coolbro contact in the Paterson area	245
Table 7.10: Key mappable criteria for assessing sandstone-hosted uranium mineral systems	253
Table 7.11: Stratigraphy in the Oakover Valley area.....	258
Table 7.12: Key mappable criteria for assessing calcrete-hosted uranium mineral systems	259
Table 7.13: Potential of calcrete-hosted uranium systems in the Paterson region.....	263
Table A3.1: Example of field sheets acquired for conductivity logs.....	313

Executive Summary

The Paterson airborne electromagnetic (AEM) survey was conducted between September 2007 and October 2008 over the Paterson region of northwestern Western Australia as part of the Australian Government's Onshore Energy Security Program. The survey was flown by Fugro Airborne Surveys Pty. Ltd. (FAS), for Geoscience Australia (GA), using the Fugro TEMPEST™ time-domain AEM system. The survey included a total of 28 200 line km flown at various line spacings (6 km, 2 km, 1 km and 200 m) and covered approximately 47 600 km² for a total survey cost of \$2 725 030. The Paterson survey was the first regional AEM survey flown in Australia.

The Paterson AEM survey was designed to deliver reliable, pre-competitive AEM data to promote exploration for uranium, uranium-copper, copper-gold, base metals and manganese minerals in the under-explored Paterson region. The survey area includes the working mines of Woodie Woodie (manganese), Nifty (copper) and Telfer (gold-copper) and the deposits at Kintyre (uranium) and Magnum (copper). All of the known deposits or prospects occur in Archean or Proterozoic rocks that outcrop within the surrounding Permian, Mesozoic and Quaternary cover, which comprises about 84% of the survey area.

Airborne electromagnetic data were subjected to quality assurance and quality control procedures before being inverted using sample-by-sample GA layered earth inversion (GA-LEI) software. Data products released to the public include the contractor-supplied data, ASCII format GA-LEI data, PDF-format multiplots of GA-LEI line data and georeferenced raster images of the GA-LEI conductivity sections, GA-LEI conductance grids, GA-LEI conductivity depth slices and GA-LEI conductivity elevation slices. The GA-LEI data were validated using confidential and public-domain drill hole conductivity data collected during field trips to the region and public-domain drill hole lithological data compiled during the data processing phase of the survey.

Interpretation of GA-LEI data for uranium systems reveals new information for uranium prospectivity in potential unconformity-related, sandstone (roll-front and tabular) and valley calcrete uranium systems. The AEM data were able to image the important Coolbro Sandstone-Rudall Complex unconformity near the Kintyre uranium deposit and highlighted other areas where this unconformity, or others assessed as having moderate to high potential for uranium mineralisation, may occur. The AEM data are particularly effective for mapping carbonaceous and pyritic metasedimentary rocks at depth that may be important reductants for reacting with uraniferous hydrothermal fluids. The AEM data also provided new interpretations for the extent of Permian palaeovalley systems, the extent of and inter-relationships between Archean and Proterozoic bedrocks and Permian and Mesozoic cover in the Canning Basin and the extent of potential redox fronts near salt lakes and playas associated with valley calcretes occupying palaeodrainage channels within the survey area.

The potential for gold and base metal mineralisation within the survey area has been reassessed in light of collated knowledge regarding the Miles mineral system, important for copper-uranium, uranium-copper and base metal mineralisation in the Nifty, Sunday Creek and Magnum deposits, and the O'Callaghans mineral system, important for gold, base metal and skarn deposits including Telfer and O'Callaghans. The Miles mineral system is the most prevalent and formed during the inversion of the Yeneena Basin. This mineral system dissolved uranium and copper and deposited them at redox boundaries near major faults. The O'Callaghans mineral system operated during and after intrusion of the O'Callaghans granite suite.

The AEM data do not appear to map the ore deposits directly, except at Woodie Woodie, however, they do map the ore host rock types for both mineral systems, especially where they have a conductivity contrast with surrounding rock types. The GA-LEI conductivity grids and sections have provided new insights into the extent of these target rocks under cover of the Paleozoic-Mesozoic Canning Basin and Cenozoic indurated regolith, sand dunes and sand sheets.

The AEM data have greatly improved understanding of the basement-cover relationships in the area, particularly between Proterozoic rocks of the Yeneena Basin and Rudall Complex and the overlying Paleozoic-Mesozoic rocks of the Canning Basin. A number of the units within the Permian and Mesozoic cover are weakly to moderately conductive, due to contained clays, saline groundwater, or a combination of both. The AEM data and the drill hole data base have also allowed the 3D stratigraphy of the Canning Basin to be interpreted over a broad area, revealing a number of large-scale sedimentary structures that were previously unknown. The data also reveal new information regarding the 3D structure of Permian palaeovalley systems around the Rudall Complex, especially those near the Kintyre uranium deposit. The AEM data are also shown to be unaffected by indurated regolith within the survey area, particularly ferruginous duricrust, which would have previously been regarded as impenetrable to electromagnetic radiation.

The AEM data show great promise for ground water studies within the region and have revealed new detail on the 3D structure of large, presumed Eocene to Oligo-Miocene age, palaeodrainage systems including the Canning Palaeovalley, the Disappointment Palaeovalley and the Wallal Palaeovalley. The AEM data show conductivity anomalies within these systems most likely related to saline ground water, especially along palaeodrainage systems that have large numbers of well developed salt lakes and playas. A number of palaeodrainage systems have resistive fill and show potential for fresh to brackish groundwater resources within the survey area.

Results from the Paterson AEM survey highlight the utility of regional AEM surveying in Australia. The survey results have provided new pre-competitive data for mineral explorers and lessened exploration risk by highlighting potential target rocks, providing more detailed depth to target information and showing new prospective areas under cover where exploration can continue.

1 Introduction

I. C. Roach and M. T. Costelloe

1.1 SURVEY CHARACTERISTICS

The Paterson Orogen (Paterson) airborne electromagnetic (AEM) survey was designed to deliver reliable, pre-competitive AEM data and scientific analysis of the energy resource potential of the Paterson region of Western Australia ([Figure 1](#)). This survey was the first regional AEM survey conducted within the Onshore Energy Security Program (OESP) at Geoscience Australia (GA). The survey was flown by Fugro Airborne Surveys Pty. Ltd. (FAS), for GA, as a combined TEMPEST™ time-domain electromagnetic (TEM) and magnetic survey between the 10th of September 2007 and the 28th of October 2008.

The survey was conducted with the aims of reducing exploration risk, stimulating exploration investment and enhancing prospectivity for various energy commodities, particularly uranium, in the Paterson area. The area covers parts of the ANKETELL, BALFOUR DOWNS, GUNANYA, NULLAGINE, PATERSON RANGE, RUDALL, RUNTON, TABLETOP and YARRIE 1:250 000 map sheets.

The Paterson AEM survey was designed as a regional mapping program, primarily for the mapping of subsurface geological features that may be associated with unconformity-related, sandstone-hosted and palaeovalley-hosted uranium mineralisation. The data are also capable of interpretation for other commodities including metals and potable water as well as for landscape evolution studies.

1.2 SURVEY LOCATION

The Paterson AEM survey area lies in the southwestern Great Sandy Desert and includes the Paterson, Throssell and Gregory ranges, Lake Waukarlycarly and parts of the Rudall Complex and Percival Lakes system in northwest Western Australia. The survey area is bisected by the Rudall River National Park. The survey area includes the working mines of Woodie Woodie (manganese), Nifty (copper) and Telfer (gold-copper) ([Figure 1.1](#)), large prospects including Kintyre (uranium), Magnum (gold-copper), Maroochydore (copper) and many smaller ones in the Paterson Orogen, Rudall Complex and parts of the Pilbara Craton and the on-lapping Canning and Officer Basins (see [Figure 1.3, Section 1.3](#))

Road access to the region is difficult. The only all-weather road is the partially sealed Telfer Access Road from Marble Bar to Telfer. The remainder of the roads are dry-weather only and include access roads to Wolf Creek, Tanami and Alice Springs in the north and the Canning Stock Route in the southeast. Tracks are formed on various substrates from hard rock to loose sand, have various grades from completely flat to steep in the ranges around Woodie Woodie and may require drivers to negotiate sand dunes up to 20 m high in the tenements. Air access is limited, with private all-weather airstrips available only at the Nifty, Telfer and Woodie Woodie mining centres. Gravel airstrips are available at Parnngurr, Punmu and Well 33 (on the Canning Stock Route to the east of the survey area) as well as the few cattle stations in the region.

The survey was flown at variable line spacings with the GA regional lines flown at 6 km, 2 km and 1 km spacing depending on location ([Figure 1.2](#)), and more detailed GA or company infill lines at 200 m line spacing in areas of interest (see [Figure 1.12, Section 1.5](#)). Survey lines were oriented east-west in the North Paterson survey area and northeast-southwest in the South Paterson survey area to lie more perpendicular to geological strike. The survey does not cover the Rudall River National Park.

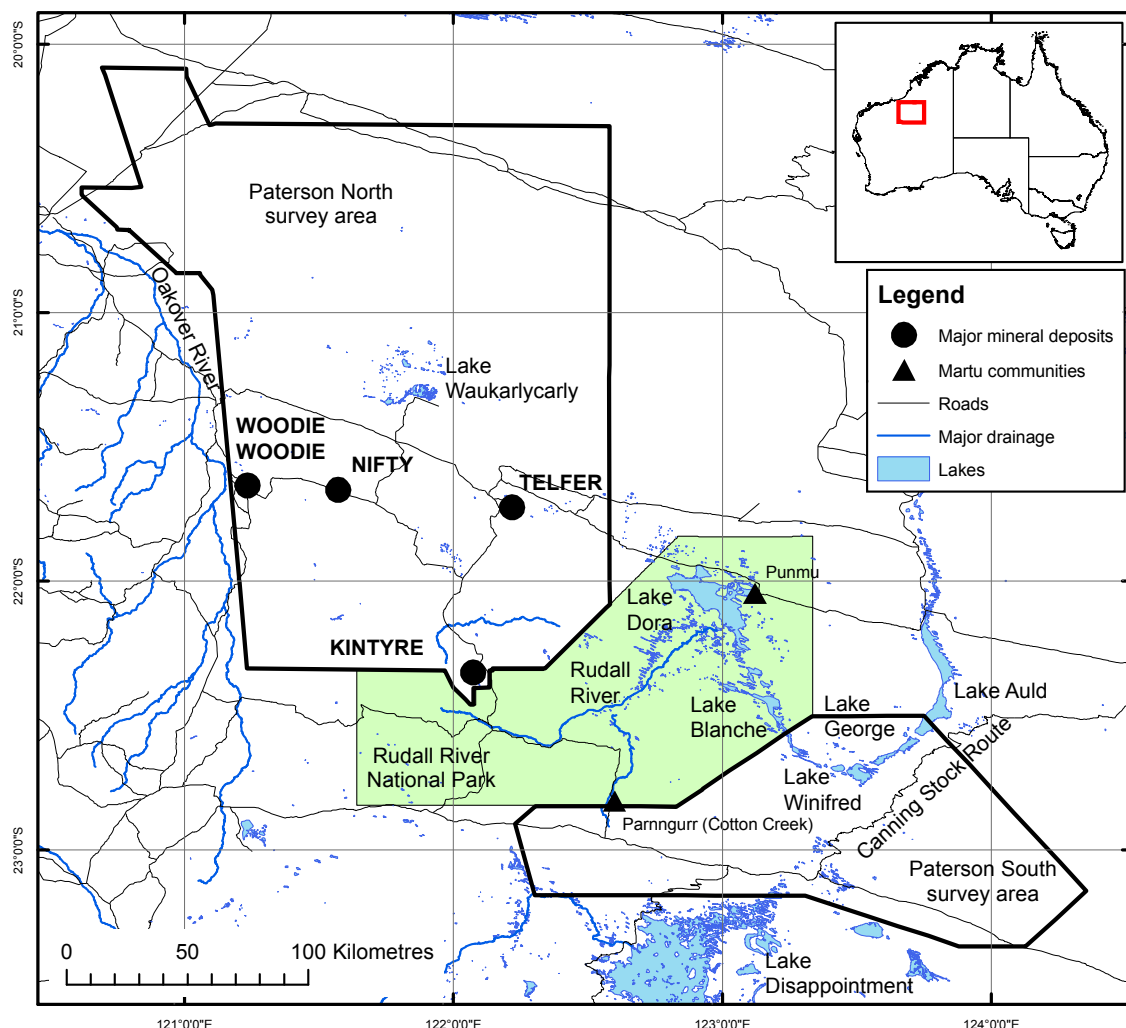


Figure 1.1: Survey location showing the principal mineral deposits, settlements, access roads and major drainage systems.

1.3 SURVEY PURPOSE

1.3.1 Uranium systems

The Paterson AEM survey was designed primarily to locate settings capable of hosting uranium mineralisation. The region is well known for its uranium potential, hosting Australia's fifth largest uranium deposit at Kintyre (36 000 t U₃O₈) after Olympic Dam (1 018 022 t U₃O₈), Jabiluka (204 000 t U₃O₈), Ranger (143 000 t U₃O₈) and Yeelirrie (52 500 t U₃O₈) (McKay and Miezitis, 2001). Through its Geological Reference Group, GA assessed Paterson as having high potential for large scale uranium deposits in unconformity-style deposits at the unconformity between the Rudall Complex and the overlying Coolbro Sandstone of the Yeneena Supergroup (Bagas *et al.*, 2000), like that at Kintyre (Andrew, 1988; Jackson and Andrew, 1990; Hickman and Clarke, 1994). There is also potential for these styles of deposit elsewhere within the Yeneena Supergroup. There is further potential within the overlying Officer Basin or Canning Basin for sandstone-style roll-front deposits or valley calcrete deposits. Most of the known uranium resources in the Paterson area are within the Rudall Complex at Kintyre (24 500 t U₃O₈ probable plus 11 500 t U₃O₈ inferred; McKay and Miezitis, 2001). Smaller deposits are also known at the Tracy, Lead Hills and Mount Cotton prospects in the Rudall Complex and the Sunday Creek and Mount Sears prospects within the

Coolbro Sandstone (McKay and Miezitis, 2001).

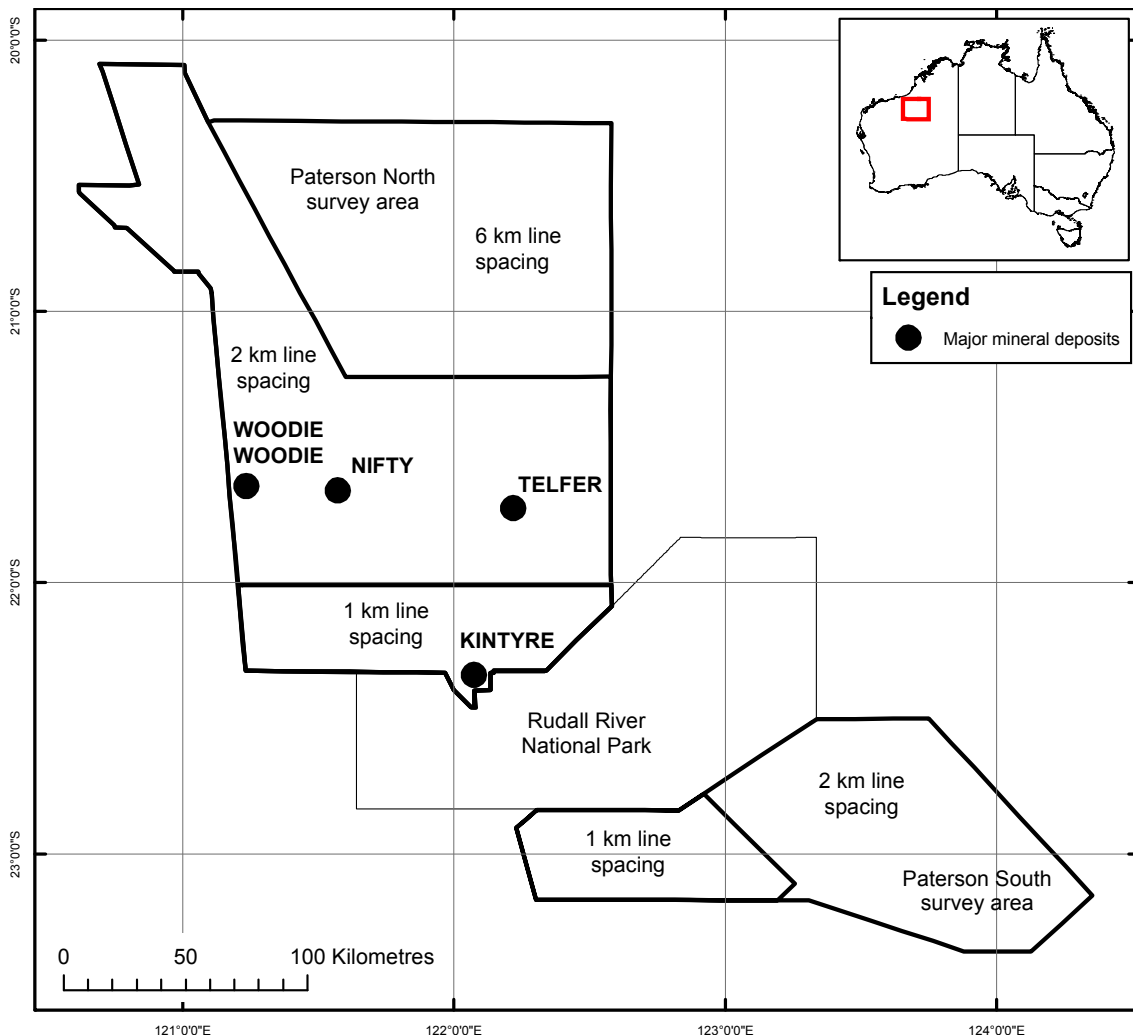


Figure 1.2: Regional survey line spacing. See Figure 1.12 for GA detail and company infill flight lines.

The descriptions below contain a brief introduction to likely uranium systems in the Paterson region summarised from McKay and Miezitis (2001). More detail on the assessment of uranium systems in the Paterson region is included in McKay and Miezitis (2001), Skirrow *et al.* (2009) and Chapter 6 of this Record.

1.3.1.1 Unconformity-related uranium deposits

The Mesoproterozoic granulite facies metamorphic rocks of the Rudall Complex host or act as source rocks for unconformity-related uranium deposits, the largest known being Kintyre (McKay and Miezitis, 2001). These types of deposits occur around the unconformity between the Rudall Complex and the overlying Coolbro Sandstone of the Neoproterozoic Throssell Group and may be several tens of metres above or below the unconformity itself (McKay and Miezitis, 2001). At Kintyre, uranium mineralisation occurs as pitchblende veins within complexly folded and faulted greenschist facies retrograde metamorphic rocks of the Yandagooge Formation (Rudall Complex) below the unconformity with overlying Neoproterozoic Coolbro Sandstone (Andrew, 1988; Jackson and Andrew, 1990; Hickman and Clarke, 1994).

In other parts of the Rudall Complex, uranium mineralisation is associated either with copper, lead and zinc mineralisation in schists (Tracy and Lead Hills prospects; Hickman and Clarke, 1994) or occurs solely as uranium in graphite-garnet-chlorite schists at Mount Cotton (Bagas *et al.*, 2000).

Uranium mineralisation is also noted within the Neoproterozoic Coolbro Sandstone overlying the Rudall Complex at Sunday Creek (Swingler, 1981) and within sheared sandstone at Mt Sears (Schwabe, 1981).

1.3.1.2 Sandstone uranium deposits

Sandstone uranium deposits may occur in sedimentary rocks or partially consolidated sediments where they are juxtaposed against fertile source rocks, nominally uranium-enriched igneous or high-grade metamorphic rocks, in on-lapping sedimentary basins. Numerous well-known examples exist in Australia, probably the best known being the Beverley deposit in the Frome Embayment of South Australia, but also the Four Mile, Goulds Dam, Oban and Honeymoon deposits in the same region (McKay and Miezitis, 2001). Uranium mineralisation may occur as tabular or roll-front deposits in sand sheets, palaeovalleys or palaeochannels buried beneath the landscape where oxidised uranium-bearing fluid meets a reductant which could include carbon (as free carbon or graphite), carbonate, lignite, hydrocarbon or other reduced sediment or ground water.

No sandstone uranium deposits are known in the Paterson region, however a number occur in the wider area including the Mulga Rock deposits (Fulwood and Barwick, 1990), 230 km ENE of Kalgoorlie in the Gunbarrel Basin, and the Oobagooma deposit (Bautin and Hallenstein, 1997), 75 km NE of Derby in the Yampi Embayment of the Canning Basin. The Paterson region is regarded as having great potential where sediments of the Canning and Officer basins, including Paleozoic to Cenozoic sediments, are juxtaposed against uranium-bearing rocks of the Rudall Complex and possibly the Mt Crofton Granite suite. The Mt Crofton Granite suite extends well north of the Rudall uplands past Telfer into the Anketell Shelf region (see [Figures 5.20](#) and [5.22](#)).

1.3.1.3 Surficial (calcrete) uranium deposits

Surficial or calcrete uranium deposits are broad, near-surface deposits associated with sediments or soils, particularly with valley calcrete accumulations, defined in Chen *et al.* (2002). In the Yilgarn Craton these deposits occur downstream of weathered uranium-bearing Archean granites and vanadium-bearing greenstones, resulting in dominantly carnotite uranium mineralisation in valley-fill sediments (Yeelirrie) and playa lake sediments (Lake Maitland) (McKay and Miezitis, 2001). A large number of surficial or calcrete uranium deposits are known within inland Australia, particularly within valley calcrites of the Yilgarn Craton. Some of the largest include Yeelirrie (Cameron, 1990), Lake Way (Brunt, 1990), Lake Maitland (Acclaim, 1999) and Centipede (Brunt, 1990).

The Paterson region has potential to host significant calcrete uranium deposits in and around the chain of lakes (the Percival Lakes) associated with the Canning Palaeovalley (Magee, 2009), also referred to as the Percival Palaeovalley (van der Graaf *et al.*, 1977), and the Lake Disappointment and Lake Waukarlycarly areas.

1.3.2 Other mineral systems

The Paterson region is highly prospective for a range of other minerals including gold, base metals and manganese and is also potentially prospective for other commodities including bauxite, iron ore, lanthanides, road construction materials, diamonds, petroleum, coal and water ([Figure 1.3](#)).

Mines currently operate at Telfer (gold-copper), Nifty (copper) and Woodie Woodie (manganese) but numerous prospects for the other commodities occur widely throughout the area. These are considered in more detail in [Chapter 6](#) of this Record.

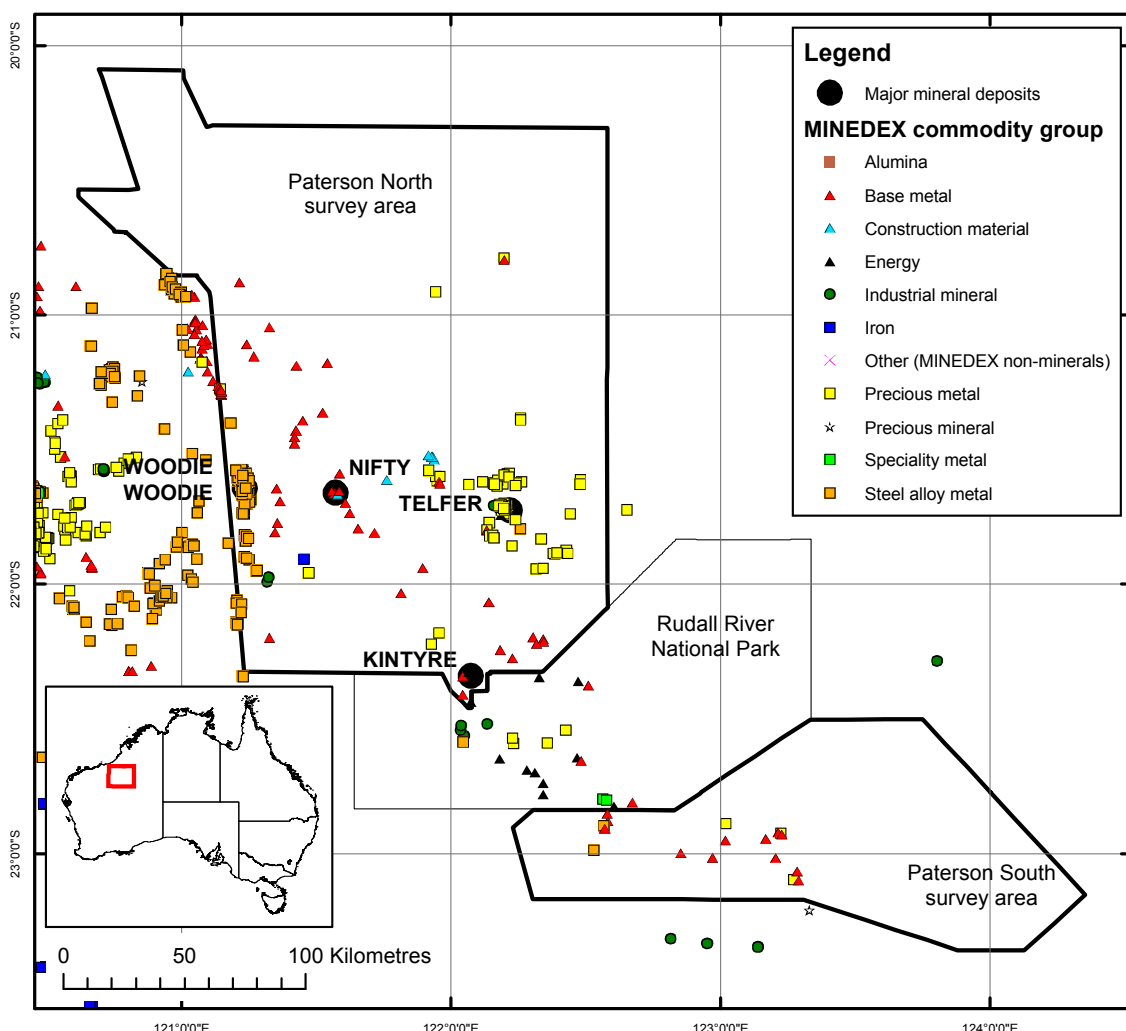


Figure 1.3: Major commodity deposits and prospects within the Paterson region. Commodity data are from the Geological Survey of Western Australia's MINEDEX database.

1.3.3 Groundwater systems

The Paterson region hosts a number of groundwater systems associated with fractured rock aquifers, palaeovalleys and sedimentary units of various ages. These systems are exploited by indigenous communities living at Punmu (Lake Dora) and Parnngurr (Cotton Creek), as well as by mining operations at Woodie Woodie, Nifty and Telfer, and are a major consideration for any new development activity.

The community at Punmu draws groundwater from bores in an aquifer in the Permian Triwhite Sandstone, which also discharges water in springs around Lake Dora (Commander, 1985; Kern, 1994). The community at Parnngurr draws water from bores in shallow alluvial and calcrete aquifers (Thorpe, 1988).

Water for the mining communities is largely drawn from fractured rock aquifers around the mine sites. At Woodie Woodie water is drawn from bores in the Archean Carawine Dolomite. At Telfer, water is drawn from bores in Yeneena Basin sediments including the Puntapunta, Wilki and Marlu formations. At Nifty, water is drawn from bores in Yeneena Basin sediments of the Broadhurst Formation, but is supplemented by water drawn from bores into Permian palaeovalleys near the site

(Lewis *et al.*, 2009). It is vital to secure water resources for the indigenous communities and to allow further development of mineral resources in the region. More detail on the palaeovalley groundwater resources of the Paterson region are considered in [Chapter 2](#) and [Chapter 5](#) of this report.

1.4 SURVEY ECONOMIC FRAMEWORK

The Australian Government provided funding under the OESP to secure energy resources for Australia's future including uranium, petroleum and geothermal energy in areas that are under-explored for these commodities. The OESP funds for the Paterson survey were directed towards providing pre-competitive data for locating unconformity, palaeovalley and calcrete-hosted uranium systems, which are described briefly above and in detail in [Chapter 6](#) of this report.

The Paterson region is under-explored; statistics calculated using the Paterson AEM survey outline and the Surface Geology of Western Australia map (Stewart, 2008; [Figure 1.4](#)) indicate that Paleozoic to Cenozoic cover comprises 84% of the total survey area, whereas the economic basement (the pre-Paleozoic) outcrops over only 16% of the total area. It is the 84% of the survey area that is the most under-explored and has just been pricked here and there by generally shallow exploration drilling ([Figure 1.5](#); Roach, 2009). Much of the drilling occurs on or near outcropping economic basement rocks along strike from known mineral deposits. Wildcat drilling has been used with partial success in the Anketell Shelf region (see [Figures 5.20](#) and [5.22](#)) in the northeast of the Paterson North survey area to measure the depth to economic basement under Mesozoic cover, and to recover samples. However, it is interesting to note that of the 402 drill holes in the database within this area, only 262 or 65% of the holes actually reached their target. The Paterson region is therefore regarded as a greenfields region in this respect. Note that the Neoproterozoic of the Yeneena Basin (in the case of Telfer, Nifty and Kintyre) and the Archean (in the case of Woodie Woodie) are mineralised and are here regarded as the economic basement, however, uranium mineralisation may also occur within the cover sequences which obscure the prospective rocks.

The producing mineral deposits were largely discovered using traditional geological and/or airborne geophysical techniques over economic basement rocks that are exposed at the surface. Prospectors discovered the Telfer gold-copper deposit by examining outcrops of Yeneena Basin rocks (Dimo, 1990). The Woodie Woodie deposit was discovered in outcrop by prospectors working in the eastern Pilbara during the late 1940s or early 1950s (Williams and Trendall, 1998a). The Kintyre deposit was discovered using a combination of airborne radiometric, magnetic and electromagnetic techniques by CRA Exploration (Jackson and Andrew, 1990). The Nifty deposit was discovered using ferruginous lag geochemical sampling to vector back to copper-stained bedrock and ironstone outcrops in dune swales (Carver, 2005).

Most of the recognisable outcropping economic basement rocks have now been visited and sampled by various exploration companies, however, a large proportion of the area remains buried by Paleozoic to Cenozoic cover, which may conceal further uranium, gold and base metal mineralisation. Thus, the aims of the Paterson AEM survey were to stimulate interest by locating potential uranium sources and sinks and to determine the depth to economic basement in those areas where basement is not exposed and where drilling has been sparse or absent.

A map of the pre- and post-survey tenement holdings ([Figure 1.6](#)) indicates considerable exploration activity and also illustrates the difference between pre-survey and post-survey tenement holdings in the Paterson region. A map of the tenement purposes is shown in [Figure 1.7](#). The total holdings before and after the survey do not appear to have altered greatly between the pre-survey and post-survey conditions, with some ground being relinquished and some taken up in other areas. This is not to say that the Paterson AEM survey had no effect on tenement holdings. A personal communication from staff at the Aditya Birla Nifty mine to GA (den Tex, 2009) and the De Grey Mining Ltd. annual report for 2009 (De Grey, 2009) confirm that both these companies have taken

up options on new ground as a direct result of the Paterson AEM survey, despite the global economic downturn in 2008.

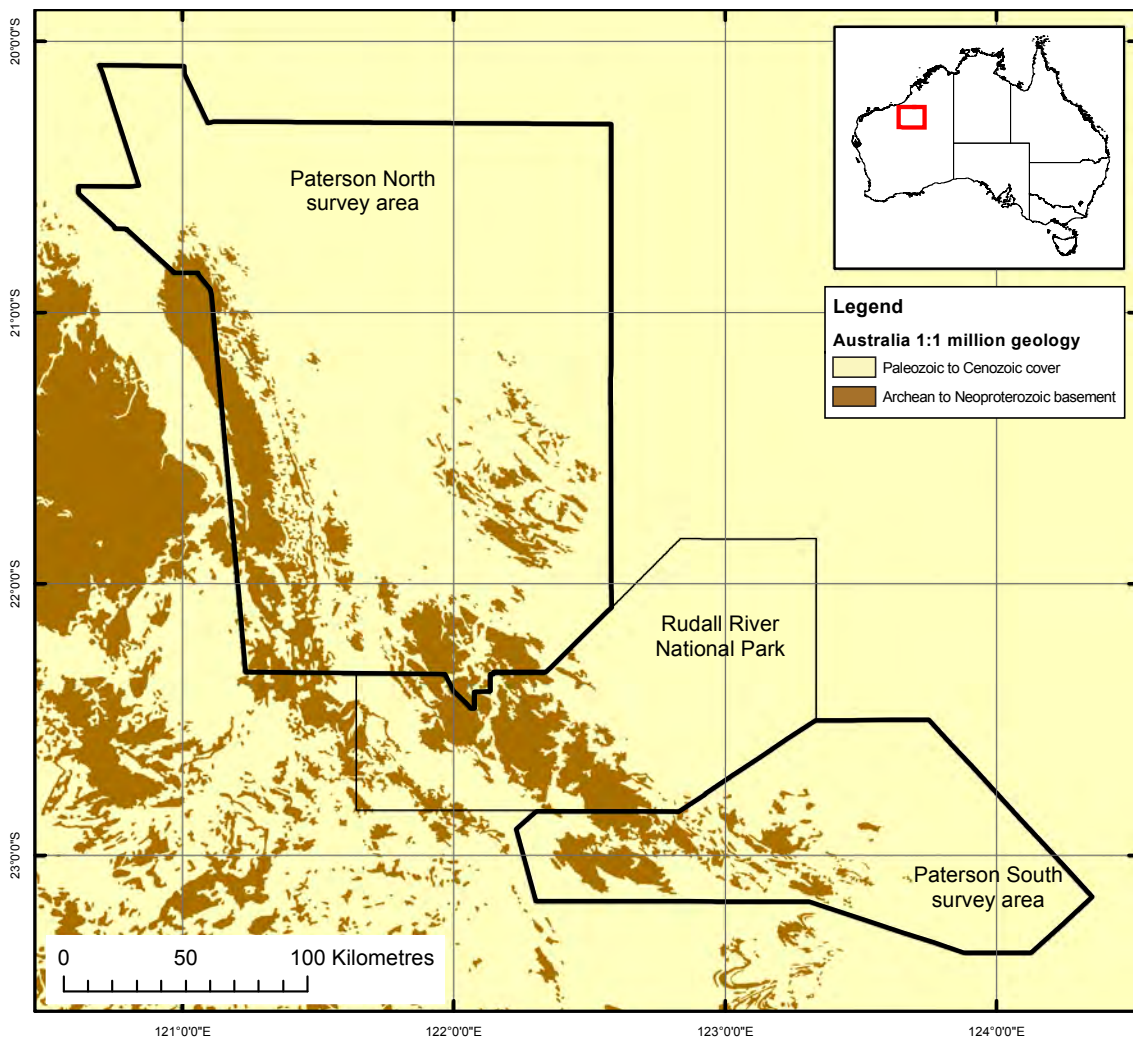


Figure 1.4: Archean to Neoproterozoic basement versus Palaeozoic to Cenozoic cover relationships for the Paterson AEM survey area.

1.5 SURVEY DESIGN CONSIDERATIONS

1.5.1 Climate

Climatic conditions are an important consideration when planning any flight operations, but particularly so when planning airborne geophysical operations which must be flown much closer to ground level than normal aircraft operations. In the case of the Paterson AEM survey acquisition the aircraft was contracted by GA to maintain an average ground clearance of 121 m and the towed receiver (the “bird”) only 81 m. Therefore, accurate knowledge of atmospheric conditions is crucial to maintain both flight safety and data reproducibility.

Air temperature plays an important role in maximum take off weight (MTOW) and aircraft endurance in aerial surveys. For some models of aircraft, particularly the Fugro CASA, as air temperature increases the flight duration decreases rapidly, up to 30 minutes duration decrease per 5°C increase in temperature. Details of survey aircraft flight considerations and other parameters

affecting flight operations are detailed in a memorandum provided by FAS included in [Appendix 1](#).

While mean wind speed at Telfer drops between 9 am and 3 pm, atmospheric turbulence anecdotally increases as daytime temperatures increase, making flying more difficult. Severe turbulence can also result in “coil knock events” that introduce noise into the processed data (Lawrence and Stenning, 2008). Personal communications with aerial survey pilots confirm that the Telfer region also experiences large amounts of airborne dust which causes increased propeller and turbine damage on the aircraft, increasing scheduled maintenance frequency, cost and survey duration.

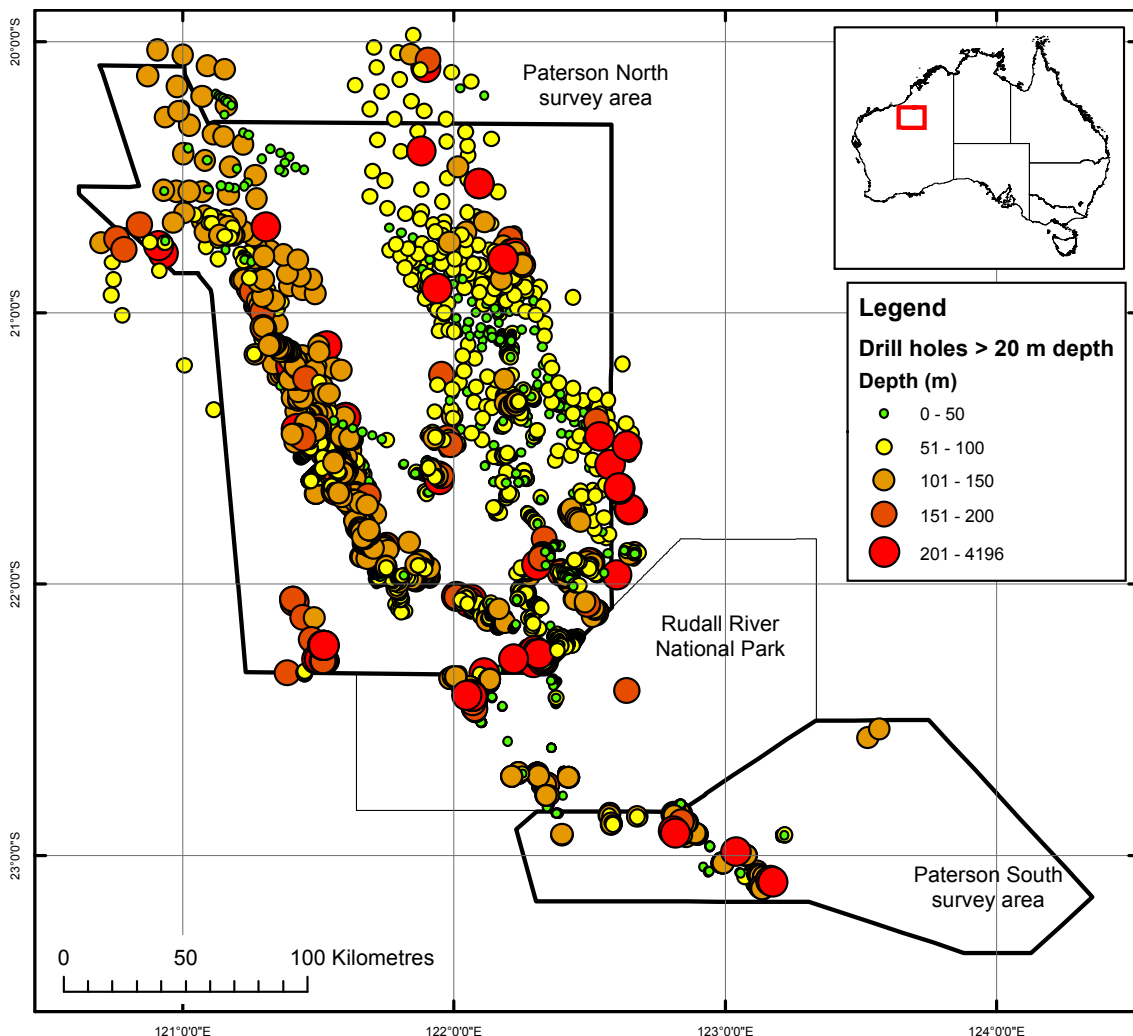


Figure 1.5: Distribution of drill holes in the Paterson AEM survey area. Data from Roach (2009).

The location and frequency of thunderstorms and lightning strikes is another consideration for AEM operations. These cause atmospheric noise (“sferics”) in AEM data. Data can be affected by storms over 1000 km away and Telfer lies within the influence of thunderstorms caused by the summer monsoon in tropical north Australia, particularly Kalumburu and Darwin. Darwin has the highest recorded number of average annual thunder days in Australia and Kalumburu the highest number of average annual lightning flashes in Australia. Most of this storm activity occurs during the build-up to the summer monsoon and during it; flight planning needs to ensure operations are scheduled away from this time. More information on the local climate is included in [Section 1.7](#) of this report and maps of storm data are included in [Appendix 2](#).

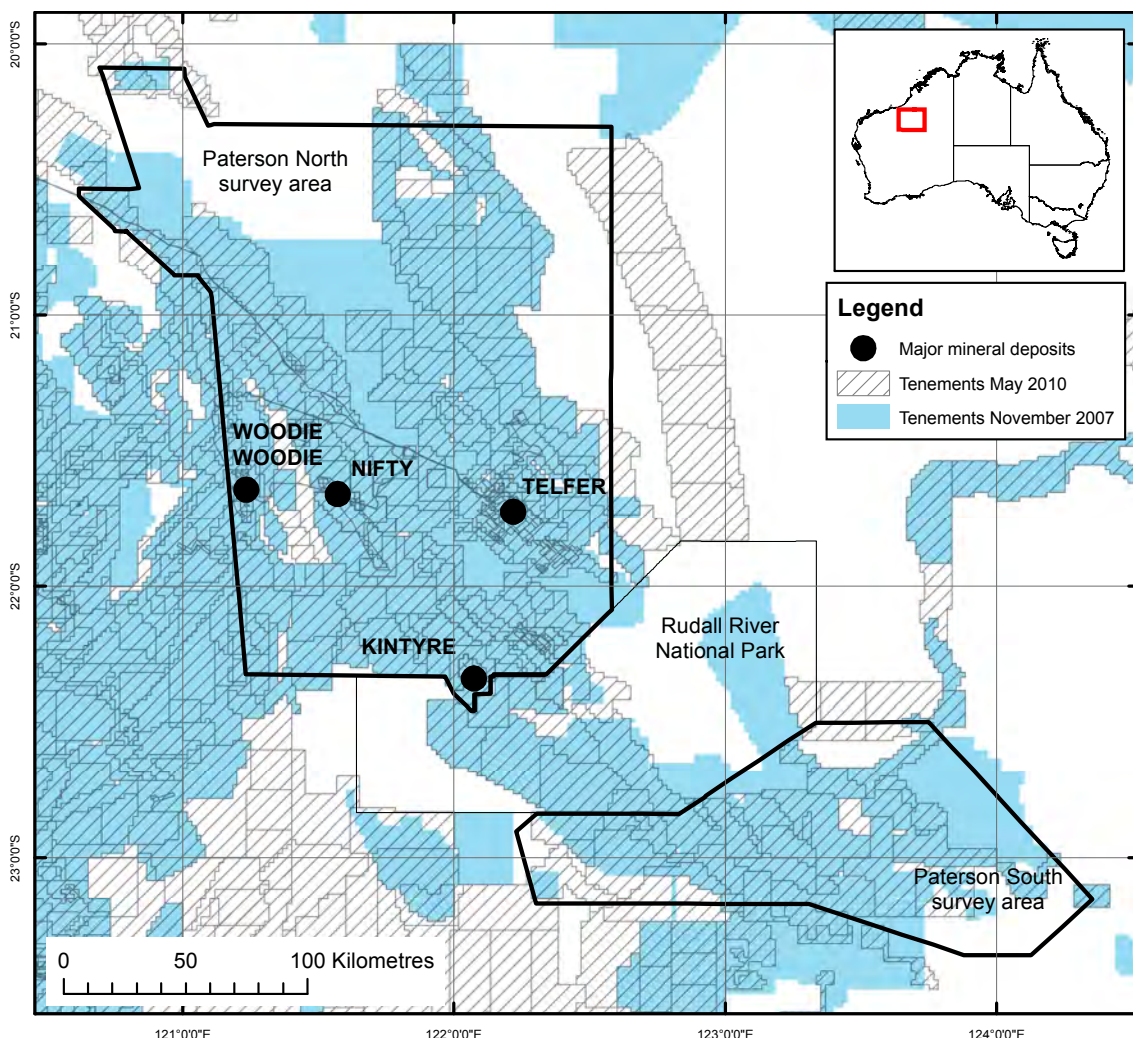


Figure 1.6: Tenement holdings before (November 2007) and after (May 2010) the Paterson AEM survey was flown. Modified from GSWA data.

1.5.2 Terrain (Drape)

Prior to requesting tenders for AEM flight operations a “drape” check is performed. The drape check tests whether the proposed survey can be performed by a nominated aircraft within its safety specifications over the survey area, or whether the proposed flight plan or aircraft type needs to be modified. The aircraft specifications are set out in a deed of standing offer between GA and survey contracting companies. The drape check is a necessary part of flight planning that ensures that it is legally possible to fly the survey with the nominated aircraft within the Federal legislation governing aerial survey operations.

The drape check is performed by entering a digital elevation model of the survey area, together with the proposed flight lines, into specialist GA-proprietary software to highlight areas where the flight lines cross terrain that would cause the aircraft to exceed its maximum rate of climb. For instance, the Fugro CASA aircraft fitted with the TEMPEST™ TEM system has an average rate of climb of only 100 m/km. [Figure 1.8](#) illustrates the results of the drape analysis, indicating that the bulk of the Paterson survey area would allow the Fugro CASA aircraft to operate within its specifications at the contracted flying height of 121 m above ground. In areas where the drape check indicated that the aircraft would exceed its specifications, permission was given to allow the aircraft to fly at slightly higher altitude to provide adequate ground clearance.

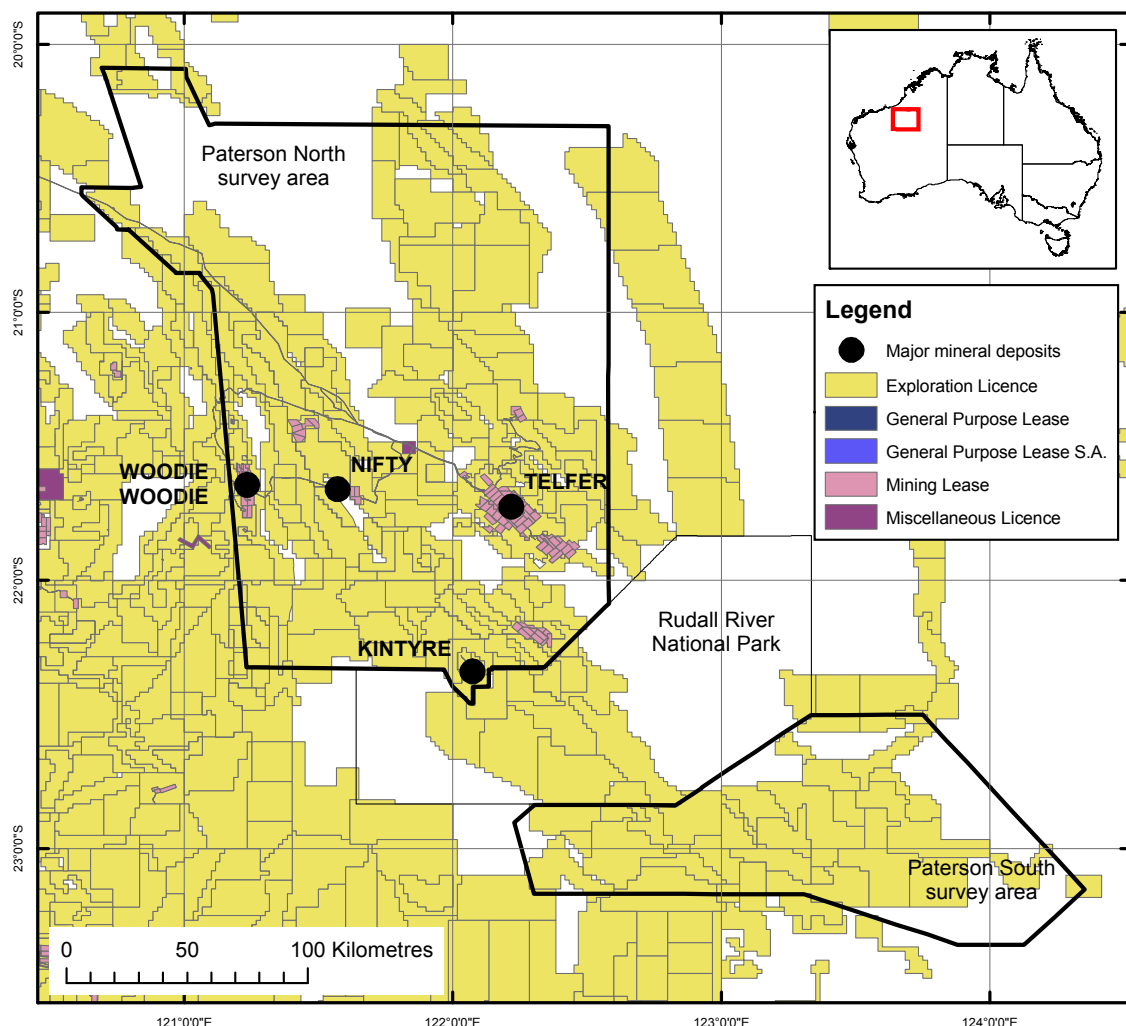


Figure 1.7: Tenement purpose. Modified from GSWA data.

1.5.3 Aircraft access

Aircraft access in the region is limited, with private all-weather airstrips available only at the Nifty, Telfer and Woodie Woodie mining centres or further afield at Newman, Port Hedland or Broome. Gravel airstrips are available at Parnngurr, Punmu and Well 33 (on the Canning Stock Route to the east of the survey area), subject to Martu People permission, as well as the few cattle stations in the western part of the region. Adequate road access to these airstrips for fuel pre-placement is also another important consideration for aerial survey operations.

1.5.4 Forward modelling

The Paterson AEM survey was advertised to aerial geophysics contractors on the GA deed of standing offer and three contractors with four different AEM systems responded with an expression of interest. Before the survey could proceed, the different AEM systems needed to be assessed by forward modelling to test each system's expected performance in the Paterson area. This was achieved by creating a series of synthetic geological settings which approximated the known target conditions for the Paterson region. These scenarios were transferred into electrical models and entered into GA-proprietary software which tests for probability of detection with a false alarm rate of 1%. When all models were deemed of equal relevance in this assessment the Fugro TEMPEST™ TEM system had a detection probability that was more successful than the other systems on the deed of standing offer. Details of the geological models, electrical models and forward model results are

discussed further in Chapter 4 of this report.

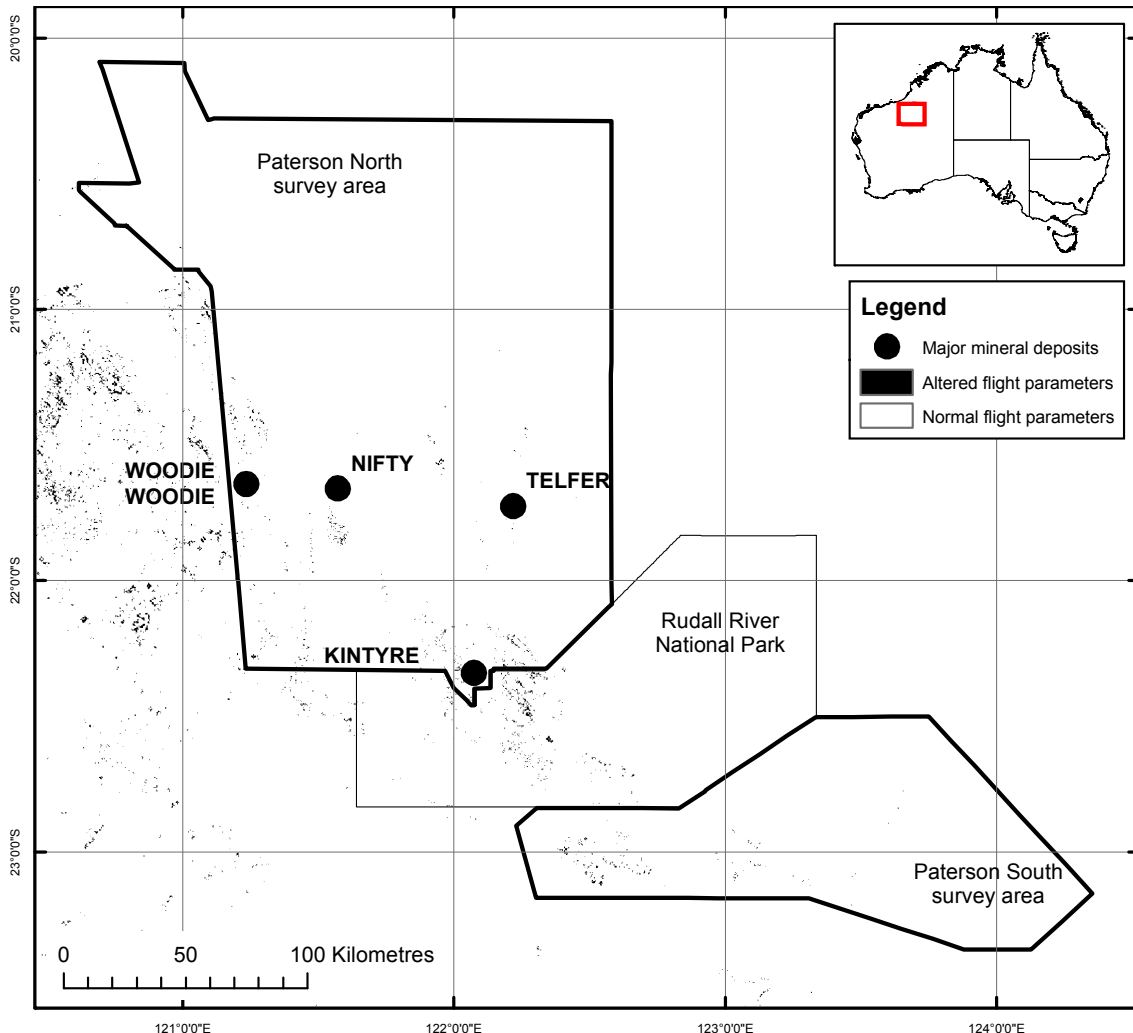


Figure 1.8: Drape analysis results for the Paterson AEM survey. Black dots indicate areas where the contracted flight parameters were altered to provide adequate terrain clearance for the aircraft and towed receiver bird.

1.5.5 Native Title and Land Access issues

The traditional owners of land within the survey boundaries were identified via the National Native Title Tribunal. The principal traditional owners were recognised as the Martu People, who have a Native Title Determination, and the Nyangumarta People, who have a Native Title Claim (Figure 1.9). Communication with the Western Desert Lands Council (WDLAC), which represents all of the traditional owners in the region, commenced in April 2007. Communication included letters, emails and personal meetings with traditional owners outlining the survey boundaries for the purpose of identifying the potential social and cultural impacts of the project, giving an outline of how the survey would be implemented and showing maps that outlined the areas where the survey would be focused.

1.5.6 Other no fly zones

Apart from the Rudall River National Park, no other no fly zones were included in the area. At the

time of survey planning, the Western Australian legislation forbade uranium mining within the State, however it was legal to explore. Also, exploration within national parks was assessed on a case-by-case basis after consideration of economic and social benefits. Given that the money made available by the Australian Government for this survey was primarily for promoting exploration for uranium resources, the Geological Reference Group at GA agreed that flying the Rudall River National Park would be counter to Western Australian State legislation and the survey proceeded on these terms. On the 17th of November 2008 the State Government of Western Australia revoked the uranium mining ban in the state, after the Paterson AEM survey had been flown.

1.5.7 Communication strategy

Geoscience Australia was aware of the probable impact this type of survey might have in the region and the amount of scientific interest it might generate within local, state and federal government agencies, exploration companies, title holders and the general public. Together with the contractors, GA developed a communication strategy including:

- Letters to the relevant national park board;
- Letters and person-to-person communication to relevant indigenous communities and councils;
- Letters to all landholders in the area; and,
- E-mails to all tenement holders in the area.

Communication also included presentations to relevant parties and the industry in general including:

- Oral and poster presentations at the Australian Society of Exploration Geophysicists' conference in 2009;
- Oral and poster presentations at the Geological Survey of Western Australia's open day in Perth, WA, in 2009;
- Oral presentations at the Australian Institute of Mining and Metallurgy's International Uranium Conference in Darwin, NT, in 2009;
- An oral presentation at the Australian Regolith Geoscientists Association conference in Arkaroola, SA, February 2010;
- A one-day workshop for state government and industry representatives at the Geological Survey of Western Australia in Perth, WA, May 2010
- Oral presentations at the Australasian Institute for mining and Metallurgy International uranium Conference in Adelaide, SA, in June 2010;
- Oral and poster presentations at the Australian Earth Science Convention in Canberra, ACT, in July 2010; and,
- Oral presentations at the Australian Society for Exploration Geophysics conference in Sydney, NSW, in August 2010.

1.5.8 Final survey design

The final survey design ([Figure 1.10](#)) was fixed after careful consideration by both the Geological Reference Group and the Geophysical Reference Group at GA. A wide range of cultural, geological, geophysical, remote sensing and topographic data were compiled covering the Paterson survey area over a period of one year to aid the final survey design process. These data included:

- Cultural data including mines, roads, tracks, pipelines;
- Cadastral data including place names;
- Topographic data;
- Hydrological data including water courses and lakes;
- Tenement boundaries from the GSWA Data and Software Centre;
- Mineral occurrences from the GSWA Data and Software Centre;
- Mineral exploration drill hole locations from the GSWA EXACT database;
- Petroleum well locations from the GSWA Data and Software Centre;
- Geoscience Australia 1:1 000 000 Surface Geology of Western Australia (Stewart, 2008);

- Geoscience Australia Radiometric Map of Australia (Minty *et al.*, 2009);
- Magnetic Anomaly Map of the Australian Region;
- Gravity Anomaly of the Australian Region Map;
- Reduced-to-pole (RTP) total magnetics;
- RTP 1st vertical derivative magnetics;
- Shuttle Radar Topography Mission (SRTM) 3 second (90 m) digital elevation model;
- Shuttle Radar Topography Mission (SRTM) 1 second (30 m) digital elevation model;
- Landsat Thematic Mapper mosaic;
- Advanced Spaceborne Thermal Emission and Reflection radiometer (ASTER) mosaic; and,
- Existing ground electromagnetic and AEM surveys.

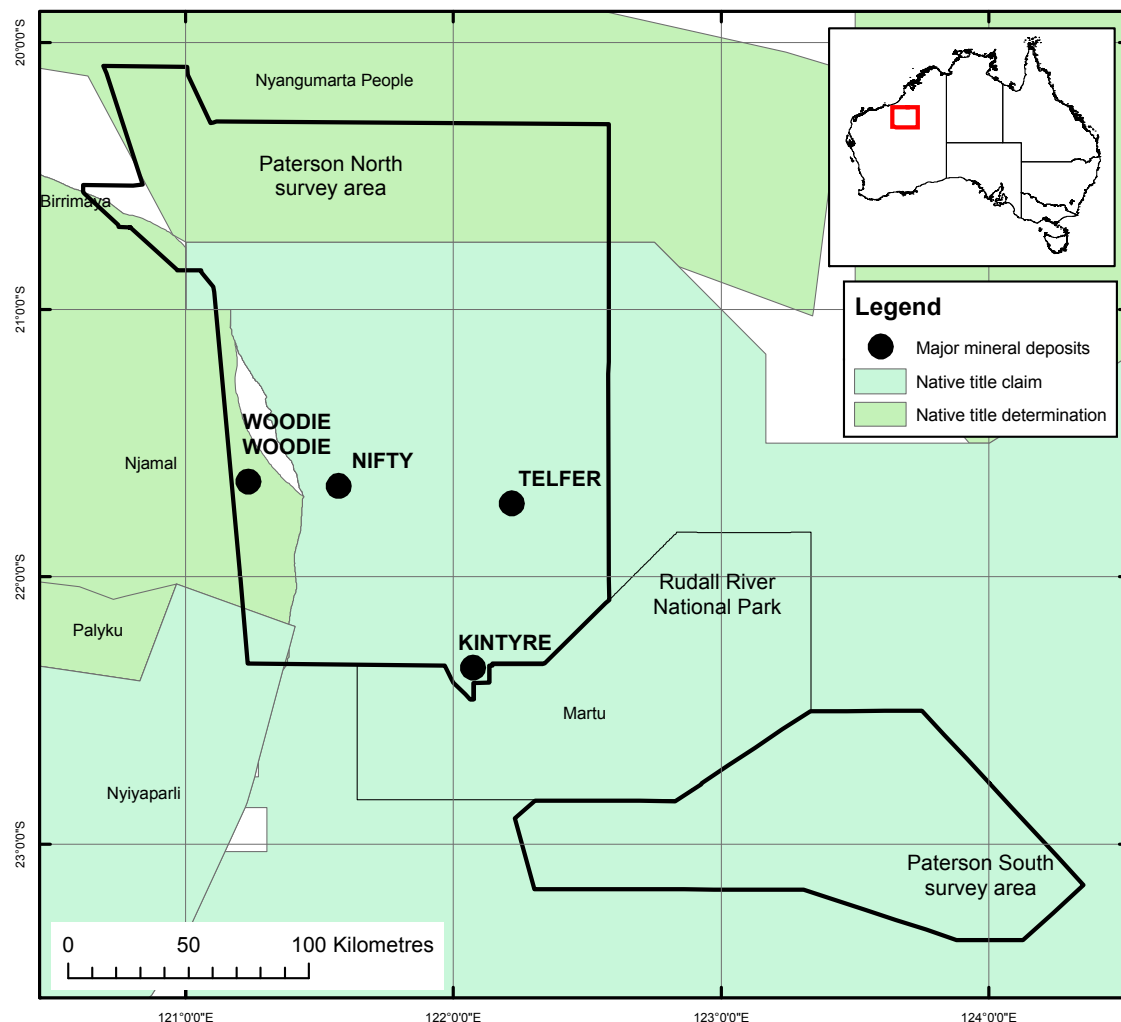


Figure 1.9: Native Title Application and Determination Areas recognised by the Federal Court (30 June 2007) for the Paterson survey areas.

Survey boundaries were determined by integrating the above data with the forward modelling parameters. Flight line spacing was determined by assessing the extents of known geological units and structures and predicted uranium potential, moving from a uranium focus with closer line spacing to regional mapping with broader line spacing. The data interpretation process used magnetics, gravity, radiometrics and geology associated with unconformity-related and paleovalley hosted uranium mineralisation to identify subsurface geological features. The process indicated that

mappable features should be 1 to 5 km in extent. This criterion helped define the final survey line spacings in the survey area.

The final survey design included the following generalisations which influenced the line spacing and survey boundaries:

- High uranium prospectivity and low risk areas:
 - Kintyre - 200 m and 1 km line spacing;
 - Cotton Creek - 1 km line spacing.
- Lower uranium prospectivity and higher risk areas:
 - Paterson North northern 2 km boundary – defined by magnetics and drill hole data indicating depth to basement to be more than 400 m (Mesozoic);
 - Paterson North western boundary - defined by Rio Tinto infill and (mineralised) Pilbara Craton boundary (Fortescue Group);
 - Paterson North eastern 2 km boundary defined by Rudall River National Park and the edge of the Paterson Province and Canning Basin;
 - Paterson North 6 km area defined by magnetics and gravity, estimated depth to basement and historical EM survey information (Anketell);
 - Boundary between Paterson North and Paterson South survey areas defined by the Rudall River National Park;
 - Paterson South western boundary – defined by magnetic low (SW) and knowledge of the Tarcunyah Group;
 - Paterson South eastern boundary 1 km lines – defined by depth of cover extending into the Canning Basin;
 - Paterson South eastern boundary 2 km lines – defined by magnetics and gravity extending into the Officer Basin;
 - Paterson South southern boundary defined by regional magnetics indicating (reasonable) depth to basement and containing outcropping or near-surface Rudall complex; and,
 - Paterson South northern boundary – defined by regional magnetics and known sub surface geology (Mesozoic-Permian-Carboniferous).

In the Paterson North survey area, the regional flight line spacing was 6 km with most of the survey conducted at 2 km line spacing and GA infill lines at 1 km line spacing across the south of the area ([Figure 1.10](#)). In the Paterson South survey area, which includes a large proportion of the Rudall Complex, flight line spacing was 2 km for the regional lines and 1 km line spacing for the GA infill lines over the most prospective area in the eastern part. A small amount of overflying is necessary at the start and end of each flight line. In this case the contractor required that a 1 km overfly was planned into the start and end of each flight line ([Figure 1.11](#)) to reduce geophysical data processing artefacts at the ends of lines.

1.6 SURVEY PARTNERS, CONTRIBUTORS AND COST

The Paterson AEM survey was opened to public subscription in the interests of stimulating further exploration in the region. The intention to fly the survey was advertised via GA's Minerals Alert email notification service and via GA's magazine publication, AusGEO News, inviting partners to purchase infill flight lines or contributors who would provide in-kind support.

A total of nine companies expressed an interest to the initial subscription request, including:

- Avalon Minerals Ltd.;
- BHP Billiton;
- Boxcut Mining Pty. Ltd. (now Mega Uranium Ltd.);
- Cameco Australia Pty. Ltd.;

- Glengarry Resources Ltd.;
- Newcrest Mining Ltd.;
- Scimitar Resources Ltd. (now Cauldron Energy Ltd.)
- Rio Tinto; and,
- Western Areas NL.

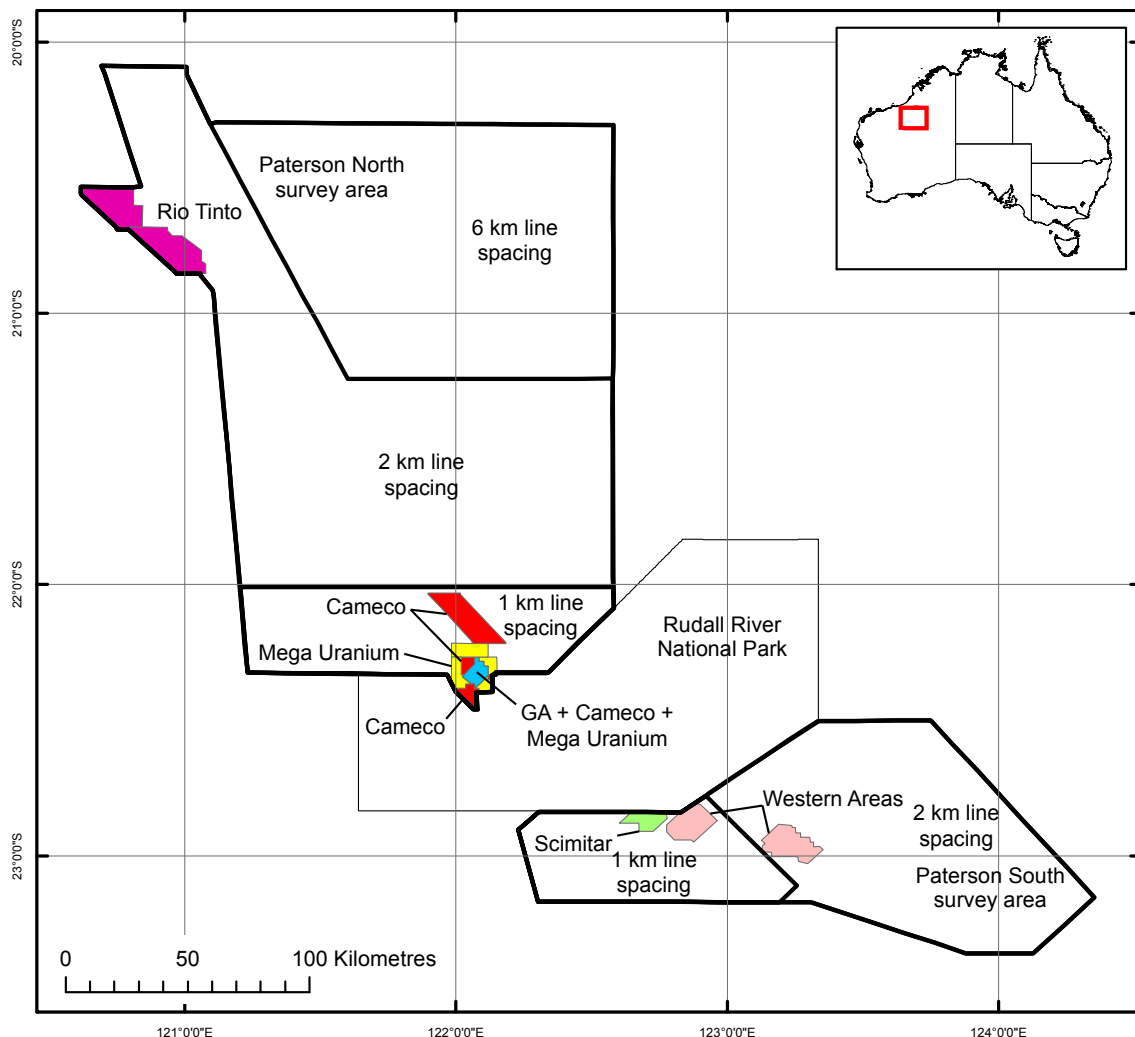


Figure 1.10: Final survey design with infill areas for the Paterson AEM survey.

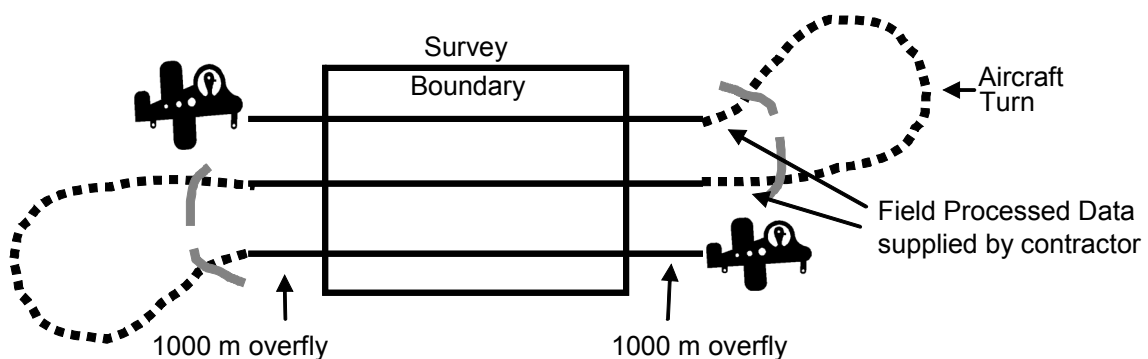


Figure 1.11: Cartoon of flight line planning including overfly areas.

Further negotiations with these interested companies resulted in five that decided to purchase infill flight lines within the survey area ([Table 1](#)). The companies matched GA funds on a dollar-for-dollar by area basis when purchasing the infill lines.

Table 1.1: Paterson AEM survey infill companies.

Company name	Commodity of interest
Boxcut (now Mega Uranium)	Uranium
Cameco Australia Pty. Ltd.	Uranium
Rio Tinto	Iron ore
Scimitar Resources Ltd. (now Cauldron Energy Ltd.)	Uranium
Western Areas NL	Base metals

A number of companies also contributed in-kind support:

- Aditya Birla Minerals (Nifty copper mine) provided a confidential drill hole database, field support in the way of accommodation, fuel and access to drill holes for conductivity logging;
- Newcrest Mining Limited (Telfer gold-copper mine) provided accommodation and access to drill holes for conductivity logging;
- Consolidated Minerals (Woodie Woodie manganese mine) provided access to drill holes for conductivity logging; and,
- Scimitar Resources Ltd. (now Cauldron Energy Ltd.) provided confidential HoistEM data.

In all, infill companies contributed \$442 620 to the survey budget and GA, through the OESP, contributed \$2 282 410 for a total survey cost of \$2 725 030, a survey area of approximately 47 600 km² and length of 28 200 line km. Infill areas to the main survey are shown in [Figure 1.10](#). All infill companies expected to spend an equal or greater amount to their contribution to the AEM survey in follow-up exploration programs after the AEM data were delivered. This is conservatively estimated to be worth an additional \$1 million in industry exploration investment in the region.

1.7 CLIMATE

Climate averages for the Paterson region presented here are taken from the Telfer Airport weather station, which commenced recording in 1974, and are available on the Australian Bureau of Meteorology (BOM) web site (BOM, 2009).

The Paterson region falls within the Desert group of the modified Koeppen climate classification system used by BOM and experiences hot, dry summers and mild winters. Average minimum and maximum monthly temperatures vary between 26°C and 40.6°C in January to 10.5°C and 25.3°C in July ([Figure 1.12](#)). The lowest and highest recorded temperatures were 2.5° in June 1976 and 48.1°C in January 1998.

Telfer lies about 100 km to the southeast of the dividing line between the Arid Zone, which has low overall rainfall, and the summer monsoon-dominated rainfall region of northern Australia. Overall rainfall patterns reflect the summer monsoon with the driest period occurring in spring time and the wettest in late summer, tailing off through autumn. Average annual rainfall is 364 mm, however, this can increase to 817 mm should a tropical cyclone cross over the area; the average annual likelihood of this occurring for all years is between 0.2 and 0.4 at Telfer. The highest average monthly rainfall of 102 mm occurs in February and the lowest average monthly rainfall of 2 mm occurs in September ([Figure 1.12](#)). Winds are dominantly from the southeast and east at 9 am ([Figure 1.13](#)) but become more variable in the afternoons at 3 pm with an increase in marine-influenced north-westerly winds.

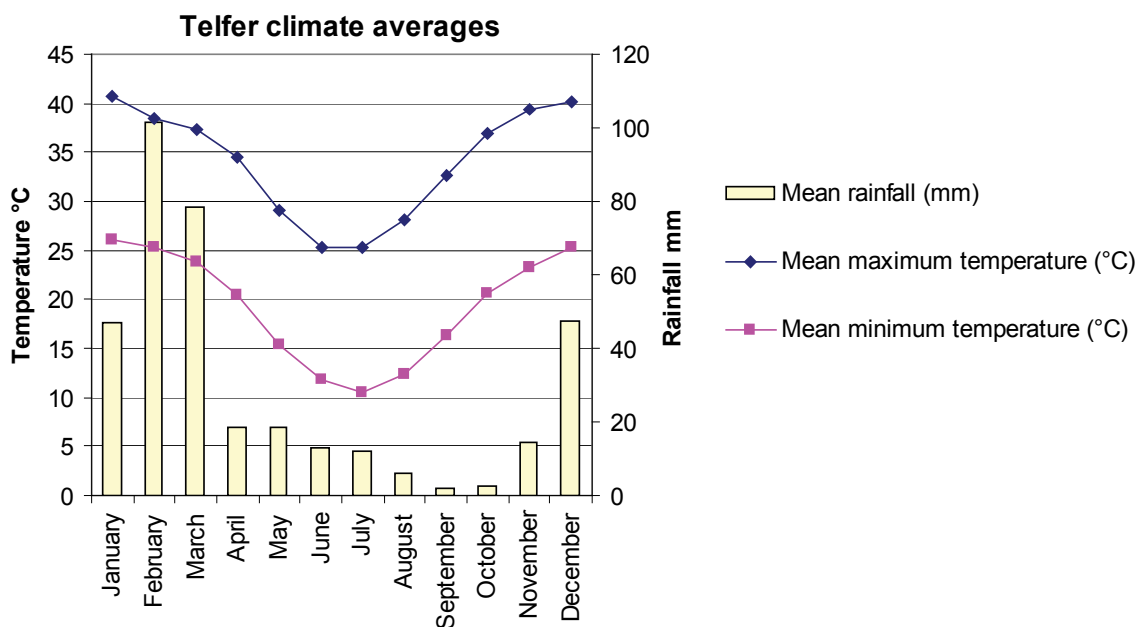


Figure 1.12: Temperature and rainfall averages for Telfer Airport since 1974 (BOM, 2009).

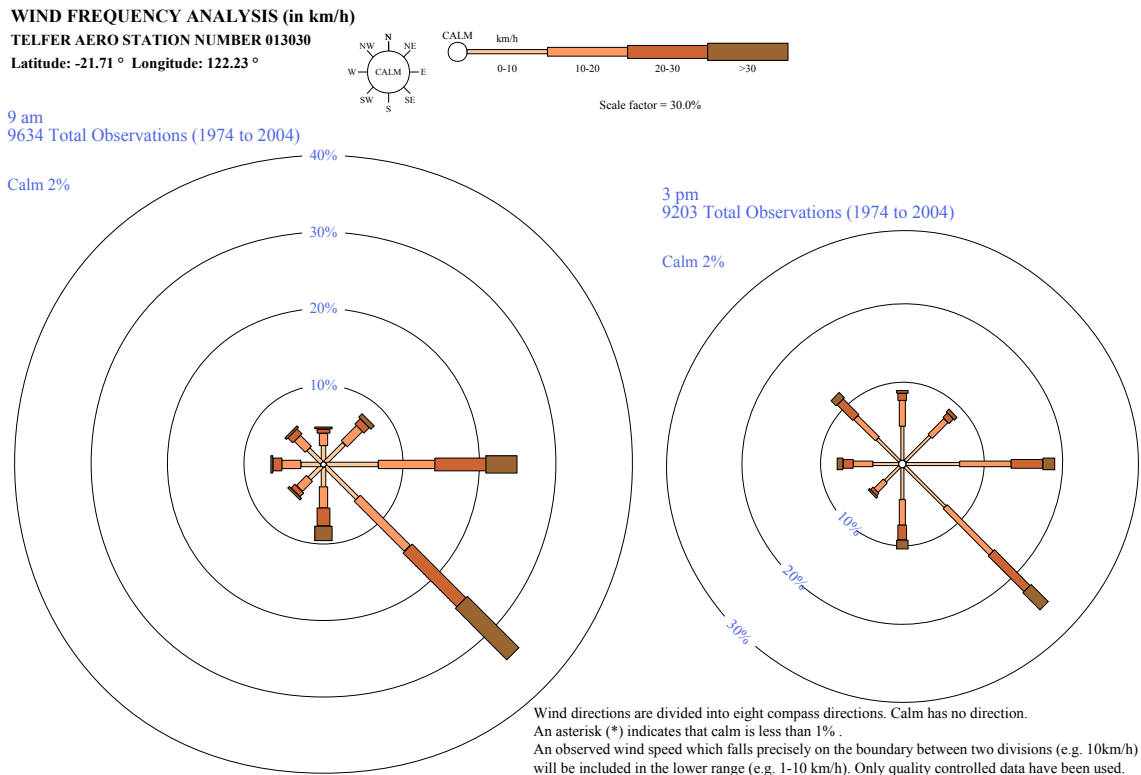


Figure 1.13: Telfer Airport 9 am and 3 pm average wind speed and direction data, modified after BOM (2009).

Average monthly wind speed decreases from 9 am to 3 pm in all months, however, air turbulence anecdotaly increases towards the afternoon as air temperature rises.

The average annual pan evaporation rate exceeds 4000 mm, the highest measured in Australia, however the average annual evapotranspiration rate is only about 300 mm, reflecting the paucity of

vegetation and surface or near-surface moisture in the Paterson region.

1.8 VEGETATION

The Paterson AEM survey area occurs principally in the Great Sandy Desert bioregion (ANRA, 2009; DEC, 2009), within the Eremaean Botanical Province of Beard (1990), but also includes a small portion of both the Little Sandy Desert and Pilbara bioregions. The Great Sandy Desert bioregion is dominantly desert grassland with low woodland and shrubs on the sand dunes and sand sheets, riparian woodland and savannah around water courses and a tree and shrub steppe with spinifex grasslands around the upland areas of the Rudall River National Park. The plant names used here are from the Council of Heads of Australian Herbaria (CHAH) Australian Plant Census (APC) database (CHAH, 2009). Examples of typical vegetation associations are shown in [Figure 1.14](#).

The grasslands over the sandhills are commonly thickly vegetated with soft spinifex (*Triodia pungens*) and feather-top spinifex (*Triodia schinzii*) with scattered trees including desert walnut (*Owenia reticulata*), sandhill bloodwood (*Eucalyptus chippendalei*) and shrubs including the sandhill grevillea (*Grevillea stenobotrya*), Wickhams grevillea (*G. wickhamii*), silver oak (*G. refracta*) and wattles, especially the bramble or prickly wattle (*Acacia victoriae*) and sandhill wattle or umbrella bush (*A. ligulata*). Occasionally jaradinty (*Hakea macrocarpa*) and *Melaleuca lasiandra* occur on the low-lying sandplains.

Between the sandhills is a mixed shrubland of *Acacia sp.* and *Spinifex sp.*, occasionally with tree species that varies with soil type. Kanji (*Acacia pyrifolia*) and waterwood (*Acacia coriacea*) grow on coarse sands, but on lighter sands *Acacia pachycarpa* are found, often with Wickham's grevillea (*Grevillea wickhami*). Thick-leaved mallee (*Eucalyptus pachyphylla*) and twin-leaf mallee (*E. gamophylla*) occur on ferruginised soils, while desert oaks (*Allocasuarina decaisneana*) can be found growing in isolated scattered clumps or dense groves in depressions, often with teatrees (*Melaleuca sp.*).

Gently undulating ferruginous duricrust uplands are dominated by shrub steppe of kanji (*Acacia pyrifolia*) on the stony plateaus and sandplains, waterwood (*A. coriacea*), cork tree (*Hakea suberea*) and other *Acacia sp.*, *Hakea sp.* and *Grevillea sp.* over soft spinifex hummock grass.

Around the watercourses and billabongs there are river red gum (*Eucalyptus camaldulensis*) savannah or riparian woodlands with coolibah (*E. microtheca*) replacing the river red gums at a distance from the water, depressions with teatree scrub including *Melaleuca lasiandra*, *M. glomerata* and *M. cajuputi* and small patches of mulga (*Acacia aneura*). Outwash plains may include teatree shrubland but other shrubs, including native willow (*Acacia salicina*) and quandong or sandalwood (*Santalum acuminatum*) may also occur.

Extensive salt lake systems support samphire (*Halosarcia sp.*) low shrubland and tea-trees (*Melaleuca glomerata*) and *M. lasiandra* shrubland.



Figure 1.14: Examples of vegetation types in the Paterson region. A: *Spinifex* sp. grassland with scattered *Grevillea* sp. and *Acacia* sp. shrubs. B: *Eucalyptus camaldulensis* (river red gum) riparian woodland either side of a water course. C: Salt lake surrounded by low samphire shrubland. D: Sand dune supporting *Spinifex* sp. grassland with scattered *Acacia* sp. shrubs looking downhill towards savannah shrubland of *Acacia aneura* (mulga) and *Spinifex* sp. in the dune swale. E: Mixed *Spinifex* Sp. grassland with *Acacia* sp. and *Eucalypt* Sp. on the dune near Well 23, Canning Stock Route, with a camel train. F: Looking west towards the Ragged Hills from the Lamil Hills across a *Spinifex* sp. grassland and scattered *Spinifex* sp., *Acacia* sp. and *Grevillea* sp. shrubs on the dune. Photos A, B and C by A. Fisher. Photo D by P. English. Photo E. by A.T. Wells from the BMR 1954 Canning Basin expedition. Photo F by A.T. Wells from the BMR 1956 Canning Basin survey.

1.9 GEOMORPHOLOGY

The geomorphology of the Paterson region has been described by a number of authors over many decades with varying degrees of detail. Most of the descriptions have been model-driven (e.g., (Jennings and Mabbutt, 1977; Payne, 2004; Tille, 2006) and describe the region in terms of morphotectonics and palaeosurface development. Here we present factual information regarding the landscape shape, without resorting to models to explain those shapes, drawn from the NASA Space Shuttle Radar Topographic Mission Digital Elevation Model (SRTM DEM; [Figure 1.15](#)), soil-landscape mapping by (Tille, 2006), land systems mapping by Van Vreeswyk *et al.* (2004), the Atlas of Australian Soils (ASRIS, 2009) ([Figure 1.16](#); [Table 1.2](#)) and the Regolith Terrain Mapping scheme of Pain *et al.* (2007) and Pain (2008).

The total relief across the Paterson survey area is approximately 410 m from the lowest point in the northwest of the Paterson North survey area (about 100 m ASL) to the highest peak in the Rudall Complex in the Paterson South survey area (about 510 m ASL). These data were determined using the 90 m ground pixel resolution SRTM DEM ([Figure 1.15](#)).

The lowlands of the Paterson AEM survey area are dominated by west- to northwest-striking seif (longitudinal) dunes of the Great Sandy Desert, depicted in [Figure 1.14E](#) and [Figure 1.15](#), which lie over plains that have a total relief of less than 100 m over tens of kilometres. Dune crests may be elevated up to approximately 30 m above the surrounding swales (averaging 12 m high in the Paterson 1:100 000 sheet area) and may be up to 3 km apart (Bagas, 2000), separated by sandsheets or plains of indurated Mesozoic basinal rocks, including large expanses of ferruginous duricrust, and residual rises or low hills of economic basement rocks. Dunes lie across most of the low-relief area apart from where they have been redistributed by water around the Percival Lakes, the Rudall River and Lake Waukarlycarly. Dunes often drape low- to moderate-relief landforms including rises and low hills.

Wide flat-bottomed drainage depressions and salt lakes associated with the Percival Lakes system ([Figure 1.15](#)) occur in the lowlands; these are interpreted to form part of a larger palaeodrainage system called the Canning Palaeoriver (Magee, 2009) or the Percival Palaeoriver (van der Graaf *et al.*, 1977), which drained northwest across the Paterson region into the extant Oakover River. This is described in more detail in [Chapter 2](#) of this report. Low relief landforms are defined in the Atlas of Australian soils landform attributes described in [Table 1.2](#) and [Figure 1.16](#) (ASRIS, 2009).

Moderate- to high-relief landforms occur along the Oakover River, the eastern Pilbara Block, Paterson Range, Throssell Range and Rudall Complex where resistant Archean, Mesoproterozoic and Neoproterozoic basement rocks occur, or where Phanerozoic sediments have been indurated by Fe-oxyhydroxides, silica or regolith carbonate to leave residual landforms. These may occur as solitary residual rises to residual low hills between sand dunes, or linear to arcuate chains of connected rises, low hills and hills in areas where resistant bedrock outcrop is more abundant, often forming rugged ranges, particularly in the western parts of the Paterson North and Paterson South survey areas around the Gregory Range, eastern Pilbara Craton, and the Rudall Complex. Moderate to high relief landforms are defined in the Atlas of Australian soils landform attributes described in [Table 1.2](#) and [Figure 1.16](#) (ASRIS, 2009).

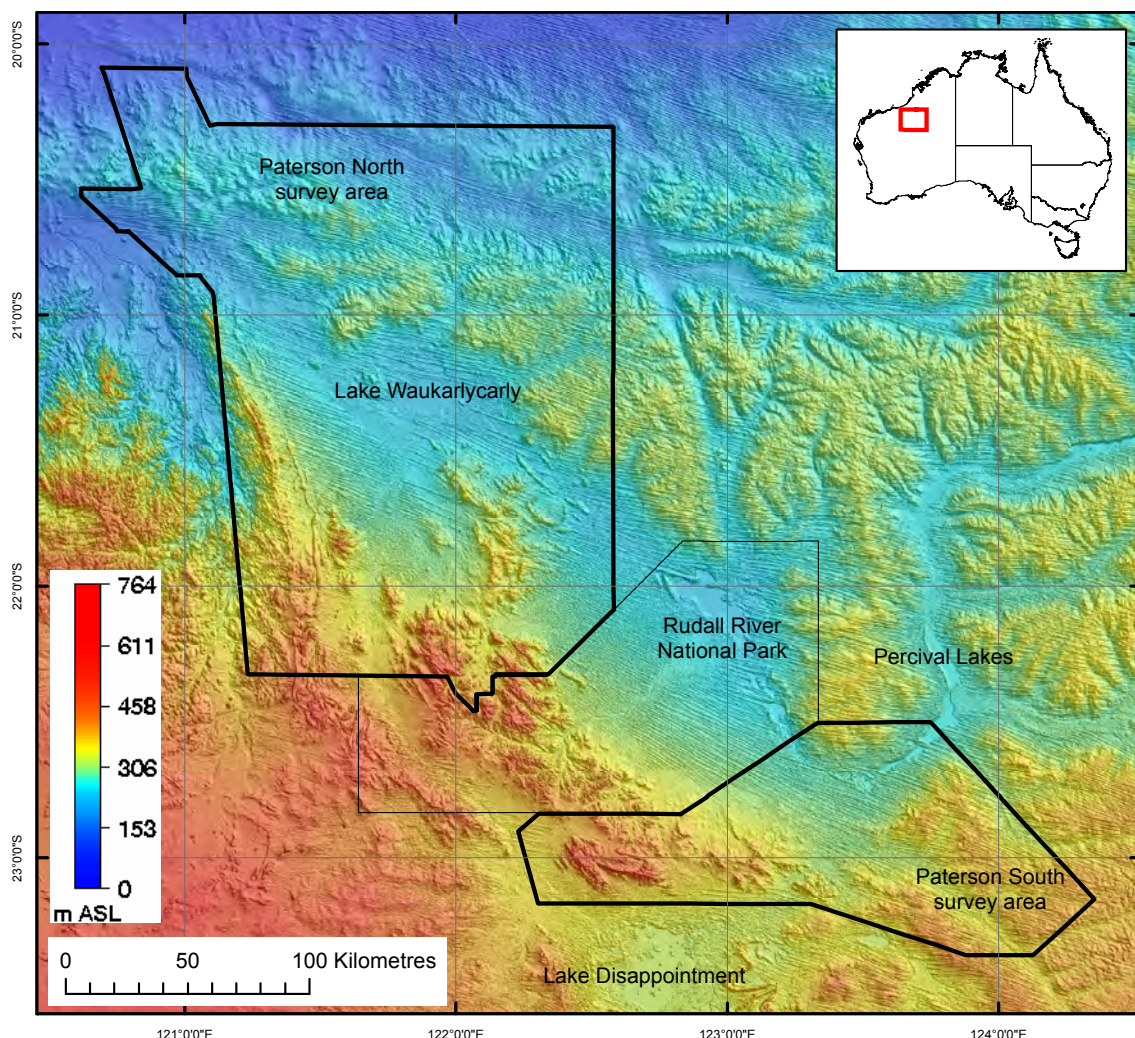


Figure 1.15: The 90 m ground pixel resolution SRTM DEM of the Paterson region. The image is sunshaded from the northeast.

A multiresolution valley bottom flatness (MRVBF) (Gallant and Dowling, 2003) image (Figure 1.17) highlights the broad geomorphological differences across the Paterson area. In this image, valley bottoms and plateaux appear white, areas of low to moderate relief appear gray and areas of higher relief appear black. The image highlights the dissected, dendritic patterned, Fe-oxyhydroxide indurated plains and rises that dominate the southern Canning Basin and the wide linear and arcuate drainage depressions associated with strings of salt lakes and claypans. Sand dunes can be seen as thin black lines running E-W to NW-SE across the image. High relief, rugged areas of resistant bedrock in the western portions of the North and South Paterson survey areas are clearly depicted as black areas with a variety of drainage patterns.

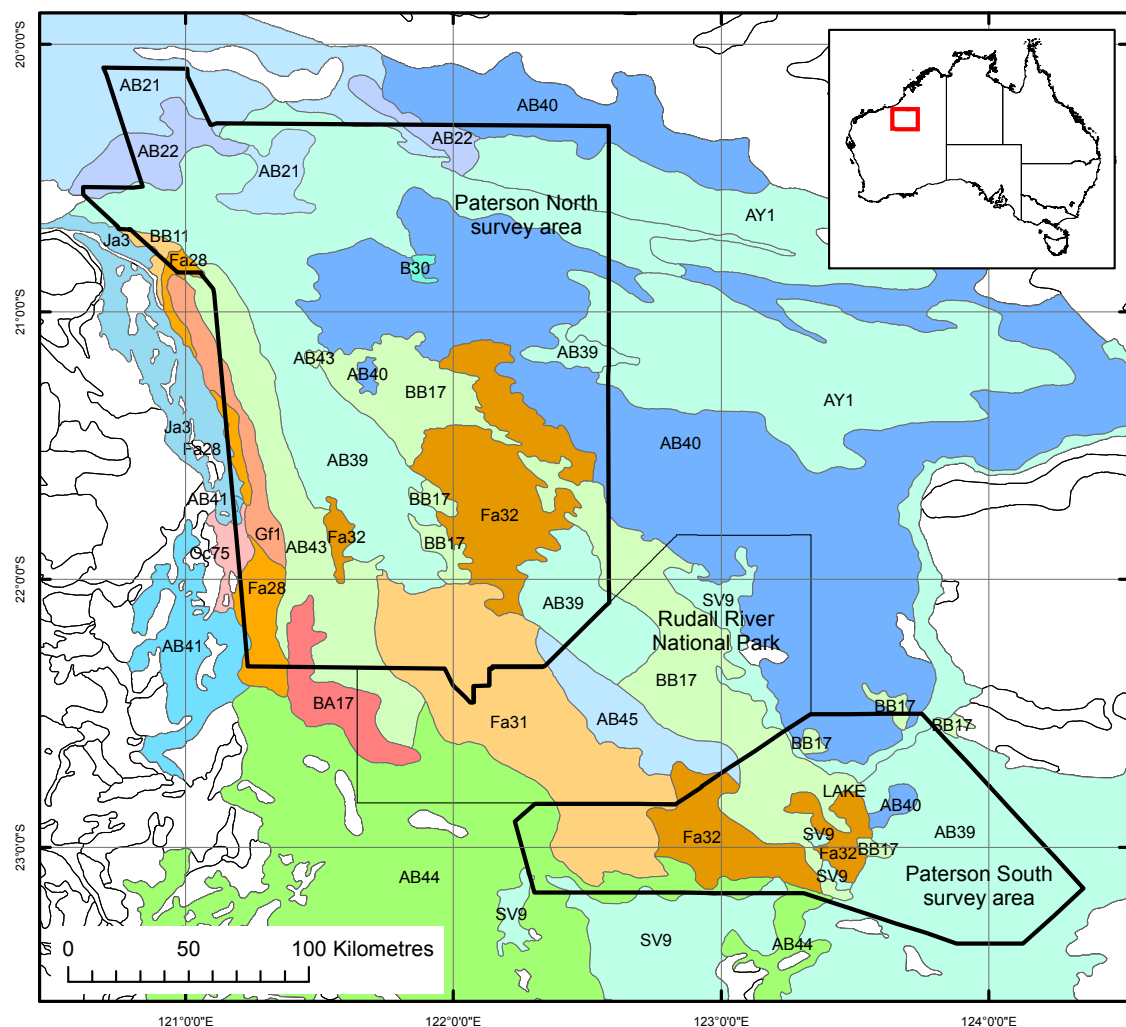


Figure 1.16: Soil-landscape polygons intersecting the Paterson AEM survey area. The key to polygon labels is given in Table 1.2. Polygons are extracted from the ASRIS (2009) database.

Table 1.2: Atlas of Australian Soils landform attributes for polygons in [Figure 1.16](#). Modified after ASRIS (2009).

MAP SYMBOL	LANDSCAPE INFORMATION
<i>Low relief landforms</i>	
AB21	Gently undulating sand plain with a few small rocky sandstone residuals; no external drainage.
AB22	Gently undulating sand plain as for unit AB21 but with many rocky sandstone residuals.
AB39	Gently undulating plain dominated by longitudinal dunes of varying frequency; some exposures of ferruginous gravels and bedrock on low rises occur in the dune swales.
AB40	Gently undulating plain slightly more elevated than unit AB39 and dominated by longitudinal dunes, many exposures of ferruginous gravels and some breakaways capped by ferruginous duricrust.
AB41	Undulating areas on chert breccia with frequent rock outcrops; these areas are elevated above the main drainage-ways but are relatively lower than adjacent ranges.
AB43	Pediplains on granite with some granitic residuals, tors, and bosses; occasional longitudinal dunes; some areas of hard calcrete.
AB44	Plains with a variable, but usually high, proportion of longitudinal sand dunes, and with some clay pans; scattered sandstone hills and ferruginous duricrust residuals are fairly common.
AB45	Plains with some longitudinal dunes.
AY1	Gently undulating upland (tableland) with much ferruginous gravel on the surface; some breakaways (mesas, buttes, and bluffs) capped by ferruginous duricrust; there is some local marginal transgression by longitudinal dunes from adjacent units.
B30	Dune fields - largely stable linear dune fields with swales opening locally into sand plains. Dune lineation is generally E-W but in the area west of 123°E the trend is NW-SE; considerable areas of clay pans and salt pans; some isolated residual sandstone hills.
BB17	Uneven rough calcrete plains with small salt lakes and pans broken by variable proportions of longitudinal sand dunes and occasional low rises or hills.
Ja3	Gently undulating pediplains and alluvial plains associated with Permian sediments.
Lake	Planar deposits of lacustrine materials.
SV9	Salt lakes, salt pans, and clay pans mostly devoid of true soils, covered with clays, silts, sodium chloride, calcium sulphate, and sodium sulphate, and underlain by brine; soft calcrete on lake margins in places; shale cliffs 15-30 m high abut the eastern edges of the lakes in places; and broken and irregularly shaped sand dunes flank the lake systems.
<i>Moderate to high relief landforms</i>	
BA17	Flat-topped but sometimes steep-sided hills with extensive areas of bare rock - sandstones and other sedimentary rocks, but including some volcanics.
BB11	Flat-topped residuals, capped by calcrete and opaline silica of the Oakover Formation.
Fa28	Steep hills and low ranges associated with various rocks including dolomite and some chert breccia; exposures of rock are extensive and soils are shallow and stony.
Fa31	Rugged ranges with extensive areas of bare rock largely on metamorphics and granites but with some inclusions of sandstones and conglomerates.
Fa32	Low ranges and hills largely on metamorphics and granites but with some inclusions of sandstones and conglomerates; extensive areas of bare rock; transgressed by dunes in places and flanked by small plains.
Gf1	Steep ranges on basic lavas along with dolomites, tuff, banded iron formations, and dolerite dykes, with some narrow valley plains and high-level gently undulating areas of limited extent. The soils are generally shallow and stony and there are large areas without soil cover.
Oc75	Dissected pediments associated with dolomites and some chert breccias.

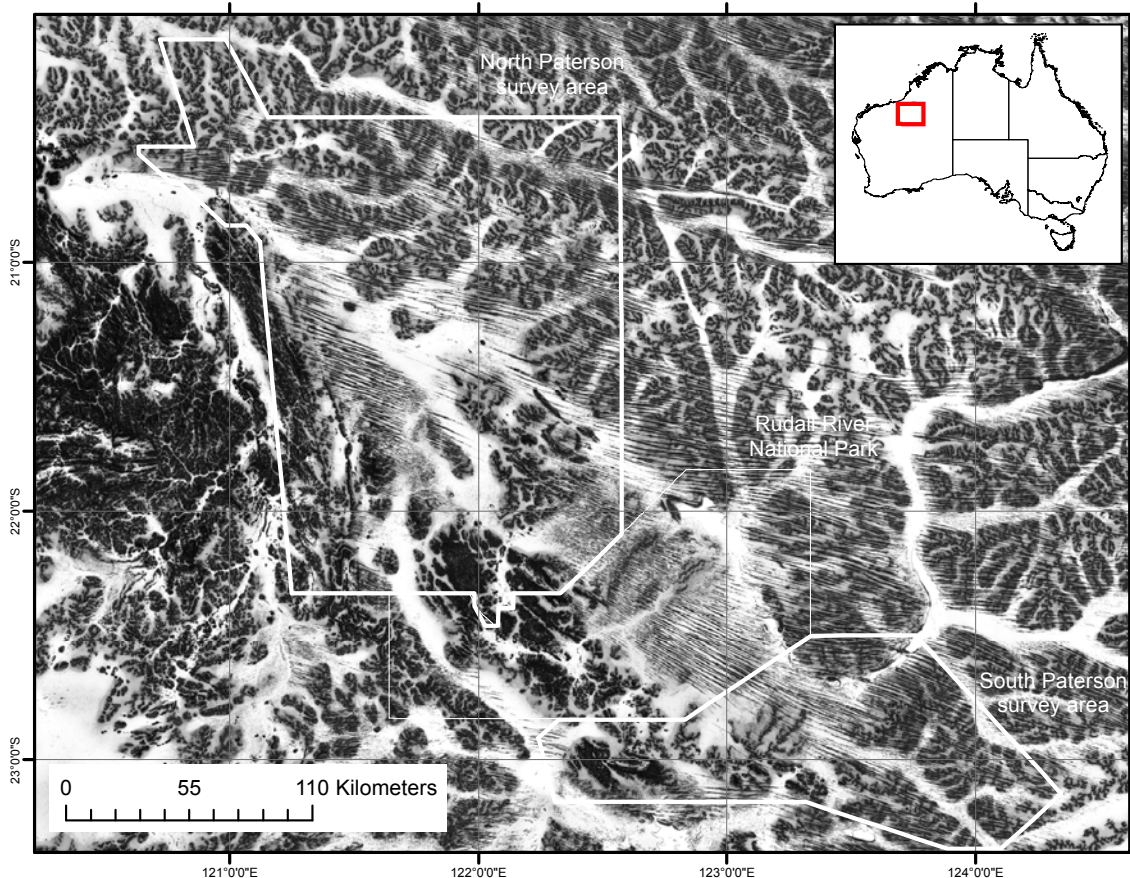


Figure 1.17: Multiresolution Valley Bottom Flatness (MRVBF) (Gallant and Dowling, 2003) image of the Paterson survey area. Image courtesy P. Kilgour, Groundwater Group, Geospatial and Earth Monitoring Division, GA.

1.10 REFERENCES

- Acclaim, 1999. Acclaim Uranium NL Annual Report 1999.
- Andrew, R. L., 1988. Kintyre uranium deposit and the Rudall Province. *Uranium Institute Symposium*, London, September 1988.
- ANRA, 2009. Australian Natural Resources Atlas. Online: <http://www.anra.gov.au/>.
- ASRIS, 2009. Australian Soil Resource Information System. Online: <http://www.asris.csiro.au/>.
- Bagas, L., 2000. Geology of the Paterson 1:100 000 sheet - Explanatory Notes. Geological Survey of Western Australia, Perth. 20 p.
- Bagas, L., Williams, I. R. and Hickman, A. H., 2000. Rudall, Western Australia (2nd Edition). 1:250 000 Geological Series - Explanatory Notes. Western Australia Geological Survey. 50 p.
- Bautin, F. and Hallenstein, C., 1997. Plans for uranium mining by COGEMA. In: *ANA 97 Conference on Nuclear Science and Engineering in Australia, 1997*. Australian Nuclear Association Inc., Sydney. 20-24 pp.
- Beard, J. S., 1990. Plant life of Western Australia. Kangaroo Press, Kenthurst NSW.
- BOM, 2009. Bureau of Meteorology. Online: <http://www.bom.gov.au/>.
- Brunt, D. A., 1990. Miscellaneous uranium deposits in Western Australia. In: Hughes, F. E. (ed) *Geology of the Mineral Deposits of Australian and New Guinea*. Australasian Institute of Mining and Metallurgy, Melbourne. 1615-1620 pp.
- Cameron, E., 1990. Yeelirrie Uranium Deposit. In: Hughes, F. E. (ed) *Geology of the Mineral*

- Deposits of Australia and New Guinea.* Australasian Institute of Mining and Metallurgy, Melbourne. 1625-1629 pp.
- Carver, R. N., 2005. Nifty Copper Deposit, Great Sandy Desert, Western Australia. In: Butt, C. R. M., Robertson, I. D. M., Scott, K. M. and Cornelius, M. (eds) *Regolith expression of Australian ore systems*. CRC LEME, Perth. 185-187 pp.
- CHAH, 2009. Council of Australian Herbaria Australian Plant Census database. Online: <http://www.anbg.gov.au/chah/apc/>.
- Chen, X. Y., Lintern, M. J. and Roach, I. C., 2002. Calcrete: characteristics, distribution and use in mineral exploration. Cooperative Research Centre for Landscape Environments and Mineral Exploration. 160 p.
- Commander, D. P., 1985. Groundwater Prospects - Punmu Aboriginal Community, Lake Dora. . Western Australia Geological Survey. 14 p.
- De Grey, 2009. De Grey Mining Ltd ASX/Media Release 8 April 2009. 3 p. Online: <http://www.degremining.com.au/news/20090408.pdf>.
- DEC, 2009. Rudall River National Park. Online: <http://www.dec.wa.gov.au/hotproperty/property-national-parks/rudall-river-national-park.html>.
- den Tex, I., 2009. Communication re: Aditya Birla Nifty taking up new tenements after release of Paterson AEM survey data.
- Dimo, G., 1990. Telfer gold deposits. *Geology of the mineral deposits of Australia and Papua New Guinea. Australasian Institute of Mining and Metallurgy Monograph 14*, 643-651.
- Fulwood, K. E. and Barwick, R. E., 1990. Mulga Rock uranium deposits, Officer Basin. In: Hughes, F. E. (ed) *Geology of the Mineral Deposits of Australia and Papua New Guinea*. The Australasian Institute of Mining and Metallurgy, Melbourne. 1621-1623 pp.
- Gallant, J. C. and Dowling, T. I., 2003. A multiresolution index of valley bottom flatness for mapping depositional areas. *Water Resource Research 39(12)*, 1347-1359.
- Hickman, A. H. and Clarke, G. L., 1994. Geology of the Broadhurst 1:100 000 sheet, Western Australia. Western Australia Geological Survey, Perth. 40 p.
- Jackson, D. J. and Andrew, R. L., 1990. Kintyre uranium deposit. In: Hughes, F. E. (ed) *Geology of the Mineral Deposits of Australia and Papua New Guinea*. The Australasian Institute of Mining and Metallurgy. 653-658 pp.
- Jennings, J. N. and Mabbutt, J. A., 1977. Physiographic outlines and regions. In: Jeans, D. N. (ed) *Australia - a geography*. Sydney University Press, Sydney. 38-52 pp.
- Kern, A. M., 1994. Groundwater Prospects - Billinooka, Jigalong and Punmu Aboriginal Communities, East Pilbara. Western Australia Geological Survey.
- Lawrence, M. and Stenning, L., 2008. Paterson North Airborne Electromagnetic (AEM) Mapping Survey - Acquisition and Processing Report for Geoscience Australia. Fugro Airborne Surveys. **Unpublished report**, 108 p.
- Lewis, S. J., English, P. M., Wischusen, J. D. H., Woodgate, M., Gow, L., Kilgour, P. and Hanna, A., 2009. Palaeovalley Groundwater Project - Detailed Demonstration Study Site Work Plans: Palaeovalley Project Milestone 4 Report. A Report by Geoscience Australia for the National Water Commission.
- Magee, J., 2009. Palaeovalley Groundwater Resources in Arid and Semi-Arid Australia. Geoscience Australia, Canberra. **Record 2009/03**, 224 p.
- McKay, A. D. and Miezitis, Y., 2001. Australia's uranium resources, geology and development of deposits. *Mineral Resource Report*, AGSO - Geoscience Australia, Canberra. **Mineral Resource Report 1**, 200 p.
- Minty, B. R. S., Franklin, R., Milligan, P. R., Richardson, L. M. and Wilford, J., 2009. The Radiometric Map of Australia. *20th International Geophysical Conference and Exhibition*, Adelaide, Australian Society of Exploration Geophysicists, 22-25 February 2009.
- Pain, C. F., 2008. Field guide for describing regolith and landforms. Cooperative Research Centre for Landscape Environments and Mineral Exploration, Perth. 96 p.
- Pain, C. F., Chan, R., Craig, M., Gibson, D., Kilgour, P. and Wilford, J. R., 2007. RTMAP Regolith Database Field Book and Users Guide. CRC LEME, Perth. **Open File Report 231**.
- Payne, A. L., 2004. Geomorphology. In: Van Vreeswyk, A. M. E., Payne, A. L., Leighton, K. A. and

- Hennig, P. (eds) *An inventory and condition survey of the Pilbara region, Western Australia*. Department of Agriculture, Government of Western Australia, Perth. 70-86 pp.
- Roach, I. C., 2009. A drill hole database for the Paterson airborne electromagnetic (AEM) survey, Western Australia. Geoscience Australia, Canberra. **Record 2009/31**, 16 p.
- Schwabe, M. R., 1981. Mt Sears Range Project, Rudall River Region, Western Australia, Annual Report 1979-80, Temporary Reserve 6883H., Occidental Minerals Corporation of Australia.
- Skirrow, R. G., Jaireth, S., Huston, D. L., Bastrakov, E. N., Schofield, A., van der Wielen, S. E. and Barnicoat, A. C., 2009. Uranium mineral systems: processes, exploration criteria and a new deposit framework. Geoscience Australia, Canberra. **Record 2009/20**, 44 pp.
- Stewart, A. J., 2008. Surface Geology of Australia 1:1 000 000 scale, Western Australia. Geoscience Australia, Canberra. http://www.ga.gov.au/minerals/research/national/nat_maps/nat_geol_maps.jsp.
- Swingler, N., 1981. Sunday Creek Project, Rudall River Region, WA - Final Report for TR 7071H. Occidental Minerals Corporation of Australia. **Western Australia Geological Survey WAMEX Open File Series; Item 1694**.
- Thorpe, P. M., 1988. Water Resources for Aboriginal Communities, Pilbara region. Western Australian Geological Survey.
- Tille, P., 2006. Soil-landscapes of Western Australia's Rangelands and Arid Interior. Department of Agriculture and Food, Government of Western Australia. Resource Management Technical Report 313, 153 p.
- van der Graaf, W. J. E., Crowe, R. W. A., Bunting, J. A. and Jackson, M. J., 1977. Relict Early Cenozoic drainages in arid Western Australia. *Zeitschrift für Geomorphologie NF* **21(4)**, 379-400.
- Van Vreeswyk, A. M. E., Payne, A. L., Leighton, K. A. and Hennig, P., 2004. An inventory and condition survey of the Pilbara region, Western Australia. Department of Agriculture, Government of Western Australia. Technical Bulletin No. 92, 424 p.
- Williams, I. R. and Trendall, A. F., 1998a. Geology of the Pearana 1:100 000 sheet, 1:100 000 Geological Series Explanatory Notes. Western Australia Geological Survey, Perth. 33 p.

2 Previous and concurrent work

I. C. Roach, M. T. Costelloe and A. J. Whitaker

2.1 GEOLOGICAL MAPPING

The Paterson AEM survey area includes a number of 1:2 500 000, 1:1 000 000, 1:250 000 and 1:100 000 scale geological maps ([Figure 2.1](#)). The entire area is mapped at 1:2 500 000 scale by the Geological Survey of Western Australia's State Geological Map and at 1:1 000 000 by the Geoscience Australia Surface Geology of Australia (released in 2009), which was compiled from 1:250 000 maps of the area. The Geological Survey of Western Australia's 1:250 000 map series dates from 1978 to the most recent, published in 2003. Mapping in the 1:100 000 series commenced in 1994 and is ongoing. A list of the available maps is given in [Table 2.1](#).

The 1:250 000 and smaller scale maps describe the regional geology of the area whilst the 1:100 000 series maps describe areas where a reasonable proportion of Archean and Proterozoic rocks are visible at the ground surface and where access is somewhat easier; these areas tend to be those where the most exploration activity is occurring.

Tectono-stratigraphic models for the evolution of the Paterson region have evolved over the span of the literature, especially with the advent of isotopic dating methods. There is continuing debate over the evolution of the Paleoproterozoic Rudall Complex and the relationships between the Neoproterozoic Yeneena Basin and lower Officer Basin. The descriptions of stratigraphy and time-space diagrams for the region have evolved as geological understanding in the 1:100 000, 1:250 000 and regional mapping has also evolved. A number of specialist volumes from the Geological Survey of Western Australia describe drilling in the Canning and Officer Basins (Perincek, 1997) and have attempted to correlate parts of the Yeneena Basin with the Officer Basin (Grey *et al.*, 2005). The tectonic evolution and metallogeny of the Paterson Orogen is also described in specialist papers including Hickman and Bagas (1994) and Ferguson *et al.* (2005).

Geological interpretations for the Paterson AEM survey rely principally on the GA 1:1 000 000 Surface Geology Map of Australia together with airborne geophysics (described below), drill hole information (described below) and a preliminary 1:250 000 solid geology interpretation of the Paterson Orogen (Czarnota *et al.*, 2009a). The solid geology interpretation was based on magnetic data, gravity data inversions, limited drill hole data and three seismic sections across the Waukarlycarly embayment.

2.2 GEOPHYSICS

The Paterson AEM survey area has been the focus of a variety of geophysical surveys since the discovery of the Woodie Woodie deposit in the late 1940s to early 1950s (de la Hunty, 1965; Williams and Trendall, 1998a) and the realisation of the petroleum potential of the Canning Basin soon after. There are a range of publicly-available airborne geophysical data covering the Paterson AEM survey area including detailed and regional magnetics, radiometrics, gravity, AEM and Digital Elevation Models (DEMs). These surveys may have been commissioned by minerals exploration companies ([Figure 2.2](#), [2.3](#)) or by State, Commonwealth or other government agencies ([Figure 2.4](#)). The Space Shuttle Radar Topographic Mission Digital Elevation Model (SRTM DEM; [Figure 2.4](#)) is also included in this compilation for completeness, although it is not exactly an “airborne” geophysical method. Most publicly-available data are held within the Geophysical Archive Data Delivery System (GADDS) at GA and are available for free download through the Australian Geoscience Portal (<http://www.geoscience.gov.au/>). The SRTM DEM is available for free download from the United States Geological Survey (USGS) at the National Map Seamless Server (<http://seamless.usgs.gov/>).

Geological and energy implications of the Paterson Province airborne electromagnetic (AEM) survey, Western Australia

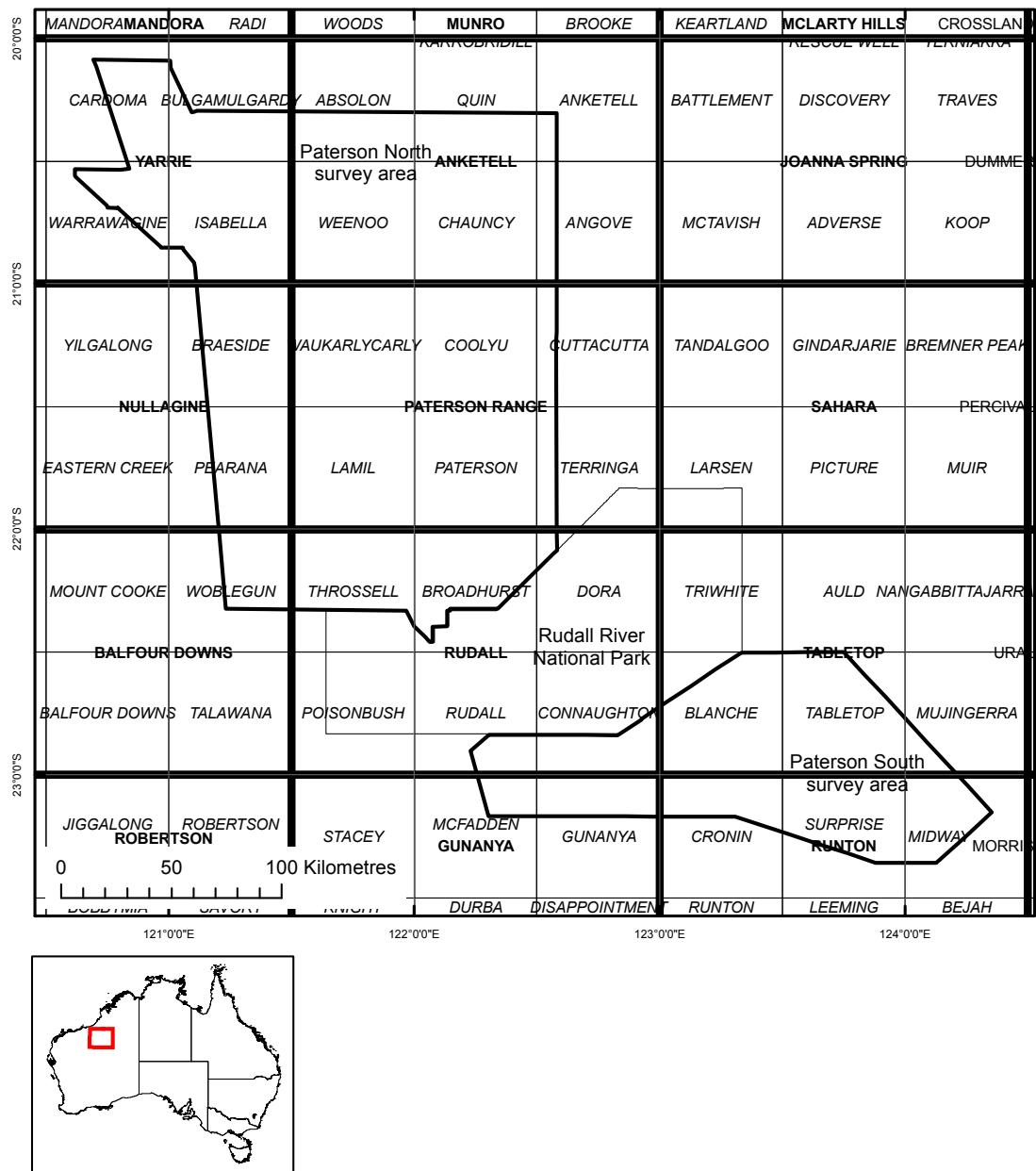


Figure 2.1: Available 1:100 000 (*italics*) and 1:250 000 (**bold**) geological maps in the Paterson region. The area is also covered at 1:1 000 000 and 1:2 500 000 scales.

Table 2.1: Available geological maps in the Paterson AEM survey area.

SCALE	NAME	AUTHOR(S), REFERENCE
1:2 500 000	Western Australia	GSWA
1:1 000 000	Australia (Western Australia)	Stewart, A.J., Sweet, I.P., Needham, R.S., Raymond, O.L., Whitaker, A.J., Liu, S.F., Phillips, D., Retter, A.J., Connolly, D.P., and Stewart, G., 2009. Surface geology of Australia 1:1,000,000 scale, Western Australia. Online: http://www.ga.gov.au/minerals/research/national/nat_maps/nat_geol_maps.jsp
1:250 000	Anketell SF 51-2	Towner R.R., 1982. 1:25,000 Geological Series Explanatory Notes – Anketell (Second Edition) - Western Australia. Department of National Development and Energy - Bureau of Mineral Resources, Geology and Geophysics, Department of Mines, Western Australia – Geological Survey of Western Australia, 22 p.
1:250 000	Balfour Downs SF 51-9	Williams, I.R., 1989. Balfour Downs – Western Australia (Second Edition). Geological Survey of Western Australia – 1:250,000 Geological Series - Explanatory Notes, 38 p.
1:250 000	Gunanya SF 51-14	Williams I.R. and Williams, S.J., 1980/. Gunanya – Western Australia. Geological Survey of Western Australia – 1:250,000 Geological Series - Explanatory Notes, 14p.
1:250 000	Nullagine SF 51-5	Hickman, A.H., 1978. Nullagine – Western Australia. Geological Survey of Western Australia – 1:250,000 Geological Series - Explanatory Notes, 21p.
1:250 000	Paterson Range SF 51-6	Chin, R.J., Hickman, A.H. and Towner, R.R., 1982. Paterson Range (Second Edition). Geological Survey of Western Australia – 1:250,000 Geological Series - Explanatory Notes, 29p.
1:250 000	Rudall SF 51-10	Bagas, L., Williams, I.R. and Hickman, A.H., 2000. Rudall – Western Australia – Second Edition. Geological Survey of Western Australia – 1:250,000 Geological Series - Explanatory Notes, 50p.
1:250 000	Runton SF 51-15	Crowe, R.W.A. and Chin, R.J., 1979. Runton – Western Australia. Department of National Development and Energy - Bureau of Mineral Resources, Geology and Geophysics, Department of Mines, Western Australia – Geological Survey of Western Australia, 16p.
1:250 000	Tabletop SF 51-11	Yeates, A.N., Chin, R.J., 1979. Tabletop – Western Australia. Department of National Development and Energy - Bureau of Mineral Resources, Geology and Geophysics, Department of Mines, Western Australia – Geological Survey of Western Australia,
1:250 000	Yarrie SF 51-1	Williams, I.R., 2003. Yarrie – Western Australia – Third Edition. Geological Survey of Western Australia – 1:250,000 Geological Series - Explanatory Notes, 84p.
1:100 000	Blanche-Cronin	Bagas, L., 1999. Geology of the Blanche-Cronin 1:100,000 sheet (part sheets 3551 and 3552). Geological Survey of Western Australia, 16p.
1:100 000	Braeside	Williams, I.R. and Trendall, A.F. 1998. Geology of the Braeside 1:100,000 sheet. Geological Survey of Western Australia, 39p.
1:100 000	Broadhurst	Hickman, A.H. and Clarke, G.L., 1994. Geology of the Broadhurst 1:100,000 sheet. Geological Survey of Western Australia, 40p.
1:100 000	Connaughton	Bagas, L. and Smithies, R.H., 1998. Geology of the Connaughton 1:100,000 sheet. Geological Survey of Western Australia, 38p.

Table 2.1: continued.

SCALE	NAME	AUTHOR(S), REFERENCE
1:100 000	Eastern Creek	Farrell T.R., 2006. Geology of the Eastern Creek 1:100,000 sheet. Geological Survey of Western Australia, 33p.
1:100 000	Gunanya	Bagas, L., 1998. Geology of the Gunanya 1:100,000 sheet. Geological Survey of Western Australia, 10p.
1:100 000	Isabella	Williams, I.R., and Trendall, A.F., 1998. Geology of the Isabella 1:100,000 sheet. Geological Survey of Western Australia, 24p.
1:100 000	Lamil	Bagas, L., 2005. Geology of the Lamil 1:100,000 sheet. Geological Survey of Western Australia, 22p.
1:100 000	Paterson	Bagas, L., 2000. Geology of the Lamil 1:100,000 sheet. Geological Survey of Western Australia, 20p.
1:100 000	Pearana	Williams, I.R. and Trendall, A.F., 1998. Geology of the Pearana 1:100,000 sheet. Geological Survey of Western Australia, 33p.
1:100 000	Poisonbush	Williams, I.R. and Bagas, L., 2000. Geology of the Poisonbush 1:100,000 sheet. Geological Survey of Western Australia, 21p.
1:100 000	Rudall	Hickman, A.H. and Bagas, L., 1998. Geology of the Rudall 1:100,000 sheet. Geological Survey of Western Australia, 30p.
1:100 000	Throssell	Williams, I.R. and Bagas, L., 1999. Geology of the Throssell 1:100,000 sheet. Geological Survey of Western Australia, 24p.
1:100 000	Warrawagine	Williams, I.R., 2001. Geology of the Warrawagine 1:100,000 sheet. Geological Survey of Western Australia, 33p.
1:100 000	Yilgalong	Williams, I.R., 2007. Geology of the Yilgalong 1:100,000 sheet. Geological Survey of Western Australia, 45p.

Airborne surveys have been flown at a variety of line spacings using a variety of sampling rates depending on the method and purpose. Company surveys may have been flown with nominal line spacings of 100–200 m for more detailed resolution, whereas regional State- and Commonwealth-based surveys may have been flown with 400 or 800 m line spacings.

Between March and December 2007 GA contracted the Australia-wide airborne geophysical tie-line survey (AWAGS 2), which included parts of the Paterson AEM survey area (Johnson and McKay, 2007). This survey featured a single aircraft acquiring magnetics and radiometrics across the whole continent at 75 km line spacing. The data were used to level magnetic and radiometric data sets across Australia to produce single, continent-wide magnetic and radiometric data sets. Data included in this report have been levelled according to the results of the AWAGS 2 survey.

Most recently (2009) GA and the GSWA conducted infill magnetic and radiometric surveys over the remainder of the Canning and Officer basins that was previously only covered by 800 m line spacing data, bringing the data to 400 m line spacing across the entire region. Some of the airborne geophysical data in the [Figure 2.4](#) reflects the lack of regional-scale data in these areas adjacent to the Paterson AEM survey area.

[Figure 2.4](#) illustrates the fundamental regional ground gravity, airborne magnetic and radiometric geophysical data and the SRTM DEM data sets covering the Paterson AEM survey area. A number of other products are calculated from each data set, including First and Second Vertical Derivative (1VD, 2VD) gravity and magnetics (or variations thereon, including 0.5 and 1.5 VD magnetics) to highlight the rate of change of the potential fields, and various filters to highlight or subdue different wavelengths and directional trends. Radiometric data can also be displayed as single channel (potassium, thorium, uranium), total counts (dose rate), channel ratio (potassium/thorium, thorium/uranium, potassium/uranium) or variants thereon including uranium²³²/thorium (U²³²/Th), which can be used to highlight surface uranium concentrations for uranium prospecting (Mernagh *et*

al., 1998; Wilford *et al.*, 2009). The SRTM DEM can be processed further to provide slope, aspect and surface drainage vector maps as well as having more advanced calculations such as the MRVBF algorithm (Gallant and Dowling, 2003) applied, to highlight areas with low, moderate and high slope for landscape and surface hydrology studies (See [Figure 1.17](#)).

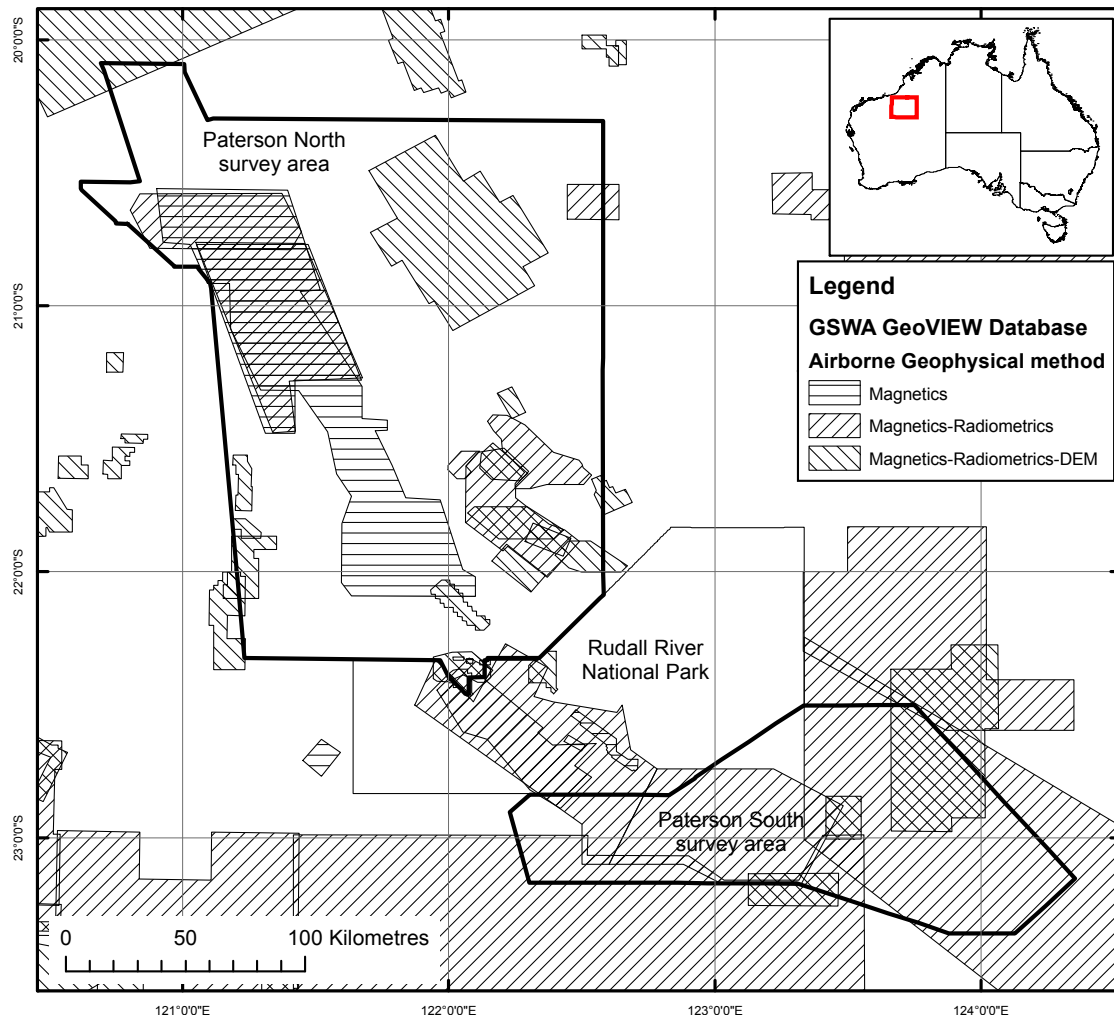


Figure 2.2: Publicly-available industry-generated airborne magnetic, radiometric and digital elevation model surveys in the Paterson region. Modified after the GSWA GeoVIEW database (GeoVIEW, 2009).

A number of seismic lines occur within or intersect the Paterson AEM survey boundaries where the Canning and Officer basins lap onto the Proterozoic basement rocks of the Rudall Complex and Yeneena Basin and within the Waukarlycarly Embayment (Figure 2.5, Table 2.2). Data are of varying quality, with the most recent survey in the Waukarlycarly Embayment by the Hunt Oil Company (Hunt, 1996) having the most recognisable stratigraphy. Unfortunately, most of the seismic lines have very poor data quality between 0 and about 0.2 seconds two-way travel time (TWT), or between the surface and approximately 500-600 m depth, effectively masking any seolith features and making interpretation of Mesozoic and Paleozoic stratigraphy difficult.

[Figure 2.6](#) depicts the three seismic lines across the Waukarlycarly Embayment in the North Paterson AEM survey area with interpretations by the Hunt Oil Company (Hunt, 1996). Interpretations depict listric faults either side of the rifted Embayment marking the boundary

between Neoproterozoic Yeneena Basin rocks (labelled “Proterozoic”), down-thrown Yeneena Basin rocks and Paleozoic to Recent infill in the rift, including Ordovician-Devonian sediments in the base of the rift, Permian fluvio-glacial and marine sediments of the Grant Group and Mesozoic sediments overlying the whole. Cenozoic sediments would form a thin layer over the top of the sections but are lost in the noise above 0.2 s TWT.

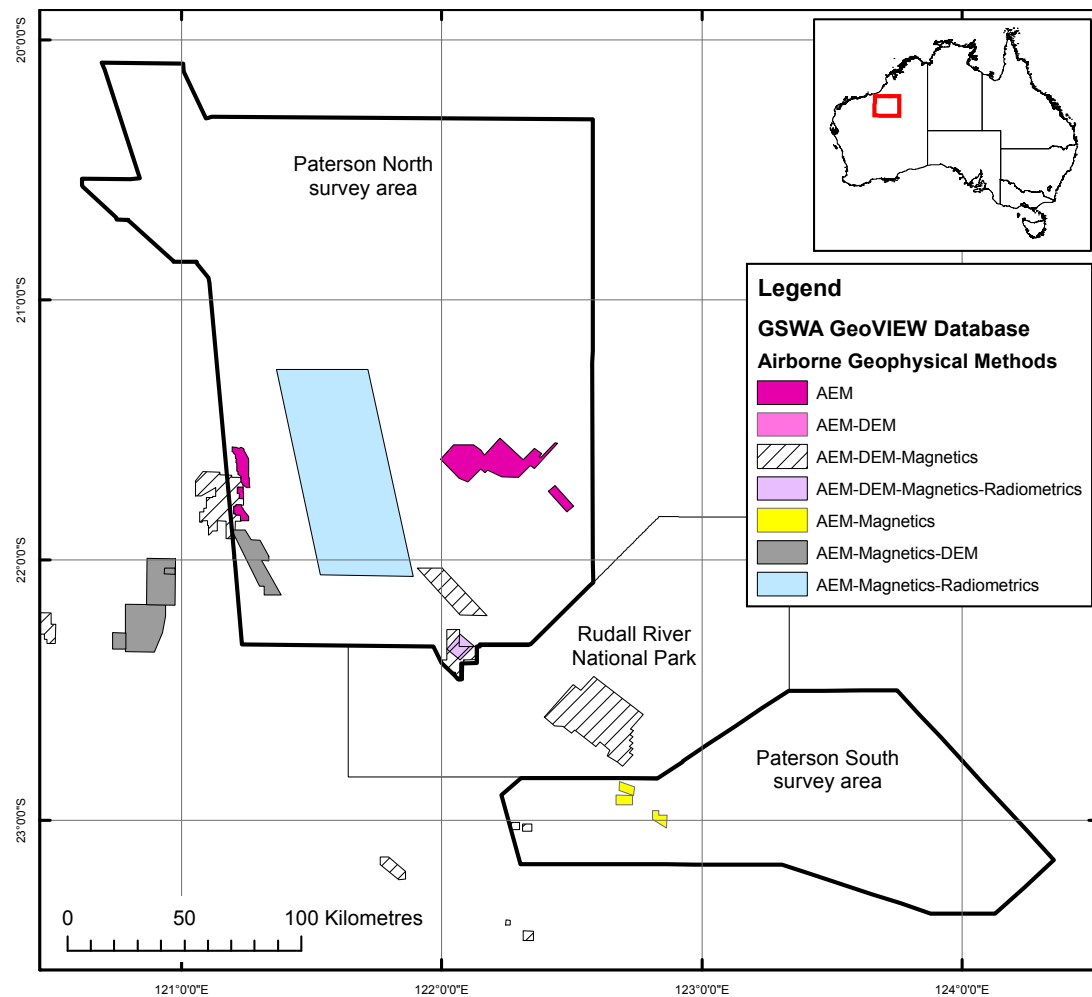


Figure 2.3: Publicly-available industry-generated AEM surveys in the Paterson region. Modified after the GSWA GeoVIEW database (GeoVIEW, 2009).

Table 2.2: Compilation of seismic surveys within or intersecting the Paterson AEM survey area.

SURVEY NAME	DATE	COMPANY	OPERATOR	REFERENCE
Anketell Hills SS	1986			GeoVIEW (2009)
Auld SS	1971			GeoVIEW (2009)
Capricorn SS	1984			GeoVIEW (2009)
Traeger SS	24 Sep–12 Nov 1983	News Corporation Ltd	Petty-Ray Geophysics	Perincek (1997)
Waukarlycarly SS	1997	Hunt Oil Company		Hunt (1997)

There is also a wide range of commercial-in-confidence company data covering the area, including ground EM, magnetics, gravity and radiometrics, which can not be included in this compilation, but were used for reference in this interpretation.

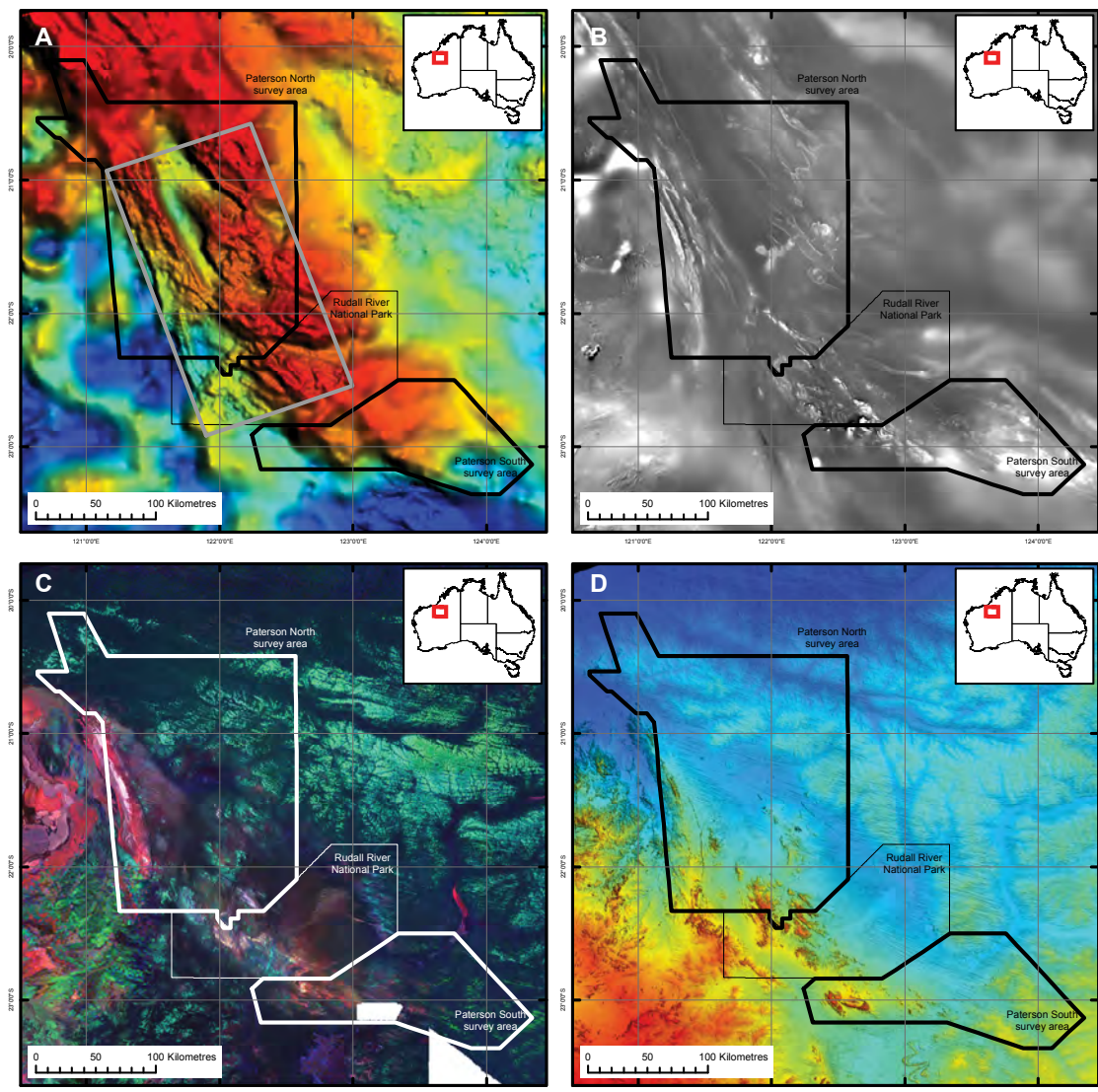


Figure 2.4: Regional geophysical data sets available for the Paterson AEM survey area. A: Bouger anomaly gravity. Grey outline highlights the higher-resolution data from the GA-GSWA 2005 1 km station spacing Paterson gravity survey, 2005; B: Reduced-to-pole total magnetic intensity (RTP TMI) image; C: Ternary radiometric (gamma-ray spectrometric) image with KThU as RGB; D: Space Shuttle Radar Topographic Mission Digital Elevation Model (SRTM DEM) with 30 m ground pixel resolution.

2.3 DRILLING DATA COMPILED

To aid with the AEM data interpretation process a database of public-domain drill hole geological information was compiled for the Paterson region between August 2008 and July 2009, described more fully in Roach (2009). This database contains over 6,500 individual drill holes of greater than 20 m depth from across the entire area, dating from the 1960s to the present, together with geological logs for over 4,300 of those holes (Figure 2.7), concentrating on areas of strategic importance to the interpretation project. The information contained within the drill hole database was used, together with other geological and geophysical data, to help interpret the EM Flow™ software fast approximate inversion AEM data products delivered by the contractor and the GA layered earth

inversion (GA LEI) AEM data products produced by the AEM Project at GA.

Drill hole location and geological data in the database are derived primarily from digital and non-digital reports lodged in the Geological Survey of Western Australia's (GSWA) WAMEX (Western Australian Mineral EXploration) database, but also some drill hole location data from the GSWA's EXACT (EXploration ACTivity) database. Both databases are available online at the Government of Western Australia's Department of Mines and Petroleum website at <http://www.dmp.wa.gov.au/>. The bulk of drill hole information is available online as reports and collar locations, however a number of reports were not available in digital form at the time of writing and were photocopied from the original paper reports at the GSWA offices in Perth, WA. A table describing the WAMEX report number, WAMEX item number and digital or non-digital status of individual reports used is included in Roach (2009).

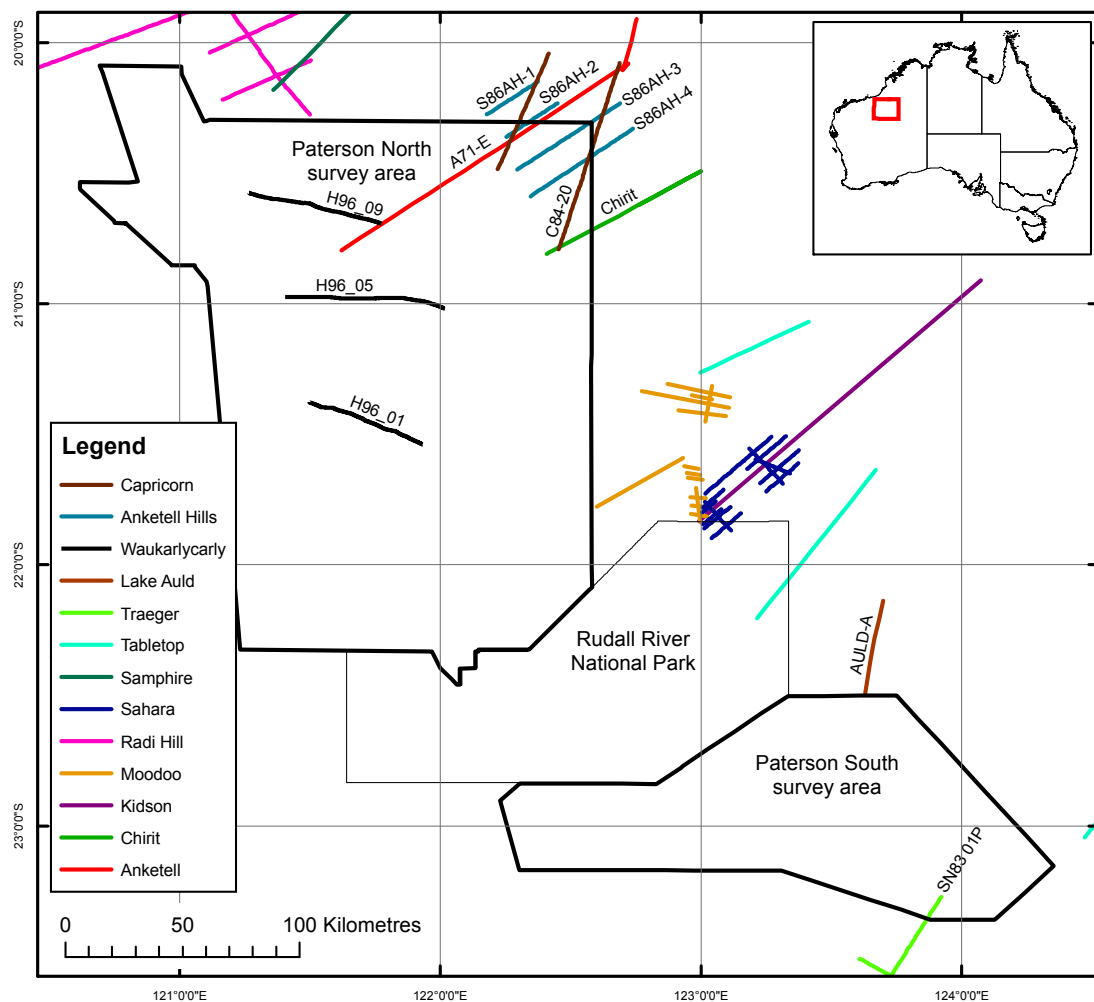


Figure 2.5: Seismic lines in and around the Paterson AEM survey area. Lines occurring within or intersecting the Paterson AEM survey area are labelled. Adapted from GeoVIEW (2009).

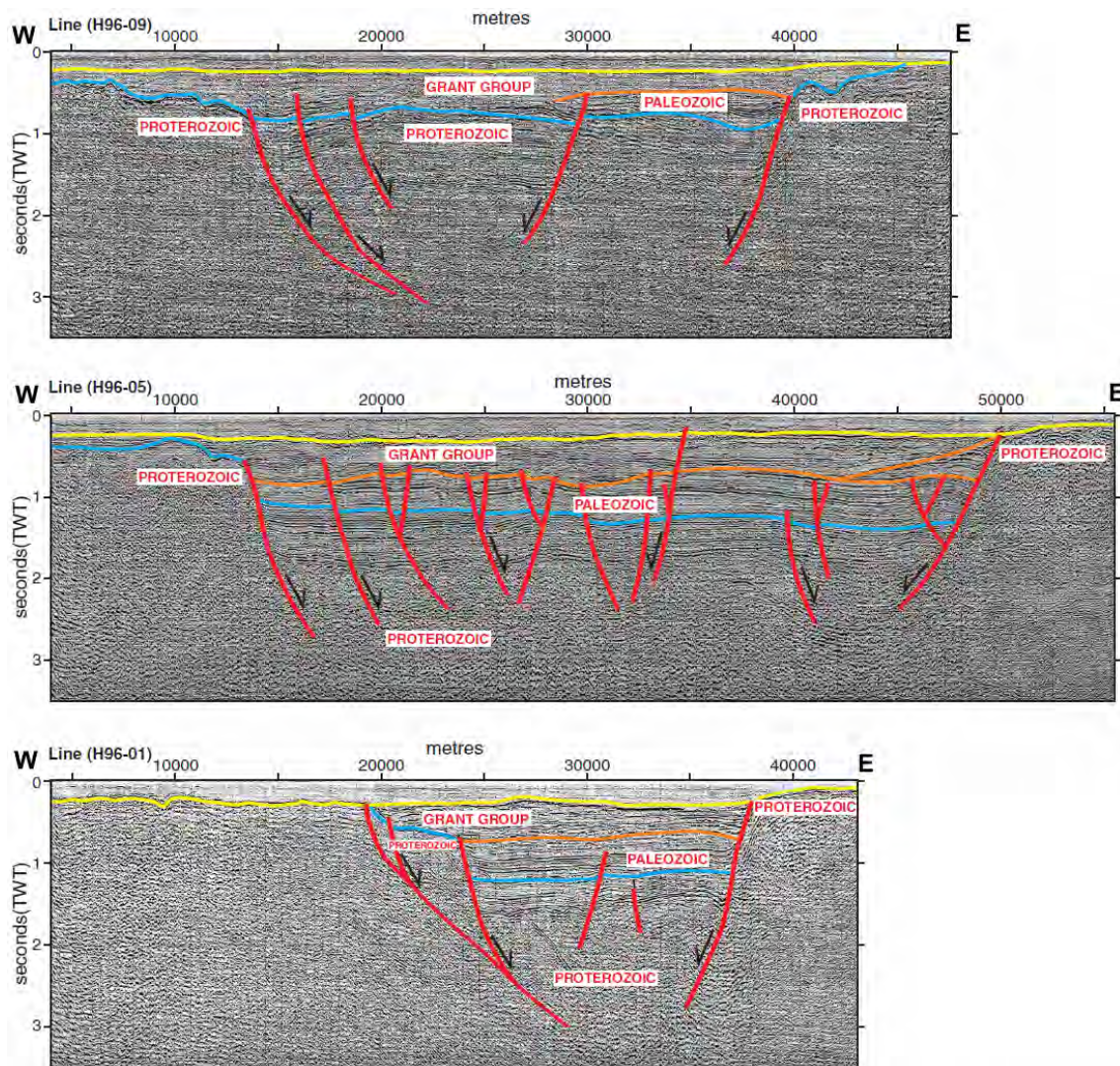


Figure 2.6: Hunt Oil Company 1996 survey interpreted seismic sections across the Waukarlycarly Embayment. From GSWA (2008) after Hunt Oil Company (Hunt, 1996).

Drill hole data were entered into a series of spreadsheets capable of being imported into a variety of drill hole management and presentation software products. Data from each hole were divided into tables based on their location, down hole geology, hole orientation and rock types, described below:

- Collar locations: Hole name, WAMEX Report and Item numbers, total depth, type of drilling activity, hole dip, hole azimuth, collar height relative to datum, easting, northing;
- Geological logs: Hole name, down hole geological log intervals (from-to depths), depth to water table, simple stratigraphy indicating economic basement or cover, GA 1:1 000 000 map sheet unit name, GA unit name geological description;
- Down hole surveys: Hole name, interval, azimuth, dip; and,
- Rock codes: original stratigraphic unit names from company reports and GA 1:1 000 000 Geological Map of Australia unit names.

Drill hole data were visualised using Geosoft Target for ArcGIS and Oasis Montaj software, allowing the data to be viewed as drill hole location plans, individual drill hole graphic logs, section plots of numerous drill hole graphic logs and 3D plots of drill holes together with geological surfaces and AEM data conductivity grids and sections or voxel data.

The drill hole data used in this record were collated from data spanning over four decades and reported in a variety of styles including hand-drafted maps, computer drawn maps and tables using a variety of datums and projections. Data have been reduced to Cartesian (easting-northing) coordinates using the Map Grid of Australia Zone 51 coordinate system using the Geocentric Datum of Australia 1994. More detail on the accuracy of collar coordinates is included in (Roach, 2009).

Drill hole locations are highly skewed towards bedrock-dominated areas, areas along strike from known deposits, or areas where other geophysical data including magnetics and gravity indicate that Proterozoic basement rocks should lie close to surface. Data and a histogram describing the frequency of drill holes versus their total depth is shown in [Table 2.3](#) and [Figure 2.8](#). The bulk of wide-spaced pattern drilling occurs along dune swales testing the depth of cover, with varying degrees of success in sampling the Proterozoic target rocks.

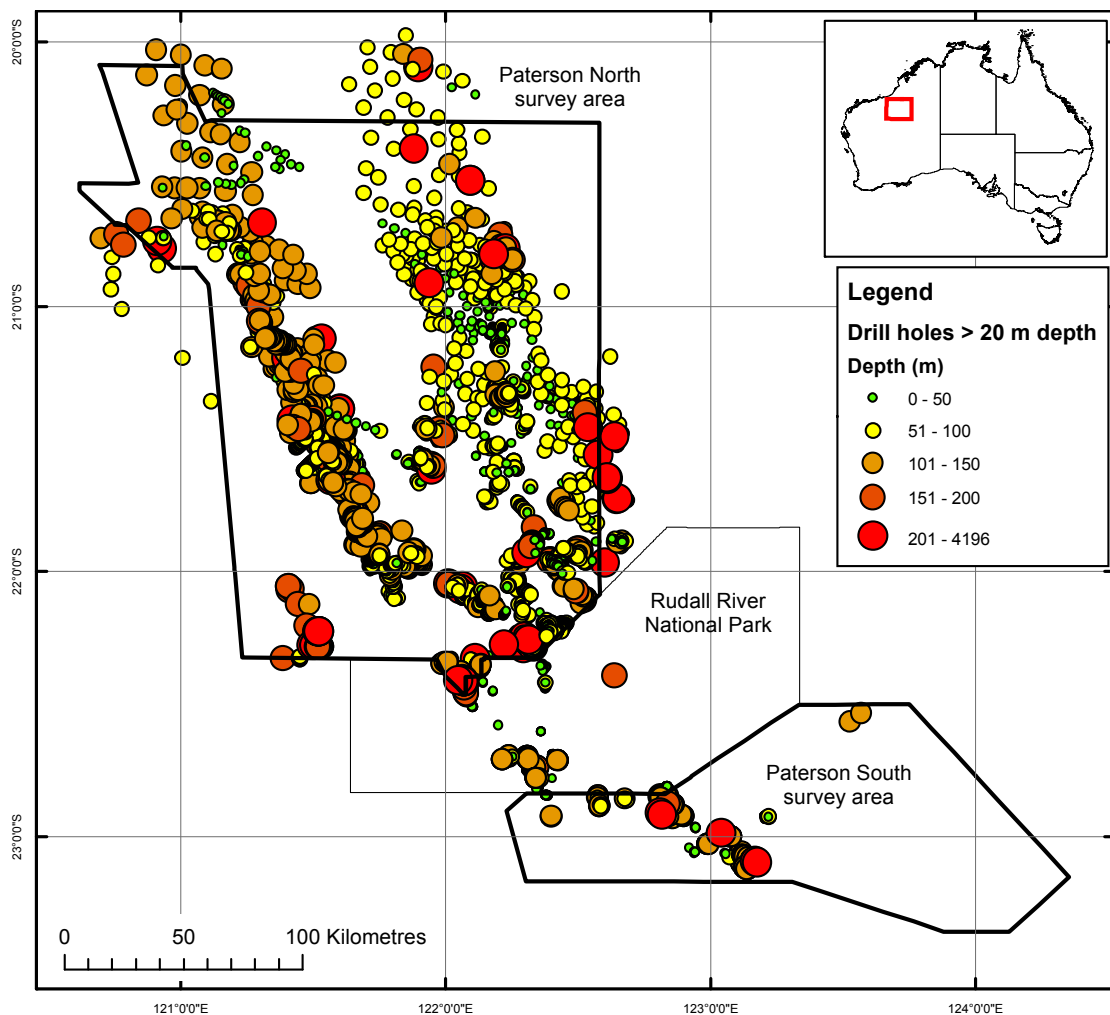


Figure 2.7: Distribution of public-domain drill holes with geological logs used in the interpretation project. From Roach (2009).

The database has been useful in showing the thickness of Cenozoic cover materials, rock types and depth to major bedrock rock groups e.g., depth to Neoproterozoic sediments and granite, depth to Paleoproterozoic metamorphic rocks. Due to the nature of much of the drilling compiled, dominated by percussion, reverse circulation percussion and rotary drilling, accurate assignment of intersections to formations, either by the logging geologist or interpreted as part of this project, was more

problematic for some rock groups. For instance, some carbonate intersections near the Broadhurst-Isdell formation boundary were assigned to Isdell Formation. However, on the basis of aeromagnetic interpretation through areas of cover, some of these intersections may more correctly be assigned to carbonate-bearing parts of the Broadhurst Formation. Furthermore, Permian and Mesozoic clastic sediments are not easily distinguished in the drill logs. With little other guidance, moderate clay content in the clastic sediments was thought to be more indicative of Permian tillite rather than cleaner, more uni-modal Mesozoic sediment. Some of these assignments may not stand when better quality drill data is acquired (e.g., diamond drill core).

Table 2.3: Drill hole depth frequency for the public domain drill hole database. Collated from data in Roach (2009).

DEPTH RANGE	FREQUENCY OF DRILL HOLES
0-50	2559
50-100	1840
100-150	1488
150-200	232
200-250	71
250-300	35
300-350	19
350-400	45
400-450	14
450-500	0
500-5000	34

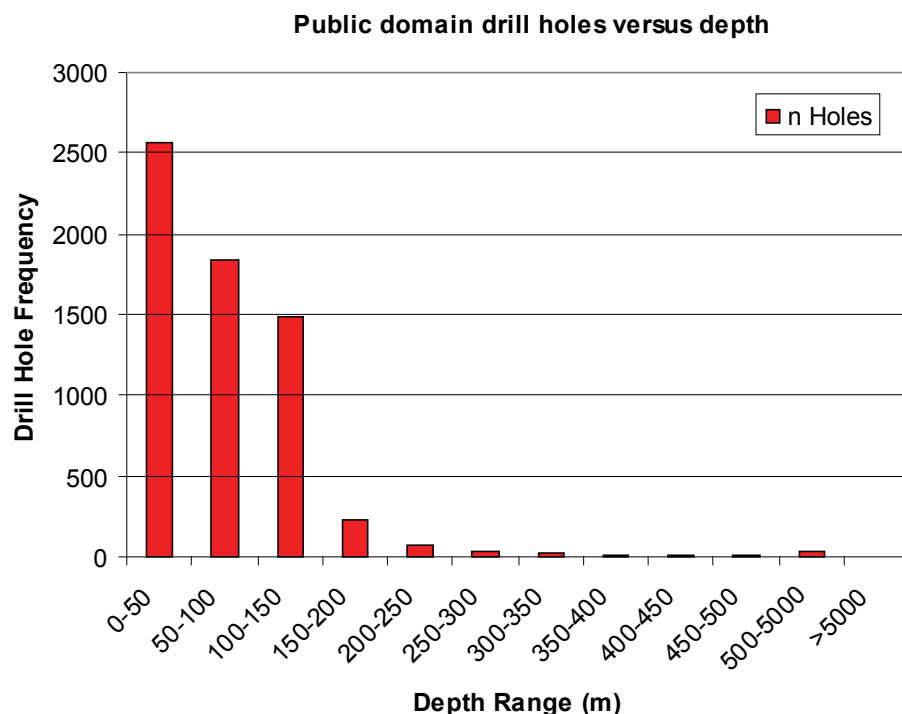


Figure 2.8: Drill hole frequency versus depth range for public domain drill holes in the database. From Roach (2009).

2.4 ROCK PROPERTIES

Accurate knowledge of rock properties is vital for the modeling and interpretation of geophysical data. In the case of the Paterson AEM survey, the review was used to collate accurate electrical conductivity data that could be used in both forward modelling for system selection and to validate the layered earth inversion model used to process the final contractor-delivered data.

Accurate data are important because the AEM response informs about the distribution of geological materials underneath the Earth's surface; inaccurate data will in turn result in inaccurate interpretations. The AEM response is a function of the conductivity of geological materials. The conductivity, in turn, is a function of a number of parameters including the porosity and permeability (including pore size and arrangement) of geological materials, pore fluid conductivity, pore fluid saturation, the conductivity of solid matter (anisotropy) and the texture of conductive solids. These properties in turn inform about the lithology, structure, alteration and groundwater conditions present in the geological materials being surveyed.

When conducting geophysical surveys it is important to collect information regarding the physical properties of geological materials within the survey area in order to accurately model their geophysical responses and to interpret survey results ([Table 2.4](#)). The forward modelling program for the Paterson AEM survey collected data on the electrical properties of target geological materials in the survey area, most particularly the electrical conductivity and electromagnetic properties of economic basement rocks and overlying Phanerozoic materials including Permian glaciogene sediments, Mesozoic and Cenozoic sediments. Information was gleaned from published papers in the "Geophysical Signatures of Western Australian Mineral Deposits" volume (Dentith *et al.*, 1994), including those regarding the Telfer gold-copper deposits (Sexton, 1994) and the Kintyre uranium deposit (Root and Robertson, 1994), company reports in the WAMEX database and personal communications with company representatives ([Table 2.5](#)). A number of suitability criteria were established in a quality assurance-quality control (QA-QC) process at GA to ensure that data were fit for purpose. These criteria were based on the documentation with the data, including information on the type of survey, instruments used, logistics information, collection techniques, location and whether the correct units were quoted. Unfortunately, some data in company reports were not included in this compilation because they were lacking in one or more of the QA-QC criteria and were consequently unusable; these data were discarded. Data that were accepted are included in [Table 2.4](#). There are also commercial-in-confidence company data pertinent to the area, which can not be included in this compilation, but were used in the interpretation.

After the literature review procedure was completed a bore hole conductivity logging program was carried out in the Paterson region in August-September 2008. This program collected conductivity values to help constrain inversions when preparing the final data products. A total of 19 holes were conductivity logged on the tenements owned by Aditya Birla Ltd. (Nifty Mine), Consolidated Minerals Ltd. (Woodie Woodie Mine) and Newcrest Ltd. (Telfer Mine) ([Figure 2.9](#)). These data are confidential between GA and the respective companies, so are not included in this Record.

Table 2.4: Rock properties important for geophysical surveying.

METHOD	PROPERTY
GRAVITY (MASS)	Density
MAGNETIC	Susceptibility (magnetisation in response to a magnetic field). Remanence (natural magnetisation by ferro- or ferri-magnetism).
ELECTRICAL	Anisotropy (directional dependence of magnetic properties). Resistivity (resistance to the flow of electric current). Anisotropy (directional dependence of electrical conductivity). Induced polarisation (IP) effect (dielectric constant; chargeability of a mineral). Dielectric Permittivity (ability to transmit an electric field). Attenuation
ELECTROMAGNETIC	Conductivity Magnetic k (inductive)
SEISMIC	Pressure (P) and Shear(S) wave velocities. Anisotropy (directional dependence of sound waves).
THERMAL	Diffusivity (rate at which a mass adjusts to ambient temperature). Conductivity (ability to conduct heat).
MECHANICAL	Rock Strength (compressive, non-compressive, tensile). Porosity (volume of a mass occupied by pore spaces). Permeability (ability to transmit a fluid through a mass).
RADIOMETRIC	Natural potassium, thorium and uranium concentrations.

Table 2.5: Electrical properties of selected geological materials in the Paterson AEM survey area.

GEOLOGICAL MATERIAL	ELECTRICAL PROPERTY	SOURCE
Quaternary surface sediment	Resistivity 112 ohm m	Richard Stuart, Western Areas Pty Ltd., pers. comm.
Telfer Permian overburden	“Conductive”	Sexton (1994)
Telfer weathered ore host rocks	Resistivity 12 ohm m	Sexton (1994)
Telfer mineralised veins	Resistivity 102 ohm m	Sexton (1994)
Telfer massive sulfides	Resistivity 406 ohm m	Sexton (1994)
Telfer disseminated sulfides	Resistivity 11 988 ohm m	Sexton (1994)
Telfer Formation (ore host)	Conductivity 2-100 mS/m	Sexton (1994)
Rudall Complex	Resistivity 400-1,000 ohm m	Root and Robertson (1994)
Kintyre mineralised units (meta-chert-carbonate metapelite)	Resistivity 1 200 ohm m	Root and Robertson (1994)
Woodie Woodie manganese ore	Resistivity 3-40 ohm m	Hashemi and Meyers (2004)
Rudall Complex base metal veins and hydrothermally-altered outcrop to 150 m	Resistivity 1 000-2 818 ohm m	Richard Stuart, Western Areas Pty Ltd., pers. comm..
Woodie Woodie	Resistivity 1 000-200 000 ohm m	Hashemi and Meyers (2004)
Carawine Dolomite (ore host)		
Pinjian Chert Brecia (ore host)		

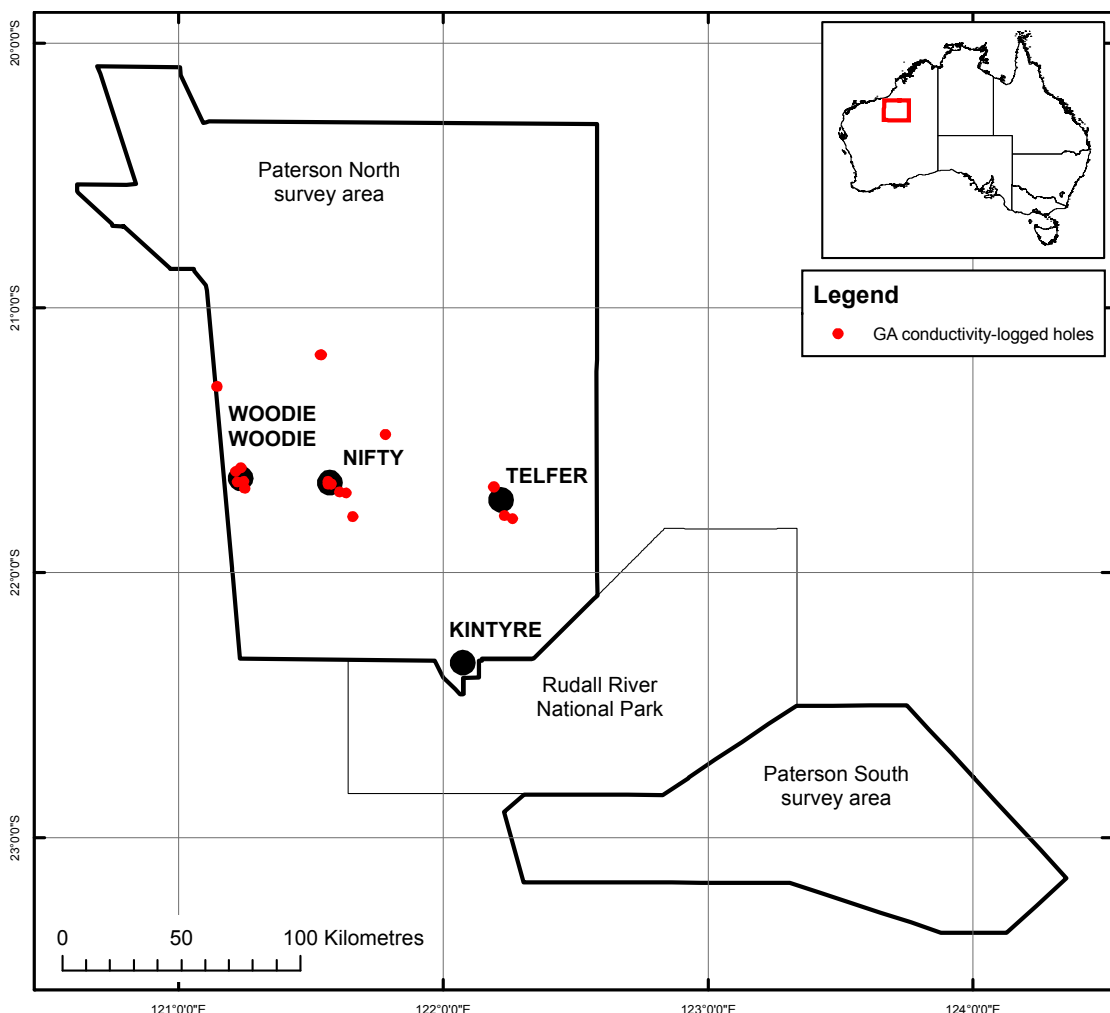


Figure 2.9: Locations of GA conductivity-logged drill holes in the Paterson AEM survey area.

2.5 SUMMARY OF HYDROGEOLOGICAL INVESTIGATIONS

Little is understood about the detailed hydrogeology of the Paterson region. There are several generalised studies covering a large area but little detailed data, which are restricted to the near-mine areas around Nifty, Telfer and Woodie Woodie and the Indigenous communities of Parnngurr and Punmu. The hydrogeology and palaeovalley ground water resources of the Paterson region are currently the subject of the Palaeovalley Groundwater project conducted jointly between GA and the National Water Commission to be reported independently following the release of the Paterson AEM data set. Detail in this record is summarised from Magee (2009) and from an unpublished milestone report by the Palaeovalley Groundwater project (Lewis *et al.*, 2009).

2.5.1 Surface water

There is little surface water available in the Paterson region and streams and most water holes are ephemeral. Semi-permanent to permanent rockholes occur in bedrock upland areas and waterholes occur within the lowland stream beds of the Rudall River and its tributary Cotton Creek (Parnngurr), within the Rudall River National Park, and the Oakover River in the far west (Figure 1.1). Surface drainage within the bulk of the Paterson AEM survey area is confined largely to the rocky upland

areas and normally only flows after intense rain events such as thunder storms or cyclones. Water draining from these areas either evaporates, flows along the Oakover River to the Indian Ocean, or from the Rudall River discharges into salt lakes and sand dune swales, evaporating or disappearing beneath the land surface into shallow aquifers. Numerous smaller streams drain from the Gregory Range, in the west of the area, and from the Rudall Complex, but these disappear into the dune fields of the Great Sandy Desert along a series of alluvial fans containing soaks.

Rockholes can retain usable water for periods of up to six months, although they frequently dry out within two months after rain (Kavanagh, 1984). Semi-permanent to permanent waterholes also occur around claypans and salt lakes in the lowland areas, but these are frequently too saline for human consumption. Fresh waterholes can be found around the flanks of salt lakes, between sand dunes, fed by runoff from nearby small creeks or by water penetrating through sand dunes (Kavanagh, 1984). Soaks and native wells are also common around the area, between sand dunes, around the flanks of granite outcrops, in ferruginous duricrust plains, at the ends of alluvial fans and along the flanks of the Gregory Range.

A number of permanent artesian springs and mound springs occur in the area, particularly around or within the Percival Lakes. Recent drilling by Aditya Birla Pty. Ltd. along the Paterson Range at the Dromedary exploration lease also intersected artesian water, resulting in a free-flowing bore which remains uncapped. Many of the soaks and artesian springs are driven by water seeping from Paleozoic-Mesozoic aquifers in the Canning Basin (see below).

2.5.2 Groundwater

Groundwater occurs within the Paterson region within shallow Phanerozoic (Paleozoic-Mesozoic-Cenozoic) sedimentary aquifers of the Canning Basin or fractured rock aquifers within the Mesoproterozoic and Neoproterozoic basement rocks.

Yeates *et al.* (1984), Commander (1985), Laws (1990) and Allen (1990; 1997) provide a regional assessment of the groundwater potential of the Canning Basin, which is the principal groundwater source in the Paterson region. [Figure 2.10](#) describes the principal Phanerozoic aquifers in a cross-section drawn from the southeast to the northwest across the Canning Basin. The dominant Mesozoic and Paleozoic aquifers include:

- Cretaceous: Broome Sandstone, Anketell Sandstone;
- Jurassic-Cretaceous: Callawa Formation;
- Jurassic: Wallal Sandstone; and,
- Permian: Triwhite Sandstone, Paterson Formation, Grant Group, Poole Sandstone.

Summarising from the references above and from Lewis *et al.* (2009), the most easily accessible aquifer in the Canning Basin near the Paterson AEM survey area appears to be the Triwhite Sandstone. This is heavily indurated by calcrete where it outcrops in valleys around Lake Dora and the South Paterson AEM survey area and is exploited by the community at Punmu, as well as having numerous wells and bores sunk into it between 1908 and 1910, roughly every 20 km along the Canning Stock Route. Potable water may be pumped from the other aquifers, although some artesian water, most likely from the Triwhite Sandstone, is also available in areas of greater relief.

Fractured rock and sandstone aquifers are present in Archean rocks of the Pilbara Craton and the Proterozoic Yeneena Basin and Rudall Complex. Little is known regarding these aquifers except where they are exploited by mining activities at Woodie Woodie (Archean Carawine Dolomite), Nifty (dolomitic Neoproterozoic Broadhurst Formation) and Telfer (Neoproterozoic Puntapunta Formation).

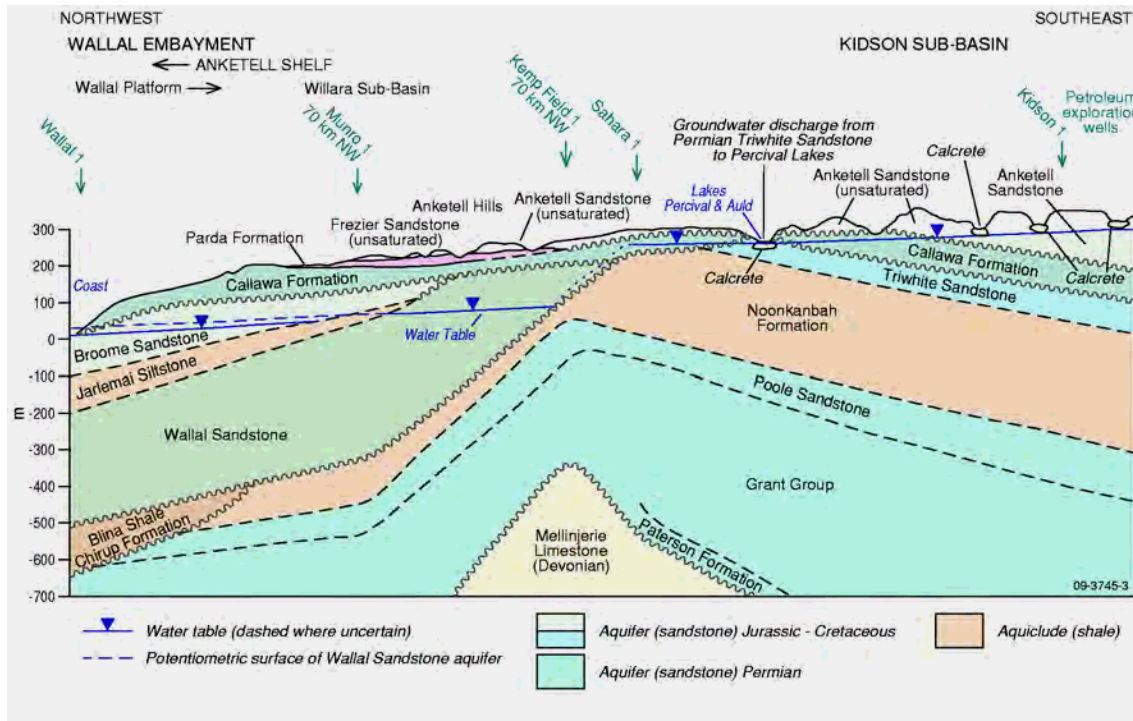


Figure 2.10: Phanerozoic aquifers of the Canning Basin. From Lewis *et al.* (2009) after Commander (1985) and Laws (1990).

2.5.3 Palaeovalleys

There is an extensive surface-visible palaeovalley system, previously interpreted by Beard (1973), van der Graaf *et al.* (1977) and Commander (1989). The palaeovalleys form parts of older drainage systems named the Percival Palaeovalley, the Disappointment Palaeovalley and the Wallal Palaeovalley by van der Graaf *et al.* (1977) (Figure 2.11). The ages of the palaeovalley systems are not known, but they are assumed to be post-Cretaceous (Beard, 1973) because the systems cut down into the Mesozoic of the Canning Basin, the Neoproterozoic of the Yeneena Basin and the Paleoproterozoic Rudall Complex. Magee (2009) summarised the palaeovalley systems in the northern Yilgarn Craton as being Mid-Late Eocene to Oligo-Miocene in age. Without further evidence, the palaeovalley systems in the Paterson could also be ascribed this age. Within the Paterson AEM survey area the palaeovalleys drain from southeast to northwest and the Percival Palaeovalley joins the Oakover River in the northwest of the area. Older palaeovalley systems are interpreted at the base of the Permian glaciogenic sediments, which are relatively common in the Paterson area (Figure 2.11). These are most visible around the Rudall Complex as outcrops following dissected dendritic channel systems from the Rudall Complex uplands, before disappearing beneath younger cover of the Waukarlycarly Embayment.

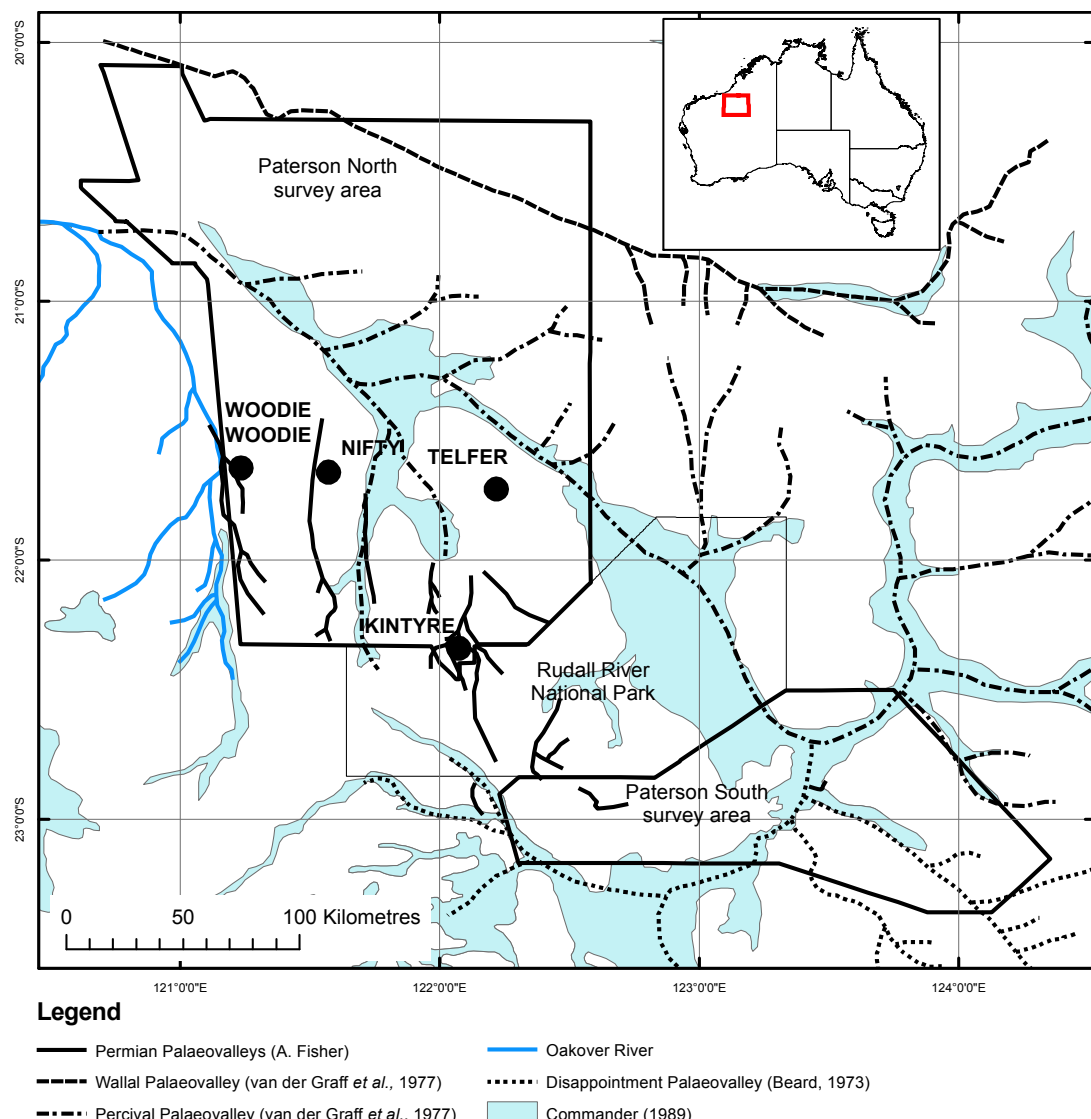


Figure 2.11: Interpreted palaeovalley traces in the Paterson AEM survey area. Data from Beard (1973), van der Graaf et al. (1977) and Commander (1989). Permian palaeovalley interpretation by A. Fisher from the GA 1:1,000,000 geological map of Western Australia.

Little data exist to describe the depths of the palaeovalleys except where exploration drilling has penetrated them in search of copper or gold near Nifty and Telfer respectively. Drill holes from the Nifty area collated in the drill hole database of Roach (2009) indicate that a palaeovalley to the east of the mine area (the East Nifty Palaeochannel) contains up to 100 m of Permian and Mesozoic sediments in a depression several kilometres across with a thin cover of Holocene to Recent sand. The valley is incised into Neoproterozoic basement which otherwise has variable cover up to about 50 m depth around the site. The larger palaeovalley systems are assumed to be several hundreds of metres deep, but little drilling data exist to support this assumption.

2.6 REFERENCES

- Allen, A. D., 1990. Groundwater resources of the Phanerozoic sedimentary basins of Western Australia. In: *Proceedings of the International Conference on Groundwater in Large Sedimentary Basins*. Department of Primary Industries and Energy. **Australian Water Resources Council Conference Series No. 20**, 16-34 pp.
- Allen, A. D., 1997. Groundwater: the strategic resource - a geological perspective of groundwater occurrence and importance in Western Australia. Geological Survey of Western Australia, Perth. 61 p.
- Beard, J. S., 1973. The elucidation of palaeodrainage patterns in Western Australia. Vegmap Publications, Perth. Occasional Paper No 1, 17 p.
- Commander, D. P., 1985. Groundwater Prospects - Punmu Aboriginal Community, Lake Dora. . Western Australia Geological Survey. 14 p.
- Commander, D. P., 1989. Hydrogeological map of Western Australia, 1:2 500 000. Geological Survey of Western Australia.
- Czarnota, K., Gerner, E., Maidment, D. W., Meixner, A. J. and Bagas, L., 2009a. Paterson Area 1:250 000 Scale Solid Geology Interpretation and Depth to Basement Model. Geoscience Australia, Canberra. **Record 2009/16**, 37 p.
- de la Hunty, L. E., 1965. Investigation of manganese deposits in the Mt Sydney-Woodie Woodie area, Pilbara goldfields. Western Australia Geological Survey, Perth. **Annual Report 1964**, 45-49 p.
- Dentith, M. C., Frankcombe, K. F., Ho, S. E., Shepherd, J. M., Groves, D. I. and Trench, A., 1994. Geophysical Signatures of Western Australian Mineral Deposits. Geology and Geophysics Department (Key Centre) & UWA Extension, The University of Western Australia, Publication 26 and the Australian Society of Exploration Geophysicists, Special Publication 7, 454p.
- Ferguson, K. M., Bagas, L. and Ruddock, I., 2005. Mineral occurrences and exploration potential of the Paterson area. Geological Survey of Western Australia, Perth. 43 p.
- Gallant, J. C. and Dowling, T. I., 2003. A multiresolution index of valley bottom flatness for mapping depositional areas. *Water Resource Research* **39(12)**, 1347-1359.
- GeoVIEW, 2009. GeoVIEW database. Online: <http://www.dmp.wa.gov.au/7113.aspx>.
- Grey, K., Hocking, R. M., Stevens, M. K., Bagas, L., Carlsen, G. M., Irimies, F., Pirajno, F., Haines, P. W. and Apak, S. N., 2005. Lithostratigraphic nomenclature of the Officer Basin and correlative parts of the Paterson Orogen Western Australia. Department of Industry and Resources, Geological Survey of Western Australia, Perth. 89 p.
- Hashemi, A. and Meyers, J., 2004. HoistEM data processing for discovery of high-grade manganese ore under regolith cover. *Exploration Geophysics* **35**, 272-276.
- Hickman, A. H. and Bagas, L., 1994. Tectonic evolution and economic geology of the Paterson Orogen - a major reinterpretation based on detailed geological mapping. In: *Geological Survey of Western Australia 1993-94 Annual Review*. Geological Survey of Western Australia, Perth. 67-76 pp.
- Hunt, 1996. Hunt Oil Company Final report Waukarlycarly Seismic Survey interpretation. Western Australia Geological Survey, Perth. **Statutory Petroleum Exploration Report S10316 A5**.
- Kavanagh, B. L., 1984. Survival Water in Australia's Arid Lands. The Australian National University, Canberra.
- Laws, A. T., 1990. Outline of the groundwater resource potential of the Canning Basin, Western Australia. In: *International Conference on Groundwater in Large Sedimentary Basins, Perth 1990*. Department of Primary Industries and Energy. **Australian Water Resources Council Conference Series No. 20**, 47-69 pp.
- Lewis, S. J., English, P. M., Wischusen, J. D. H., Woodgate, M., Gow, L., Kilgour, P. and Hanna, A., 2009. Palaeovalley Groundwater Project - Detailed Demonstration Study Site Work Plans: Palaeovalley Project Milestone 4 Report. A Report by Geoscience Australia for the National Water Commission.
- Magee, J., 2009. Palaeovalley Groundwater Resources in Arid and Semi-Arid Australia. Geoscience

- Australia, Canberra. **Record 2009/03**, 224 p.
- Mernagh, T. P., Wyborn, L. A. I. and Jagodzinski, E. A., 1998. 'Unconformity-related' U +/- Au +/- platinum-group-element deposits. *AGSO Journal of Australian Geology and Geophysics* **17(4)**, 197-205.
- Perincek, D., 1997. A compilation and review of data pertaining to the hydrocarbon prospectivity of the Officer Basin. Geological Survey of Western Australia, Department of Minerals and Energy, Perth. **Record 1997/6**, 209 p.
- Roach, I. C., 2009. A drill hole database for the Paterson airborne electromagnetic (AEM) survey, Western Australia. Geoscience Australia, Canberra. **Record 2009/31**, 16 p.
- Root, J. C. and Robertson, W. J., 1994. Geophysical signature of the Kintyre uranium deposit, Western Australia. In: Dentith, M. C., Frankcombe, K. F., Ho, S. E., Shepherd, J. M., Groves, D. I. and Trench, A. (eds) *Geophysical Signatures of Western Australian Mineral Deposits*. Geology and Geophysics Department (Key Centre) & UWA Extension, The University of Western Australia, Publication 26 and the Australian Society of Exploration Geophysicists, Special Publication 7, 454p. 371-382 pp.
- Sexton, M. A., 1994. Geophysical characteristics of the Telfer gold deposits, Western Australia. In: Dentith, M. C., Frankcombe, K. F., Ho, S. E., Shepherd, J. M., Groves, D. I. and Trench, A. (eds) *Geophysical Signatures of Western Australian Mineral Deposits*. Australian Society of Exploration Geophysicists, Special Publication 7, 454p. 199-212 pp.
- van der Graaf, W. J. E., Crowe, R. W. A., Bunting, J. A. and Jackson, M. J., 1977. Relict Early Cenozoic drainages in arid Western Australia. *Zeitschrift für Geomorphologie NF* **21(4)**, 379-400.
- Wilford, J., Worrall, L. and Minty, B., 2009. Radiometric Map of Australia provides new insights into uranium prospectivity. In: *AusGeo News*. Geoscience Australia. No. 95.
- Williams, I. R. and Trendall, A. F., 1998a. Geology of the Pearana 1:100 000 sheet, 1:100 000 Geological Series Explanatory Notes. Western Australia Geological Survey, Perth. 33 p.
- Yeates, A. N., Gibson, D. L., Towner, R. R. and Crowe, R. W. A., 1984. Regional Geology of the Onshore Canning Basin. In: Purcell, P. G. (eds) *The Canning Basin, Western Australia. Proceedings of the Geological Society of Australia/Petroleum Exploration Society of Australia Symposium*. Perth. 23-55 pp.

3 Geology

A. J. Whitaker, I. C. Roach, S. F. Liu and J. R. Wilford

3.1 INTRODUCTION

The Paterson region includes geological materials ranging from Archean to Recent in age and a regolith overprint perhaps beginning in the Paleozoic and extending until the present day. Consequently the region has a complex geological and regolith-landscape history. This chapter describes the geological materials, regolith and landscapes of the region, discusses their origins and highlights some of the problems with earlier interpretations.

3.2 BEDROCK GEOLOGY

3.2.1 Introduction

The following summary of the regional geology draws extensively on 1:100 000 and 1:250 000 scale geological mapping of the Paterson region. Maps in the 1:100 000 scale series used include PEARANA (Williams and Trendall, 1998a), BRAESIDE (Williams and Trendall, 1998b), LAMIL (Bagas, 2005), PATERSON (Bagas, 2000), THROSSELL (Williams and Bagas, 1999), BROADHURST (Hickman and Clarke, 1993), RUDALL (Hickman and Bagas, 1998), CONNAUGHTON (Bagas and Smithies, 1996) and BLANCHE-CRONIN (Bagas, 1999b). Maps in the 1:250 000 scale series include ANKETELL 2nd edition (Towner, 1982), NULLAGINE (Hickman, 1978), PATERSON RANGE 2nd edition (Chin *et al.*, 1982), and RUDALL 2nd edition (Bagas *et al.*, 2000). The Paterson area solid geology explanatory notes by Czarnota *et al.* (2009a; 2009b) were also consulted.

The Paterson survey area covers parts of four main Tectonic Units (Tyler and Hocking, 2002b): the Pilbara Craton in the west; the Paterson Orogen distributed more centrally through the survey area and the main focus of AEM acquisition; Officer Basin sediments in the south; and, sediments of the Canning Basin to the north and east ([Figure 3.1](#)). The Pilbara Craton, of Archean age, includes granite of the Gregory Range Suite and volcanics and sediments of the Fortescue and Hamersley basins. Interpretation of gravity and aeromagnetic data suggests that the Pilbara Craton is in tectonic contact with rocks of the Paterson Orogen to its east, however, the contact is obscured by overlying Officer Basin and Cenozoic sediments. The Paterson Orogen consists of the high grade metamorphic Paleoproterozoic Rudall Complex and overlying low to moderate metamorphic grade Yeneena Basin sediments. These rocks were subsequently deformed as a result the Miles (<950 & > 650 Ma) and Paterson orogenies (ca. 650 to 550? Ma). Gently folded and disrupted Officer Basin sediments are in faulted contact or partially overlie the Paterson Orogen in the south and west of the project areas.

Sedimentation commenced in the Canning Basin in the Ordovician Period. In the project area these rocks are completely covered by Permian and Mesozoic sediments. During Permian times, tillite and fluvioglacial sediments were deposited in glacial valleys which trend north to north-easterly across the palaeolandscape towards more laterally continuous sedimentation in the Canning Basin and related Waukarlycarly Embayment. Mesozoic sediments are more extensively preserved in the north and east of the survey area. Ferruginous duricrust is widely distributed but is laterally more continuous where developed on Mesozoic sediments as evidenced by outcrop and inferred from interpretation of gamma-ray spectrometric data. The region has undergone further erosion and incision during the Cenozoic Era with accumulation of materials in salt lakes and development of calcrete in valley sediments. Sand plains and west-northwest oriented longitudinal dunes are prevalent in widespread areas of low relief.

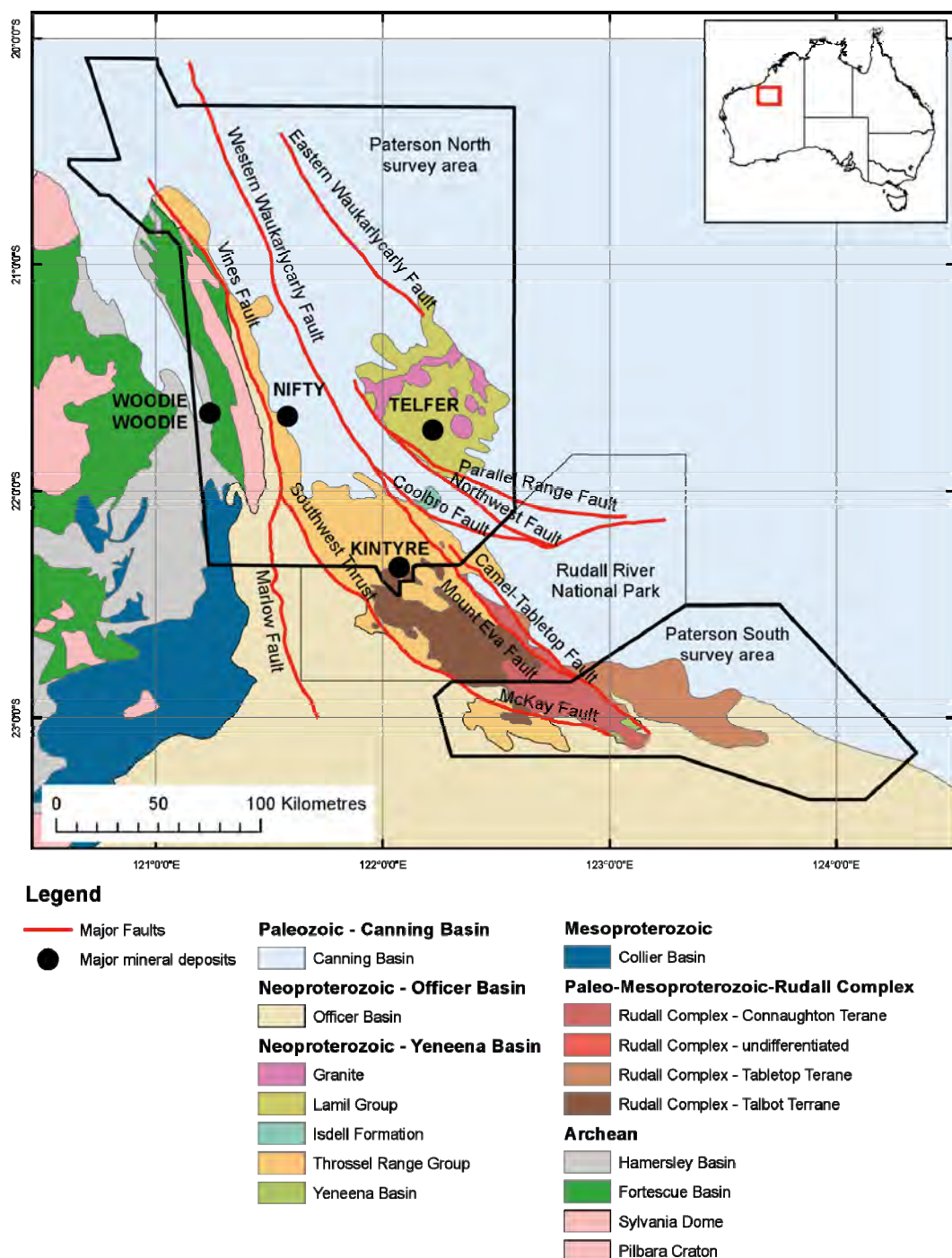


Figure 3.1: Simplified province map of the Paterson Project area also showing the AEM acquisition areas, Paterson North and Paterson South. Major faults (labelled) are from GSWA outcrop mapping and interpretation of gravity and aeromagnetic data. Airborne Electromagnetic acquisition was directed at areas of Rudall Complex, the overlying Yeneena Basin and regions thought to have less than 500 m of younger cover.

Airborne electromagnetic acquisition by Geoscience Australia and five infill companies was undertaken in two areas north and south of the Rudall River National Park. These areas are referred to below as 'Paterson North' and 'Paterson South'.

In the following description of the Precambrian geology, reference will be made to regional gravity (Bacchin *et al.*, 2008; Wynne and Bacchin, 2009) and aeromagnetic data (Percival, 2010) and their interpretation. The whole of the area is covered by an 11 km spaced regional gravity grid acquired by the Bureau of Mineral Resources, predecessor of Geoscience Australia. Most of Paterson North has also been covered by a 2.5 km spaced gravity survey acquired in 2005 by the Geological Survey of Western Australia. Some additional complementary infill gravity data was acquired from Barrick Gold Corporation. All of Paterson North and much of Paterson South are covered with 400 m line-spaced aeromagnetic data acquired at a ground clearance of 60-80 m and ca. 15 m along-line sampling. The southern part of Paterson South on GUNANYA and RUNTON is covered with older regional 1500 m line-spaced aeromagnetic data acquired at a ground clearance of 150 m and ca. 60 m along-line sampling.

The sample- and line-spacing of these surveys places relative constraints on their ability to resolve near-surface geological features. Other factors that influence resolution of geological features include the distribution and variability of rock properties (density, susceptibility and remanence) and the drop in anomaly amplitude with distance (depth) to the source: gravity anomalies decrease with the square of the distance; and, aeromagnetic anomalies decrease with the cube of the distance. Thus, in combination with respective station spacings, gravity data often show deeper, and aeromagnetic data shallower, information on lithology and structural patterns.

3.2.2 The Precambrian rocks

3.2.2.1 Pilbara Craton (Archean Fortescue and Hamersley basins, Mesoproterozoic Collier Basin)

3.2.2.1.1 Fortescue Group (Archean; Fortescue Basin; thickness >7 km)

The oldest rocks in the project area belong to the Fortescue Group and are located in the west of the Paterson North ([Figure 3.1](#)). These rocks are inferred to overlie older granite-greenstone terrane of the eastern Pilbara. The formations of the Fortescue Group outcrop in a generally north-northwest oriented, westward-younging sequence to the west of the Gregory Range Suite. However, they are also distributed around the northern end and in a synform preserved on the eastern flank of the suite. The basal unit of the Fortescue Group, the Mount Roe Basalt, does not crop out in the survey area. Rhyolite within the overlying Hardey Formation, which does outcrop in the west of Paterson North, has been dated at 2764 Ma (Arndt *et al.*, 1991).

The Hardey Formation is commonly in faulted contact with granite of the Gregory Range Suite which outcrops in a narrow, north-trending, 5-10 km wide linear belt exceeding 150 km in length. Syenogranite, granitic gneiss and granophyre are the main constituents of the suite and samples of metamorphosed syenogranite yielded isotopic ages of ca. 2760 Ma (Nelson, 1996). The emplacement of granite in the East Pilbara granite-greenstone terrane to the west largely occurred between 3470 and 2840 Ma (Huston *et al.*, 2002). The Gregory Range Suite was emplaced after this period (ca. 80 Ma after) at about the same time as the youngest granititic intrusions elsewhere in the East Pilbara granite-greenstone terrane (Huston *et al.*, 2002) but some 700 Ma before the earliest granitic protolith to augen gneiss (2015 Ma) in the Rudall Complex (Hickman and Bagas, 1998) to the east. The rocks of the Gregory Range Suite are considered to be coeval and comagmatic with the felsic volcanic rocks of the Hardey Formation, but have been juxtaposed in outcrop through uplift on multiple sub-parallel, steep easterly-dipping reverse faults (Williams and Trendall, 1998a).

Overlying the Hardey Formation in sequence are the Kylena Basalt, Tumbiana Formation, Maddina Basalt and Jeerinah Formation. This sequence consists largely of basalt flows but includes considerably thinner units of volcaniclastic sediments. Thus, the Fortescue Group includes bimodal volcanics with basaltic flows dominating the lower (not exposed in the survey area) and upper parts separated by felsic volcanics of the Hardey Formation ([Table 3.1](#)).

Table 3.1: Fortescue Group stratigraphy, after Williams and Trendall (1998a).

Top

- Jeerinah Formation. Thickness ca. 350 m. Mixed volcanoclastic and epiclastic succession of tuffaceous siltstone, lapilli tuff, shale, wacke, conglomerate and chert.
- Maddina Basalt. Thickness ca. 1 km. Subaerial basalt flows to 50 m thick, minor interbedded siltstone and tuffaceous volcanoclastic sediments.
- Tumbiana Formation. Thickness 100 to 150 m. Tuffaceous siltstone and minor interbedded fine-grained sandstone.
- Kylena Basalt. Thickness > 3 km. Subaerial basalt flows to 20 m thick.
- Hardey Formation. Thickness > 3 km. Rhyolite, rhyodacite, quartzite, siltstone, basalt, pelitic schist and tuffaceous volcanoclastic sandstone.
- Mount Roe Basalt. Thickness ca. 2.4 km, Does not crop out in the survey area.

Bottom

In the survey area, the Fortescue Group is gently to moderately folded with dips of 20-40° and is considerably disrupted by north-northwest to north oriented faults. While most of these faults dip steeply to the north-northeast with evidence of reverse movement (Trendall, 1991), several demonstrate a more complex history including earlier sinistral strike slip movement (Williams and Trendall, 1998a). Epithermal base metal mineralisation hosted by faults disrupting the Fortescue Group on BRAESIDE has yielded Pb isotope model ages in the range 2720-2620 Ma (Williams and Trendall, 1998a), whereas other similarly oriented faults were active during deposition of the unconformably overlying Neoproterozoic Waltha Woora Formation. Tectonic reactivation of these structures is therefore inferred to have occurred over a broad timeframe (Williams and Trendall, 1998a). Neoproterozoic Officer Basin sediments unconformably overlie the Fortescue Group to the east, Cenozoic sediments to the north and northwest and Archean Carawine Dolomite disconformably overlies the group to the west.

3.2.2.1.2 Hamersley Group-Carawine Dolomite

The Carawine Dolomite outcrops to the west of, and disconformably overlies, the Jeerinah Formation in central western Paterson North ([Figure 3.1](#)). It is composed of grey dolomite with minor shale and chert interbeds and is over 500 m thick. Deposition in a shallow water platform environment is inferred from the presence of sedimentary features including wave ripple marks, oolites and pseudomorphs of evaporitic minerals (Simonson and Jarvis, 1993; Simonson *et al.*, 1993). Jahn and Simonson (1995) obtained a Pb-Pb isochron age of ca. 2540 Ma for the dolomite which was considered to date either regional or early diagenesis.

3.2.2.1.3 Pinjian Chert Breccia (Proterozoic)

The Pinjian Chert Breccia unconformably overlies the Carawine Dolomite and has the same spatial distribution. The breccia consists of angular chert fragments in a siliceous chert matrix. The lower contact with the Carawine Dolomite is highly irregular and thought to represent a palaeokarst environment (Hickman, 1978; Williams and Trendall, 1998a).

3.2.2.1.4 Woblegun Formation (Collier Basin, Mesoproterozoic)

In the southwest of Paterson North, the Woblegun Formation of the Collier Basin unconformably overlies the Pinjian Chert Breccia and the Fortescue Group ([Figure 3.1](#)). The Formation is composed of shale, mudstone and chert with local sandstone and conglomerate and is ca. 300 m thick. Williams and Trendall (1998b) suggested deposition in shallow near-shore marine or lagoonal environments. The Woblegun Formation has been deformed by the Miles or Paterson orogenies giving rise to broad open folds disrupted by north-northwest-trending faults and was subsequently intruded by the Davis Dolerite at ca. 523 Ma (Hickman, 1978).

3.2.2.2 Pilbara Craton and overlying basins - gravity and aeromagnetic interpretation

Gravity data in areas of outcropping Pilbara Craton to the west of Paterson North show a coincidence of broad (20-60 km wide), ovoid-shaped Bouguer anomaly lows (ca. $-600 \mu\text{m.sec}^{-2}$) corresponding to large, similarly shaped granite complexes. Moderate to high amplitude Bouguer anomaly highs (ca. $-200 \mu\text{m.sec}^{-2}$) correspond with intervening greenstone sequences which include abundant dense basalt and common highly-magnetised banded iron formation. This pattern of regional gravity and magnetic anomalies continues eastward into the western Paterson North up to the position of the north-northwest-trending Vines Fault (Figure 3.2). Crust of the East Pilbara granite-greenstone terrane is therefore inferred to underlie the Fortescue, Hamersley, and Collier Basins in the area. The station spacing of the gravity data in this region is 11 km and is not suited to resolving detail in basins overlying the craton.

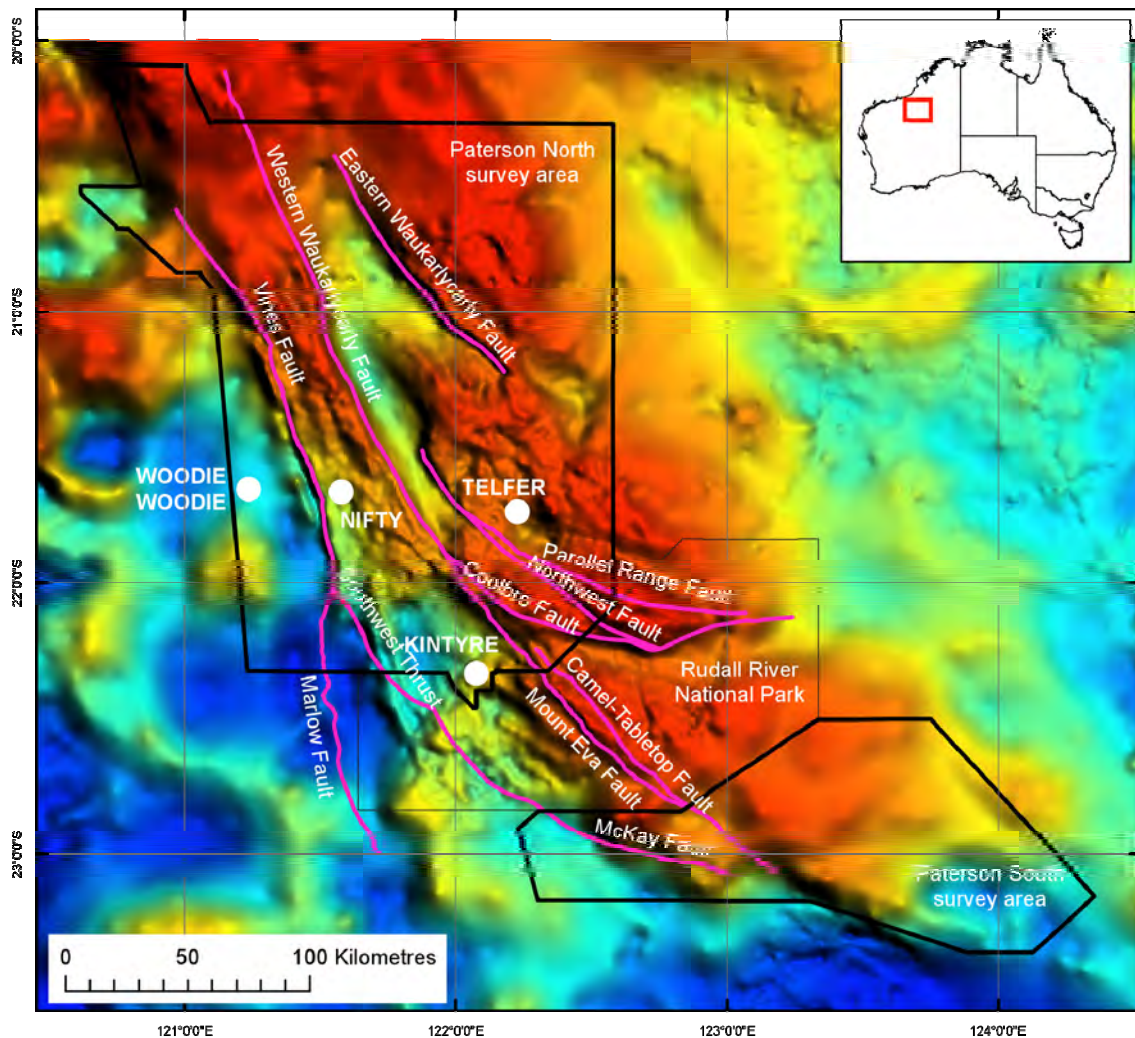


Figure 3.2: Gradient-enhanced Bouguer anomaly gravity with a 500 m grid cell size. Red corresponds with high, and blue low, Bouguer anomaly. Anomalies typical of granite greenstone terrane of the Pilbara Craton extend eastward under the Fortescue and Hamersley Basins to the Vines Fault. Rudall Complex in outcrop and underlying the Yeneena Basin is thought to be responsible for the 150 km wide zone of general north-northwest-trending gravity high to the east of the Vines Fault. Local gravity lows in this zone are attributed to: overlying Coolbro Sandstone, between the Southwest Thrust and Mount Eva Fault; Paleozoic sediments in the Waukarlycarly Embayment, central Paterson north; and, in some instances, intruded granite. Major faults are inferred to disrupt the Rudall Complex and influence the distribution of overlying sediments.

Aeromagnetic data in northwest Paterson North show an easterly-trending, high amplitude total magnetic intensity anomaly (Figure 3.3) inferred to be due to banded iron formation in greenstone underlying the Fortescue Group. The Fortescue Group, with the exception of the Maddina Basalt, which is poorly- to moderately-magnetised, is poorly-magnetised and not readily subdivided using aeromagnetic data. The Carawine Dolomite, Pinjian Chert Breccia and Woblegun Formation are also poorly magnetised and are not discriminated in aeromagnetic data. The Gregory Range Suite is poorly- to moderately-magnetised and is inferred to extend under adjacent Hardey Formation to the west and north and under Tarcunyah Group of the Officer Basin in south-western Paterson North. Images of the first vertical derivative of total magnetic intensity (Figure 3.4) show possible conjugate north-northwesterly and northerly-trending, poorly-magnetised faults cutting and dislocating the suite. Geologically mapped faults are not well imaged in the poorly-magnetised formations due to a lack of magnetisation contrast.

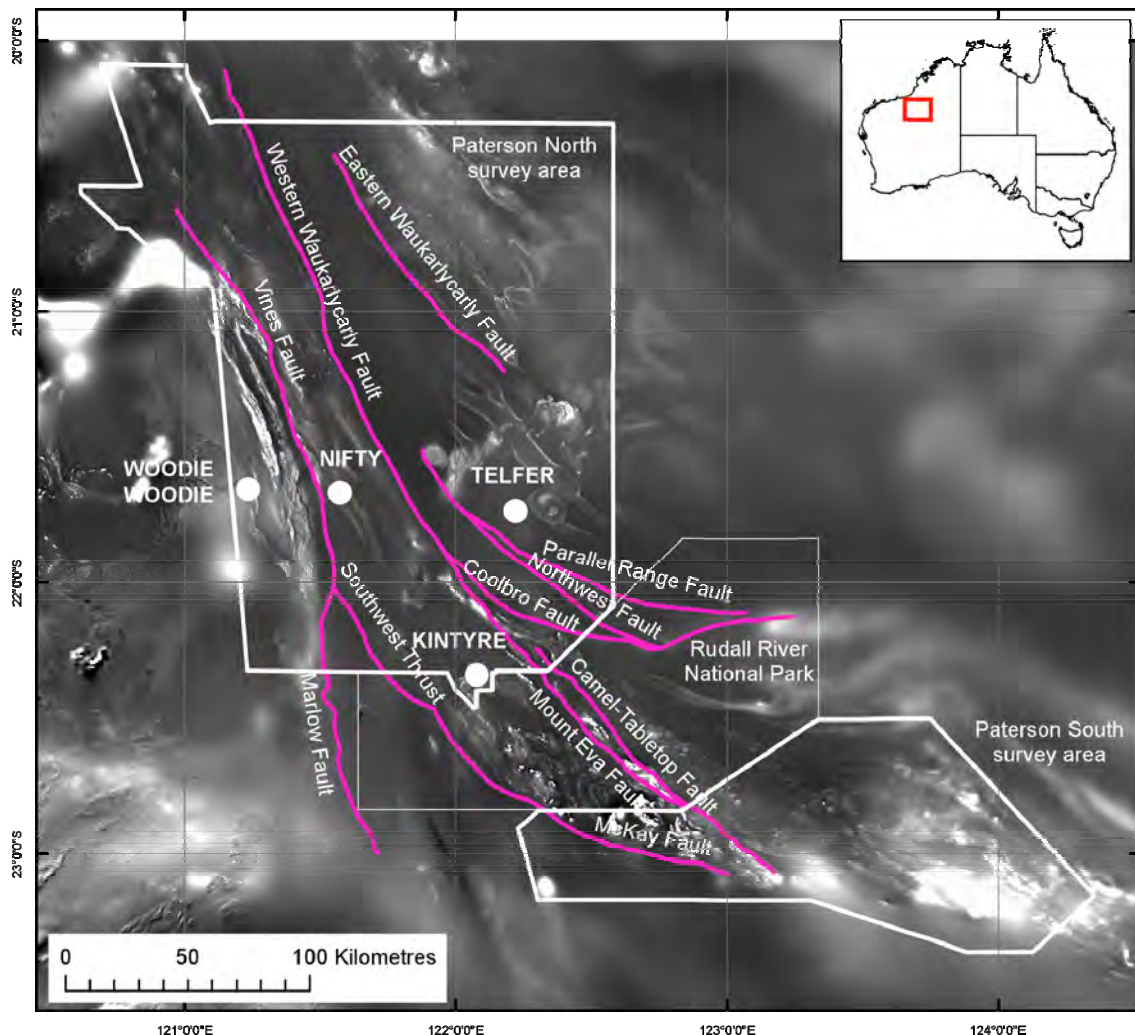


Figure 3.3: Image of total magnetic intensity data with an 80 m grid cell size. White corresponds with high-magnetisation and black with low-magnetisation. Highly magnetised banded iron formation in greenstone of the Pilbara Craton extends under the Fortescue Group to the west of the Vines Fault. In the Rudall Complex, Paterson South and southern-most Paterson North, folded compositional layering in the Talbot and Connaughton terranes southwest of the Camel-Tabletop Fault contrasts with textures attributed to abundant granite in the Tabletop Terrane to the northeast and east

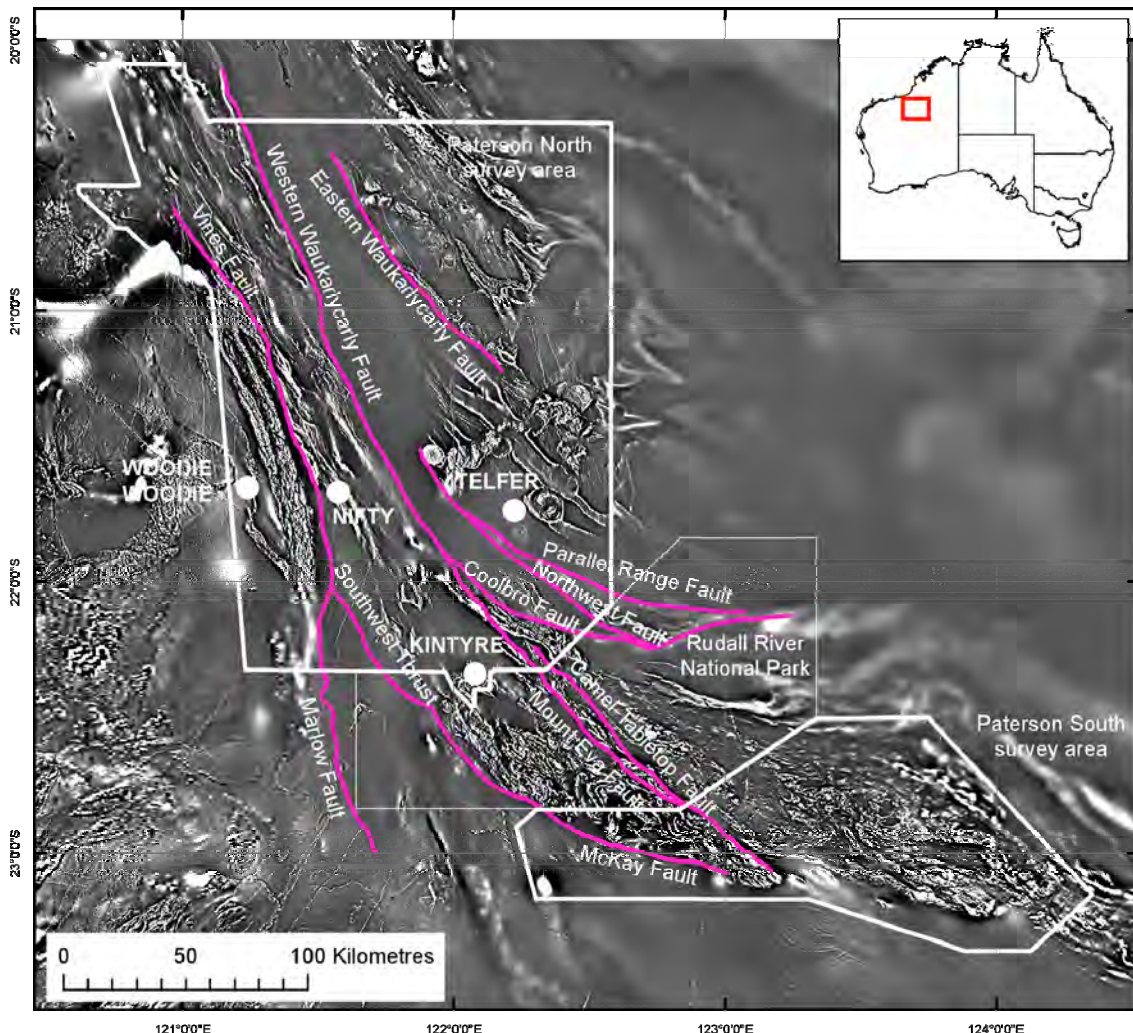


Figure 3.4: Image of the first vertical derivative of total magnetic intensity with an 80 m grid cell size. Structural trends and complexity of the Rudall Complex in Paterson South and southern-most Paterson North contrast with simpler bedding trends of the Lamil Group in northeast Paterson North. Granite of the Mount Crofton and O'Callaghans suites cut dominantly northwest bedding trends and faults in the Lamil Group. Fault-disrupted gentle folds in the Tarcunyah Group are seen to the south of the McKay Fault.

3.2.2.3 Paterson Orogen

The Paterson Orogen (Tyler and Hocking, 2002a) consists of metamorphosed Paleoproterozoic to Neoproterozoic sediments and igneous rocks which were variably deformed during the Miles (ca. 1070 & > 650 Ma; Bagas, 2000) and Paterson (ca. 650-550 Ma; Bagas *et al.*, 1995; Bagas *et al.*, 1999) orogenies. The Rudall Complex forms the basement of the Paterson Orogen and underwent amphibolite to granulite facies metamorphism during the Yapungku Orogeny (ca. 2015-1760 Ma; Bagas *et al.*, 2000). The Complex consists of supracrustal and igneous rocks of Paleoproterozoic to Mesoproterozoic age. Unconformably overlying these rocks are greenschist facies Neoproterozoic sediments of the Yeneena Basin. These sediments were folded and faulted during the Miles Orogeny and were subsequently intruded by granite. Faulting during the Paterson Orogeny further deformed the Rudall Complex and the south-western margin of the Yeneena Basin. The Rudall Complex is host to the Kintyre uranium deposit, whereas sediments of the Yeneena Basin host the Telfer (gold-copper), Nifty (copper) and O'Callaghans (tungsten-base metal skarn) deposits. Numerous other

small mineral occurrences occur throughout the Paterson Orogen. See [Chapter 6](#) of this Record for further information.

3.2.2.3.1 The Rudall Complex (Paleo- to Mesoproterozoic)

The Rudall Complex crops out from central southern Paterson North, through the Rudall River National Park, southeast into western and central Paterson South. The complex was previously subdivided into three terranes with distinct lithological make up: the Talbot; Connaughton; and Tabletop Terranes (Bagas, 2004a) ([Figure 3.1](#)). While the Talbot and Connaughton Terranes are inferred to have undergone similar geological evolution, the Tabletop Terrane is considered to be significantly different, particularly in the timing of voluminous felsic magmatism.

The Talbot Terrane is composed largely of orthogneiss and metamorphosed siliciclastic sedimentary rocks. While the Terrane has been significantly disrupted by faulting and thrusting, sufficient detail of lithostratigraphic relationships have been preserved in the metasedimentary rocks to enable development of a stratigraphic succession ([Table 3.2](#)).

Table 3.2: Talbot Terrane metasedimentary stratigraphy, after Hickman and Bagas (1998).

Top

- Poynton Formation. Thickness ca. 1 km. Quartzite, meta-greywacke, quartz-muscovite schist, minor pelitic schist and banded iron formation.
- Butler Creek Formation. Thickness >1 km. Pelitic schist, paragneiss and local banded iron formation.
- Yandagooge Formation. Thickness < 1500 m. Quartz-muscovite schist, meta-pelitic rocks, banded iron formation, chert, graphitic schist and biotite schist.
- Fingoon Quartzite. Thickness > 1500 m. Quartzite and micaceous quartzite.
- Larry Formation. Unknown thickness. Quartz-feldspar-mica paragneiss and quartz mica schist.

Bottom

Widespread orthogneiss was derived mostly from monzogranite to granodiorite compositions and rarely tonalite. Emplacement ages for protoliths of orthogneiss of between 2015 and 1765 Ma (Hickman and Bagas, 1998) are inferred to provide minimum depositional ages of paragneiss in the terrane. While some paragneiss must be older than 2015 Ma, the Fingoon Quartzite is younger than 1790 Ma, the age of contained detrital zircons (Nelson, 1995). The stratigraphically or structurally overlying Yandagooge and Butler Creek formations were intruded by, and must be older than, granite ranging in age from 1790 to 1756 Ma (Nelson, 1995). A greater abundance of intrusive ages for the granitic protolith of orthogneiss, in the range of 1790 to 1765 Ma (Nelson, 1995; 1996), is considered to be coincident with the second phase, including D2 deformation and high pressure metamorphism, of the Yapungku Orogeny (Bagas, 2004a). Orthogneiss, Fingoon Quartzite and Yandagooge Formation outcrop in southern Paterson North and western Paterson South.

The Connaughton Terrane is located to the east and southeast of the Talbot Terrane and is composed of approximately 50% mafic and ultramafic rocks with successively lesser quantities of gneiss and schist of unknown protolith, orthogneiss, metasedimentary rocks, granite and pegmatite. Stratigraphic relationships are poorly defined due to structural dismemberment and lack of well defined primary layering. Rocks of the Connaughton Terrane underwent high pressure amphibolite to granulite metamorphism during the latter part of the Yapungku Orogeny (Smithies and Bagas, 1997; Bagas *et al.*, 2000) and were intruded by similarly-aged protoliths to the orthogneiss during that event.

The Tabletop Terrane abuts the Connaughton Terrane to the northeast across the northwest-trending Camel-Tabletop Fault. Granite and pegmatite account for approximately 70% of the terrane with lesser abundances of mafic, ultramafic and metasedimentary rocks. Tonalite is the dominant granitic

rock type and is largely undeformed except adjacent to the Camel-Tabletop Fault (Bagas, 2004a). The terrane has undergone low pressure metamorphism to lower amphibolite grade and was extensively intruded by granite between 1590 and 1310 Ma (Nelson, 1995; 1996). Augen gneiss, abundant in the adjacent Talbot and Connaughton terranes, is absent from the Tabletop Terrane. The contrast in rock type abundances, pressure of metamorphism and lack of 1590-1310 Ma granite in the adjacent terranes is thought to indicate that the Tabletop Terrane developed separately and was subsequently tectonically emplaced (Bagas, 2004a).

The Rudall Complex is overlain unconformably to the north by sediments of the Yeneena Basin and to the southeast by sediments of the Tarcuryah Group. Permian glacial sediments of the Paterson Formation were subsequently deposited in palaeovalleys that cut across the region of outcrop of the complex. The whole is over-topped by Mesozoic sediments of the Canning Basin.

3.2.2.3.2 *Yeneena Basin (Neoproterozoic)*

The Yeneena Basin crops out largely to the north of exposures of the Rudall Complex, underlies much of the Paterson North survey area and consists of the Throssell Range Group and the Lamil Group ([Figure 3.1](#)). Precise depositional ages of the groups are not known and contacts between the groups are not observed in outcrop. The Throssell Range and Lamil groups are younger than contained ca. 950 Ma detrital zircons (Bagas *et al.*, 2002) and the Lamil Group is older than the ca 650-630 sensitive high-resolution ion microprobe (SHRIMP) uranium-lead (U-Pb) isotopic age of the Mount Crofton Granite Suite (Dunphy and McNaughton, 1998) which intrudes it. On BROADHURST, carbonate-rich Isdell Formation lies between the two groups, but again no stratigraphic relationships have been determined as contacts with the Throssell Range Group to the south are obscured by Cenozoic sediment and the Isdell Formation is in tectonic contact with the Lamil Group across the Parallel Range Fault to the north-northeast. The Isdell Formation is older than monzonite and gabbro intrusives dated at ca. 830 Ma (Maidment pers. comm. in Czarnota *et al.*, 2009a).

3.2.2.3.3 *Throssell Range Group (thickness > 7km)*

In Paterson North, the Coolbro Sandstone is the lowermost unit of the Throssell Range Group and unconformably overlies the Rudall Complex. The formation is up to 4 km thick (Hickman and Clarke, 1994) and is largely composed of fine- to coarse-grained sandstone. The sandstone tends to have finer grain sizes in the upper parts where siltstone lenses are interbedded. These finer grained sandstone and siltstone units mark a transition to the overlying Broadhurst Formation. Deposition occurred in a fluvio-deltaic environment (Turner, 1982) with sediment derived from the adjacent Rudall Complex. Hickman and Bagas (1998) suggested the regional depositional setting was that of a strike-slip basin with initiation associated with the onset of the Miles Orogeny.

The Broadhurst Formation conformably overlies the Coolbro Sandstone and consists of upper and lower sections, dominantly composed of carbonaceous shale/pelitic schist, with an intervening interval of argillaceous turbiditic greywacke and sandstone. The shale-dominated sections include beds with up to 10% pyrite and pyrrhotite, the latter giving rise to aeromagnetic highs. Beds of limestone and dolomite, generally less than 100 m thickness, are particularly associated with the carbonaceous shale components. The Formation is estimated to be 2-3 km thick and is inferred to have been deposited in a fault-controlled, sediment-starved basin under euxinic conditions (Hickman *et al.*, 1994). A generalised lithological column for Coolbro Sandstone and Broadhurst Formation is presented in [Figure 3.5](#) and a generalised stratigraphy for the Throssell Range Group is given in [Table 3.3](#).

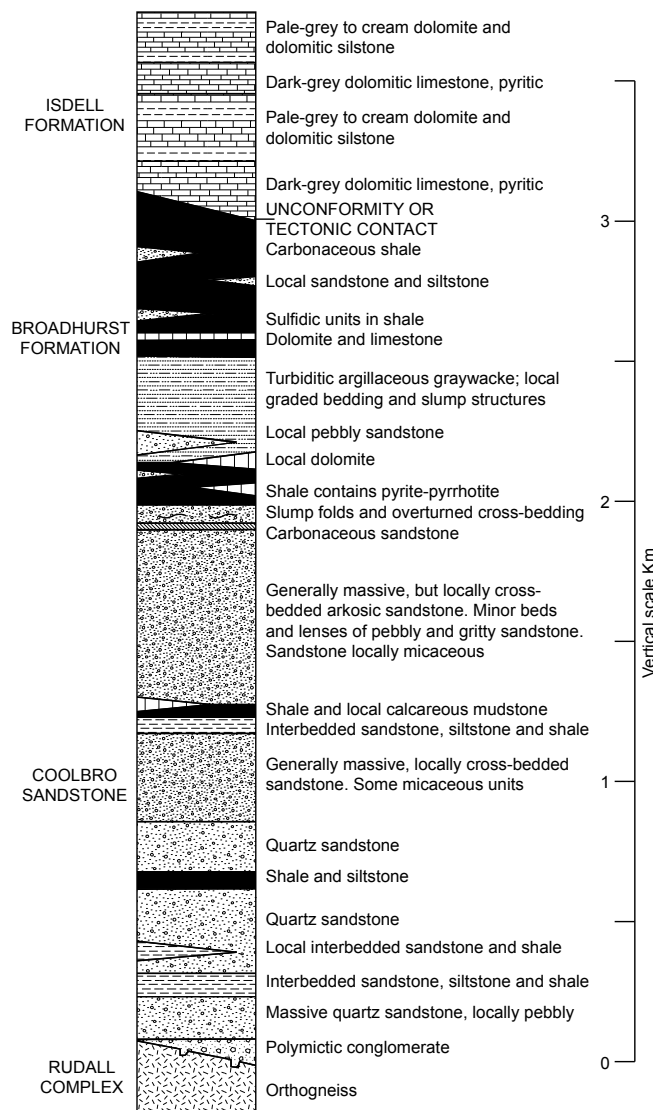


Figure 3.5: Generalised stratigraphy of the Throssell Range Group and Isdell Formation, redrawn from Hickman and Clarke (1994).

Table 3.3: Throssell Range Group stratigraphy, Paterson North, after Hickman and Clarke (1994).

Top

- Broadhurst Formation. Thickness 2 to 3 km. Carbonaceous shale (pyrite and pyrrhotite to 10%) with minor carbonate lenses, argillaceous turbiditic greywacke and sandstone.
- Coolbro Sandstone. Thickness, 3 to 4 km. Fine- to coarse-grained sandstone with local basal conglomerate.

Bottom

In Paterson South and to the immediate north, polymictic conglomerate and arkosic sandstone of the Taliwanya Formation lies unconformably on the Rudall Complex. The Formation is up to 170 m thick and is overlain by the Pungkuli Formation, which is composed of up to 900 m of black shale, sandstone and pyritic shale. These two formations have also been assigned to the Throssell Range Group and may be correlatives of Coolbro Sandstone and overlying Broadhurst Formation outcropping further north (Bagas *et al.*, 2000).

3.2.2.3.4 Isdell Formation (*Thickness > 1km*)

The Isdell Formation outcrops poorly in a region between better exposed Broadhurst Formation to the south and Lamil Group to the north. The Formation is estimated to be over 1 km thick and is composed of dolomitic limestone and limestone intercalated with calcareous siltstone and shale. Stratigraphic relationships with the adjacent groups have not been determined due to Cenozoic sediment cover of the contact with Broadhurst Formation and faulted contacts with the Lamil Group. Hickman and Clarke (1994) noted a discontinuity in aeromagnetic data corresponding to the position of the Broadhurst-Isdell formation boundary which they attributed to either an unconformity or a tectonic contact.

Minimum depositional age constraints for the Isdell Formation are provided by monzonite and gabbro intrusives which yielded emplacement ages of ca. 830 Ma (Maidment pers. comm. in Czarnota *et al.*, 2009a). An unpublished pooled lead-lead isotopic (Pb-Pb) age of 858 +/- 29 Ma from thinly bedded limestone, calcareous siltstone and argillaceous siltstone samples is thought to date diagenesis of the Formation (Maas and Huston, unpublished data).

3.2.2.3.5 Lamil Group (*Thickness 4-5 km*)

The Lamil Group is a sandstone-shale-carbonate succession which Turner (1982) suggested was deposited in an intracratonic setting at a continental margin or in a failed rift. The stratigraphy is outlined in [Table 3.4](#). The lowermost unit, the Malu Formation, is in the order of 1-2 km thick and consists of shale, sandstone and siltstone with thin carbonate units present towards the top. The Puntapunta Formation conformably overlies the Malu Formation and consists of dolomitic siltstone, rare limestone, dolomitic sandstone, chert and shale. The Puntapunta Formation is up to 1.5 km thick and was deposited in a carbonate-dominated shelf environment (Turner, 1982). The Wilki Formation is inferred to conformably overlie the Puntapunta Formation, however, contacts are not exposed. The Wilki Formation is approximately 1.4 km thick and is composed of a lower section of graphitic shale, siltstone and fine grained silty sandstone overlain by fine- to medium-grained sandstone with interbedded silty sandstone. A shallow marine environment was proposed by Turner (1982) for deposition of the Wilki Formation.

In recent mapping of Yeneena Basin sediments on PATERSON, several outcrops have not been assigned to named formations. For instance, massive sandstone with minor interbedded dolomitised shale in the northeast, although having similar descriptions, outcrop pattern and aeromagnetic characteristics to the Wilki Formation, is separated by a major concealed structural break from the Wilki Formation and therefore could not be correlated with certainty (Bagas, 2000). Also, dolomite with interbedded siltstone to the south of the Parallel Range Fault, which was previously correlated with the Isdell Formation by Chin *et al.* (1982), remains unassigned in the most recent mapping (Bagas, 2000). The 10 km distance between these exposures and outcropping Isdell Formation to the south, lithological similarity with Puntapunta Formation and lack of known stratigraphic context due to the faulted contact with Malu Formation to its north were the reasons given for lack of assignment.

Table 3.4: Lamil Group stratigraphy, after Bagas (2000).

Top

- Wilki Formation. Thickness 1.4 km. Graphitic shale, siltstone, fine grained silty sandstone and fine- to medium-grained sandstone.
- Puntapunta Formation. Thickness 1.5 km. Dolomitic siltstone and sandstone, chert and shale.
- Malu Formation. Thickness 1-2 km. Shale, sandstone and siltstone with thin carbonate units in the upper part.

Bottom

The Lamil Group extends under gently deepening cover to the north of outcropping areas in a structural high known as the Anketell Shelf. In this area the Group is unconformably overlain by Mesozoic sediments immediately and Paleozoic and Mesozoic sediments farther north. Both to the west and east cover increases more rapidly and includes Ordovician to Permian sediments in the Waukarlycarly Embayment to the west and Canning Basin to the east. Because of the inferred prospectivity of the Lamil Group, which hosts the Telfer gold-copper deposit, much exploration drilling has been undertaken in the vicinity of the Shelf. However, nearly 50% of this drilling failed to reach the prospective rocks underneath the cover materials (Roach, 2009). A lack of knowledge of the distribution of cover thickness is a likely factor in the relatively ineffective drilling.

3.2.2.3.6 Intrusions of the Yeneena Basin

The Lamil Group has been intruded extensively by generally undeformed, highly fractionated granites with compositions ranging from monzogranite to syenogranite. The Mount Crofton and associated granite suites have yielded inferred intrusive ages in the range of 650 to 630 Ma (Dunphy and McNaughton, 1998). Surrounding contact metamorphic aureoles of varying widths of up to 2 km have been developed and reached the pyroxene hornfels facies of metamorphism (Bagas, 2000).

The Paterson Orogen has also been intruded by numerous mafic dykes and sills. Dolerite on BROADHURST has yielded rubidium-strontium (Rb-Sr) isotopic ages of 700 to 750 Ma, however, some dykes intruding the Rudall Complex are inferred to postdate all deformation (Hickman and Clarke, 1994).

3.2.2.3.7 The Miles and Paterson orogenies

The Yeneena Basin has been deformed by two main orogenic events, the Miles and Paterson orogenies, but the ages of these orogenies are not well constrained. The Miles Orogeny is younger than the ca. 950 Ma detrital zircons in both the Throssell Range and Lamil groups (Bagas *et al.*, 2002), and older than the 650-630 Ma intrusive age of the Mount Crofton Granite (Dunphy and McNaughton, 1998) which intrudes the Lamil Group and imposed structure. The Orogeny (D3-4) (Bagas and Smithies, 1998) produced large scale northwest-trending faults and widespread, similarly aligned folds in the Throssell Range and Lamil groups. Local thrusts and recumbent folds were developed in the Throssell Range Group. Southwest-directed shortening also produced conjugate north-northeast- and east-southeast-trending faults with dextral and sinistral movements respectively. Widespread soft sediment deformation of the Lamil Group is thought to indicate the orogeny occurred early in the history of the Group. Both the Throssell Range and Lamil groups underwent lower or sub-greenschist metamorphism during this event (Bagas, 2005) while the Rudall Complex underwent extensive retrogressive metamorphism to greenschist facies.

The Paterson Orogeny occurred after the Miles Orogeny, but more detailed constraints are not well documented from within the Paterson Orogen. Howard *et al.* (2005) inferred the timing of the Orogeny was closely linked with intrusion of granite and thermal metamorphism in the Telfer area and therefore occurred about 650-630 Ma. However, Williams (1992) and Williams and Tyler (1991) state that the Orogeny occurred after deposition of the ca. 610 Ma Boondawari Formation of the northwest Officer Basin. The Orogeny has been correlated with the Petermann Orogen of central Australia (Myers, 1993; Bagas *et al.*, 1995; Perincek, 1996) at about 550 Ma but this speculative view requires more factual constraints to firm a tectonic connection.

Deformation resulting from south-southwest directed shortening produced folds with east to east-southeast fold axes and north-northwest and east-southeast, near-vertical strike-slip faults with dextral and sinistral movements respectively. The Camel-Tabletop Fault is inferred to have been reactivated during the Orogeny with evidence for both vertical and strike-slip movements (Bagas, 2004a). There is no evidence in the regional geophysical data to suggest that the Lamil Group was subsequently deformed around the Mount Crofton and O'Callaghans Suite granites after intrusion, or, that there was any significant disruption of the granites by reactivated movement on northwest-trending faults. Thus, if the Paterson Orogeny occurred after the 650-630 Ma, deformation of the

Lamil Group was relatively minor. Perhaps the main effects of the Orogeny were constrained between the Vines Fault in the west, the western Waukarlycarly-Camel-Tabletop faults to the east and the Southwest Thrust–McKay Fault system to the southwest and south respectively.

3.2.2.3.8 Paterson Orogen - gravity and aeromagnetic interpretation

Outcropping Rudall Complex corresponds with high Bouguer anomalies in the range -350 to $-50 \mu\text{m.sec}^{-2}$ ([Figure 3.2](#)). The region of high gravity extends in a 150 km wide zone from the Southwest Thrust-McKay Fault Zone in Paterson South, north-northwest through Paterson North and is bounded in the west by the Vines Fault. In the east, gravity values drop off over about a 30 km wide margin which corresponds with increasing thickness of Canning Basin sediments. The eastern boundary of the zone is disrupted by interpreted west- to northwest-trending faults. Further east, basement to the Canning Basin and the overlying sediments corresponds with a different anomaly pattern and a lower average Bouguer anomaly (ca. -350 to $-450 \mu\text{m.sec}^{-2}$). The zone of the Bouguer gravity high is inferred to map the Rudall Complex from outcrop northward under the Yeneena Basin. Crust of the Rudall Complex differs from that of the East Pilbara granite-greenstone terrane to the west by having a higher average Bouguer anomaly and lacking large diameter (+30 km), moderate amplitude Bouguer gravity lows attributed to granite complexes. Rudall Complex crust is inferred to be dislocated by several major faults. Some of these faults define the margins of a north-northwest-trending gravity low (ca. $-430 \mu\text{m.sec}^{-2}$) coincident with the Waukarlycarly Embayment. Interpretation of seismic data indicates that Paleozoic sediment fill of the Embayment exceeds 2 km (Hunt, 1996), assuming a seismic velocity in basin sediment of ca. 3 km.sec^{-1} . A gravity lineament, here termed the Coolbro Fault, cuts west to west-northwest across the Complex in southern Paterson North ([Figure 3.6](#)), disrupts the eastern margin of the Rudall Complex and approximates the buried contact between the Broadhurst and Isdell formations. Outcrop patterns of both Neoproterozoic and Permian sediments change across the structure, which is speculated to be a major, long-lived fault.

The western margin of the Rudall Complex, between the Vines Fault and the Waukarlycarly Embayment, is cut by numerous north-northwest-trending lineaments. The crust in this area appears to have undergone more intense disruption than crust to the east. Further west, crust of the Pilbara Craton and overlying basins is covered by broad 11 km spaced data (c.f. 2.5 km data over the Yeneena Basin/Rudall Complex) which does not provide sufficient resolution for effective comparison of near-surface structural disruption.

Much of northeast Paterson North is underlain by the Lamil Group, either in outcrop or at shallow depth. Broad (ca. 20 km wide) gravity highs within this area are 50 to $100 \mu\text{m.sec}^{-2}$ higher in amplitude than those associated with outcropping Rudall Complex to the south. By comparison, substantial areas of Coolbro Sandstone overlying Rudall Complex in south-western Paterson north correlate with gravity anomalies which are 200 - $300 \mu\text{m.sec}^{-2}$ lower than that associated with outcropping Rudall Complex. Coolbro Sandstone is likely to be less dense than Rudall Complex and to be the cause of the local gravity lows in that area. The Lamil Group contains significantly more carbonate than the Throssell Range Group and should therefore be of higher average density. However, the distribution of rock units as mapped in outcrop or inferred from interpretation of aeromagnetic data does not easily explain the distribution and shape of gravity highs in northeast Paterson North. A simple (speculative) explanation may be that the Rudall Complex, perhaps with a greater abundance of dense mafic material than in outcropping regions, directly underlies the Lamil Group in this area and probably lies at shallow but variable depth. Certainly, it is less likely that a substantial thickness of lower density Coolbro Sandstone lies between Rudall Complex and Lamil Group in the vicinity of these gravity highs.

A broad (5-10 km wide) gravity gradient to lower values approaching the Coolbro Fault from the south corresponds with outcropping or interpreted near-surface Throssell Range Group. This gradient may result from a thickening wedge of the Group overlying Rudall Complex up to the Fault. The distribution of Mount Crofton and associated granites, as interpreted from aeromagnetic data, also partially corresponds with variable-amplitude, local gravity lows, commonly 50 to 100

$\mu\text{m.sec}^{-2}$ lower than the surrounding region. The foregoing examples, plus the distribution and varying thickness of Permian, Mesozoic and Cenozoic sediment, give rise to a number of possible causes for local variation in gravity anomaly. However, the regional 2.5 to 11 km station spacing of the gravity surveys precludes the development of a detailed model of density distribution in the near surface. Therefore, meaningful correlation of anomalies with surface geology and aeromagnetic data is difficult for all but the largest features.

The gravity data provide a perspective of the province-scale variation in crustal materials and distribution of major disrupting faults. Aeromagnetic data, particularly because of the more appropriate station spacing, depict greater detail of many aspects of the near-surface geology. However, for the Paterson Orogen, many rock groups are poorly magnetised and are not easily discriminated.

In aeromagnetic data ([Figure 3.3](#)), the Rudall Complex can be subdivided into two main parts either side of a broad northwest-trending structural corridor corresponding with the Camel-Tabletop-Mount Eva Fault system: a more poorly-magnetised western part corresponding with the Talbot and Connaughton terranes; and, a generally, but not consistently, more highly-magnetised eastern part corresponding with the Tabletop Terrane. In the west, poorly- to moderately-magnetised paragneiss and sparse moderately- to highly-magnetised amphibolite provide some detail of the internal structure of the Talbot and Connaughton Terranes. As observed in the geological mapping, broad folds with axes oriented from the northeast to southeast are truncated by many northwest-trending faults. Thrusts are not discriminated from other faults in these data and are not discriminated at all where they parallel compositional layering. To the east, the Tabletop Terrane contains rare compositional banding attributed to paragneiss and is dominantly composed of large areas of irregularly shaped, poorly- to highly-magnetised granite. Poorly- to highly-magnetised circular to ovoid plutons inferred to be granite are common, and small (< 2 km diameter) moderately- to highly-magnetised plugs of unknown composition are distributed sparsely through the terrane. The Rudall Complex is inferred to underlie most of Paterson South. In the west, the Talbot and Connaughton terranes are bound to the south by the Southwest Thrust-McKay Fault system which places these rocks in contact with poorly-magnetised sediments of the Officer Basin. To the east, the Tabletop Terrane is interpreted to continue from outcrop, across Paterson south in a south-easterly direction, under relatively shallow sediment cover (largely Permian and Mesozoic sediments). The Terrane is bound to the south-southwest by a poorly defined east-southeast-trending splay from the Camel-Tabletop-Mount Eva Fault system. In this region, poorly-magnetised sediments, with those of the Officer Basin uppermost, thicken rapidly to the south-southwest. Continuity of Rudall Complex under the Throssell Range and Lamil Groups to the north is not readily discerned from aeromagnetic data.

Most of the Yeneena Basin sediments are poorly magnetised ([Figure 3.3](#)). However, parts of the Broadhurst and Wilki formations, and rare units in the Isdell Formation, are poorly to moderately magnetised and provide a perspective of the local lithological structure. North of the Talbot Terrane, Coolbro Sandstone and Broadhurst Formation are much disrupted by faults at 1 to 5 km intervals. Intense, close-spaced north-northwest oriented faulting is inferred for the region between the Vines Fault and the western bounding fault of the Waukarlycarly Embayment (the Western Waukarlycarly Fault; [Figure 3.1](#)) and its continuation into the Camel-Tabletop-Mount Eva Fault system. To the east, north of outcropping Tabletop Terrane, inferred Coolbro Sandstone and Broadhurst Formation continue eastward under cover, are much less disrupted by faulting and exhibit broad scale folding with axes spaced at about 20 km intervals. To the north of this area, a west to west-northwest discontinuity between bedding trends, previously noted by Hickman and Clarke (1994), was thought to map either an unconformity or tectonic boundary between the Broadhurst Formation and the Isdell Formation. The discontinuity in bedding trends is supported in this interpretation of the data and correlates with both a change in fold patterns (fold amplitude and wavelength) and with the position of a major gravity lineament, termed the Coolbro Fault above (see [Figure 3.1](#)). Thus a tectonic boundary between the Broadhurst and Isdell Formations in this area is favoured here.

The Isdell Formation is, for the most part, very poorly-magnetised, but contains rare, folded, relatively continuous, weakly-magnetised compositional layering inferred to be bedding. Bedding and fold axes are generally aligned to the northwest. The boundary of the Isdell Formation with similarly poorly-magnetised Lamil Group to the north is not well expressed in aeromagnetic data.

In outcropping areas of Lamil Group, moderately magnetised compositional layering corresponds with part of the Wilki Formation ([Figures 3.3 & 3.4](#)). Inferred bedding trends dominantly strike to the northwest and are less disrupted by faulting than Coolbro Sandstone and Broadhurst Formation to the west and southwest. Further north, in regions of cover, similarly magnetised units, considered to be likely correlatives of Wilki Formation, are folded with northwest-trending axes spaced at about 20 km intervals. Limbs of these folds are commonly truncated on faults that parallel the fold axes.

The area of the Lamil Group has been intruded by much poorly- to moderately-magnetised granite. Isolated plutons are present, but emplacement in possible structurally controlled; linear corridors with contact between adjacent intrusions are common. The intrusion corridors are aligned to the northeast, north-northeast to north and northwest and cut folded bedding and northwest-trending faults that developed during the Miles Orogeny (Bagas, 2000).

Dykes have intruded all components of the Paterson Orogen and are easily observed in the first vertical derivative of total magnetic intensity image ([Figure 3.4](#)). In areas of Rudall Complex, and Officer Basin to the south, broadly spaced (5 to 40 km spacing) dykes trend north-south and to the northeast. In southwest Paterson North, several dykes intrude Coolbro Sandstone and Broadhurst Formation with trends that splay between north-northeast and north at about 5 to 10 kilometre intervals. By far the greatest abundance of dykes evident in aeromagnetic data occurs in the area of the Lamil Group in central and northern Paterson North. In this area, swarms of sub parallel dykes intrude with spacings of < 1-5 kilometres. These dykes compose at least three groups which cross-cut with apparent progressive changes in trend northwards, from north to north-northwesterly.

The interpretation of the gravity and aeromagnetic data described above differs most from that of Czarnota *et al.* (2009a; 2009b) in the following ways: an inferred tectonic contact between the Isdell and Broadhurst formations across the west-oriented Coolbro Fault, interpreted here (c.f. conformable boundary); and, continuation of the Camel-Tabletop–Mount Eva Fault system through to join the Western Waukarlycarly Fault (c.f. Camel-Tabletop–Mount Eva Fault system terminates in Broadhurst Formation). The Coolbro Fault disrupts the Rudall Complex as inferred from interpretation of gravity data, may have influenced sediment deposition in the Yeneena Basin and has affected the distribution of deformation with differing fold patterns in the Isdell Formation to the north and the Throssell Range Group to the south. The fault is thought to be a major regional structure and may have influenced crustal scale mineralising fluids. The Camel-Tabletop Fault is inferred to be a major long lived fault and terrane boundary in the Rudall Complex (Bagas and Smithies, 1998). Field evidence indicates the Paterson Orogeny reactivated the Fault with both vertical and strike slip movement apparent (Bagas and Smithies, 1998). Thus the Fault should disrupt fully, and not terminate in, overlying Throssell Range Group. This view is supported by mapped linear gravity gradients and near-coincident discontinuities in aeromagnetic data inferred to map the continuation of the fault system. In both this and the interpretation of Czarnota *et al.* (2009b), evidence of maximum fault disruption and folding attributed to the Miles and Paterson orogenies occurs between the Vines Fault in the west and the Western Waukarlycarly Fault and Camel-Tabletop faults in the east. The Southwest Thrust and McKay faults were interpreted to be a sole thrust system, bounding most of the deformation to the southwest and south (Williams and Bagas, 1999). To the east of this zone of high deformation, sediments of the Yeneena Basin are much less disrupted by faulting and axes of large scale folds are much further apart. In this area there is no geophysical evidence that northwest-trending faults established during the Miles Orogeny and subsequently intruded by the Mount Crofton Granite Suite have been reactivated by tectonism associated with the Paterson Orogeny.

3.2.2.4 Officer Basin (Neoproterozoic)

The Officer Basin lies largely to the south and west of outcropping Rudall Complex in Paterson South. However, formations of the Tarcuryah Group and correlatives overlie the Archean Fortescue Group and Gregory Range Suite to the west of the Vines Fault in western Paterson North.

3.2.2.4.1 Tarcuryah Group (*Thickness > 3 km*)

Sediments of the Tarcuryah Group crop out in a north-northwest-trending, narrow, 2-5 km wide strip down much of the western part of the Paterson North survey area and intermittently through the western, and more extensively in the central, Paterson South (Figure 3.1). In western Paterson North, the Tarcuryah Group unconformably overlies the Fortescue Group and the eastern margin of the Gregory Range Suite. The north-northwest-trending Vines Fault bounds the Tarcuryah Group to the east where it is in tectonic contact with the Throssell Range Group.

In southwest Paterson North, the basal Googhenama Formation unconformably overlies the Woblegun Formation of the Collier Basin. Deposition occurred in a fluvial environment with palaeocurrent directions to the northeast and southeast, trending away from the Pilbara Craton (Williams and Trendall, 1998b). Overlying formations of the Tarcuryah Group (Table 3.5, 3.6) were deposited conformably in a variety of shallow to deeper water marginal marine and marine shelf settings. The uppermost unit, the Nooloo Formation, appears to conformably overlie the Wangarlong Formation in the west but overlies conglomerate and sandstone of the Choorun Formation in the east, adjacent to the Southwest Thrust. The Choorun Formation has also been assigned to the Tarcuryah Group, is at least 1800 m thick, and unconformably overlies Rudall Complex in this area (Williams and Bagas, 2000). The interpreted stratigraphy of the Tarcuryah Group is given in Figure 3.6.

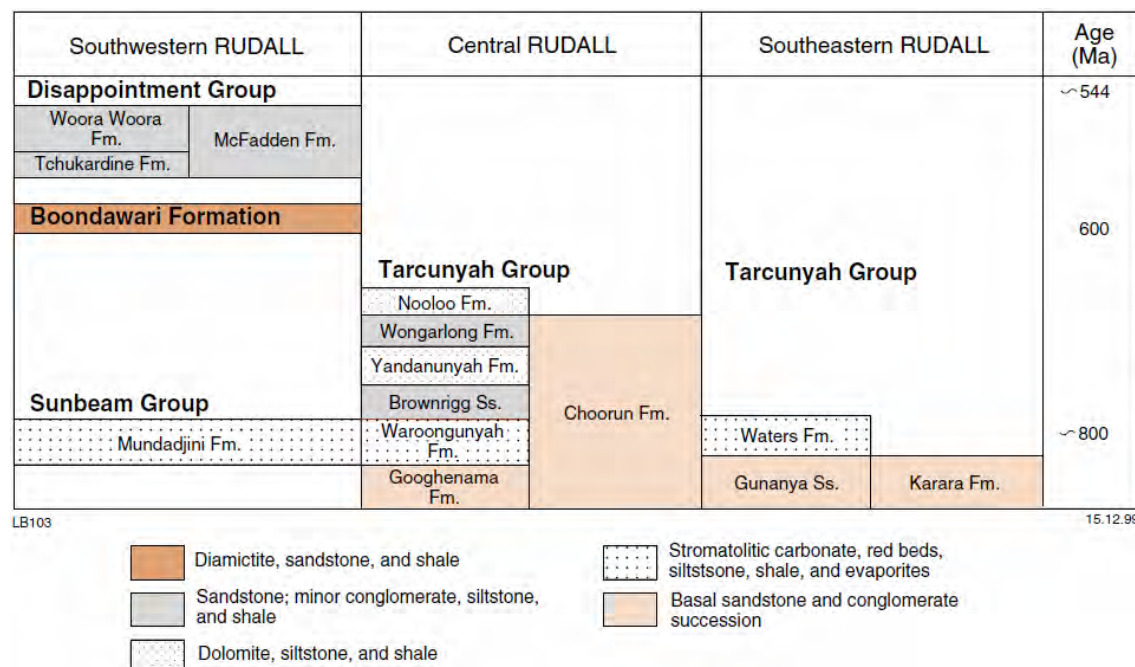


Figure 3.6: Stratigraphic correlations of formations in the Tarcuryah and Disappointment groups in the northwest Officer Basin, from Bagas et al. (2000).

Table 3.5: Tarcunyah Group - Paterson north stratigraphy after Williams and Bagas (1999) and Williams and Trendall (1998b).

Top

- Nooloo Formation. Thickness unknown. Thinly bedded dolomite and limestone, calcareous shale and siltstone. Deep-water shelf environment.
- Wongarlong Formation. Thickness >1200 m. Fine- to medium-grained sandstone and orthoquartzite with gypsum casts, interbedded with laminated siltstones and shale. Shallow marine shelf.
- Yandanunyah Formation. Thickness 450 m. Thick silicified shale, dolomite, calcareous shale and fine-grained sandstone. Transgressive shallow marine environment.
- Brownrigg Sandstone. Thickness 400 m. Fine- to coarse grained sandstone and orthoquartzite. Shallow water marine shelf environment.
- Waroongunyah Formation. Thickness 300 m. Calcareous siltstone and fine- to medium-grained sandstone. Transgressive shallow marine environment.
- Googhenama Formation. Thickness 500 m. Mixed sandstone and conglomerate sequence. Braided stream environment.

Bottom

Table 3.6: Other Tarcunyah Group units.

Southwestern Paterson North, adjacent to the Southwest Thrust (Williams and Bagas, 2000).

- Choorun Formation. Thickness 1800 m. Cobble to pebble conglomerate, pebbly sandstone and coarse- to medium-grained sandstone. Fluvial environment.

Western Paterson South (Hickman and Bagas, 1998).

Top

- Waters Formation. Thickness 350 m. Carbonaceous shale, sandstone, siltstone, finely laminated carbonate, shaly units locally sulphidic. Czarnota *et al.* (2009a; 2009b) correlated Waters Formation with Broadhurst Formation.
- Gunanya Sandstone. Conglomerate, arkose, coarse- to medium-grained sandstone, siltstone. Czarnota *et al.* (2009a; 2009b) correlated Gunanya Sandstone with Coolbro Sandstone.

Bottom

Central Paterson South (Bagas, 1999a).

- Karara Formation. Thickness ca. 350 m. Coarse grained arkosic sandstone, pebble conglomerate and thinly-bedded dolomite.

Gunanya Sandstone and overlying Waters Formation crop out in western Paterson South and have been assigned to the Tarcunyah Group in the published RUDALL (Bagas *et al.*, 2000) and GUNANYA (Bagas, 1998) map sheets. A recent interpretive solid geology map by Czarnota *et al.* (2009b) has reinterpreted these formations as southern exposures of the Coolbro Sandstone and Broadhurst Formation respectively. However, this correlation is at odds with previous correlations of the underlying Taliwanya and Pungkuli Formations with Coolbro Sandstone and Broadhurst Formation respectively (Bagas *et al.*, 2000). The issue has not been resolved in this review of the regional geology and geophysics. A minimum depositional age for Gunanya Sandstone is provided by the youngest contained detrital zircon ages of ca. 950 Ma (Bagas and Nelson, 2007).

Further east, the Karara Formation unconformably overlies, and is in faulted contact with, the Rudall Complex in a 2-5 km wide northwest-trending graben along the Camel-Tabletop Fault. The Formation is composed of conglomerate and arkose and has been speculatively correlated with the Choorun and Googhenama formations to the west.

In summary, the basal units of the Tarcuryah Group are of fluvial origin whereas overlying units are dominated by marine sedimentation. The Tarcuryah Group is strongly deformed adjacent to the Vines Fault and Southwest Thrust, but has only seen one phase of deformation and has not undergone significant metamorphism, c.f. Throssell Range Group, which has undergone two major phases of deformation and metamorphism to lower greenschist facies.

3.2.2.4.2 *Waltha Woora Formation, western Paterson North*

The Waltha Woora Formation was deposited in palaeochannels scoured in Pinjian Chert Breccia, Carawine Dolomite and the Fortescue Group in western Paterson North and is between 250 and 300 m thick. The Formation consists of shale, siltstone, sandstone and dolomitic beds with a locally distributed basal conglomerate. Correlation with the Waroongunyah Formation of the Tarcuryah Group has been proposed based on commonality of stromatolite taxa on PEARANA (Grey, 1978; 1984). The Waltha Woora Formation is unconformably overlain by Permian Paterson Formation and Cenozoic sediments.

3.2.2.4.3 *Disappointment Group, Tchukardine Formation*

The Tchukardine Formation unconformably overlies Tarcuryah Group in southwest Paterson North. Outcrop extends from southwest Paterson North, southeast to just west of Paterson South. The Formation consists mainly of medium-grained quartz sandstone but includes thin basal units of pebble to cobble conglomerate, pebbly sandstone, mudstone and siltstone. Accumulated sediment is at least 700 m thick and was deposited in a sandy marine shelf environment (Williams, 1992).

3.2.2.4.4 *Officer Basin gravity and aeromagnetics interpretation.*

In the south of Paterson South, to the south of the Southwest Thrust-McKay Fault system, sediments of the Officer Basin correspond with low Bouguer anomaly (to $-600 \mu\text{m.sec}^{-2}$, [Figure 3.2](#)). The pattern of gravity anomaly differs from that associated with crust of the Pilbara Craton to the west in lacking the pattern of contrasting highs and lows attributed to underlying granite-greenstone terrane. The low average Bouguer anomaly is attributed to a thick accumulation of sediment over basement of unknown affinity.

Tarcuryah Group sediments are poorly magnetised ([Figure 3.3](#)). However, to the south of outcropping Rudall Complex in Paterson South, subtle variations in magnetisation, brought out in images of the first vertical derivative of total magnetic intensity ([Figure 3.4](#)), outline broad gentle folds with axes oriented between west and northwest. The folds are inferred to be dominantly synformal with limbs disrupted by west to northwest oriented faults. Sparse poorly- to moderately-magnetised dykes with north-northwest alignment have intruded the sequence.

In southwestern Paterson north, Tarcuryah Group sediments are not resolved in gravity data, are poorly magnetised and are not readily delimited in aeromagnetic data.

3.2.4 Canning Basin

The onshore segment of the Phanerozoic Canning Basin lies mainly within the Great Sandy and Gibson deserts, spreading over 430 000 km². Its geological history began in the Early Ordovician and was largely completed by the Early Cretaceous (Yeates *et al.*, 1984). The Paterson area is located at the northwest margin of the Canning Basin where the Basin onlaps the Archean Pilbara Craton, Paleoproterozoic Rudall Complex and Neoproterozoic Yeneena Basin.

In the Paterson area the exposed Canning Basin rocks are the Permian and Late Jurassic to Early Cretaceous sedimentary rocks; older rocks are interpreted in seismic sections across the Waukarlycarly Embayment (Hunt, 1996). In the following section these rocks are briefly summarised in terms of distribution, lithology and thickness. This information will be used in the geological interpretation of AEM data ([Chapter 5](#)) and assessment of uranium mineral systems for the area ([Chapter 7](#)). Permian and Mesozoic stratigraphy and solid geology are presented in [Table 3.7](#) and [3.8](#) and [Figure 3.7](#) and [3.8](#).

3.2.4.1 Permian

Exposed and interpreted Permian sedimentary sequences in the Paterson area include the fluvioglacial Paterson Formation and the shallow marine facies of the Poole Sandstone, Noonkanbah Formation and Triwhite Sandstone (Table 3.8, Figure 3.7). The Paterson Formation was placed under the Grant Group by Towner *et al.* (1980) and Chin *et al.* (1982), but it is not recognised in many wells in the Canning Basin. It is probably a correlative of parts of the Grant Group (Towner and Gibson, 1980). The Poole Sandstone, Noonkanbah Formation and Triwhite Sandstone were placed under the Liveringa Group by Towner *et al.* (1980).

Table 3.7 Permian sediments in the Paterson area after Towner *et al.* (1980).

UNIT	LITHOLOGY	DEPOSITION ENVIRONMENT
Liveringa Group	Sandstone and siltstone	
Triwhite Sandstone	Sandstone, fine- to medium-grained, silty, micaceous, interbedded with siltstone, shale; laminated to medium bedded, cross-bedded; minor intraformational conglomerate; micaceous, trace fossils.	Shallow marine
Noonkanbah Formation	Siltstone, poorly bedded and laminated; shale, carbonaceous; minor fine-grained sandstone, micaceous, feldspathic.	Shallow marine
Poole Sandstone	Interbedded mudstone and fine- to coarse-grained sandstone, thin-bedded, ripple-marked, cross-bedded; minor conglomerate, macrofossils.	Shallow water marine
Paterson Formation (time equivalent with upper Grant Group)	Sandstone and mudstone with dropstones, poorly sorted. Sandstone, fine- to coarse-grained, cross-bedded, minor mudstone and conglomerate; dropstones. Mapped on PATERSON RANGE and RUNTON.	Glacial Fluvioglacial
	Mudstone, massive to poorly bedded, very poorly sorted, with dropstones; minor sandstone. Mapped on PATERSON RANGE and RUNTON.	Glacial-lacustrine
Grant Group	Fine to coarse sandstone; shale, siltstone, conglomerate (mapped on PATERSON RANGE and TABLETOP).	Glacial, partly marine

Permian sediments in much of the AEM survey area belong to the Paterson Formation. The Paterson Formation consists of a basal unit of very poorly sorted, unstratified mudstone containing abundant dropstones, ranging up to boulder size, and minor fine-grained, thinly-bedded quartz wacke. This is overlain by an upper unit of cross-bedded fluvial sandstone and conglomerate with lenses of pebbles and boulders of Precambrian rocks (quartz, quartzite, granite, chert, chert breccia, sandstone, dolomite, basalt, gabbro and schist). The Paterson Formation is 33 m thick at the type section, ranging to over 250 m in the Canning Basin with some drill holes indicating > 400 m. Cross-bedding in the upper unit is planar, with some ripple cross-bedding and scour-and-fill structures present. Some beds are bioturbated (Hickman, 1978; Towner and Gibson, 1980; Chin *et al.*, 1982).

The Paterson Formation as a whole is interpreted to be a fluvioglacial deposit. Towner and Gibson (1980) considered that it was initially deposited in lakes during an early stage of glaciation. These lakes were connected with a sea into which the rivers flowed, still under the influence of a glacial climate.

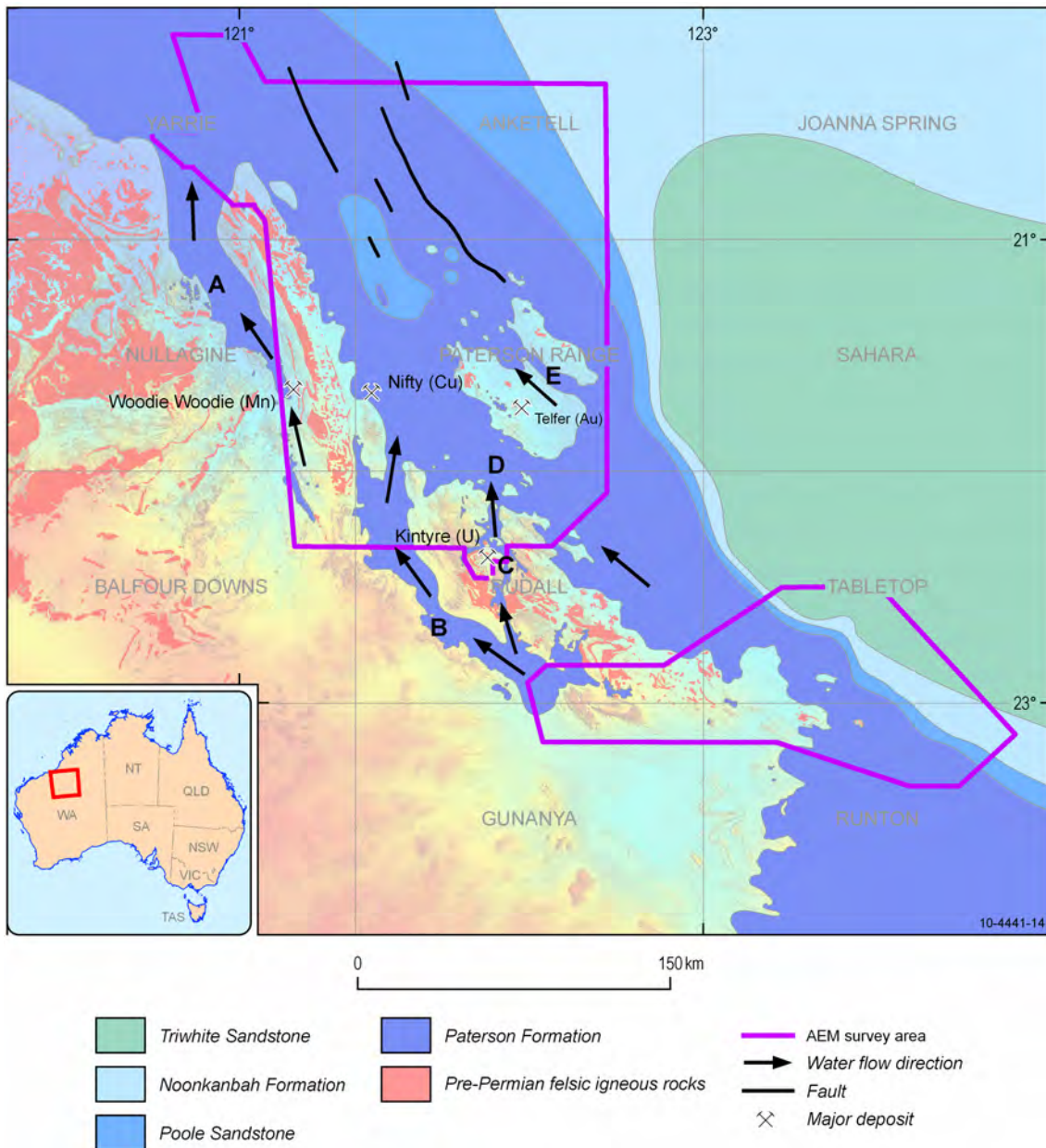


Figure 3.7: Permian solid geology with glacial flow directions in the Paterson area, modified after Towner et al. (1980).

The most characteristic feature of the Paterson Formation is glacially-derived dropstones of various Precambrian rock types, some of which are faceted and striated (Crowe and Chin, 1979). In the glacio-lacustrine facies on RUNTON, these dropstones are randomly set in a massive mudstone matrix, which forms low, rounded cliffs. Such exposures commonly contain purple and red liesegang banding. In the fluvio-glacial facies the dropstones occur throughout the sequence together with lenses of fluvially derived conglomerate. A glaciated pavement with overlying tillite occurs 11 km west-southwest of the Cronin Hills.

In the northern portion of PATERSON RANGE, well-bedded sandstone is folded into zones of disharmonic, tight, concentric folds which are commonly cut by thrusts and steeply dipping faults.

These structures are interpreted to be resultant of deformation caused by the movement of glaciers, or slumping of sediments made unstable by the melting of ice (Chin *et al.*, 1982). Several regional scale faults are interpreted from the AEM data through Paterson Formation sediments in the Waukarlycarly Embayment, probably as growth faults along the basin boundary ([Figure 3.7](#)). No organic materials have been mapped or mentioned in the Paterson Formation in the 1:100 000 and 1:250 000 surface geology maps and explanatory notes.

Exposures of the Poole Sandstone are mainly confined to PATERSON RANGE, largely between the eastern and western bounding faults of the Waukarlycarly Embayment ([Figure 3.1](#)). It is about 33 m thick at the type section and fossils indicate deposition in a marine environment. The ripple-marked, thin interbeds of sandstone and mudstone were interpreted as having been deposited in a shallow sea, probably above wave base, by Towner and Gibson (1980).

The Noonkanbah Formation is very poorly exposed within the area. The presence of a very rich marine fauna indicates an unrestricted marine environment and the abundance of fine calcareous mudstone in the sequence suggests continuous deposition in a quiet standing body of water. Pyritic zones indicate some reducing anaerobic conditions. The thickness of the Formation varies, with 6 m exposed in TABLETOP and nearly 290 m encountered in Tappers Inlet 1 well (Towner and Gibson, 1980).

The Triwhite Sandstone is confined to the area around SAHARA and TABLETOP in the Paterson area. No more than 8 m is exposed in the area, however in the WAPET Kidson 1 well it is 77 m thick (WAPET, 1966). Towner *et al.* (1976) postulated that the gradual upward increase in grainsize from mudstone of the Noonkanbah Formation to sandstone of the unit indicates a shallow-water regressive marine environment.

3.2.4.2 Mesozoic

In the Paterson area Mesozoic sedimentary sequences occur north and northeast of the Percival Palaeovalley system west of Lake Winifred and east of the Disappointment Palaeovalley system ([Figure 3.8](#)). The total thickness of Mesozoic units is probably less than 100-200 meters in this part of the Canning Basin.

The oldest Mesozoic unit in the Paterson area is the Late Jurassic Alexander Formation, consisting of sandstone interbedded with mudstone (20-92 m thick). It is a shallow marine to tidal facies, occurring on JOANNA SPRING and to the north. The Bardwine Sandstone (Late Jurassic) is a fluvial facies and occurs as a small patch only on DUMMER, well outside the survey area. The Late Jurassic to Early Cretaceous Cronin Sandstone is confined to the RUNTON area east of Lake Disappointment. It was interpreted as a correlative of the Callawa Formation by Towner *et al.* (1980).

Much of the northeast part of the Paterson area (OAKOVER 1:1 000 000 sheet area) is thinly blanketed by the fluvial facies of the Late Jurassic to Early Cretaceous Callawa Formation, consisting of poorly sorted sandstone and conglomerate (52 m thick at the type section, elsewhere > 80 m). It is overlain on YARRIE and west ANKETELL by thin-bedded and massive mudstone and fine sandstone (up to 30 m thick) of the Early Cretaceous Parda Formation. The Early Cretaceous Frezier Sandstone is a unit of sandstone and minor conglomerate (about 15 m exposed). It rests on the Callawa Formation and the Parda Formation on ANKETELL. It is thought to be a basinward facies of the Callawa Formation. The Anketell Sandstone (Early Cretaceous, less than 50 m thick) disconformably overlies the Frezier Sandstone and Callawa Formation (Towner and Gibson, 1980; Towner *et al.*, 1980; Towner, 1982).

Table 3.8: Mesozoic sedimentary sequences in the Paterson area, after Towner *et al.* (1980).

UNIT	LITHOLOGY	DEPOSITION ENVIRONMENT
Lake George Beds	Sandstone, granule conglomerate, poorly sorted, massive.	Continental, partly pedogenic
Anketell Sandstone	Fine-grained sandstone, siltstone, interbedded with coarse sandstone and conglomerate, laminated to thin bedded.	Shallow marine
Frezier Sandstone	Sandstone, fine- to coarse-grained, minor conglomerate, poorly sorted, feldspathic in part; commonly ferruginised or pedogenically altered.	Fluvial to deltaic
Parda Formation	Mudstone, fine-grained sandstone, thin-bedded or massive.	Lagoonal or shallow marine beach
Callawa Formation	Sandstone, conglomerate, poorly sorted, minor siltstone.	Fluvial
Cronin Sandstone	Sandstone, fine- to coarse-grained, bioturbated, minor conglomerate, mudstone	Fluvial
Bardwine Sandstone	Sandstone, fine- to coarse-grained, conglomerate, minor siltstone.	Fluvial
Alexander Formation	Sandstone, interbedded mudstone, cross-bedded, ripple marked, minor conglomerate.	Shallow marine, tidal

It was most likely that Mesozoic sediments were much more laterally continuous prior to the incision of the three major palaeovalley systems, namely, the Wallal Palaeovalley, the Percival Palaeovalley and the Disappointment Palaeovalley. The palaeovalley systems most likely eroded and reworked much of the Mesozoic sedimentary sequence. The palaeovalley systems have incised underlying Permian sediments and even older basement in places. See [Section 5.7](#) for more information.

3.2.4.3 Cenozoic bedrocks

The Oakover Formation is composed of lacustrine carbonates and is up to 50 m thick. It consists of a lower carbonate-rich unit and an upper chalcedonic unit and occupies much of the Oakover River valley in Paterson North.

Other Cenozoic materials are regarded as regolith and are discussed in [Section 3.3](#).

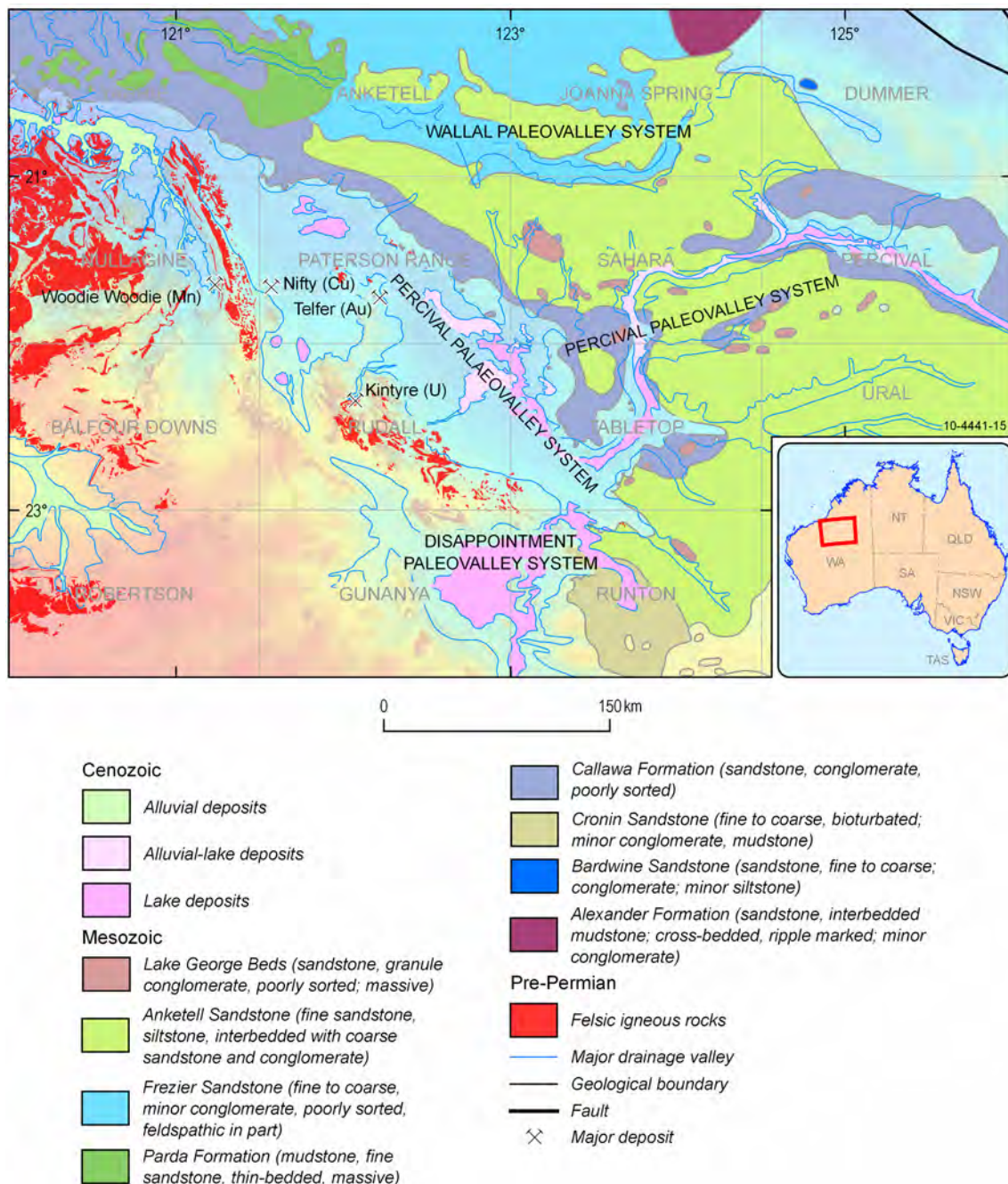


Figure 3.8: Mesozoic solid geology and major drainage systems in the Paterson area.

3.3 REGOLITH GEOLOGY

3.3.1 Introduction

The Paterson region has complex regolith and landscapes, but little has been written about either aside from what is mentioned in passing in the various geological explanatory notes (see references in Section 3.2) or in the broad discussions of palaeovalleys by Beard (1973; 2005), van der Graaf (1977) and Commander (1989). There are no existing regolith-landform maps of the area apart from a small area around the Telfer gold-copper mine. Further detailed regolith-landform mapping was

outside the scope of this report, therefore, the regolith and landscapes of the Paterson region are here summarised from existing knowledge and are broadly characterised using geophysical and geomorphological surrogates at a scale that is applicable to the regional AEM surveying. The following describes the known regolith and landscape characteristics of the Paterson region, describes the process used to construct the regional regolith map ([Figure 3.9](#)) and discusses the observations and implications of the regional regolith-landform map.

The great span in the geological ages of materials within the Paterson region can lead to scientific and philosophical problems with determining what is transported regolith and what is weathered bedrock. There are numerous examples from around Australia where Mesozoic and Cenozoic sedimentary materials may be classed as transported regolith because they are largely unconsolidated and have not undergone significant diagenesis (lithification). Many descriptions contained within company progress reports from the Paterson region indicate that Permian tillites are unconsolidated, but have ferruginous (ferricrete) and siliceous (silcrete) indurated overprints. The question remains as to whether they have remained unconsolidated since deposition, or have since been weathered. In this Record, we regard older Phanerozoic materials (Paleozoic, Mesozoic and Early Cenozoic) as being *in situ* regolith (bedrock) for simplicity. Late Cenozoic (mapped as Quaternary) materials are regarded as transported regolith. All of the materials, from Archean to Recent, may have a surface regolith overprint including weathering and induration, which may be buried underneath younger materials.

3.3.2 Previous work

Very little information exists regarding regolith-landforms within the Paterson area, however, limited regolith information is contained within 1:100 000 and 1:250 000 geological map explanatory notes. The following is synthesised from 1:250 000 geological sheet notes of the area, describing first transported regolith materials, then *in situ* regolith materials and lastly regolith overprints.

3.3.2.1 Transported regolith

The Paterson region is dominated by sand sheets and seif (longitudinal) dunes of the Great Sandy Desert and the Little Sandy Desert. Sand sheets commonly have a lag of ferruginised or quartzose sediment as pisoliths, nodules and broken fragments noted around the Oakover River on BALFOUR DOWNS (Williams, 1989). Dunes range in size up to about 30 m tall, may be spaced between 300 m and 3 km apart and may be over 70 km long on YARRIE (Williams, 2003). Dunes trend dominantly north-westerly, but trends vary according to their location with relation to the Australian dune whorl of Bowler (1976). Dunes are partially active today, however they are believed to have been most active during the last glacial maximum between 17 500 and 16 000 years ago (Bowler, 1976). The dunes also probably have a complex history of activity related to glacial cycles throughout the Pleistocene and Holocene. Fitzsimmons (2005) and Fitzsimmons *et al.* (2007) discussed the results of optically-stimulated luminescence (OSL) dating of seif dune strata from the Strzelecki and Tirari deserts of Central Australia and noted that dunes were active many times over the last 100 ka, activity peaking during glacial maxima when climates were cool and dry. Dunes are composed of red-yellow slightly ferruginised sands and vary in morphology according to landscape position. Net dunes are noted in depressions on GUNANYA (Williams and Williams, 1980) and chain dunes on YARRIE (Williams, 2003); these two terms probably describe the same features and these morphological types also most likely occur to lesser amounts on other map sheets within the Paterson region. Dunes continue over low-relief features (rises, breakaways, buttes and mesas), noted on ANKETELL (Towner, 1982) but are stopped against larger hills often as sand ramps on the windward (eastern) side, as noted on PATERSON RANGE (Chin *et al.*, 1982).

Salt lakes and claypans commonly occur within low-lying parts of the Paterson region. These include large salt lakes such as Lake Disappointment on GUNANYA (Williams and Williams, 1980) and RUNTON (Crowe and Chin, 1979), Lake Waukarlycarly on PATERSON RANGE (Chin *et al.*, 1982) and the Percival Lake system on RUDALL (Bagas *et al.*, 2000) and TABLETOP (Yeates and

Chin, 1979). Smaller salt lakes and clay pans occur along ephemeral drainage lines and within dune swales, noted on RUDALL (Bagas *et al.*, 2000) and RUNTON (Crowe and Chin, 1979). These lakes are filled by rains from passing cyclones and thunder storms. Salt lakes and clay pans commonly have halitic or gypseous crusts and gypseous lunette dunes on their leeward sides. Clay pans may have well-developed gilgai formed on their surfaces, as noted on YARRIE (Williams, 2003). Many of these geographical features are noted in [Figure 1.1](#).

The Paterson survey area features several large alluvial systems based around the Oakover River and Rudall River. There are numerous small creeks draining from the Gregory Range and Rudall Complex, draining into alluvial fans in the dune fields. In the broader area, there are well-developed alluvial systems containing braided, incised channels and alluvial plains entering Lake Disappointment, including Savory Creek on GUNANYA (Williams and Williams, 1980). Savory Creek is deeply incised (20 m) into the foothills to the west of Lake Disappointment and divides into salt-laden creeks < 10 m deep towards the Lake. The Rudall River on RUDALL (Bagas *et al.*, 2000) rises in the Rudall Complex, has a well-developed channel featuring numerous semi-permanent water holes and has incised up to 10 m below the surrounding plains. The river drains into a prominent alluvial-colluvial fan system that overprints the dune field southwest of Lake Dora. The Oakover and Nullagine rivers on NULLAGINE (Hickman, 1978) have well developed channels and floodplains with gilgai formed in silty deposits. Both drain into the Indian Ocean.

Colluvial systems occur throughout the Paterson survey area as high-relief scree slopes, as moderate-to low-relief pediments around hills and breakaways, as low-relief surfaces associated with alluvial-colluvial outwash fans at the terminations of alluvial systems and as low-relief pavements between sand dunes. High-relief landforms on NULLAGINE (Hickman, 1978), RUDALL (Bagas *et al.*, 2000), RUNTON (Crowe and Chin, 1979) and YARRIE (Williams, 2003) are all flanked by scree, colluvium and lag deposits consisting of local bedrocks and ferruginous pisoliths, nodules and fragments. Scree slopes may lead into colluvial-alluvial fans at footslopes. On YARRIE (Williams, 2003) broad sheets of partially indurated colluvium occur adjacent to the Callawa Formation near the Callawa Hills, indicating re-cementation of previously indurated materials. Low-relief landforms occur at the terminations of colluvial-alluvial fan systems, on floodplains and within the dune fields between seif dunes. In these areas contour-banded (Dunkerley and Brown, 1995; Wakelin-King, 1999) colluvial sheetwash fans are commonly reported where alluvium and quartzose and ferruginous lag are being reworked by colluvial processes. On BALFOUR DOWNS Williams (1989) reported “buckshot” plains consisting of ferruginous pisoliths and nodules being colluvially-reworked into sand.

3.3.2.2 *In situ* regolith

The Paterson survey area contains numerous bedrock outcrops and all have a regolith overprint. *In situ* regolith commonly ranges from slightly weathered bedrock to well-developed lateritic weathering profiles. Lateritic profiles include a ferruginous duricrust capping, a kaolinite-rich bleached (plasmic) zone and a mottled zone above saprolite, conforming to the description provided by Eggleton (2001). On RUDALL (Bagas *et al.*, 2000) most Precambrian outcrops are variably ferruginised, leached or silicified, typical of lateritic profiles, and dolomites can have a chert breccia cap. Incision through the profiles occurs as cliffs, gorges or ravines. On YARRIE (Williams, 2003) the Carawine Dolomite and carbonate-bearing ultramafics may have massive, nodular and cavernous calcrete formed *in situ*. Phanerozoic materials including Permian, Mesozoic and Cenozoic deposits may also have lateritic weathering profiles developed on them. On ANKETELL (Towner, 1982) ferruginous and siliceous duricrusts (ferricrete and silcrete) occur over highly weathered kaolinite-rich weathering zones on outcrops of the entire Mesozoic sequence. On NULLAGINE (Hickman, 1978) mesas and plateaux of the Tertiary Oakover Fm consist of partly silicified calcrete after lacustrine limestone. On RUDALL (Bagas *et al.*, 2000) Cenozoic deposits are commonly indurated by ferricrete or silcrete. On RUNTON (Crowe and Chin, 1979) Phanerozoic rocks form mesas and buttes where capped by ferruginous duricrust. Ferruginous duricrust up to 10 m thick occurs in undulating plains with a well developed dendritic palaeodrainage system over the Cenozoic and

Mesozoic units. On TABLETOP (Yeates and Chin, 1979) dissected hills, ridges and mesas have ferruginous duricrust caps up to 5 m thick over moderately well developed lateritic weathering profiles in the Anketell Sandstone. On YARRIE (Williams, 2003) numerous sand-covered mesas, buttes and rock pavements are armoured by ferruginous duricrust and pisolithic ferruginous gravel. Scattered exploration drill holes have intersected ferruginous duricrust up to 20 m thick, with rare intersections up to 35 m thick, which are interpreted to be channel-fills. The Oakover Formation consists of white vuggy opaline silica and chalcedony overprinting calcareous sandstone and limestone. Mesozoic material is commonly armoured with massive, pisolithic and nodular ferruginous duricrusts and the Paterson Formation near the Gregory Range has a well-developed siliceous duricrust.

3.3.2.3 Indurated regolith

Indurated materials are reported from all 1:250 000 geological sheets within the Paterson survey area. These most commonly comprise calcrete, ferricrete, silcrete and gypcrete.

Calcrete is common throughout the area, occurring mostly in the bottoms of palaeodrainage channels including the Wallal, Canning and Disappointment palaeovalleys (see [Figures 5.27](#) and [7.21](#)) and flanking well-established extant drainage channels, particularly the larger salt lakes including Lake Dora, Lake Waukarlycarly and Lake Disappointment (see [Figures 1.1](#) and [7.23](#)). These are defined as valley calcretes (Butt *et al.*, 1977; Chen *et al.*, 2002) because they lie in the bases of valleys and are regarded as having precipitated from groundwater. Valley calcrete is also reported from low-lying areas between sand dunes on ANKETELL (Towner, 1982) and over a ferruginous hardpan in the banks of Savory Creek on GUNANYA (Williams and Williams, 1980). Calcrete also occurs as pedogenic types, reported as earthy calcrete beneath ferricrete in a lateritic weathering profile on NULLAGINE (Hickman, 1978). Valley calcrete with karstic depressions is reported on TABLETOP (Yeates and Chin, 1979). Calcrete may also form as a karstic cap over carbonate-bearing bedrocks including the Carawine Dolomite on YARRIE (Williams, 2003). Valley calcrete occurrences are shown in [Figure 7.21](#).

Silcrete occurs widely throughout the Paterson survey area, however, it is not a common surface material. Silcrete occurs as a duricrust over the Pinjian Chert Member and the Carawine Dolomite on BALFOUR DOWNS (Williams, 1989) and over dolomite on RUDALL (Bagas *et al.*, 2000). It may also be found as a minor component within valley calcrete deposits as chalcedonic veins. It occurs within exposed lateritic profiles on Mesozoic and Paleozoic sediments of the Canning Basin underneath the ferruginous duricrust, on exposed weathering profiles in the Rudall Complex and in drill holes where Mesozoic or Paleozoic sediments, particularly the Paterson Formation, are indurated.

Ferricrete is abundant and occurs as an indurating overprint over most *in situ* regolith materials, see [Section 3.2.2.2](#).

Gypcrete is common bordering and within salt lakes and claypans within the region, particularly occurring in lunettes on the leeside of playa lakes where it has been deflated (blown) from the lake surface. These leeside deposits may also be described as "kopi". Gypcrete consists of cemented gypsum crystals which have been partially dissolved and reprecipitated, creating a solid but highly porous mass of secondarily-cemented gypsum.

3.3.2.4 Regolith mapping

Only one regolith-landform map is known to exist within the AEM survey area. This was created by Henderson (1996) over the Telfer area at 1:50 000 scale as part of a University of Western Australia Masters research program. This map incorporates the relict-erosional-depositional (RED) scheme developed by the CSIRO Division of Exploration and Mining. The map was completed using Landsat TM and SPOT satellite imagery and airborne radiometric imagery to identify regolith-landforms and place them in a model-driven classification scheme of "relict", "erosional" or

“depositional” regimes. The map offers great spatial detail but covers insufficient area to be of benefit to this study.

3.3.2.5 Regolith geochemistry

Several studies exist detailing the geochemistry of regolith surrounding mines within the region. Wilmhurst (1999) described the geochemistry of a cross-section of weathered Malu Formation rocks in the Telfer gold-copper mine pit and gossanous Malu Formation outcrops from around the mine site. This study discussed the bulk geochemistry and mineralogy of a vertical succession of regolith materials.

Carver (2005) discussed the regolith materials and landscape surrounding the Nifty copper deposit as part of a detailed ferruginous lag sampling program of the deposit surrounds. Carver, paraphrasing Chin *et al.* (1982), described the most dominant landscape feature as being seif dunes up to 30 m high and 1.0-1.5 km apart. Carver noted that the dune swales were sandy and contained minor scattered rock outcrops (“siliceous ironstone after dolomite”) with thin skeletal soils, ferruginous gravel and colluvium. The effects of weathering on the Nifty deposit have not been well described, however Carver (2005) described the presence of a > 10 km diameter secondary mineral alteration halo around the Nifty deposit and associated deposits (Rainbow, Hakea, Bloodwood and Finch) that was formed by weathering processes. This alteration halo was discovered in a lag sampling program by Western Mining Corporation in 1980, resulting in the ultimate discovery of the Nifty deposit after initial geophysical targeting.

Cornelius (2008) interpreted geochemical data from a single soil geochemical traverse in a dune swale across the Rainbow prospect near the Nifty Copper deposit. Soils were sieved into different size fractions and analysed. Only limited regolith or landform information was recorded, but useful observations were made regarding the nature of surface lags between the dunes and dune swales as well as recommendations for future soil geochemical sampling programs.

3.3.3 Regolith map development

Regolith-landform maps describe discrete landforms and the regolith materials that occur within them as polygons encompassing individual regolith-landform units (RLUs). Mapping at large scales is normally accomplished using aerial photography and detailed field observations (points and traverses) to ground-truth observations, paying close attention to vegetation occurring within each polygon. Undisturbed vegetation can be used as a surrogate for regolith materials and landforms because most vegetation prefers to grow in materials and landscape positions that best suit an individual plant's survival strategy; there can be a geobotanical relationship between regolith, landform and vegetation. Aerial photography is used because texture, tone or colour and pattern on photography may be used as surrogates for regolith materials and vegetation, and the stereoscopic effect is used to separating different landforms to divide photography into different RLUs. Large scale mapping may also be accomplished using high-resolution remote sensing including Quickbird, Ikonos or SPOT satellite imagery and a high-resolution digital elevation model (DEM) such as LIDAR (light detection and ranging) to provide landform information.

Small scale mapping can be accomplished using remote sensing imagery like Landsat, Advanced Spaceborne Thermal Emission and Reflection Radiometer (ASTER) or other similar imagery and airborne geophysics (principally radiometrics) as regolith material surrogates and topographic maps or medium- to low-resolution DEMs such as the GEODATA 9-second DEM (Hutchinson, 2008) or one of the Shuttle Radar Topography Mission (SRTM) products (3-second DEM, 1-second DEM) to provide the landform information. Limited ground checking is necessary to validate the correlations made between the surrogates and RLUs.

In this study only very limited ground checking was possible, so a regolith-only map was created principally using the Weathering Intensity Index—WII (Wilford, in prep), the SRTM 3-second DEM and the Geoscience Australia 1:1 000 000 Surface Geology of Western Australia (Stewart, 2008).

Other geophysical and remotely sensed derivatives used included a multi-resolution valley bottom flatness (MRVBF; Gallant and Dowling, 2003) image derived from the SRTM 1-second DEM and a ternary (potassium-thorium-uranium) radiometric image. The WII is a new regolith classification method based on radiometric imagery and a DEM which makes predictions on regolith materials by their potassium, thorium, uranium and total counts responses and their landscape position, or solely uses the DEM to make predictions where radiometric data are unavailable.

A WII image of the Oakover 1:1 000 000 geological sheet area was added to an ArcGIS project as a 100 m ground pixel resolution raster image, together with the other data sets. A series of rules were then developed using ArcGIS Model Builder to characterise known pixels, extrapolate them within the Oakover sheet bounds and classify them according the regolith-terrain mapping (RTMAP) scheme of Pain *et al.* (2007).

Because no regional-scale regolith-landform mapping was available, and the creation of such was beyond the scope of this study, mapped bedrock polygons from the 1:1 000 000 scale Geological Map of Western Australia were used as the primary surrogate for *in situ* regolith polygons. Rules were developed using the WII to group pixels occurring over mineralogically-similar bedrocks according to weathering grade. Mapped bedrock polygons were used to derive *in situ* regolith polygons because they were regarded as being authoritative. However, mapped polygons describing ferruginous duricrusts in the Canning Basin were found to be unreliable, so other data were used to develop regolith polygons of these areas, including the WII and radiometric data, most particularly thorium abundance. Mapping surrogates and rules used to define regolith pixels are listed in [Table 3.9](#). The abundance of thorium in the radiometric image was used to separate ferruginous duricrust from other material. Thorium and ferruginous duricrust are strongly associated in the regolith because thorium is scavenged by hematite and goethite (two important regolith minerals in ferruginous duricrusts) during weathering processes and is retained in duricrust outcrops, or can be scattered throughout the landscape as ferruginous duricrusts are alluvially or colluvially reworked.

The Great Sandy Desert, over which the Paterson AEM survey area partially lies, is dominated by a highly complex network of seif dunes which may be up to 3 km apart, several hundred metres wide and over 50 km long. At the scale of mapping, the dunes are almost invisible, however their influence is seen in DEMs and consequently in the WII model. Rather than map individual or groups of dunes, we have instead used digitised dune crest polylines taken from the GA GEODATA TOPO 250K map series (GEODATA, 2006).

The WII method depends highly on accurate geological mapping for locating most regolith classes (*in situ*, some indurated, transported), but on radiometric imagery for determining weathering grade and for locating some classes of indurated regolith not in the mapped geology. This was, however, deemed acceptable for a wide area regolith map of the Paterson survey area to more completely identify areas with significant amounts of ferruginous duricrust, which are under-represented in current geological mapping.

3.3.4 Regolith mapping scheme

The RTMAP regolith-landform mapping scheme of Pain *et al.* (2007) characterises regolith materials and the landforms in which they occur according to an alphanumeric scheme. The scheme characterises materials according to two main criteria: transported materials; and, *in situ* materials. Transported materials may be terrestrial sediments including alluvial, colluvial and aeolian sediment. *In situ* materials are unweathered or weathered bedrocks. Indurated materials are regarded as an overprint over the *in situ* and transported regolith classes.

For this report, polygons are labelled with regolith attributes only, thus the regolith unit (RU) descriptor uses a capitalised regolith descriptor and a digit to describe variations in regolith materials, such as:

SM1

The uppercase letters indicate saprolite (S), moderately weathered (M) of type 1. Regolith units used in this report are tabulated in [Table 3.10](#).

Table 3.9: Data sets and rules used to develop the Paterson regolith map.

REGOLITH UNIT	DATA SETS USED	RULES
<i>In situ</i> regolith		
Felsic bedrocks – Archean and Proterozoic bedrocks with felsic affinities.	1:1 000 000 Surface Geology of Western Australia, WII.	All geological polygons with “felsic word” affinities, WII classes 1, 2 and 3 for “slightly”, “moderately” and “highly” weathered.
Mafic bedrocks – Archean and Proterozoic bedrocks with mafic affinities.	1:1 000 000 Surface Geology of Western Australia, WII.	All geological polygons with “mafic” word affinities, WII classes 1, 2 and 3 for “slightly”, “moderately” and “highly” weathered.
Silica-rich Archean and Proterozoic bedrocks – BIF, quartzite, chert.	1:1 000 000 Surface Geology of Western Australia, WII.	All geological polygons with “silica-rich” and “medium-high grade metamorphic” word affinities, WII classes 1, 2 and 3 for “slightly”, “moderately” and “highly” weathered.
Archean and Proterozoic sedimentary rocks.	1:1 000 000 Surface Geology of Western Australia, WII.	All geological polygons with “sedimentary rock” and “low grade metamorphic” word affinities, WII classes 1, 2 and 3 for “slightly”, “moderately” and “highly” weathered.
Phanerozoic sedimentary rocks – Permian, Mesozoic and Cenozoic rocks .	1:1 000 000 Surface Geology of Western Australia, WII.	All Phanerozoic, but not Quaternary, rock affinities, WII classes 1, 2 and 3 for “slightly”, “moderately” and “highly” weathered.
Indurated regolith		
Indurated regolith – ferricrete.	1:1 000 000 Surface Geology of Western Australia.	All ferricrete polygons (Czl).
Indurated regolith – silcrete.	1:1 000 000 Surface Geology of Western Australia.	All silcrete polygons (Czz).
Indurated regolith – calcrete.	1:1 000 000 Surface Geology of Western Australia.	All calcrete polygons (Czk, Czik).
Transported regolith		
Alluvium – alluvium, valley calcrete, sand dunes, sand sheets.	1:1 000 000 Surface Geology of Western Australia, MRVBF6, thorium.	All alluvial polygons, MRVBF6 > 5.2 and all pixels without previous data and Th < 18 ppm, not lacustrine polygons.
Colluvium – ferruginous lag, sand dunes, sand sheets, minor valley calcrete and silcrete.	1:1 000 000 Surface Geology of Western Australia, MRVBF6, thorium.	All colluvial polygons, MRVBF < 5.2 and all pixels without previous data and Th > 18 ppm.
Lacustrine sediments.	1:1 000 000 Surface Geology of Western Australia.	All lacustrine sediment polygons.

Table 3.10: Regolith unit code explanations.

REGOLITH UNIT CODE	DESCRIPTION
SDA	Sediment, detrital, alluvium.
SDC	Sediment, detrital, colluvium.
SDL	Sediment, detrital, lacustrine.
IN1	Indurated regolith, ferruginous duricrust.
IN2	Indurated regolith, siliceous duricrust.
IN3	Indurated regolith, calcareous duricrust.
SS1-5	Saprolite, slightly weathered, type 1 to 5 (see text below).
SM1-5	Saprolite, moderately weathered, type 1 to 5 (see text below).
SH1-5	Saprolite, highly weathered, type 1 to 5 (see text below).

3.3.5 Regolith units (RUs)

The following summarises regolith materials within the classification scheme used for the Paterson survey area regolith map ([Figure 3.9](#)).

3.3.5.1 Transported regolith

Alluvial sediments - SDA

Alluvial RUs include all geological polygons mapped as containing alluvium including streams, rivers and overbank deposits (flood plains), all pixels where $\text{MRVBF6} > 5.2$ (these are deemed to be of sufficiently low slope to be classed as alluvium) and where thorium $< 18 \text{ ppm}$ (these are deemed to not contain low-relief ferruginous duricrust outcrops and are therefore alluvium), except where *in situ* regolith polygons already exist. This RU also contains a large amount of valley calcrete, which is not mapped separately on the geological mapping, but is common in valley floors especially around salt lakes and clay pans. The RU also contains a large proportion of sand dunes and sand sheets.

Regolith materials include gravel-filled channel beds, silt and clay overbank deposits and reworked aeolian sand. Materials may include quartz sand or reworked lithic clasts of local bedrocks and fragments of indurated regolith materials (ferricrete, silcrete, calcrete) as described in [Section 3.2.2.1](#).

Colluvial sediments - SDC

Colluvial RUs include all geological polygons mapped as containing colluvium, all pixels where $\text{MRVBF6} < 5.2$ (these are deemed to be of sufficiently high slope to be classed as colluvium) and where thorium $> 18 \text{ ppm}$ (these are deemed to contain ferruginous duricrust which is being colluvially reworked), except where *in situ* regolith polygons already exist. Colluvial polygons may also contain small amounts of valley calcrete or pedogenic calcrete formed on slopes, and a large proportion of sand dunes and sand sheets.

Regolith materials include reworked lithic and indurated regolith materials (ferricrete, silcrete, calcrete) as footslopes around higher-relief features and also colluvial sheetwash developed over low-relief, low-angle landforms including old alluvial plains and around indurated bedrocks in the Canning Basin. Colluvial RUs include significant amounts of ferruginous duricrust reworked from the local landscape as pisoliths, nodules and fragments plus sand dunes and sand sheets as described in [Section 3.2.2.1](#).

Lacustrine sediments – SDL

Lacustrine sediment polygons include all geological polygons mapped as containing lacustrine sediments (Ql). This includes lake bottoms and may also include lunettes and source-bordering dunes (Qdl).

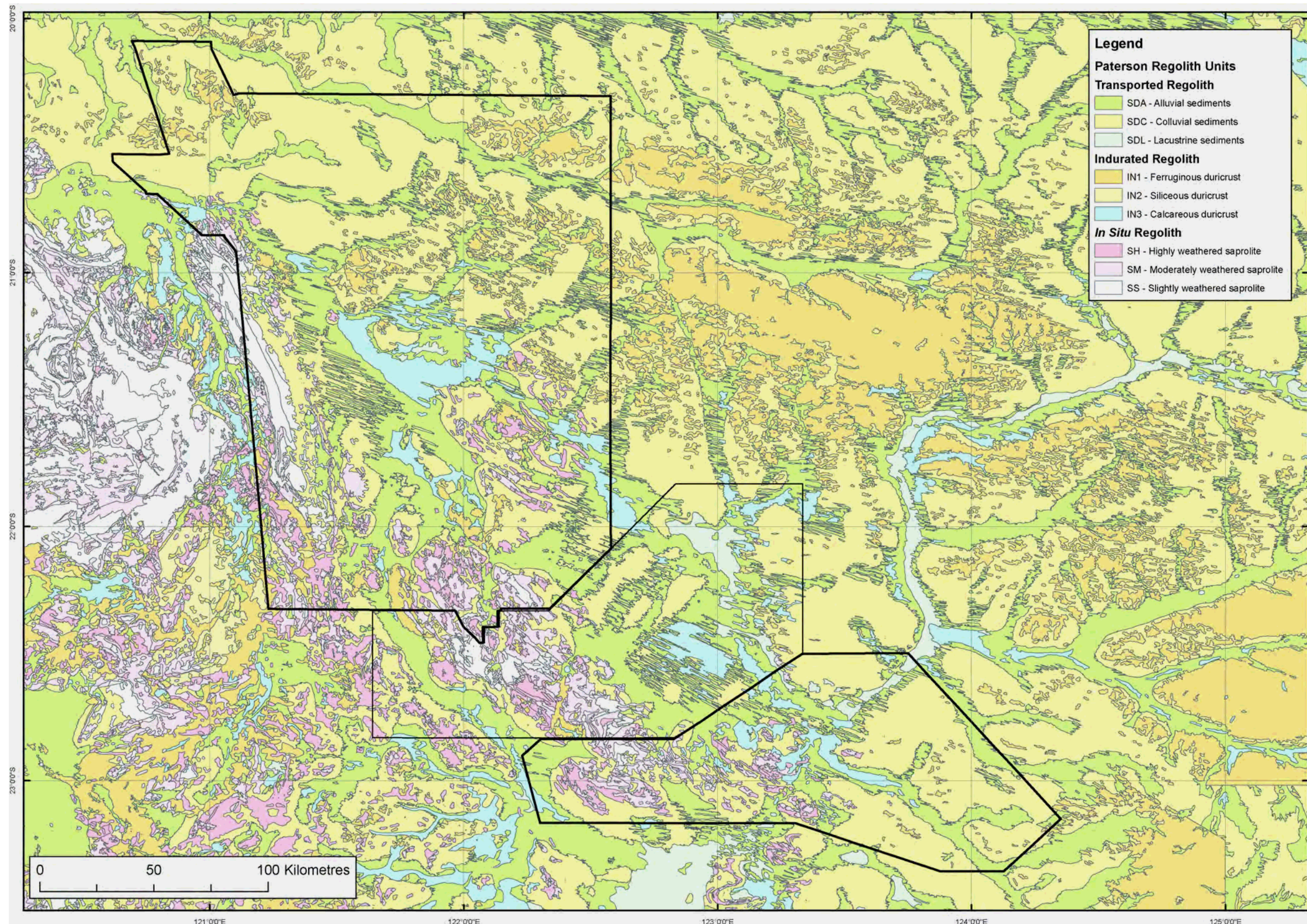


Figure 3.9: Regolith map of the Paterson area, sand dunes removed.

3.3.5.2 Indurated regolith

Ferruginous duricrust – IN1

Ferruginous duricrust (ferricrete) RUs include all geological polygons mapped as containing “laterite” or “lateritic duricrust” (Czl) plus all pixels identified as having significant amounts of ferruginous duricrust by having thorium > 18 ppm in areas not already occupied by *in situ* regolith polygons. Ferricrete RUs occur most commonly over Permian and Mesozoic strata in the Canning Basin.

Regolith materials may include ferruginised bedrock with minor colluvium, sand dunes and sand sheet cover as described in [Section 3.2.2.3](#).

Siliceous duricrust – IN2

Siliceous duricrust (silcrete) RUs contain all geological polygons mapped as containing silcrete (Czz). Silcrete is common in areas where Phanerozoic sediments occur, commonly forming duricrust-capped mesas and buttes, for instance Permian outcrops.

Regolith materials include highly silicified quartzose fragments with minor accessory minerals such as anatase and zircon and other resistant lithic fragments including quartzite.

Calcareous duricrust – IN3

Calcareous duricrust (calcrete) RUs contain all geological polygons mapped as containing calcrete (Czk, Czik). Calcrete is common in the Oakover River valley where the carbonate-rich Tertiary Oakover Formation is overprinted by calcrete (Czik) with numerous chalcedonic veins. Calcrete also commonly occurs in alluvial RUs as valley calcrete included in the alluvial sediment (SDA) RUs and may occur in colluvial sediment (SDC) RUs.

3.3.5.3 In situ regolith

Weathered felsic rocks – SS1, SM1, SH1

Weathered felsic rocks contain all geological polygons mapped as including Archean and Proterozoic volcanic, volcanoclastic and intrusive rocks dominant over other rocks such as clastic and chemical sedimentary and metasedimentary rocks.

Weathering grades (SS-slightly weathered; SM – moderately weathered; and, SH – highly weathered) reflect the weathering grade calculated using the WII.

Weathered mafic rocks – SS2, SM2, SH2

Weathered mafic rocks contain all geological polygons mapped as including Archean and Proterozoic volcanic, volcanoclastic and intrusive rocks dominant over other rocks such as clastic and chemical sedimentary and metasedimentary rocks

Weathering grades (SS-slightly weathered; SM – moderately weathered; and, SH – highly weathered) reflect the weathering grade calculated using the WII.

Weathered silica-rich and high-grade metamorphic rocks – SS3, SM3, SH3

Weathered silica-rich and high-grade metamorphic rocks contain all geological polygons mapped as including Archean and Proterozoic banded iron formation (BIF), chert, quartzite and silica-rich high-grade metamorphic rocks dominant over other classes of rocks.

Weathering grades (SS-slightly weathered; SM – moderately weathered; and, SH – highly weathered) reflect the weathering grade calculated using the WII.

Weathered low-grade metamorphic rocks – SS4, SM4, SH4

Weathered low-grade metamorphic rocks contain all geological polygons mapped as including Archean and Proterozoic rocks with no or low-grade (greenschist facies) metamorphism dominant

over other classes of rocks.

Weathering grades (SS-slightly weathered; SM – moderately weathered; and, SH – highly weathered) reflect the weathering grade calculated using the WII.

Weathered Phanerozoic rocks – SS5, SM5, SH5

Weathered Phanerozoic rocks contain all geological polygons mapped as including Permian, Mesozoic and Cenozoic (except Quaternary) rocks.

Weathering grades (SS-slightly weathered; SM – moderately weathered; and, SH – highly weathered) reflect the weathering grade calculated using the WII.

3.4 REFERENCES

- Arndt, N. T., Nelson, D. R., Compston, W., Trendall, A. F. and Thorne, A. M., 1991. The age of the Fortescue Group, Hamersley Basin, Western Australia, from ion microprobe zircon U-Pb results. *Australian Journal of Earth Sciences* **38**(3), 261-281.
- Bacchin, M., Milligan, P., Tracey, R. and Wynne, P., 2008. New gravity anomaly map of the Australian region. *AUSGEO News* **91 September 2008**.
- Bagas, L., 1998. Geology of the Gunanya 1:100 000 sheet, 1:100 000 Geological Series Explanatory Notes. Western Australia Geological Survey, Perth. 10 p.
- Bagas, L., 1999a. Rudall, WA Sheet SF51-10. *1:250 000 Geological Series*, Western Australia Geological Survey Perth. 2nd edition.
- Bagas, L., 1999b. Geology of the Blanche-Cronin 1:100 000 sheet (part sheets 3551 and 3552), 1:100 000 Geological Series - Explanatory Notes. Geological Survey of Western Australia, Perth. 16 p.
- Bagas, L., 2000. Geology of the Paterson 1:100,000 sheet - Explanatory Notes. Geological Survey of Western Australia, Perth. 20 p.
- Bagas, L., 2004a. Proterozoic evolution and tectonic setting of the northwest Paterson Orogen, Western Australia. *Precambrian Research* **128**(3-4), 475-496.
- Bagas, L., 2005. Geology of the Lamil 1:100 000 sheet, Explanatory Notes. *1:100 000 Geological Series*, Western Australia Geological Survey.
- Bagas, L., Camacho, A. and Nelson, D. R., 2002. Are the Neoproterozoic Lamil and Throssell Groups of the Paterson Orogen allochthonous? In: *Annual Review 2000–2001*. Western Australia Geological Survey, Perth. 45-52 pp.
- Bagas, L., Grey, K., Hocking, R. M. and Williams, I. R., 1999. Neoproterozoic successions of the northwestern Officer Basin: a reappraisal. In: *Annual Review*. Western Australia Geological Survey, Perth. 39-44 pp.
- Bagas, L., Grey, K. and Williams, I. R., 1995. Reappraisal of the Paterson Orogeny and Savory Basin. In: *Annual Review 1994-95*. Western Australia Geological Survey. 55-63 pp.
- Bagas, L. and Nelson, D. R., 2007. Provenance of Neoproterozoic sedimentary rocks in the northwest Paterson Orogen, Western Australia. *Central Australian Basins Symposium Special Publication*, Northern Territory Geological Survey.
- Bagas, L. and Smithies, R. H., 1996. Connaughton, WA Sheet 3452. *1:100 000 Geological Series*, Western Australia Geological Survey. 1st edition.
- Bagas, L. and Smithies, R. H., 1998. Geology of the Connaughton 1:100 000 sheet, 1:100 000 Geological Series Explanatory Notes. Western Australia Geological Survey, Perth. 38 p.
- Bagas, L., Williams, I. R. and Hickman, A. H., 2000. Rudall, Western Australia (2nd Edition). *1:250,000 Geological Series - Explanatory Notes*. Western Australia Geological Survey. 50 p.
- Beard, J. S., 1973. The elucidation of palaeodrainage patterns in Western Australia. Vegmap Publications, Perth. Occasional Paper No 1, 17 p.

- Beard, J. S., 2005. Drainage evolution in the Lake Disappointment Catchment, Western Australia - a discussion. *Journal of the Royal Society of Western Australia* **88**, 57-64.
- Bowler, J. M., 1976. Aridity in Australia: Age, origins and expression in aeolian landforms and sediments. *Earth-Science Reviews* **12(2-3)**, 279-310.
- Butt, C. R. M., Horwitz, R. C. and Mann, A. W., 1977. Uranium occurrence in calcrete and associated sediments in Western Australia. CSIRO Minerals Research Laboratories, Division of Mineralogy, Perth. **Report FP16**.
- Carver, R. N., 2005. Nifty Copper Deposit, Great Sandy Desert, Western Australia. In: Butt, C. R. M., Robertson, I. D. M., Scott, K. M. and Cornelius, M. (eds) *Regolith expression of Australian ore systems*. CRC LEME, Perth. 185-187 pp.
- Chen, X. Y., Lintern, M. J. and Roach, I. C., 2002. Calcrete: characteristics, distribution and use in mineral exploration. Cooperative Research Centre for Landscape Environments and Mineral Exploration. 160 p.
- Chin, R. J., Hickman, A. H. and Towner, R. R., 1982. Paterson Range, Western Australia. 1:250 000 Geological Series - Explanatory Notes. Geological Survey of Western Australia, Perth. 29 p.
- Commander, D. P., 1989. Hydrogeological map of Western Australia, 1:2 500 000. Geological Survey of Western Australia.
- Cornelius, M., 2008. Interpretation of soil geochemical data from Rainbow Prospect, Nifty, WA. CRC LEME, Perth. **Open File Report 181**. Online: <http://crcleme.org.au/Pubs/OFRSIndex.html>.
- Crowe, R. W. A. and Chin, R. J., 1979. Runton, Western Australia. 1:250 000 Geological Series - Explanatory Notes. Bureau of Mineral Resources, Geology and Geophysics, Geological Survey of Western Australia, Canberra, Perth. 16 p.
- Czarnota, K., Gerner, E., Maidment, D. W., Meixner, A. J. and Bagas, L., 2009a. Paterson Area 1:250 000 Scale Solid Geology Interpretation and Depth to Basement Model. Geoscience Australia, Canberra. **Record 2009/16**, 37 p.
- Czarnota, K., Gerner, E., Maidment, D. W., Meixner, A. J. and Bagas, L., 2009b. Proterozoic Solid Geology of the Paterson Province, 1:250 000 scale map. Geoscience Australia.
- Dunkerley, D. L. and Brown, K. J., 1995. Runoff and runon areas in a patterned chenopod shrubland, arid western New South Wales, Australia: characteristics and origin. *Journal of Arid Environments* **30**, 41-55.
- Dunphy, J. M. and McNaughton, N. J., 1998. Geochronology of the Telfer granitoids: zircon and titanite U-Pb SHRIMP data. In: *Geological Society of Australia Abstracts*, v. 49, 127 pp.
- Fitzsimmons, K. E., 2005. From little things big things grow: reconstructing past environments from Quaternary desert dune sediments and stratigraphy. In: Roach, I. C. (ed), *Regolith 2005: Ten Years of CRC LEME*, Canberra, Adelaide, CRC LEME, 102-106 pp. Online: <http://crcleme.org.au/Pubs/Monographs/regolith2005/Fitzsimmons.pdf>.
- Fitzsimmons, K. E., Rhodes, E. J., Magee, J. W. and Barrows, T. T., 2007. The timing of linear dune activity in the Strzelecki and Tirari Deserts, Australia. *Quaternary Science Reviews* **26(19-21)**, 2598-2616.
- Gallant, J. C. and Dowling, T. I., 2003. A multiresolution index of valley bottom flatness for mapping depositional areas. *Water Resource Research* **39(12)**, 1347-1359.
- GEODATA, 2006. GEODATA TOPO 250K Series 3. Geoscience Australia, Canberra. **GEOCAT # 63999**. Online: https://www.ga.gov.au/products/servlet/controller?event=GEOCAT_DETAILS&catno=63999.
- Grey, K., 1978. Re-examination of stromatolites from the Nullagine map sheet, Waltha Woora Formation. Western Australia Geological Survey, Perth. **Palaeontological Report 79/84**, 4 p.
- Grey, K., 1984. Field studies of Precambrian stromatolites from the Nabberu Basin and eastern Pilbara. Western Australia Geological Survey, Perth. **Palaeontological Report 79/84**, 18 p.
- Henderson, I., 1996. A study of the regolith landforms in the Telfer district, Western Australia. University of Western Australia, Perth. MSc.
- Hickman, A. H., 1978. Nullagine, Western Australia. 1:250 000 Geological Series - Explanatory Notes. Geological Survey of Western Australia, Perth. 21 p.

- Hickman, A. H. and Bagas, L., 1998. Geology of the Rudall 1:100 000 sheet. Geological Survey of Western Australia, Perth. 30 p.
- Hickman, A. H. and Clarke, G. L., 1993. Broadhurst, W.A. Sheet 3353. *1:100 000 Geological Series*, Western Australian Geological Survey.
- Hickman, A. H. and Clarke, G. L., 1994. Geology of the Broadhurst 1:100 000 sheet, Western Australia. Western Australia Geological Survey, Perth. 40 p.
- Hickman, A. H., Williams, I. R. and Bagas, L., 1994. Proterozoic geology and mineralization of the Telfer-Rudall region, Paterson Orogen. *Excursion Guidebook 5*, Geological Society of Australia, Perth. 56 p.
- Howard, G. R., Maxlow, J., Helm, S., Inglis, R., Carlson, R. and Hansen, T., 2005. Telfer gold-copper mine: 26 million ounces and growing. *Proceedings of Newgengold 2005*, Perth, 28-29 November.
- Hunt, 1996. Hunt Oil Company Final report Waukarlycarly Seismic Survey interpretation. Western Australia Geological Survey, Perth. **Statutory Petroleum Exploration Report S10316 A5**.
- Huston, D. L., Sun, S.-S., Blewett, R., Hickman, A. H., Kranendonk, M. V., Phillips, D., Baker, D. and Brauhart, C., 2002. The Timing of Mineralization in the Archean North Pilbara Terrain, Western Australia. *Economic Geology* **97(4)**, 733-755.
- Hutchinson, M. F., 2008. GEODATA 9 second DEM and D8: Digital Elevation Model Version 3 and Flow Direction Grid 2008. Geoscience Australia, Canberra. **GEOCAT #66006**. Online: https://www.ga.gov.au/products/servlet/controller?event=GEOCAT_DETAILS&catno=66006.
- Jahn, B. M. and Simonson, B. M., 1995. Carbonate Pb-Pb ages of the Wittenoom Formation and Carawine Dolomite, Hamersley Basin, Western Australia (with implications for their correlation with the Transvaal Dolomite of South Africa). *Precambrian Research* **72**, 247-261.
- Myers, J. S., 1993. Precambrian tectonic evolution of part of Gondwana, southwestern Australia. *Geology* **18**, 537-540.
- Nelson, D. R., 1995. Compilation of SHRIMP U-Pb zircon geochronology data, 1994. Geological Survey of Western Australia. **Record 1995/3**, 244 p.
- Nelson, D. R., 1996. Compilation of SHRIMP U-Pb zircon geochronology data, 1995. Geological Survey of Western Australia, Perth. **Record 1996/5**, 168 p.
- Pain, C. F., Chan, R., Craig, M., Gibson, D., Kilgour, P. and Wilford, J. R., 2007. RTMAP Regolith Database Field Book and Users Guide. CRC LEME, Perth. **Open File Report 231**.
- Percival, P., 2010. Index of airborne geophysical surveys. Geoscience Australia, Canberra. **Record 2010/013**. Online: https://www.ga.gov.au/products/servlet/controller?event=GEOCAT_DETAILS&catno=70295.
- Perincek, D., 1996. The stratigraphic and structural development of the Officer Basin, Western Australia. In: *Annual Review 1995-96*. Western Australia Geological Survey, Perth. 135-148 pp.
- Roach, I. C., 2009. A drill hole database for the Paterson airborne electromagnetic (AEM) survey, Western Australia. Geoscience Australia, Canberra. **Record 2009/31**, 16 p.
- Simonson, B. M. and Jarvis, D. G., 1993. Microfabrics of oolites and pisolithes in the Early Precambrian Carawine Dolomite of Western Australia. In: Rezak, R. and Lavai, D. (eds) *Carbonate microfabrics*. Springer-Verlag, Berlin. 227-237 pp.
- Simonson, B. M., Schubel, K. A. and Hassler, S. W., 1993. Carbonate sedimentology of the Precambrian Hamersley Group of Western Australia. *Precambrian Research* **60**, 287-335.
- Smithies, R. H. and Bagas, L., 1997. High pressure amphibolite-granulite facies metamorphism in the Paleoproterozoic Rudall Complex, central Western Australia. *Precambrian Research* **83**, 243-265.
- Stewart, A. J., 2008. Surface Geology of Australia 1:1 000 000 scale, Western Australia. Geoscience Australia, Canberra. http://www.ga.gov.au/minerals/research/national/nat_maps/nat_geol_maps.jsp.

- Towner, R. R., 1982. Anketell (Second Edition) Western Australia 1:250 000 Series Explanatory Notes. Bureau of Mineral Resources, Geology and Geophysics, Geological Survey of Western Australia. 22 p.
- Towner, R. R., Crowe, R. W. A. and Yeates, A. N., 1976. Notes on the geology of the southern part of the Canning Basin. Bureau of Mineral Resources, Geology and Geophysics, Canberra. **BMR Record 1976/095**, 42 p.
- Towner, R. R. and Gibson, D. L., 1980. Geology of Late Carboniferous and younger rocks of the onshore western Canning Basin, Western Australia. Bureau of Mineral Resources, Geology and Geophysics, Canberra. **BMR Record 1980/30**.
- Towner, R. R., Gibson, D. L., Young, G. A. and P., M., 1980. Geology of the Canning Basin, Western Australia (1:1 000 000 surface geology map and 1:3 000 000 simplified geology and structure). Bureau of Mineral Resources, Geology and Geophysics, Canberra.
- Trendall, A. F., 1991. Progress report on the stratigraphy and structure of the Fortescue Group in the Gregory Range area of the eastern Pilbara Craton. Geological Survey of Western Australia, Perth. **Record 1990/10**, 38 p.
- Turner, C. C., 1982. The Telfer Gold Deposits, Western Australia. Stratigraphy, sedimentology and mineralisation of the Proterozoic Yeneena Group. Unpublished Ph.D. thesis, University of New England, 296 p.
- Tyler, I. M. and Hocking, R. M., 2002a. A revision of the tectonic units of Western Australia. In: *Annual Review 2000-01*. Geological Survey of Western Australia, Perth. 33-44 pp.
- Tyler, I. M. and Hocking, R. M., 2002b. A revised geological framework for Western Australia. In, Geological Survey of Western Australia 6pp.
- van der Graaf, W. J. E., Crowe, R. W. A., Bunting, J. A. and Jackson, M. J., 1977. Relict Early Cenozoic drainages in arid Western Australia. *Zeitschrift für Geomorphologie NF* **21(4)**, 379-400.
- Wakelin-King, G. A., 1999. Banded mosaic ('tiger bush') and sheetflow plains: a regional mapping approach. *Australian Journal of Earth Sciences* **46(1)**, 53-60.
- WAPET, 1966. West Australian Petroleum Pty Ltd Kidson No. 1 well completion report. Bureau of Mineral Resources, Geology and Geophysics, Canberra. **File 65/4177**.
- Wilford, J., in prep. A weathering intensity index for the Australian Continent using airborne gamma-ray spectrometry and digital terrain analysis. *Geoderma*.
- Williams, I. R., 1989. Balfour Downs, Western Australia (Second Edition). 1:250 000 Geological Series - Explanatory Notes. Geological Survey of Western Australia, Perth. 38 p.
- Williams, I. R., 1992. Geology of the Savory Basin, Western Australia. Western Australia Geological Survey, Perth. **Bulletin 141**, 115 p.
- Williams, I. R., 2003. Yarrie, Western Australia. 1:250 000 Geological Series - Explanatory Notes. Geological Survey of Western Australia, Perth. 84 p.
- Williams, I. R. and Bagas, L., 1999. Geology of the Throssell 1:100 000 sheet, 1:100 000 Geological Series Explanatory Notes. Western Australia Geological Survey, Perth. 24 p.
- Williams, I. R. and Bagas, L., 2000. Geology of the Poisonbush 1:100 000 sheet, 1:100 000 Geological Series Explanatory Notes. Western Australian Geological Survey, Perth. 21 p.
- Williams, I. R. and Trendall, A. F., 1998a. Geology of the Pearana 1:100 000 sheet, 1:100 000 Geological Series Explanatory Notes. Western Australia Geological Survey, Perth. 33 p.
- Williams, I. R. and Trendall, A. F., 1998b. Geology of the Braeside 1:100 000 sheet, 1:100 000 Geological Series Explanatory Notes. Western Australia Geological Survey, Perth. 39 p.
- Williams, I. R. and Tyler, I. M., 1991. Roberston, WA (2nd Edition), 1:250 000 Geological Series Explanatory Notes. Western Australia Geological Survey, Perth. 36 p.
- Williams, I. R. and Williams, S. J., 1980. Gunanya, Western Australia. 1:250 000 Geological Series - Explanatory Notes. Geological Survey of Western Australia, Perth. 13 p.
- Wilmshurst, J. R., 1999. Geochemistry of weathered rocks at the Telfer Gold deposit, Paterson Province, WA. CRC LEME, Perth. **Open File Report 70**. Online: <http://crcleme.org.au/Pubs/OFRSindex.html>.
- Wynne, P. and Bacchin, M., 2009. Index of Gravity Surveys. Geoscience Australia, Canberra. **Record 2009/07**. Online: <https://www.ga.gov.au/products/servlet/controller?event=>

- GEOCAT_DETAILS&catno=68264.
- Yeates, A. N. and Chin, R. J., 1979. Tabletop, Western Australia. 1:250 000 Geological Series - Explanatory Notes. Bureau of Mineral Resources, Geology and Geophysics, Geological Survey of Western Australia, Canberra, Perth. 19 p.
- Yeates, A. N., Gibson, D. L., Towner, R. R. and Crowe, R. W. A., 1984. Regional Geology of the Onshore Canning Basin. In: Purcell, P. G. (eds) *The Canning Basin, Western Australia. Proceedings of the Geological Society of Australia/Petroleum Exploration Society of Australia Symposium*. Perth. 23-55 pp.

4 AEM Geophysics

M. T. Costelloe, D. K. Hutchinson and I. C. Roach

4.1 INTRODUCTION

Airborne Electromagnetic (AEM) surveys are commonly used to map the electrical conductivity of the subsurface over large areas. As an AEM system flies over the ground it carries a transmitter loop through which a time-varying current is passed, thereby inducing eddy (secondary) currents to flow in any electrically conductive subsurface material. These eddy currents may be detected via the voltage that they induce in receiver coils that are towed by the aircraft. Since the amount of current that flows in the subsurface is related to its conductivity, analysis of the received signals allows estimates of the conductivity to be made. The depth to which the signals can be used to map conductivity depends on the system configuration and the subsurface conductivity (Smith, 2001; Lane *et al.*, 2004b).

The following introduces the survey method used for the Paterson AEM survey and the considerations and methods used to process the AEM dataset and produce the final inversions.

4.2 PREVIOUSLY RELEASED DATA

The survey was flown and Phase-1 data were released in two separate blocks, Paterson South and Paterson North, due to industry delivery requirements. The blocks are shown on the locality map ([Figure 1.10](#)). Internal to these two main survey blocks are eight sub-areas of infill flying that were funded by exploration companies. The flight lines that were funded by these companies were not included in the Phase-1 data release as, under the terms of the funding agreement, there was a moratorium on the data release until April 2010.

The Phase-1 data release included contractor-supplied data that had been quality assured and quality controlled (QA-QC) by Geoscience Australia (GA). The GA-funded portion of the Paterson South contractor-supplied data were released on 4 March 2009 and the Paterson North data were released on 17 April 2009.

The Phase-1 data release contained:

1. Survey operations and processing report;
2. Point-located electromagnetic response data without correction to a standard geometry;
3. Point-located electromagnetic response data with correction to a standard geometry;
4. Point-located conductivity depth image data derived using EM FlowTM software;
5. Gridded electromagnetic response and conductivity depth interval (CDI) data; and,
6. Graphical multiplot profiles showing electromagnetic, CDI and ancillary data for each line.

These data are available from the GA Sales Centre and are also available by free download from the GA web site using the links below:

1. Paterson South Phase-1 data and processing report;
https://www.ga.gov.au/products/servlet/controller?event=GEOCAT_DETAILS&catno=68430.
2. Paterson North Phase-1 data and processing report;
https://www.ga.gov.au/products/servlet/controller?event=GEOCAT_DETAILS&catno=68761.
3. Entire Paterson Phase-1 data including the infill data funded by private companies:
https://www.ga.gov.au/products/servlet/controller?event=GEOCAT_DETAILS&catno=70312.

Phase-1 data included CDIs generated by Fugro Airborne Surveys (FAS) using the EM FlowTM software package. The EM FlowTM CDI program is an industry standard method of deriving conductivity estimates from AEM surveys.

The conductivity estimates that are contained in the Phase-2 data, and detailed in this chapter, have been produced by the GA layered earth inversion (GA-LEI) algorithm developed at GA. The Phase-2 data release contained the GA-LEI 1D “sample-by-sample” inversion data, including:

1. Paterson AEM Survey Inversion Report;
2. Point-located GA-LEI inversion data;
3. Point-located GA-LEI inversion data (secondary) used to calculate the percent data influence (PDI);
4. GA LEI georeferenced jpeg sections;
5. GA LEI multiplots;
6. ER MapperTM grids of depth slices, elevation slices (10 and 50 m slices), 0-200 m conductance, 0-400 m conductance, AEM depth of investigation (DOI) Go Map;
7. Shape files: flight lines, survey boundary and National Park; and,
8. JPEG images of depth slices, elevation slices (10 and 50 m slices), 0-200 m conductance, 0-400 m conductance, AEM DOI Go Map.

Phase-2 data are available from the GA Sales Centre and are also available by free download from the GA website. Downloads are available through the link below:

1. Entire Paterson Phase-2 data including the infill data funded by private companies:
https://www.ga.gov.au/products/servlet/controller?event=GEOCAT_DETAILS&catno=70297

4.3 THE TEMPESTTM AEM SYSTEM

The Paterson survey was flown with FAS’ TEMPESTTM AEM system (Lane *et al.*, 2000) which was installed on the CASA C-212-200 aircraft registered VH-TEM on the Australian civil aircraft register. A summary of the system configuration used in the Paterson survey is provided in Table 4.1. The acquisition and processing of the Paterson North and Paterson South survey data is detailed in Lawrence and Stenning (2007a) and Lawrence and Stenning (2007b), respectively.

TEMPESTTM is a fixed-wing, time-domain system. It employs an approximate square-wave, 50% duty cycle current waveform with a base frequency of 25 Hz. The current is transmitted through a single turn transmitter (TX) loop draped around the nose, wings and tail of the aircraft. The survey was flown with the TX loop at an average of 122.4 m above ground level.

The receiver (RX) coils are housed in a ‘bird’ that was towed at approximately 120 m behind and 35 m below the aircraft. The RX consists of three orthogonal coils that sense the rate of change of the magnetic field (dB/dt) flux threading each coil. The axes of the three coils are nominally aligned in the horizontal flight line direction (X-component), horizontal direction perpendicular to the flight line (Y-component), and vertical directions (Z-component). However, only the X and Z-components are recorded and processed at full resolution and are available for interpretation.

The TX height and the orientations and relative separations of the TX and RX are also known as the system geometry. The system geometry continuously varies as the aircraft moves along a flight line. The TEMPESTTM instrumentation includes a GPS unit for the aircraft’s position, RADAR and LASER altimeters to measure its height above ground level and gyroscopes to measure its roll, pitch and yaw angles (i.e., its orientation). The relative separations of the TX and RX and the orientation of the RX are not measured by the system because of the logistical difficulty in doing so.

Since the system geometry affects the measured response, it must be input into quantitative forward

modelling of the system response, and hence estimation of subsurface conductivity from the recorded data. Therefore, in the data processing the unmeasured elements of the system geometry need to be estimated. For the TEMPEST™ system this involves separation of the measured total field response into its primary field (due to direct coupling between TX and RX) and secondary field (due to eddy currents induced in the ground) components. This requires an assumption to be made about the unknown subsurface conductivity, which typically is that the subsurface is resistive at depth. Once separated into primary and secondary components, the horizontal and vertical offsets between the TX and RX can be analytically determined from the primary field if it is assumed that the receiver bird is orientated with zero roll, pitch and yaw. It is these estimated and assumed values of system geometry that are taken to be the real values in standard algorithms for estimating subsurface conductivity from the measured data.

Table 4.1: TEMPEST™ AEM system specifications, from Lane et al. (2000).

ATTRIBUTE	SPECIFICATION
Base frequency	25 Hz
Transmitter area	221 m ² (VH-TEM)
Transmitter turns	1
Waveform	Square
Duty cycle	50%
Transmitter pulse width	10 ms
Transmitter off time	10 ms
Peak current	280 A (VH-TEM)
Peak moment	61880 Am ² (VH-TEM)
Average moment	30940 Am ² (VH-TEM)
Sample rate	75 kHz on X and Z
Sample interval	13.333 microseconds
Samples per half cycle	1500
System bandwidth	25 Hz to 37.5 kHz
Tx Loop Flying height nominal	121.1 m (subject to safety considerations)
Tx Loop Flying height average	122.4 (VH-TEM)
EM sensor	Towed bird with 3 component dB/dt coils
Tx Rx horizontal separation average	120.1 (VH-TEM)
Tx Rx vertical separation average	34.5 (VH-TEM)
Tx Rx horizontal separation standard	120 m (geometry-corrected standard)
Tx Rx vertical separation standard	35 m (geometry-corrected standard)
Stacked data output interval	200 ms (ca. 12 m)
Number of output windows	15
Window centre times	13 µs to 16.2 ms
Magnetometer	Stinger mounted caesium vapour
Magnetometer compensation	Fully digital
Magnetometer output interval	200 ms (ca. 12 m)
Magnetometer resolution	0.001 nT
Typical noise level	0.2 nT
GPS cycle rate	1 second

4.4 BACKGROUND ON THE GA-LEI INVERSION

Conversion of the non-linear electromagnetic response data into estimates of subsurface conductivity allows for much easier and more accurate integration with independent subsurface information and facilitates better interpretation. The conversion can use either approximate transformation methods or geophysical inversion, both of which produce model-dependent conductivity estimates.

The Phase-1 data release of Paterson data included conductivity predictions produced by FAS from the industry standard EM Flow™ algorithm (Macnae *et al.*, 1998; Stolz and Macnae, 1998). EM Flow™ is a fast approximate transformation method based on the concept that the response of a quasi-layered earth can be approximately represented by a mirror image of the transmitter dipole that recedes below the surface and expands with delay-time. By determining the vertical depth distribution of the mirror image dipoles a quasi-layered estimate of the subsurface conductivity can be estimated.

Since the routine relies on the estimates of the system geometry that are made during the FAS data processing (c.f. [Section 4.3](#)) the accuracy of the resultant conductivity estimates are dependent on the accuracy of the geometry estimates. Accordingly, the estimates tend to be biased towards producing results that are consistent with the assumptions made in the FAS data processing, namely a resistive basement earth model. This bias can in turn create an overestimate of the conductivity near the surface, since the model must compensate for the lack of conductance at depth (Lane *et al.*, 2004a; Brodie and Fisher, 2008).

A further problem is caused by the assumptions made in the system geometry estimation that the receiver is orientated in its nominal position (i.e., with zero roll, pitch, and yaw). If the receiver is in fact rotated from its nominal position, which is generally the case, it may be impossible to simultaneously fit both the X- and Z-component data using the same subsurface conductivity distribution because the data are inconsistent with the system geometry information provided to the routine. For this reason it is often necessary to calculate the EM Flow™ estimates using just the X- or the Z-component data. While this is possible, a different conductivity model will result from each component.

These issues led to the development of the GA-LEI algorithm (Lane *et al.*, 2004b). In the GA-LEI inversion algorithm, the idea is to not rely on the primary field separation and hence geometry estimates made in the standard FAS data processing. Instead, the total field (primary plus secondary) data are inverted directly. The inversion solves not only for a layered earth conductivity model, but it simultaneously solves for the horizontal and vertical separations between the TX and RX and the pitch of the receiver coils. By solving for the system geometry during the final inversion the method allows the information from both the X- and Z-components to be simultaneously fitted using a single common conductivity model. It prevents the assumptions made during the standard data processing from being automatically imposed onto the inversion results. Furthermore, if prior information exists about the electrical structure of the survey area, these can be included as specific constraints on the inversion results.

Previous work at GA, in which downhole conductivity log data were compared to conductivity estimates (Lane *et al.*, 2004a; Reid and Brodie, 2006; Brodie and Fisher, 2008), has shown that improvements on the standard FAS EM Flow™ conductivity estimates can be made using the GA-LEI algorithm. The inversion products included in this data release have been derived with the GA-LEI algorithm. [Section 4.5](#) of this report contains details of settings used in the GA-LEI for the Paterson survey. [Section 4.6](#) of this report details the products derived from the GA-LEI inversions that available for free download on the GA website. For details on the product list and image enhancements refer to [Appendix 3.1](#).

4.5 GA-LEI INVERSIONS

4.5.1 Description

The GA-LEI is a 1D “sample-by-sample” inversion in which each of the airborne samples, acquired at approximately 12 m intervals along a flight line, are inverted independently of their neighbours. The inversion of each individual sample involves the estimation of a 1D layered earth conductivity structure, and three elements of the system geometry, that are consistent with the data. A 1D layered

earth conductivity structure means that the earth is considered to be a series of horizontal layers stacked in layer-cake fashion. Each layer extends to infinity in the horizontal direction and the conductivity within each layer is constant. Once all samples are inverted they are compiled into a pseudo-3D model by ‘stitching’ the 1D model together. A detailed technical description of the GA-LEI is provided in [Appendix 3.2](#).

Since the data are non-linear with respect to the model parameters, an iterative inversion technique is used. Starting from an initial estimate, the layer conductivities and system geometry parameters are iteratively updated until the forward response of the model replicates the measured data satisfactorily (i.e., to within the noise levels). The estimated conductivity model is constrained to be vertically smooth and to be as close as possible to a reference conductivity model. The aim of these smoothness and reference model constraints is to ensure that the model is as simple as possible, and complex structure is only permitted where necessary, see for example Constable *et al.* (1987).

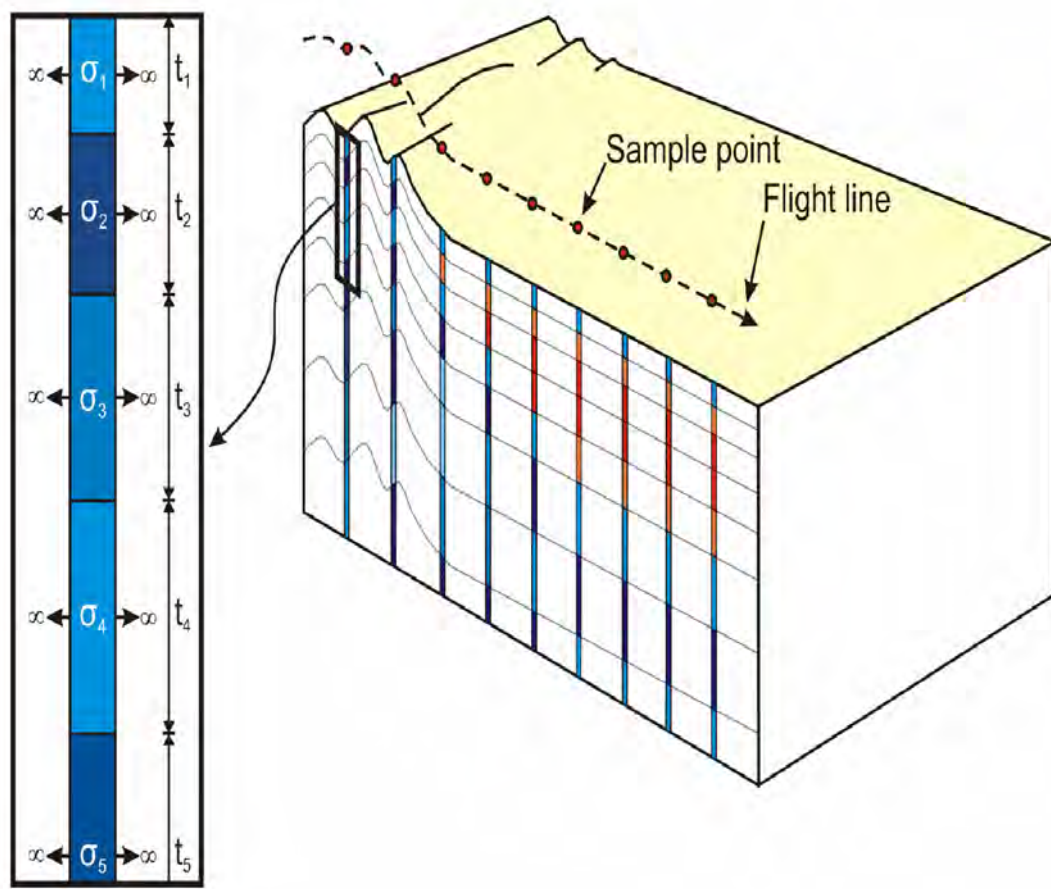


Figure 4.1: Schematic diagram of 1D vertically smooth layered earth model used in the GA-LEI. The thickness of each layer (t_n) is fixed, but the conductivity (σ_n) is not fixed and can vary between layers. From Brodie and Fisher (2008).

In this work the subsurface was parameterized with 30 layers whose thicknesses were chosen and remained fixed throughout the inversion (i.e., they were not solved for). The layer thicknesses gradually increase from 4 m in the top layer of the model up to approximately 60 m in the second deepest layer. The bottom layer was set to infinite thickness and thus represents a halfspace below all other layers. The parameters of each layer used in the GA-LEI are shown in [Table 4.2](#).

Table 4.2: GA-LEI model layer thicknesses and depths from surface.

LAYER NUMBER	THICKNESS (m)	DEPTH TO TOP (m)	DEPTH TO BOTTOM (m)
1	4.00	0.00	4.00
2	4.40	4.00	8.40
3	4.84	8.40	13.24
4	5.32	13.24	18.56
5	5.86	18.56	24.42
6	6.44	24.42	30.86
7	7.09	30.86	37.95
8	7.79	37.95	45.74
9	8.57	45.74	54.31
10	9.43	54.31	63.74
11	10.37	63.74	74.11
12	11.41	74.11	85.52
13	12.55	85.52	98.07
14	13.81	98.07	111.88
15	15.19	111.88	127.07
16	16.71	127.07	143.78
17	18.38	143.78	162.16
18	20.22	162.16	182.38
19	22.24	182.38	204.62
20	24.46	204.62	229.08
21	26.91	229.08	255.99
22	29.60	255.99	285.59
23	32.56	285.59	318.15
24	35.82	318.15	353.97
25	39.40	353.97	393.37
26	43.34	393.37	436.71
27	47.67	436.71	484.38
28	52.44	484.38	536.82
29	57.68	536.82	594.50
30	∞	594.50	∞

The inversion is run using an in-house Matlab script. The input or control file is included in Hutchinson *et al.* (2010). The inversion output ASCII header information from the inversion is in [Appendix 3.3](#).

4.6 REFERENCE MODEL

In principle, conductivity logs can be used to create a detailed reference model that varies across the survey in order to constrain the inversion when the solution becomes non-unique. In the Paterson survey, just 19 conductivity logs were available for use in the inversion. Since there were relatively few conductivity logs available over a large survey area, it was not feasible in this case to define a conductivity reference model that was spatially variable. Therefore the reference model used in this inversion is simply a half-space of homogeneous conductivity across the survey area. A conductivity reference value of 0.004 S/m was based on the average value of the resistive basement obtained from the logs. The reference model was also used as the starting model for the iterative inversion.

The TX to RX horizontal and vertical separation inversion model parameter values for each sample were estimated during the standard FAS data processing as the starting and reference model values. The starting and reference model value for the receiver coil pitch parameter is zero.

4.7 GEO-ELECTRICAL MODELS

Geo-electrical models were created utilising *a priori* knowledge of conductivity ranges for the targeted geological units. [Table 4.3](#) is a summary of the conductivity ranges used for geological targets in the forward modelling exercise (Sorensen, 2007).

Table 4.3: Conductivities used in the forward modelling.

GEOLOGICAL TARGET	CONDUCTIVITY (mS/m)
Regolith	10-250
Coolbro Sandstone	0.5-5
Broadhurst Formation	200-1000
Rudall Complex	0.5-5

An example forward model for the Coolbro Sandstone and the Broadhurst Formation is provided in [Figure 4.2](#).

Model 5.1: Coolbro Sandstone/Broadhurst Formation

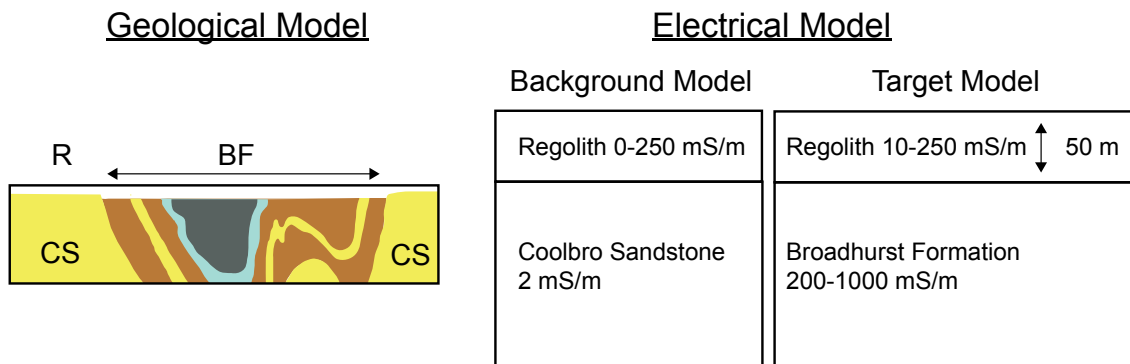


Figure 4.2: An example of a forward model from the Paterson AEM Survey. Forward model 5.1 modelled the theoretical response of the Broadhurst Formation under 50 m of regolith. Abbreviations: BF – Broadhurst Formation; R – regolith; CS – Coolbro Sandstone.

The results of the forward model in [Figure 2](#) indicated that all of the AEM systems considered for the Paterson survey had a 100% success rate in detecting the target of Broadhurst Formation under 50 m of regolith. Further modelling increased the regolith thickness to 150 m where fewer AEM systems were predicted to successfully detect the target.

4.8 GA-LEI INVERSION PRODUCTS

4.8.1 Depth of Investigation

The conductivity model estimated by the inversion is determined not only by the AEM data, but it is also influenced by an *a priori* estimate of conductivity. This estimate of conductivity, known as the reference model, is used as the initial model which is iteratively updated until an acceptable solution is reached. It is important to ascertain how much the solution is determined by the reference model and how much it is determined by the AEM data itself.

The relative contributions of the data and the reference model can be estimated by defining a parameter called the PDI; which compares two inversions created from different reference models. In this work, the PDI is defined as:

$$PDI = 100 \left(1 - \frac{\log(\sigma_{i1}) - \log(\sigma_{i2})}{\log(\sigma_{r1}) - \log(\sigma_{r2})} \right)$$

where σ_{i1} and σ_{i2} are the two inverted conductivities at a given location and σ_{r1} and σ_{r2} are the corresponding reference model conductivities (Lane *et al.*, 2004a). We define the PDI using the logarithm of the conductivity, since this is the quantity used in each inversion.

If the PDI is greater than 50% then the inversion is deemed to be more influenced by the AEM data than the reference model, whereas if it is less than 50% then the reference model is deemed to be dominant. The depth of investigation (DOI) is defined as the depth at which the PDI is 50%. Thus the DOI marks the depth to which the inverted conductivity is relatively robust. Note that the 50% PDI threshold is arbitrary and a different threshold could be chosen. [Figure 4.3](#) illustrates the effect of the DOI, showing an inverted section of line number 10040 data with two inverted solutions. In [Figure 4.3a](#) the inversion uses a reference conductivity of 0.04 S/m, whereas in [Figure 4.3b](#) the inversion uses a reference conductivity of 0.004 S/m.

As shown in [Figure 4.3](#) in the resistive areas of the inversion (predominantly blue), the solution is nearly identical under both reference models. This is reflected by the DOI threshold line being deeper in these areas. In more conductive areas, notably on the right hand side of the section, the deeper parts of the inversion are dominated by the reference model. Below the DOI the conductivity steadily approaches the homogeneous reference model value in both cases.

Assessment of the forward models in resistive areas, for example the Coolbro Sandstone overlying Rudall Complex and regolith over Coolbro Sandstone (see [Figure 4.2](#), [Section 4.7](#)), showed that the least probability of detection was at 400 m. This was considered the theoretical maximum depth of investigation. The probability of detection assumption required to cap the percent data influence (PDI) threshold was set to 400 m, based on forward modelling in resistive terrain. The DOI grid was therefore set to a maximum of 400 m depth.

4.8.2 Grids

The Phase-2 data release contains a selection of 2D grids, presenting the inverted data across the whole Paterson survey. These 2D grids have been created in three different categories:

1. As single inversion layers (the fundamental parameters from the 30 layer GA-LEI model);
2. As depth slices; and,
3. As elevation slices.

A conductivity depth slice is the average estimated conductivity over a given constant depth interval below the topographic surface. In contrast, an elevation slice is the average estimated conductivity over a given constant height interval above sea level.

All of these grids present the data using the base-10 logarithm (\log_{10}) of conductivity, since this is the value that enters into the inversion. For interpretation purposes we have found that geological structures are more evident in grids that use the logarithm of conductivity, rather than conductivity itself. Users who wish to grid the data without logarithms may obtain the data from the raw inversion output file: *master.inversion.dat* (see [Appendix 3.1](#)).

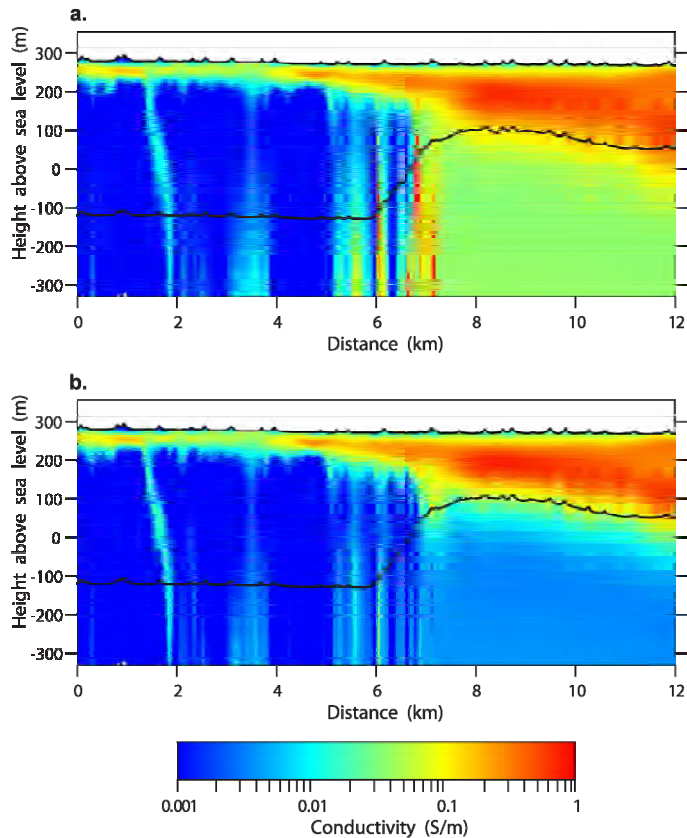


Figure 4.3: Sample conductivity depth sections comparing the results of inversions using reference models of (a) 0.04 S/m and (b) 0.004 S/m. The black line marks the depth of investigation (DOI) in each case. Above the DOI the results are similar for both inversions, whereas below the DOI the conductivity differs according to the reference model value. From Hutchinson et al. (2010b).

4.8.3 Gridding parameters

The AEM survey data were gridded using IntrepidTM Software and are stored in binary files as ER MapperTM single band IEEE 4 Byte Real data types. A comprehensive ER MapperTM header (.ers) file is associated with each grid file, which describes the data type and the coordinate system used to geographically position the grid. Gridded data are stored in a projected coordinate system only, in this case Universal Transverse Mercator (metric) coordinates of the Map Grid of Australia Zone 51 using the Geodetic Datum of Australia 1994. Technical details of the projection used are given in Appendix 3.4.

In the north-east corner of the survey the line spacing is 6 km. It was deemed more appropriate to not interpolate data across 6 km to reduce artefacts that obscure the structure evident in the data. In this area the data appears as coloured stripes with null values in between. This “Venetian blind” effect can be seen in the DOI grid, the depth slices and elevation slices ([Figures 4.4, 4.5](#) and [4.6](#)).

4.8.4 AEM DOI Go map

The DOI (described in [Section 4.7.1](#)) is presented as a 2D grid in [Figure 4.4](#). The probability of detection assumption required to cap the PDI threshold was set to 400 m, based on forward modelling in resistive terrain. In the resistive areas of the survey the DOI reaches this maximum depth. The yellow and red colours (40-150 m) in [Figure 4.4](#) are areas where the DOI is much shallower, and in some places is less than 100 m. These shallower areas of the DOI correspond closely to conductive regions of the survey area.

The DOI grid can be interpreted as an AEM “Go map”. AEM surveys are relatively costly, and carry an inherent risk since the depth of penetration is highly variable. This DOI grid can reduce the risk of exploration using EM surveys in the Paterson region, making EM surveying a more attractive tool for mineral exploration(Hutchinson *et al.*, 2010a; 2010b).

The main grid products of this AEM inversion are the depth slices and elevation slices. These grids present the inverted conductivity values in 2D spanning the entire survey area. The DOI surface has been incorporated into these depth and elevation slice grids in order to mask out results that are predominantly driven by the choice of reference model. The purpose of this masking is to focus attention on the data-driven results of the inversion and to ensure that spurious features from model-driven results are not misinterpreted as real structures or objects.

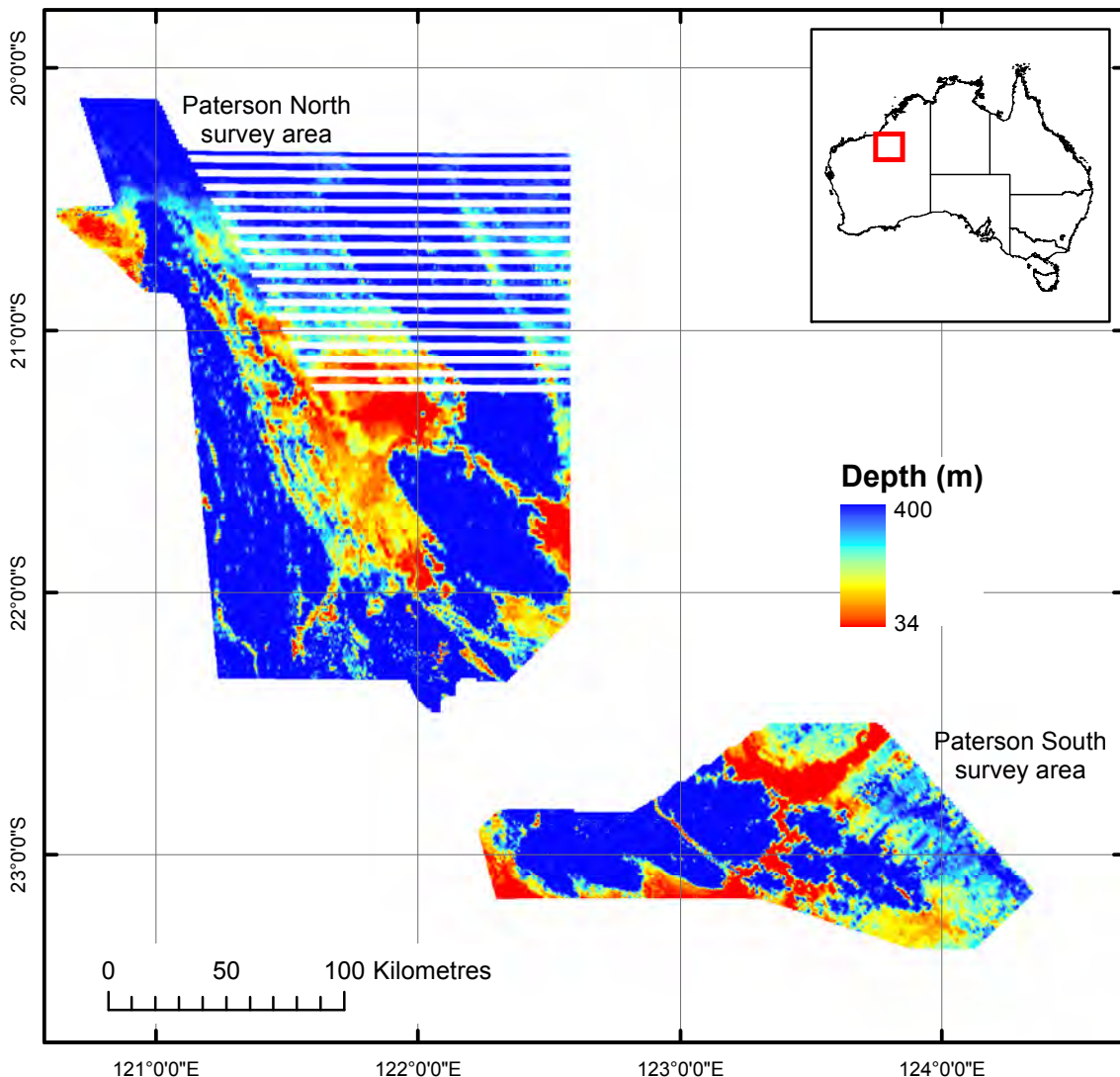


Figure 4.4: The DOI grid (AEM Go map).

4.8.5 Depth Slices

A series of 13 depth slices have been created between 0 and 300 m, with the slices becoming progressively thicker with depth. The depth slices are set to 5 m thickness between 0 and 20 m depth, 10 m thickness between 20 and 40 m depth, 20 m thickness between 40 and 100 m depth, and 50 m thickness between 100 and 300 m depth. These increases in thickness reflect the higher

sensitivity of the inversion at shallower depths.

A selection of four depth slices is illustrated in [Figure 4.5a-d](#), showing the: a) 0-5 m; b) 30-40 m; c) 100-150 m; and, d) 200-250 m depth intervals. Both [Figure 4.5a](#) and [Figure 4.5b](#) show a range of conductive and resistive areas and there is no DOI masking, since the depth slices are relatively shallow. However, [Figure 4.5c](#) shows some isolated areas of DOI masking, and [Figure 4.5d](#) shows substantial masking in broad conductive regions. This masking reflects the different penetration of the AEM signal in resistive (deep penetration) and conductive (shallow penetration) areas.

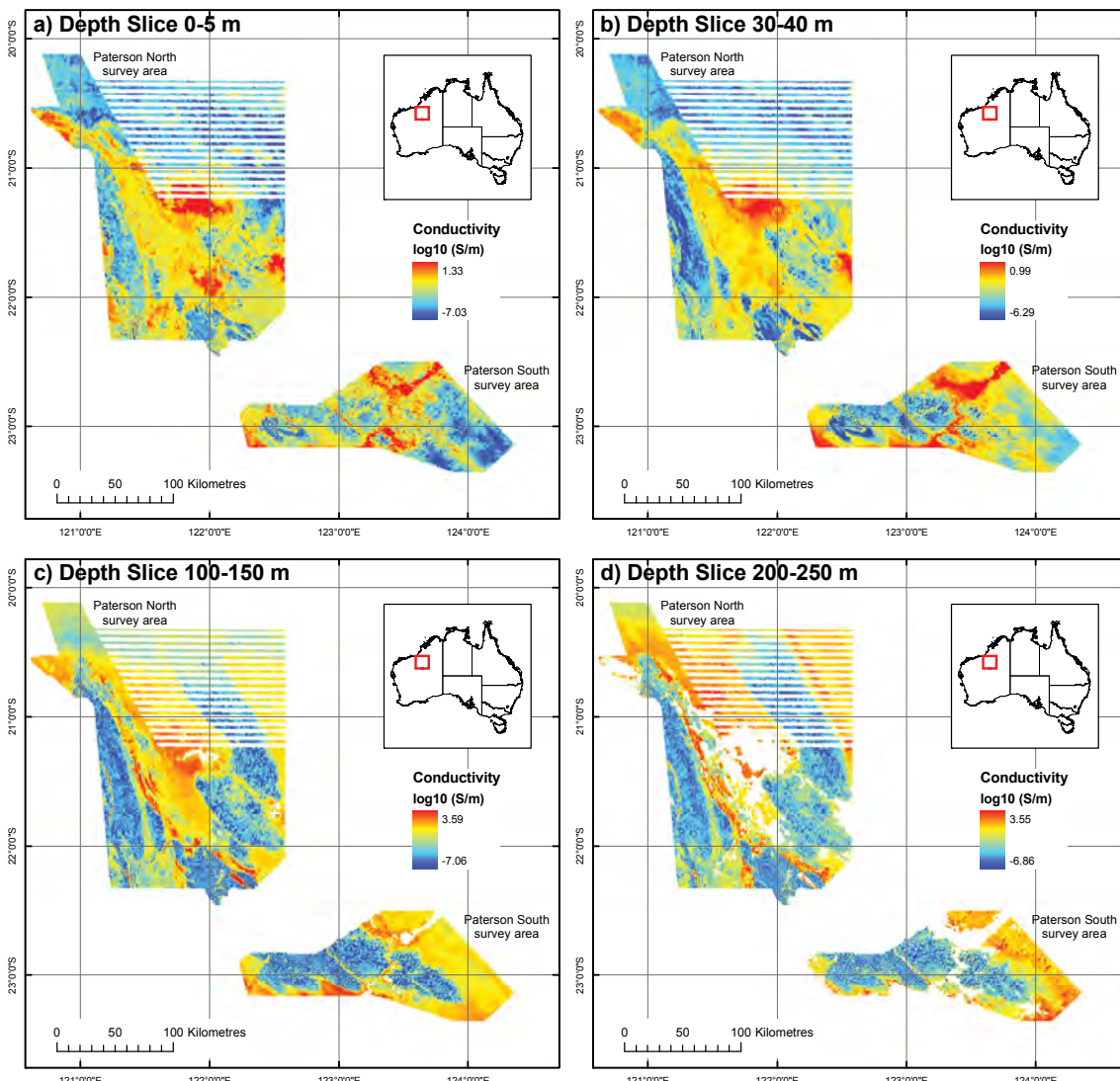


Figure 4.5: A selection of depth slices showing: a) 0-5 m; b) 30-40 m; c) 100-150 m; and, d) 200-250 m. Data falling below the DOI are masked out, and appear white.

4.8.6 Elevation slices

The elevation slices present the same inversion results, but the slices are referenced to the height above sea level rather than depth below surface. This gives the option of viewing data plotted along horizontal planes. The one drawback of using elevation slices over the entire survey is that there is a substantial altitude difference across some parts of the Paterson survey—up to 400 m of relief between the highest and lowest points of the survey. Therefore, a given elevation slice may compare near-surface data from one corner of the survey with much deeper data from other parts of the

survey.

Elevation slices were created from 490 m below sea level to 540 m above sea level at 10 m intervals. Figure 4.6a-d shows a selection of the elevation slices, with: a) 0-10 m; b) 100-110 m; c) 200-210 m; and, d) 300-310 m above sea level. In both Figure 4.6a and Figure 4.6b there are substantial areas of masking due to the DOI, as parts of these slices lie deep below the surface. In Figure 4.6c and Figure 4.6d there is little or no masking from the DOI, but there are still substantial areas of null data values due to the land surface being lower than the elevation slice itself. These null data values are especially prevalent in the north-west, where the surface elevation is significantly lower, and hence much of this area is below the 300 m altitude of the elevation slice.

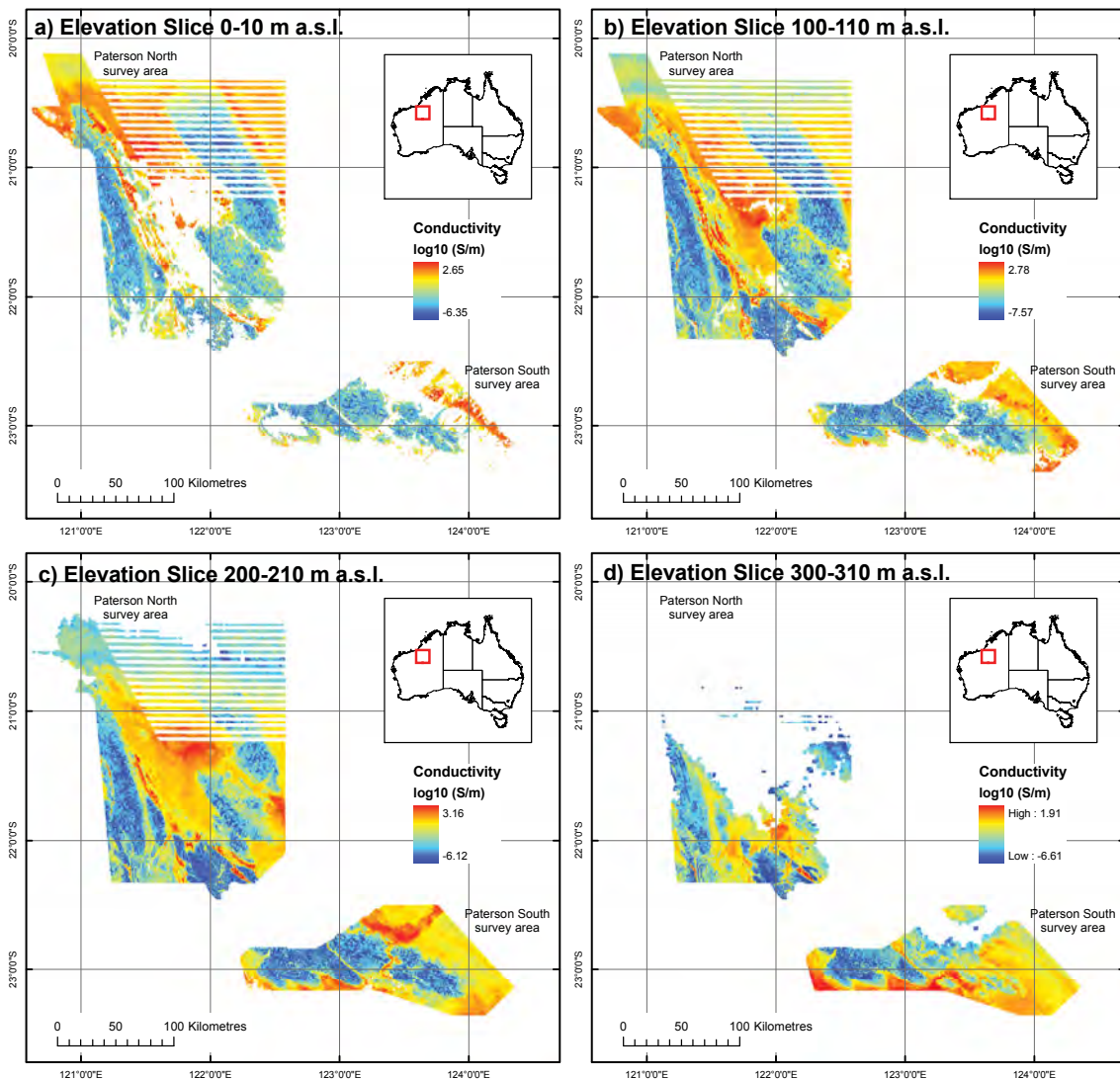


Figure 4.6: Selection of elevation slices, showing: a) 0-10 m above sea level (a.s.l.); b) 100-110 m a.s.l.; c) 200-210 m a.s.l.; and, d) 300-310 m a.s.l.

4.9 SECTIONS

Vertical sections of GA-LEIs and multiplots are provided as a quick reference tool as both georeferenced Joint Photographic Experts Group-format images (JPEGs) and non-georeferenced

multiplots. The PDI is marked in black on the GA-LEI JPEGs and is contained within the associated databases.

4.9.1 Georeferenced JPEGs

The JPEG World File (.jgw) is used to georeference JPEG (.jpg) files. The .jgw files provide coordinate information to the associated file. Each of the Paterson flight lines has a GA-LEI image stored as a JPEG image (.jpg) file and an associated (.jgw) file ([Table 4.4](#)).

Table 4.4: JPEG world file contents for line 10000.

LINE	VALUE
1 x scale (per pixel)	4.225161
2 rotation about y axis	0.020241
3 rotation about x axis	0.020241
4 y scale	-4.225161
5 x reference point	397076.753108
6 y reference point	7541178.552010

Georeferenced JPEGs have been included in the Phase-2 data release as a convenient way to image inversion data in GIS software ([Figure 4.7](#)). A colour scale bar can be found in the georeferenced JPEG data file directory in the data release and applies to all sections ([Figure 4.8](#)).

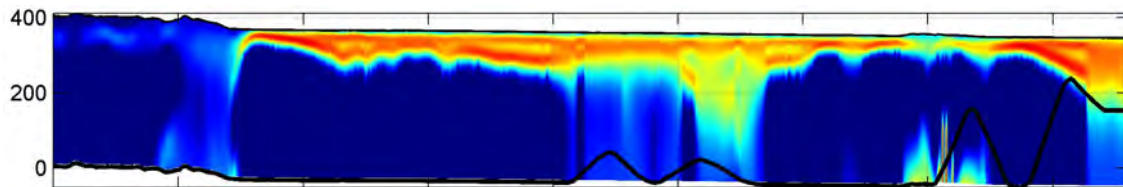


Figure 4.7: Georeferenced JPEG for line 10000. Elevation above sea level is in metres and is labelled on the left hand side of each image. The horizontal scale and real-world coordinate information is provided in the accompanying .jgw world file.

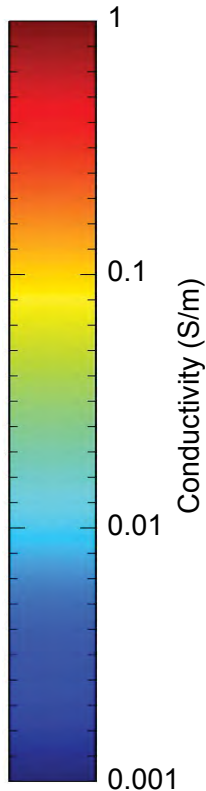


Figure 4.8: Colour scale bar for georeferenced JPEGs.

4.9.2 GA-LEI multiplots

The GA-LEI multiplots (example shown in [Figure 4.9](#)) for the Paterson AEM survey contains a number of panels, described in [Table 4.5](#).

Table 4.5: Panel descriptions for GA-LEI multiplots.

Φ_D	The data misfit of the inversion, the target misfit is less than 1.0.
TX Height	Transmitter height in metres.
TX att	Transmitter attitude in degrees with two traces measuring the pitch and roll.
D_x	Inline horizontal separation between the transmitter and the receiver coils in metres. Two traces measuring the processing estimate and inversion output.
D_z	Inline vertical separation between the transmitter and the receiver coils in metres. Two traces measuring processing estimate and inversion output.
R_p	Receiver pitch in degrees. Two traces measuring the processing assumption and inversion output.
$\text{asinh}(X)$	Window amplitude profiles for X component data (fT) compressed using the asinh function to give an overview of the decay along line for non-geometry corrected data.
$\text{asinh}(Z)$	Window amplitude profiles for Z component data (fT).
GA-LEI	Image in depth below surface (m) with conductivity colour bar in (S/m).
Easting	Labelled every 5000 m.
Northing	Labelled every 5000 m.

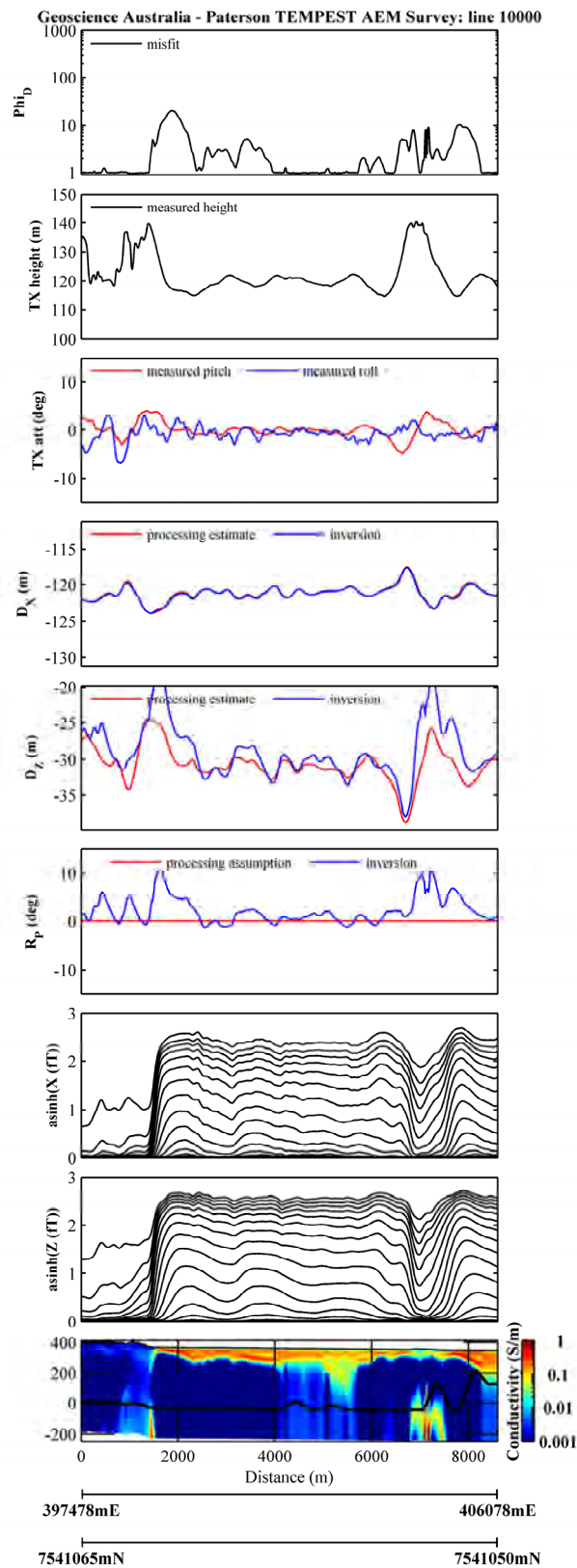


Figure 4.9: GA-LEI multiplot for line 10000.

4.10 COMPARISON WITH CONDUCTIVITY LOGS

4.10.1 Conductivity Logging

A conductivity logging program was conducted in the Paterson survey area to assist the interpretation of the survey data. Some of the company data remain in-confidence and are not expanded upon further in this Record.

Induction conductivity data logs were acquired in boreholes (referred to as conductivity logs) during September 2008 in support of the Paterson AEM survey. The logs were acquired from a number of widespread boreholes across different geological units. The logs were used to assist in generating reference models for geophysical inversions of the AEM data, as well as allowing the results of those inversions to be assessed against an independent dataset (Sorensen, 2008).

Nineteen boreholes distributed across the Paterson North area were logged with an induction conductivity logging tool. No boreholes in the Paterson South area were logged because there were no open holes available at the time of the fieldwork. Three boreholes were located at Telfer mine (Newcrest), five were at the Woodie Woodie mine (Consolidated Minerals) and two were waterbores located on Telfer Access Road. The remaining bores were either waterbores or exploration bores at and around the Nifty mine (Aditya Birla). Most of the holes were cased with PVC, but a few were open, un-cased holes. The majority of the holes had steel casing in the top 6 m (Sorensen, 2008). [Table 4.6](#) provides location coordinates and depths of the logged boreholes and [Figure 4.10](#) shows the location of the logged boreholes plotted over the conductance from 0-200 m. The five logs collected at Woodie Woodie are in-confidence, and are not displayed.

Table 4.6: Coordinates (MGA94 Zone 51) and depths of the 19 conductivity-logged boreholes.

BOREHOLE	EASTING	NORTHING	DEPTH (m)
08DKRCD011	348403	7657601	428
08DKRCD012	348074	7657600	561
08FCHDD002	361302	7590049	285
THRP155	356024	7600376	119
THRP161B	358531	7600035	159
THRP162D	351524	7603738	60
Waterbore B	351524	7604678	125
YNC219	352665	7603678	200
YNC224	352750	7603643	100
WW1	In confidence	In confidence	101
WW2	In confidence	In confidence	120
WW3	In confidence	In confidence	39
WW4	In confidence	In confidence	120
WW5	In confidence	In confidence	62
HB405	373788	7624508	46
HB419	307618	7643890	34
HB326	423671	7589789	148
HB315	420467	7590932	150
HB227	416363	7602972	156

Induction conductivity logging tools measure the electrical conductivity of the material surrounding the borehole and provide a detailed indication of changes in conductivity with depth. These tools permit measurements of the electrical conductivity of the ground outside PVC cased boreholes, generally without being sensitive to the presence of more conductive borehole fluid within the casing. These tools are capable of making reliable scientific measurements, however, their method of use has not been standardised. The principle of operation of induction conductivity borehole logging

tools and other conductivity logging information can be found in McNeill (1986), McNeill *et al.* (1990), Appendix 3.5 and also Sorensen and Lane (2007b).

In order to assess the predictions of the inversion, we compare the results of the GA-LEI at selected points to the borehole conductivity logs collected in the survey area. Since there are only 19 borehole logs compared to 29 000 line km of AEM data, this validation applies to only a small sample of the inversion.

An example of the results of these comparisons for the 14 publicly available conductivity logs are shown in Figure 4.11. The remainder of the comparisons are included in Appendix 3.6. Each borehole log is compared to the inversion of the nearest AEM line data sample. On each plot, “PhiD” quantifies the data misfit of the inversion (the target misfit is less than 1.0), and “distance” represents the distance from the nearest point of the inversion to the borehole location. The distances vary from 137 m to 769 m, and the average distance is 441 m. These distances are generally larger than the footprint of the AEM signal, thought to be approximately 470 m (Reid and Vrbancich, 2004). Since the conductivity logs are on average located outside the AEM system footprint, a square of side length 470 m (Reid and Vrbancich, 2004), and the conductivity logs only has a footprint of approximately 4 m, the comparisons should be treated as indicative only.

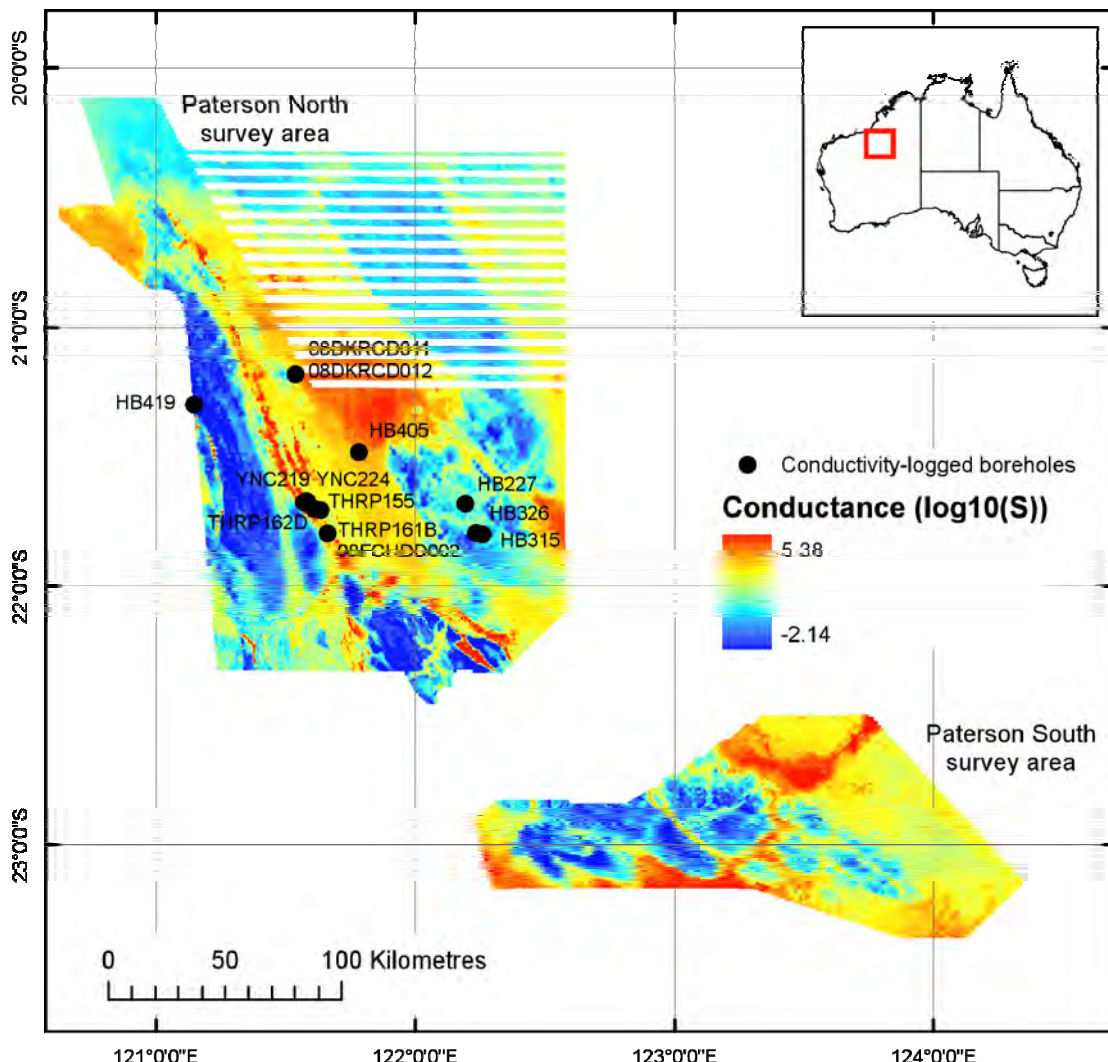


Figure 4.10: Location of conductivity-logged boreholes plotted over 0-200 m conductance.

Generally, the GA-LEI results show agreement with the borehole logs in close proximity to flight lines. The GA-LEI results are smoother than the borehole logs, due to the vertical smoothness constraints of the GA-LEI.

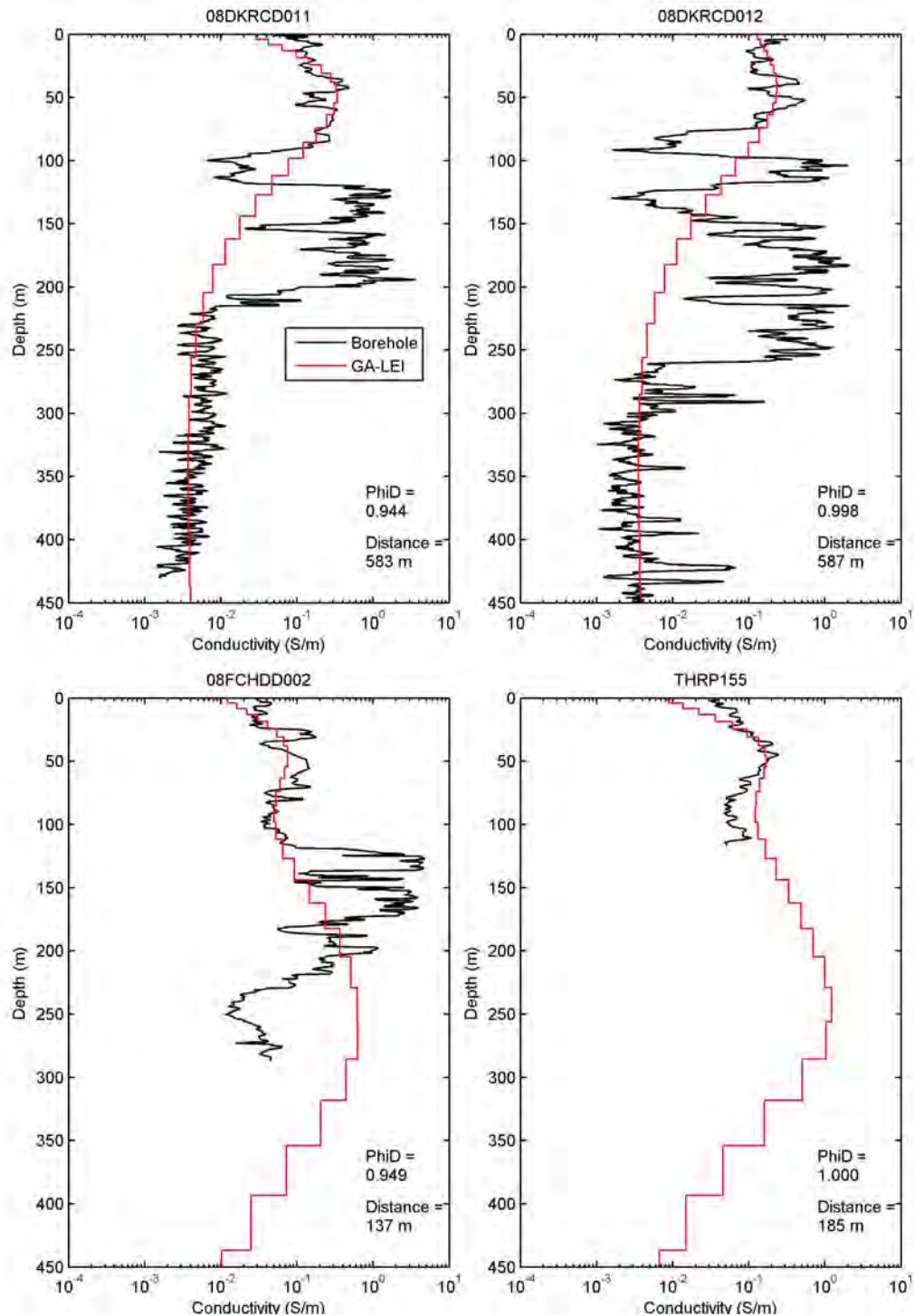


Figure 4.11: Conductivity logs compared to GA-LEI results.

4.11 REFERENCES

- Brodie, R. and Fisher, A., 2008. Inversion of TEMPEST AEM survey data, Honeysuckle Creek, Victoria. Geoscience Australia for the Bureau of Rural Sciences, Canberra. Unpublished.
- Constable, S., Parker, R. and Constable, C., 1987. Occam's inversion; a practical algorithm for generating smooth models from electromagnetic sounding data. *Geophysics* **52**, 289-300.
- Hutchinson, D. K., Costelloe, M. T., Roach, I. C. and Sorensen, C., 2010. Paterson TEMPEST AEM Survey, Western Australia, 2010 Final Inversion Data and Conductivity Models. Geoscience Australia, Canberra. Unpublished report. Online: https://www.ga.gov.au/products/servlet/controller?event=GEOCAT_DETAILS&catno=70297.
- Hutchinson, D. K., Roach, I. C. and Costelloe, M. T., 2010a. Reducing Exploration Risk for Airborne Electromagnetic Surveys in the Paterson Region, WA and Pine Creek, NT. In: *Australian Society of Exploration Geophysicists Abstracts*, Sydney.
- Hutchinson, D. K., Roach, I. C. and Costelloe, M. T., 2010b. Depth of Investigation Grid for Regional Airborne Electromagnetic Surveys. *Preview April 2010(145)*, 38-39.
- Lane, R., Brodie, R. and Fitzpatrick, A., 2004a. Constrained inversion of AEM data from the Lower Balonne area, Southern Queensland, Australia. Cooperative Research Centre for Landscape Environments and Mineral Exploration, Perth. Open File Report 163. Online: <http://crcleme.org.au/Pubs/OPEN%20FILE%20REPORTS/OFR%20161-162-163-164-166-167/OFR163.pdf>.
- Lane, R., Brodie, R. and Fitzpatrick, A., 2004b. A revised inversion model parameter formulation for fixed wing transmitter loop – towed bird receiver coil time-domain airborne electromagnetic data. In: *ASEG 17th Geophysical Conference and Exhibition*, Sydney.
- Lane, R., Green, A., Golding, C., Owers, M., Pik, P., Plunkett, C., Sattel, D. and Thorn, B., 2000. An example of 3D conductivity mapping using the TEMPEST airborne electromagnetic system. *Exploration Geophysics* **31(2)**, 162-172.
- Lane, R. and Worrall, L., 2002. Interpretation of Airborne Electromagnetic Data: Summary report on the Challenger Workshop. Geoscience Australia Gawler Craton Mineral Promotion Project Canberra. **Geoscience Australia Record 2002/2**.
- Lawrence, M. and Stenning, L., 2007a. Paterson North Airborne Electromagnetic (AEM) Mapping Survey Acquisition and Processing Report for Geoscience Australia. Unpublished report.
- Lawrence, M. and Stenning, L., 2007b. Paterson South Airborne Electromagnetic (AEM) Mapping Survey Acquisition and Processing Report for Geoscience Australia. Unpublished report.
- Macnae, J., King, A., Stoltz, N., Osmakoff, A. and Blaha, A., 1998. Fast AEM processing and inversion. *Exploration Geophysics* **29**, 163-169.
- McNeill, J. D., 1986. Geonics EM39 borehole conductivity meter-theory of operation. Geonics Ltd, Mississauga, Ontario. **Technical Note 20(11)**. Online: <http://www.geonics.com/pdfs/technicalnotes/tn20.pdf>.
- McNeill, J. D., Bosnar, M. and Snelgrove, F. B., 1990. Resolution of an electromagnetic borehole conductivity logger for geotechnical and ground water applications. Geonics Limited, Mississauga, Ontario. Technical Note TN-25, 29 p. Online: <http://www.geonics.com/pdfs/technicalnotes/tn25.pdf>.
- Reid, J. E. and Brodie, R. C., 2006. Preliminary inversions of Honeysuckle Creek airborne electromagnetic data: Comparison with borehole conductivity logs and previously derived conductivity models. Geoscience Australia for the Bureau of Rural Sciences. Unpublished report.
- Reid, J. E. and Vrbancich, J., 2004. A comparison of the inductive-limit footprints of airborne electromagnetic configurations. *Geophysics* **69**, 1229-1239.
- Smith, R. S., 2001. On removing the primary field from fixed wing time-domain airborne electromagnetic data: some consequences for quantitative modelling, estimating bird position and detecting perfect conductors. *Geophysical Prospecting* **49**, 405-416.
- Sorensen, C., 2007. Assessment of AEM systems for the Paterson survey. Geoscience Australia. Unpublished report.
- Sorensen, C., 2008. Logistics report for down-hole conductivity logging in the Paterson AEM

- Survey area, Western Australia, September 2008. Geoscience Australia. Unpublished report.
- Sorensen, C. and Lane, R., 2007b. Guidelines for conductivity borehole logging procedures. Geoscience Australia. Unpublished report.
- Stoltz, E. and Macnae, J., 1998. Evaluating EM waveforms by singular-value decomposition of exponential basis function. *Geophysics* **63**, 64-74.

5 Interpretations of AEM data

I. C. Roach, M. T. Costelloe and D. K. Hutchinson

5.1 INTRODUCTION

This chapter describes and discusses interpreted correlations between the AEM data and geological features known from surface regolith and geological mapping, solid geology interpretation and other geophysical data sets.

5.2 DETERMINE “FIT-FOR-PURPOSE”

Predicting Earth conductivities from measured electromagnetic responses depends on window amplitudes, terrain clearance, aircraft attitude and estimates of changes in transmitter loop-to-receiver coil geometry, as described in [Chapter 4](#) and [Appendix 3.2](#). Before interpreting AEM data, it must be determined whether they are fit-for-purpose and contain sufficient information to justify being modelled and interpreted according to the survey objectives. To achieve this Geoscience Australia (GA) continually assessed the contractor’s supplied data during survey flying and completed a data check list prior to inverting the data. The project geophysicist worked with the contractor to resolve any problems or discrepancies between delivered data and the contractual specifications.

5.2.1 Quality control and quality assurance of the contractor supplied data

The contractor performed numerous compensations and calibration flights in accordance with industry best practice. The validation of electromagnetic calibration, navigation and flight path recovery, magnetic, diurnal, altimeter, RADAR, LASER, barometer, thermometer, video tracking and elevation data are conducted by the contractor and GA assessed the results prior to quality assurance and quality control (QA-QC) of the AEM data. The QA-QC checks on the Paterson AEM dataset, once flying was complete, are summarised in [Table 5.1](#).

High altitude (zero-level) flights are used to characterise system noise in the absence of any ground effect. The high-altitude noise is considered as two components:

1. The mean of the processed data in each channel, that is, the window and component combination is calculated and termed the ‘bias’; and,
2. The standard deviation of the processed data in each channel which is calculated and termed the ‘additive noise’.

The high altitude noise analysis of the data revealed that flights 13, 23 and 29 contained above-average values in window 14 and 15, but the noise was still within acceptable levels. Additive noise analysis is summarised in [Tables 5.2a](#) and [b](#). The additive noise is used as an input into the GA Layered Earth Inversion (GA-LEI).

Repeat line data is used to characterise the system noise at the specified survey altitude. The repeatability of the processed data is used to calculate the multiplicative noise for the survey (Green and Lane, 2003). For this survey multiplicative noise for the X component is calculated to be 2.9%, and Z component multiplicative noise is calculated to be 3.11%. The multiplicative noise is an input parameter in the GA-LEI.

Flight path checks confirmed that no lines deviated more than 40 m off course over a continuous distance of 1500 m from the planned flight path.

The terrain clearance contract specification was that the average terrain clearance for any one flight

should be within ± 5 m of the nominal aircraft terrain clearance (121 m). Several lines were outside this specification, for example:

- Line 10390 due to large sand dunes; and,
- Lines 30860 and 30890 due to overflying the Nifty and Telfer mine pits.

Other lines with the mean transmitter height above or below the contract specifications occurred in areas of hilly topography.

Table 5.1: Quality control and quality assurance steps.

NUMBER	DESCRIPTION
1	Check that all data has been delivered against contract specifications.
2	Check data has been supplied (format and detail) as per contract.
3	Noise analysis of high altitude data (X and Z component): <ul style="list-style-type: none"> • Calculate the additive noise, standard deviation and bias noise.
4	Repeat line analysis on repeat lines: <ul style="list-style-type: none"> • Calculate multiplicative noise estimates and assess system repeatability.
5	Create survey line database and assess statistics on all fields: <ul style="list-style-type: none"> • Note number of nulls, minimum, maximum, average.
6	Check flight path: <ul style="list-style-type: none"> • That all lines are flown, in the right direction, in the right location, that no flight line is more than 40 m off course over a continuous distance of 1500 m or more unless the deviation is required by civil aviation requirements.
7	Check flight path and terrain clearance: <ul style="list-style-type: none"> • The average transmitter terrain clearance for any one flight line shall be within ± 5 m of the nominal transmitter terrain clearance.
8	Check altimeter corrections: <ul style="list-style-type: none"> • Compare LIDAR and RADAR altimeters.
9	Assess GPS height field: <ul style="list-style-type: none"> • Corrected altimeter-nvalue \approx SRTM DEM or gravity spot heights.
10	Grid elevation and magnetics: <ul style="list-style-type: none"> • Assess for nulls, level shifts and coherency.
11	Grid non-height-pitch-roll-geometry (HPRG) corrected and HPRG windows: <ul style="list-style-type: none"> • Assess for nulls, level shifts and coherency.
12	Grid all monitor channels: <ul style="list-style-type: none"> • Assess for nulls, level shifts.
13	Compute and tabulate minimum, maximum, mean and standard deviation of transmitter height (tx_height), transmitter-received x-separation distance (txrx_dx) and transmitter-receiver z-separation distance (txrx_dz) for each line, each flight and whole survey and assess.
14	Assess EM Flow™ HPRG data: <ul style="list-style-type: none"> • Compare to drill hole data, known geology and geological targets.
15	Multiplot assessment: <ul style="list-style-type: none"> • For noise, interpretability and data consistency.
16	Check the logistics report and associated metadata.
17	Conductivity Logging: <ul style="list-style-type: none"> • Compare conductivity logs to geology.
18	GA layered earth inversion (GA-LEI) inversion: <ul style="list-style-type: none"> • Assess inversion parameters and compare to <i>a priori</i> information.

Corrections to the RADAR and LIDAR were applied accurately by the contractor; it was found that the final contractor supplied elevation equalled the GA calculated elevation (GPS height - corrected

LIDAR altimeter minus the nvalue) to within 0.2 m. The final elevation approximates the AUSLIG 9 second DEM to within 0.26 m, and the SRTM 1 second DEM to within 3.3 m. The GPS height field was within 0.2 m of the GA calculated DTM (assuming the GPS-to-LIDAR sensor offset is 2.3 m).

Table 5.2a: X component additive noise (standard deviation of high altitude data) for the Paterson survey.

X WINDOW NUMBER	ADDITIVE NOISE (FT) SURVEY DATA	ADDITIVE NOISE CONTRACT SPECIFICATIONS (FT)
1	0.0108	0.0362
2	0.0079	0.0348
3	0.0077	0.0315
4	0.0057	0.0260
5	0.0049	0.0238
6	0.0049	0.0206
7	0.0046	0.0190
8	0.0044	0.0182
9	0.0042	0.0176
10	0.0042	0.0174
11	0.0043	0.0170
12	0.0048	0.0163
13	0.0033	0.0146
14	0.0023	0.0126
15	0.0024	0.0134

Table 5.2b: Z component additive noise (standard deviation of high altitude data) for the Paterson survey.

Z WINDOW NUMBER	ADDITIVE NOISE (FT) SURVEY DATA	ADDITIVE NOISE CONTRACT SPECIFICATIONS (FT)
1	0.0072	0.0267
2	0.0063	0.0160
3	0.0056	0.0141
4	0.0042	0.0134
5	0.0041	0.0122
6	0.0041	0.0123
7	0.0038	0.0117
8	0.0037	0.0118
9	0.0035	0.0110
10	0.0032	0.0102
11	0.0032	0.0099
12	0.0028	0.0084
13	0.0023	0.0075
14	0.0016	0.0070
15	0.0021	0.0087

The simplest method to assess the AEM and associated noise and magnetic fields is to grid the survey data. Gridded data was used to check for data spikes, along-line data level shifts (drift) and system noise within flights. The EM Flow™ software conductivity depth interval (CDI) sections provided by the contractor for field data and repeat line analysis were also assessed for data coherency, relevance to known geology and noise.

Multiplot assessment was another important step in the quality control and interpretation of the Paterson AEM data. The contractor-supplied multiplots are a visual representation of relevant data in one frame at the highest possible resolution. They contain line data that has not been re-sampled and smoothed, unlike data in a gridded format. Discrete conductors are most effectively interpreted from line data presented in this multi-panel stacked profile format. However, multiplots can also be used to assess artefacts that result from noise, system geometry and topography. For the Paterson AEM survey the multiplots delivered contain seven information panels ([Figure 5.1](#)). The individual panels in the multiplot are described in [Table 5.3](#).

Table 5.3: Panel descriptions for sample multiplot in [Figure 5.1](#).

PANEL (FROM THE TOP)	DESCRIPTION
1. Transmitter data	Terrain clearance, pitch and roll of the transmitter.
2. X EM monitors	X component monitor values tracking sferics, coupling to the transmitter loop, low frequency signals induced by variations in the coupling of the receiver coils with the ambient magnetic field, powerline noise and coupling with VLF transmissions.
3. X Component data	X component window amplitude profiles compressed using an asinh function. HPRG and non-HPRG profiles are plotted.
4. Z EM monitors	Z component monitor values tracking sferics, coupling to the transmitter loop, low frequency signals induced by variations in the coupling of the receiver coils with the ambient magnetic field, powerline noise and coupling with VLF transmissions.
5. Z Component data	Z component window amplitude profiles compressed using an asinh function. HPRG and non-HPRG profiles are plotted.
6. Conductivity Depth Image	EM Flow™ conductivity depth section Z component.
7. Magnetic data	Total magnetic intensity (TMI) and 1st vertical derivative TMI.
8. Location	Easting and northing information.

The multiplot panels are arranged to aid interpretation as well as being a quality control tool. The ability to assess if a response in the X and Z component is geological, or is just a variation in system geometry, topography or noise, is invaluable. Primary sources of EM noise include sferics, powerlines, VLF transmissions, electric fences and man-made metal objects on or just under the ground such as sheds, mining structures or pipes.

In the top panel of [Figure 5.2](#) the transmitter terrain clearance pitch and roll varies along the line, significantly affecting the signal response. The panel second from the top shows sferic “spikes” along the base in a black trace. Panel three shows the X component height-pitch-roll-geometry (HPRG) corrected data in colour and non-HPRG data in black.

[Figure 5.3](#) is an example of weakly elevated conductivity artefacts apparently linking near-surface flat-lying conductors to each other within the CDI section. The artefacts are a result of 1D algorithm limitations in EM Flow™ and the GA-LEI, as well as the AEM system footprint (Sattell, 2004) and noise.

Metadata attached to the survey data are assessed for accuracy to facilitate data exchange and archiving between organisations with different hardware and software systems. Details such as a text descriptions of the data and survey parameters, map datum and projection details, field names, units of measurement, format, comments and missing data substitution values (nulls) are essential for the usefulness and longevity of the dataset. The metadata text describes the survey database which is in simple, multi-column ASCII files.

Geological and energy implications of the Paterson Province airborne electromagnetic (AEM) survey, Western Australia

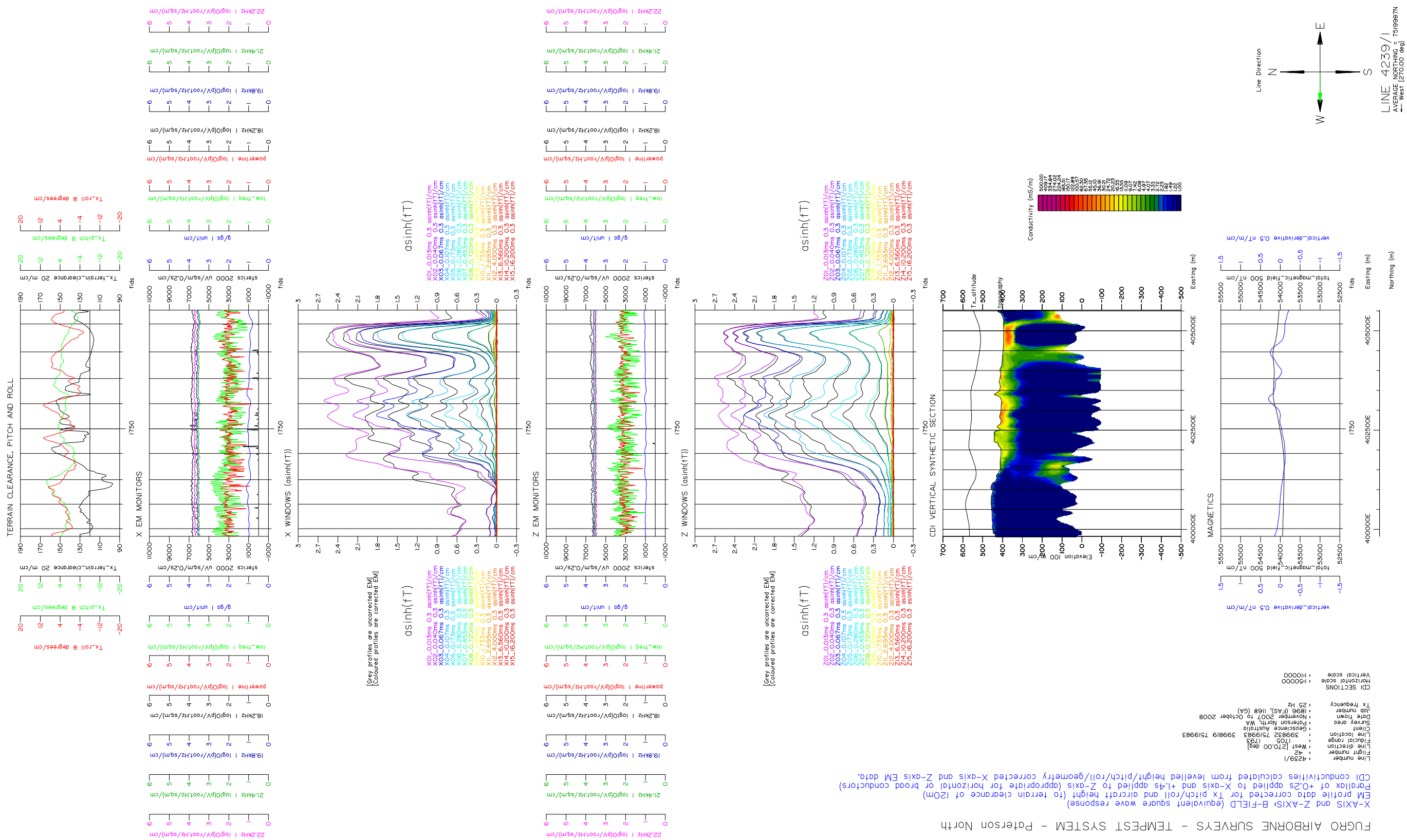


Figure 5.1: An example of a multiplot from the Paterson survey.

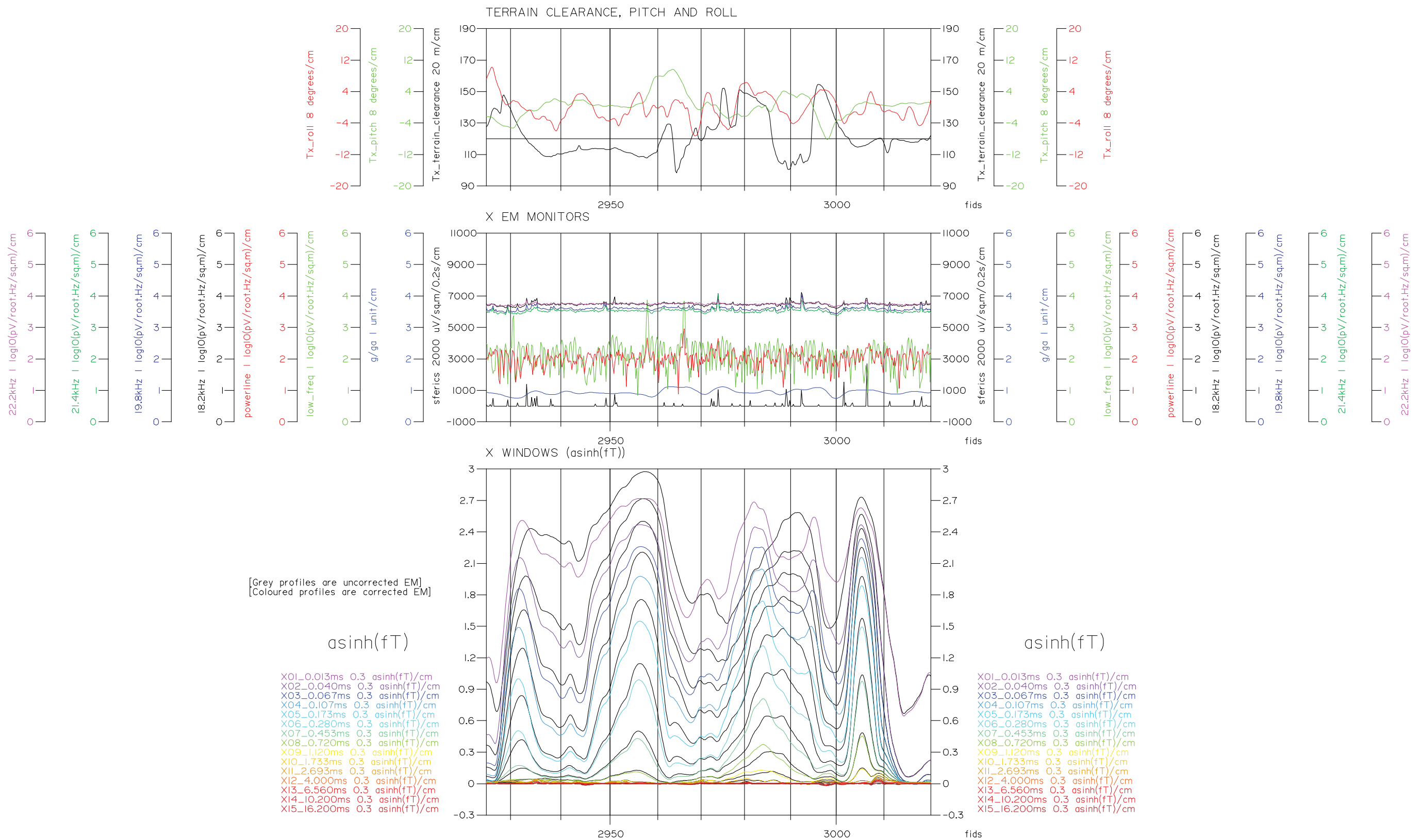


Figure 5.2: Subsection of multiplot for line 42321. In the bottom panel, the HPRG-corrected data are displayed in colour, non-corrected data are displayed in black.

The accuracy, integrity and useability of AEM data are reliant on many factors including topography, system geometry, noise and location. Successful QA-QC of all these factors allows the data to be deemed “fit-for-purpose”. The QC steps undertaken in this survey assessed the data as being fit to be interpreted, inverted and manipulated. Fit-for-purpose data provides the highest standard of information for successful exploration decision-making.

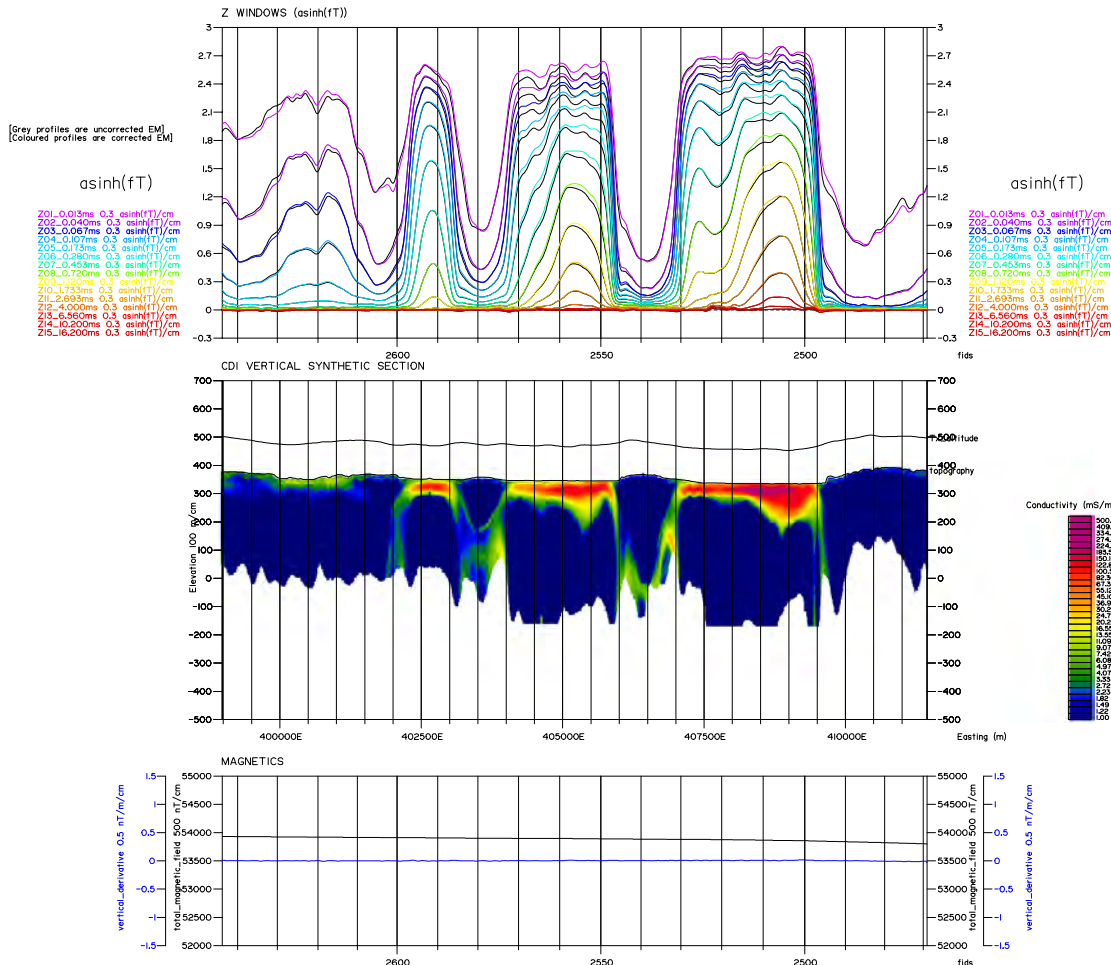


Figure 5.3: Subsection of multiplot for line 43530. The rapid change in system response produces artefacts in the CDI section. These artefacts occur where the EM FlowTM transform misrepresents the sharp contact between a near surface conductor and the resistor surrounding it. Notice in the bottom panel there is no magnetic signal associated with these near-surface conductors.

5.2.2 Depth of Investigation grid

A key objective of this analysis was to determine where AEM surveys are likely to be effective as an aid to exploration in the Paterson Region. Airborne electromagnetic surveys carry an inherent risk, as the depth of penetration of the signal is highly variable. Furthermore, AEM surveys are relatively expensive compared to other geophysical techniques. The Depth of Investigation (DOI) grid presented in Chapter 4 reduces the risk for further AEM and ground EM surveys in the Paterson region by showing where AEM and ground EM systems are likely to penetrate to a usable depth.

The DOI tends to be shallower in conductive regions and deeper in resistive regions. This correlation can be seen by comparing the DOI grid (Figure 4.4) with the shallower conductivity depth slices shown in Figures 4.5a and 4.5b. Conductive material creates a stronger secondary field response

than resistive material, and this strong secondary response reduces the penetration of the AEM signal. The shallowest values of DOI (less than 100 m) are around salt lakes, since these provide a highly conductive layer that masks signals from any resistive material below.

The DOI also tends to be shallower in palaeochannels, since they are relatively conductive. However, since much of the surrounding material is resistive, the DOI returns to deep values (up to 400 m) at the edges of the many of the palaeochannels. Thus the horizontal extents of the palaeochannels are well mapped, even though the AEM signal has shallower penetration in the centre of the channels. Similarly it is possible to map other conductive features where there are strong contrasts with neighbouring resistive rocks.

The DOI grid can also be used to estimate the effectiveness of AEM surveys in areas outside of the Paterson region, where geological units have similar conductivities. An accurate down hole conductivity logging assessment and comparison of the conductivity signatures within a tenement to the Paterson DOI can be used as an interpretative tool reducing risk when planning an AEM survey.

5.3 METHODS USED TO DEFINE CORRELATIONS

A variety of geological and geophysical data sets were used to validate the AEM data set. These include:

- Drill holes: a publicly-available drill hole compilation (Roach, 2009);
- Solid geology: a compilation by Czarnota *et al.* (2009a; 2009b);
- Surface geology: the 1:1 000 000 scale Surface Geology of Western Australia (Stewart, 2008);
- Magnetics: GA Magnetic Map of Australia compilation (Percival, 2010);
- Gravity: GA gravity compilation (Bacchin *et al.*, 2008; Wynne and Bacchin, 2009);
- Radiometrics: GA Radiometric Map of Australia (Minty *et al.*, 2008; 2009); and,
- Conductivity logs (see [Section 4.11](#)).

Correlations were interpreted between conductivity sections and conductivity grids (conductivity depth slices and conductivity elevation slices; [Figures 5.4](#) and [5.5](#)) from the AEM data set and the geological and geophysical data sets mentioned above. Data were added to a GIS project, allowing individual layers to be switched on and off or made transparent. Drill hole data were used to validate the geological interpretations. Graphic representations of drill hole logs were added to conductivity sections, allowing for the rapid interpretation of conductivity anomalies and validation of the AEM data ([Figures 5.6](#) and [5.7](#)).

Conductivity sections and conductivity grids were added as georegistered raster images and could be displayed as stacked sections or grids, together with other geological and geophysical data. The conductivity sections were very high resolution, with X (horizontal) and Z (vertical) pixel sizes of 12.5 and 5 m respectively. Conductivity grids were lower resolution, commonly 300 m in the X (east) and Y (north) directions for 6, 2 and 1 km line spacing data, but higher-resolution (50 m) grids were used where flight line spacing was 200 m in infill areas. The AEM data set resolutions are detailed in [Table 5.4](#).

Table 5.4: XYZ resolutions of AEM raster data sets used for validation and correlation.

DATA SET	X (m)	Y (m)	Z (m)	PROJECTION
Conductivity elevation slices	300	300	-	X-Y: MGA Z51; Z: mean sea level
Conductivity depth slices	300	300	-	X-Y: MGA Z51; Z: aircraft DEM
Conductivity sections	12.5	-	5	X-Y: MGA Z51; Z: Mean sea level

Broad correlations between the AEM data and geological features were noted in the conductivity sections and conductivity grids. A number of unconformities were recognised within the AEM data set, the most prominent being the sub-Permian unconformity that separates Archean and Proterozoic rocks of the Pilbara Craton, Rudall Complex and Yeneena Basin from Permian and younger sediments of the Canning Basin (see [Section 5.5](#)). The unconformity between the Coolbro Sandstone and the Rudall Complex (the Coolbro-Rudall unconformity), which is important for uranium systems models in the Paterson area (see [Section 5.6](#)), was also located during the interpretation phase of this project. Where possible, as indicated by the DOI grid ([Figure 4.4](#)), the pre-Permian unconformity surface was interpreted and contoured from the 300 m gridded conductivity elevation slices using average sea level as the datum. Where necessary, contours were also interpreted from the conductivity sections, which allowed for a much higher-resolution interpretation of the unconformity elevation. The contours are presented in [Section 5.5](#). Details of the Coolbro-Rudall unconformity are presented as sections only because it occurs on too few sections to be accurately contoured in 3D.

5.4 GEOLOGICAL VALIDATION OF THE AEM DATA

The AEM data set was geologically validated using surface geology, solid geology and drill hole data. Gridded conductivity depth slice and conductivity elevation slice data were initially displayed against surface geology (Stewart, 2008) and solid geology (Czarnota *et al.*, 2009a; 2009b) to highlight areas where conductivity anomalies could be correlated to large geological features. In the surface conductivity depth slice ([Figure 5.4](#)) most surface conductivity anomalies correlate to known salt lakes and (palaeo)drainage systems. Some of the other surface conductivity anomalies do not correlate to known lake or (palaeo)drainage features and are discussed further in the sections below.

The solid geology interpretation of Czarnota *et al.* (2009a; 2009b) was used to help interpret deeper features in the GA-LEI conductivity depth slices, conductivity elevation slices and conductance images ([Figure 5.5](#)). In this example, the 0-400 m conductance image illustrates the correlation between conductive features and Neoproterozoic units under cover near the Nifty copper mine. Conductive features are mostly associated with interpreted geological units that are known to be conductive from rock property data collected from surface exposures in other areas, particularly the carbonaceous and pyritic parts of the Broadhurst Formation (NYbc in [Figure 5.5](#)).

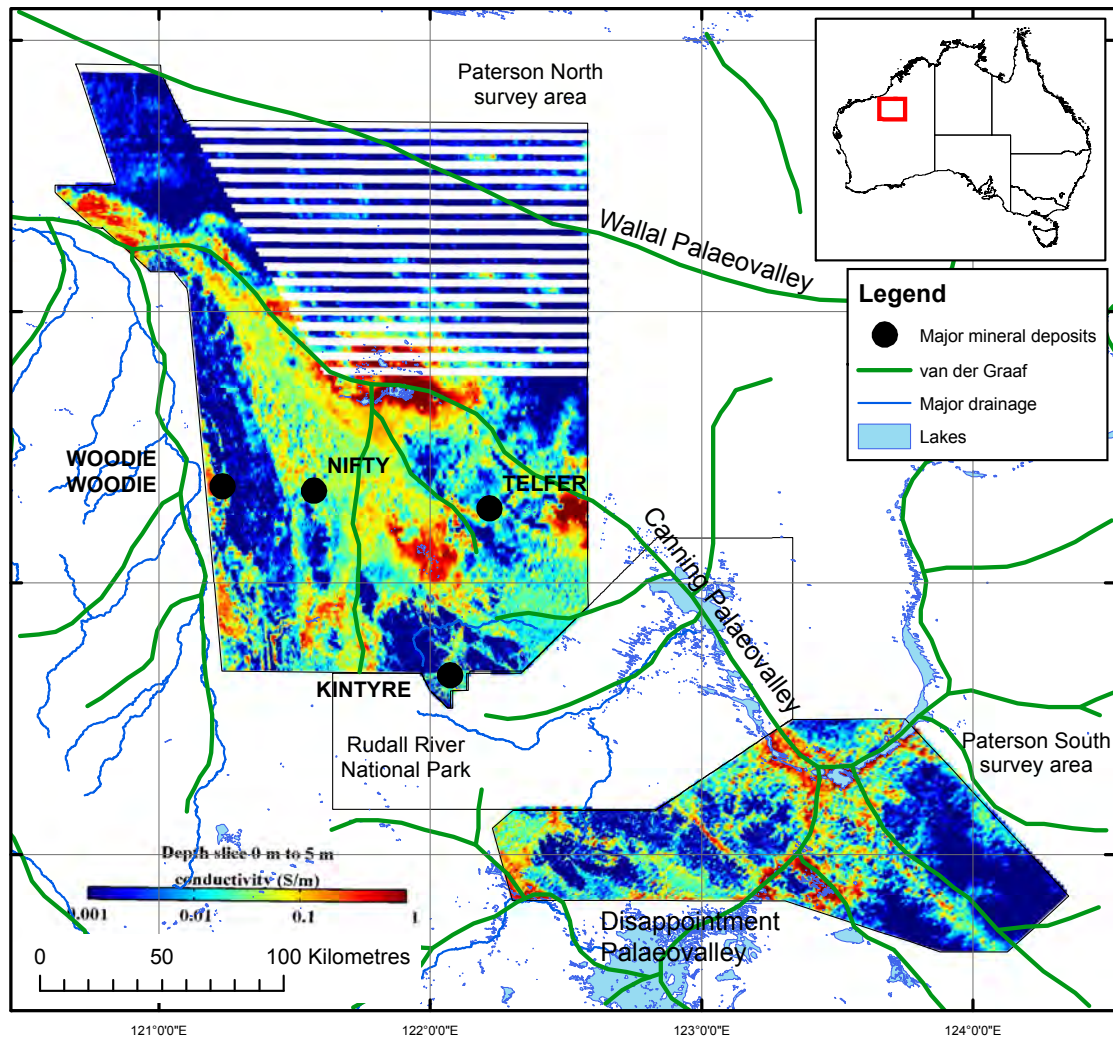


Figure 5.4: 0-5 m GA-LEI conductivity depth slice overlain by surface features including lakes from the 1:1 000 000 Surface Geology of Western Australia (Stewart, 2008) and the interpreted palaeovalley net from van der Graaf et al. (1977).

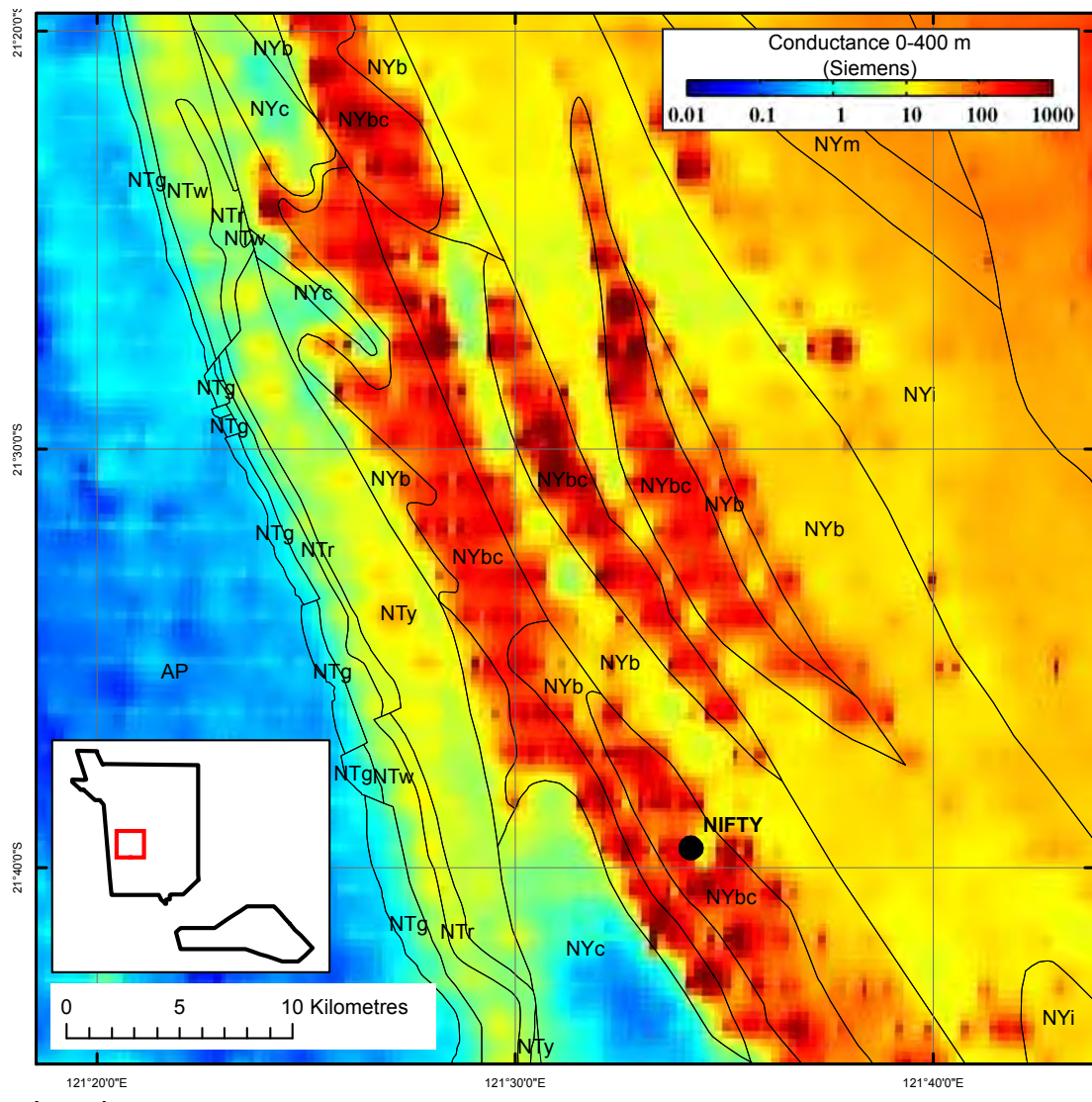


Figure 5.5: GA-LEI 400 m \log_{10} conductance image compared to solid geology (Czarnota et al., 2009a; 2009b) highlighting the correlation between conductive features in the Neoproterozoic bedrocks in the Nifty copper mine area with interpreted solid geology derived from magnetic and gravity imagery.

The drill hole database (Roach, 2009) ([Figure 1.5](#)) was used to more accurately validate the AEM data set by comparing individual GA-LEI conductivity sections to drill holes lying near selected flight lines. Drill holes from less than 2.5 km north and south of selected flight lines were overlain on conductivity sections for the validation process. [Figure 5.6](#) illustrates the onlapping relationship between conductive units in the Canning Basin and the Neoproterozoic rocks of the Anketell Shelf. On the western portion of the section Neoproterozoic rocks of the Lamil Group are intruded by Mt Crofton Granite, both of which are resistive. These are overlain by small thicknesses of Permian Paterson Formation, Mesozoic Anketell Sandstone and Cenozoic sand. To the east of the section the Permian and Mesozoic units thicken into the Canning Basin, with two, distinct, flat lying conductors present in the far east of the section. Stratigraphic interpretations of the conductors conforms to knowledge of Canning Basin stratigraphy from drill hole data on the Anketell Shelf and further into the Basin from petroleum exploration drilling.

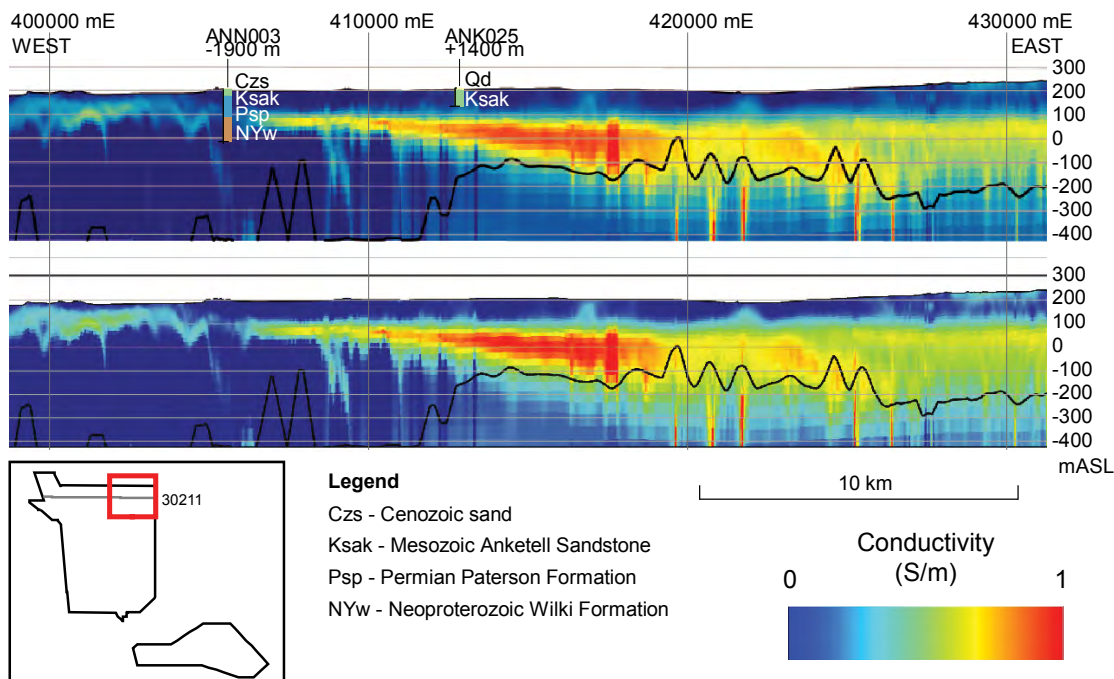


Figure 5.6: GA-LEI conductivity sections for line 30211 with (top), and without (bottom), drill hole graphic logs overlaid. The section shows conductors in Permian and Mesozoic Canning Basin sediments (right) lapping onto Neoproterozoic rocks of the Anketell Shelf (left). Numbers quoted below drill hole labels indicate the distance the holes lie behind (-, north) and in front (+, south) of the section line.

[Figure 5.7](#) illustrates a more complex bedrock-cover relationship near the Nifty copper mine where moderately resistive Permian Paterson Formation and Permian-Mesozoic Poole Sandstone or Callawa Formation sediments overlie folded and faulted, conductive and resistive Broadhurst Formation rocks. The highly conductive material under cover in the section conforms to the mapped carbonaceous and pyritic shale facies of the Broadhurst Formation, whereas the resistive material conforms to the carbonate-rich or greywacke facies of the Broadhurst Formation.

Overall, the validation process revealed that, where conditions were suitable according to the DOI ([Figure 4.4](#)), conductivities within the AEM data set could be reasonably well-correlated with, and could be explained by, the geological data.

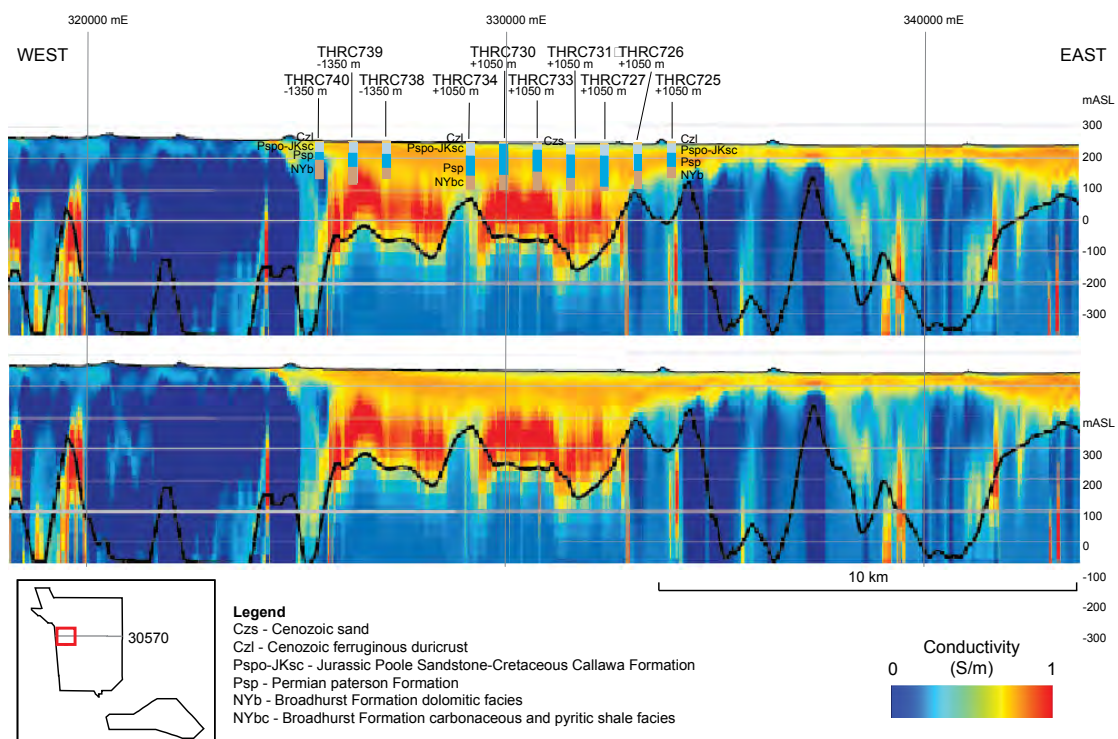


Figure 5.7: GA-LEI conductivity sections for line 30570 with (top) and without (bottom) drill hole graphic logs. Section shows conductive Permian and Mesozoic cover sediments overlying conductive and resistive Broadhurst Formation rocks near the Nifty copper mine. Numbers quoted below drill hole labels indicate the distance the holes lie behind (-, north) and in front (+, south) of the section line.

5.5 BROAD GEOLOGICAL CORRELATIONS

The regional nature of the AEM data set lends itself to the recognition of large-scale geological features within the data, both in sections and grids. A number of the Archean and Proterozoic bedrocks feature prominently in the AEM data because they are either very resistive or are moderately to highly conductive, providing a conductivity contrast between themselves and overlying weakly to moderately conductive cover. So too, a number of cover sequences have reasonable conductivity contrasts with underlying bedrocks, allowing them to be delineated. Figure 4.4 depicts the regional DOI grid of the entire survey highlighting areas where it is possible to interpret regional geological correlations.

A number of significant geological correlations are visible in the gridded conductivity depth slices or conductivity elevation slices. A representative range of these are discussed in the following sections.

5.5.1 Pinjian Chert Member and Jeerinah Formation

The Paleoproterozoic Pinjian Chert Breccia is associated with the manganese deposits of the Woodie Woodie mine. The Jeerinah Formation occurs within the Archean Fortescue Group stratigraphically below the Archean Carawine Dolomite of the Hamersley Group. The Paleoproterozoic Pinjian Chert Breccia unconformably overlies the Carawine Dolomite in palaeokarst depressions (Williams and Trendall, 1998a). Both the Carawine Dolomite and the Pinjian Chert Breccia host manganese deposits in karstic depressions.

The Jeerinah Formation is associated with a linear, arcuate conductivity anomaly in the far west of

the Paterson North AEM data set within the otherwise resistive rocks of the Fortescue Basin (Figure 5.8). The Jeerinah Formation is moderately conductive over much of its length within the conductivity depth slices, conductivity elevation slices, conductivity sections and conductance images. The Jeerinah Formation is a shale-rich unit with intercalated chert, dolomite and basalt. The conductivity anomaly may be more associated with the conductive shales within the unit rather than being a feature of saline groundwaters.

The Pinjian Chert Breccia is associated with a diffuse low to moderate conductivity anomaly in the far west of the Paterson North AEM data set. The conductivity anomaly may result from manganese and iron enrichment within the rock mass.

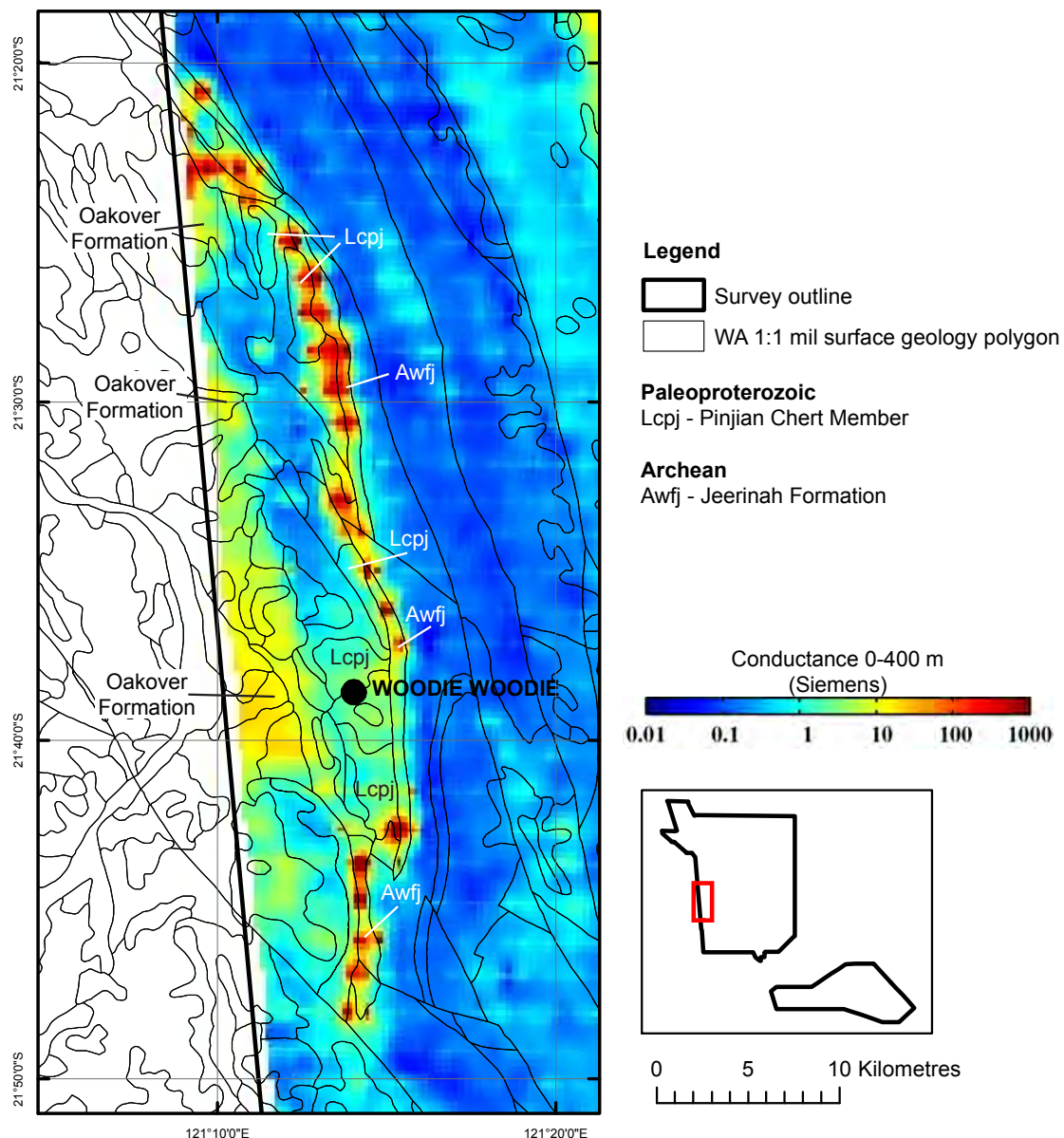


Figure 5.8: Conductive Jeerinah Formation and Pinjian Chert Member highlighted in the 0-400 m GA-LEI conductance image. Conductive Tertiary Oakover Formation occurs along the survey boundary. Geological polygons are from the Surface Geology of Western Australia (Stewart, 2008).

5.5.2 Rudall Complex

The Rudall Complex consists of Paleoproterozoic rocks including high-grade metamorphic rocks and granitoids of the Connaughton, Tabletop and Talbot terranes (Bagas *et al.*, 2000). The Rudall Complex has limited outcrop over much of its area, with (semi-)continuous outcrop limited more-or-less to the Rudall River National Park and Kintyre areas, consisting of ranges and isolated rises and hills surrounded by Permian, Mesozoic and Quaternary sedimentary cover. Conductivity depth slices and conductivity sections indicate that the Rudall Complex has low overall bulk conductivity. However, some units within the Rudall Complex are graphite-bearing, and these units will have moderate to high conductivity. There are a number of discrete conductors associated with the Rudall Complex, especially in the Yandagooge Formation near Kintyre (see [Chapter 6](#)), which do suggest the presence of graphite-bearing units.

[Figure 5.9a](#) shows the 0-10 m conductivity depth slice over the Rudall Complex area. Continuous outcrop is limited largely to the Connaughton and the Talbot terranes, consisting mostly of numerous small ranges or "islands" of outcrop surrounded by cover. There are numerous small conductors occurring with dendritic shapes over outcrop that reflect conductive sediments in Quaternary surface drainage. The dendritic patterns are especially noticeable in the high-resolution data within the infill areas around Kintyre and in the Connaughton Terranes in the Paterson South survey area. The bulk of the Tabletop Terrane in the east is covered by moderately to highly conductive sediments occurring in salt lake systems or Permian and Mesozoic sediments of the Canning and Officer basins. [Figure 5.9b](#) illustrates the 200-210 m conductivity depth slice of the same area and highlights the extent of the resistive Rudall Complex under cover. The complicated, relatively short wavelength magnetic anomalies associated with the Rudall Complex can also be used to help correlate the extent of the Rudall Complex under cover ([Figure 5.10](#)). In this image it is noted that the magnetic anomalies are strongly correlated with the conductivity anomaly associated with the under-cover extension of the Rudall Complex, confirming that it extends much further to the southeast than is shown in surface mapping. The magnetic anomalies also show sharp, fault-related boundaries along the southern margin of the Tabletop Terrane. The unconformity surface between the Permian and Proterozoic cover can be traced with some certainty to a depth of over 300 m below surface in this area, as shown in a perspective view of the southeastern Rudall Complex (see [Section 5.5.5](#) and [Figure 5.15](#)). The AEM data can be used to validate depth to magnetic basement modelling in this region (Czarnota *et al.*, 2009a; 2009b), adding certainty to both geophysical data sets.

5.5.3 Broadhurst Formation

The Broadhurst Formation of the Neoproterozoic Throssell Range Group is one of the most important geological units in the Paterson region for its uranium and copper mineral potential (discussed in [Chapter 6](#)). The Broadhurst Formation consists of two major facies: a greywacke ±dolomite facies; and, a carbonaceous, pyritic black shale facies (Hickman and Clarke, 1994), which hosts the Nifty copper deposit and numerous other base metal prospects. The black shale facies is highly conductive and is easily recognised within the AEM data set.

The Broadhurst Formation outcrops sporadically along the length of the Throssell Range, continuing to the west and north of the Rudall Complex, however, much of it is covered by Permian and Mesozoic sediments. [Figure 5.11](#) illustrates the overall extent of the conductivity anomalies associated with the black shale facies of the Broadhurst Formation under cover within the Paterson North survey area. The black shale facies of the Broadhurst Formation is well correlated to known outcrop patterns on 1:100 000, 1:250 000 and 1:1 000 000 scale geological mapping, and largely conforms to the interpreted solid geology of Czarnota *et al.* (2009a; 2009b), an example of which is shown in [Figure 5.5](#). Multiple conductors are visible within the known Broadhurst Formation sequence around the Nifty copper mine and these conform to earlier interpretations of the fault duplication of the Broadhurst Formation in this region (Czarnota *et al.*, 2009a; 2009b).

Conductivity sections of the Broadhurst Formation show far more detail of the conductive stratigraphy than the gridded data. The conductive Broadhurst Formation appears to have a

weathering profile approximately 50 m thick between the base of the Permian sediment cover and fresh, highly conductive bedrock. The conductivity anomaly gradually disappears upwards to merge with the anomaly associated with the Permian sediments (Figure 5.7). The top of the highly conductive Broadhurst Formation undulates in the sections, which may be reflective of kilometre-scale folding or faulting within the rocks.

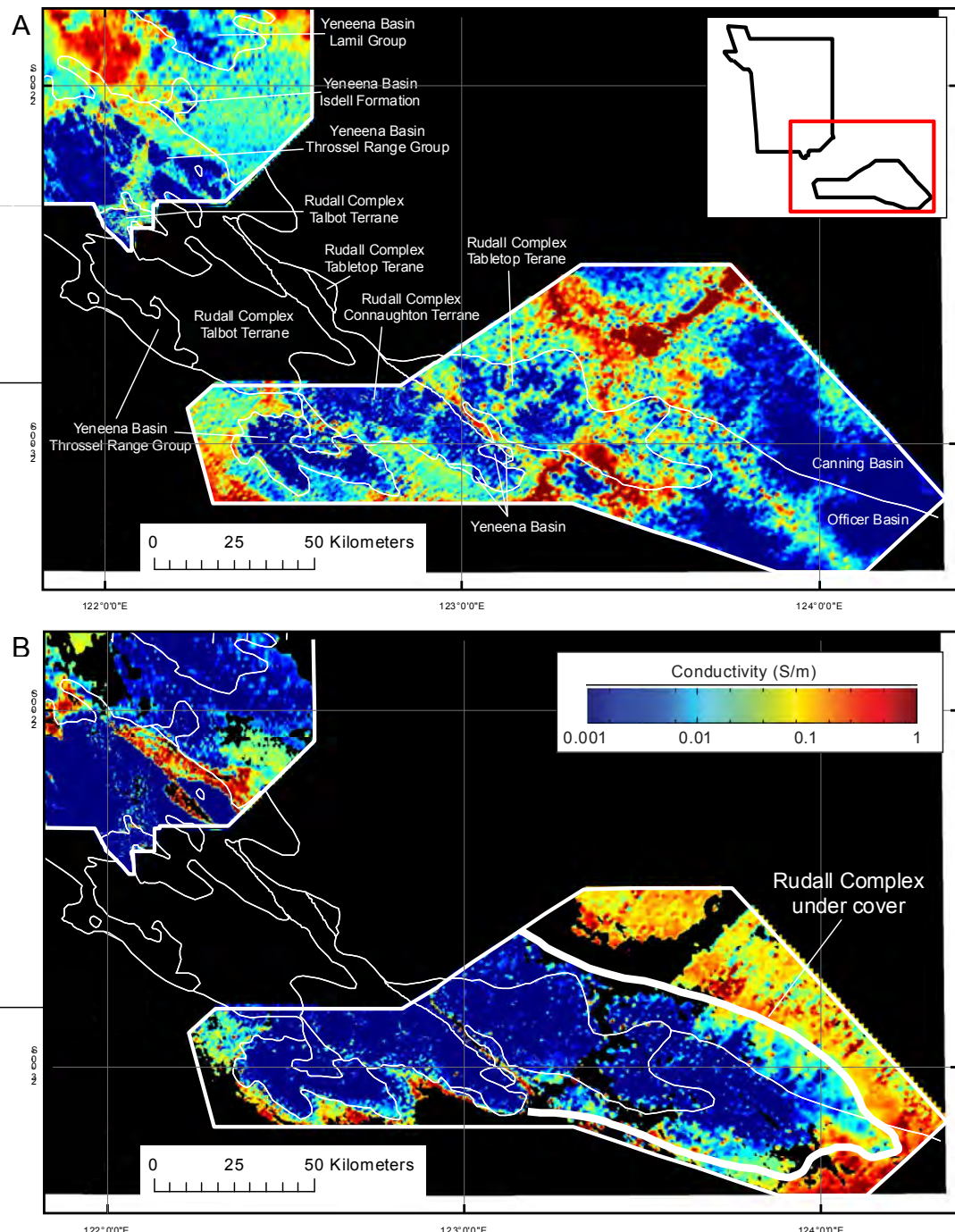


Figure 5.9: GA-LEI conductivity depth slices of the Rudall Complex showing simplified geological provinces. A: 0-5 m conductivity depth slice. B: 200-250 m conductivity depth slice showing the under-cover extension of the Rudall Complex to 250 m depth below surface.

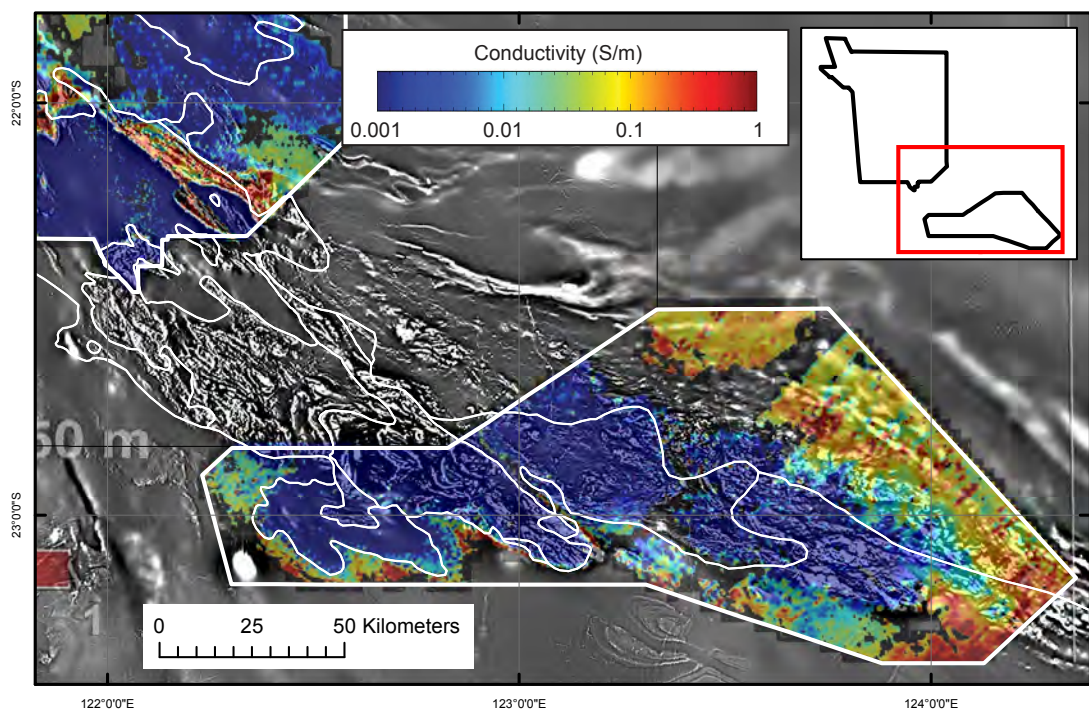


Figure 5.10: GA-LEI 200-250 m conductivity depth slice and 1st vertical derivative magnetics (grey scale) of the Rudall Complex. Image highlights the close correlation between the resistive conductivity anomaly and the complex magnetic fabric of the Rudall Complex.

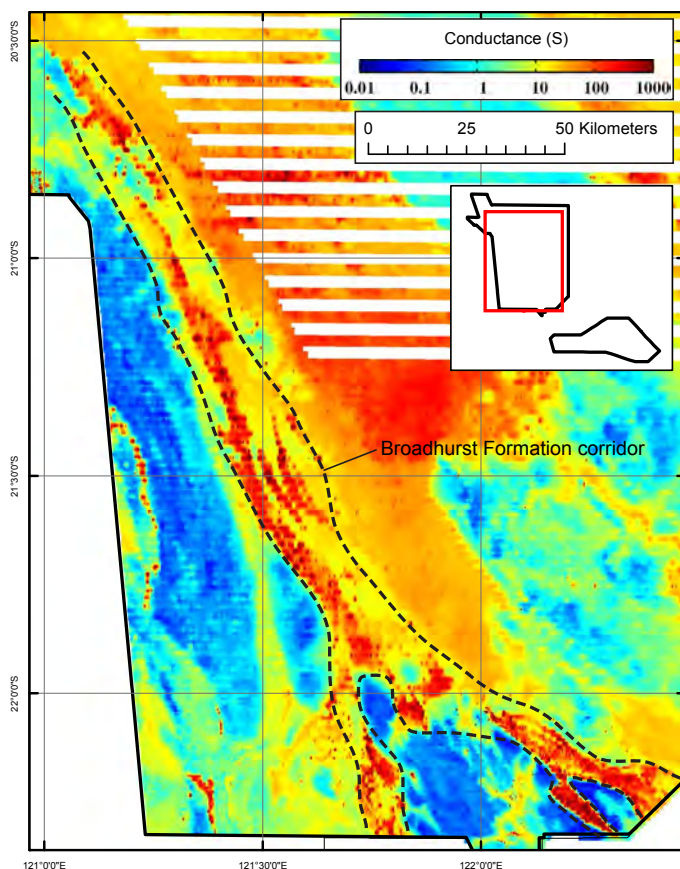


Figure 5.11: 0-400 m GA-LEI conductance image of the Paterson North AEM data set highlighting conductivity anomalies associated with the conductive black shale facies of the Broadhurst Formation.

5.5.4 Tarcunyah Group

Tarcunyah Group rocks occur in the Paterson South area (RUDALL 1:250 000 sheet area) as a moderately to highly conductive feature. Karara Formation rocks of the Tarcunyah Group are shown in the AEM data in a linear feature aligned to the Camel-Tabletop Fault Zone separating the Tabletop and Connaughton Terranes of the Rudall Complex (Figure 5.12).

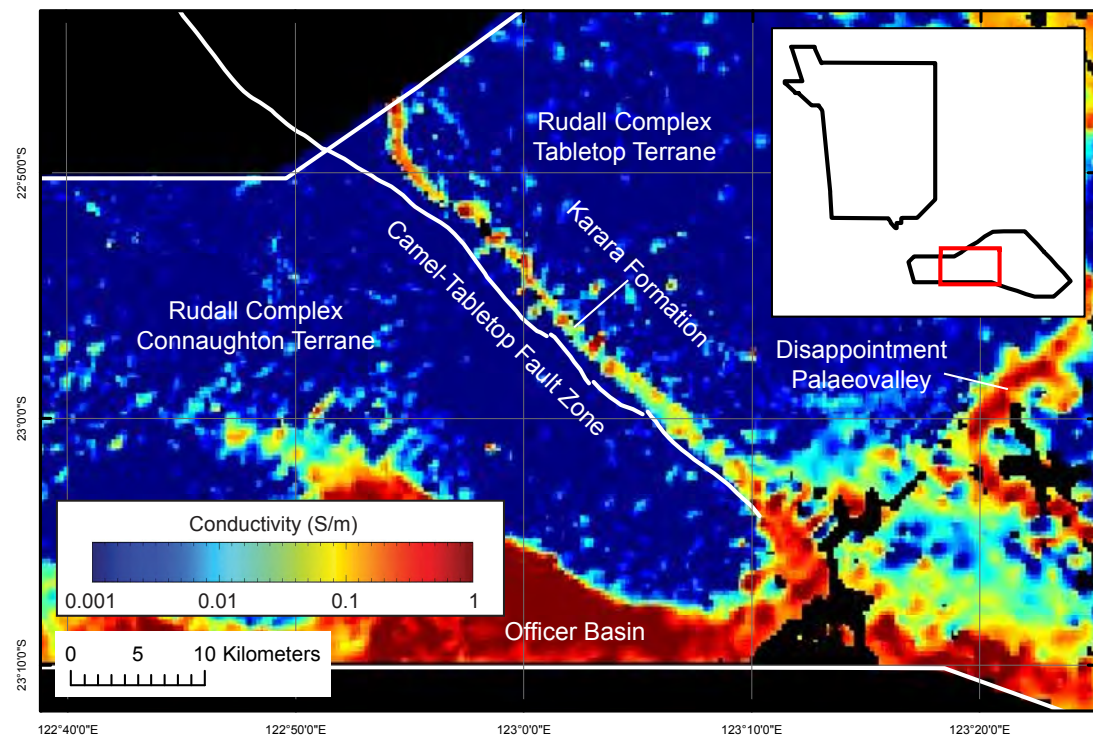


Figure 5.12: Conductive Karara Formation, Tarcunyah Group, in Paterson South shown in the 100–150 m GA-LEI conductivity depth slice.

Other Tarcunyah group rocks are visible in the southwest corner of the Paterson North survey area (Figure 5.13) as weakly conductive linear to arcuate features within conductivity sections, conductivity depth slices and conductivity elevation slices. Here, Tarcunyah Group rocks are faulted against more conductive Jeerinah Formation rocks, so are difficult to distinguish based on conductivities alone and are only mapped approximately.

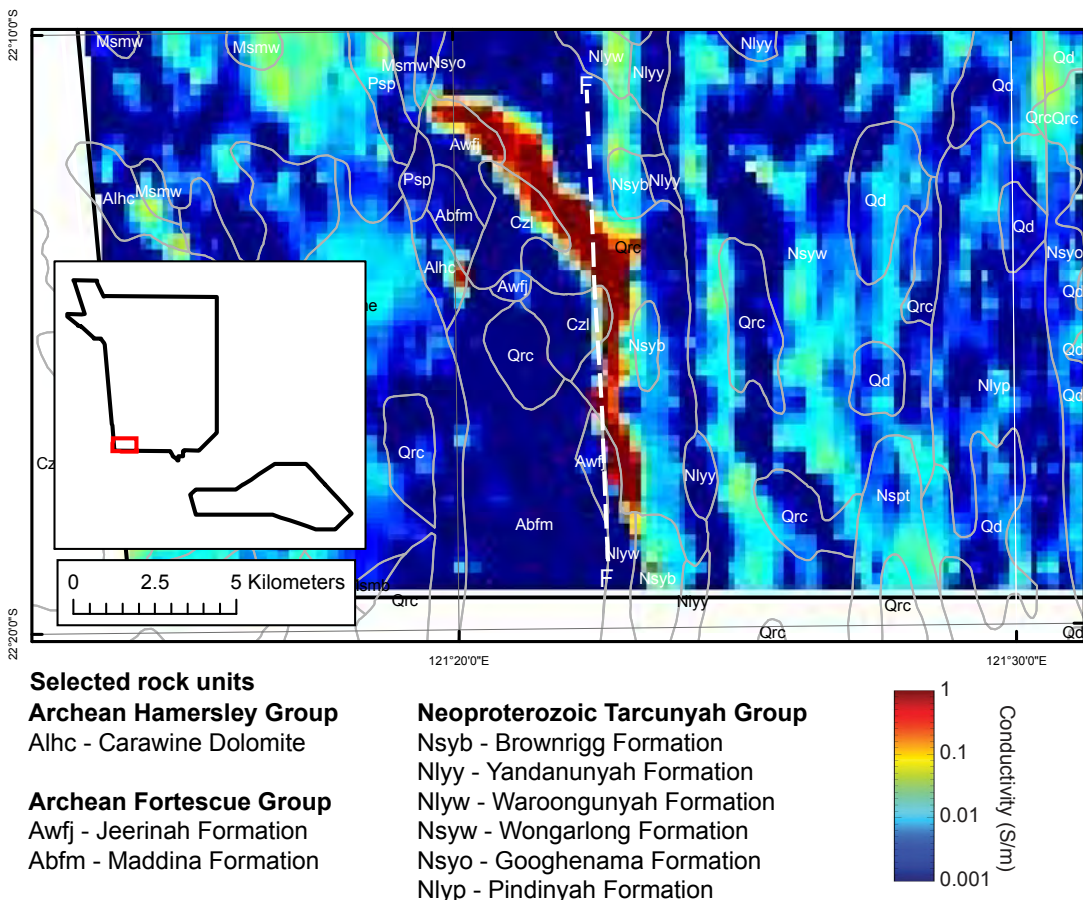


Figure 5.13: Conductive Tarcunyah Group faulted against Jeerinah Formation in Paterson North shown in the 100-150 m GA-LEI conductivity depth slice. Geological polygons are from the 1:1 000 000 Surface Geology of Western Australia by Stewart (2008).

5.5.5 Permian-Mesozoic strata

Where conditions allow, according to the DOI grid (Figure 4.4), it is possible to interpret Permian and Mesozoic strata within the survey area. Permian and Mesozoic strata are visible as sheet-like conductivity anomalies lapping onto the eastern edges of the Anketell Shelf in the Paterson North survey area and the Rudall Complex in the Paterson South survey area. Permian rocks are generally gently E- to NE-dipping, whereas Mesozoic rocks are nearly flat-lying. These are visible in both the conductivity grid and conductivity sections (e.g., Figure 5.14, Figure 5.15). Conductivity anomalies conform relatively well with known stratigraphy in the Canning Basin, surface outcrop patterns and the limited drilling available. A number of gently northeast-dipping conductors are visible in conductivity sections, especially in the Canning Basin to the northeast of the Rudall Complex in the South Paterson survey area (Figure 5.15).

Much of the Throssell Shelf, Waukarlycarly Embayment and the Anketell Shelf area are covered by Permian to Mesozoic sediments with a thin cover of Quaternary sand sheets and sand dunes. It is difficult to image the stratigraphy in the Waukarlycarly Embayment area because of the prevalence of salt lakes and saline groundwater. However, it is possible to detect at least two horizons within most conductivity sections through the Waukarlycarly Embayment (Figure 5.16). These are interpreted to be related to the Permian Paterson Formation and possibly the Permian Poole Sandstone, which lies stratigraphically above the Paterson Formation. Much of the Mesozoic strata appear to be relatively resistive within the Waukarlycarly Embayment except where they interact

with saline groundwater associated with the Lake Waukarlycarly-Canning Palaeoriver groundwater flow system. The Permian palaeovalley systems are described later.

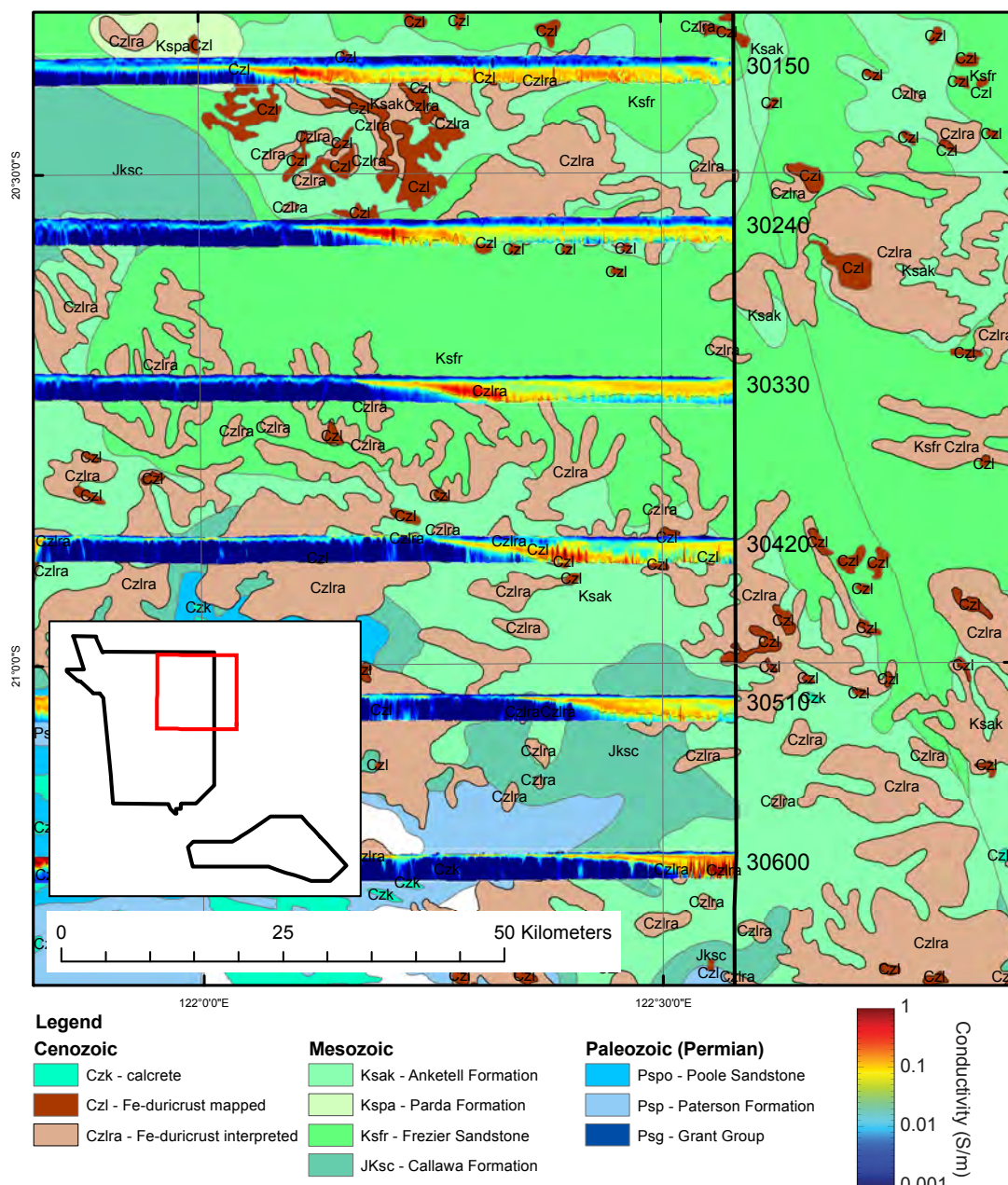


Figure 5.14: Stacked GA-LEI conductivity sections showing Permian and Mesozoic strata lapping onto the eastern side of the Anketell Shelf using a Canning Basin solid geology interpretation by A. J. Whitaker.

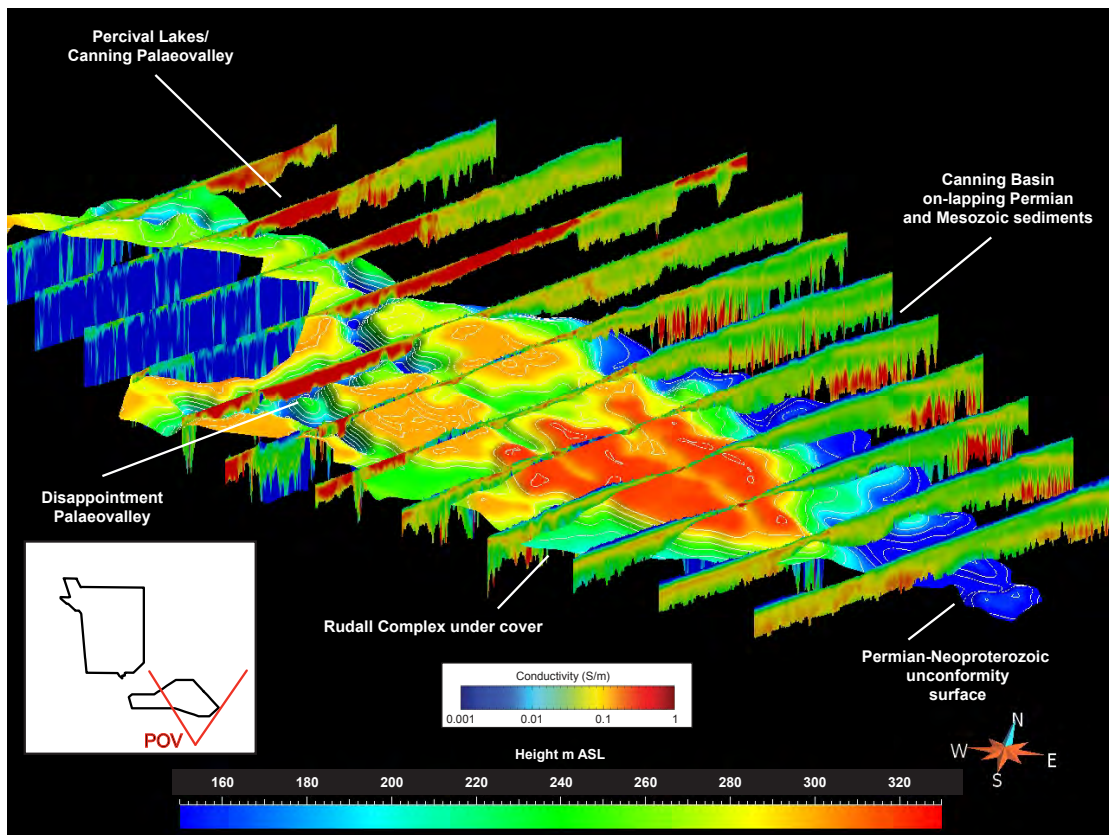


Figure 5.15: Perspective view of the Paterson South survey area showing a shaded relief model of the interpreted Canning Basin basal unconformity surface and selected GA-LEI conductivity sections showing onlapping Permian and Mesozoic sediments of the Canning Basin on the northeast of the Rudall Complex and conductive sediments in the Percival Lakes (Canning Palaeovalley) and Disappointment Palaeovalley systems. The inset map (lower left) shows the point of view.

5.5.6 Waukarlycarly Embayment

The Waukarlycarly Embayment occupies the region between the Throssell Shelf and the Anketell Shelf in the Paterson North survey area and is named after Lake Waukarlycarly, which occurs in its approximate centre. The Waukarlycarly Embayment is a deep (> 3.5 km) rift basin filled with Canning Basin sediments, perhaps as old as Ordovician at its deepest point (Hunt, 1996). A number of seismic sections cross the region (Figure 2.6), however, there are no deep drill holes within the survey area to confirm interpretations of the stratigraphy. Sediments within the upper stratigraphy of the Waukarlycarly Embayment are moderately to highly conductive and AEM signal penetration is very low, as indicated by the DOI grid (Figure 4.4). The borders of the Waukarlycarly Embayment are, however, quite visible in the AEM data set and have been mapped. Figure 5.16 illustrates the surface geology of the Waukarlycarly Embayment together with a number of conductivity sections showing the subsurface stratigraphy. Figure 5.17 illustrates the extent of the Waukarlycarly Embayment using conductivity elevation slice and conductivity section data. Saline sediments and/or groundwater associated with Lake Waukarlycarly and the Canning Palaeoriver partially obscure the central eastern edge of the Waukarlycarly Embayment where drill hole and magnetic data indicate that Neoproterozoic rocks lie close, within 200 m, of the surface. However, for the most part the conductivity anomalies clearly outline the eastern and western edges of the Waukarlycarly Embayment. The boundary faults for the eastern and western edge of the Waukarlycarly Embayment have been termed the East Waukarlycarly Fault and the West Waukarlycarly Fault, respectively (see Chapter 6).

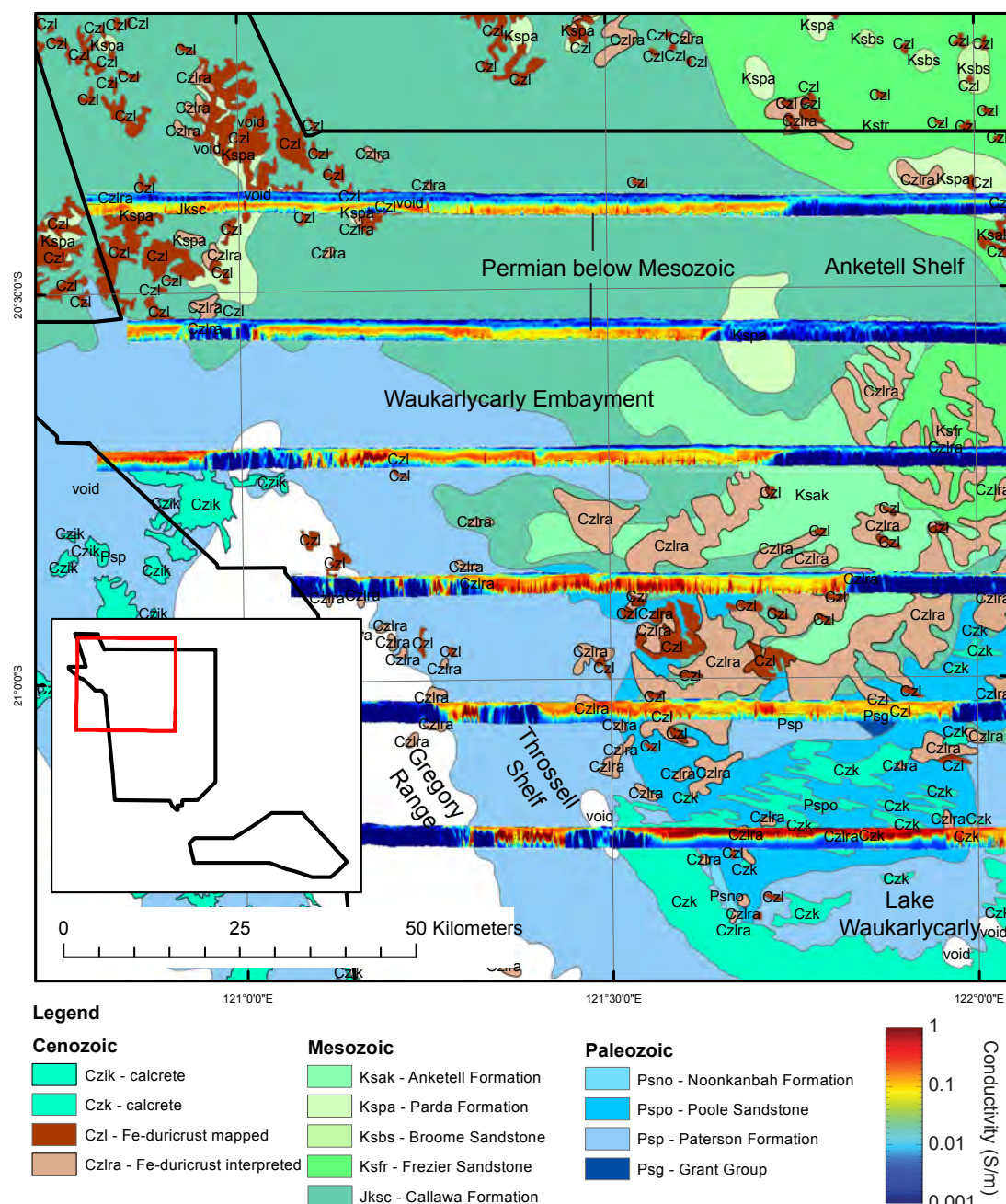


Figure 5.16: Stacked GA-LEI conductivity sections through the Waukarlycarly Embayment depicting Permian stratigraphy using a Canning Basin solid geology interpretation by A.J. Whitaker.

5.5.7 Anketell Shelf

The Anketell Shelf is described as “*a broad, poorly-controlled area of flat-lying to very gently dipping, shallow basement*” (Towner, 1982). The Anketell Shelf was originally recognised by gravity, magnetic and seismic profiling, but has since been more accurately defined through exploration company drilling, detailed magnetics and gravity. The Anketell Shelf consists of a large mass of Neoproterozoic Lamil Group rocks (Wilki Formation, Malu Formation and possibly Isdell Formation) intruded by granitoids and minor coeval volcanoclastics of the Mt Crofton Suite (described in more detail in Chapter 3). The Shelf is here regarded as the Neoproterozoic rocks

extending northwards underneath Paleozoic and Mesozoic sediments of the Canning Basin from the limited outcrop north of the Canning Palaeoriver.

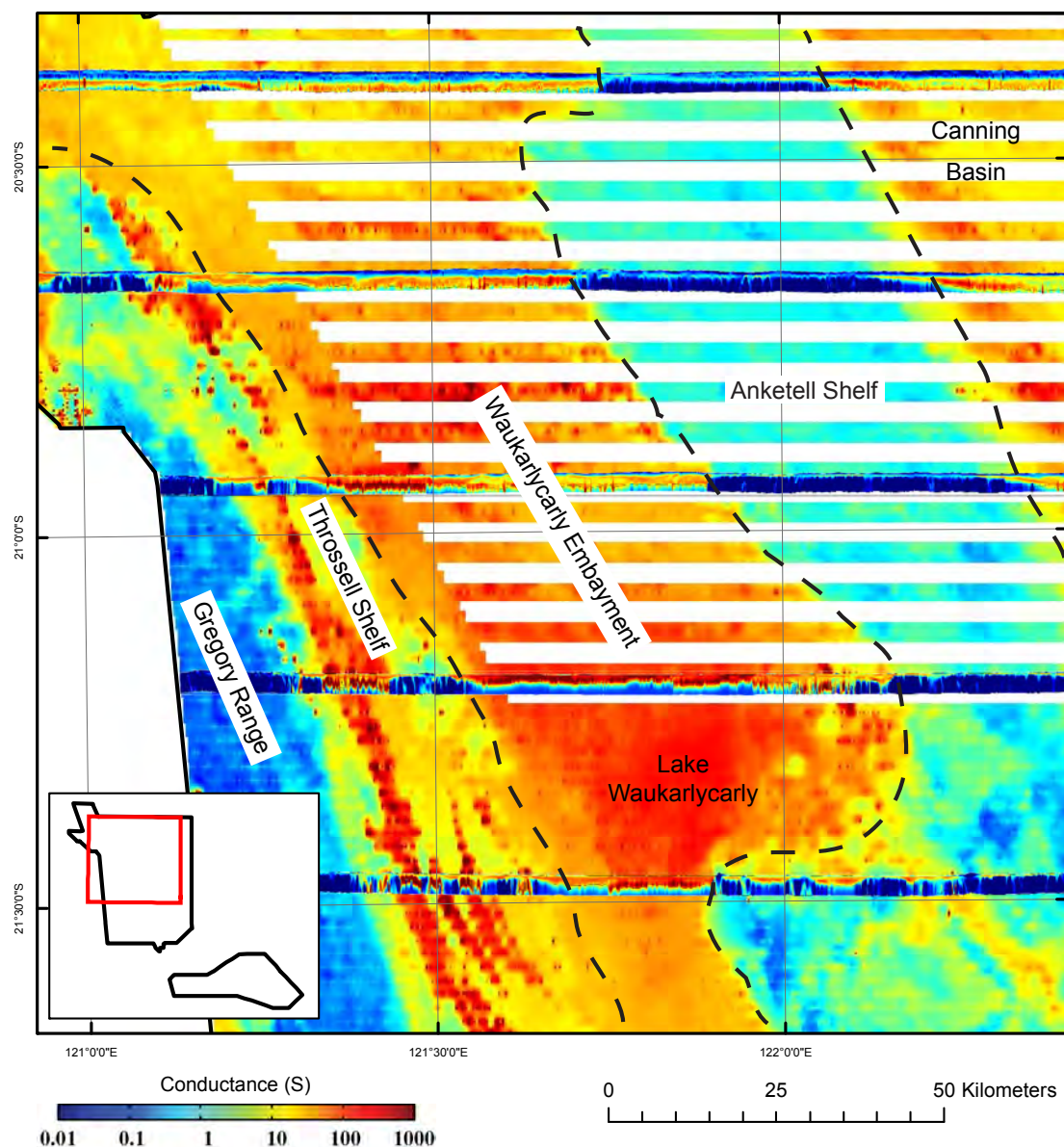


Figure 5.17: GA-LEI 0-400 m conductance image and conductivity sections showing the extent of the Waukarlycarly Embayment in the central Paterson North survey area.

The Anketell Shelf is a prominent, generally resistive feature in the conductivity elevation slices and conductivity sections (Figure 5.17, 5.18) generated from the AEM data set. The western and eastern edges of the Anketell Shelf are clearly defined. The western edge is abrupt against the Waukarlycarly Embayment on a NNW-trending laterally continuous feature and is interpreted to be fault-bound by the East Waukarlycarly Fault (see Chapter 6 of this record). The eastern edge against the Canning Basin is more gentle and is interpreted to be an onlapping margin, where Permian sediments that once covered the Shelf have been eroded and reworked into Mesozoic sediments. Small amounts of weakly to moderately conductive material are visible in conductivity sections across the Shelf underneath resistive Mesozoic sediment. These occurrences are interpreted as Permian valley-bottoms inset into the Anketell Shelf. These conductivity anomalies are

discontinuous and can not be traced across adjacent conductivity sections, which are spaced every 6 km. The Neoproterozoic rocks of the Anketell Shelf are generally resistive, however, a number of weak conductors are visible in conductivity sections. These may conform to different geological units within the Neoproterozoic bedrock, however, the broad line spacing of the survey in the region does not allow for detailed correlation of discrete conductors that may be of interest to mineral explorers.

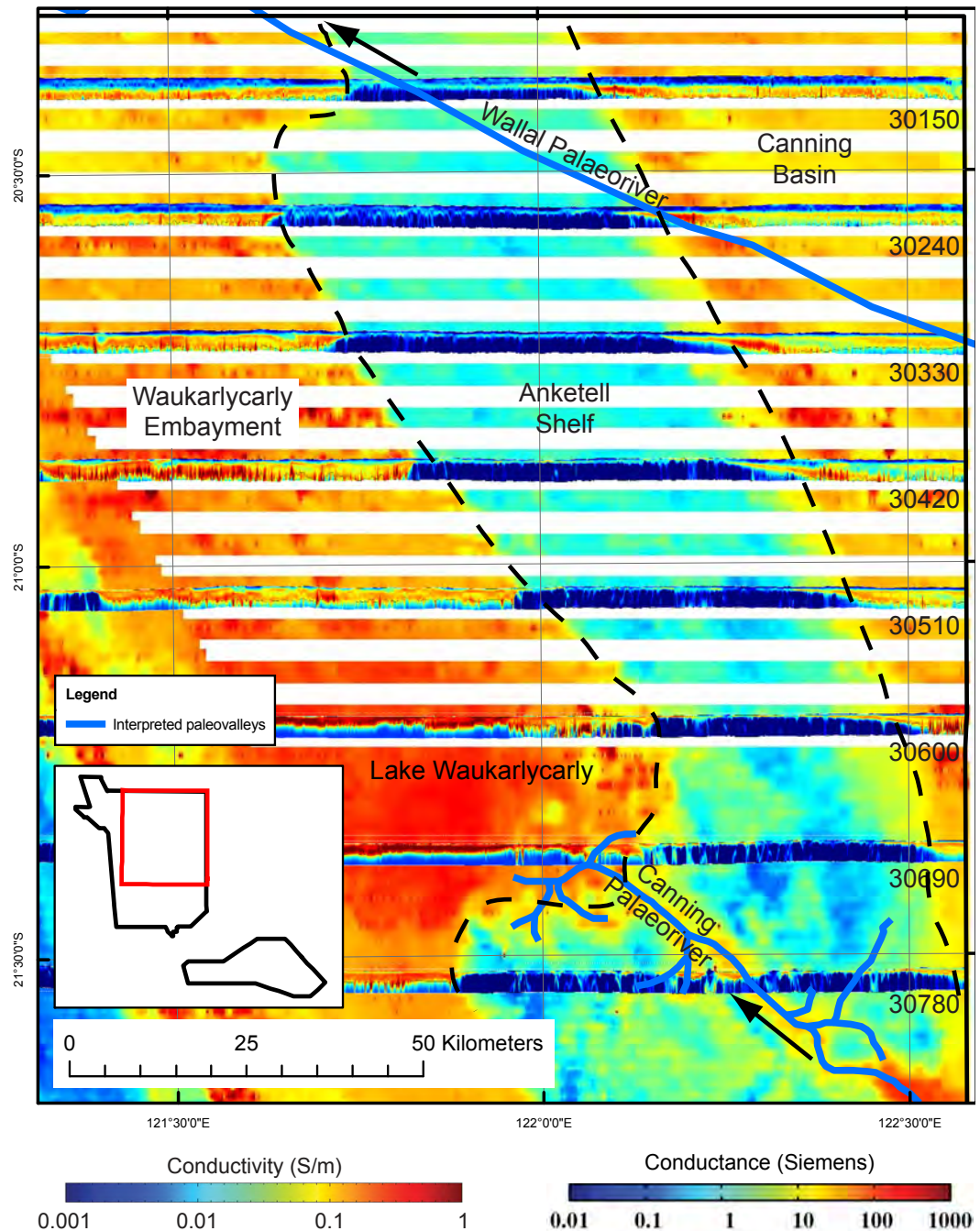


Figure 5.18: The Anketell Shelf depicted using the GA-LEI 0-400 m conductance image (background) and stacked GA-LEI conductivity sections. Selected geological and geographical features are marked. Line numbers are shown on the right hand side. The Wallal Palaeoriver course is derived from van der Graaf et al. (1977) and the Canning Palaeoriver course is derived from conductivity anomaly contours described in Figure 5.19.

The conductivity contrast between the upper moderately-conductive materials and the lower resistive materials approximates the Permian-Proterozoic (basal Canning Basin) unconformity in this area, as indicated by drill hole logs from the area (e.g., [Figure 5.6](#)). The conductivity contrast has been traced using a combination of conductivity elevation slices and conductivity sections and converted into 20 m interval contours and an elevation surface. [Figure 5.19](#) illustrates the conductivity anomaly contours over the 0 to -10 m above sea level conductivity elevation slice (the approximate limit of the deepest reliable data) and [Figure 5.20](#) illustrates the surface made from the contours that approximates this important unconformity surface.

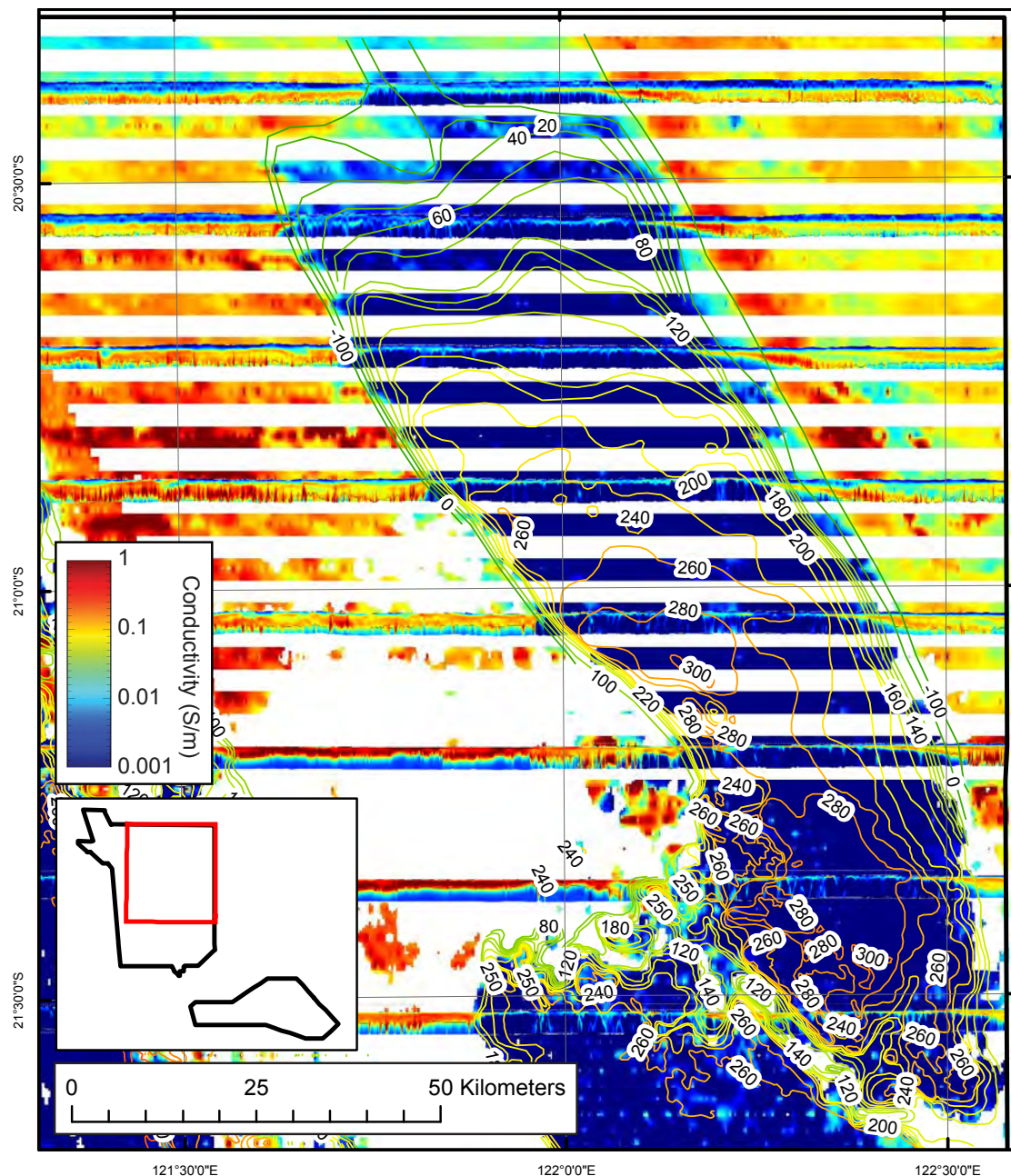


Figure 5.19: Conductivity anomaly contours approximating the Canning Basin basal unconformity over the Anketell Shelf. The Anketell Shelf is depicted using the 0 to -10 m GA-LEI conductivity elevation slice and selected GA-LEI conductivity sections (see [Figure 5.18](#) for line numbers). Data below the DOI in the conductivity elevation slice have been nulled (white).

The conductivity anomaly contours confirm previous interpretations that the Anketell Shelf is a gently north-dipping undulating surface, however, the AEM data can add more information than was previously available.

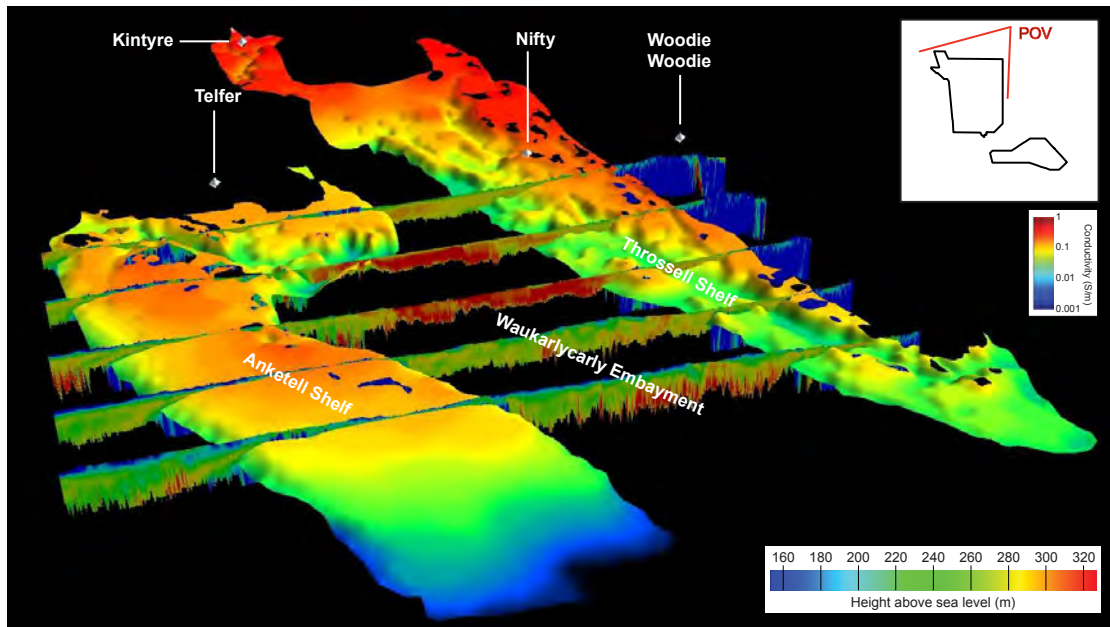


Figure 5.20: Perspective views of the Proterozoic-Paleozoic unconformity over the Anketell Shelf and Throssell Shelf interpreted from conductivity anomaly contours.

5.5.8 Throssell Shelf

The Throssell Shelf is a new term to describe a NNW-trending, covered area in the north Paterson survey area between the Gregory Range-Vines Fault in the west and the Waukarlycarly Embayment boundary fault (the West Waukarlycarly Fault, described in [Chapter 6](#)) in the east. The Throssell Shelf extends from the Isabella Range-Snell Well area in the north, past the Nifty copper mine to the Throssell Range in the south ([Figure 5.20, 5.21](#)). The Throssell Shelf is an area of discontinuous outcrop, mostly of Broadhurst Formation rocks, but also some Coolbro Sandstone, and dominant cover that may hide Lamil Group rocks according to the solid geology interpretation map of Czarnota *et al.* (2009a; 2009b). The Throssell Shelf is marked by prominent magnetic and gravity anomalies indicating intense reverse faulting and shearing in the Throssell Range Group rocks and sharply-defined magnetic anomalies that indicate a shallow depth to magnetic basement. The Throssell Shelf has a variable-thickness (< 100 m to 200 m) cover of Permian, Mesozoic and Cenozoic sediments visible in the AEM data and may extend underneath highly saline sediments of the southern Waukarlycarly Embayment where AEM data fail to image it.

The Throssell Shelf is interpreted to have an undulating surface with 300-400 m of relief using the base of the conductivity anomaly associated with the Permian to approximate the Permian-Proterozoic unconformity. The surface is cut by known small palaeovalleys near the Nifty copper mine, but also has numerous conductivity anomalies between bedrock outcrops that are filled with Permian sediments. These are interpreted to be larger Permian glacial palaeovalleys gouged between prominent bedrock "islands" of the Gregory Range and the eastern Throssell Shelf. Drill hole logs in the area confirm the thicknesses of Permian and younger cover seen in the conductivity slices and sections. Permian sediments are weakly to moderately conductive and provide a reasonable contrast with underlying resistive Neoproterozoic sediments of the dolomitic facies of the Broadhurst Formation (e.g., [Figure 5.7](#)) and Coolbro Sandstone. Where this situation occurs conductivity elevation slices were used to develop the conductivity anomaly model that approximates the

unconformity. Locating the unconformity is more problematic, however, in areas where the conductive black shale facies of the Broadhurst Formation occurs. In this situation individual conductivity sections were used to define the conductivity anomaly to model the unconformity surface.

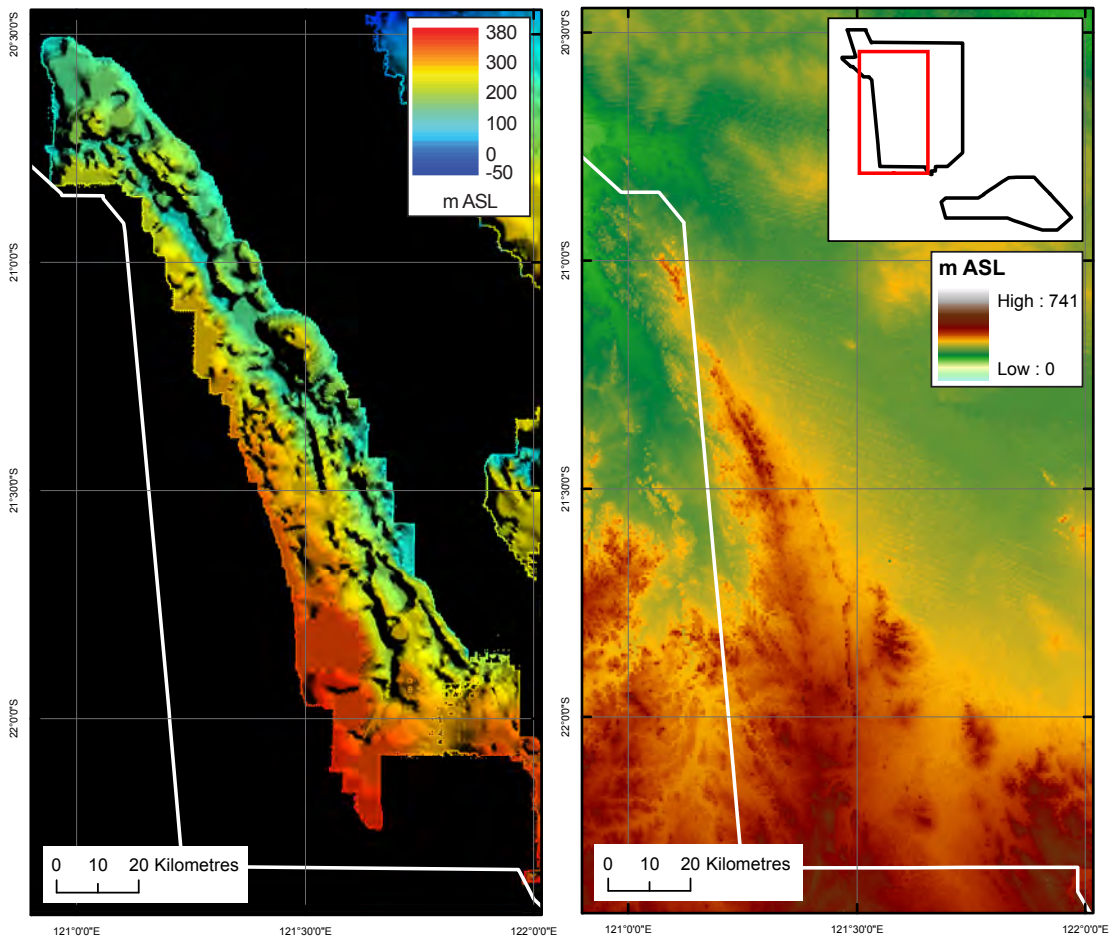


Figure 5.21: Shaded relief model of the Throssell Shelf (left) derived from interpreted conductivity anomaly contours compared to a shaded relief model of the SRTM DEM land surface (right).

5.6 Unconformities

A number of unconformities are visible within the AEM data set. The most obvious is the Permian-Proterozoic unconformity marking the base of the Canning Basin, visible over much of the survey area above the limit set by the DOI surface (Figure 4.4). The basal unconformity of the Canning Basin is actually interpreted to be at the Ordovician-Neoproterozoic boundary in the Waukarlycarly Embayment (Hunt, 1996), except Ordovician sediments are not present within the surface geology of the survey area, nor are they expressed within the AEM data set. This unconformity is interpreted throughout much of the survey area where it occurs above the DOI limit (Figure 4.4) and is shown in Figures 5.11, 5.15, 5.19-21, 5.27 and 5.28 as contours or as a 3-dimensional surface. This unconformity may be the most economically-important one in the Paterson region, because it determines the depth to Proterozoic basement and therefore the cover thickness for base metal and gold exploration in the region. It may also define regions with potential for sandstone-hosted uranium deposits (see Chapter 6).

Several other unconformities are visible within the data set, however these are more difficult to

image because of weak conductivity contrasts between the different materials, or because of their limited geographic extent. (see [Chapter 7](#)).

The uppermost major unconformity is the Permian-Mesozoic unconformity, occurring between the Permian Poole Sandstone and Jurassic-Cretaceous Callawa Formation within the Canning Basin ([Figure 5.22](#)). Although this unconformity may be inferred within the data set, its actual location is difficult to accurately determine because there is little or no conductivity contrast between the different strata. There are indications in the Canning Basin area that the Mesozoic units have scoured into the underlying Permian units. This is evidenced by undulations in the conductivity surface of the top Permian unit ([Figure 5.23](#)). There are also indications in the Waukarlycarly Embayment that Permian units have been offset by later faulting. These are discussed in [Chapter 6](#).

For uranium energy purposes, the most important unconformity in the Paterson region is between the Neoproterozoic Coolbro Sandstone and the Paleoproterozoic Rudall Complex (the Coolbro-Rudall unconformity). The structure and economic importance of this unconformity is discussed in more detail in [Section 7.2.2](#) of this record.

The Coolbro-Rudall unconformity occurs near the Kintyre uranium deposit in the Paterson North survey area and is also interpreted in the Paterson South survey area. The unconformity is difficult to locate on the surface because of extensive Permian and Quaternary cover, but is exposed in several places (see [Section 7.2.2](#)). The unconformity has been drilled in a number of exploration drill holes within the Kintyre region; a typical hole is depicted in [Figure 5.24](#).

The unconformity is marked by an undulating zone of weak conductivity contrast between the otherwise resistive Coolbro Sandstone and the underlying Rudall Complex. This zone is interpreted to consist of metamorphosed weathering products including a small amount of magnetite. This zone with its included weathering and/or metamorphic products may account for the elevated conductivity but the amount of magnetite is not sufficient to generate a magnetic anomaly. The unconformity is shown in [Figure 5.25](#). More detail of the Coolbro-Rudall unconformity is included in Costelloe *et al.* (2010b) and [Section 7.2.2](#).

A similar feature also possibly occurs at the Coolbro Sandstone-Rudall Complex interface in the Paterson South survey area ([Figure 5.26](#)). Here, similar possible weak conductors with weak conductivity contrasts and similar wavelength undulations occur and could be interpreted as the southern extension of the Coolbro-Rudall unconformity.

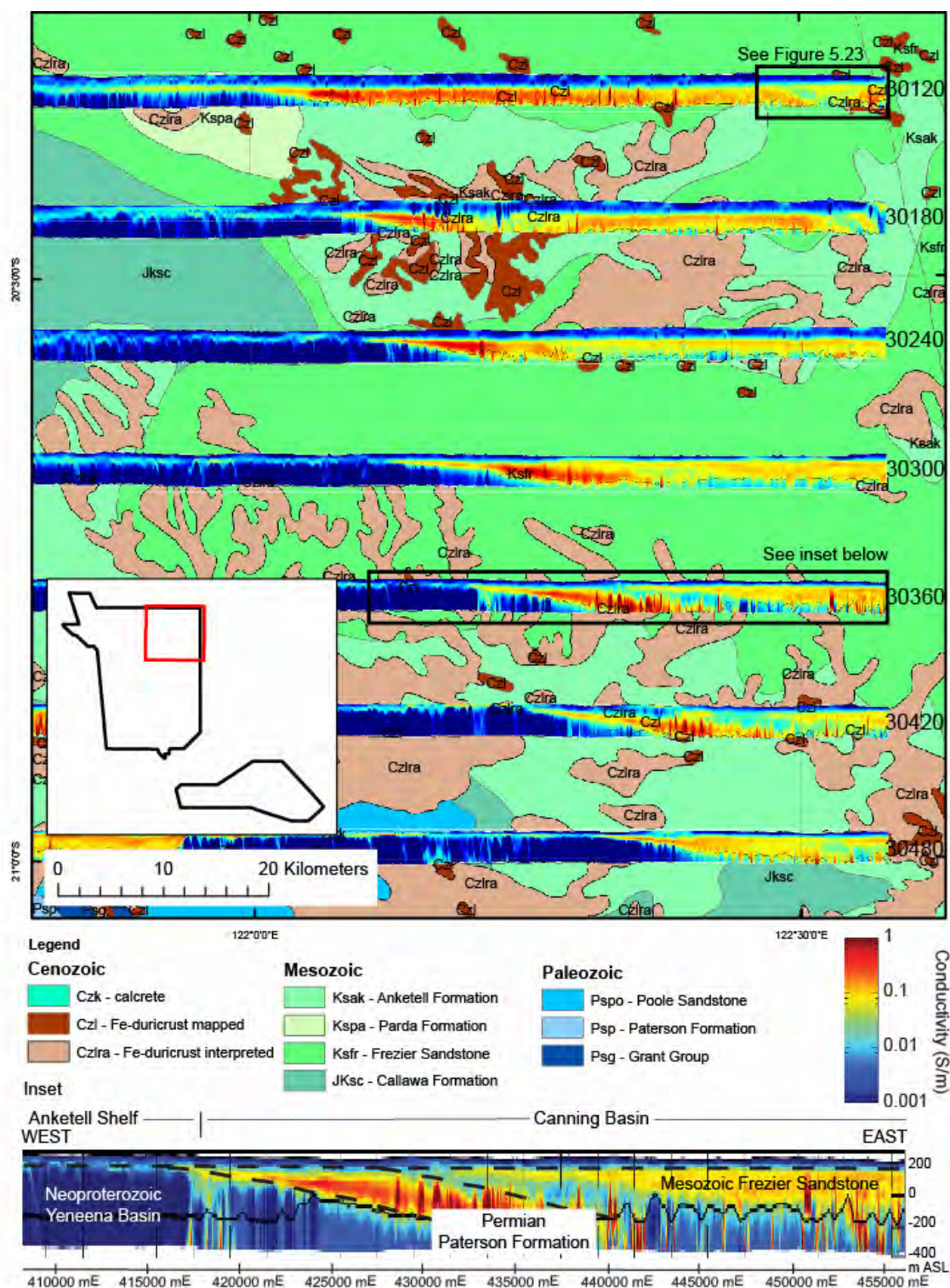


Figure 5.22: Stacked GA-LEI conductivity sections of the eastern edge of the Anketell Shelf showing Mesozoic sediments unconformably overlying Permian sediments. The basement-cover relationships of the Neoproterozoic, Permian and Mesozoic for the box in line 30360 are interpreted in the inset. Canning Basin solid geology interpretation by A.J. Whitaker.

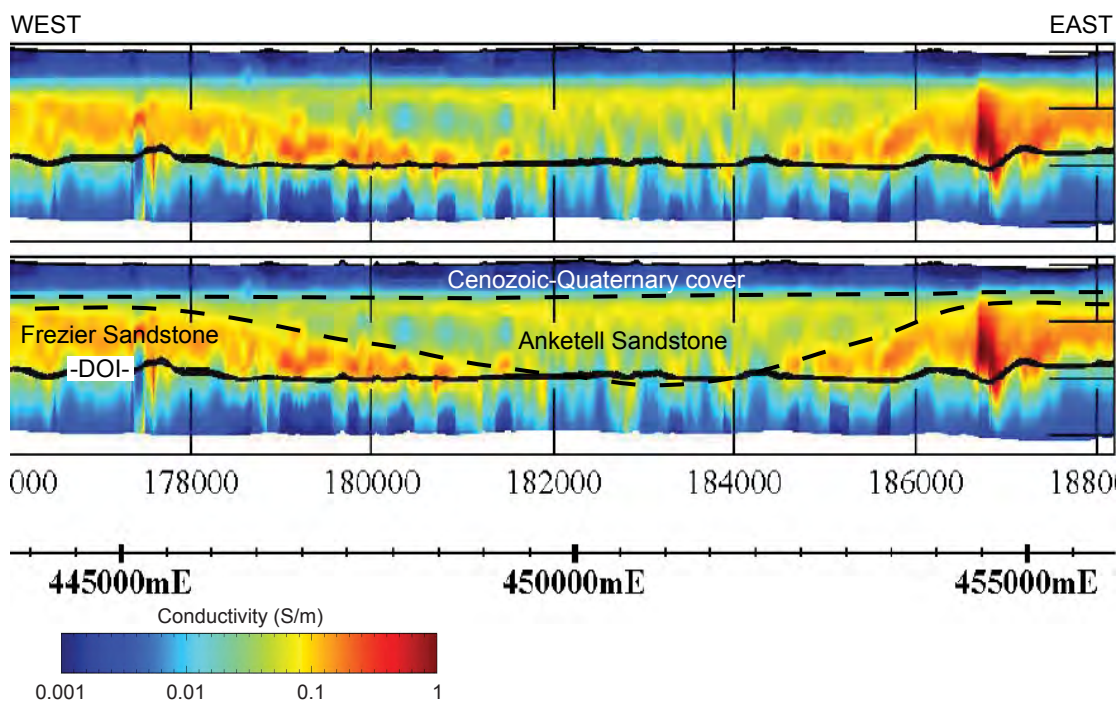


Figure 5.23: An interpreted scour by Anketell Sandstone into Frezier Sandstone in line 30120 showing (above) original GA-LEI conductivity section and (below) interpretation.

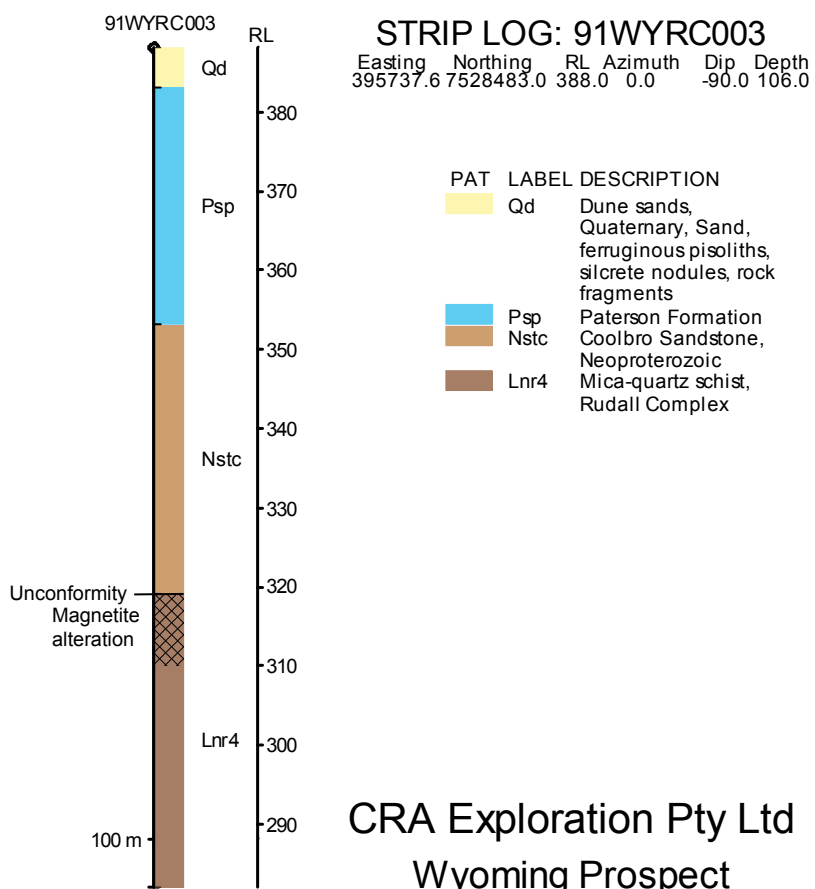


Figure 5.24: Graphic log for drill hole 91WYRC003 containing the Coolbro-Rudall unconformity. Drill hole data from CRA Exploration (CRA, 1991).

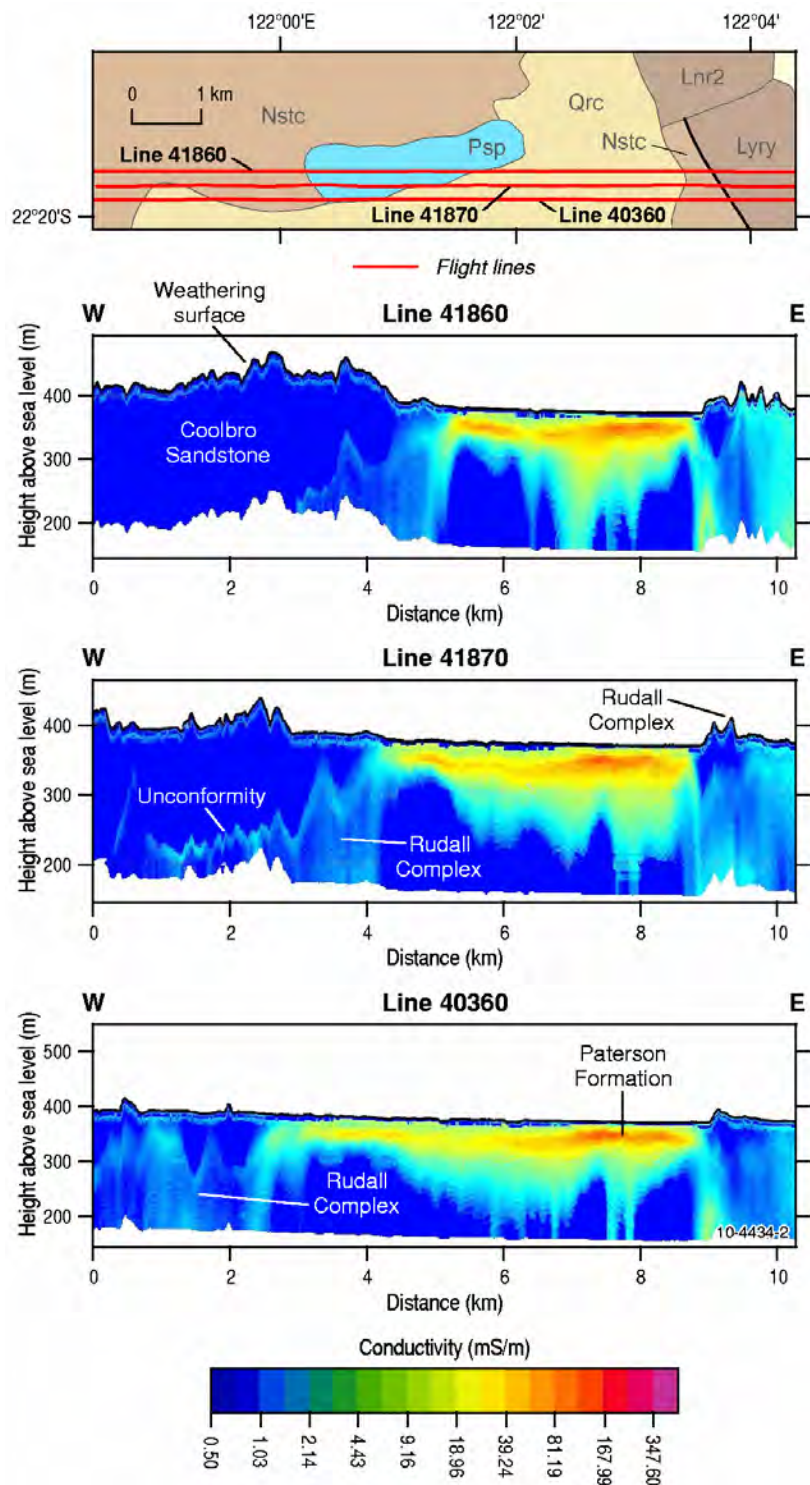


Figure 5.25: Surface Geology of Western Australia Map (Stewart, 2008) and stacked conductivity sections showing the Coolbro-Rudall unconformity in the Paterson South survey area, from Costelloe et al. (2010b).

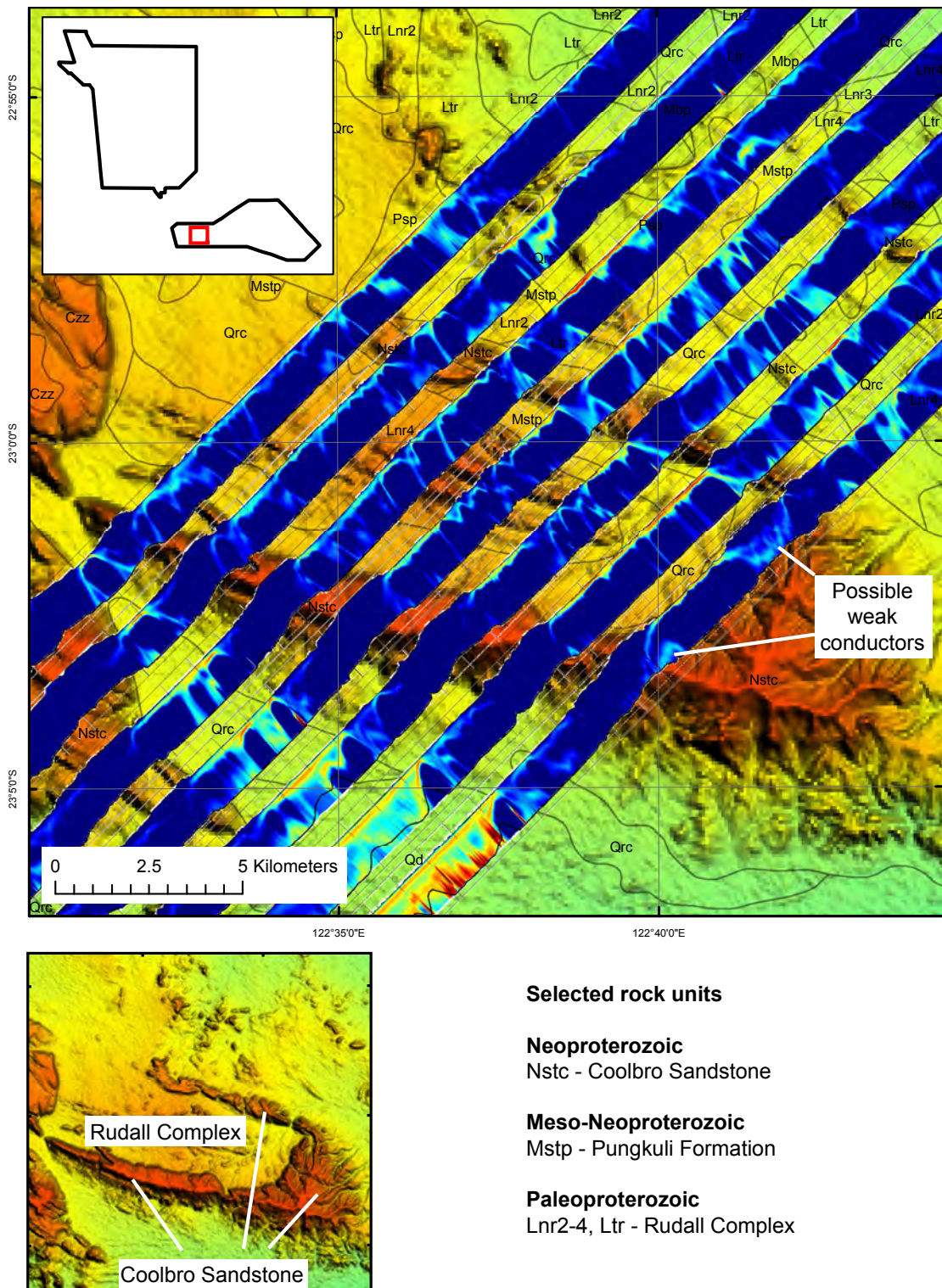


Figure 5.26: Stacked GA-LEI conductivity sections showing conductivity anomalies near the Coolbro-Rudall unconformity in the Paterson South survey area. Data are overlain with polygons from the 1:1 000 000 Surface Geology of Western Australia Map (Stewart, 2008), with selected rock units shown, and a shaded relief model of the SRTM 3-second DEM.

5.7 PALAEOVALLEYS

It is important to be able to recognise palaeovalley or palaeochannel systems because they can host sandstone-style uranium deposits (as described in [Section 1.3](#) and [Chapter 6](#) of this record) and can host potable groundwater in arid landscapes (as described in [Sections 1.3.3](#) and [2.5](#) of this record).

Prior to the Paterson AEM survey a number of large palaeovalley or ‘palaeoriver’ systems of different ages had been recognised within the Paterson region ([Figures 2.11](#) and [5.4](#)) using a range of techniques. Early work by Beard (1973), updated in Beard (2005), recognised a series of Tertiary palaeovalleys, including the Disappointment Palaeoriver, principally by using geobotanical associations. Beard (1973) recognised the changes in vegetation community type and structure between different regolith substrates and used these as a proxy for mapping modern drainage and palaeodrainage lines. Later, when accurate topographic maps of the region finally became available, Beard (2005) updated his interpretation of the Lake Disappointment catchment and the north-flowing Disappointment Palaeoriver joining the Percival Lakes system at Lake Winifred north of the Rudall Complex.

van der Graaf *et al.* (1977) systematically interpreted palaeodrainage lines across inland Australia using aerial photography, surface geology and topography, by joining lines of playas and recognising the value of regolith materials and relict landforms for determining landscape evolution history. van der Graaf *et al.* (1977) described the courses of the Wallal Palaeoriver and the Percival Palaeoriver and slightly modified Beard’s (1973) course for the Disappointment Palaeoriver in the southeastern Rudall Complex area. The Percival Palaeoriver of van der Graaf *et al.* (1977) is also known as the Canning Palaeoriver (Magee, 2009).

Both Beard (1973; 2005) and van der Graaf (1977) interpreted the palaeoriver systems as being Miocene or older, and attributed their relict status to the overall drying of Australia due to northward continental drift. Unfortunately, there has been no attempt at dating the sediments in the playa lake systems in the Paterson region, so their absolute age remains unknown. van de Graaf *et al.* (1977) noted that palaeovalleys in the Gibson Desert were incised into Lower Cretaceous (Aptian-Albian) marine sediments and could, therefore, be no older. Similar palaeovalley systems have been dated around the Yilgarn Craton to the south of Paterson (Magee, 2009). In this region palaeovalleys commonly have a two-stage stratigraphic sequence consisting of Early to Middle Eocene (de Broekert and Sandiford, 2005) channel or estuarine sediments overlain by finer-grained Oligo-Miocene overbank or alluvial plain deposits. The Eocene sediments are typically coarse-grained and contain abundant organic material and lignite, signifying that they were deposited under wet climatic conditions. Late Oligocene to Middle Miocene sediments are typically finer grained and are interpreted to have been deposited in much lower-energy environments, and now typically host post-depositional valley calcrete, ferricrete and silcrete deposits. There is the possibility of a redox interface existing between the Eocene (reducing) sediments and the Oligocene-Miocene (oxidising) sediments allowing uranium to be trapped. The palaeovalley systems in the Paterson area are assumed to be of a similar age to those of the Yilgarn.

More modern analysis of topography in the region through the use of photogrammetry, but more particularly satellite-based radar systems, has allowed greater knowledge of surface features that may be related to the Eocene to Oligo-Miocene palaeodrainage systems. The MRVBF image of the Paterson area ([Figure 1.17](#), [5.27](#)) shows many of the surface features related to the palaeodrainage systems. The MRVBF algorithm (Gallant and Dowling, 2003) can be used to classify landscape into areas of similar relief. In this case, the image ([Figure 5.27](#)) has been broadly classified into areas with low relief (white), moderate relief (grey) and high relief (black).

It is entirely likely that the palaeovalley systems have re-occupied older Permian glacial valley systems in places. van der Graaf *et al.* (1977) suggested that parts of Ponton Creek near Lake Disappointment occupy a Permian glacial valley. Other areas where this may have occurred within

the Paterson area are discussed below. The implications of the mineralogy of valley-fill sediments for uranium systems are discussed in [Chapter 6](#) of this record.

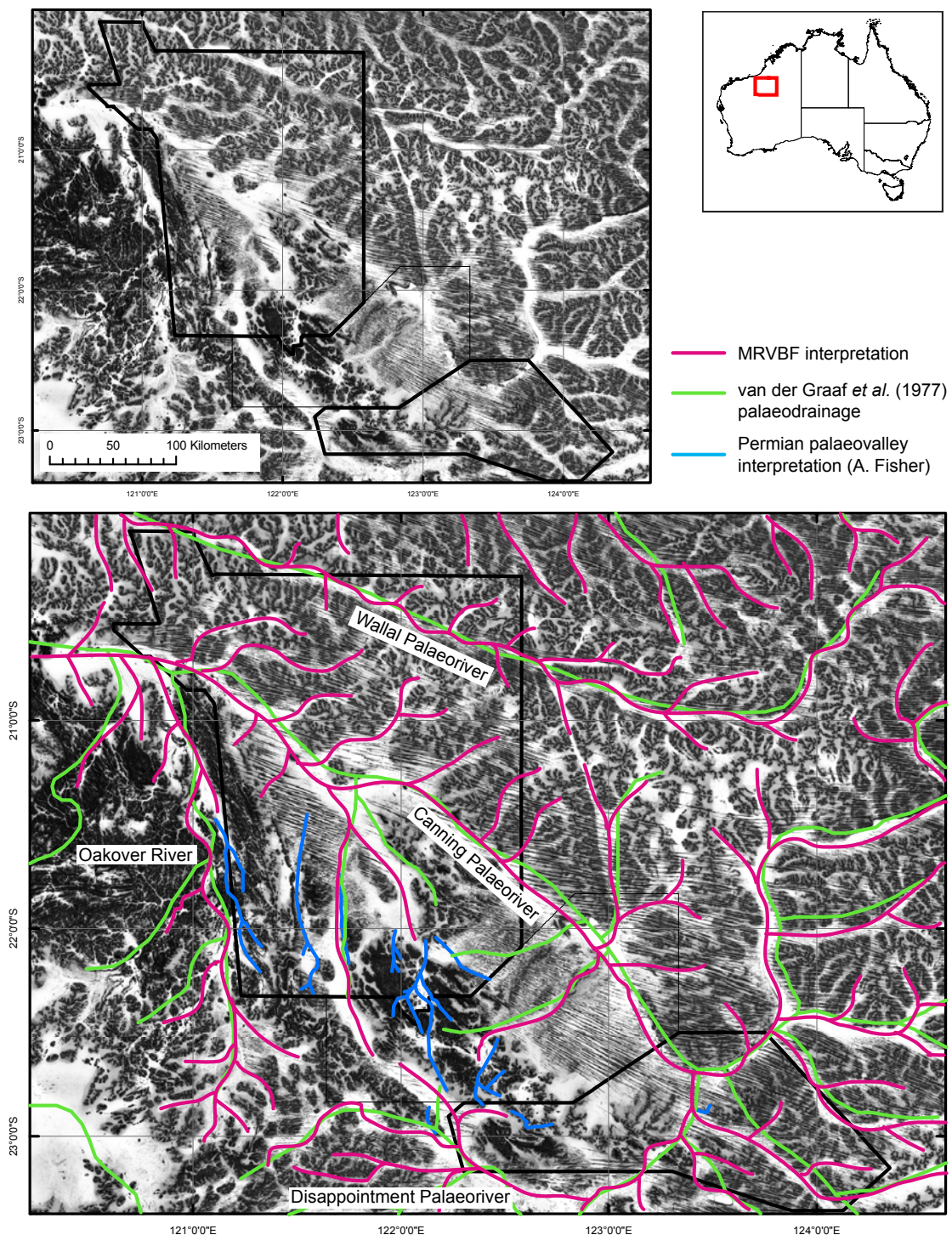


Figure 5.27: Multi resolution valley bottom flatness (MRVBF) images of the Paterson AEM survey area showing interpreted palaeodrainage-related surface features from van der Graaf et al. (1977) and Permian palaeovalley systems interpreted by A. Fisher, together with an interpretation of palaeodrainage-related features.

Older palaeovalley systems are recognised within the Paterson region, principally in Permian flavioglacial systems. In the BROADHURST 1:100 000 geological sheet area Hickman and Clarke (1994) described buried U-shaped valleys up to 100 m deep (discovered during company exploration drilling) that are filled with glacial tillite including striated boulders up to 5 m diameter. The valleys are north-trending and have prominent glacial striae and chatter marks on their pavements indicating ice movement vectors pointing northwest to northeast, generally north. Similar valleys are described on the RUDALL 1:100 000 geological sheet by Hickman and Bagas (1998), again with striae on pavements indicating generally northward ice movement. Permian sediments lap onto Proterozoic bedrocks throughout much of the Paterson region, ranging from tillite of the Paterson Formation at base through fluvial and fluviacustrine sediments further up-sequence in the Poole Sandstone and Noonkanbah Formation.

A number of small Permian palaeovalley systems are already known from the Paterson region from mineral company drilling around the Nifty copper mine and the Telfer gold-copper mine. These systems were located during exploration drilling programs and are now exploited for potable and process water for the mining operations. Small palaeovalley systems are difficult to locate using regional AEM surveys because of their small footprint, which is generally less than that of the AEM system. The flight line spacing may also be too broad to resolve fine dendritic drainage patterns in the regional data. However, some small modern drainage systems are resolved in the south of Paterson North and Paterson South where flight line spacings are 200 m. Palaeovalley systems may also be difficult to recognise because they can contain potable to brackish groundwater and therefore would not provide a good conductivity contrast to allow recognition in the regional AEM data set.

Some examples of Permian and younger palaeovalley features detected during the AEM survey are shown below in [Figures 5.28-32](#).

The most obvious Permian palaeovalley systems are those around the Kintyre uranium deposit in the Paterson North survey area, which have already been recognised by Bagas *et al.* (2000) because they crop out at the surface as a series of inverted remnants on top of the Rudall Complex. A number of these palaeovalleys have a conductivity anomaly associated with them and can be modelled in plan view and 3D using conductivity elevation slices ([Figure 5.28](#)). These palaeovalleys are observed disappearing under the cover of a Permian tillite sheet to the north of the Rudall Complex once they cross the Coolbro Fault. From the different outcrop patterns on either side of the fault, there is a suggestion that the Coolbro Fault has been reactivated at some time after the Permian (and may still be neotectonically active), eroding the Permian tillite sheet and exposing the valley bottoms to its south, but retaining the tillite sheet with buried valley bottoms to the north.

Permian palaeovalley systems are also interpreted within the AEM data set in the Throssell Shelf to the north of the Nifty copper mine, using a combination of conductivity elevation slices, conductivity sections and company exploration drilling. Here, the valley systems are interpreted parallel to the Gregory Range, but also flowing between bedrock topographic highs between outcropping and subcropping Throssell Group rocks ([Figure 5.29](#))

Several large Cenozoic palaeovalley systems are visible within the AEM data set, including the Canning and Disappointment palaeovalleys (Magee, 2009), also referred to as the Percival and Disappointment palaeorivers by van der Graaf *et al.* (1977). These palaeovalley systems, shown in [Figure 2.11](#) and [5.27](#), can be interpreted in 3D by using the AEM dataset. The Canning Palaeovalley is a linear feature visible in the MRVBF image ([Figure 1.17, 5.27](#)) as a linear feature striking northwest from the Percival Lakes system to Lake Waukarlycarly to the north of the Telfer gold-copper mine. Sediments in the palaeovalley have a reasonable conductivity contrast with the underlying Neoproterozoic rocks of the Lamil Group. It is possible to contour the conductivity anomaly as a proxy for the Permian-Proterozoic unconformity in this region and to interpret the extent of palaeovalley fill. [Figure 5.30](#) illustrates the interpreted Permian-Proterozoic unconformity in the vicinity of the Canning Palaeovalley across the southern Anketell Shelf. The Disappointment

Palaeovalley had been described by Beard (1973; 2005) and van der Graaf *et al.* (1977) as a hydraulic connection between Lake Disappointment and the Percival Lakes system, allowing water to drain from the inland to the coast through the Canning Palaeoriver and the Oakover River. Until now the actual course of the Disappointment Palaeovalley had been conjectural, but the AEM data set has allowed the course to be traced, again using the conductivity contrast between sediments in the palaeovalley and the underlying resistive basement as a proxy for the location of the Permian-Proterozoic unconformity. [Figure 5.31](#) illustrates the interpreted Permian-Proterozoic unconformity in the vicinity of the Disappointment Palaeovalley.

Both the Canning and Disappointment palaeovalleys are estimated to be up to 150 m deep and are mostly likely filled with Eocene to Oligo-Miocene sediments in keeping with dated palaeovalley fills from the Yilgarn (Magee, 2009) that were incised into Permian sediments and Proterozoic bedrock. It is not possible to separate the conductivity anomaly associated with the Eocene to Oligo-Miocene palaeovalley fill from that of the Permian sediments because they both have similar mineralogy, and are likely to be saturated with brackish to saline groundwater.

The Wallal Palaeovalley is not visible within the AEM data set. This disparity is discussed below.

5.8 GROUNDWATER

The AEM data set contains much useful information related to conductivity anomalies within the Precambrian and Phanerozoic sequences of the Paterson region. These may be correlated with different geological features or saline groundwater in the near-surface environment or within sandstone aquifers in the Phanerozoic cover of the region. However, the data may also be used to locate fresh groundwater resources, some examples of which are discussed below.

The palaeovalleys described in [Section 5.7](#) are each associated with distinct conductivity anomalies indicating that they are filled with conductive sediments and/or saline groundwater that makes the bulk conductivity of the sediments higher than that of the surrounding material.

There are a number of surface features related to broad groundwater flow systems or valley systems on the DEM and MRVBF images that may also be expected to show similar conductivity anomalies, but do not. These features either contain resistive sediments, or relatively fresh groundwater that lowers the bulk conductivity in a relative sense.

The Wallal Palaeovalley, in the northeast of the Paterson North survey area ([Figure 5.32](#)), is a large feature that was expected to be highly conductive, in keeping with the sediments filling the Canning and Disappointment palaeovalleys (c.f. [Figure 5.9, 5.18](#)). The Wallal Palaeovalley actually has only a very subtle conductivity anomaly associated with it, visible only in conductivity sections—the conductance image ([Figure 5.32](#)) shows no obvious conductance anomaly. The Wallal Palaeovalley is related to the other Eocene-Oligocene palaeovalleys in the region (van der Graaf *et al.*, 1977; Magee, 2009)) and is likely to have a similar-age sediment fill. However, it is not generally conductive and, short of containing vastly different sediments (which is unlikely), must therefore be filled with relatively fresh groundwater, unlike other palaeoriver systems in the region. Further evidence to support this includes the fact that the Wallal Palaeovalley does not drain a large salt lake system, unlike the Canning and Disappointment palaeovalleys, and therefore will not be charged with saline groundwater and may be a potential source of potable to brackish groundwater suitable for future exploitation.

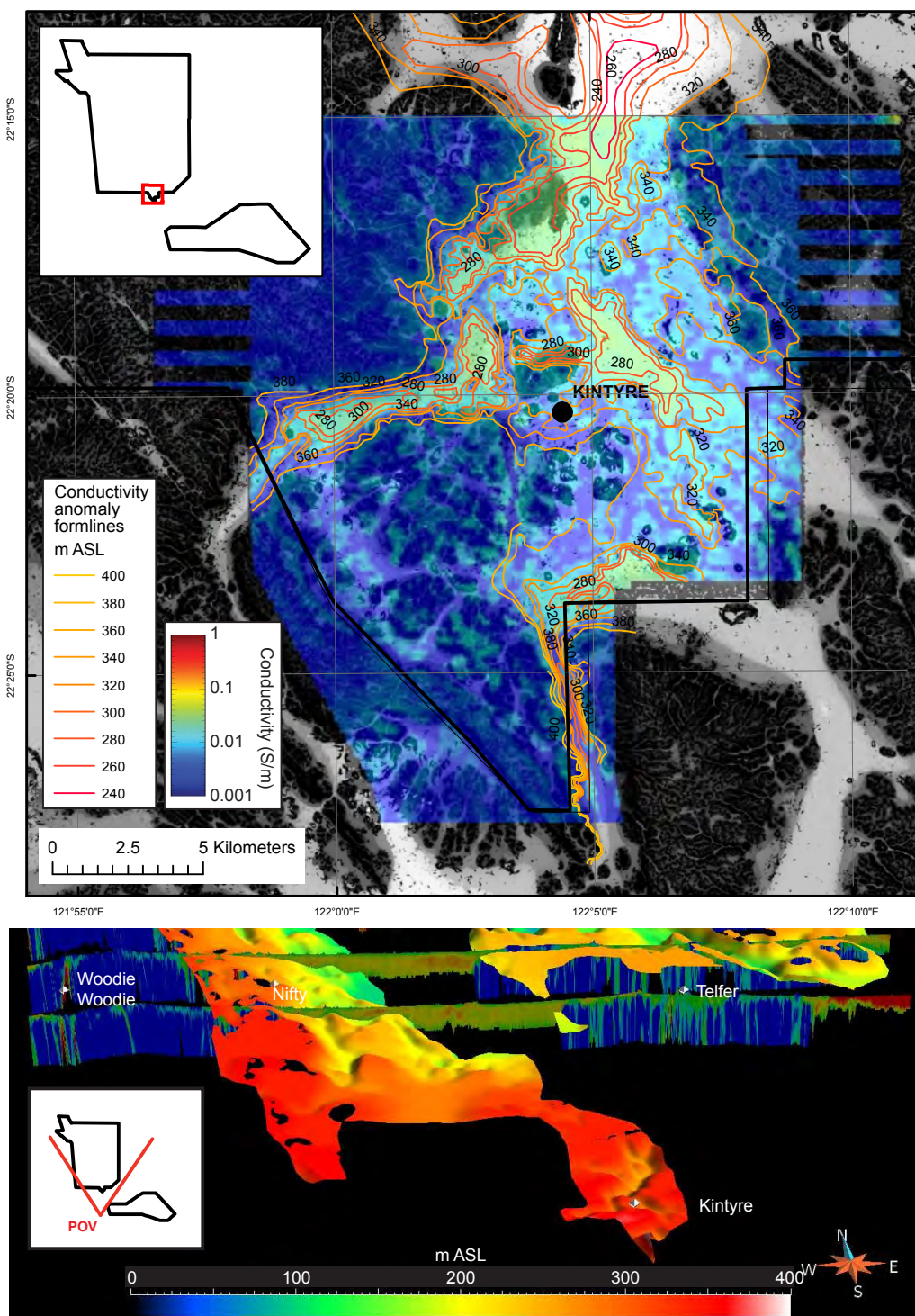


Figure 5.28: (Top) 20 m interval conductivity anomaly contours associated with the conductive Permian palaeovalleys in the Kintyre area. Contours are drawn on the interpreted Permian-Proterozoic unconformity surface. Image includes a 50 m ground pixel resolution grid of the 300-310 m GA-LEI conductivity elevation slice of 200 m line flight spacing AEM data (in colour) and the MRVBF6 image of the SRTM DEM (grey scale). (Bottom) Perspective view of the 3D Permian-Proterozoic unconformity surface shaded relief model generated from conductivity anomaly contours also showing selected GA-LEI conductivity sections.

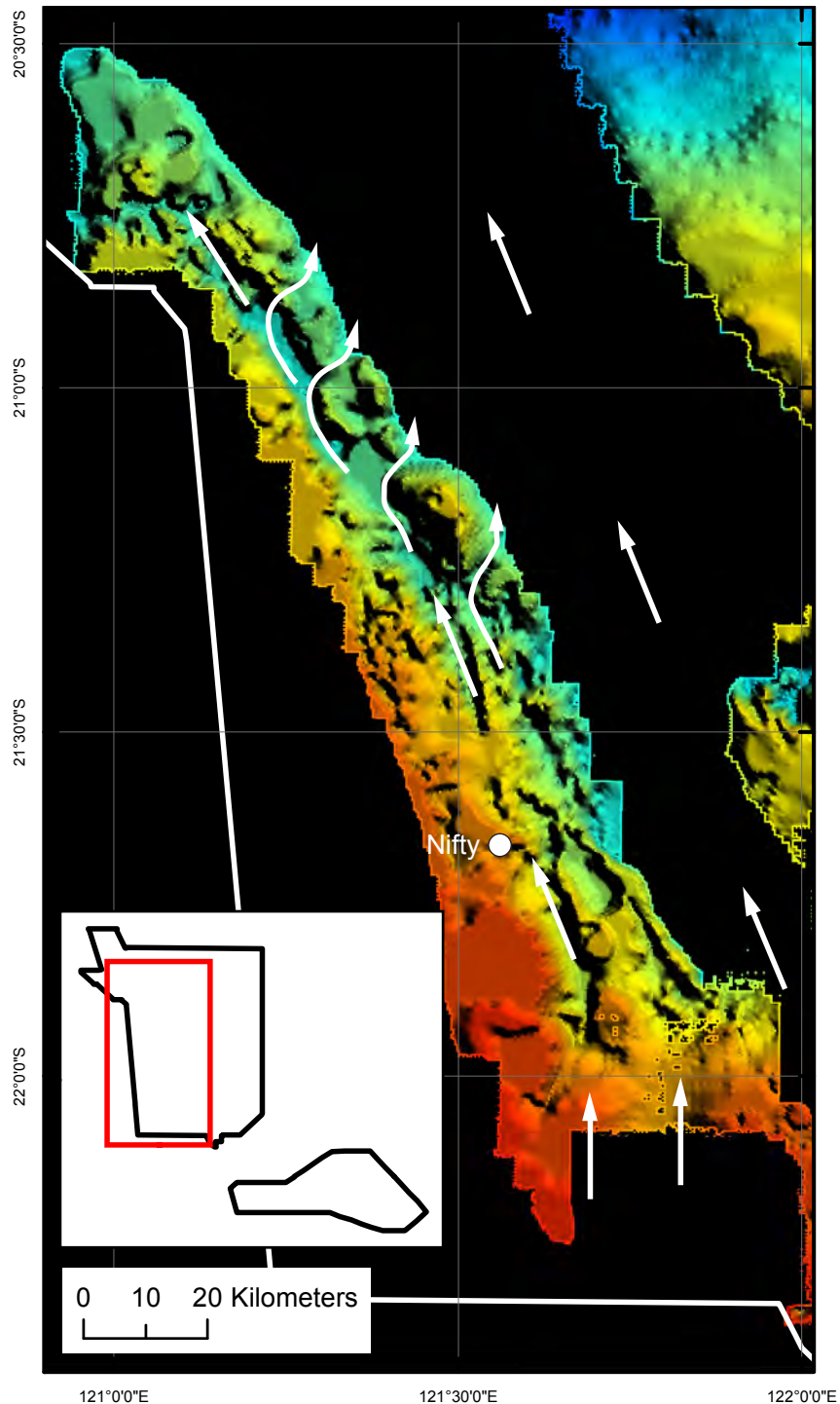


Figure 5.29: Shaded relief model of the interpreted Permian palaeovalley systems in the Throssell Shelf area with interpreted ice flow directions.

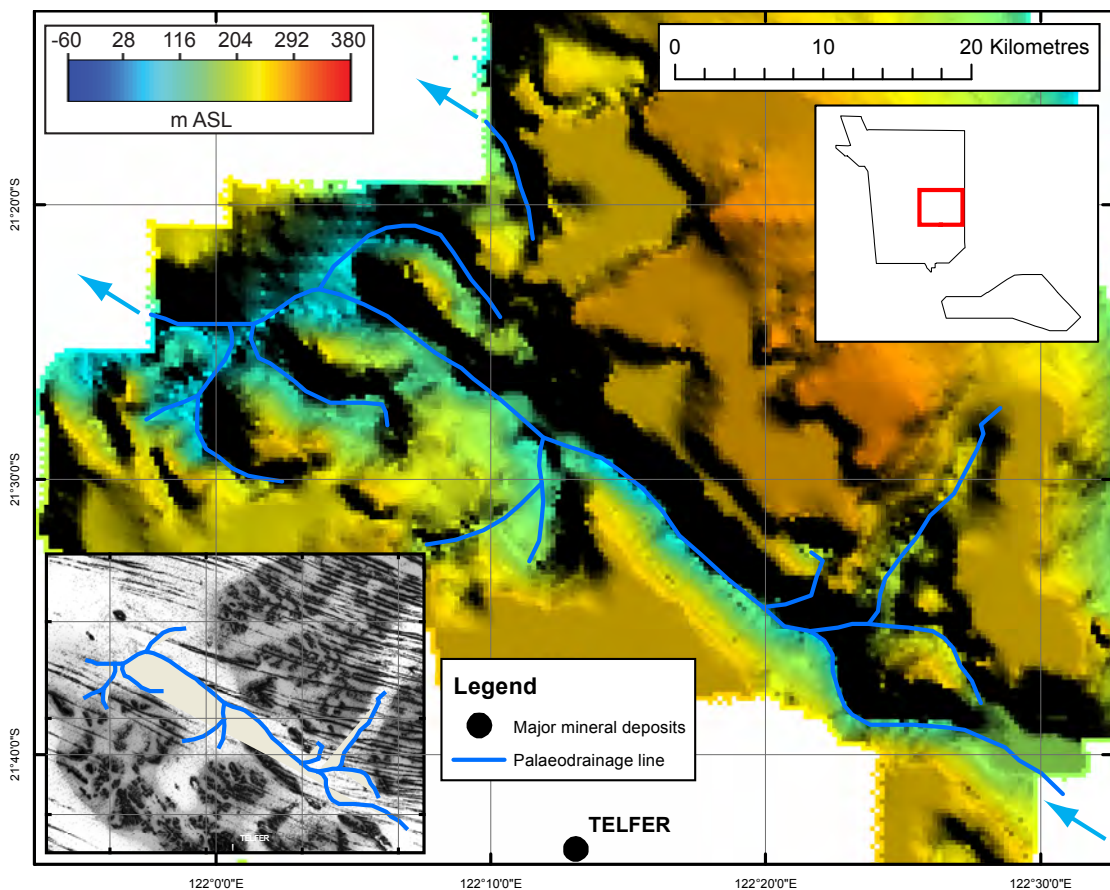


Figure 5.30: Shaded relief model of the unconformity surface of the Canning Palaeovalley interpreted from GA-LEI conductivity elevation slice data. Sediment fill in the Canning Palaeovalley is interpreted from drilling and literature review data to be a combination of Permian and Eocene to Oligo-Miocene sediment incised into Neoproterozoic Lamil Group rocks. The inset shows the MRVBF image for the same area, highlighting the low relief palaeodrainage system visible at surface.

The Telfer and Nifty palaeovalleys are smaller, fresh to brackish, palaeovalley groundwater systems in the region and are used to draw potable and process water for mining operations. While the regional-scale saline palaeovalley systems can be seen in the AEM data set, it is difficult to locate smaller palaeovalley systems like the Telfer and Nifty systems as the regional grids have a pixel size of 300 m. It may be possible to locate palaeovalley remnants within conductivity sections, however, it is difficult to connect these to adjacent flight lines, especially when they may be 6 km apart. Higher-resolution gridded data are required to make sense of landscape features and the conductivity data. The area flown around the Kintyre uranium deposit is ideal for this kind of analysis because the flight line spacing is 200 m and the grids have a pixel size of 50 m. Figure 5.33 depicts the conductivity anomalies around the Kintyre area, overlain on the 50-55 m conductivity depth slice with interpreted conductivity contours. The MRVBF image forms the backdrop to this image. For the most part, the conductivity anomaly follows the flat-lying areas within the MRVBF image that conform to valley bottoms, indicating that the valley bottoms are filled with conductive (saline) sediments. However, there are a number of areas where there are no conductivity anomalies across valley bottoms. There are several possibilities to explain these occurrences:

- The valley segment contains a thin sheet of sediments covering resistive bedrock close to surface;

- The sediments within the valley segment have different mineralogy and are resistive;
- The sediments within the valley segment are dry; or,
- The groundwater in the valley segment is fresh, resulting in a relatively low bulk conductivity for the valley segment.

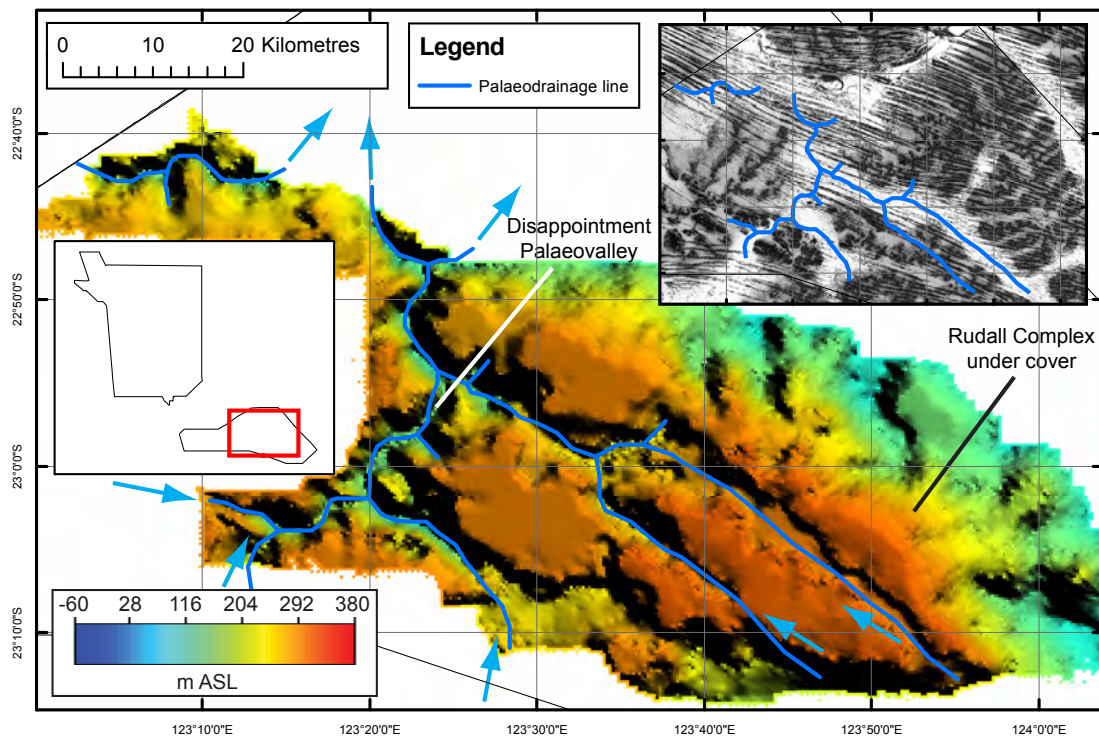


Figure 5.31: Shaded relief model of the Disappointment Palaeovalley interpreted from GA-LEI conductivity elevation slice data. The Rudall Complex in this image is covered by Permian and Mesozoic sediments of the Canning Basin and Quaternary fluvial and aeolian sediments. Sediment fill in the Disappointment Palaeovalley is interpreted from regional mapping and literature review data to be a combination of Permian and Eocene to Oligo-Miocene sediment incised into Paleoproterozoic Rudall Complex rocks. The inset shows the MRVBF image for the same area, highlighting the low relief palaeodrainage system visible at surface.

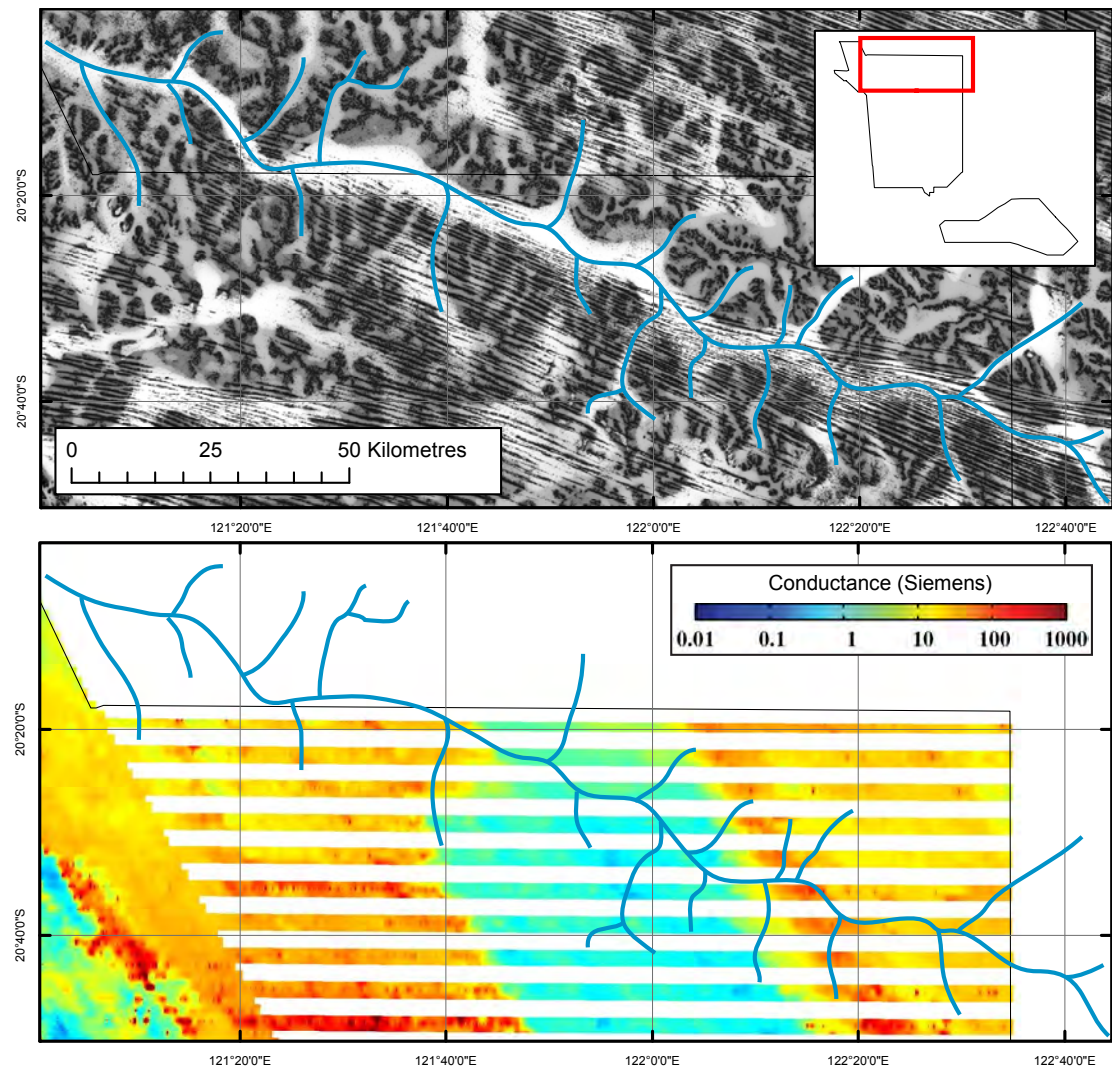


Figure 5.32: The Wallal Palaeovalley and tributaries (blue lines) highlighted over (top) a MRVBF image and (bottom) the GA-LEI 0-400 m conductance image. The Wallal Palaeovalley has no appreciable conductance anomaly associated with it, unlike the Canning and Disappointment palaeovalleys.

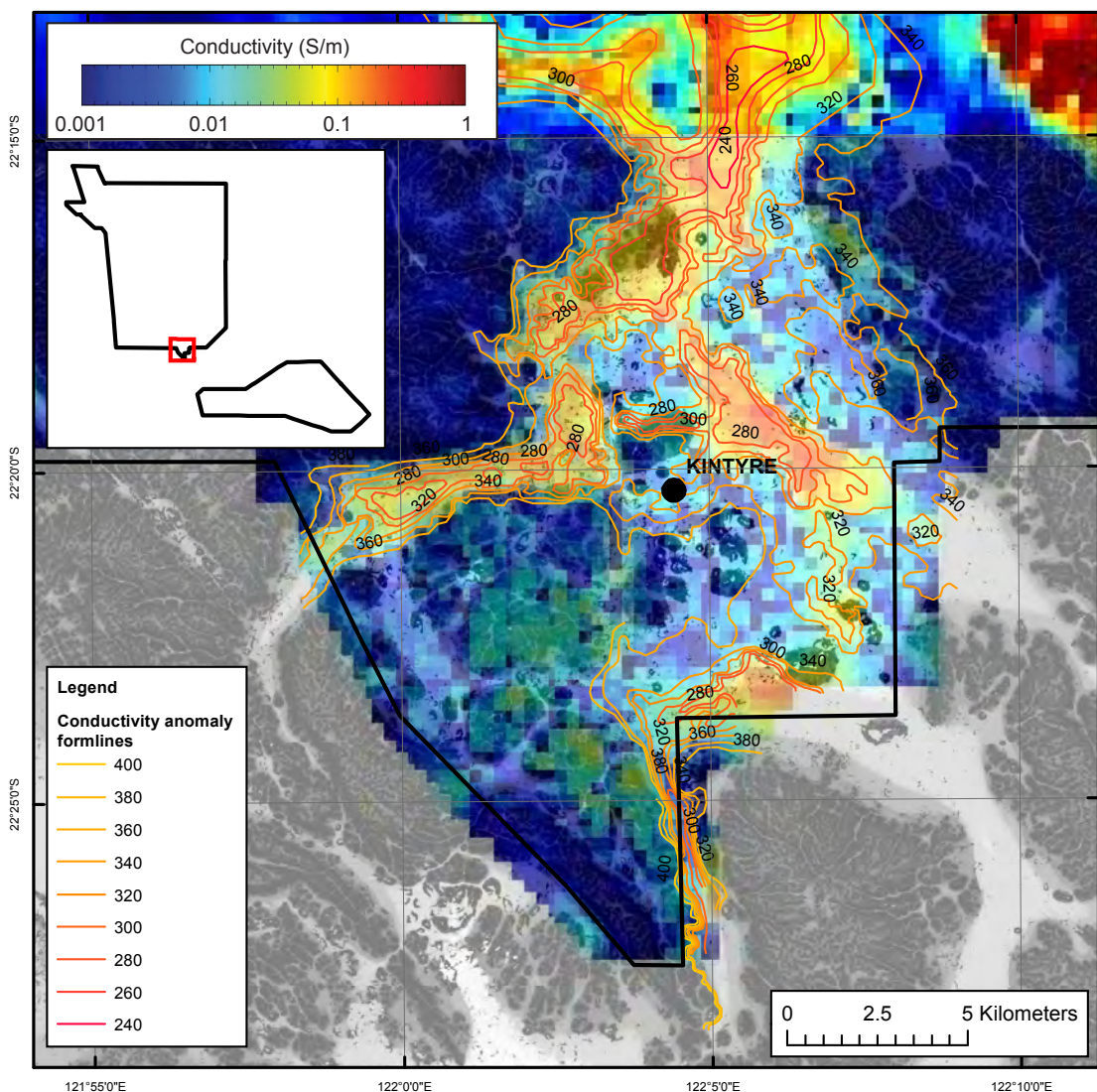


Figure 5.33: GA-LEI 40-60 m depth slice of AEM data in the Kintyre area highlighting the difference between conductive and resistive Permian sediment-filled palaeovalleys. The MRVBF image in the background (greyscale) highlights surface relief. Resistive valleys include examples about 8 km SW and 10 km ENE of Kintyre. The contours highlight the extent of the conductivity anomaly associated with conductive Permian valley fill sediments.

5.9 KNOWN MINERAL DEPOSITS

5.9.1 Nifty

Flight line 30860 is located over the Nifty copper mine, which is owned and operated by Aditya Birla Minerals. The section of flight line 30860 between 345000 mE and 360000 mE (Figure 5.34) shows the mine pit in the surface topography. The infrastructure around the mine site is seen in the X and Z component powerline monitors (not shown). The X and Z component data quality are negatively impacted by the transmitter height as well as the mining infrastructure. The GA-LEI conductivity section shows surficial anthropogenic materials with conductivity ranges of 35 to 500 mS/m on either side of the open cut indicating relocated conductive material in mine waste piles. Consistent with current understanding, the Nifty Member is a strongly silicified, pyritic and

carbonaceous black shale sequence that has conductivities ranging from 150 to 1000 mS/m at 200 m below surface. One-dimensional assumptions in the GA-LEI calculations result in edge artefacts at strong lateral contrasts in conductivity, which are visible in [Figure 5.34](#). The other geophysical responses over Nifty are discussed further in [Chapter 6](#).

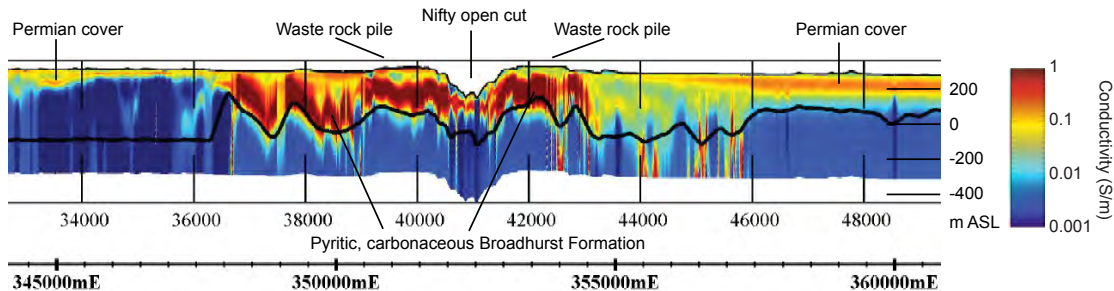


Figure 5.34: Subsection of conductivity section of line 30860 over the Nifty copper mine. The black line in the section is the DOI.

5.9.2 Telfer

Flight line 30890 is located over the Telfer gold-copper mine, owned and operated by Newcrest Mining Limited. The section of flight line 30860 between 415000 mE and 420000 mE ([Figure 5.35](#)) shows the Main Dome and West Dome open pits in the surface topography. The infrastructure around the mine site is seen in the X and Z component powerline monitors (not shown). The X and Z component data quality are negatively impacted by the transmitter height as well as the mining infrastructure. The GA-LEI conductivity section shows surficial anthropogenic materials with low conductivity of ca. 0.01 S/m indicating relocated resistive material in mine waste piles. A discrete conductor at 417000 mE, 400 m below Telfer Dome, is anomalous at 0.4 S/m and may represent the Telfer Deep deposit. The other geophysical responses over Telfer are discussed further in [Chapter 6](#).

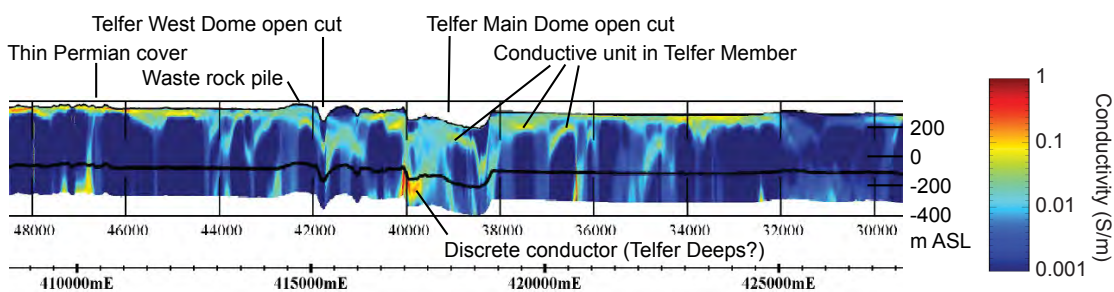


Figure 5.35: GA-LEI subsection of line 30890 over Telfer. The black line in the section is the DOI.

5.9.3 Kintyre

Flight line 41920 is located over the Kintyre uranium prospect, owned and under development by Cameco Australia and Mitsubishi Development Pty. Ltd. The section of flight line 30860 between 402500 mE and 406000 mE ([Figure 5.36](#)) shows the Rudall Complex outcropping with conductivity < 0.01 S/m. The Rudall Complex contains basement conductors (1 S/m) seen in this line and more extensively within the survey area. The flat lying, near-surface (to 100 m) conductors are Quaternary sediments (ca. 0.1 S/m) and Paterson Formation (0.1-0.5 S/m). The Coolbro Sandstone to the west of the section under the Paterson Formation is uniformly resistive at < 0.005 S/m. The other geophysical responses over Kintyre are discussed further in [Chapter 6](#).

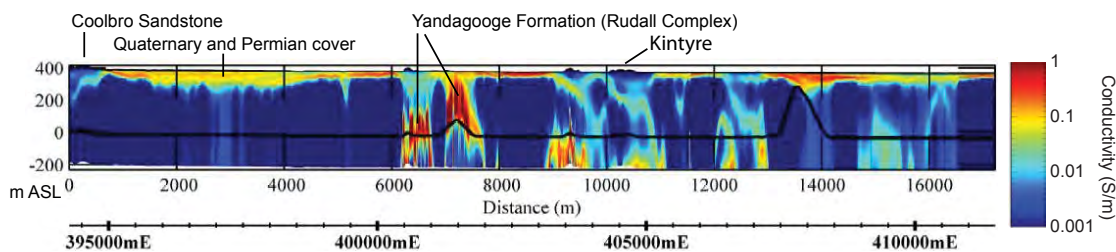


Figure 5.36: GA-LEI Line 41920 over Kintyre. The black line in the section is the DOI.

5.9.4 Woodie Woodie

Flight line 30850 is approximately 500 m to the north, and flight line 30860 is approximately 1500 m south, of Consolidated Minerals Ltd's Woodie Woodie manganese mine (Figure 5.37). The infrastructure around the mine site is still seen in the X and Z component powerline monitors for both lines (not shown). The X and Z component data quality are negatively impacted by the mining infrastructure. The GA-LEI conductivity section shows thin, flat-lying surface conductors to 0.3 S/m interpreted as palaeochannels. Below the surficial palaeochannels are weaker conductors, up to 0.04 S/m, showing similar electrical properties to the manganese ore as reported by Hashemi and Meyers (2004). The conductivity surfaces below 50 m appear to follow the palaeokarst topography within the Carawine Dolomite.

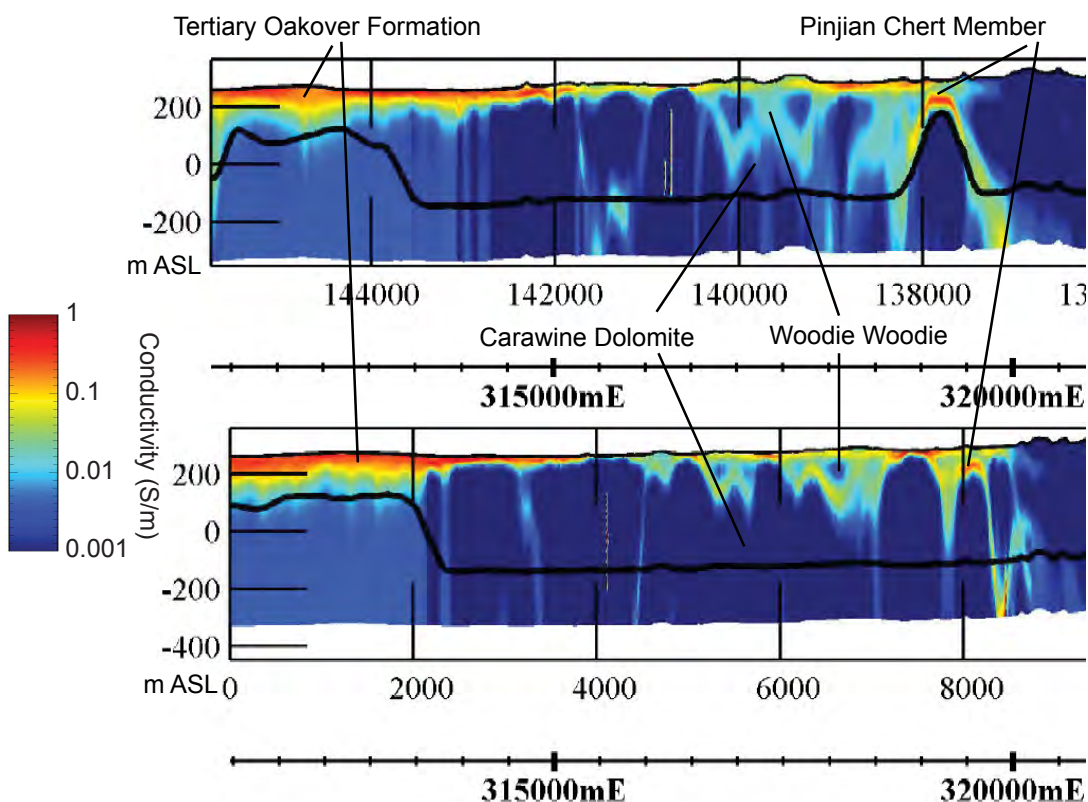


Figure 5.37: GA-LEI conductivity sections of lines 30850 (north of) and 30860 (south of) Woodie Woodie.

5.10 DISCRETE ANOMALIES

The primary goal of the AEM survey in the Paterson area was to provide context and to map potential unconformity, palaeochannel and calcrete uranium deposit host rocks. However, as a procedural step in the QA-QC process, the data were also examined for the presence of discrete conductors.

The multiplots delivered by FAS were the tool used for the interpretation of discrete conductors in a process described by Lane and Worrall (2002). The transmitter loop and receiver coil variations are observed in window amplitude responses when system geometry, receiver coil vibration and sferics exist. It is important to determine if the source of the discrete conductor effect is noise or variations in the subsurface conductivity distribution. Figure 5.38 shows an example of an X and Z component multiplot for line 20641, with a discrete conductor feature at fiducial 1410.

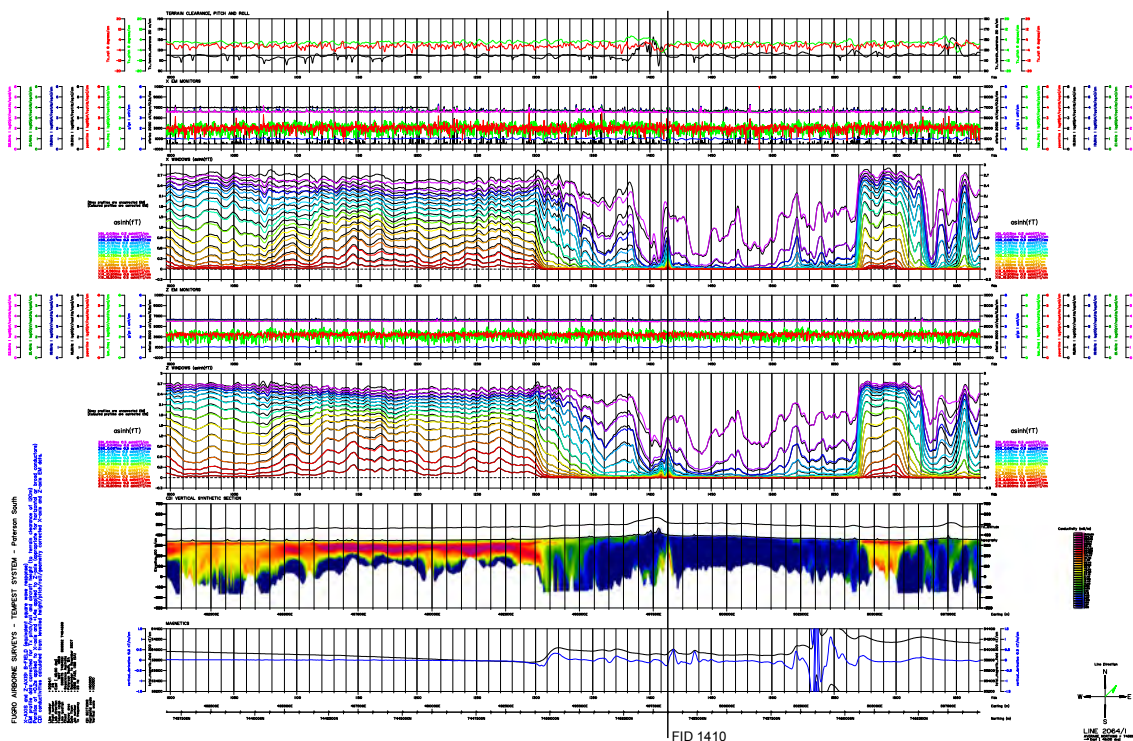


Figure 5.38: EM Flow multiplot created by FAS for line 20641 from the Paterson South survey area.

The discrete anomaly in the multiplot of line 20641 is expanded in [Figure 5.39](#) to highlight the discrete anomaly that is present at fiducial 1410.

Discrete anomalies are most prolific within the Rudall Complex. The conductors are associated with metamorphosed banded iron formation and/or graphitic schist and amphibolites. These discrete conductors could represent graphite-bearing fault zones in the sandstone or basement and as such may be prospective sites for uranium mineralisation (Energia, 2010). Copper and base metal mineralisation are often associated with such basement anomalies.

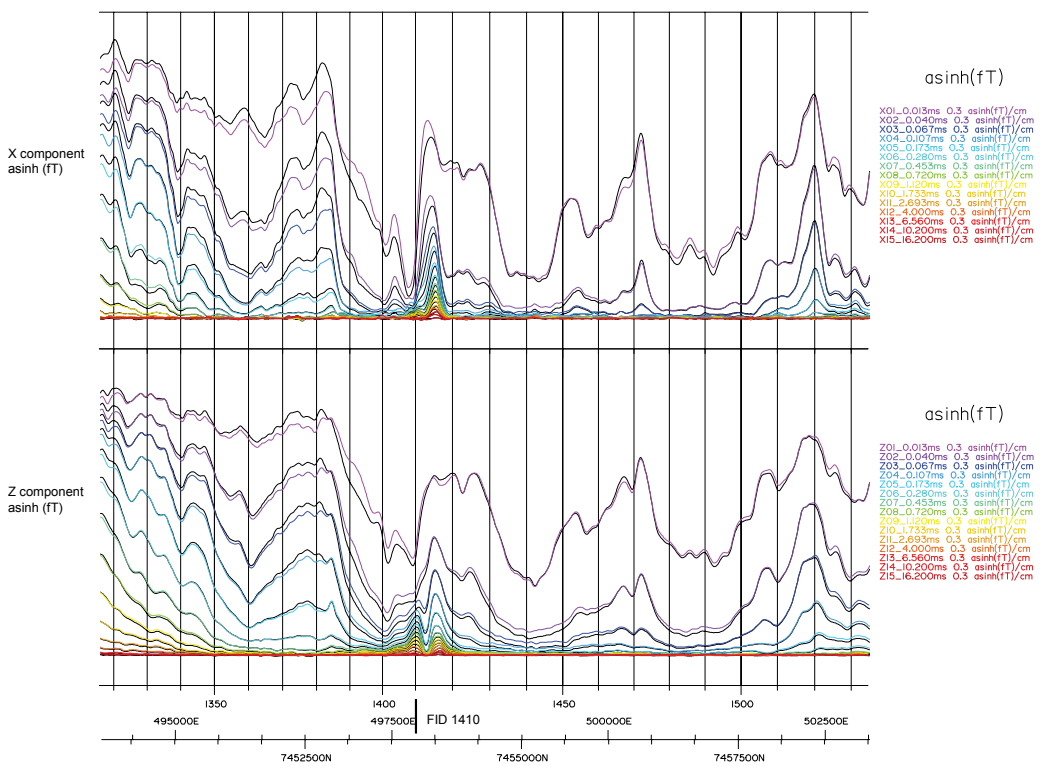


Figure 5.39: Sub-sections of the multiplot for line 20641 highlighting the discrete conductor response in the X and Z component windows.

Figure 5.40 shows a comparison subsection of EM FlowTM to the GA-LEI georeferenced jpeg for line 20641.

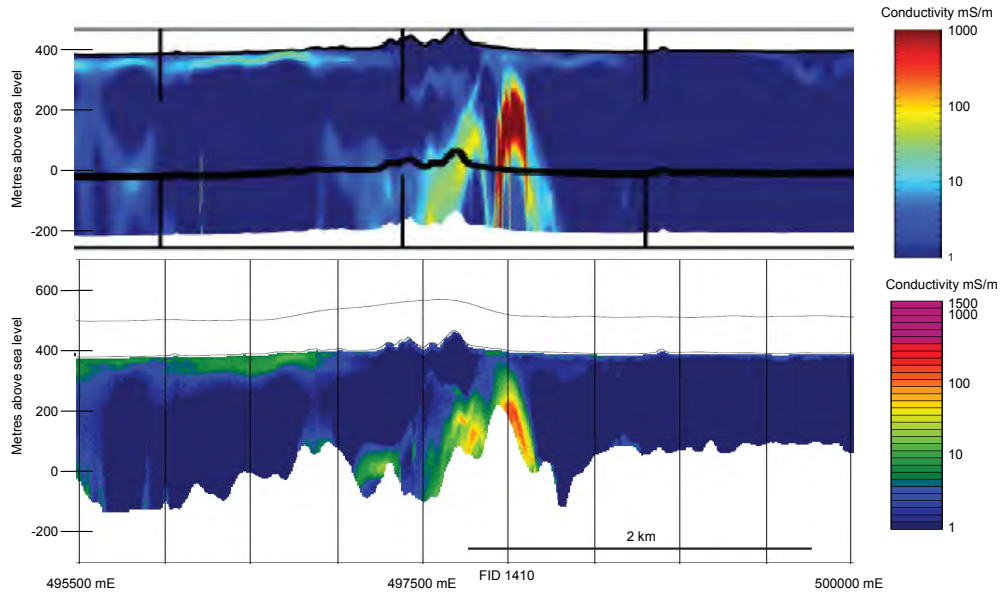


Figure 5.40: A comparison between EM FlowTM and GA-LEI for line 20641. The top panel is a subsection of the GA-LEI inversion for line 20641 highlighting the discrete conductor response. The bottom panel is a subsection of the FAS-supplied EM FlowTM CDI for line 20641. Please note the vertical exaggeration differs between plots.

5.11 REFERENCES

- Bacchin, M., Milligan, P., Tracey, R. and Wynne, P., 2008. New gravity anomaly map of the Australian region. *AUSGEO News 91 September 2008*.
- Bagas, L., Williams, I. R. and Hickman, A. H., 2000. Rudall, Western Australia (2nd Edition). 1:250,000 Geological Series - Explanatory Notes. Western Australia Geological Survey. 50 p.
- Beard, J. S., 1973. The elucidation of palaeodrainage patterns in Western Australia. Vegmap Publications, Perth. *Occasional Paper No 1*, 17 p.
- Beard, J. S., 2005. Drainage evolution in the Lake Disappointment Catchment, Western Australia - a discussion. *Journal of the Royal Society of Western Australia* **88**, 57-64.
- Costelloe, M. T., Roach, I. C. and Hutchinson, D. K., 2010b. Paterson AEM survey directly detects major unconformity near Kintyre, WA. *Preview April 2010(145)*, 40-41.
- CRA, 1991. Annual report for 1990 on exploration completed in the Rudall region, Rudall, WA SF510-10. Available via Western Australian Mineral Exploration Index (WAMEX). Report No. A33618. Online: <http://www.dmp/wa/gov/au/5136.aspx>.
- Czarnota, K., Gerner, E., Maidment, D. W., Meixner, A. J. and Bagas, L., 2009a. Paterson Area 1:250 000 Scale Solid Geology Interpretation and Depth to Basement Model. Geoscience Australia, Canberra. *Record 2009/16*, 37 p.
- Czarnota, K., Gerner, E., Maidment, D. W., Meixner, A. J. and Bagas, L., 2009b. Proterozoic Solid Geology of the Paterson Province, 1:250 000 scale map. Geoscience Australia.
- de Broekert, P. P. and Sandiford, M., 2005. Buried inset-valleys in the eastern Yilgarn Craton, Western Australia: geomorphology, age and alloigenic control. *Journal of Geology* **113**, 471-493.
- Energia, 2010. Energia Minerals Limited, Table Top. Online: <http://www.energaminerals.com/projects/westernaustralia.html>.
- Gallant, J. C. and Dowling, T. I., 2003. A multiresolution index of valley bottom flatness for mapping depositional areas. *Water Resource Research* **39(12)**, 1347-1359.
- Green, A. and Lane, R., 2003. Estimating Noise Levels in AEM Data. ASEG 16th Geophysical Conference and Exhibition, Adelaide, Australian Society of Exploration Geophysicists, February 2003.
- Hickman, A. H. and Bagas, L., 1998. Geology of the Rudall 1:100 000 sheet. Geological Survey of Western Australia, Perth. 30 p.
- Hickman, A. H. and Clarke, G. L., 1994. Geology of the Broadhurst 1:100 000 sheet, Western Australia. Western Australia Geological Survey, Perth. 40 p.
- Hunt, 1996. Hunt Oil Company Final report Waukarlycarly Seismic Survey interpretation. Western Australia Geological Survey, Perth. Statutory Petroleum Exploration Report **S10316 A5**.
- Lane, R. and Worrall, L., 2002. Interpretation of Airborne Electromagnetic Data: Summary report on the Challenger Workshop. Geoscience Australia Gawler Craton Mineral Promotion Project Canberra. *Record 2002/2*.
- Magee, J., 2009. Palaeovalley Groundwater Resources in Arid and Semi-Arid Australia. Geoscience Australia, Canberra. *Record 2009/03*, 224 p.
- Minty, B. R. S., Franklin, R., Milligan, P. R., Richardson, L. M. and Wilford, J., 2008. Radiometric Map of Australia (1st edition), scale 1:5 000 000., Geoscience Australia, Canberra.
- Minty, B. R. S., Franklin, R., Milligan, P. R., Richardson, L. M. and Wilford, J., 2009. The Radiometric Map of Australia. 20th International Geophysical Conference and Exhibition, Adelaide, Australian Society of Exploration Geophysicists, 22-25 February 2009.
- Percival, P., 2010. Index of airborne geophysical surveys. Geoscience Australia, Canberra. Record 2010/013. Online: https://www.ga.gov.au/products/servlet/controller?event=GEOCAT_DETAILS&catno=70295.
- Roach, I. C., 2009. A drill hole database for the Paterson airborne electromagnetic (AEM) survey, Western Australia. Geoscience Australia, Canberra. *Record 2009/31*, 16 p.
- Sattell, D., 2004. The resolution of shallow horizontal structure with airborne EM. *Exploration Geophysics* **35**, 208-216.

- Stewart, A. J., 2008. Surface Geology of Australia 1:1 000 000 scale, Western Australia. Geoscience Australia, Canberra. http://www.ga.gov.au/minerals/research/national/nat_maps/nat_geol_maps.jsp.
- van der Graaf, W. J. E., Crowe, R. W. A., Bunting, J. A. and Jackson, M. J., 1977. Relict Early Cenozoic drainages in arid Western Australia. *Zeitschrift für Geomorphologie NF* **21(4)**, 379-400.
- Williams, I. R. and Trendall, A. F., 1998a. Geology of the Pearana 1:100 000 sheet, 1:100 000 Geological Series Explanatory Notes. Western Australia Geological Survey, Perth. 33 p.
- Wynne, P. and Bacchin, M., 2009. Index of Gravity Surveys. Geoscience Australia, Canberra. Record 2009/07. Online: https://www.ga.gov.au/products/servlet/controller?event=GEOCAT_DETAILS&catno=68264.

6 Mineral systems of the Paterson region

D. L. Huston, K. Czarnota, S. Jaireth, N. Williams, D. Maidment, K. F. Cassidy, P. Duerden and D. Miggins

6.1 INTRODUCTION

Despite its remoteness, the Paterson region has, over the last four decades, become one of Western Australia's premier mineral provinces, containing deposits that are among the largest uranium (Kintyre), copper (Nifty), gold-copper (Telfer) and tungsten (O'Callaghans) deposits known in the state. Available data suggest that these deposits formed in two discrete geological intervals, between 840 and 810 Ma, possibly related to initial inversion of the Yeneena Basin, and between 655 and 615 Ma, temporally associated with intrusion of granites of the O'Callaghans Supersuite. The first metallogenic event includes major copper deposits at Nifty and, probably, Maroochydore, the Kintyre uranium deposit and, possibly, the Warrabarty zinc-lead deposit. The second metallogenic event produced the world-class Telfer gold-copper deposit, the Magnum gold-copper prospect, the O'Callaghans tungsten-zinc-lead-copper deposit and other minor, epigenetic gold-bearing deposits. The discussion below describes deposits formed during these two events and then uses these data, along with regional geological data, to formulate mineral system models considering geodynamic (or tectonic) setting, architecture, the origin of fluids and metals, fluid drivers and pathways, depositional processes at the site of mineralisation and post-depositional modifications (Barnicoat, 2007). A description of the regional geology is presented in [Chapter 3](#).

6.2 MINERAL SYSTEMS ASSOCIATED WITH THE MILES OROGENY

As discussed in [Chapter 3](#), geochronological data constrain deposition of the rocks that form the Yeneena Basin ([Figure 6.1](#)) to between 910 Ma, the age of the youngest detrital zircon in the basal Coolbro Formation (Bagas and Nelson, 2007), and ca. 830 Ma, the age of intermediate to mafic rocks that intrude the lower part of the basin (D. Maidment, unpublished data). These constraints are compatible with a Pb-Pb isochron age for carbonate rocks of the Isdell Formation of ca. 860 Ma (R. Maas and D.L. Huston, unpublished data), interpreted as a diagenetic age. Considering the uncertainties inherent in the age determinations, Czarnota *et al.* (2009a) inferred that sedimentation in the Yeneena Basin occurred between 850 and 830 Ma. Ages of 840-830 Ma for the Kintyre deposit (Maas and Bagas, in prep.; A. Cross, unpublished data), and of ca. 815 Ma for the Nifty deposit (Huston *et al.*, 2007; Huston *et al.*, 2009; see below) suggest mineralisation occurred during or after the latest period of sedimentation in the Basin, probably during the Miles Orogeny, which we interpret as the initial inversion of the Yeneena Basin between 850 and 800 Ma (see below).

6.2.1 Uranium-bearing deposits associated with the Coolbro Sandstone and Rudall Complex

Most uranium-bearing deposits and prospects in the Paterson region ([Figure 6.2](#)) are spatially associated with the Coolbro Sandstone, either hosted by this unit, by rocks of the unconformably underlying Paleoproterozoic and Mesoproterozoic Rudall Complex, or by rocks of the conformably overlying Broadhurst Formation. The largest known hydrothermal uranium deposit in Western Australia, Kintyre, is hosted by rocks of the Rudall Complex just below the unconformity with the Coolbro Sandstone. Other significant uranium prospects, including Sunday Creek and Mount Sears, are hosted by the upper part of the Coolbro Sandstone. Deposits hosted by the Broadhurst Formation are copper-dominated, although some, such as the Nifty deposits, contain local zones of uranium enrichment to 1000 ppm (Huston *et al.*, 2007). All of these deposits are polymetallic; other metals associated with uranium include copper, zinc-lead, gold and platinum group elements. This suggests that potential for all of these metals is present within the Coolbro Sandstone or in immediately adjacent units and requires assessment.

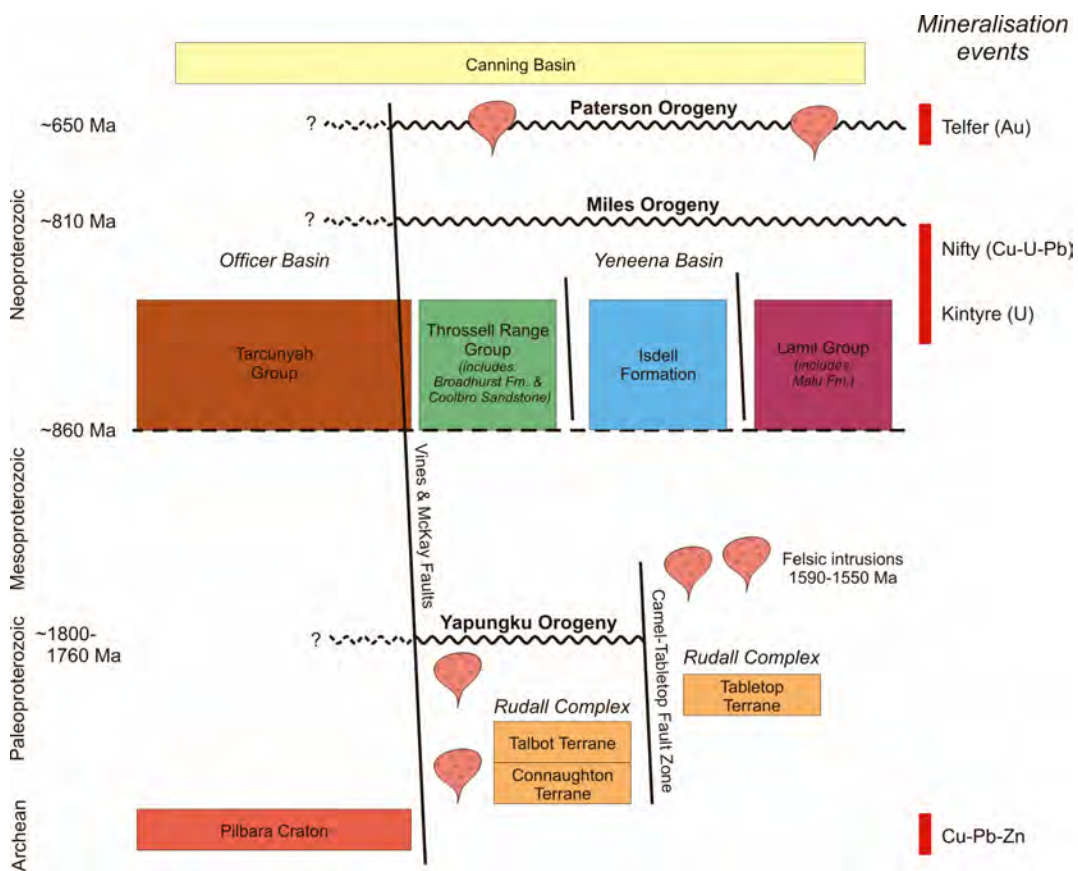


Figure 6.1: Simplified event history of the Paterson region, emphasising the main units within the AEM survey area.

6.2.1.1 Kintyre deposit

Following up anomalies generated from a detailed helicopter-based radiometric survey, CRA Exploration Pty. Ltd. (now Rio Tinto Exploration Pty. Ltd.) discovered uranium mineralisation cropping out at the Kintyre deposit in April 1985. Drilling commenced in October 1985, with the first drill hole intersecting 77 m grading 0.25 wt. % U_3O_8 . In 1988, a non-JORC compliant resource of 36,000 t U_3O_8 was announced at grades between 0.15 and 0.40 wt. % U_3O_8 (Jackson and Andrew, 1990). Kintyre, which is the largest hydrothermal uranium deposit, and the second largest uranium deposit in Western Australia, is the most significant of a number of polymetallic mineral occurrences hosted by the Paleo- to Mesoproterozoic Rudall Complex. Other occurrences include the Tracy (also known as Yandagooge) and Lead Hills prospects to the north and the Wellington and several other prospects to the south (Hickman and Clarke, 1993). Despite the importance of the Kintyre discovery, very little public data are available about this deposit. Important references include Jackson and Andrew (1990), Gauci and Cunningham (1992), Hickman and Clarke (1993), Root and Robertson (1994), Gauci (1997), and McKey and Miezitis (2001). The following description is based on these references and discussions with A. McKay (Geoscience Australia).

6.2.1.1.1 Geology, age and origin

The Kintyre and nearby deposits are hosted by the Paleo- to Mesoproterozoic Rudall Complex, with the Kintyre deposit and prospects to the north and west hosted by metasedimentary rocks of the Yandagooge Formation, and the Wellington and nearby prospects hosted by an unnamed quartzite that contains thin units of banded iron formation. Most of these deposits are located within two kilometres to the northeast of northwest-striking thrust faults mapped by Hickman and Clarke (1993).

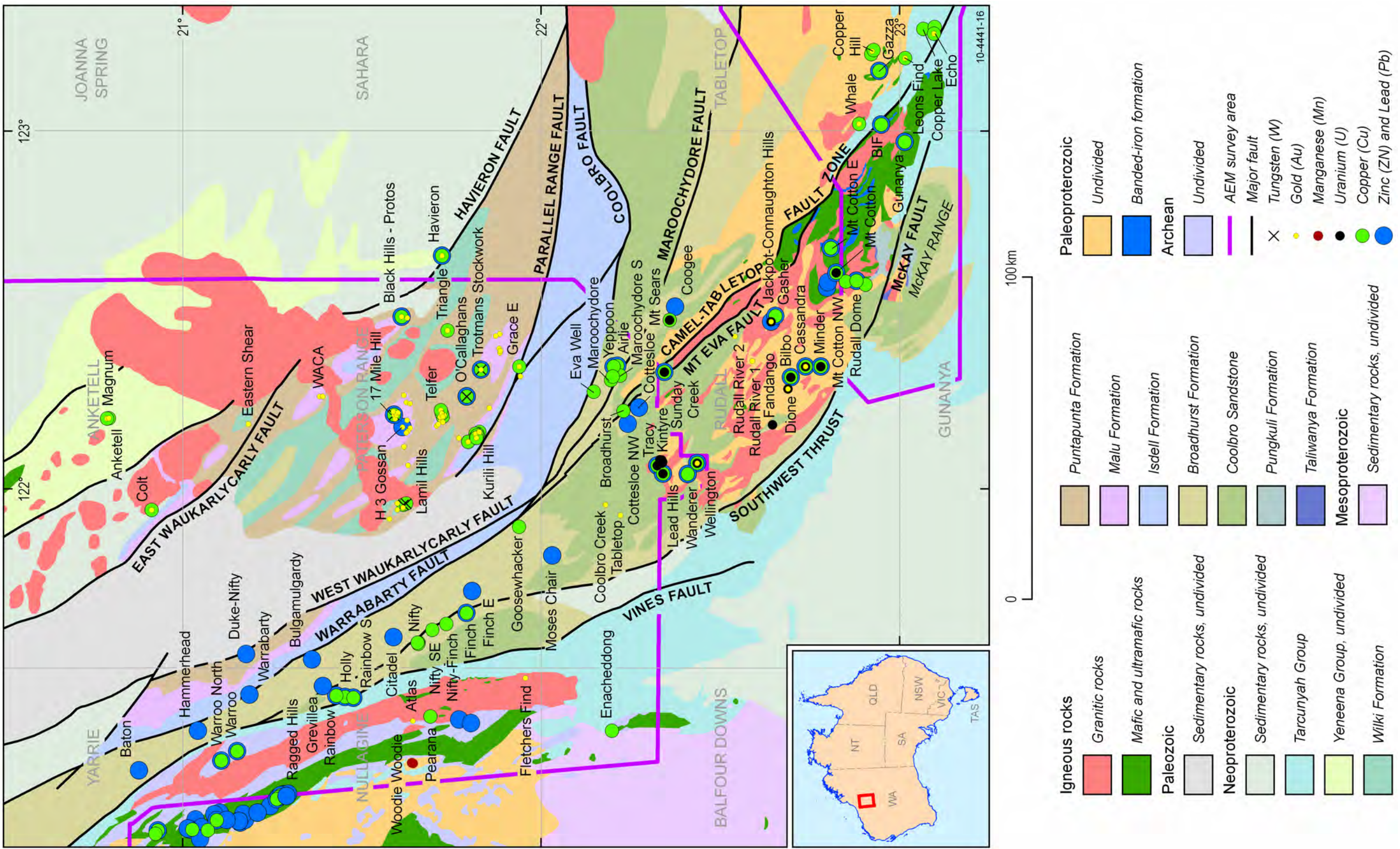


Figure 6.2: Simplified solid geology of the Paterson region showing the location of uranium, copper and zinc-lead deposits and prospects.

In detail, the Kintyre deposit comprises five ore zones: Kintyre-East Kintyre; Whale; East Whale; Pioneer; and, Nerada. [Figure 6.3](#) shows the most recent interpretation of the geology of the Kintyre lens, which is based upon the results of underground mapping on exploratory workings developed in 1996 (Gauci, 1997; McKay and Miezitis, 2001). Uranium occurs mostly as pitchblende in a series of narrow, closely-spaced carbonate-chlorite veins. These veins, which dip ca. 60° to the northeast (McKay and Miezitis, 2001), have a similar orientation to the regional thrust faults mapped by Hickman and Clarke (1993).

The veins are hosted by chlorite-quartz schist, chlorite-carbonate-quartz schist and chloritic and garnetiferous quartzite (Jackson and Andrew, 1990), which form a stratigraphic unit that is structurally overlain by dolomite and underlain by biotite-graphite schist ([Figure 6.3](#); Gauci, 1997; McKay and Miezitis, 2001). This succession is folded by a recumbent (regional F2; local F1: Bagas, 2004a)¹ fold with a shallowly east-dipping axial plane, which appears, based on trend lines in bedding within the host unit, to be refolded by an asymmetric regional F₄ (local F₂) fold with an axial plane dipping moderately to the northeast. The uraniferous veins tend to be concentrated in the hinges of these folds and have an orientation sub-parallel to the axial planes ([Figure 6.3](#)). Northwest-striking faults, parallel to the axial planes of the F₄ folds, separate the ore lenses (Bagas, 2004a). Before the existence of underground development, the veins were interpreted to occur in east-west-striking bedding-plane faults, breccia zones and shears (Root and Robertson, 1994).

Although the host unit contains a wide variety of rock types, the more competent siliceous chloritic and garnetiferous quartzite preferentially host the uraniferous veins (Root and Robertson, 1994). The host rocks are extensively chloritised, with primary garnet totally altered to chlorite near mineralised zones. Other alteration minerals include carbonate and martite (hematite), which replaces magnetite. The veins are dominated by the assemblage chlorite-carbonate, with carbonate minerals including dolomite, ankerite and calcite. Colloform pitchblende is the dominant ore mineral, with minor bismuthinite, chalcopyrite, bornite and galena, and trace native bismuth and gold. Platinum group elements have also been noted with gold, which has a geochemical association with copper and bismuth (Jackson and Andrew, 1990). Small quantities of pitchblende are present as microscopic disseminated grains in the wall rock, although this style of mineralisation is much lower grade than the vein-hosted style, and forms only a minor part of the total resource (Jackson and Andrew, 1990).

Maas and Bagas (in preparation) reported an age of 841 ± 10 Ma based on TIMS analysis of large pitchblende separates. Currently this is the best estimate for the age of the Kintyre deposit, and, by inference, the age of other uranium prospects hosted by the Rudall Complex (see below).

6.2.1.1.2 Geophysical characteristics

Root and Robertson (1994) reported the results of a systematic assessment of the geophysical signature of the Kintyre deposit. These surveys, which included ground and aircraft-based magnetics, radiometrics and electromagnetic surveys, and ground-based gravity, resistivity and induced polarisation surveys, along with a down-hole IP-resistivity survey, yielded varying responses. Many of the geophysical characteristics they describe can be observed with public domain, regional-scale datasets reproduced in [Figure 6.4](#). As discussed above, the deposit was discovered as a radiometric anomaly in the bismuth-214 (²¹⁴Bi) channel (a decay product of uranium-238 [²³⁸U]), and this is evident as a 300-400 m wide anomaly of up to 8 ppm uranium equivalent in the regional radiometric data.

The host rocks at Kintyre are associated with a series of other regional geophysical anomalies, although the radiometric anomaly is the only one unequivocally related to mineralisation. The deposit is associated with one of several low amplitude, short wavelength magnetic highs, and lies on the shoulder of a gravity high (Root and Robertson, 1994). The complex nature of the magnetic

¹ In this section we use the regional structural nomenclature of Hickman and Clarke (1993); where appropriate we also indicate local structural nomenclature.

response makes resolution of discrete, ore-related magnetic features difficult. The gravity high is interpreted to be a consequence of the high-density metapelitic rocks that host the deposit, and not the ore lenses. Similarly, the resistivity anomaly described by Root and Robertson (1994) and the relatively resistive subsurface in conductivity depth slices is interpreted to reflect the resistive host rocks—metachert, carbonate and quartzite.

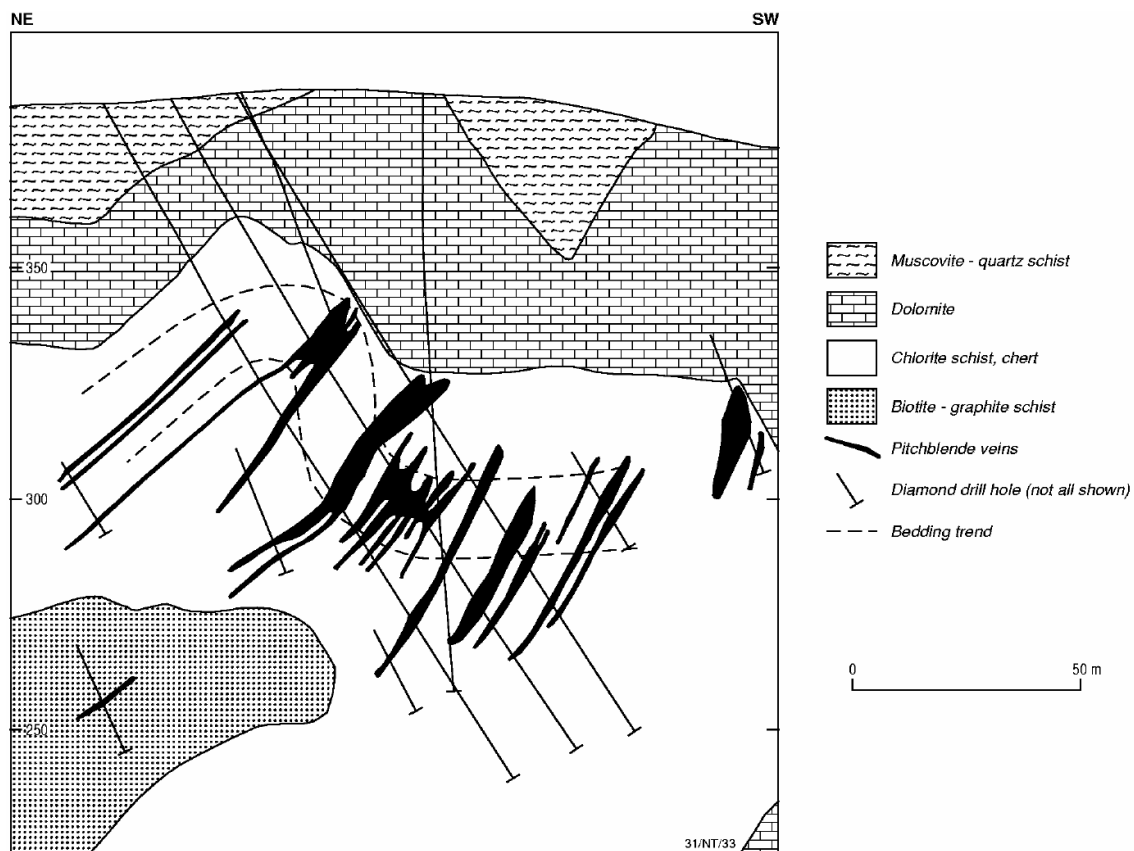


Figure 6.3: Geological cross section of the Kintyre ore lens, Kintyre uranium deposit, from McKay and Miezitis (2001) after Gauci (1997).

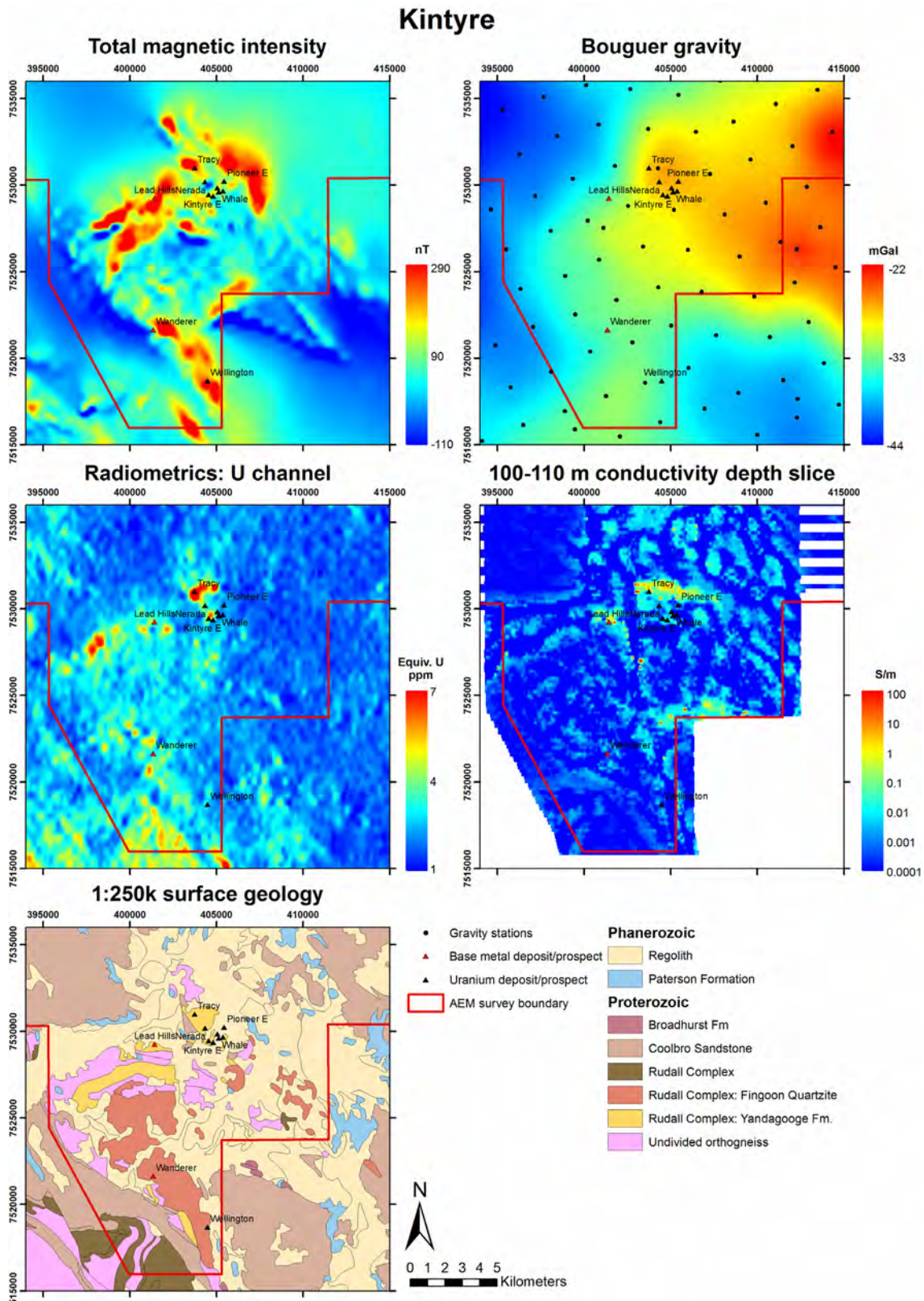


Figure 6.4: Geophysical signature of the area surrounding the Kintyre uranium deposit. Total magnetic intensity, Bouguer gravity and radiometric data are extracted from the Geophysical Archive Data Delivery System (GADDS: <http://www.ga.gov.au/gadds>). The conductivity depth slice was prepared in this study (Chapter 4). The surface geology is simplified from Bagas et al. (2000).

From their detailed surveys, Root and Robertson (1994) identify a strong IP conductivity response spatially associated with mineralisation, but note that it could be explained by minerals other than sulfides, including pitchblende and graphite. In fact, the conductivity Geoscience Australia layered earth inversions (GA-LEIs) described in [Chapter 5](#) indicate that there may be more conductive (and potentially chargeable) features at depth either associated with the Kintyre Fault or pyritic graphite schist in the Yandagooge Formation of the Rudall Complex. These successions shallow to the north and can be seen in the 100-110 m conductivity depth section 1-2 km north of Kintyre ([Figure 6.4](#)), where they outcrop at Tracy Hills and Lead Hills (below; Clarke, 1991).

6.2.1.2 Other uranium prospects hosted by the Rudall Complex

The other uranium deposits in the vicinity of Kintyre, in most cases consisting of an occurrence at the surface, are poorly described. The Tracy prospect comprises a 20-30 m wide, folded, stratabound pyritic zone that passes along strike into ankerite-siderite-quartz "iron formation" and goethitic chert. This zone is located near the contact between graphite-quartz-sericite schist and quartz-sericite-biotite schist. Base metals, though present, are generally below 1000 ppm, with galena present in sulfide veinlets. Mineralisation at Lead Hills is similar to the Kintyre deposit, although lenticular siderite veins with galena are present in carbonate units (Hickman and Clarke, 1993). Both of these prospects are hosted by the Yandagooge Formation, with the Tracy prospect less than 1 km to the northeast of a northwest-striking (in the hanging wall), northeast-dipping thrust fault that juxtaposes the Coolbro Sandstone against basement.

About 10 km to the south of Kintyre, Hickman and Clarke (1993) report a series of uranium-bearing prospects along a north-northwest trend, including the Wellington prospect in the southeast ([Figure 6.2](#)). These prospects also contain gold, copper and lead. The prospects are hosted by sulfide-bearing chlorite-muscovite schist in Rudall Complex quartzite and gossans commonly contain more than 1000 ppm total base metal, more than 100 ppm bismuth and molybdenum and up to 0.12 wt. % U_3O_8 (Hickman and Clarke, 1993). At one of these prospects, Wanderer, which is hosted by sulfidic chlorite schist and quartzite, a pre-JORC resource of 0.2 Mt grading 1-2 wt. % copper was identified. Many of these prospects are within 2 km of mapped northwest-striking thrust faults ([Figure 6.2](#)).

The Tracy and Lead Hills prospects, which are hosted by the Yandagooge Formation, are associated with magnetic highs and relatively conductive rocks ([Figure 6.4](#)), more conductive than those that host Kintyre. In contrast, the series of quartzite-hosted prospects between Wellington and Wanderer are associated with magnetic highs and more resistive rocks. All are associated with stronger magnetic responses than Kintyre. Notable magnetic and conductive rocks indicative of the Yandagooge Formation are identified under cover near the AEM survey boundary 5 km northeast of Wanderer.

Hickman and Bagas (1999) describe a series of polymetallic, uranium-bearing prospects hosted by the Yandagooge Formation located ca. 50 km south-southeast of the Kintyre deposit ([Figure 6.2](#)). These prospects, which include the Bilbo, Dione, Cassandra and Minder prospects, also contain base metals, gold, silver and bismuth and are spatially related to northwest-striking faults. At Bilbo and Dione, secondary mineralisation occurs in flat-lying zones within the regolith and is interpreted to be developed from primary, shear-zone-related mineralisation which contains uraninite in addition to pyrite, galena, chalcopyrite, nickel-cobalt-arsenate minerals and bismuth-antimony minerals (Hickman and Bagas, 1999).

At Cassandra, uraninite and coffinite are hosted by veins in D_4 fractures and shears in association with silicified pegmatite and with sericite, hematite and albite hydrothermal alteration. At Minder, uraninite is associated with albite-altered D_4 shear zones in iron-rich pelite along pegmatite margins. Traces of galena, chalcopyrite, sphalerite and lead-bismuth sulfides are also present with the uraninite (Hickman and Bagas, 1999). Unlike the deposits near Kintyre, these latter two deposits seem to be associated with albite alteration assemblages more characteristic of metasomatic uranium deposits.

6.2.1.3 Summary of the characteristics of prospects hosted by the Rudall Complex

Geological features that seem to characterise most uranium-bearing deposits hosted by the Rudall Complex include:

1. A spatial association with northwest-striking D₄ faults;
2. A lithological association with the magnetic and conductive Yandagooge Formation, particularly iron-rich or carbonaceous successions (Kintyre, Tracy, Lead Hills and Minder) or quartz-rich rock with interbedded banded iron formation (Wellington and Wanderer); and,
3. A polymetallic character, including one or more of copper, lead, zinc, silver, gold, platinum group elements, bismuth, molybdenum and antimony.

Although limited by the amount of data available, there is also what appears to be some important differences in the styles of mineralisation. For instance, prospects in the northwestern part of the Rudall Complex have a close association with remnant outliers of Coolbro Sandstone, particularly where northwest-striking faults juxtapose Coolbro Sandstone against basement rocks, and with hematite- and albite-bearing alteration assemblages. This association is not observed in the southeastern prospects, where the Coolbro Sandstone has been eroded. The style of alteration also differs between the northwestern deposits, which are characterised by chlorite-dominated assemblages, and the southeastern deposits, which are associated with sericite-albite-dominated assemblages. However, in both cases, uranium is associated with hematite alteration.

6.2.1.4 Prospects hosted along the Coolbro Sandstone and Broadhurst Formation contact

In addition to deposits hosted by the Rudall Complex, uranium-bearing prospects are also present at the contact between the Coolbro Sandstone and the overlying Broadhurst Formation. These prospects are generally associated with faults, and include the Sunday Creek, Mount Sears, and Fandango prospects ([Figure 6.2](#)). In addition, there are a number of other unnamed uranium-bearing (> 100 ppm equivalent U₃O₈ [eU₃O₈]) occurrences along this contact. Like deposits hosted by the Rudall Complex, these prospects are polymetallic, containing copper and lead (Sunday Creek and Mount Sears) and zirconium (Fandango).

6.2.1.4.1 Geology, age and origin

As all uranium prospects and occurrences in the Coolbro Sandstone are at very early stages of exploration, very little information is publicly available, with the most useful descriptions in Swingler (1981), Schwabe (1981), Hickman and Clarke (1993), Hickman and Bagas (1999) and de Angelis (2009). At Sunday Creek, surface samples were collected to follow up a radiometric anomaly and yielded grades of up to 7 wt. % uranium, 1.12 wt. % lead and 0.85 wt. % copper. Subsequent drilling yielded a best intersection of 603 ppm eU₃O₈ over 1.3 m (Hickman and Clarke, 1993; de Angelis, 2009). Although associated with a north-northwest-striking faults (c.f. 1:100 000 geological map: Hickman and Clarke, 1993), the mineralised zone is strataform. It is localised on the contact between the Coolbro Sandstone and the overlying Broadhurst Formation and can be traced for 800 m along strike (Swingler, 1981). The mineralisation consists of disseminated pitchblende, chalcopyrite, covellite and torbernite hosted by both massive, black, carbonaceous and pyritic quartzite of the Coolbro Formation and by black carbonaceous shale of the Broadhurst Formation (Swingler, 1981).

At Mount Sears, uranium-copper mineralisation is described as being associated with a synclinal cross fold with a northeast plunge (Schwabe, 1981). The fold closure is characterised by an increase in the intensity of east-striking quartz veining, taken to indicate faulting and shearing. The Mount Sears prospect extends from the fold closure to the north and along its west limb for at least 400 m. The mineralised zone is strataform, being localised along the contact between the Coolbro Sandstone and Broadhurst Formation, and occurring in both units (Schwabe, 1981). Bedding and the mineralised zone have dips of around 50-70° to the east.

Petrographic reports by H.W. Fander (in Schwabe, 1981) describe both disseminated and veinlet-hosted sulfide minerals, including pyrite, pyrrhotite, chalcopyrite and galena, inferring an epigenetic (although possibly remobilised) origin in most cases. The same report cited colloform coffinite, but noted that this mineral could also be pitchblende, and that thulcite could also be present. The colloform coffinite had a close association with carbonaceous matter. Schwabe (1981) also reported disseminated pyrite, covellite, chalcopyrite and pitchblende as well as sulfide minerals associated with quartz-carbonate veinlets.

Down-hole gamma-ray logs on holes drilled at Mount Sears all indicated local uranium enrichment, with highest grades of ca. 1300 ppm eU₃O₈, although the intersections were, in general, narrow, the thickest being 1.9 m grading 1306 ppm eU₃O₈. Copper grades up to 0.16 wt. % are also reported. In both drill holes SC2 and SC3, uranium enrichment (as established from both gamma-ray logs and geochemical analysis) is best developed in the Coolbro Sandstone and copper enrichment is restricted to the overlying Broadhurst Formation. In drill hole SC1, the greatest uranium enrichment is in Coolbro Sandstone, described as black, feldspathic sandstone which becomes white with depth (see Plates 5 to 7 in Schwabe, 1981).

In addition to these prospects, a series of percussion drill holes targeted radiometric anomalies along the contact between the Coolbro Sandstone and Broadhurst Formation on the northeastern limb of the Cottesloe Syncline. These drill holes successfully intersected narrow uranium mineralised zones (for details see de Angelis, 2009). The best intersection was 1.9 m grading 893 ppm eU₃O₈ at BR7.

Further to the south, the Fandango uranium-zirconium prospect ([Figure 6.2](#)) is hosted by the Coolbro Sandstone near its contact with the Broadhurst Formation and close to the closure of the Camelot Syncline. At this locality, the sandstone is strongly fractured, with the fractures infilled by quartz-limonite veins. The host sandstone is strongly brecciated, with the matrix being extensively sericitised and kaolinitised. The matrix is also rich in zircon (>1 %), which may account for part of the uranium enrichment (Hickman and Bagas, 1999).

Finally, in the northern part of the Paterson region, the Rainbow copper-zinc prospect (no reported uranium) is hosted just above the contact between the Coolbro Sandstone and the Broadhurst Formation and has been traced for over 4 km of strike length. This prospect has been described as a sheet-like body, less than 1 m thick, of disseminated to massive sulfide, with a sulfide assemblage of chalcopyrite and subordinate bornite (Haynes *et al.*, 1993). A best intersection of 54 m grading 0.3 wt. % copper has been reported for this deposit (Anderson *et al.*, 2001). Haynes *et al.* (1993; their Figure 6) indicate the presence of a lead-zinc-enriched zone several tens of metres above the copper zone.

6.2.1.4.2 Geophysical characteristics

Regional geophysical data over Sunday Creek, Mt Sears Range and the Cottesloe prospects is shown in [Figure 6.5](#). The most notable feature is the degree to which rocks of the Broadhurst Formation in the Cottesloe Syncline are mapped out as a magnetic high, gravity low, uranium and potassium channel radiometric highs and most clearly a conductive high. The surrounding Coolbro Sandstone has lower magnetic, radiometric, and conductivity responses, but perhaps a slightly higher gravity response.

The Sunday Creek, Mt Sears, and the Cottesloe prospects all lie in less magnetic rocks adjacent to magnetic highs and the close association with a magnetic gradient may be important. Mt Sears and the Cottesloe prospects are associated with high uranium-channel radiometric anomalies, but the deposit anomalies may be indistinguishable from the background value for the Broadhurst Formation. The Cottesloe prospects are associated with the high conductivity Broadhurst Formation; the Sunday Creek and Mt Sears prospects lie outside of the AEM survey area.

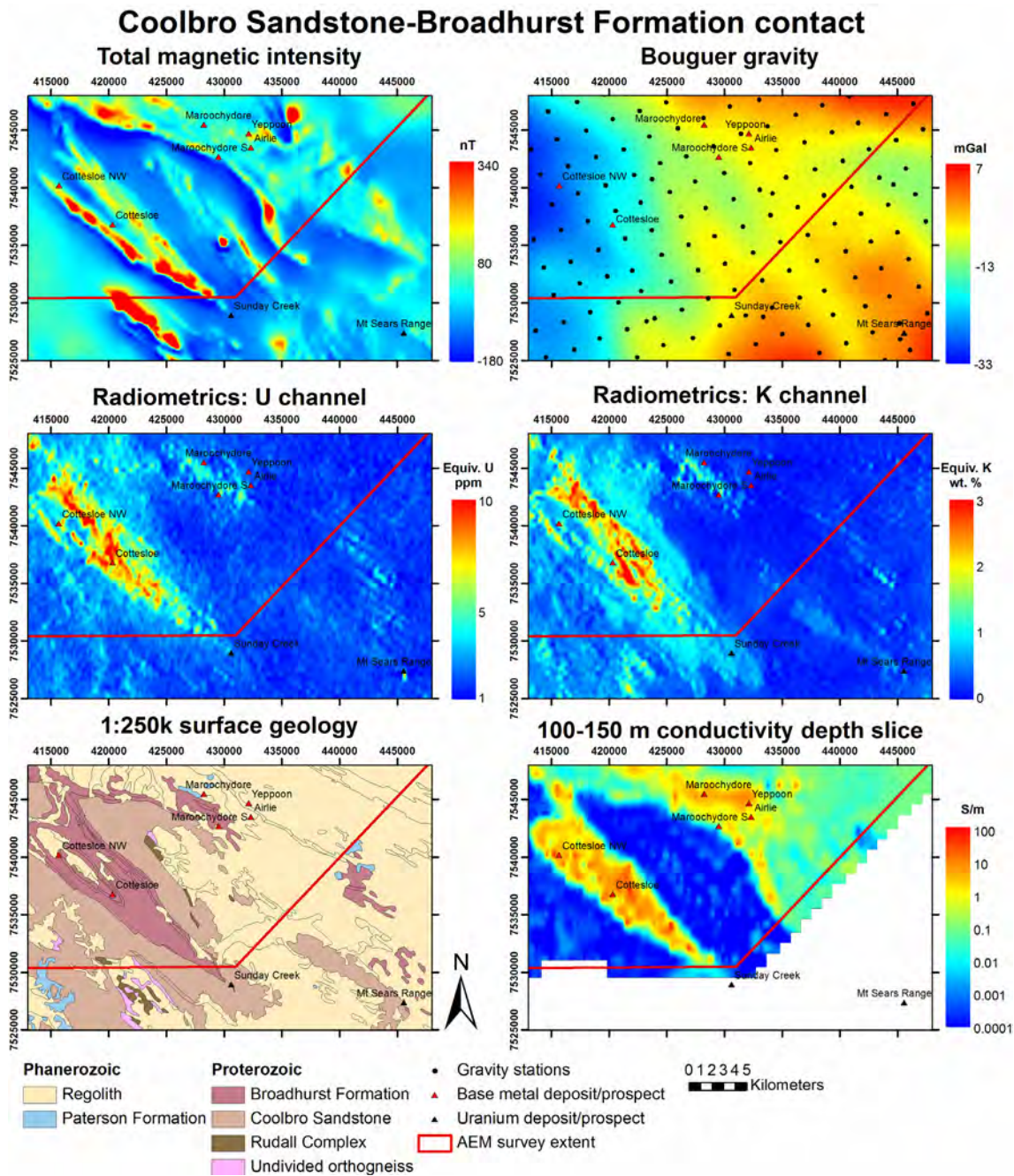


Figure 6.5: Geophysical signature of the area surrounding the Sunday Creek, Mt Sears and Maroochydore prospects. Total magnetic intensity, Bouguer gravity and radiometric data are extracted from the Geophysical Archive Data Delivery System (GADDS: <http://www.ga.gov.au/gadds>). The conductivity depth slice was prepared in this study (Chapter 4). The surface geology is simplified from Bagas *et al.* (2000).

6.2.2 Sediment-hosted copper deposits

In addition to major uranium and gold deposits at Kintyre and Telfer, respectively, exploration in the Paterson region in the 1970s and 1980s discovered two major copper deposits, Nifty and Maroochydore, as well as a number of prospects. Initially, as discussed by Haynes *et al.* (1993), a

sediment-hosted, syn- or diagenetic model (e.g., a Zambian copper belt type model) was used for these discoveries. More recent studies (Reed, 1996; Anderson *et al.*, 2001), however, suggest that the deposits are structurally controlled. Most, if not all, of these deposits and prospects are hosted in the upper part of the Broadhurst Formation, in close spatial association with conductive zones as determined from ground and airborne electromagnetic data (Czarnota *et al.*, 2009a). These conductive zones most likely represent portions of the Broadhurst Formation that are carbonaceous and/or sulfide-bearing. In the following section, the geology, age and origin of the Nifty and Maroochydore deposits are described in detail, with other prospects, including Goosewhacker, and occurrences described briefly.

6.2.2.1 Nifty

After discovery in 1981, mining of the Nifty deposit began in 1993, initially in the oxide zone, and in 2004 in the sulfide zone. Production to 2009 totalled 16 Mt grading 2.4 wt. % copper. At 31 March 2009, JORC-compliant mineral resources totalled 45.29 Mt grading 2.3 wt. % copper, including ore reserves of 27.14 Mt grading 2.1 wt. % copper (Aditya Birla Minerals, 2010). In addition to these resources, a JORC-compliant recoverable inventory under leach of 15.67 Mt grading 0.4 wt. % copper was reported. Cumulatively, these total >1.1 Mt of contained copper, making the Nifty deposit one of the largest copper deposits in Western Australia.

6.2.2.1.1 Geology, age and origin

The Nifty deposit is hosted by the upper part of the Broadhurst Formation, which consists of carbonaceous shale and siltstone with minor dolomite beds. Although strongly controlled by structures (see below), the ores are stratabound, localised within the "Nifty member" of Anderson *et al.* (2001). This unit is characterised by interbedded carbonaceous shale and dolomitic mudstone. The presence of the dolomitic rocks distinguishes this unit from the underlying and overlying units, which consist of shale. The underlying chloritic unit lacks carbonaceous material and the upper unit contains abundant carbonaceous material and minor interbedded siltstone (Anderson *et al.*, 2001). The overlying unit also contains a 1-20 m thick unit of highly pyritic carbonaceous shale termed the "pyrite marker bed" which is located several tens of metres above the mineralised Nifty member. The uppermost unit within the host succession is the upper carbonate bed, a 5-60 m thick unit of finely laminated dolomitic and calcareous silty shale, which is located 50-100 m stratigraphically above the Nifty member (Anderson *et al.*, 2001).

6.1.2.1.1.1 Structure

The Nifty deposit is located close to the junction of the underlying northwest-striking Camel-Tabletop Fault zone and the north-northwest striking dextral transpressional Vines Fault. The deposit is located at the culmination of two synclines that are imaged particularly well by electromagnetic techniques (Czarnota *et al.*, 2009a). The presence of these two synclines at the site of the deposit seems to indicate the presence of the sulfides has localised deformation around them but the genesis of these two synclines is problematic. They either are related to progressive deformation along the Vines Fault supported by the presence of only one dominant foliation or due to two discrete periods of deformation in the Miles and Paterson Orogenies.

Anderson *et al.* (1997) recognised five deformational events in the Nifty open cut. The earliest event, D_{Y1}, which produced recumbent isoclinal and angular upright folds, was interpreted as the onset of bedding-plane slip associated with north-northeast-directed contraction, probably during the earliest Miles Orogeny. This event most likely correlates with the regional D₃ event of Hickman and Clarke (1993). The Nifty deposit is localised along the northern limb and closure of a southeast plunging, open, F₄ syncline, which is the equivalent of F_{Y2} reported by Anderson *et al.* (2001; [Figure 6.6](#)). The D₄ (D_{Y2}) event is the main folding and cleavage-forming event at Nifty, and corresponds to the main phase of the Miles Orogeny (Bagas, 2005). It also involved contraction verging from the north-northeast. Anderson *et al.* (1997) recognised three additional deformational events in the Nifty open cut: 1. an unnumbered event, which is localised in the Nifty pit and involved upright folds and a north-northeast-striking slaty cleavage; 2. D_{Y3}, which formed folds with horizontal folds coaxial

with F_{Y2} folds and was interpreted as the consequence of extensional collapse at the end of the Miles Orogeny; and, 3. D_{Y4} , a late brittle event. Peak metamorphic conditions during D_4 (D_{Y2}) were sub-greenschist, with illite crystallinity measurements indicating temperatures of 200–300°C (Anderson, 1999). The Nifty syncline is transected by a north-striking, east-dipping dolerite dyke.

6.1.2.1.1.2 Primary ores

Three types of copper ores are recognised at Nifty (Figure 6.6): 1. shale-hosted secondary ore; 2. carbonate-hosted secondary ore; and, 3. carbonate-hosted primary ore. The first two ore types were mined early in the development of the Nifty deposit and were extracted using solvent extraction-electro-winning metallurgical techniques. Since 2005 the primary ores, which are localised in the closure of the syncline at depths of 300–600 m below surface, have been the main ore type extracted, with the copper extracted using conventional hydrometallurgical techniques. This fold plunges at 15°/125°, and the deposit extends for over 1200 m along plunge, estimated from Figure 3 of Anderson *et al.* (2001). Three dimensional modelling of ore shells indicate that high grade zones are controlled by a north-northwest trend in addition to the plunge direction, particularly along the northeastern limb of the syncline (Huston *et al.*, 2007).

The primary ores are mineralogically simple; chalcopyrite is the only major ore mineral and is accompanied by pyrite as the only other major sulfide mineral. Chalcopyrite is mostly concentrated in the Nifty member, but is also present in the pyrite marker bed. Although some chalcopyrite occurs in bedding-parallel bands, it is dominantly cross-cutting, occurring in veins, vein networks, as the matrix to breccias (Anderson *et al.*, 2001), along S_4 (S_{Y2}) foliation and as replacement of carbonate (D.L. Huston and K. Czarnota, unpublished data). These relationships led Anderson *et al.* (2001) to infer a syn- S_4 (S_{Y2}) timing for chalcopyrite introduction. Alternatively, the present siting of chalcopyrite could be the result of remobilisation of pre-existing syngenetic or diagenetic chalcopyrite.

Pyrite is present as both framboids, most likely formed diagenetically, and variably corroded and fractured euhedra, interpreted as hydrothermal pyrite. Framboidal pyrite is most abundant in carbonaceous shales surrounding the Nifty member, particularly in the pyrite marker bed (Anderson *et al.*, 2001). Euhedral pyrite is described as having a number of habits, both containing chalcopyrite inclusions and being corroded by chalcopyrite (Anderson *et al.*, 2001).

Other sulfide minerals present at Nifty include minor sphalerite and galena. Sphalerite is localised in the hanging wall succession, particularly the pyrite marker bed, whereas galena is restricted to the pyrite marker bed. This mineralogical zonation is mimicked by a geochemical zonation, with copper concentrated in the Nifty member and zinc and lead concentrated in the hanging wall succession. Zones of zinc and lead concentration commonly do not coincide (Anderson *et al.*, 2001).

Huston *et al.* (2007) described the presence of 2–10 mm apatite veins and stockworks along the margins of high grade ore zones, particularly along the southeastern margin of the orebody. In addition to apatite and quartz, these veins contain accessory to minor chalcopyrite, pyrite, disordered carbon and sphalerite, variable sericite, dolomite and trace galena and rutile. These veins are locally folded and partly recrystallised. Although these veins were identified using uranium anomalies in assay data (to 1300 ppm), the veins do not contain uranium minerals. Rather, uranium is present as ningyoite associated with framboidal pyrite and carbonaceous material immediately adjacent to the veins. The presence of uranium minerals, both in association with these veins and in the ore zone suggest untested potential for uranium mineralisation in the vicinity of the Nifty deposit.

Based on fluid inclusion studies, Anderson *et al.* (2001) inferred that the fluids that formed the Nifty deposit were moderate temperature (>270°C) and relatively saline (8–27 eq. wt. % NaCl).

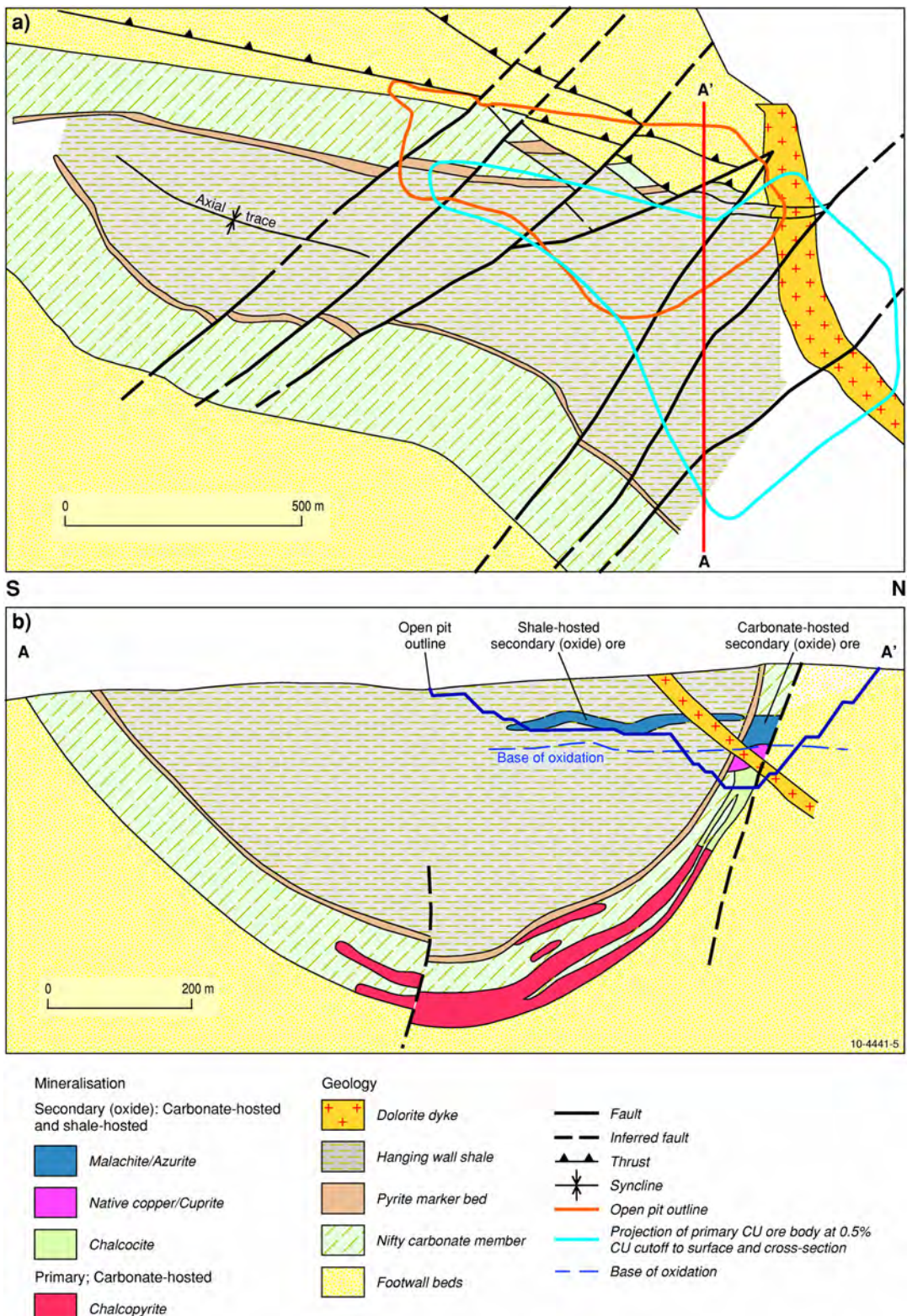


Figure 6.6: Geological plan and cross section of the Nifty deposit, modified after Anderson et al. (2001) and Ferguson et al. (2005).

6.1.2.1.1.3 Alteration assemblages and zonation

Anderson *et al.* (2001) describe silicification as the dominant ore-related alteration process. They define four assemblages involving silicification. A black quartz-dominated assemblage is restricted to the highest grade ore zones. This assemblage consists of microcrystalline quartz with abundant carbonaceous material, euhedral pyrite and irregular chalcopyrite blebs. In addition to these sulfide minerals, this assemblage is characterised by abundant fluorapatite and minor uraninite and pitchblende associated with carbonaceous material (Huston *et al.*, 2007). Anderson *et al.* (2001) report the presence of rare, coarsely crystalline dolomite inclusions within ore zones. Comparison of the immobile element geochemistry of these inclusions with that of the black quartz assemblage suggests that the black quartz assemblage formed by replacement of the inclusions, which are interpreted as the remnants of an original dolomite lens that the high grade ore zone at Nifty replaced (D. Huston and K. Czarnota, unpub data). This interpretation is consistent with early interpretations that the copper lens at Nifty replaced a carbonate lens within the Broadhurst stratigraphy (Hickman and Clarke, 1993).

Anderson *et al.* (2001) indicate that the black quartz assemblage grades outwards to silicified dolomitic shale and then into hydrothermal quartz-dolomite. They also described a chloritic shale assemblage, which has limited extent marginal to the quartz-dolomite assemblage, and a silicified pyritic shale assemblage, which is restricted to the pyrite marker bed. Ferguson *et al.* (2005) indicate the presence of a barite halo and then a K-feldspar halo above the pyrite marker bed.

6.1.2.1.1.4 Secondary ores

Ferguson *et al.* (2005) indicate the presence of two styles of secondary copper ores, both of which were exploited during the early history of mining at Nifty. The first style consists of silicified carbonate-hosted ore, which is developed along the northern limb of the fold at depths of above 300 m. Secondary carbonate-hosted ores are mineralogically zoned and stratabound within the Nifty member. The uppermost zone, above the base of oxidation, is composed of malachite and azurite and passes downward into a malachite-cuprite-tenorite-native copper zone, which in turn passes into a chalcocite-rich supergene zone ([Figure 6.6](#)). At a depth of about 300 m, the chalcocite zone passes into the primary ore zone.

The second style of secondary copper ore is developed as a blanket-like zone, approximately 15 m thick, that is hosted by shale between 40 and 80 m below surface. This zone is located at the same level at which the secondary carbonate-hosted ores begin. Hickman *et al.* (1994) interpreted shale-hosted secondary ores to have formed at a paleo-water table.

6.1.2.1.1.5 Age of mineralisation

Huston *et al.* (2007) undertook uranium-lead (U-Pb) and samarium-neodymium (Sm-Nd) analysis of apatite and galena from the apatite veins to establish their age. Samarium-neodymium and lead-lead (Pb-Pb) arrays from these analyses indicated ages of 791 ± 42 Ma and 811 ± 39 Ma, respectively, and were interpreted to indicate the age of apatite veining and, therefore, the age of the Nifty deposit. These ages are within error of each other and the age (835 ± 23 Ma) derived from pitchblende analyses from the Kintyre deposit, suggesting that the uranium and copper deposits were broadly coeval and probably formed during the Miles (D₄) orogeny.

6.2.2.1.2 Geophysical characteristics

The geophysical signature of the Nifty deposit is shown in [Figure 6.7](#). The deposit, and a series of prospects to the southeast of Nifty (see below), are located in a corridor of less magnetic rocks between the strongly magnetic limbs of the southeast-striking Nifty syncline. Along the length of the syncline the Broadhurst Formation, and its abundant graphitic schists, is mapped as a strong northwest-striking, 6 km wide conductivity anomaly ([Figure 6.8](#)). The syncline is also coincident with a broad gravity gradient, separating apparently less dense rocks to the west from more dense rocks to the east. Although there is limited outcrop surrounding the Nifty deposit, radiometric data identifies a strong uranium channel anomaly over an area of about 9 km² centred on the deposit.

Comparison with satellite imagery suggests that this anomaly is broader than the area of mine infrastructure and disturbed ground around Nifty, and may indicate remobilisation of uranium in the regolith surrounding the deposit. Potassium and thorium radiometric channels show a similar anomalous area surrounding Nifty, but with more subdued anomalies.

The geophysical signature of the Nifty deposit is similar to that observed for the Cottesloe prospects described above. The association of the conductive graphitic units of the Broadhurst Formation with magnetic gradients, and potentially uranium channel radiometric anomalies where deposits are close to surface, is clearly a prospective association for base metal targets in the Paterson region that can be effective under cover.

6.2.2.2 Maroochydore

The Maroochydore deposit, which contains a global resource of 41.2 Mt grading 0.8 wt. % copper and 0.04 wt. % cobalt (Aditya Birla Minerals, 2008a), is the second largest known copper deposit hosted by the Broadhurst Formation. This deposit differs from other copper deposits in the Paterson region in being located away from the Vines Fault system. As it is a less advanced prospect, less information is available about the deposit, although a thesis by Reed (1996) provides a comprehensive description of the host succession, structure, and the ore and alteration assemblages, as well as a model for mineralisation and its timing.

6.2.2.2.1 Geology, age and origin

The Maroochydore deposit is hosted in the upper part of the Broadhurst Formation, approximately 1.5 km stratigraphically above the contact with the Coolbro Sandstone (Reed, 1996). Locally the deposit is hosted within the "mineralised horizon", a 75 m thick succession characterised by carbonaceous and dolomitic shales with a recrystallised dolostone near the centre ([Figure 6.9](#)). The mineralised succession differs from the underlying footwall succession in that the latter has only minor carbonate and lacks frambooidal pyrite.

The footwall succession is characterised by interbedded carbonaceous shale and chloritic mudstone, with at most 5 wt. % carbonate (dolomite and/or ankerite; Reed, 1996). A single analysis of carbonaceous shale from this unit indicated a total organic content of 2.9 wt. %, whereas an analysis of mudstone yielded a total organic content of 0.5 wt. % (Reed, 1996). The hanging wall succession consists of dolomitic and weakly carbonaceous shales that have very minor or no pyrite. Based on two shale analyses, the total organic content of the hanging wall succession is 0.5-0.9 wt. %.

Reed (1996) subdivided the mineralised horizon into two carbonaceous shales separated by a dolostone unit, which is up to 15 m in thickness. The upper carbonaceous unit is between 25 m and 40 m thick and consists of 1-100 mm thick carbonaceous shale beds interbedded with 1-15 mm pyritic and dolomitic beds. The unit is very organic carbon-rich, with the only sample analysed returning a total organic carbon content of 2.6 wt. %. Thicker shale beds commonly grade upward from dolomitic siltstones into highly carbonaceous and sulfide shale, with some examples consisting of up to 80 % frambooidal pyrite (Reed, 1996).

The upper carbonaceous unit overlies the dolostone unit, which comprises massive dolostone to dolomitic siltstone, with individual bed thickness to 1 m. Unlike the surrounding carbonaceous shale, the dolostone contains only minor to trace carbonaceous matter and frambooidal pyrite (Reed, 1996).

The lower carbonaceous unit is also between 25 and 40 m thick and comprises individual beds that are between 5 and 400 mm in thickness and grade from a carbonate-rich base that fines upwards into carbonaceous and pyritic shale. This grading is best developed in the upper part of this unit, and the pyrite is typically frambooidal. The lower carbonaceous unit is also characterised by the presence of polymictic conglomerate units up to 2-m-thick, which also grade upwards.

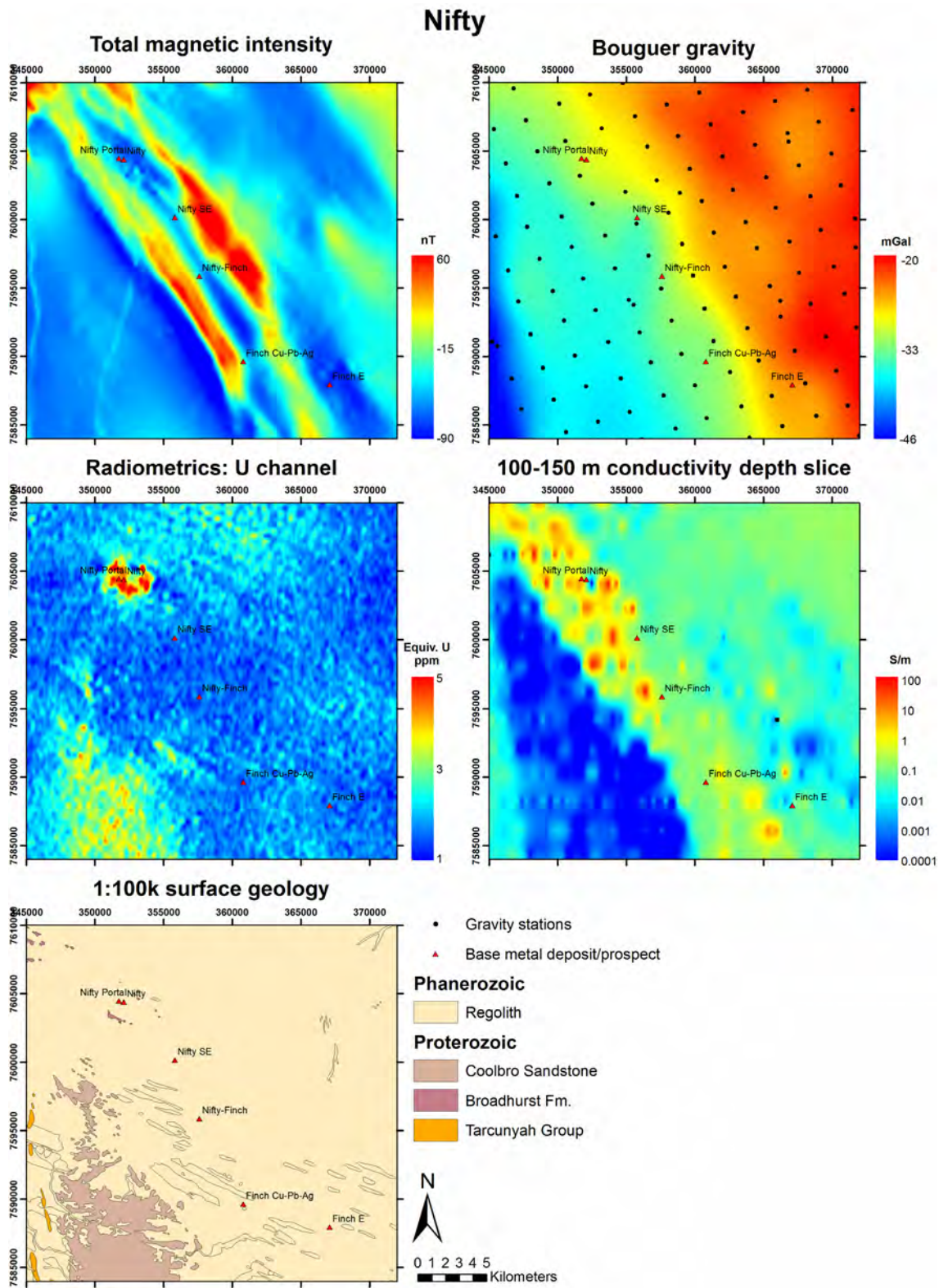


Figure 6.7: Geophysical signature of the area surrounding the Nifty copper deposit. Total magnetic intensity, Bouguer gravity and radiometric data are extracted from the Geophysical Archive Data Delivery System (GADDS: <http://www.ga.gov.au/gadds>). The conductivity depth slice was prepared in this study (Chapter 4); the checkerboard pattern is due to gridding across the 2-km-spaced AEM flight lines in this area. The surface geology is simplified from Bagas (2005).

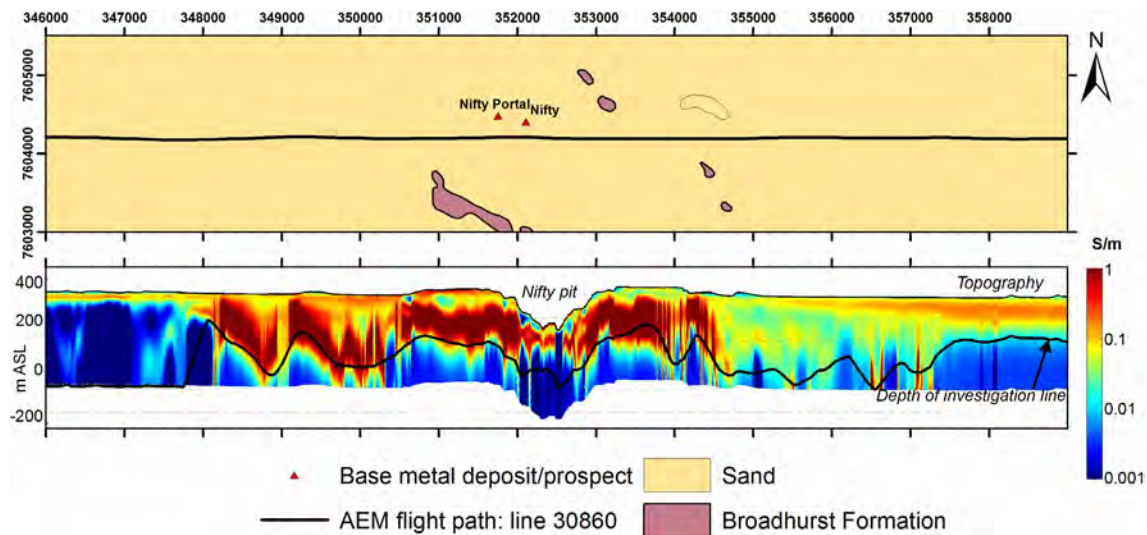


Figure 6.8: A portion of a layered earth inversion conductivity section (with 3 times vertical exaggeration) for flight line 30860 across the Nifty deposit, compared with surface geology simplified from 1:100 000 scale surface mapping by Bagas (2005). The AEM data clearly maps the conductive portions of the Broadhurst Formation to depths of 300 m, and provides some evidence of structural complexity west of Nifty, in the same position as the magnetic response in Figure 6.7.

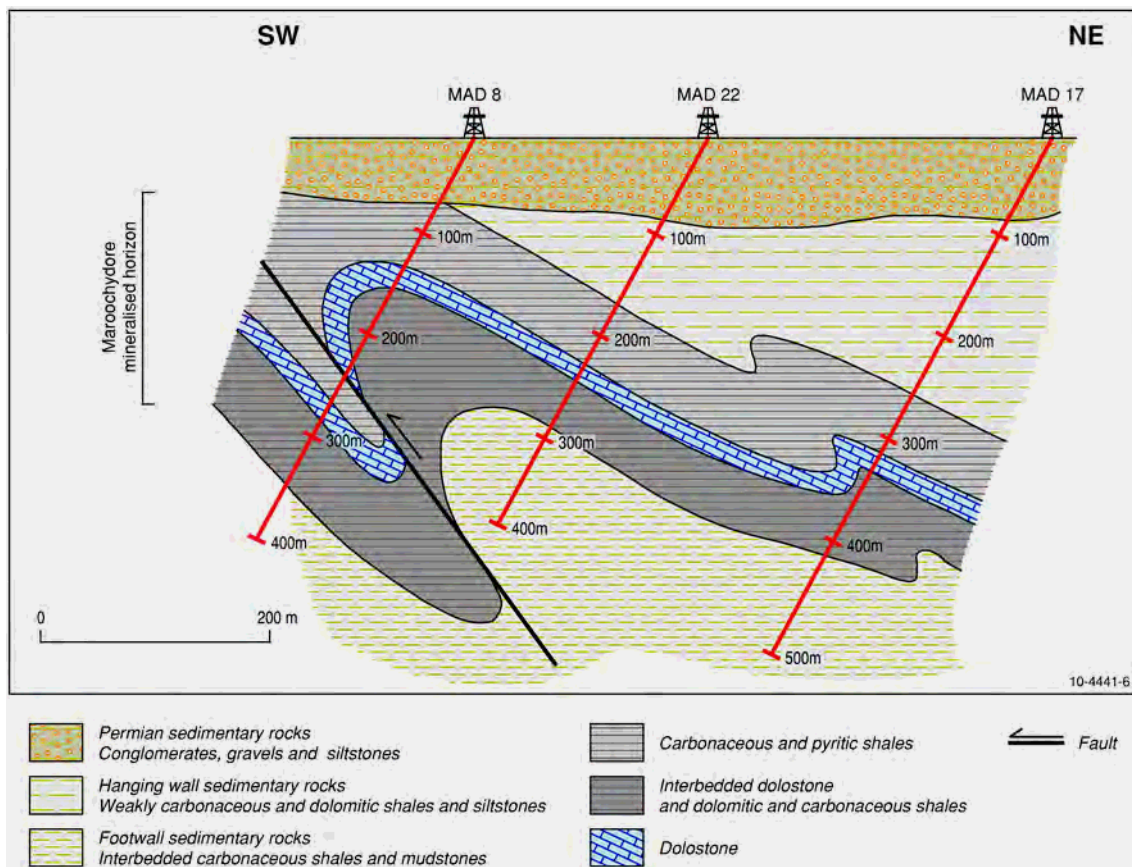


Figure 6.9: Geological cross section of the Maroochydore deposit, modified after Reed (1996).

6.2.2.2.1.1 Structure

Based on widely-spaced oriented drill core, the presence of marker beds within the host succession, and ground electromagnetic data (see below), Reed (1996) interpreted a series of southwest-verging, tight to open, recumbent folds with axial planes dipping 45–65° to the northeast ([Figure 6.9](#)). Saddle reefs are present along fold closures, particularly where dolostone beds are interlayered with carbonaceous shale. The saddle reefs are infilled by sulfide minerals, dolomite and quartz. This folding event is also associated with an axial planar cleavage, developed as an alignment of phyllosilicates and carbonaceous matter in shales and stylolites in dolomitic rocks. This folding event was interpreted by Reed (1996) as local D₂, which correlates with regional D₄ (Hickman and Clarke, 1993).

Reed (1996) also interpreted a series of northeast-dipping thrust faults developed along the overturned limbs of local D₂ (regional D₄) folds ([Figure 6.9](#)), with offsets of up to 150 m. The abundance of silica-dolomite veins oriented parallel to S₂ increases towards these fault zones (Reed, 1996). Based on the mineral assemblage of chlorite-phlogopite-green biotite-ankerite-dolomite-talc in the footwall succession, Reed (1996) inferred a peak metamorphic grade of middle greenschist.

6.2.2.2.1.2 Mineralisation and alteration

Mineralised zones at Maroochydore are mineralogically simple, consisting of pyrite, pyrrhotite and chalcopyrite as the main sulfide minerals, with minor to trace sphalerite and galena, and with a gangue assemblage, in decreasing abundance, of dolomite, quartz, phlogopite, chlorite, apatite and feldspar (Reed, 1996). Chalcopyrite is commonly developed in the hinge of local D₂ folds, where it is accompanied by pyrite, quartz, dolomite and phlogopite. All sulfide minerals increase in abundance toward D₂ stylolitic cleavage planes. Saddle reefs developed in fold closures are dominantly dolomite, but include subsidiary pyrite and chalcopyrite. Sulfide minerals are also concentrated along thrust faults and fracture zones adjacent to them. Foliation-parallel dolomite-quartz veins also contain minor galena, sphalerite and chalcopyrite. Pyrrhotite appears to be restricted to the footwall succession (Reed, 1996).

6.2.2.2.1.3 Age of mineralisation

Based on relationships of sulfide minerals to structural elements, Reed (1996) inferred a syn-local D₂ (regional D₄) timing for mineralisation, similar to the timing inferred at Nifty by Anderson *et al.* (2001) and the likely timing of the Kintyre deposit. To determine the age of mineralisation, Reed (1996) analysed phlogopite, which paragenetically accompanies chalcopyrite at Maroochydore, using argon-argon (⁴⁰Ar-³⁹Ar) methods. The analysis yielded a well-defined plateau with an age of 717 ± 5 Ma. This age is problematic in that it is significantly younger than the mineralisation ages obtained from the Nifty and Kintyre deposits (840–790 Ma) and significantly older than ages of ca. 650 Ma obtained from ⁴⁰Ar-³⁹Ar dating from the Rudall Complex and the Yeneena Basin (Durocher *et al.*, 2003). The significance of this Maroochydore age is unclear as it is based on very limited data.

6.2.2.2.2 Geophysical characteristics

Reed (1996) noted that pyritic and carbonaceous shales that characterise the mineralised horizon and footwall are conductive, with values of 70 S/m, significantly higher than non-carbonaceous and pyrite-poor rocks, which have conductivities of 5–10 S/m. Reed (1996) used this conductivity contrast to map out the host succession at Maroochydore and structure in the subsurface.

The regional geophysical signature of Maroochydore ([Figure 6.5](#)) is similar to that of other deposits hosted by the Broadhurst Formation. In addition to the strong conductivity anomaly identified by Reed (1996), and demonstrated in [Figure 6.10](#), the deposits occur on a broad gravity gradient, and in rocks with a subdued magnetic response adjacent to much more magnetic features. Exposed host rocks are associated with moderate uranium and potassium radiometric anomalies. Based on this association, there are several areas under cover west, east, and southeast from Maroochydore that exhibit similar responses, in particular around 433 900 mE, 7 536 550 mN (MGA Zone 51).

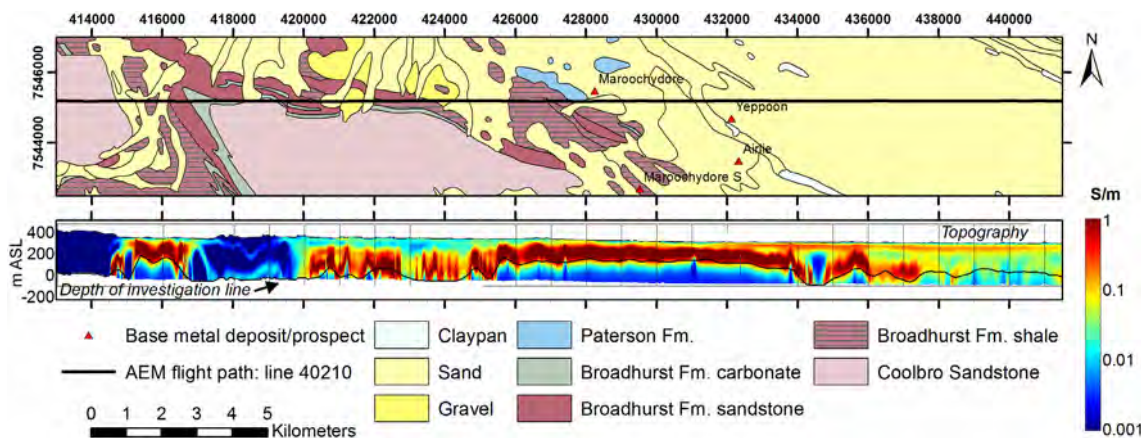


Figure 6.10: A portion of a layered earth inversion conductivity section (with 3 times vertical exaggeration) for flight line 40210 across the Maroochydore deposit compared with surface geology simplified from 1:100 000 scale surface mapping by Hickman and Clarke (1993). The AEM data map the conductive Broadhurst Formation in both limbs of the fold (left hand side), with resistive Coolbro Sandstone in the nose of the fold.

6.2.2.3 Other sediment-hosted copper prospects and occurrences in the Broadhurst Formation

In addition to the two major deposits at Nifty and Maroochydore, the Broadhurst Formation hosts a series of other prospects, including Nifty Northwest, Nifty Southeast, Finch (and nearby prospects) and Goosewhacker (several are included in Figure 6.7). Other prospects, such as Grevillea, Citadel, Moses Chair and Cottesloe, though hosted at a similar stratigraphic level in the Broadhurst Formation, are dominated by zinc and lead. These prospects are hosted by conductive parts of the Broadhurst Formation as mapped by Czarnota *et al.* (2009a) and the AEM data. Very little data are available for these prospects, with the most important sources being Hickman and Clarke (1993), Froud (1997), Anderson *et al.* (2002) and Ferguson *et al.* (2005).

As it was the subject of a B.Sc. Honours thesis (Froud, 1997), the Goosewhacker deposit has the most comprehensive description. This deposit is hosted by the upper part of the Broadhurst Formation, within a succession characterised by carbonaceous shale, siltstone, sandstone and conglomerate. The prospect consists of syn-regional D₄ veins characterised by quartz ± siderite ± sulfide assemblages. Unlike other copper prospects hosted by the Broadhurst Formation, the sulfide mineralogy of these veins is relatively complex, containing pyrite, galena, chalcopyrite, sphalerite, and pyrrhotite along with minor to trace bornite, covellite, marcasite, bismuth, wittichenite and hematite. Geological data for the other copper prospects is limited to drilling intersections reported by Ferguson *et al.* (2005), the best of which include 4 m grading 2.95 wt. % copper at Nifty Southeast and 2 m grading 1.5 wt. % copper at Finch.

Of the zinc-lead-rich prospects, most information is available for the Grevillea prospect, which is hosted by carbonaceous siltstone and carbonate of the lower Broadhurst Formation. This prospect is characterised by structurally-controlled replacement bodies dominated by pyrite with minor sphalerite and galena (Anderson *et al.*, 2002). The Cottesloe (Eva Well) prospect crops out as a gossan within the southeastern closure of the doubly plunging Cottesloe syncline (Hickman and Clarke, 1993). Drilling indicated that the mineralisation was stratiform, yielding best grades of 4 m grading 3.8 wt. % lead and 80 g/t silver (Ferguson *et al.*, 2005).

6.2.2.4 Summary of the characteristics of sediment-hosted copper deposits in the Broadhurst Formation

The above descriptions of sediment-hosted copper deposits in the Broadhurst Formation highlight a number of commonalities between the deposits, including stratigraphic position, lithological associations, ore and alteration mineralogy, structural timing, geophysical signature and, most likely, the age of mineralisation. With the exception of the Grevillia prospect, both copper-rich and zinc-lead-rich deposits are hosted in the upper part of the Broadhurst Formation. Maroochydore is located approximately 1500 m stratigraphically above the base of the formation. At the well described Nifty and Maroochydore deposits, and the less well described Grevillea prospect, the mineralised zones are closely associated with a carbonate-rich part of the stratigraphy, with some of the ores at Nifty formed by replacement of the carbonate. The host successions are also carbonaceous and commonly rich in frambooidal pyrite. This characteristic is reflected in the close association of the ores with conductive zones mapped using ground electromagnetic data (Czarnota *et al.*, 2009a) and airborne electromagnetic data (above; [Figures 6.5](#) and [6.7](#)). Deposits typically occur near magnetic and gravity gradients, but the resolution of the regional geophysical data may be insufficient to tightly define this association.

Although the copper deposits in the Broadhurst Formation are stratiform, in detail, the deposits are epigenetic, consisting of veins or replacement bodies. Most deposits have a relatively simple mineralogy and metallogeny, with copper being the only or major economic metal. In most cases, the ores are dominated by pyrite and chalcopyrite, with minor to accessory sphalerite, galena and, in some cases, pyrrhotite. The presence of zinc-lead-rich deposits, such as Grevillia, combined with the presence of zinc-lead-rich zones in the Nifty deposit, however, suggest a more complex metallogeny. As an example, uraninite and pitchblende have been described in Nifty ores, and local uranium-enriched zones associated with apatite veins, are present along the southeastern margin of the deposit. At present, the understanding of the distribution and geological control on uranium in these deposits is poor.

Like the uranium deposits hosted by the Rudall Complex, data from all prospects in the Broadhurst Formation suggest a close spatial association with D₄ structures, particularly fold closures, and to a lesser extent thrust faults. This association has been interpreted by both Anderson *et al.* (2001) and Reed (1996) to indicate a syn-D₄ timing of mineralisation. Data for the age of mineralisation is conflicting, with Reed (1996) reporting an age of ca. 720 Ma for the Maroochydore deposit based on ⁴⁰Ar-³⁹Ar dating of ore-related phlogopite, whereas Huston *et al.* (2009) reported overlapping ages of ca. 790 Ma and ca. 810 Ma for the Nifty deposit based on Sm-Nd and Pb-Pb isochrons of apatite veins. The latter also overlap with ages determined from the Kintyre deposit and mafic-to-intermediate magmatism (see above) and are compatible with the age range initially inferred for the Miles Orogeny (900-800 Ma: Hickman and Bagas, 1998). In contrast, the ca. 720 Ma age does not correspond to any other age event known in the Paterson region; hence, we interpret the 810-790 Ma age range as the most likely period for copper (and uranium) mineralisation in the Broadhurst Formation.

6.2.3 Other zinc-lead deposits

In addition to the uranium and copper deposits described above, the Paterson region hosts significant zinc-lead deposits, including the Warrabarty deposit and the recently-discovered Dromedary deposit. These deposits differ from the copper deposits in being hosted by carbonate-dominated units, the Isdell Formation or uppermost Broadhurst Formation, in the case of Warrabarty, and the Puntapunta Formation in the case of Dromedary. The deposits are substantially different from each other. The Warrabarty deposit has been interpreted as a Mississippi Valley-type deposit (Smith, 1996), whereas the Dromedary deposit appears to be a skarn deposit related to the ca. 830 Ma Duke monzonite (D. Maidment, pers. comm.).

6.2.3.1 Warrabarty

The Warrabarty deposit is located in the northwestern part of the Paterson region, within carbonate rocks of either the upper Broadhurst Formation or the Isdell Formation. The deposit has been described thoroughly by Smith (1996), upon whose description the following is largely based. Smith (1996) described the Warrabarty deposit as a relatively large (strike length of over 2.5 km; [Figure 6.11](#)), low grade zinc-lead (typically 3-6 wt. % zinc + lead) epigenetic deposit hosted by dolomitised carbonates, which are part of the upper Broadhurst Formation, although he noted that the host units could also be Isdell Formation. This succession consists dominantly of organic-rich dolostone, with lesser organic-poor dolostone and minor fine-grained limestone. This dolomitisation is inferred to have occurred during late diagenesis, and was then overprinted by a second dolomitisation event that just predated or accompanied mineralisation (Smith, 1996).

As elsewhere in the Throssell Range Group ([Figure 6.1](#)), deformation was dominated by an event (local D₂, regional D₄), which produced northwest-striking open to tight folds with a northeast-dipping axial planar cleavage. Main-stage mineralised breccias are overprinted by this cleavage (Smith, 1996), indicating a pre-tectonic timing relative to the Miles Orogeny.

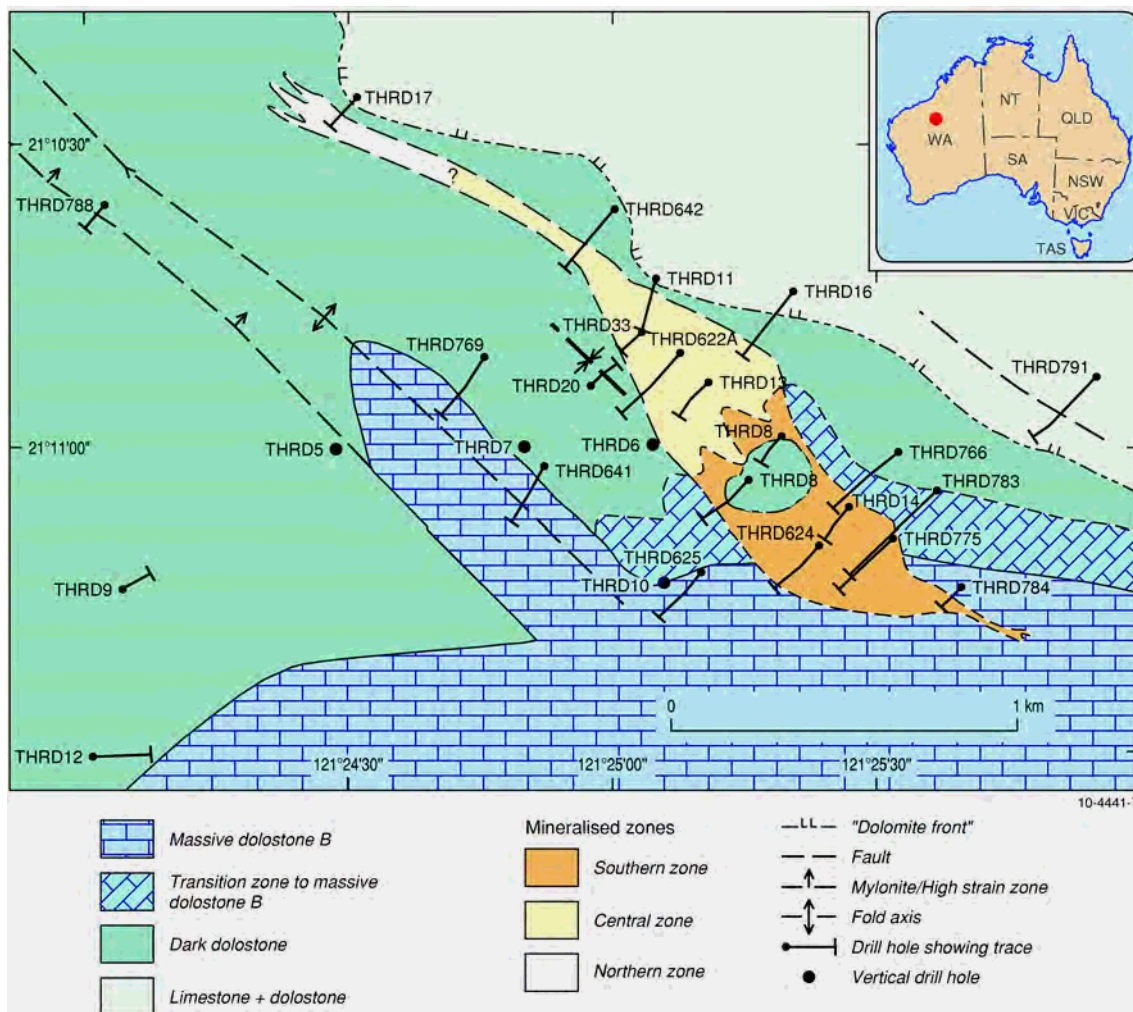


Figure 6.11: Geological map of the Warrabarty deposit, modified after Smith (1996).

Mineralised rock at Warrabarty consists of breccia, veins and zones of disseminated to massive sulfide. Smith (1996) recognised two paragenetic stages: an early, main stage with a simple assemblage consisting of low-iron sphalerite, pyrite, galena, dolomite and pyrobitumen; and, a later stage with a more complex assemblage of white dolomite accompanied by quartz and pyrite with minor sphalerite and galena, and trace chalcopyrite, arsenopyrite, bornite, chalcocite and phlogopite. Smith (1996) interpreted this latter assemblage to have formed syn-kinematically.

Primary fluid inclusion data from growth-zoned sphalerite in the main stage assemblage indicated moderately saline (22-26 wt. % total salt) calcic brines with trapping temperatures of 165-250°C, whereas primary inclusions from chalcopyrite-diseased sphalerite from the later paragenetic stage indicates similar salinities (15-26 wt. % total salt) but higher trapping temperatures between 300 and 400°C (Smith, 1996).

Smith (1996) noted that lead isotope data from Warrabarty and the copper deposits hosted by the Broadhurst Formation define a linear array on a ^{207}Pb - ^{204}Pb versus ^{206}Pb - ^{204}Pb diagram. He interpreted this array as an isochron with an age of ca. 840 Ma. Although this age is highly model dependent, it is compatible with age estimates for the Nifty and Kintyre deposits (see above).

6.2.3.2 Dromedary

The Dromedary (also known as Duke) prospect is hosted within the Puntapunta Formation (Czarnota *et al.*, 2009a), a laminated to thinly bedded succession of dolarenite, dolomite, siltstone and shale (Ferguson *et al.*, 2005). Zinc-rich massive sulfide zones have been intersected within this unit and also within the Duke monzonite ([Figure 6.12](#)). The best intersection to date, located within the Puntapunta Formation, yielded 17 m grading 7.36 wt. % zinc (Aditya Birla Minerals, 2008b). This deposit is most likely a skarn deposit related to the Duke monzonite.

6.2.4 Model for mineral systems associated with inversion of the Yeneena Basin

Geological observations and limited geochronological data suggest that uranium deposits in the Rudall Complex and at the contact between the Coolbro Sandstone, copper deposits in the Broadhurst Formation, and possibly zinc-lead deposits in overlying units, are associated with structures active during regional D₄, with absolute ages between ca. 840 and ca. 810 Ma. Geochronological data suggest that the most likely ages for the Kintyre deposit are ca. 840 Ma, followed by emplacement of mafic intrusions at ca. 830 Ma and then by deposition of the Nifty deposit at ca. 810 Ma. All of these ages are younger than the best estimate for the Throssell Range Group of ca. 860 Ma. Although it is recognised that there is uncertainty in these apparent age relationships due to the large errors associated with some of the ages, these deposits are interpreted to have formed in a two-stage, evolving mineral system that formed before and during the Miles Orogeny ([Figure 6.13](#)), which we informally term the Miles mineral system.

The first stage of the model ([Figure 6.13a](#)) is interpreted to have occurred at 840-830 Ma, toward the end of the development of the Yeneena Basin. At this time, basin thickness most likely exceeded 10 km, causing the evolution of basinal brines during diagenesis. Continued extension and heat flow associated with the emplacement of 835-830 Ma mafic intrusions (equivalent to the Gairdner Dyke Swarm in South Australia) triggered flow of these dense brines downwards into an aquifer developed in the upper part of the Coolbro Sandstone. Where these fluids encountered extensional faults, they continued to flow downward into the basement. Where suitable trap rocks were present in the basement (e.g., graphitic or iron-rich rocks), uranium, along with variable amounts of copper, other base metals, gold and platinum group elements, was deposited by reduction caused by interaction with the trap rocks or with fluids in equilibrium with the trap rocks. Although we have interpreted fluid flow to have occurred during the final stage of basin formation, these processes may have continued into the earliest part of basin inversion.

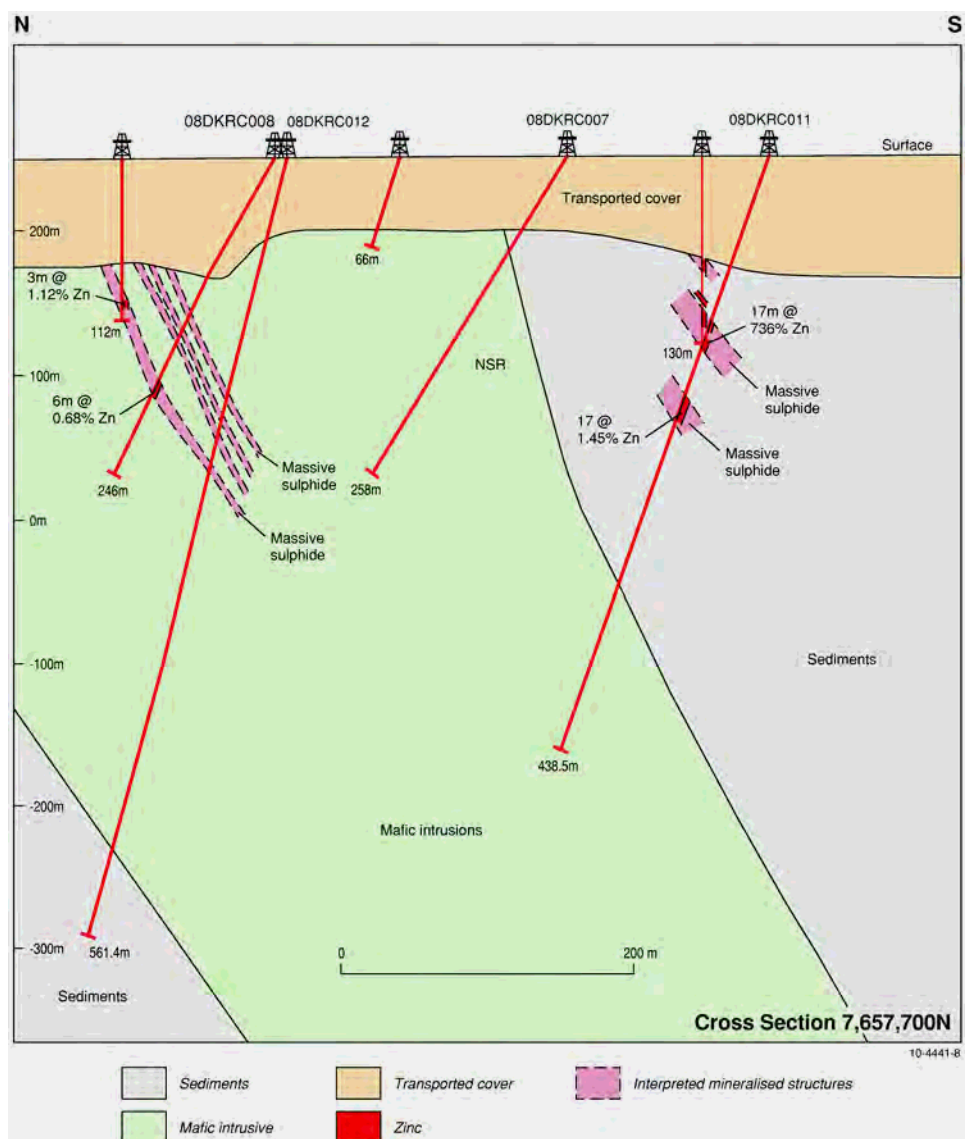


Figure 6.12: Geological cross section of the Dromedary prospect, after Aditya Birla Minerals (2008b).

The second stage of the model (Figure 6.13b) is interpreted to have occurred at 830-810 Ma, during initial inversion of the Yeneena Basin. Although a residual thermal anomaly associated with earlier extension and mafic magmatism persisted and drove fluid flow, the change in stress from extension to contraction changed the dynamics of structural elements and fluid flow. Normal faults developed during basin formation were inverted to become thrust faults; this was accompanied by the development of folds with axial planes parallel to the faults. As the change in stress to contraction was not compatible with downward fluid flow, brines began to flow upward from the aquifer in the Coolbro Sandstone, utilising the inverted extensional faults and new thrusts nucleated during contraction. When these fluids interacted with suitable traps, in this case either the contact between the Coolbro Sandstone and the carbonaceous Broadhurst Formation or carbonaceous, carbonate-rich intervals at higher levels in the Broadhurst Formation, copper, uranium and other metals were deposited, again as the consequence of reduction. Deposits formed during this stage are enriched in copper as mafic rocks introduced at ca. 830 Ma acted as a source for copper.

Due to uncertainties associated with geochronological data, the ages of mineralisation and mafic intrusion all overlap and could have happened coevally. In this case, the Miles mineral system

should be considered as a single stage, probably during inversion of the Yeneena Basin, but with both upward and downward fluid flow from the Coolbro aquifer. We prefer a two-stage model, however, as a change in stress patterns best accounts for this change in fluid flow patterns. In either case, most of the mappable characteristics identified in the mineral system analysis still apply.

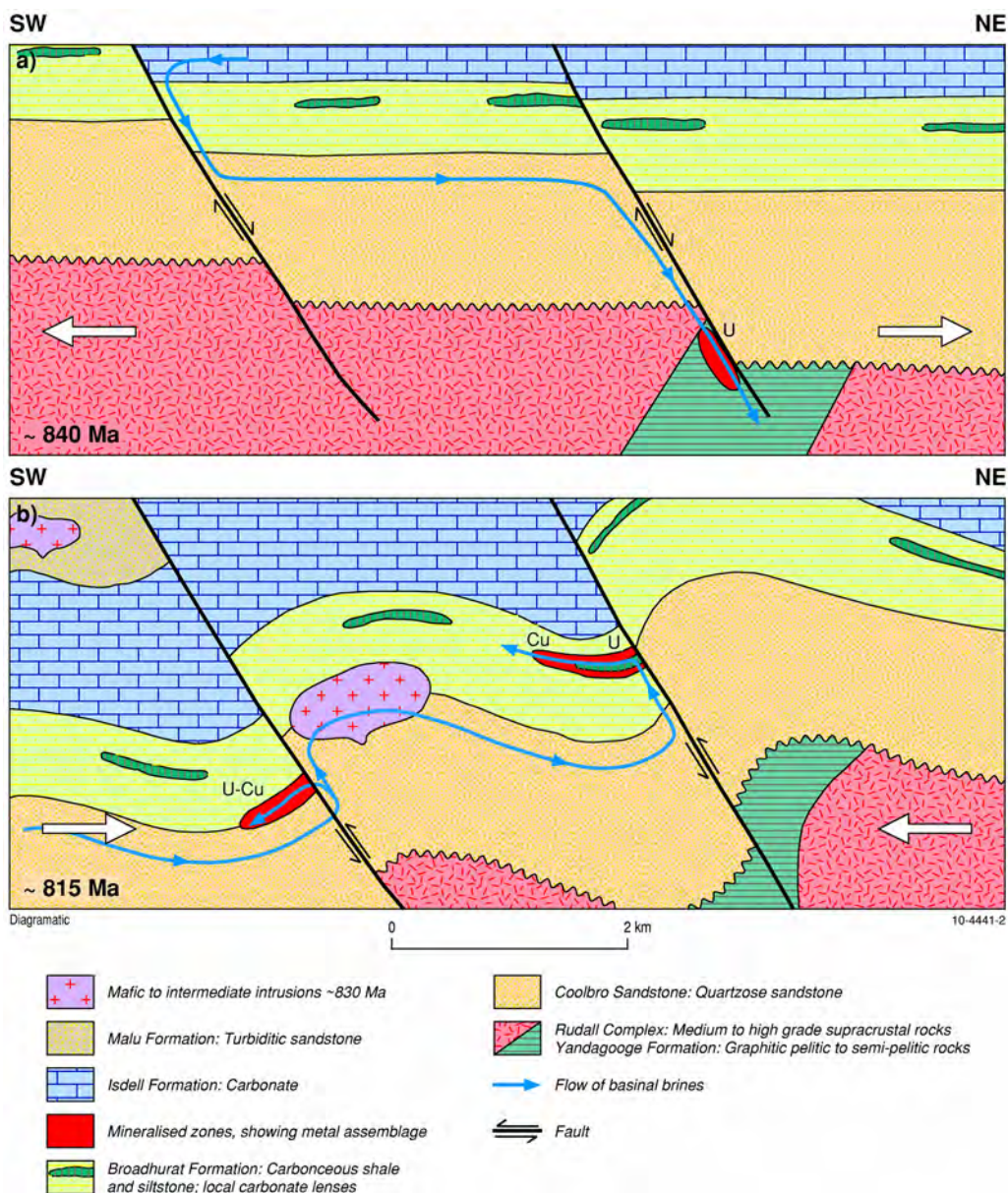


Figure 6.13: Mineral system model for the Miles mineral system.

The evidence for and details of this model are considered below according to six features that characterise the mineral system: 1. geodynamic setting; 2. architecture, including basin, structure and igneous architecture; 3. the origin of the ore fluids and metals; 4. fluid pathways and drivers; 5. depositional mechanisms; and, 6. post-depositional modifications. In describing these features, attention is paid to characteristics whereby these features can be mapped using regional to semi-regional geological and geophysical data. These features are summarised in [Table 6.1](#), and can be used in identifying and assessing other provinces, e.g., parts of the Centralian Superbasin (Walter *et al.*, 1995), in which mineral systems analogous to the Miles system may have been active.

Table 6.1: Features and mappable characteristics of the Miles mineral system.

MINERAL SYSTEM FEATURE	STAGE ONE	MAPPABLE CHARACTERISTICS STAGE TWO
Geodynamic setting	<p>Evidence of extension:</p> <ul style="list-style-type: none"> • Thickness changes in basin units; • Presence of extension-related magmatism. 	<p>Evidence of inversion:</p> <ul style="list-style-type: none"> • Thrust and inverted extensional faults; • Folding associated with thrust and inverted extensional faults.
Architecture	<ul style="list-style-type: none"> • Basin 	<p>Thick basin fill deposited in environments evolving from fluvial to marine conditions.</p>
	<ul style="list-style-type: none"> • Structure 	<p>Development of strong redox gradients, particularly along the basal unconformity.</p>
	<ul style="list-style-type: none"> • Igneous 	<p>Distribution of extensional faults, and indicated by structural timing relationships and changes in stratigraphic thicknesses.</p>
	<ul style="list-style-type: none"> • Igneous 	<p>Evidence of extension as indicated by emplacement of mafic to intermediate magmatic rocks.</p>
Origin of ore fluids and metals	<p>Presence of evaporative minerals within basin, indicating production of basinal brines.</p>	<p>Presence of evaporative minerals within basin, indicating production of basinal brines.</p>
	<p>Presence of uranium-enriched rocks, either within the basin or in the basement as indicated by gamma-ray spectrometric and whole rock geochemical data.</p>	<p>Presence of uranium-enriched rocks, either within the basin or in the basement as indicated by gamma-ray spectrometric and whole rock geochemical data.</p>
	<p>Presence of copper-enriched rocks, either within the basin or in the basement as indicated by mafic to intermediate intrusive rocks (determined from mapped geology and from aeromagnetic and gravity data).</p>	<p>Presence of copper-enriched rocks, either within the basin or in the basement as indicated by mafic to intermediate intrusive rocks (determined from mapped geology and from aeromagnetic and gravity data).</p>
Fluid pathways and drivers	<p>Distribution of potential aquifers, including stratigraphic units and extensional faults.</p>	<p>Distribution of potential aquifers, including stratigraphic units, inverted extensional faults, and thrust faults.</p>
	<p>Semi-regional alteration assemblages indicative of flow within aquifers and along faults:</p> <ul style="list-style-type: none"> • Variations in muscovite crystallinity (as determined from ASTER and PIMA data); • Distribution of aluminous alteration minerals (as determined from ASTER data). 	<p>Semi-regional alteration assemblages indicative of flow within aquifers and along faults:</p>
		<ul style="list-style-type: none"> • Variations in muscovite crystallinity (as determined from ASTER and PIMA data); • Distribution of aluminous alteration minerals (as determined from ASTER data).

Table 6.1: Features and mappable characteristics of the Miles mineral system (continued).

MINERAL SYSTEM FEATURE	MAPPABLE CHARACTERISTICS STAGE ONE	STAGE TWO
Metal trap sites and depositional mechanisms	<p>Evidence of uranium deposition as indicated from gamma-ray spectrometric data.</p> <p>Evidence of other metal deposition as indicated by the distribution of mineral occurrences and gossans.</p>	<p>Evidence of uranium deposition as indicated from gamma-ray spectrometric data.</p> <p>Evidence of other metal deposition as indicated by the distribution of mineral occurrences and gossans.</p>
Post-depositional modifications	<p>Reduction of ore fluids:</p> <ul style="list-style-type: none"> • Proximity to reduced rock packages, including reduced carbon and/or iron-rich rocks, as indicated by mapped lithology and geophysical responses in aeromagnetic and electromagnetic data; • Zonation in metals, uranium → copper → zinc-lead, down redox gradient. 	<p>Reduction of ore fluids:</p> <ul style="list-style-type: none"> • Proximity to reduced rock packages, including reduced carbon and/or iron-rich rocks, as indicated by mapped lithology and geophysical responses in aeromagnetic and electromagnetic data; • Zonation in metals, uranium → copper → zinc-lead, down redox gradient. <p>Neutralisation of ore fluids and creation of permeability:</p> <ul style="list-style-type: none"> • Extent of carbonate-rich successions, as indicated by mapped lithology and by the distribution of calcrete as mapped using ASTER.
Post-thermal and tectonic overprints.	Post-ore thermal and tectonic overprints.	<p>Post-ore thermal and tectonic overprints.</p> <p>Weathering.</p>

6.2.4.1 Geodynamic setting

Lithological similarities and limited geochronological data suggest that the Yeneena Basin correlates with the basal part of the Centralian Superbasin, a Neoproterozoic to Paleozoic basin that developed through much of central Australia and includes the Amadeus, Georgina and Officer Basins (Walter *et al.*, 1995). Using this correlation, the Coolbro Sandstone corresponds to, for instance, the Heavitree Sandstone of the Amadeus Basin.

The Centralian Superbasin is traditionally interpreted as an intracratonic basin initiated by thermal subsidence (Walter *et al.*, 1995). It is possible, however, that this basin was, at least in part, extensional. Walter *et al.* (1995) recognised four supersequences within the Centralian Basin. The Yeneena Group corresponds to the first of these, which was terminated by a superbasin-wide unconformity-disconformity which is loosely constrained to ca. 800 Ma (Walter *et al.*, 1995; Grey *et al.*, 1999).

In the Yeneena Basin, evidence for extension is present as growth faults (Table 6.1), for example a change in thickness of the Coolbro Sandstone along the southwest limb of the Cottesloe Syncline. The emplacement of mafic to intermediate intrusions between 835 and 830 Ma implies extension continued until this time (Table 6.1). This timing corresponds to the emplacement of the Gairdner Dyke swarm in the Adelaide rift system (Pirajno and Bagas, 2008), which is interpreted as an early stage of the break-up of Rodinia. It is likely that the extension that formed the Yeneena Basin, and possibly the Centralian Superbasin, is related to this breakup (Bagas and Nelson, 2007). Stage one of the Miles mineral system is associated with the later stages of this extension.

Geological and geochronological data suggest that after emplacement of these mafic bodies, the Yeneena Basin went into inversion, resulting in the Miles Orogeny. The main phase of the Miles Orogeny (D_4) is characterised by east-northeast-dipping thrust faults, which are parallel to a foliation developed parallel to the axial planes of recumbent folds, and indicate vergence of northeast over southwest (Bagas, 2004a; [Table 6.1](#)). These relationships suggest northeast over southwest contraction or transpression, although it is not clear at this time the cause of this contractional event. One possible mechanism is ridge push, which developed once the rifting that formed the Yeneena Basin went to completion and ocean spreading occurred. In this mechanism, ridge push forces acted upon a weakened lithosphere. This does not have to have been directly outboard from the Paterson region and could have occurred on the other side of the North Australian Craton. The widespread ca. 800 Ma unconformity-disconformity noted in the Centralian Superbasin could also be an expression of tectonism related to ridge push. Stage two of the Miles mineral system is best interpreted as the consequence of the change from extension to contraction in the Yeneena Basin. Given the many geological similarities between the Yeneena Basin, other basins within the Centralian Superbasin system, and the Adelaide rift system, it is probable that similar mineral systems to the Miles system operated in these basins.

6.2.4.2 Architecture

Deposition and subsequent inversion of the Yeneena Basin during the Miles Orogeny provided the architecture that allowed operation of the Miles mineral system. This architecture is linked fundamentally to geodynamic processes and consists of stratigraphic architecture, which was set up during basin formation, structural architecture, which was established and-or reactivated during basin formation and inversion, and igneous architecture, which appears to have accompanied late stage basin formation, and possibly the early stages of basin inversion.

6.2.4.2.1 Basin architecture

The Yeneena Basin, which consists of the basal Throssell Range Group and overlying Lamil Group ([Figure 6.1](#)), unconformably overlies medium- to high-grade metamorphic rocks of the Rudall Complex. The basal unit of the Throssell Range Group is the Coolbro Sandstone, a unit composed dominantly of quartz-rich sandstone with ubiquitous planar and trough cross bedding. Hickman and Clarke (1993) interpret this unit to have formed in a fluvial-deltaic environment, becoming shallow marine at the contact with the Broadhurst Formation. Palaeocurrent directions indicate that the source of detritus was from the southwest. Although there is uncertainty due to structural complexities, Hickman and Clarke (1993) and Hickman and Bagas (1998) indicate that this unit thins from 3000-4000 m thickness in the northwest to hundreds of metres thickness in the southeast, with shales being present mostly to the southeast. This unit is extensively altered (see below) and may have acted as an aquifer during mineralisation.

The overlying Broadhurst Formation consists of a 1000-2000 m thick succession dominantly of carbonaceous shale and turbiditic sandstone-shale beds (described as wackes in [Chapter 3](#)), with minor sandstone and carbonate units, interpreted to have been deposited in shallow water (Hickman and Clarke, 1993). Very localised basalt is also present, although the relationship (extrusive versus intrusive) to the enclosing rocks could not be established. Sandstone is present in the lower half of the Broadhurst Formation, up to 500 m stratigraphically above the contact with the Coolbro Sandstone. Carbonate units, including both limestone and dolomite up to 100 m thick, are present at all levels of the Broadhurst Formation (Hickman and Clarke, 1993). The Broadhurst Formation is variably sulfidic, with up to 10 vol. % pyrite and pyrrhotite present near the base of the unit, where the abundant basal pyrrhotite provides a distinctive aeromagnetic signature (Hickman and Clarke, 1993). Although the Broadhurst Formation was likely an aquiclude, the sandstone, and possibly the carbonate, units may have been local aquifers. The presence of high quantities of carbonaceous material, combined with the presence of significant carbonate-dominated intervals, and local sulfide-rich zones, make the Broadhurst Formation highly reactive with hydrothermal fluids, particularly oxidised fluids.

The overlying Isdell Formation, which is the uppermost unit of the Throssell Range Group, consists almost exclusively of carbonate (dolomite and dolomitic limestone) rocks with thin units of calcareous siltstone and shale. This unit is up to 1000 m thick (Hickman and Clarke, 1993).

The Isdell Formation appears to be structurally overlain by rocks of the Lamil Group, which include, from bottom to top, the Malu, Puntapunta and Wilki Formations (Bagas, 2000) (see [Section 3.2.2.3.2](#) for a discussion of this). The Malu Formation consists of turbiditic sandstone interbedded with calcareous siltstone, whereas the Puntapunta Formation comprises silty to sandy carbonate and the Wilki Formation consists of mature quartzitic sandstone (Czarnota *et al.*, 2009a). Although these upper units are not known to be mineralised by the Miles mineral system, it is possible that down-flowing brines formed in these units may have been involved in mineralisation at deeper levels of the Yeneena Basin.

McIntyre *et al.* (2005) suggested that Throssell Range Group is characterised by a fining upwards sequence, consistent with transgression and a deepening water column. This is consistent with interpretations based on sedimentology suggesting a progression from fluvialite sandstones (Coolbro Sandstone), through a shallow marine shale-carbonate-sandstone package (Broadhurst Formation) into deep water carbonates (Isdell Formation). In contrast, McIntyre *et al.* (2005) further suggested that the Lamil Group is a coarsening-upward sequence and indicative of regression and a shallowing water column, consistent with sedimentological data of Turner (1982). The combined Throssell and Lamil Groups are best interpreted as a single supersequence, during which the Yeneena Basin initially opened (Throssell Range Group) and was subsequently filled (Lamil Group), with the Isdell and Malu Formations representing the deepest water environments. The sequence of events described above is conjectural; the known boundaries between the Throssell Range Group, Isdell Formation and Lamil Group are all faulted, as illustrated in [Figure 6.1](#).

If rocks of the Yeneena Basin correlate with Supersequence 1 of the Centralian Superbasin (Bagas *et al.*, 1995; Walter *et al.*, 1995), the Yeneena Basin would be the thickest depocentre for the Superbasin. Using the estimates of unit thickness documented above, the Throssell Range Group has a total thickness of between 4000 and 7000 m, and the total thickness (in the direction of progradation) of the combined Yeneena Supergroup is ca. 13 km (McIntyre *et al.*, 2005), making it significantly thicker than any measured section of equivalent rocks elsewhere in the Centralian Superbasin (Walter *et al.*, 1995). This thickness meets the empirical requirement that basin thickness must exceed 5-6 km before unconformity-type uranium deposits form (Kyser *et al.*, 2000). More detail on the geology of the Yeneena Basin can be found in [Chapter 3](#) of this Record.

6.2.4.2.2 Structural architecture

The Yeneena Basin is located where the exposed Broadhurst Formation overlies the Camel-Tabletop Fault Zone which separates the Tabletop Terrane from the Connaughton and Talbot terranes of the Rudall Complex. This is a major feature of the Mesoproterozoic geology. The McKay Fault-Southwest Thrust system, which marks the southern thrust front in the Yeneena Basin, is parallel to the Camel-Tabletop system. The other major basement structure in the region is the NNW-striking Vines Fault which bounds the eastern margin of the Pilbara Craton. The intersection of these two features in the vicinity of the Nifty Deposit controls the overall crescent shape of the Yeneena Basin outcrop and controlled the site of extension and later inversion of these systems and hence the overall geometry of the Basin.

As documented by Hickman and Clarke (1993), Hickman and Bagas (1998) and Bagas (2004a), the Yeneena Basin and the Rudall Complex underwent six contractional deformational events. Of these, two (D_1 and D_2) predated deposition of the Yeneena Basin and are restricted to the Rudall Complex, two (D_3 and D_4) comprise the Miles Orogeny and two (D_5 and D_6) occurred later. The last two deformational events are not considered further in the Miles mineral system as they post-date mineralisation. An important aspect not included in the structural history is the extensional history, particularly associated with the formation of the Yeneena Basin.

The earliest deformational event is recorded as a layer-parallel, penetrative foliation, interpreted to be the consequence of either isoclinal folding or thrusting. This fabric is folded by F₂ isoclinal folds and is deformed by S₂ schistosity. After removal of tilting by later deformational events, S₂ is thought to have originally dipped 20–40° to the north-northeast (Hickman and Bagas, 1998). Although D₂ structures did not play a direct role in localising mineralisation, they probably influenced the geometry of distribution of favourable host units.

Although the restricted exposure of much of the Yeneena Basin makes identification of extensional structures difficult, the thickness of the Coolbro Sandstone changes across an east-northeast striking fault on the Broadhurst 1:100 000 sheet (Hickman and Clarke, 1993) as well as clearly thickening across northwest-striking faults southwest of Kintyre. It is likely that these early extensional faults may have localised later deformation during the Miles Orogeny.

The earliest contractional deformational event to affect the Yeneena Basin was D₃, the first of two deformational events that make up the Miles Orogeny. This event resulted in bedding-parallel faulting and quartz veining along the unconformity between the Basin and the Rudall Complex. It was very localised, however, and does not appear to have any control on mineralisation and may represent compaction during the extensional event.

An important structural control on the Miles mineral system was D₄, which produced an anastomosing set of largely thrust faults, with moderate dips to the northeast, and a series of locally overturned folds with axial planes parallel to the faults. Uranium deposits in the Rudall Complex are closely associated with, or hosted by D₄ faults, whereas copper deposits in the upper Broadhurst Formation are associated with D₄ folds. Uranium-copper deposits along the contact between the Coolbro Sandstone and Broadhurst Formation appear to be associated with the northeast-dipping faults and with a second set of subvertical faults with a northerly trend and predominantly sinistral displacements.

6.2.4.2.2 Igneous architecture

In the Rudall Complex, there are two major igneous events. The first, at 1800–1760 Ma, corresponds to the Yambah Event in the North Australian Craton, and involves felsic intrusives of the Kalkan Supersuite in the Talbot and Connaughton terranes. The Kalkan Supersuite constitutes 50% of the areal extent of the Talbot Terrane (Smithies and Bagas, 1997; Czarnota *et al.*, 2009a).

In the Tabletop Terrane, which appears to be a separate crustal block to the Talbot and Connaughton terranes (Bagas and Lubieniecki, 2000), extensive magmatism involving felsic and mafic intrusions has been dated at between 1590 Ma and 1550 Ma (D. Maidment, unpub. data; Czarnota *et al.*, 2009a). Younger magmatism in the Tabletop Terrane includes granites with ages of ca. 1476 Ma and 1310 Ma (Nelson, 1996; Bagas, 2004a).

The earliest magmatic activity in the Yeneena Basin is mafic-dominated, consisting of basaltic rocks with an unknown timing (extrusive or intrusive) relative to the host Broadhurst Formation and dolerite and monzonite bodies that intrude both the Throssell Range and Lamil groups. Sensitive high-resolution ion microprobe (SHRIMP) U-Pb dating of these intrusive bodies has yielded ages of 816 ± 6 Ma (Eva Well Intrusion; Reed, 1996), 837 ± 6 Ma (Hasties Gabbro; D. Maidment pers. comm.) and 835 ± 4 Ma (Duke Monzonite; Maidment pers. comm.). These mafic bodies, which are both spatially and stratigraphically widespread, correlate with the 827 ± 6 Ma Gairdner Dyke Swarm (Wingate *et al.*, 1998), which extends from the Gawler Craton, through the Musgrave Complex and into the Paterson region (Pirajno and Bagas, 2008), and probably with the Bitter Springs Basalt in the Amadeus Basin. As some of these intrusions are deformed, it is likely that they predated, or were intruded very early during, the Miles Orogeny.

6.2.4.3 Origins of fluids and metals

With the exception of the Nifty and Maroochydore deposits, very little information is available which bears on the characteristics and source of ore fluids and metals in the Miles mineral system. Detailed fluid inclusion studies by Anderson *et al.* (2001) and Reed (1996), combined with fluid inclusion observations by Huston *et al.* (2007), suggest that the ore fluids at Nifty and Maroochydore had relatively high salinity (to 27 eq. wt. % NaCl) and were, possibly, evolved basinal brines.

Saline brines may have been produced at two periods during the deposition of the Yeneena Basin: during shallow water deposition of the Broadhurst Formation as the Basin initiated; and, of the Wilki Formation as the Basin filled. Both Reed (1996) and Anderson *et al.* (2001) reported the presence in mineralised successions of dolomite and sulfide pseudomorphs after minerals interpreted to be sulfate, either gypsum or anhydrite, and halite. Such evaporative minerals are consistent with a shallow water environment of deposition for at least part of the Broadhurst Formation and the formation of evaporative brines.

Although insufficient data are available to assess the origin of the main ore metals, uranium and copper, radiogenic isotopes can be used as tracers as to the rocks the ore fluids have encountered. Initial strontium ($^{87}\text{Sr}/^{86}\text{Sr}$) ratio values of ca. 0.722-0.723 from the apatite veins at the Nifty deposit are compatible with interaction of the ore fluids with rocks of the Yeneena Supergroup or rocks from the Rudall Complex to derive strontium. In contrast, at 825 Ma, epsilon neodymium (ϵ_{Nd}) values of -3.6 to -1.3 from the same apatite veins are not compatible with derivation from either Yeneena Group rocks (ϵ_{Nd} ca. -16.4 to -6.5, at 825 Ma: calculated from unpublished data, R Maas pers. comm.) or the Rudall Complex (ϵ_{Nd} ca. -25.6 to -4.5, mostly -17.9 to -6.2), at 825 Ma: calculated from unpublished data, D Maidment). Rather, the epsilon neodymium data are more compatible with an input from ca. 830 Ma mafic rocks, which have ϵ_{Nd} at 825 Ma of -4.6 to 7.5. These mafic rocks may have been key to formation of copper deposits in the Miles mineral system, as these rocks are typically enriched in copper (Figure 6.13). Uranium was most likely derived from crustal rocks of the Rudall Complex or detritus within the Yeneena Supergroup, consistent with the $^{87}\text{Sr}/^{86}\text{Sr}$ data.

Data and observations presented above suggest that the ore fluid that formed the Nifty deposit, and probably the other deposits in the Miles mineral system, was a basinal brine that had reacted with the Yeneena Supergroup, ca. 830 Ma mafic rocks and probably the Rudall Complex. Geochemical modelling of unconformity-related uranium deposits and sediment-hosted copper deposits (Bastrakov *et al.*, 2010) suggests that the ore fluid was oxidised. The dominance of quartz-rich sandstone and carbonate rocks within the Yeneena Supergroup maintained the fluids at a relatively high redox state, allowing uranium and copper to readily be transported from sources, as discussed above, to reduced trap sites, as discussed below.

6.2.4.4 Fluid drivers and pathways

As described and discussed above, mineral deposits and prospects hosted by the Rudall Complex and Throssell Range Group have both stratigraphic and structural controls on mineralisation. The stratigraphic controls are best illustrated by the uranium-copper prospects localised along the Coolbro-Broadhurst contact and by localisation of copper deposits within carbonate-rich intervals of the upper Broadhurst Formation. The structural control is best illustrated by the association of uranium deposits in the Rudall Complex with D₄ thrust faults and by the spatial association of the copper deposits in the upper Broadhurst Formation to D₄ folds. These relationships suggest that fluid flow was controlled both by permeable zones within the stratigraphic succession and by crosscutting faults (Figure 6.13). Moreover, the temporal association with D₄ structures suggest that deformation associated with the Miles Orogeny was an important driver for fluid flow.

More direct evidence of stratigraphically-controlled fluid flow is present in ASTER images showing variations in the crystallinity of white mica in the Throssell Subgroup in the Cottesloe Syncline area (Figure 6.14). These data define a conformable zone of crystalline white mica in the upper part of the Coolbro Sandstone that is characterised by low Al-OH absorption features. Many of the

uranium-copper prospects (e.g., Sunday Creek) are located where this zone is transected by northwest- to north-striking faults (Figure 6.14). A number of uranium occurrences have also been identified in this area, both in drilling (BR series) and in outcrop (GA series). Geoscience Australia sampled two uranium-enriched rocks at or near the contact between the Coolbro Sandstone and Broadhurst Formation. The first, labelled GA1 on Figure 6.14 (sample 2006678163), consisted of siliceous medium- to coarse-grained sandstone with 2-3% limonite after disseminated pyrite and with possible covellite and assayed 93 ppm arsenic, 166 ppm copper and 107 ppm uranium. This sample was collected just below the contact with the Broadhurst Formation. The second, labelled GA2 on Figure 6.14 (sample 2006678123-02) sampled a bedding-parallel gossanous vein in the Broadhurst Formation. This vein assayed 240 ppm arsenic, 1060 ppm copper, 21 ppm molybdenum and 48 ppm uranium.

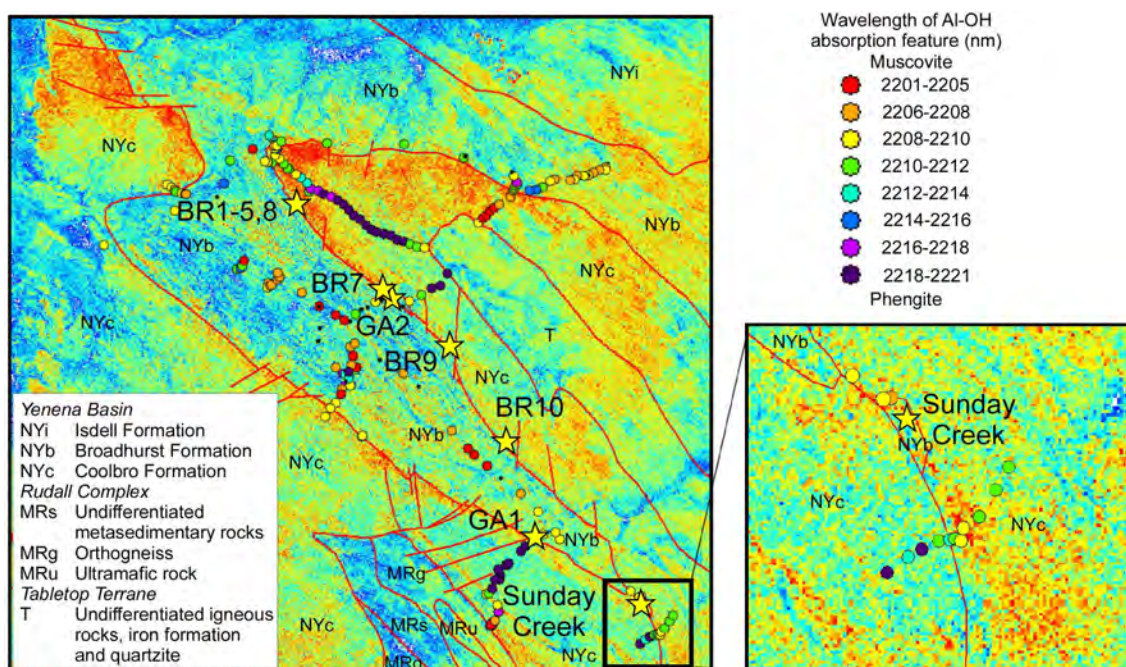


Figure 6.14: Image of the Cottesloe Syncline area showing variations in the Al-OH absorption feature of white mica, as determined from ASTER data and PIMA analyses, and the locations of uranium-copper and copper deposits, occurrences and prospects.

Petrographic studies suggest that this alteration is also characterised by the presence of crandallite-group minerals (K. Czarnota, unpub. data). Such minerals also have been identified in alteration zones developed in basins associated with unconformity-related uranium deposits in the Athabasca district in Saskatchewan, Canada, and the Pine Creek area of the Northern Territory (Quirt *et al.*, 1991; Gaboreau *et al.*, 2005). Additionally, ASTER mapping indicates that the zones of more crystallised white mica correspond to zones apparently characterised by aluminous alteration minerals.

We interpret this zone of crystalline white mica as a fluid pathway. Structures tapping the pathway allowed fluids to react with carbonaceous rocks along the Coolbro-Broadhurst contact, or to migrate into the upper part of the Broadhurst Formation, where interaction with carbonaceous, carbonate-rich successions caused deposition of copper and, to an unknown extent, uranium (Figure 6.13b). Limited geochronological data from the Nifty deposit suggests that this upward-directed fluid flow may have occurred later during the Miles mineral system as basin inversion neared completion. This model is

compatible with that presented by Anderson *et al.* (2001), although our inferred age of mineralisation is about 100 million years earlier.

Earlier, during the Miles mineral system, it is possible that fluid flowed downward from the Coolbro Sandstone fluid pathway, reacting with reduced rocks in the Rudall Complex and forming unconformity-related deposits such as Kintyre (Figure 6.13a). The D₄ faults that host the Kintyre and related deposits may be reactivations during inversion of faults which were initiated during extension that led to the formation of the Yeneena Basin. Geochronological data indicate that Kintyre may have formed 25 million years before the Nifty deposit, although the 2 σ errors overlap. In the case of the Kintyre deposit and related prospects, fluids are inferred to have flowed downward along thrust faults as inversion of the Yeneena Basin initiated.

6.2.4.5. Depositional mechanisms

As discussed above, fluid flow associated with the Miles mineral system appears to have largely occurred through the Coolbro Sandstone, a highly siliceous, oxidised unit. The ferric/ferrous iron ratio ($\text{Fe}_2\text{O}_3/\text{FeO}$) of the Coolbro Sandstone ranges from 1.7 to 32, with most values in the range 4–17 based on whole rock geochemical analyses of fresh or weakly weathered surface samples. These rocks would have been inert to the highly oxidised fluids generally interpreted as ore fluids in uranium-bearing mineral systems (Skirrow *et al.*, 2009; Bastrakov *et al.*, 2010). Hence, ore deposition would have occurred only when the fluids encountered a chemical gradient, in this case a redox gradient. Basin evolution from fluvial to submarine environments produces such chemical gradients, including gradients from oxidised fluvial sandstone to reduced, graphitic rocks in the basement and to reduced, carbonaceous rocks in overlying shallow marine successions.

These considerations, along with empirical observations of a close association between uranium and copper deposits with graphitic or carbonaceous rocks, suggest that the main cause of metal deposition in the Miles mineral system was reduction of originally oxidised fluids. Thermodynamic modelling of this process indicates that uranium will be deposited first, during initial reduction of the fluid, followed by copper when pyrite becomes stable, and then by lead and zinc when sufficient dihydrogen sulfide (H_2S) becomes available (Figure 6.15; Bastrakov *et al.*, 2010). This H_2S could be produced either from reduction of aqueous sulfate in the ore fluids, reaction with sulfide-rich rocks, or mixing with a second H_2S -rich fluid. Hence, the expected zonation, down the redox gradient, of metals is uranium → copper → zinc-lead, a zonation that is observed at the deposit and, possibly, the district scale. At the district scale there is a broad zonation from uranium ± copper deposits in the basement and along the upper contact of the Coolbro Sandstone, copper-dominated deposits (± uranium) in the upper part of the Broadhurst Formation, and zinc-lead deposits in the Isdell Formation.

This zonation can be used to predict potential locations of other metals. For example, at the Nifty and Maroochydore deposits, uranium deposition is predicted up the redox gradient from copper deposition. At Nifty, the presence of enriched uranium along the southeast margin of the deposit suggests fluid flow from the southeast and untested uranium potential in this direction.

Although there is an empirical relationship that many of the uranium and copper deposits in the Miles mineral system are associated with, or are hosted by, carbonaceous and/or graphitic rocks, at temperatures of likely ore deposition (200–300°C), the kinetics of redox reactions between carbon species is slow (Ohmoto, 1986), raising the likelihood that deposition did not occur as a consequence of direct fluid-rock interaction. Rather, it is more likely, although not proven, that mineral deposition occurred when oxidised basinal fluids reacted with fluids in equilibrium with, or buffered by, reduced rocks, including reduced carbon-bearing siltstone, shale or schist, or iron-rich rocks. Although these fluids are more likely to be hosted by reduced rock packages, expulsion of these fluids could lead to mineral deposition in rocks not characterised by high organic carbon, graphite or iron. Hence, uranium and copper deposition could occur outside, although in proximity, to the reduced packages.

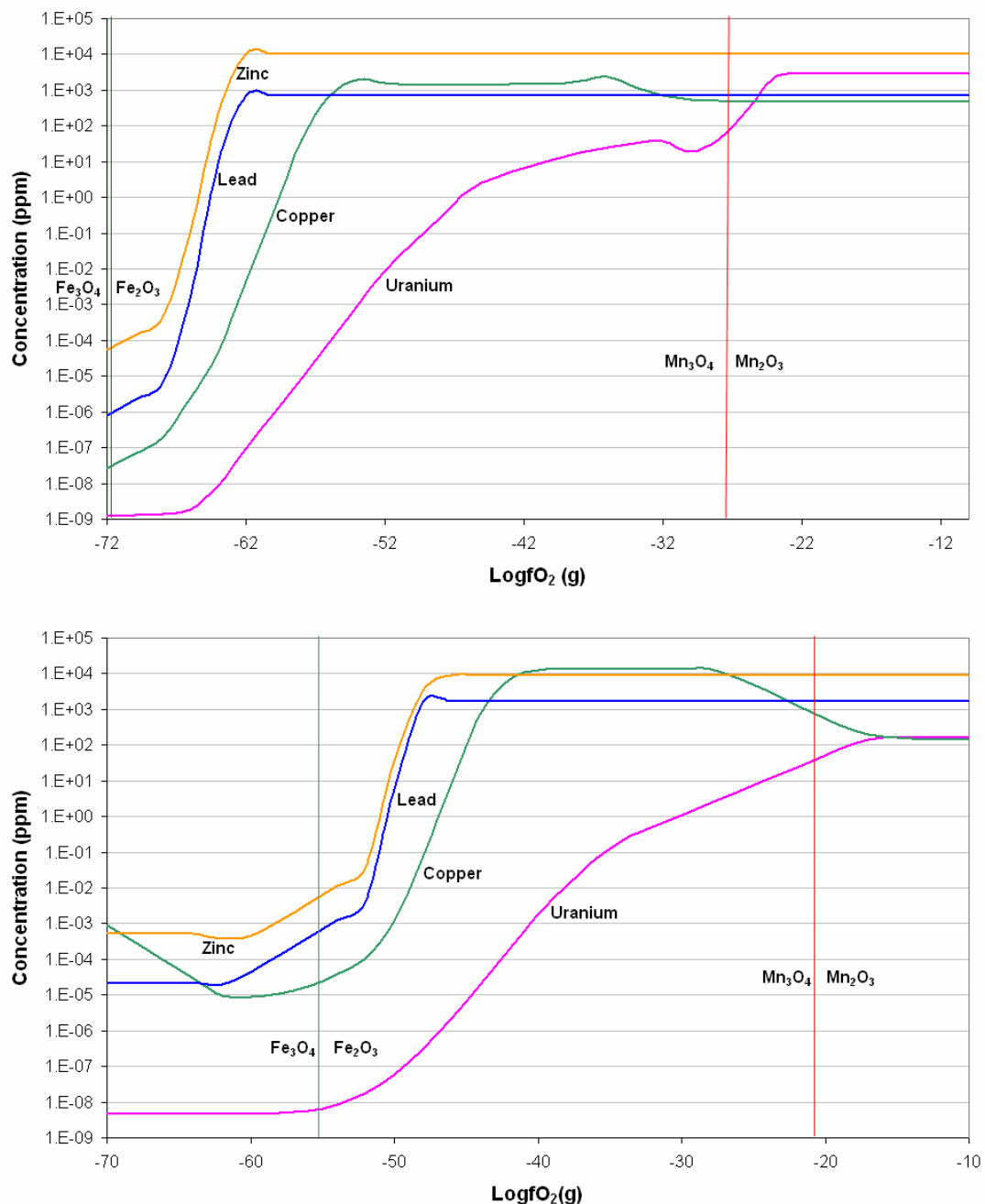


Figure 6.15: Diagrams showing solubility of uranium, copper, lead and zinc in a 5 wt. % NaCl fluid in equilibrium with quartz-potash-feldspar-albite-muscovite-paragonite assemblage as a function of oxidation state at 25°C (upper diagram) and 100°C (lower diagram). Vertical straight lines labelled $\text{Fe}_3\text{O}_4/\text{Fe}_2\text{O}_3$ and $\text{Mn}_3\text{O}_4/\text{Mn}_2\text{O}_3$ show oxygen fugacity ($f\text{O}_2$) levels corresponding to these buffers at 25°C and 100°C (after Bastrakov et al., 2010).

Copper deposits such as Nifty and Maroochydore appear to be closely associated with carbonate-rich intervals within the upper part of the Broadhurst Formation. At the Nifty deposit, the ores, at least in part, have replaced carbonate lenses, suggesting that the presence of carbonate is essential for

formation of these deposits. Carbonate rocks are common host rocks to many types of hydrothermal ore deposits, including skarns and Mississippi Valley-type deposits, as these rocks are highly reactive when they interact with hydrothermal fluids. This interaction dissolves carbonate, leading to the production of CO₂ and porosity. Both of these factors enhance rock permeability, with the production of CO₂ increasing fluid pressure and causing rock fracturing. In addition, interaction with carbonate neutralises fluids, a process that can lead to metal deposition. Hence, carbonates, particularly carbonates within organic-rich successions, are effective trap rocks for ore deposition, including within the Miles mineral system.

6.2.4.6 Post-depositional modifications

After cessation of the Miles Orogeny, the Paterson region experienced a major thermotectonic event associated with the emplacement of granites at 650–615 Ma (Goellnicht *et al.*, 1991; Goellnicht, 1992; Dunphy and McNaughton, 1998; Czarnota *et al.*, 2009a). As has been documented by Nash *et al.* (1981) and others, uranium deposits are highly susceptible to post-depositional modifications. These include remobilisation of ores, as well as the resetting of radiogenic isotopic systems. The effects of post-depositional processes on the deposits formed during the Miles mineral system are unclear, although these events have partially reset isotopic systematics (Huston *et al.*, 2007). The effects on the copper deposits are probably less, although localisation of ores at the Nifty and Maroochydore systems may have been affected by syn- to post-ore deformation.

The most significant post-depositional modifications relate to weathering, which has strongly affected the Nifty deposit. The effects of weathering on geochemical dispersion are beyond the scope of this chapter, but are also discussed in [Section 3.3.2.5](#).

6.3 MINERAL SYSTEMS ASSOCIATED WITH THE O'CALLAGHANS TECTONOTHERMAL EVENT

The interval between ca. 655 and 615 Ma (Goellnicht, 1992; Nelson, 1995; Dunphy and McNaughton, 1998; Czarnota *et al.*, 2009a), was a period of extensive granitic magmatism in the northern part of the Paterson region. The age of this felsic magmatism is uncommon in Australia (Goellnicht *et al.*, 1991) and unusual globally. A broad spatial association between the granites and a series of gold-copper and tungsten-copper-zinc-lead deposits and prospects have led to the interpretation that these deposits are genetically associated with the magmatism (Goellnicht *et al.*, 1989; Goellnicht *et al.*, 1991; Ferguson *et al.*, 2005), although the nature of this relationship is debated (Rowins *et al.*, 1997).

6.3.1 Granite-related gold-copper and tungsten-copper-zinc-lead deposits

Known examples of granite-related deposits are located in the northern part of the Paterson region and are hosted mostly by the Lamil Group, in particular the Malu Formation ([Figure 6.16](#)). Gold-copper deposits include the major Telfer deposit, numerous nearby prospects and the Magnum prospect ca. 100 km to the north. The recent discovery of the O'Callaghans tungsten-copper-zinc-lead deposit, located 10 km south of Telfer, highlights the polymetallic character of granite-related deposits in the northern Paterson region.

Granites that intrude the upper Yeneena Supergroup in the northern Paterson region form the O'Callaghans Supersuite of Budd *et al.* (2001). This has been divided into groupings by Goellnicht *et al.* (1991) and Budd *et al.* (2001). Goellnicht *et al.* (1991) divided it into two groups, the Minyari (Minyari Granite, Koolyu Granite and O'Callaghans Granite) and Mt Crofton (Mt Crofton Granite, Wilki Granite and minor plutons) groups, based on silica content, lead isotope characteristics and deformation. The Minyari group granites are less fractionated (< 74 wt. % silica [SiO₂]), are less deformed and are characterised by more radiogenic lead isotope ratios, whereas the Mt Crofton group are more fractionated (> 74 % wt. SiO₂), are generally undeformed and have less radiogenic lead isotope ratios.

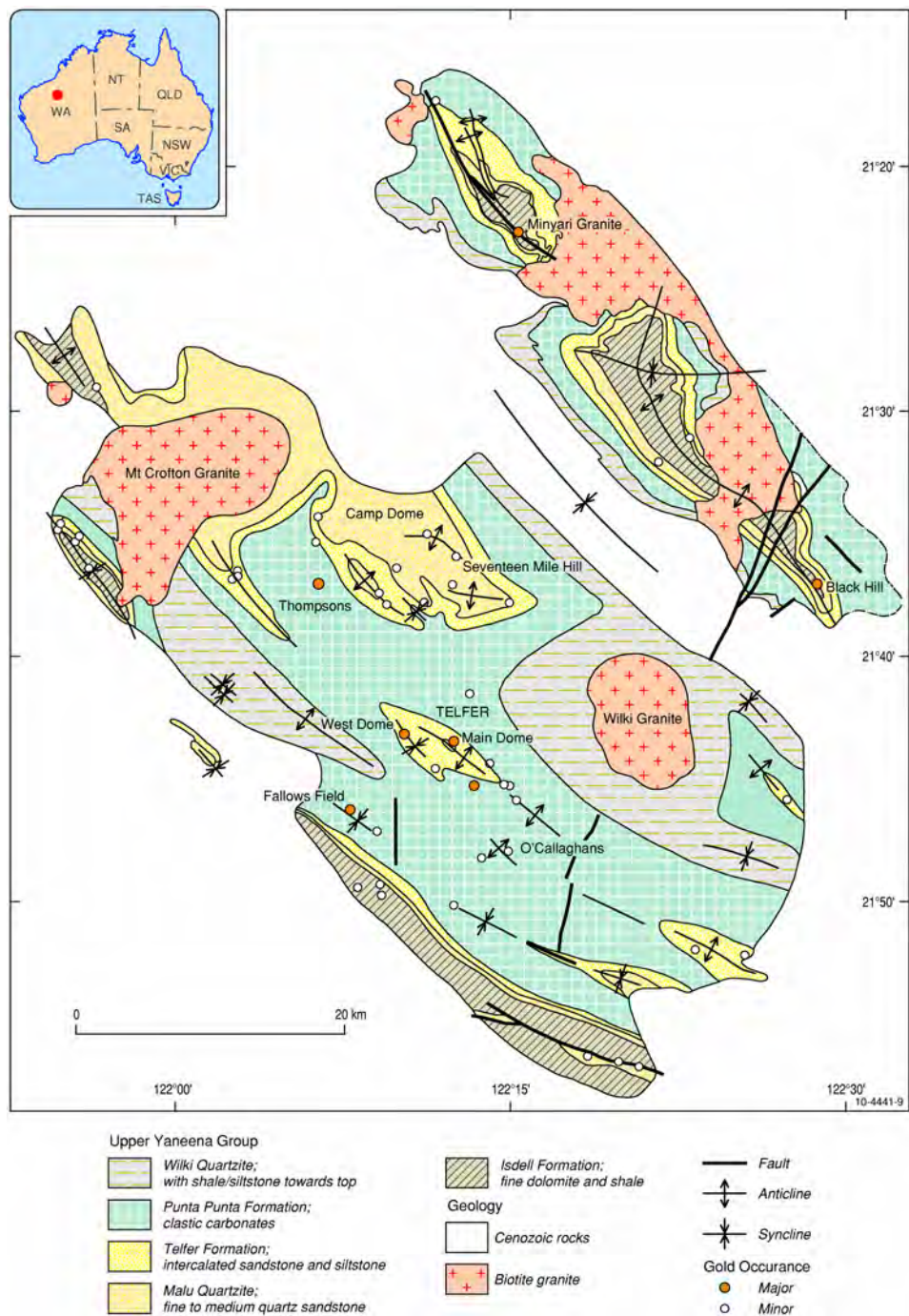


Figure 6.16: Geology of the northern part of the Paterson region, showing the location of gold deposits and prospects, modified after Rowins *et al.* (1997).

In contrast, Wyborn (1997) and Budd *et al.* (2001) divided the O'Callaghans Supersuite into the magnetite-stable Mount Crofton Suite and the ilmenite-stable O'Callaghans Suite. This classification differs from that of Goellnicht *et al.* (1991) in that the Wilki Granite and minor plutons have been classified into the O'Callaghans Suite (Minyari group). As the solid geology map of Czarnota *et al.* (2009a) uses magnetic character as a primary criterion for differentiating granites, the classification

used differentiates the Mount Crofton Suite from the O'Callaghans Suite. Budd *et al.* (2001) noted that fluids evolved from the O'Callaghans Suite would be reduced and could carry gold, copper, tungsten and molybdenum. They also suggested that mineralisation associated with the more oxidised Mt Crofton Suite would be more copper-rich.

Granites of the O'Callaghans Supersuite align along a number of geographic trends, the most prominent of which are east-northeast and north-northeast. The NE trend of the Mount Crofton Suite of granites, and particularly the parting of the trend at its south-western margin, is indicative of a mode one (i.e., opening) fracture. Based on this interpretation these granites were intruded under a northeast-southwest oriented maximum principle stress (σ_1) direction and northwest-southeast oriented minimum principal stress direction (σ_3). Similar granite trends have been observed within subduction-related volcanic arcs. This principle stress direction is consistent with the dominant structures found in the area—NW striking thrusts and folds as well as dextral transpression along the Vines fault (Czarnota *et al.*, 2009a).

Published ages for granite emplacement range from ca. 690 Ma (Mount Crofton Granite; Goellnicht *et al.*, 1991) to ca. 617 Ma (O'Callaghans Granite; Goellnicht, 1992). These ages, however, are based upon $^{207}\text{Pb}/^{206}\text{Pb}$ isochrons and have inherently high uncertainties. More precise ages range from 654 ± 8 Ma (Crofton Granite SHRIMP titanite; Dunphy and McNaughton, 1998) to ca. 630 Ma (Minyari Granite; D Maidment, unpub. data in Czarnota *et al.*, 2009a).

6.3.1.1 Telfer

Prior to closure in July 2000, the Telfer gold-copper mine produced over 180 t of gold. Following closure, a reassessment of the geology and resources of the deposit resulted in the announcement in 2003 of a JORC-compliant total remaining resource of 890 t gold and 960 kt copper (Howard *et al.*, 2005), making Telfer the third largest gold deposit in Western Australia (after the Golden Mile and Boddington) and the largest Neoproterozoic gold deposit in the world. Its discovery in 1971 was the first realisation of the mineral potential of the Paterson region.

6.3.1.1.1 Geology, age and origin

The Telfer deposit is hosted by the Malu Formation of the Lamil Group (Figure 6.1), which is dominated by turbiditic sandstone interbedded with calcareous siltstone (Czarnota *et al.*, 2009a). Rocks that host the Telfer deposit, termed the Telfer Member (Bagas, 2000), are transitional between sandstone of the Malu Formation and carbonate-rich rocks of the overlying Puntapunta Formation. The Telfer Member consists of fine- to medium-grained sandstone interbedded with clayey sandstone, siltstone and shale, with minor dolomite near the top (Bagas, 2000). In detail, the Telfer Member has been divided into a series of local units that define the northwest-striking Telfer Dome (Figure 6.17).

6.3.1.1.1.1 Structure

The Telfer Dome consists of two smaller-scale, *en echelon*, doubly-plunging anticlines with an intervening syncline (Figure 6.17). These folds are asymmetric, with northeast-dipping limbs steeper (30–55°) than southwest-dipping limbs (10–20°; Goellnicht *et al.*, 1989; Rowins *et al.*, 1997). Goellnicht *et al.* (1989) and Rowins *et al.* (1997) recognised three structural fabrics in the rocks: 1. an early foliation developed at a low angle to bedding (S_1); 2. a steeply southwest-dipping spaced cleavage (S_2) which crenulates S_1 and is axial planar to the major folds; and, 3. a weakly developed steeply southeast- or northwest-dipping spaced cleavage (S_3) that is oblique to S_2 and defined by sericite. Goellnicht *et al.* (1989) interpreted the first two fabrics to be linked and related to the formation of the folds that define the Telfer Dome. Rowins *et al.* (1997) interpreted the third fabric to have formed during a later deformational event.

Hewson (1996) recognised the two early fabrics observed by Goellnicht *et al.* (1989) and Rowins *et al.* (1997), but inferred that they formed in separate deformational events. In addition, he recognised three later, less well-developed structural elements: 1. mesoscale, recumbent, asymmetric folds (F_3)

with axial planes dipping shallowly to the northwest or north; 2. mesoscale cross-folds (F_4) of D_2 structures with subvertical axial planes that strike obliquely to the F_2 axial trend; and, 3. late, small-scale monoclinal kink folds (F_5). The F_4 folds of Hewson (1996) may relate to the S_3 fabric observed by Rowins *et al.* (1997).

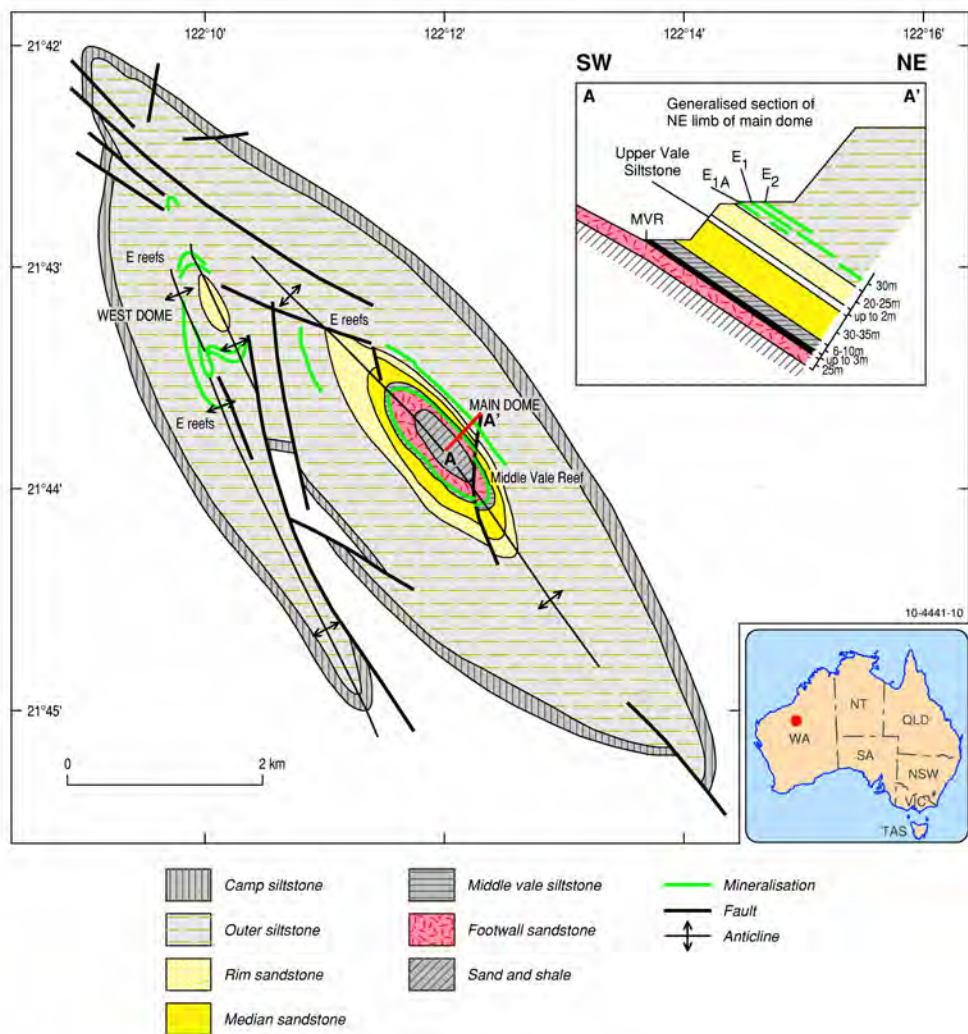


Figure 6.17: Geological map of the Telfer Dome showing the surface expression of mineralised reefs, modified after Rowins *et al.* (1997).

6.3.1.1.1.2 Mineralisation and alteration

Detailed studies of the Telfer deposit (Goellnicht *et al.*, 1989; Dimo, 1990; Rowins *et al.*, 1997; Howard *et al.*, 2000; Howard *et al.*, 2005) have identified five types of ore (Figure 6.18): 1. reefs concordant to stratigraphy; 2. stockwork ore; 3. boundary ore; 4. halo ore; and, 5. monocline ore. These ores are known to extend for over 1500 m vertically, and are present in the both the Malu (including the Telfer Member) and Isdell Formations (Howard *et al.*, 2005).

Concordant reefs, which include the Middle Vale and E Reefs, are remarkably persistent, stratabound thin sheets that extend over areas of up to 20 km² (Dimo, 1990; Figure 6.17). In the upper part of the deposit these veins are typically hosted by interbedded pelitic and arenaceous siliciclastic rocks, commonly within carbonate-rich sandstone or black carbonaceous shale-siltstone

(Goellnicht *et al.*, 1989; Howard *et al.*, 2005). Oxidation and supergene enrichment significantly upgraded the veins. Along the northeast flank of the Main Dome, supergene and mixed supergene-oxide ores averaged 27-29 g/t gold and 2-10 wt. % copper, significantly higher than hypogene ores, which graded 1.6-12.8 g/t gold and 0.0-0.1 wt. % copper (Goellnicht *et al.*, 1989). Other reefs deeper down in the stratigraphy, such as M30 (Figure 6.18), lack a quartz component and are dominated by dolomite, with lesser pyrite and chalcopyrite (Hewson, 1996).

The latter four types of ore are stockwork in style and vary according to the consistency of grade and geological setting. With the exception of the monocline ores, these ore types generally form haloes around, or link, concordant reefs at different stratigraphic levels (Figure 6.17). Stockwork ores, as defined by Howard *et al.* (2005), are characterised by consistent gold grades above 0.3 g/t, and are localised in the upper parts of the mine, largely within the Telfer Member. Boundary ore consists of patchy gold zones that are generally adjacent to stockwork ore (Figure 6.18). Halo ore zones consist of stockworks that envelope and link concordant reefs, including the lower M reefs (M20 to M50: Howard *et al.*, 2005).

The monocline ores differ from the other stockwork ores in that they are not as closely linked to the main concordant reefs (Figure 6.18). These ores form a southeast-dipping zone that appears to be controlled by the northeast limb of the Main Dome anticline.

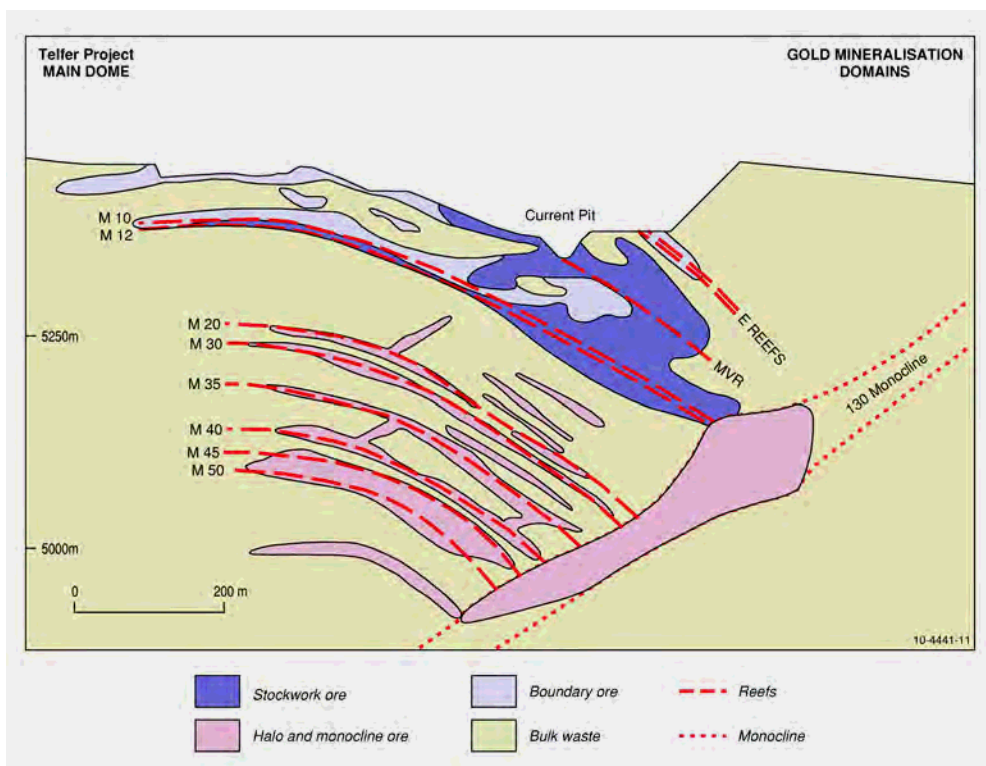


Figure 6.18: Schematic cross section showing the geology of the Telfer, modified after Howard *et al.* (2005).

At a depth of approximately 1 km below surface, the Telfer Deep zone forms a body discrete from the shallower ore zones. This ore zone contains most of the ore types present in the upper parts of the deposit. It includes the down-dip extension of the I30 monocline orebody, the I30 quartz reef and adjacent stockwork zones. These stockwork zones also extend to the west and below the economic ore zone (Figure 6.18).

Mineralogically these veins are relatively simple. The major gangue is either quartz or dolomite,

which is accompanied by varying amounts of pyrite and chalcopyrite, with minor to trace pyrrhotite. Other hypogene minerals that have been recognised in the veins include sericite, tourmaline, rutile, albite, galena, pentlandite, chalcocite, bornite, sphalerite, cobaltite, xenotime, monazite and gold (Goellnicht *et al.*, 1989; Dimo, 1990; Hewson, 1996; Howard *et al.*, 2005).

Most rocks in the Telfer Dome are altered, with more pelitic units characterised by sericite-carbonate assemblages and quartz-rich sandstones characterised by silicification. Alteration zones associated directly with veins have variable mineral assemblages, including sericite-silica ± pyrite ± adularia ± albite ± tourmaline (Goellnicht *et al.*, 1989), muscovite-dolomite, carbonate-sericite-sulfide, carbonate-chlorite-muscovite-tourmaline ± scheelite, and dolomite-sericite-tourmaline-epidote assemblages (Hewson, 1996).

6.3.1.1.3 Age and timing of mineralisation

Although originally thought to be syngenetic due to the concordant character of early discovered reefs (Tyrwhitt, 1979; Turner, 1982), the Telfer deposit is now generally considered to be epigenetic as further exploration and research identified clearly cross-cutting veins and demonstrated that the concordant veins, though bedding-parallel at the local scale, were discordant at the deposit scale (Goellnicht *et al.*, 1989; Hewson, 1996; Rowins *et al.*, 1997; Howard *et al.*, 2005). Based on paragenetic studies relating the timing of veining to deformational events, Hewson (1996) inferred that gold and copper were introduced after the "major terrane deformation", the D₂ event which corresponds with the Miles Orogeny, because sericite alteration accompanying mineralisation overprinted the S₂ fabric. A D₃ to D₄ timing was preferred based on microstructural observations (Hewson, 1996). This timing is broadly compatible with inferences by Goellnicht *et al.* (1989) that mineralisation occurred either late during, or following, formation of the Telfer Dome, and conclusions by Howard *et al.* (2005) that the main stage of mineralisation occurred during the early part of the Paterson Orogeny, when structures that developed in the Miles Orogeny were reactivated. Taken together, these observations suggest that the main stage of mineralisation post-dated the Miles Orogeny, and accompanied the Paterson Orogeny. However, L. Bagas (pers. comm., 2010) indicates that fabrics assigned to the Paterson Orogeny postdate the Telfer Dome and must be younger than ca. 630 Ma.

Although direct ages for mineralisation are not available, most workers (Goellnicht *et al.*, 1989; Rowins *et al.*, 1997; Howard *et al.*, 2005) have inferred that mineralisation was coeval with granite emplacement, which, from limited data by Dunphy and McNaughton (1998) and D. Maidment (unpub. data in Czarnota *et al.*, 2009a), occurred between ca. 654 Ma and ca. 630 Ma. The lower end of this range corresponds with the age inferred for the Magnum gold-copper deposit (below) and the entire range falls within the range of ⁴⁰Ar/³⁹Ar ages reported for Rudall Complex and Throssell Range Group by Durocher *et al.* (2003).

6.3.1.1.4 Controls and origin of mineralisation

Howard *et al.* (2005) indicated that the controls on ore localisation at Telfer are largely rock competency and rock chemistry, identifying three mineralisation domains: 1. concordant domains; 2. discordant domains; and, 3. chemically reactive domains. In the concordant domains reefs are localised within well-bedded sandstone-siltstone successions, with mineralisation controlled by bedding plane shears or faults. In discordant domains, the ores are hosted by crosscutting shears, stockworks and breccia veins that are concentrated in more massive arenaceous sandstones, particularly where these rocks have been silicified and bedding is poorly developed (Howard *et al.*, 2005). These controls are largely structural and related to the competency of the rocks. The third domain, in contrast, relates to the chemical composition. This domain is hosted by carbonate-rich sandstone and by pyrite-rich, carbonaceous shale-siltstone units. Although the gold and copper are hosted by structurally-controlled veins, the rock types appear to have enhanced mineralisation. The presence of different styles of mineralisation within different lithological and structural domains indicates a complex interplay between chemical gradients and structural elements for ore deposition.

Goellnicht *et al.* (1989; 1991) originally proposed a link to magmatism for the Telfer deposit, largely based upon high fluid inclusion salinities and lead isotope characteristics. Although acknowledging that the ore fluids were saline, Rowins *et al.* (1997) suggested that stable isotope data, including sulfur, carbon, oxygen and boron, radiogenic lead isotope data, the composition of tourmaline, and sulphur/selenium (S/Se) ratios were more consistent with derivation from the succession in the Yeneena Basin. Hence, although there appears to be a broad spatial and possible temporal link to 650-630 Ma felsic magmatism, a direct link between the ore fluids and magmatic emanations is less certain, and, perhaps, unlikely. Fluid flow, however, could still be driven by magma emplacement.

6.3.1.1.2 Geophysical characteristics

Sexton (1994) reported the results of a series of geophysical surveys over the Telfer deposit designed to test responses of the ores. Techniques reported included aeromagnetic, gravity, time-domain electromagnetic and induced polarisation-resistivity surveys. In addition, seismic velocity measurements were undertaken to determine the suitability of various rocks in the mine environment for machine excavation, although these measurements did not have direct application to exploration. The results indicate that the ores were not detectable using either magnetic or gravity data, but could be imaged using time-domain electromagnetic and induced polarisation-resistivity techniques.

Despite limitations for detecting ore lenses, magnetic and gravity data were found to be useful in mapping regional and semi-regional geological features, such as granite intrusions, structures and rock units. Regionally, these methods mapped dolerite intrusions, and at the Telfer deposit detailed gravity successfully mapped exposed Camp Sandstone and Outer Siltstone (informal mine terms) as these units are more resistive to weathering and the associated decrease in density (Sexton, 1994).

Time domain electromagnetic techniques (using the Newmont Electromagnetic Pulse system) successfully identified the down-dip extension of the Middle Vale Reef as a conductor and gradient-profiling induced polarisation surveys mapped E reefs around the Main Dome (Sexton, 1994). These results led Sexton (1994) to conclude "before oxidation the MVR contained a substantial amount of sulphide and, given its areal extent, would have made a good target for IP and possibly EM".²

The regional geophysical response around Telfer is shown in [Figure 6.19](#). As indicated by Sexton (1994), there is no notable magnetic signature other than that from mining infrastructure and the 2.5 km spaced regional gravity does not have sufficient resolution to show the subtle gravity high attributed to the Telfer main dome. In contrast, the host rocks around Telfer show a subtle but widespread uranium channel radiometric anomaly up to ca. 5 ppm equivalent uranium (eU) over an area 6 km wide and 10 km long, and a matching thorium channel anomaly up to ca. 14 ppm equivalent thorium (eTh). As observed around Nifty (above), these anomalies extend well beyond the disturbed ground from mining infrastructure into areas of well developed, undisturbed regolith, and may indicate mobilisation of uranium out of the host rocks or alteration system during weathering.

The GA-LEIs clearly map several folded conductive layers in the subsurface below the Telfer deposit ([Figure 6.20](#)). At several locations these appear to correlate with mapped or projected positions of the Telfer Member, but more generally may be responding to carbonaceous units within the Lamil Group.

6.3.1.2 Magnum

The Magnum prospect, located approximately 150 km to the north of Telfer, was discovered in the mid-1990s under Permian cover. The description below is based upon data obtained in 2005-2008 by collaborative research between Geoscience Australia and NGM Resources Ltd.

² MVR denotes Middle Vale Reef, IP induced polarisation and EM electromagnetics.

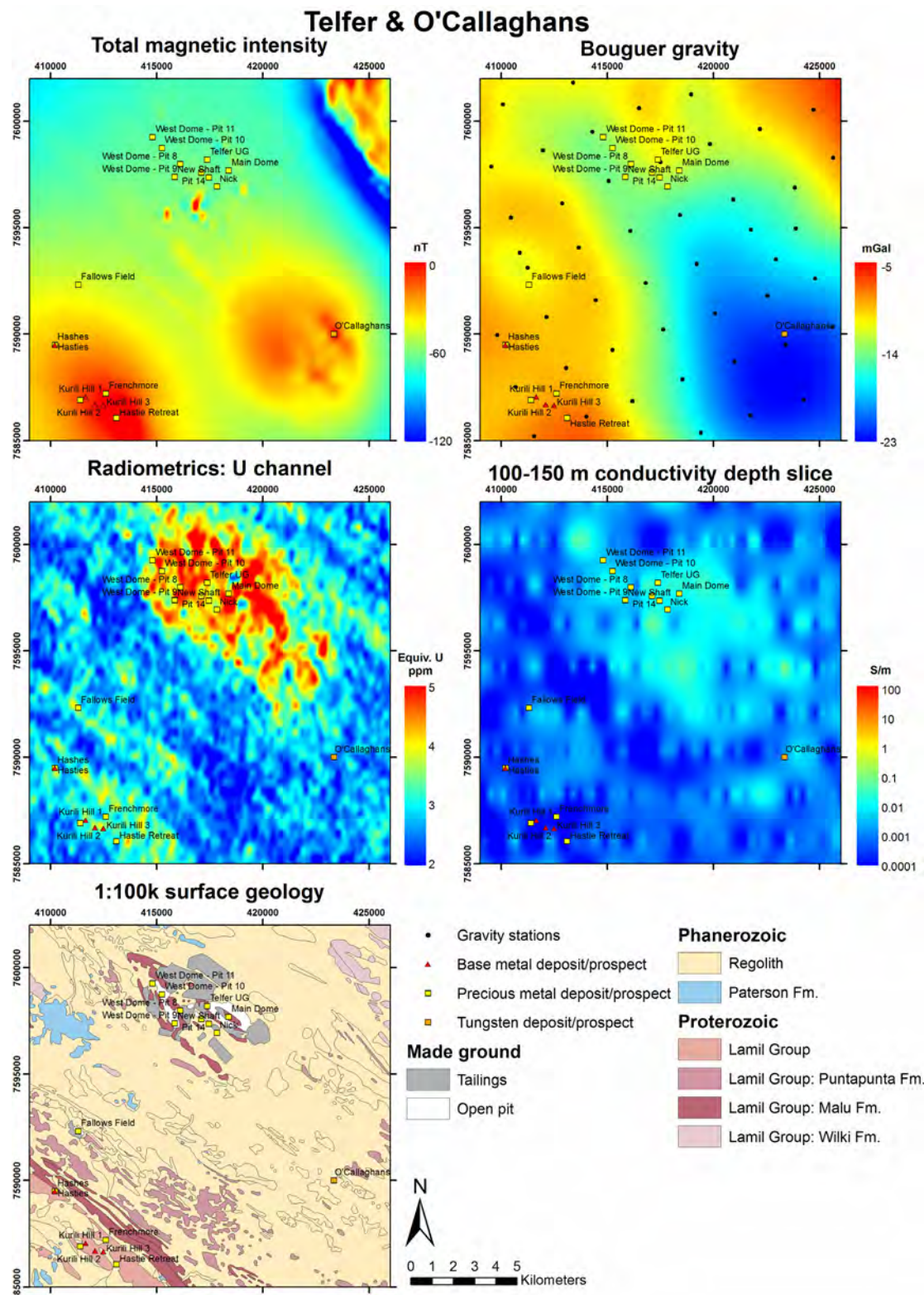


Figure 6.19: Geophysical signature of the Telfer area. Total magnetic intensity, Bouguer gravity, and radiometric data are extracted from the Geophysical Archive Data Delivery System (GADDS: <http://www.ga.gov.au/gadds>). The conductivity depth slice was prepared in this study (Chapter 4); the checkerboard pattern is due to gridding across the 2-km-spaced AEM flight lines in this area. The surface geology is simplified from Bagas (2000).

6.3.1.2.1 Geology, age and origin

The Magnum prospect is hosted by an undifferentiated siliciclastic sedimentary succession of the Yeneena Supergroup. The presence of metamorphic biotite and amphibole suggest these rocks have been metamorphosed to upper greenschist grade. The sedimentary succession comprises interlayered pelitic metasandstone and metasiltstone units with gold mineralisation localised within or near the margins of a 250 m thick gabbro body ([Figure 6.21](#)). The gabbro has chilled margins and shows metasomatism of the host sequence up to 100 m from the contact.

Two structural elements have been recognised in drill core: 1. early tight to isoclinal mesofolds (F_1) associated with the development of an axial-planar fabric (S_1) defined by muscovite and biotite that dips 60° to 045° (D_1); and, 2. a later crenulation cleavage (S_2) developed in finer-grained units that dip 70° to 320° (D_2). Early, folded quartz-carbonate veins (V_1) are interpreted to have formed during D_1 . Detailed logging of drill core suggests two main structural elements within the succession: 1. early tight to isoclinal mesofolds (F_1), often defined by folded narrow quartz-carbonate veins (V_1) and associated with an axial-planar fabric (S_1) defined by muscovite and biotite dipping 60° to 045° (D_1); and, 2. a later crenulation cleavage (S_2), best developed in finer-grained units dipping 70° to 320° (D_2).

In addition to the early quartz-carbonate veins, three later sets of veins are recognised. The first two (V_2 and V_3), which dip 60° to 235° and 85° to 038° respectively, are interpreted to have formed contemporaneously, but are only weakly mineralised. These quartz-dominant veins are characterised by a highly strained, laminar, mylonitic fabric ([Figures 6.22a](#) and [6.22B](#)) with common highly undulose quartz.

The V_2 and V_3 veins are commonly associated with a 10-20 mm thick zone of wall rock bleaching against the vein margin ([Figure 6.22G](#)). Mineralogically, these vein-controlled alteration zones are dominated by quartz, with accessory plagioclase (andesine), sericite and apatite. The alteration appears to overprint the main foliation (S_1) in [Figure 6.22G](#), however, it is not clear which vein set it may be related to.

Sulfide-rich spider veins (V_4 ; [Figure 6.22B](#) to [6.22D](#)) cut and brecciate the earlier vein sets. Sulfide minerals in these veins are dominated by pyrrhotite, with lesser chalcopyrite, minor pyrite with trace amounts of native bismuth, possible bismuth sulfosalts and electrum. Gangue minerals in the spider veins include amphibole, pyroxene, plagioclase, epidote and unstrained quartz. Unlike the earlier vein sets, the spider veins are relatively undeformed, with the preservation of acicular amphibole intergrown with pyrrhotite and chalcopyrite ([Figure 6.22E](#)). Some examples of spider veins contain non-foliated biotite with minor intergrown muscovite and are observed cross cutting V_2 and V_3 veins ([Figure 6.22F](#)).

The sulfide-rich veins within the host gabbro also appear to have alteration halos up to 30 mm from the vein margin. Alteration assemblages associated with the sulfide-rich veins differ from those associated with V_2 - V_3 veins, having variable mineralogy, including pyroxene, amphibole, plagioclase, carbonate, epidote and rutile along with disseminated pyrrhotite, chalcopyrite and minor pyrite. These calc-silicate-dominated assemblages are similar to the gangue present within many of the sulfide spider veins.

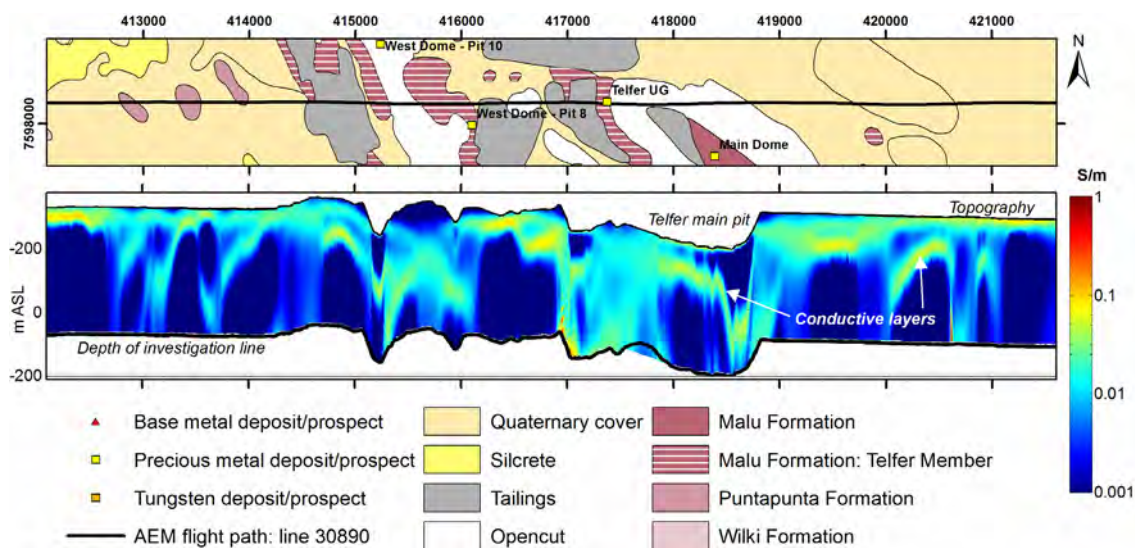


Figure 6.20: A portion of a GA-LEI conductivity section (with 3 times vertical exaggeration) for flight line 30890 across the Telfer deposit compared with surface geology simplified from 1:100 000 scale surface mapping by Bagas (2000). The AEM data are clearly able to map several folded conductive horizons in the subsurface that match the geometries shown in Figures 6.17 and 6.18. Note that the pit outlines have changed slightly between the 2000 mapping and the 2007-2008 AEM survey.

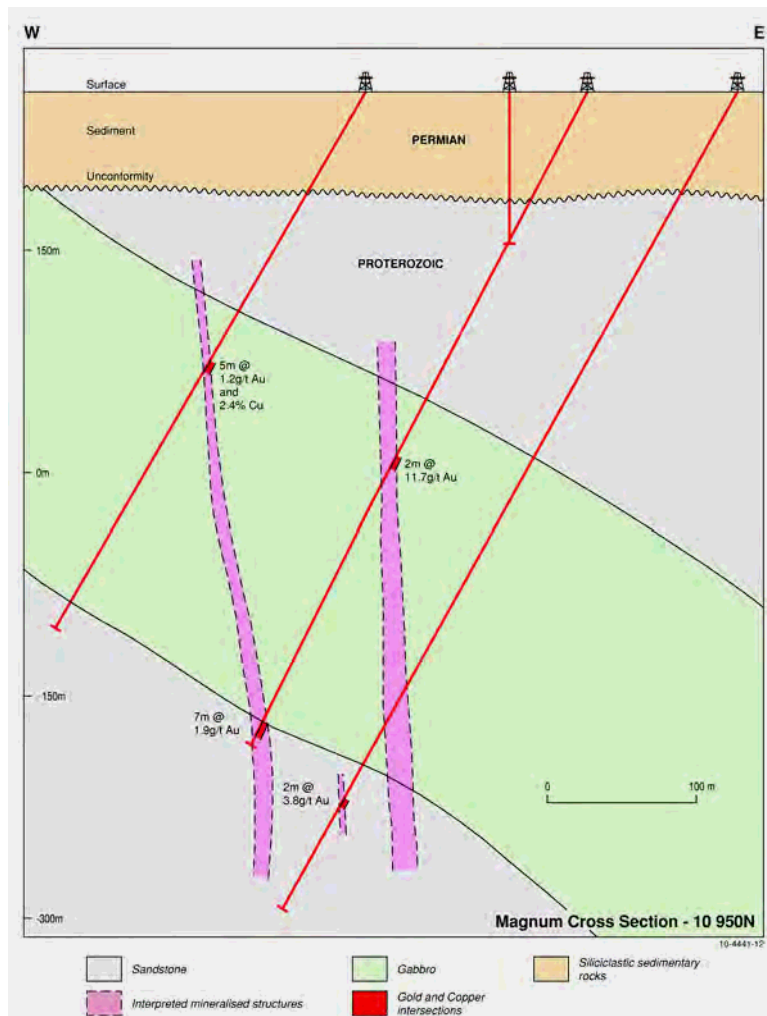


Figure 6.21: Geological section through the Magnum prospect, after Glengarry Resources Limited (2010).

Very minor carbonate veinlets with accessory pyrite and chlorite and minor to trace chalcopyrite, sphalerite and galena also crosscut the V₂-V₃ veins, but have an unknown relationship to the spider veins.

To constrain the age of quartz veining, biotite and muscovite were separated from two samples of mica-rich veins or domains that cut the earlier V₂-V₃ veins (e.g., [Figure 6.22F](#)). [Figure 6.23](#) shows the results of ⁴⁰Ar/³⁹Ar analysis of these separates. All four separates yielded plateau ages within error of each other, with an average age of ca. 628 Ma, which is the likely crystallisation age of the micas. Although a direct link to sulfide spider veins was not established, the paragenetic similarity relative to V₂-V₃ veins between the mica and sulfides suggests that this age is the most likely age of mineralisation.

Textural observations, both in drill core and in thin-section, indicate that the early (V₂-V₃) quartz veins have had a significantly different tectonic history to the sulfide-rich spider veins. The V₂-V₃ veins are highly deformed and are mylonitic in places, whereas the sulfide veins are virtually undeformed, suggesting that they formed after the last major deformation event. In addition, calc-silicate minerals that characterise both the spider vein assemblage and the associated alteration assemblage are typical of metasomatic skarn assemblages.

6.3.1.3 O'Callaghans

As the O'Callaghans deposit was only recently recognised (initial mineral resource announced June 2009), very limited public-domain data are available. This description is based on data available (mostly from presentations to conferences and workshops) on the Newcrest Ltd. website (www.newcrest.com.au: accessed March 2010).

6.3.1.3.1 Geology, age and origin

The O'Callaghans deposit, located ca. 10 km south-southeast of the Telfer deposit ([Figure 6.16](#)), consists of a blanket-like, magnetite-bearing (Sexton, 1994) skarn deposit localised along the contact between the O'Callaghans Granite and carbonate rocks of the Puntapunta Formation. The deposit is sub-horizontal, located ca. 350 m below surface, with thicknesses of up to 70 m ([Figure 6.24](#)). In plan, the deposit is elongate, approximately 1300 m × 900 m in maximum dimension and the long axis oriented to the northwest. An updated JORC-compliant mineral inventory totalling 78 Mt grading 0.33 wt. % tungsten trioxide (WO₃), 0.50 wt. % zinc, 0.25 wt. % lead and 0.29 wt. % copper was announced in February 2010, making O'Callaghans one of the largest tungsten deposits in Australia.

6.3.1.3.2 Geophysical characteristics

Although no data specifically regarding the geophysical response of the O'Callaghans skarn have been previously reported publicly, Sexton (1994) indicated that this skarn was associated with a magnetic high along the eastern margin of the associated granite, and this is observed in the regional magnetic data ([Figure 6.19](#)). The granite is also associated with a strong gravity low, but lacks a distinctive conductivity response; it is as resistive as surrounding rocks.

6.3.1.4 Other deposits, occurrences and prospects

In addition to the Telfer, O'Callaghans and Magnum deposits, the northern Paterson region is characterised by a large number of prospects and mineral occurrences at various stages of exploration ([Figure 6.16](#); Ferguson *et al.*, 2005). Although dominantly gold prospects, these also include prospects in which copper is the commodity of most interest. Most of these deposits are associated with structural domes or anticlines and they are hosted by both the Malu and Puntapunta Formations. Typically the gold and copper are hosted by veins, stringers and breccias. Ferguson *et al.* (2005) provide a more comprehensive description of these deposits. Of particular note is that the Haveiron prospect was discovered through over 400 m of Permian cover by drilling coincident magnetic and gravity anomalies (Henderson, 1993).

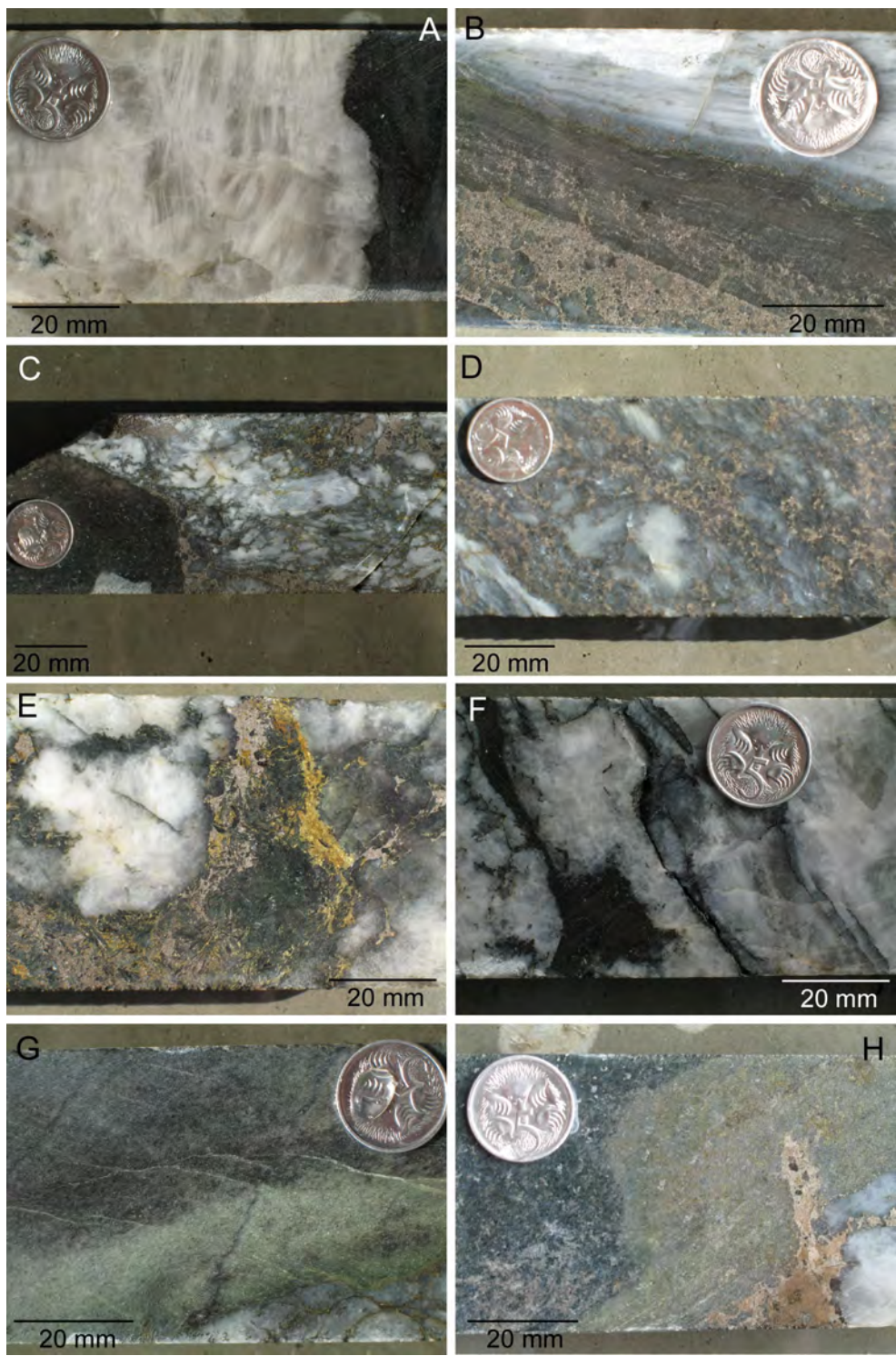


Figure 6.22: Photographs of core from the Magnum prospect: A. early V_2 - V_3 quartz vein; B. early V_2 - V_3 quartz vein adjacent to V_4 spider sulfide-quartz vein; C. vein breccia, with V_4 sulfides infilling brecciated V_2 - V_3 quartz; D. vein breccia, with V_4 sulfides infilling brecciated V_2 - V_3 quartz; E. pyrrhotite-chalcopyrite-amphibole intergrowth in V_4 spider vein infilling V_2 - V_3 quartz; F. non-foliated biotite-muscovite domain within V_2 - V_3 vein; G. bleached selvage associated with V_2 - V_3 vein; and H. calc-silicate alteration assemblage as selvage associated with V_4 pyrrhotite vein.

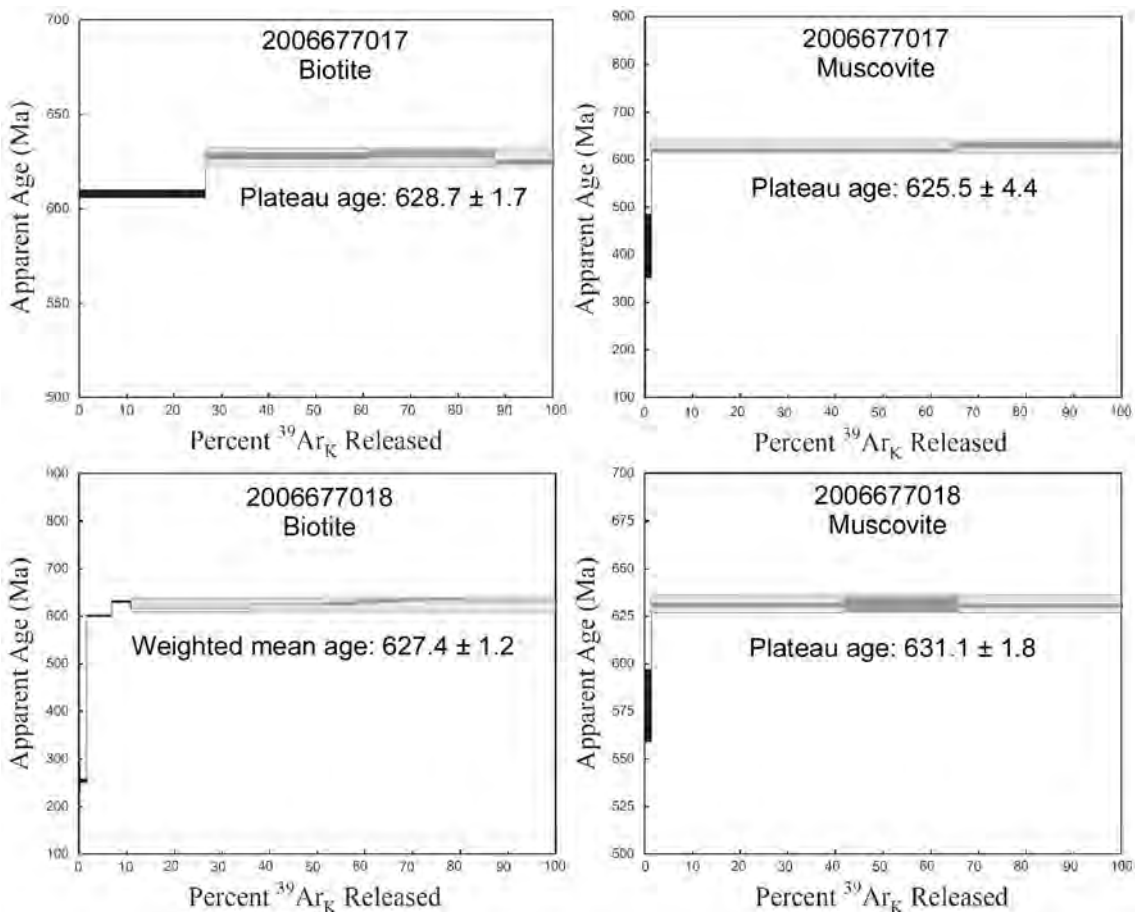


Figure 6.23: ^{40}Ar - ^{39}Ar age spectra of biotite and muscovite from the Magnum deposit. Prior to analysis, samples were irradiated for 50 megawatt hours in the central thimble of the U.S Geological Survey TRIGA reactor in Denver, Colorado (Dalrymple et al., 1981). Neutron fluence was monitored using sanidine standard FCT-3 (Fish Canyon Tuff) with an internally calibrated age of 28.03 Ma. Argon isotopic compositions were measured at the U.S. Geological Survey Argon Geochronology Laboratory in Denver, Colorado using analytical techniques, which, in general, followed procedures given in Miggins et al. (2002; 2004).

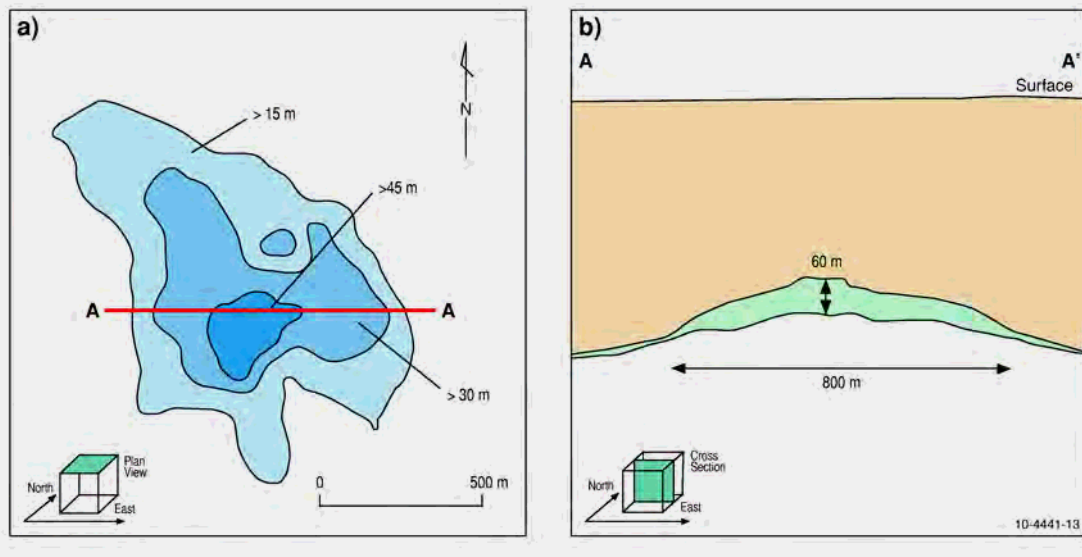
6.3.2 Model for mineral systems associated with the O'Callaghans tectonothermal event

Geological observations and limited geochronological data suggest that gold-copper and tungsten-copper-zinc-lead deposits in the upper part of the Yeneena Basin, collectively termed the O'Callaghans mineral system, overlap temporally and spatial with granites of the 655-630 Ma O'Callaghans Supersuite. Figure 6.25 presents a model for this mineral system. In it we consider tungsten-dominated systems separately from gold-copper-dominated systems as these have different metallogenetic characteristics and the granite associated with the O'Callaghans deposit differs geochemically from the other granites of the O'Callaghans Supersuite.

Available geochronological data for granites of the O'Callaghans Supersuite, combined with the demonstrated (in the case of the O'Callaghans skarn deposit) and inferred (in the case of Telfer) linkage with granite emplacement, and with ^{40}Ar - ^{39}Ar data from the Magnum deposit, suggest an age for the O'Callaghans mineral system of between 655 and 630 Ma. The O'Callaghans tungsten-copper-zinc-lead deposit is hosted within skarn along the contact with the O'Callaghans Granite.

Hence, we infer a genetic and temporal link between the tungsten-bearing skarns and granite emplacement, with a direct magmatic-hydrothermal source for the metals in these deposits.

Figure 6.24: Plan and schematic cross section of the O'Callaghans tungsten-zinc-lead-copper skarn,



after Newcrest Mining Limited (2010).

The link between gold-copper deposits, such as Telfer, and granite emplacement, however, is not as well established. Although most workers (Goellnicht *et al.*, 1989; Goellnicht, 1992; Rowins *et al.*, 1997; Howard *et al.*, 2000; Howard *et al.*, 2005) accept that granite emplacement and mineralisation were coeval, the linkages between mineralisation and magmatism are not as robust. In fact, Rowins *et al.* (1997) advocated a non-magmatic origin. Hence, in [Figure 6.25](#) we present, in effect, two models for the formation of these deposits, a magmatic-hydrothermal model with some modification of the fluids by interaction with wall rocks (e.g., Howard *et al.*, 2005), and a model in which the fluids were derived from the Yeneena Basin (e.g., Rowins *et al.*, 1997) and/or the basement and driven by emplacement of granites.

As with the Miles mineral system, we consider the O'Callaghans mineral system in terms of the six features that characterise the system: 1. geodynamic setting; 2. architecture, including basin, structure and igneous architecture; 3. the origin of the ore fluids and metals; 4. fluid pathways and drivers; 5. depositional mechanisms; and, 6. post-depositional modifications. In describing these features, which are summarised in [Table 6.2](#), attention is paid to characteristics whereby these features can be mapped using regional to semi-regional geological and geophysical data.

6.3.2.1 Geodynamic setting

Based largely on structural studies at the Telfer mine, Howard *et al.* (2005) interpreted that the Paterson Orogeny involved a progressive rotation of contraction from northeast-southwest through to near east-west, resulting in sinistral transpression of previously developed structures and the development of a steeply dipping, northwest-striking foliation that accompanied upright folds (Hewson, 1996; Rowins *et al.*, 1997). Without further structural analysis utilizing exposures at Telfer and linking these to large architectural considerations, it is not possible to determine whether this described change in paleo-stress field is related to a progressive regional change in the paleo-stress direction or local perturbations around faults during the Paterson Orogeny. The most reliable feature indicative of the paleo-stress field is the regional orientation of the folds and the trend of the Crofton Granites which indicates a NE-SW compression vector. Howard *et al.* (2005) interpreted that this deformational event overlapped granite emplacement and gold-copper mineralisation, although L. Bagas (pers. comm., 2010) suggested it post-dated granite emplacement. The

geodynamic setting of this event is unclear but most likely represents the initiation of Gondwana Supercontinent amalgamation. Consequently the entire Neoproterozoic history of the Paterson province can be viewed in terms of one Wilson-type Super Continent cycle (Wilson, 1968).

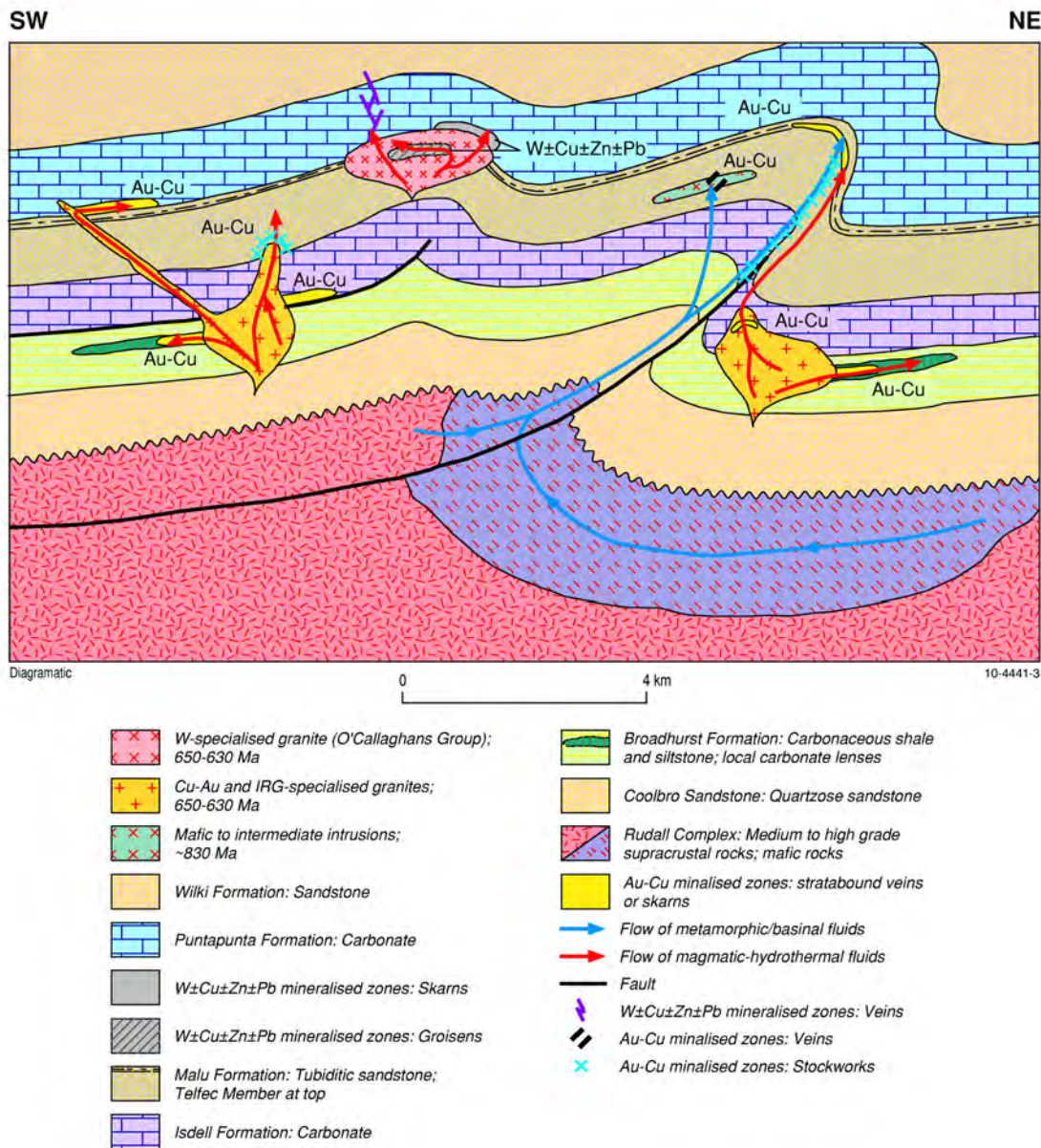


Figure 6.25: Mineral system model for the O'Callaghans mineral system.

Table 6.2: Features and mappable characteristics of the O'Callaghans mineral system.

MINERAL SYSTEM FEATURE	MAPPABLE CHARACTERISTICS
Geodynamic setting	Post-tectonic thermal relaxation after Paterson Orogeny
Architecture	
• Basin	Thick basin-fill deposited in environments ranging from deep to shallow water.
• Structure	Development of strong chemical (redox and pH) gradients, particularly between units.
• Igneous	Distribution of domal structures and anticlines, particularly the cores and northeast limbs. Evidence for late- to post-kinematic hydrothermal activity. Underlying basement control on the distribution of granites, as indicated by spatial trends.
Origin of ore fluids and metals	Distribution of W-specialised and Au-Cu specialised granites in space and time. Alternative 1. Direct sourcing of fluids and metals from magma: <ul style="list-style-type: none">• Geochemical trends indicating W-specialised or Au-Cu-specialised granites;• Evidence for volatile-rich granites (geochemical fractionation and/or textural evidence; and,• Proximity (<10 km) to granite at district-deposit scale. Alternative 2. Granites act as heat sources driving basinal-metamorphic fluids: <ul style="list-style-type: none">• Distribution of evaporites within basin;• Distribution of potential source rocks for gold and copper (e.g., mafic igneous rocks as mapped using regional and, possibly, magnetic data; and,• Proximity (<10 km) to granite at regional-district scale.
Fluid pathways and drivers	Domal-anticlinal structures, possibly related to blind thrusts. Distribution of regional silicification and albite alteration. Skarn assemblages, as mapped using gravity and/or magnetic data.
Metal trap sites and depositional mechanisms	Chemically receptive rocks, including: <ul style="list-style-type: none">• Carbonaceous and pyritic (black) shale and siltstone;• Dolomitic or calcareous sandstone;• Carbonate; and,• Mafic magmatic rocks. Strong gradients in rock competency, including: <ul style="list-style-type: none">• Interbedded competent in incompetent rocks including interbedded psammite-pelite; and,• Massive igneous rocks intruding sedimentary successions. Brittle rock units, including: <ul style="list-style-type: none">• Massive silicified sandstone.
Post-depositional modifications	Weathering leading to grade upgrading within oxidised and supergene zones.

6.3.2.2 Architecture

As the O'Callaghans and Miles mineral systems share many architectural features, such as basin architecture and, to a lesser extent structural architecture, differences in the architecture, and, in particular igneous architecture, will be emphasised.

6.3.2.2.1 Basin architecture

As the basin architecture was described in [Section 6.2.4.2.1](#), it is not discussed further here. As discussed below, chemically-reactive rocks, including carbonaceous rocks and carbonate-bearing rocks, appear to be important as trap rocks.

6.3.2.2.2 Structural architecture

Rocks hosting deposits of the O'Callaghans mineral system have been affected by five recognised deformational events, the first two of which correspond to the Miles Orogeny, which pre-dated mineralisation. The third and fourth events, although relatively minor, overlapped with mineralisation at the Telfer deposit. The last event is also minor and post-dated mineralisation and is not considered further.

The consensus interpretation (Goellnicht *et al.*, 1989; Hewson, 1996; Rowins *et al.*, 1997) is that the *en echelon* anticlines that form the Telfer Dome formed during D₂, that is, during the Miles Orogeny. As these anticlines have steeply dipping (even overturned; Howard *et al.*, 2005) northeast limbs and shallow dipping southwest limbs, tectonic transport appears to have been northeast over southwest. Outcrop patterns suggest that this vergence applies over much of the area to the northeast of the Warrabarty-Coolbro fault system. This contrasts with the southwest over northeast vergence to the southwest of this fault system, based on fold asymmetry and fault geometries.

The geometry of the folds in the Telfer Dome and other domes in the north central Paterson region are compatible with the presence of blind, southwest-dipping thrusts ([Figure 6.25](#)). The *en echelon* nature of the anticlines and their extent over typically 10s rather than 100s of kilometres indicate they most likely represent inversion anticlines above inverted extensional faults rather than thin-skinned thrust sheets. Consequently, the vergence direction as deduced from the fold asymmetry is unrelated to the regional tectonic transport direction but rather is controlled by the extensional architecture. Structures such as the Warrabarty, Coolbro and Trotman Hill faults ([Figure 6.2](#)) may be surface expressions of these inferred blind thrusts. However, the lack of clear fault outcrop traces indicates the Lamil Group was likely mostly deposited during the post-rift thermal subsidence of the Yeneena Basin's history.

Although the Miles Orogeny appears to have set up the structural architecture used by the mineralising fluids, fluid flow post-dated this orogeny. As shown in [Figure 6.2](#), granites of the O'Callaghans Supersuite cut the folds developed during the Miles Orogeny. This observation, combined with timing relationships at the Telfer deposit, implies that granite emplacement and mineralisation accompanied a later deformational event.

Mineralisation accompanied the local D₃ or D₄ events (Hewson, 1996), which are interpreted to have formed during the Paterson Orogeny (Howard *et al.*, 2005). The D₄ event produced a subvertical fabric oblique to the main S₂ fabric and open upright folds, suggesting that contraction associated with the Miles and Paterson Orogenies was broadly similar, with a northeast-southwest shortening direction. Given the similarities in stress orientations, it is likely that the D₄ event also reactivated structures formed during the Miles Orogeny, creating permeable zones in fault zones, which allowed fluid flow, and tightening of the D₂ existing folds. These structures are most likely inverted extensional faults rather than thin-skinned thrust and newly developed reverse faults.

6.3.2.2.2 Igneous architecture

[Figure 6.2](#) illustrates that the northeastern part of the Paterson region, which contains known deposits formed by the O'Callaghans mineral system, also contains abundant granite bodies. The

distribution of these bodies defines several apparent trends: a well-defined northeast trend; a less well-defined north trend; and, a poorly-defined northwest trend. The origin of these trends is unclear; they could be controlled by basement features, related to changes in the direction of transpression during magmatism, or indicate migration of magmatism with time. Granitic bodies are not known to be abundant to the south and east of the Warrabarty-Coolbro fault system, that is, areas that lack gold-copper and tungsten-copper-zinc-lead deposits.

Figure 6.26 illustrates the composition of granites of the O'Callaghans Supersuite on a rubidium/strontium ratio (Rb/Sr) versus $\text{Fe}_2\text{O}_3/\text{FeO}$ diagram, which reflects the redox state and fractionation of granites, respectively. These compositions are overlain on the fields of magmatic-hydrothermal mineral systems from Blevin *et al.* (1996) and Blevin (2008). Based on this discrimination diagram, the O'Callaghans and Minyari granite groups, and the Deserts Revenge Granite, are within the intrusion-related gold field, and the O'Callaghans group overlays the tungsten field. The oxidation state of the Crofton granite group, however, is too oxidised for the intrusion-related gold field, although it is compatible with copper-molybdenum systems. If less fractionated granites of the Crofton group are present in the Paterson region, although they are not evident in the data, these granites may have potential for copper-gold systems.

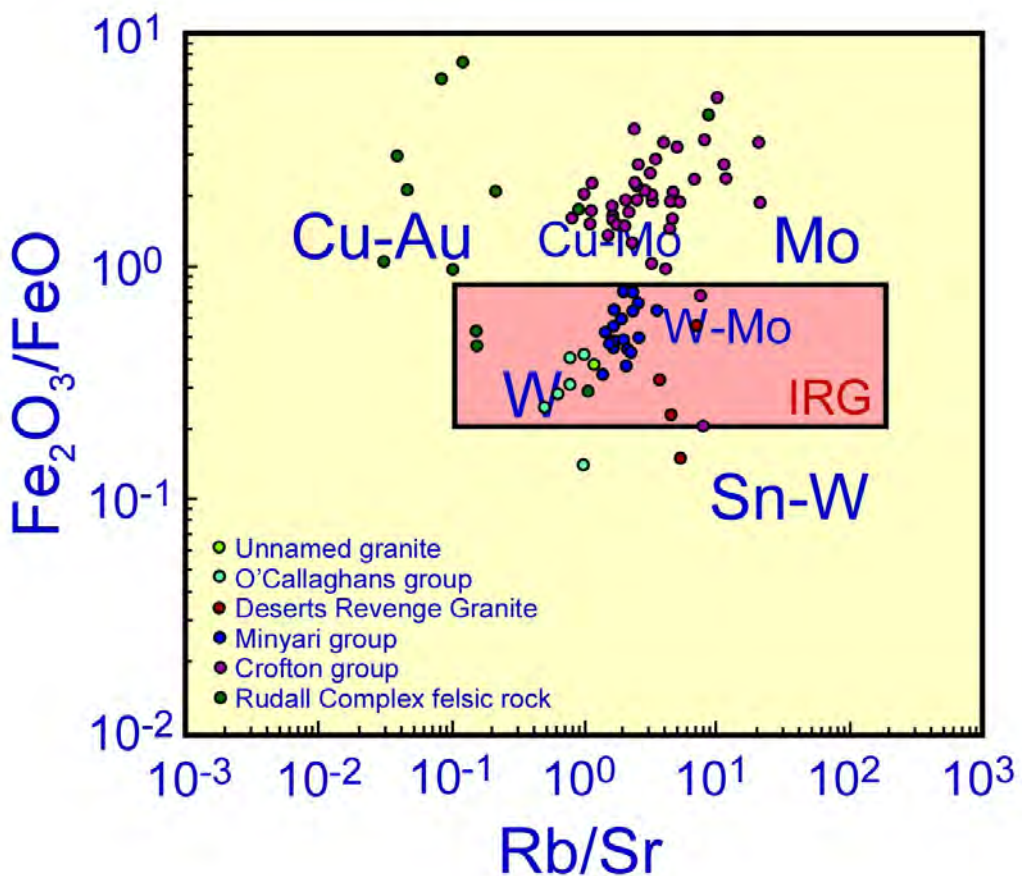


Figure 6.26: Rb/Sr versus $\text{Fe}_2\text{O}_3/\text{FeO}$ diagram (both ratios by mass) showing the composition of granites from the Paterson region overlain on the fields of granites associated with various types of magmatic-hydrothermal deposits. IRG is intrusion-related gold. Fields from Blevin *et al.* (1996) and Blevin (2008).

Granites with greatest affinity for copper-gold systems (**Figure 6.26**) are located within the Rudall Complex, to the south and west of the Warrabarty-Coolbro fault system (**Figure 6.2**). As these granites appear to be Paleo- to Mesoproterozoic in age, some potential for similarly-aged copper-

gold systems is present in the Rudall Complex; this analysis is beyond the scope of this report.

The other group of magmatic rocks that may bear significance on the O'Callaghans mineral system are mafic bodies, both within the Yeneena Basin and in the basement. As discussed in [Section 6.2.4.2.2](#), 835-815 Ma mafic to intermediate intrusive bodies are present within the many units which make up the Yeneena Basin. These bodies are known to host ca. 630 Ma gold-copper-bearing veins at Magnum ([section 6.2.2.1.2](#)). Ultramafic and mafic bodies are also extensively developed in parts of the Rudall Complex. Where interpreted on the solid geology ([Figure 6.2](#)), these bodies are associated with gravity highs, suggesting that gravity highs in the central north and east-central parts of the Paterson region may indicate mafic rocks in the basement (see also section [Chapter 3](#)).

6.3.2.3 Origins of fluids and metals

Since the earlier results of Goellnicht *et al.* (1989) a consensus has developed that formation of the Telfer deposit and other gold-copper deposits has involved magmatic processes, although the exact involvement has been debated (Rowins *et al.*, 1997). Concepts on the involvement of magmatic processes range from a direct magmatic-hydrothermal contribution of fluids and metals (Goellnicht *et al.*, 1991) through to the granites only providing heat with the fluids and metals derived from the Yeneena Basin (Rowins *et al.*, 1997). Howard *et al.* (2005) inferred that the fluids were originally derived from granites but interacted with basinal rocks. Although the data provided by Rowins *et al.* (1997) are strong indications that the ore fluids did interact with basinal rocks, the data cannot exclude an original magmatic-hydrothermal origin. Hence we consider two possible sources of fluid and metal in our mineral system model for gold-copper deposits. In the first scenario, fluids are interpreted to evolve off granitic bodies and then migrate through the Yeneena Basin along structures. In this scenario, the mineralisation would only be linked to granites in a broad way, and a direct spatial link is not implied.

In the second scenario, granites either directly provide heat or are evidence for a high geothermal gradient, both of which drive fluid flow. In this case the fluid is derived either from basinal brines or metamorphic dewatering as per the lode orogenic gold system model. Metals and sulfur are derived from the Yeneena basin or from the basement Rudall Complex. A possible source of gold and copper are mafic rocks in the basement ([Figure 6.25](#)), which may be indicated by major gravity highs (c.f., [Chapter 3](#)).

The granitophile metal assemblage and a close spatial association with granites of the tungsten-copper-zinc-lead deposits suggest that the ore fluids and metals were derived directly from the associated granite.

6.3.2.4 Fluid drivers and pathways

Unlike the Miles mineral system, in which permeable stratigraphic units appear to have been important fluid conduits, structures are the most likely fluid conduits in the O'Callaghans mineral system when fluids evolve from magmas. As discussed above, it is likely that the major structures, both faults and folds, initiated during the Miles Orogeny or earlier during basin formation. These structures include domes and thrust faults ([Figure 6.25](#)), both of which focus fluid flow. It is probable that reactivation of these early-formed structures during the Paterson Orogeny produced permeable zones through which fluids flowed.

The spatial and apparent temporal association of granites with gold-copper and tungsten-copper-zinc-lead deposits in the northeastern Paterson region indicates a link between magmatism and mineralisation. This suggests that if granite emplacement did not directly drive fluid flow, a regional thermal anomaly associated with magmatism likely drove fluid flow.

Unlike fluid flow paths in the Miles mineral system, which can be mapped at a semi-regional scale using ASTER and other data sets, fluid flow paths in the O'Callaghans mineral system are difficult to map. Goellnicht *et al.* (1989) described sericite-carbonate alteration zones and silicified zones in the

Telfer Dome. Such assemblages, however, are difficult to recognise at a regional scale and are not necessarily related to gold-copper mineralising processes. Part of the fluid flow path for tungsten-bearing fluids may be mapped by skarns. These metasomatic rocks, which form along flow paths, are denser than the surrounding rocks and may be magnetite-bearing. However, in most cases, the skarn zone will approximate the depositional site, so more regional fluid flow cannot be mapped.

6.3.2.5 Depositional mechanisms

At the Telfer deposit, gold-copper ores appear to have been deposited both along chemical gradients, such as increases in the abundance of carbonaceous matter or carbonate, and in rheological traps, such as major contrasts in rock rheology, or highly brittle units, such as silicified sandstone (Howard *et al.*, 2005). The chemical traps are best developed in the Telfer Member (Bagas, 2000), which forms the uppermost unit of the Malu Formation and consists of a large range of rock types, including carbonate-rich rocks. In contrast, rheological traps are best developed in the underlying, silicified and massive sandstones of the Malu Formation.

Contrasts in lithology, including changes in organic carbon and carbonate content, are present through many units of the Yeneena Basin, including, most importantly, the Broadhurst and Malu formations. In addition, both the Isdell and Puntapunta formations would be highly reactive with gold-copper-bearing fluids. This suggests that, in addition to the known deposits in the Telfer Member, carbonate lenses within the Broadhurst Formation or the lower parts of the Isdell and Puntapunta formations are potential hosts for gold-copper deposits ([Figure 6.25](#)).

Rheological traps include both units with large lithological variations, such as the Telfer Member, and homogeneous rock types that can easily be fractured, such as silicified sandstone and dolerite. In the latter case, dolerite hosts the Magnum deposit. Hence, ca. 830 Ma mafic rocks in the Yeneena Basin, which could be mapped using a combination of gravity and magnetic data, should be considered potential trap rocks for gold and copper.

The traps discussed above apply for deposition in both granite-derived and basinal-metamorphic fluids. The possibility of granite-derived fluids, however, raises potential for other trap sites, specifically as stockworks or greisens within the granite ([Figure 6.25](#)) by analogy with the Timbarra deposit in New South Wales (Mustard, 2001), or in skarns, stockworks or breccia pipes along the margins or above apophyses or cupolas of the granites (Thompson and Newberry, 2000; Blevin, 2008).

Depositional sites for granitophile tungsten-copper-zinc-lead deposits are more restrictive and more closely related to granite bodies. The O'Callaghan deposit is developed in a skarn along the upper contact of the tungsten-specialised O'Callaghans Granite, where it intrudes the Puntapunta Formation. In addition to the known proximal skarns, depositional sites for tungsten-rich deposits include griesens within tungsten-specialised granites and veins proximal to the granites.

6.3.2.6 Post-depositional modifications

As gold-copper and tungsten-bearing mineral assemblages are less susceptible to remobilisation than uranium-bearing mineral assemblages, and as the Paterson region was relatively tectonically inactive following the Paterson Orogeny, post-depositional modifications, other than weathering, of deposits formed in the O'Callaghans mineral system are not likely to be significant. However, at Telfer, weathering and supergene enrichment have enriched supergene and mixed supergene-oxide zones by factors of ten or greater in both gold and copper relative to primary ores (Goellnicht *et al.*, 1989).

6.4 CALCRETE-HOSTED URANIUM SYSTEMS

Geologically significant uranium is associated with non-pedogenic calcrete or dolocrete formed within Cenozoic drainage systems incised into rocks containing leachable uranium and vanadium. Non-pedogenic calcrete (also known as groundwater or valley calcrete) forms predominantly near the water table from groundwater moving along extremely low gradients (Carlisle, 1984). The formation of non-pedogenic calcrete is generally controlled by climate and the type of soil. In the Yilgarn Craton, the distribution of non-pedogenic and pedogenic calcrites is defined by the Menzies Line (Butt *et al.*, 1984). North of the Menzies Line, the zone dominated by non-pedogenic calcrites, the soils are generally neutral to acid and the groundwaters are less saline and neutral to alkaline. South of the Menzies Line, dominated by pedogenic calcrites, the soils are neutral to alkaline and the groundwaters are saline and neutral to acidic. The southern zone is characterised by relatively higher annual rainfall (> 225 mm), which is winter-dominated, and lower annual evaporation (< 2500 mm) with average temperatures below 19°C . The northern zone is characterised by summer-dominated rainfall.

6.4.1 Types of calcrete-hosted uranium deposits

Butt *et al.* (1984) classify calcrete-hosted uranium deposits by their geomorphological setting into three main types:

1. The valley deposits, such as Yeelirrie, Hinkler-Centipede, Lake Way and Lake Raeside in the Yilgarn Craton, occur in calcrites and associated sediments in the central channels of major (palaeo)drainages, and in the platforms and chemical deltas where the drainage enter playas. The calcrites generally change downwards into an alluvial clay-quartz unit. Uranium mineralisation is not limited to the calcrites but transgresses into underlying units, with the greatest concentration located in the vicinity of the groundwater table. Mineralisation occurs almost entirely as carnotite, generally as a late-stage precipitate in cavities lined by thin coatings of minerals such as calcite, dolomite, silica and/or sepiolite. Carnotite may also form fine disseminations in the clay-quartz units.
2. The playa deposits, such as the Lake Maitland and Lake Austin deposits in the Yilgarn Craton, occur in near-surface evaporitic and alluvial sediments. The calcrites near playas act as principle aquifers to the playas. In the Yilgarn, mineralised playas are usually closely associated with calcrites in the channels, often enriched in uranium. Mineralisation is generally concentrated near the groundwater table in sediments consisting of gypsumiferous clays and muds. The sandy and silty clays locally contain calcareous nodules. In some deposits, such as Lake Maitland, the mineralisation is in thin calcrites in the playa itself.
3. The terrace deposits are less common and occur in calcrete terraces in dissected valleys mainly in the Gascoyne Province.

6.4.2 Source of uranium, vanadium and potassium

All known calcrete-hosted uranium deposits are located in palaeochannels incised into potential source rocks of potassium, uranium and vanadium. Felsic rocks in the Yilgarn Craton contain up to 20 ppm uranium (Schofield, 2009) and a granite in the upstream area of Lake Way deposit contains up to 25 ppm uranium (Mann and Deutscher, 1978). Intensive weathering and erosion of such felsic rocks can provide uranium as well as potassium to the calcrete system. High uranium concentrations (up to 400 ppb) in groundwaters in the Lake Way area supports leaching of uranium from the felsic rocks (Mann and Deutscher, 1978).

Mafic igneous rocks, sediments with vanadium-rich clays, ironstone such as banded iron formation and ferricrete are often enriched in vanadium (Bastrakov *et al.*, 2009). Such rocks are generally present in the vicinity of calcrete-hosted uranium deposits (Mann and Deutscher, 1978; Karner and Becker, 2009) and can provide vanadium.

6.4.3 Drainage system

The calcrete-hosted uranium system is driven by shallow groundwater drainage in extremely low gradients, ca. 10 m/km (Karner and Becker, 2009), established in permeable sediments infilling palaeochannels. Groundwaters in mineralised areas are generally neutral to alkaline with maximum median salinity of ca. 10 wt. % (Mann and Deutscher, 1978; Gray, 2001). The high salinities are more common along palaeovalley axes (Gray, 2001). The drainage in the region is controlled by a recharge area upstream and a system of playa lakes in the discharge area. In addition of the infill sediments, calcretes formed near the water table also function as aquifers which allow groundwaters to actively interact with the calcretes. The presence of playa lakes creates conditions where groundwaters in the palaeovalleys can mix with relatively more saline waters in the playas.

6.4.4 Geochemical factors controlling precipitation of carnotite in calcrete-hosted uranium deposits

Carnotite is a uranium bearing potassium vanadate with the formula $K(U^{+6}O_2)(V^{+5}O_4).xH_2O$.

Its solubility and precipitation depend on:

- The concentration/activity of potassium, uranium and vanadium in the fluid;
- The oxidation state of the fluid, because in oxygen-saturated, low-temperature surficial fluids, uranium and vanadium form aqueous complexes of uranyl ($U^{+6}O_2$) and V^{+4} and V^{+5} respectively; and,
- The type of oxidation-reduction reaction. As the valence state of uranium and vanadium in carnotite is U^{+6} and V^{+5} respectively, oxidation-reduction reactions are important with respect to vanadium only in conditions where vanadium forms complexes containing V^{+3} and V^{+4} . In such cases precipitation of carnotite will require oxidation and not reduction of the fluid (see discussion below).

Calculations on speciation of uranium and vanadium and on the stability of carnotite in shallow-level groundwaters show that geologically realistic concentrations of uranium and vanadium (> 0.01 ppm each of uranium and vanadium) can be transported in oxidised fluids (Bastrakov *et al.*, 2009). In such conditions uranium forms aqueous complexes of uranyl and vanadium forms complexes containing either V^{+4} or V^{+5} . The calculations also show that precipitation of carnotite can occur due to changes in any of the following:

1. pH; decrease in pH if the groundwater is alkaline (pH >8) or increase in pH if the groundwater is acidic;
2. Oxidation state. At oxidation states where vanadium is transported as complexes of V^{+3} and/or V^{+4} , an increase in the oxidation state is essential to form carnotite;
3. Concentration of dissolved potassium. An increase in the concentration of potassium will cause precipitation of carnotite;
4. Partial pressure of carbon dioxide (CO_2), which controls the concentration of carbonate complexes in the groundwater. As uranium in these conditions is transported as a uranyl-carbonate complex, any decrease in the concentration of carbonate ions in groundwater will favour precipitation of carnotite;
5. Concentration of dissolved calcium in the groundwater. As addition of calcium to the groundwater can cause precipitation of carbonate, the associated decrease in the concentration of dissolved carbonate ions in the groundwater can cause precipitation of carnotite; or,
6. Concentration of dissolved sulfur in the groundwater. In oxidised groundwater, sulfur is dissolved to form sulfate ions which control the solubility of uranium as uranium forms uranyl-sulfate complexes. A decrease in the concentrations of sulfate ions, caused often by the deposition of gypsum and barite, can thus favour precipitation of carnotite.

The formation of carnotite in valley calcretes is closely related to the seasonal fluctuation of the groundwater table. The fluctuation is associated with evaporation of groundwaters which can lead to

an increase in the concentration of dissolved potassium, vanadium and uranium (Butt *et al.*, 1984). It can also change the concentration of carbonate ions in the water, affecting the solubility of uranium.

Evaporation is also important in the playa deposits, where it can control the salinity of lake waters and the precipitation of gypsum-bearing sediments. However, mixing of more saline lake waters, relatively enriched in potassium and calcium, and the incoming groundwaters from the drainage channel can be equally important in the formation of carnotite. Such mixing can cause an increase in the concentration of potassium and calcium in groundwater which may lead to the precipitation of carnotite. In a similar way, an increase in the concentration of calcium can destabilise uranyl-carbonate or uranyl sulphate complexes by precipitating calcite and gypsum, respectively, and thereby facilitate the formation of carnotite (Mann and Deutscher, 1978).

According to Mann and Deutscher (1978), redox process can also contribute to the formation of carnotite in some calcrete-hosted uranium deposits. In this model the interaction of mildly reduced groundwaters with mafic rocks in the greenstones can cause dissolution of vanadium to form V^{+4} -bearing complexes. Vanadium from these groundwaters mixes with overlying uranium-bearing fluids either through diffusion and/or by upwelling of the waters caused by a subsurface hydromorphic barrier. Mixing causes oxidation of vanadium from V^{+4} to V^{+5} to form carnotite. The presence of dark-green coloured (relatively reduced with V^{+4}) carnotite deep in the calcrete profile, and of more yellow coloured (relatively oxidised, with V^{+5}) carnotite towards the surface in some deposits is cited in support of this model.

The formation of calcrete-hosted uranium deposits is illustrated in a three stage model (Figure 6.27) and is also described in a minerals systems approach (Table 6.3). The first stage represents the filling of palaeovalleys with coarse-grained sediments of high permeability (Figure 6.27a). This is followed by the initiation of an active groundwater drainage system. In arid zones dominated by intensive evaporation the drainage system generates calcrete zones near the water table (generally in the vadose zone, Figure 6.27b). Intensive evaporation in the playa lakes causes deposition of evaporites and calcrete. Like other infill sediments, calcrete also begins to act as aquifers and is affected by chemical process caused by evaporation and a fluctuating water table. Potassium and uranium are leached from felsic rocks (located upstream or in the incised bedrock of the palaeovalley) by saline and oxidised groundwaters, whereas vanadium is extracted from sources such as mafic rocks or iron-rich (meta)sediments. Evaporation of groundwaters can cause changes in the concentration of dissolved potassium, uranium, vanadium and carbonate triggering precipitation of carnotite (Figure 6.27b). In the vicinity of playa lakes, precipitation of carnotite can occur due to mixing of valley groundwaters with more saline lake waters.

6.4.5 Lamil Hills Prospect

The Lamil Hills calcrete-hosted uranium prospect was explored by CRA in 1980 (Muggeridge, 1980). The prospect is located at the southern margin of the Lake Waukarlycarly where an east-west trending channel merges with the playa lake. The drainage is defined by a meandering zone (ca. 1 km wide) of gypsum-bearing calcareous clays, flanked on the southern side by a zone of massive calcretes. The northern part of the channel is represented by gypsum-rich clays with abundant crystalline gypsum and may represent part of the playa lake.

Drilling shows that a zone of massive calcrete capped by a gypsum-rich clay zone lies above the water table. Below the water table the massive calcrete changes into a zone of calcareous clays. The gamma- (γ -) logs of drill holes suggest that uranium-anomalous zones are located in close proximity to the groundwater table, both above and below it. The anomalous zone above the water table is associated with gypsum-rich calcareous clays, whereas the zone below the water table is associated with calcareous clays only. In general, massive calcretes do not record anomalous counts (Muggeridge, 1980). The concentration of uranium reported lies between 2 and 7 ppm uranium equivalent. The presence of Lamil Hills prospect indicates that a fertile calcrete-hosted uranium system operated in the study area.

Table 6.3: Features and mappable characteristics of calcrete-hosted uranium systems.

MINERAL SYSTEM FEATURE	MAPPABLE CHARACTERISTICS
<i>Geodynamic setting</i>	Not significant.
<i>Architecture:</i>	
Basin	Cenozoic palaeovalleys and channels in arid zones filled with coarse-grained permeable sediments. Playa lakes with evaporitic sediments. Concentration of non-pedogenic (or valley-type) calcretes near water table in the alluvial valley infill. Calcrete-rich zones in playa lake sediments.
Structure	Valleys with low gradients (ca. 10 m/km). Structures in the incised bedrock could be important for the groundwaters to access source rocks of potassium, uranium and vanadium.
Igneous	Felsic rocks in upstream area or in the bedrock incised by the palaeochannel. Mafic igneous rocks, ferruginous sediments (ferricrete, banded iron formation) and sediments with vanadium-rich clays significant as sources of vanadium.
<i>Origin of ore fluids and metals</i>	Groundwaters recharged with oxidised surface waters. Moderately high salinity (up to ca. 10 wt. %); generally neutral to alkaline. Uranium-rich felsic rocks in upstream area or in the bedrock incised by the palaeochannel, which also provide potassium. Mafic igneous rocks, ferruginous sediments (ferricrete, banded iron formation) and sediments with vanadium-rich clays significant as sources of vanadium.
<i>Fluid pathways and drivers</i>	Distribution of aquifers in palaeovalleys. Distribution of playa lakes. Main driver: hydrostatic head and seasonal fluctuation of water table.
<i>Metal trap sites and depositional mechanisms</i>	Calcretes in proximity to water table and calcretes in playa sediments. Deposition of uranium (carnotite) caused by any to the following: evaporation of groundwater; mixing of vanadium and uranium-bearing groundwaters; mixing of waters near playa lakes. Map: <ul style="list-style-type: none"> • Groundwater analysis (salinity, pH, potassium, uranium and vanadium); and, • Presence of gypsum-rich sediments.
<i>Post-depositional modifications</i>	Any movement that leads to increase the gradient of the palaeovalley will cause flushing of the system with oxidised waters which can redistribute or destroy carnotite-rich zones.

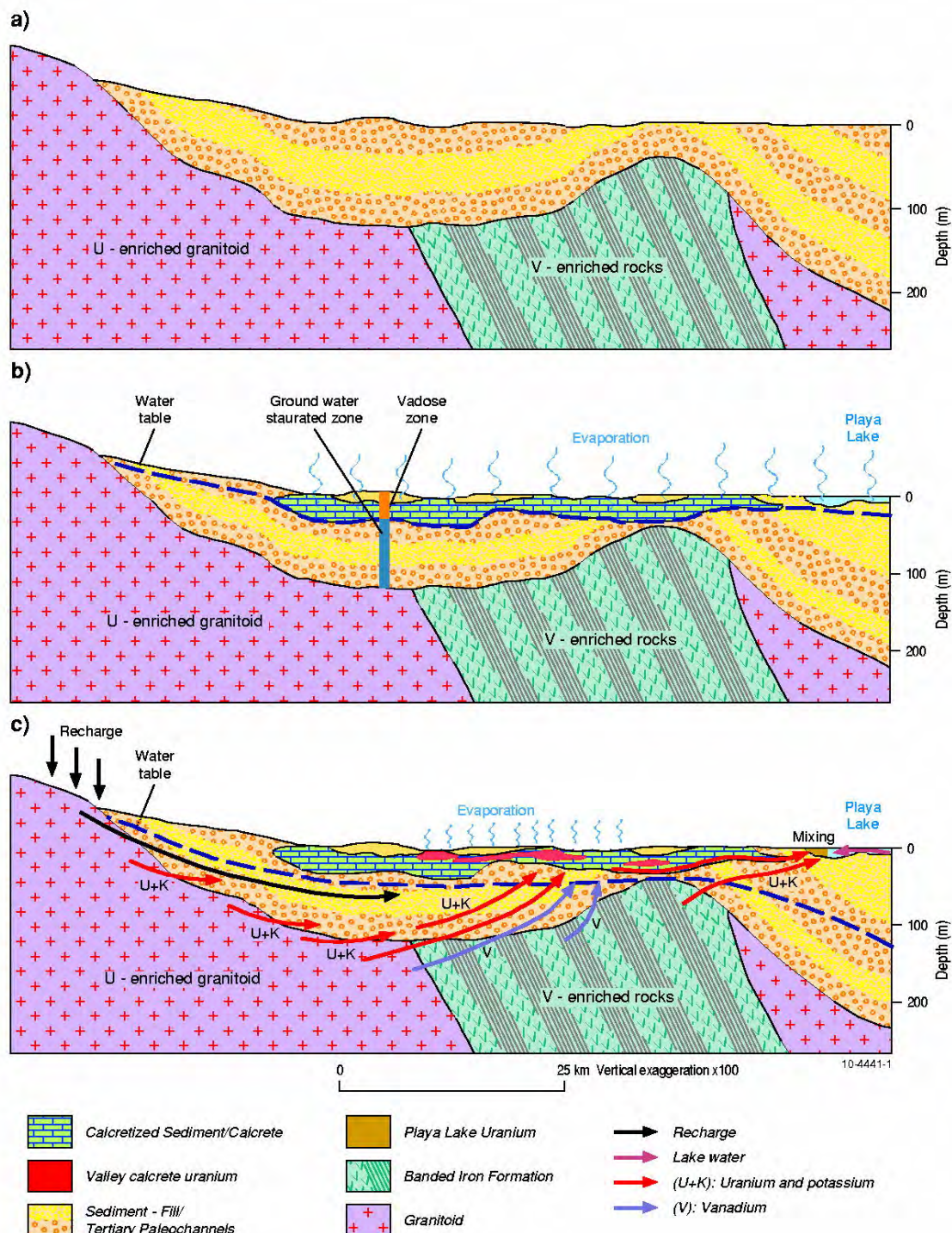


Figure 6.27: Model depicting the formation of calcrete-hosted uranium deposits.

6.5 REFERENCES

- Aditya Birla Minerals, 2008a. Aditya Birla Minerals Annual Report 2007-2008. Online: http://www.adityabirlaminerals.com.au/media/Final_Annual_Report07-08.pdf.
- Aditya Birla Minerals, 2008b. Aditya Birla Minerals Ltd 31th October 2008 Steven Oxenburgh (Presentation to Mining 2008, Brisbane). Online: http://www.adityabirlaminerals.com.au/media/Mining_2008_Conference_Brisbane.pdf.
- Aditya Birla Minerals, 2010. Birla Nifty Copper Operation. Online: <http://www.adityabirlaminerals.com.au/birlaniftyoperation.asp>.
- Anderson, B. R., 1999. Structure, alteration and mineralisation of the Nifty copper deposit, Western Australia: implications for ore genesis. Unpublished Ph. D. thesis, University of Tasmania, 225 p.
- Anderson, B. R., Dare, P., Berry, R. F. and Gemmell, J. B., 1997. The Nifty copper deposit - geology and structure. In: *Geological Society of Australia Abstracts* **44**, 2 pp.
- Anderson, B. R., Gemmell, J. B. and Berry, R. F., 2001. The geology of the Nifty copper deposit, Throssell Group, western Australia: Implications for ore genesis. *Economic Geology* **96**(7), 1535.
- Anderson, B. R., Gemmell, J. B. and Nelson, D. R., 2002. Lead isotope evolution of mineral deposits in the Proterozoic Throssell Group, western Australia. *Economic Geology* **97**(4), 897.
- Bagas, L., 2000. Geology of the Paterson 1:100,000 sheet - Explanatory Notes. Geological Survey of Western Australia, Perth. 20 p.
- Bagas, L., 2004a. Proterozoic evolution and tectonic setting of the northwest Paterson Orogen, Western Australia. *Precambrian Research* **128**(3-4), 475-496.
- Bagas, L., 2005. Geology of the Lamil 1:100 000 sheet, Explanatory Notes. 1:100 000 Geological Series, Western Australia Geological Survey.
- Bagas, L., Grey, K. and Williams, I. R., 1995. Reappraisal of the Paterson Orogeny and Savory Basin. In: *Annual Review 1994-95*. Western Australia Geological Survey, 55-63 pp.
- Bagas, L. and Lubieniecki, Z., 2000. Copper and associated polymetallic mineralization along the Camel-Tabletop Fault Zone in the Paterson Orogen. Geological Survey of Western Australia Perth. *Annual Review 1998-99*, 39-44 pp.
- Bagas, L. and Nelson, D. R., 2007. Provenance of Neoproterozoic sedimentary rocks in the northwest Paterson Orogen, Western Australia. Central Australian Basins Symposium Special Publication, Northern Territory Geological Survey.
- Bagas, L., Williams, I. R. and Hickman, A. H., 2000. Rudall, Western Australia (2nd Edition). 1:250,000 Geological Series - Explanatory Notes. Western Australia Geological Survey. 50 p.
- Barnicoat, A. C., 2007. Mineral systems and exploration science: Linking fundamental controls on ore deposition with the exploration process. In: *Digging Deeper: Proceedings of the Ninth Biennial SGA meeting, Dublin*, 1407-1411 pp.
- Bastrakov, E. N., Jaireth, S. and Mernagh, T. P., 2010. of uranium in hydrothermal fluids at 25°-300°: Implications for the formation of uranium deposits. Geoscience Australia, Canberra. **Geoscience Australia Record 2010/29**, 91 p.
- Blevin, P. L., 2008. Redox and compositional parameters for interpreting the granitoid metallogeny of eastern Australia: Implications for gold-rich ore systems. *Resource Geology* **54**(3), 241-252.
- Blevin, P. L., Chappell, B. W. and Allen, C. M., 1996. Intrusive metallogenic provinces in eastern Australia based on granite source and composition. *Transactions - Royal Society of Edinburgh: Earth Sciences* **87**(1-2), 281-290.
- Budd, A. R., Wyborn, L. A. I. and Bastrakova, I. V., 2001. The metallogenic potential of Australian Proterozoic granites. Geoscience Australia, Canberra. **Record 2001/12**.
- Butt, C. R. M., Mann, A. W. and Horwitz, R. C., 1984. Regional setting, distribution and genesis of surficial uranium deposits in calcretes and associates sediments in Western Australia. In: *Surficial Uranium Deposits*, TECDOC-322. Vienna. 121-127 pp.
- Carlisle, D., 1984. Surficial uranium occurrences in relation to climate and physical setting. In:

- Surficial Uranium Deposits* TECDOC. IAEA, Vienna. 322, 121-227 pp.
- Clarke, G. L., 1991. Proterozoic tectonic reworking in the Rudall complex, Western Australia. *Australian Journal of Earth Sciences* **38(1)**, 31-44.
- Czarnota, K., Gerner, E., Maidment, D. W., Meixner, A. J. and Bagas, L., 2009a. Paterson Area 1:250 000 Scale Solid Geology Interpretation and Depth to Basement Model. Geoscience Australia, Canberra. **Record 2009/16**, 37 p.
- Dalrymple, G. B., Alexander, E. C., Lanphere, M. A. and Kraker, G. P., 1981. Irradiation of samples for $^{40}\text{Ar}/^{39}\text{Ar}$ dating using the Geological Survey TRIGA reactor. United States Geological Survey. **Professional Paper 1176**, 55 pp.
- de Angelis, M., 2009. Uranium exploration potential -- Rudall River region (Sunday Creek Project: EL 45/3278, EL 45/3345, EL 45/3292) and Gascoyne region (Nanutarra Project: EL 08/1689, EL 08/1889, EL 09/1563). Unpublished report to Raisama Pty Ltd. 68 p.
- Dimo, G., 1990. Telfer gold deposits. Geology of the mineral deposits of Australia and Papua New Guinea. *Australasian Institute of Mining and Metallurgy Monograph* **14**, 643-651.
- Dunphy, J. M. and McNaughton, N. J., 1998. Geochronology of the Telfer granitoids: zircon and titanite U-Pb SHRIMP data. In: *Geological Society of Australia Abstracts* **49**, 127 pp.
- Durocher, K. E., Kyser, T. K., Marlatt, J. and Hanly, A., 2003. New $^{40}\text{Ar}/^{39}\text{Ar}$ ages from the central Paterson Orogen, Western Australia. *Australian Journal of Earth Sciences* **50(4)**, 601-610.
- Ferguson, K. M., Bagas, L. and Ruddock, I., 2005. Mineral occurrences and exploration potential of the Paterson area. Geological Survey of Western Australia, Perth. 43 p.
- Froud, J., 1997. Mineralization and alteration of the Goosewhacker prospect, Western Australia. Unpublished B.Sc. Honours thesis, University of Tasmania, 116 p.
- Gaboreau, S., Beaufort, D., Vieillard, P., Patrier, P. and Bruneton, P., 2005. Aluminum phosphate-sulfate minerals associated with Proterozoic unconformity-type uranium deposits in the East Alligator River uranium field, Northern Territory, Australia. *Canadian Mineralogist* **43(2)**, 813.
- Gauci, G., 1997. The Kintyre Advancement Program. Twenty-second Annual Symposium, London, Uranium Institute, p. 1-6.
- Gauci, G. C. and Cunningham, C. C., 1992. A holistic approach to project design for cost effective yellowcake production at Kintyre. Annual Symposium, London, Uranium Institute.
- Glengarry Resources Limited, 2010. Citadel - Gold, Copper and Uranium. Online: <http://www.glengarry.com.au/projects/citadel.htm>.
- Goellnicht, N. M., 1992. Late Proterozoic fractionated granitoids and their role in the genesis of gold and base-metal mineralisation in the Telfer district, Western Australia. Unpublished Ph.D. thesis, University of Western Australia, 132 p.
- Goellnicht, N. M., Groves, D. I. and McNaughton, N. J., 1991. Late proterozoic fractionated granitoids of the mineralized Telfer area, Paterson province, Western Australia. *Precambrian Research* **51(1-4)**, 375-391.
- Goellnicht, N. M., Groves, D. I., McNaughton, N. J. and Dimo, G., 1989. An epigenetic origin for the Telfer gold deposit. *Economic Geology Monograph* **6**, 151-167.
- Gray, D., J., 2001. Hydrogeochemistry in the Yilgarn Craton. *Geochemistry: Exploration, Environment, Analysis* **1(3)**, 253-264.
- Grey, K., Apak, S. N., Eyles, C., Eyles, N., Stevens, M. K. and Carlsen, G. M., 1999. Neoproterozoic glaciogenic succession, western Officer Basin, Western Australia. *Western Australia Geological Survey Annual Review 1998-99*, 74-80.
- Haynes, D. W., Brook, W. J. L. and Mazzoni, P. P., 1993. Application of conceptual models for sediment-hosted ore deposits in the discover of the Nifty copper and adjacent zinc-lead deposits, Yeneena basin, Western Australia. Geological Association of Canada, Ottawa. **Special Paper 40**, 75-88 p.
- Henderson, I., 1993. Annual technical report to the Department of Mines on the Anketell Group, period ending December 1992. Newcrest Mining Limited unpublished report.
- Hewson, S. A., J., 1996. A structural examination of the Telfer gold-copper deposit and surrounding region, northwest Western Australia: the role of polyphase orogenic deformation in ore

- deposit development and implications for exploration. Unpublished Ph. D. thesis, Townsville, James Cook University.
- Hickman, A. H. and Bagas, L., 1998. Geology of the Rudall 1:100 000 sheet. Geological Survey of Western Australia, Perth. 30 p.
- Hickman, A. H. and Bagas, L., 1999. Geological evolution of the Palaeoproterozoic Talbot Terrane and adjacent Meso and Neoproterozoic successions, Paterson Orogen, Western Australia. Geological Survey of Western Australia, Perth. Report 71, 91 p.
- Hickman, A. H. and Clarke, G. L., 1993. Broadhurst, W.A. Sheet 3353. 1:100 000 Geological Series, Western Australian Geological Survey.
- Hickman, A. H., Williams, I. R. and Bagas, L., 1994. Proterozoic geology and mineralization of the Telfer-Rudall region, Paterson Orogen. Excursion Guidebook 5, Geological Society of Australia, Perth. 56 p.
- Howard, G. R., Hansen, T., Moore, C., Moffitt, P. J., Inglis, R. J., Carlson, R. D., Kirchner, I., Coupland, D., Leary, S. and Tomsett, A., 2000. Current geological understanding of Telfer Mine. Australian Institute of Mining and Metallurgy Publications Series 3, 135-142.
- Howard, G. R., Maxlow, J., Helm, S., Inglis, R., Carlson, R. and Hansen, T., 2005. Telfer gold-copper mine: 26 million ounces and growing. Proceedings of Newgengold 2005, Perth, 28-29 November.
- Huston, D. L., Maas, R. and Czarnota, K., 2007. The age and genesis of the Nifty copper deposit: back to the future. Geoscience Australia, Canberra. **Professional Opinion 2007/03**, 26 p.
- Huston, D. L., Maas, R., Miggins, D., Maidment, D. W., Czarnota, K., Preiss, W. and Cassidy, K., 2009. Neoproterozoic mineralisation in Australia: timing and geodynamic setting. In: *Proceeding of the 10th Biennial SGA Meeting of the Society for Geology Applied to Mineral Deposits*, Townsville, Australia, 285-287 pp.
- Jackson, D. J. and Andrew, R. L., 1990. Kintyre uranium deposit. In: Hughes, F. E. (ed) *Geology of the Mineral Deposits of Australia and Papua New Guinea*. The Australasian Institute of Mining and Metallurgy. 653-658 pp.
- Karner, K. and Becker, E., 2009. Geological setting of the Langer Heinrich uranium mine, Namibia. In: *AusIMM International Uranium Conference 2009*, Darwin, AusIMM, 97-98 pp.
- Kyser, K., Hiatt, E., Renac, C., Durocher, K., Holk, G. and Deckart, K., 2000. Diagenetic fluids in Paleo-and Meso-Proterozoic sedimentary basins and their implications for long protracted fluid histories. *Mineralogical Association of Canada Short Course 28*, 225-262.
- Mann, A. W. and Deutscher, R. L., 1978. Genesis principles for the precipitation of carnotite in calcrete drainages in Western Australia. *Economic Geology* **73(8)**, 1724-1737.
- McIntyre, A., Bagas, L., Cassidy, K., Czarnota, K., Neumann, N., Meixner, T. and Huston, D., 2005. Proterozoic geology of the northwest Paterson Orogen, Western Australia: prospectivity, possibilities, progress, and the Permian problem. *Central Australian Basins Symposium Abstracts*, Darwin, Northern Territory Geological Survey.
- McKay, A. D. and Miezitis, Y., 2001. Australia's uranium resources, geology and development of deposits. Mineral Resource Report, AGSO - Geoscience Australia, Canberra. **Mineral Resource Report 1**, 200 p.
- Miggins, D. P., Blome, C. D. and Smith, D. V., 2004. Preliminary 40 Ar/39 Ar geochronology of igneous intrusions from Uvalde County, Texas: defining a more precise eruption history for the southern Balcones volcanic province. *US Geological Survey Open File Report 2004-1031*, 31.
- Miggins, D. P., Thompson, R. A., Pillmore, C. L., Snee, L. W. and Stern, C. R., 2002. Extension and uplift of the northern Rio Grande Rift: Evidence from 40Ar/39Ar geochronology from the Sangre de Cristo Mountains, south-central Colorado and northern New Mexico. *Geological Society of America Special Paper 362*, 47-64.
- Muggeridge, G. D., 1980. Final report on exploration compiled within temporary reserve 7012H Lamil Hills, Paterson Range, Western Australia. CRA Exploration.
- Mustard, R., 2001. Granite-hosted gold mineralization at Timbarra, northern New South Wales, Australia. *Mineralium Deposita* **36(6)**, 542-562.
- Nash, J. T., Granger, H. C. and Adams, S. S., 1981. Geology and concepts of genesis of important

- types of uranium deposits. *Economic Geology Seventy-fifth Anniversary Volume 1905-1980*, 63-116.
- Nelson, D. R., 1995. Compilation of SHRIMP U-Pb zircon geochronology data, 1994. Geological Survey of Western Australia. **Record 1995/3**, 244 p.
- Nelson, D. R., 1996. Compilation of SHRIMP U-Pb zircon geochronology data, 1995. Geological Survey of Western Australia, Perth. **Record 1996/5**, 168 p.
- Newcrest Mining Limited, 2010. BMO Capital Markets Global Metals & Mining Conference 1st to 3rd March 2010, Miami Florida. Online: http://www.newcrest.com.au/upload/640_3x1x201054316PM.pdf.
- Ohmoto, H., 1986. Stable isotope geochemistry of ore deposits. *Reviews in Mineralogy* **16**, 491-559.
- Pirajno, F. and Bagas, L., 2008. A review of Australia's Proterozoic mineral systems and genetic models. *Precambrian Research* **166(1-4)**, 54-80.
- Quirt, D., Kotzer, T. and Kyser, T. K., 1991. Tourmaline, phosphate minerals, zircon and pitchblende in the Athabasca group: Maw Zone and McArthur River areas, Saskatchewan. *Saskatchewan Geological Survey Technical Report 91-4*, 181-191.
- Reed, A., 1996. The structural, stratigraphic and temporal setting of the Maroochydore copper prospect, Paterson orogen, Western Australia. Unpublished Ph. D. thesis, Perth, Australia, University of Western Australia, 289 p.
- Root, J. C. and Robertson, W. J., 1994. Geophysical signature of the Kintyre uranium deposit, Western Australia. In: Dentith, M. C., Frankcombe, K. F., Ho, S. E., Shepherd, J. M., Groves, D. I. and Trench, A. (eds) *Geophysical Signatures of Western Australian Mineral Deposits*. Geology and Geophysics Department (Key Centre) & UWA Extension, The University of Western Australia, **Publication 26** and the Australian Society of Exploration Geophysicists, **Special Publication 7**, 454p. 371-382 pp.
- Rowins, S. M., Groves, D. I., McNaughton, N. J., Palmer, M. R. and Eldridge, C. S., 1997. A reinterpretation of the role of granitoids in the genesis of Neoproterozoic gold mineralization in the Telfer Dome, Western Australia. *Economic Geology* **92(2)**, 133-160.
- Schofield, A., 2009. Uranium content of igneous rocks of Australia 1:5 000 000 maps - Explanatory notes and discussion. Geoscience Australia Record, Geoscience Australia, Canberra. **Record 2009/17**, 20 p.
- Schwabe, M. R., 1981. Mt Sears Range Project, Rudall River Region, Western Australia, Annual Report 1979-80, Temporary Reserve 6883H., Occidental Minerals Corporation of Australia.
- Sexton, M. A., 1994. Geophysical characteristics of the Telfer gold deposits, Western Australia. In: Dentith, M. C., Frankcombe, K. F., Ho, S. E., Shepherd, J. M., Groves, D. I. and Trench, A. (eds) *Geophysical Signatures of Western Australian Mineral Deposits*. Australian Society of Exploration Geophysicists, **Special Publication 7**, 454p. 199-212 pp.
- Skirrow, R. G., Jaireth, S., Huston, D. L., Bastrakov, E. N., Schofield, A., van der Wielen, S. E. and Barnicoat, A. C., 2009. Uranium mineral systems: processes, exploration criteria and a new deposit framework. Geoscience Australia, Canberra. **Record 2009/20**, 44 pp.
- Smith, S. G., 1996. Geology and geochemistry of the Warrabarty carbonate-hosted Zn-Pb deposit, Paterson Orogen, Western Australia. Unpublished Ph.D. thesis, University of Tasmania, 162 p.
- Smithies, R. H. and Bagas, L., 1997. The Tabletop terrane of the Proterozoic Rudall Complex: preliminary notes on the geology, granite geochemistry and tectonic implications. *Geological Survey of Western Australia Perth. Annual Review 1996-97*, 89-94 pp.
- Swingler, N., 1981. Sunday Creek Project, Rudall River Region, WA - Final Report for TR 7071H. Occidental Minerals Corporation of Australia. Western Australia Geological Survey WAMEX Open File Series; Item 1694.
- Thompson, J. F. H. and Newberry, R. J., 2000. Gold deposits related to reduced granitic intrusions. *Reviews in Economic Geology* **13**, 377-400.
- Turner, C. C., 1982. The Telfer Gold Deposits, Western Australia. Stratigraphy, sedimentology and mineralisation of the Proterozoic Yeneena Group. Unpublished Ph.D. thesis, University of New England, 296 p.
- Tyrwhitt, D. S., 1979. Stratabound gold deposits of Proterozoic age at Telfer, Western Australia.

- Proceedings of the 85th Annual Northwest Mining Convention, Spokane, Washington.
- Walter, M. R., Veevers, J. J., Calver, C. R. and Grey, K., 1995. Neoproterozoic stratigraphy of the Centralian Superbasin, Australia. *Precambrian Research* **73(1)**, 173-195.
- Wilson, J. T., 1968. Static or mobile earth: The current scientific revolution. *Proceedings of the American Philosophical Society* **112**, 309-320.
- Wingate, M. T. D., Campbell, I. H., Compston, W. and Gibson, G. M., 1998. Ion microprobe U-Pb ages for Neoproterozoic basaltic magmatism in south-central Australia and implications for the breakup of Rodinia. *Precambrian Research* **87(3)**, 135-159.
- Wyborn, L. A. I., 1997. The metallogenic potential of Australian Proterozoic granites – Paterson Orogen. The metallogenic potential of Australian Proterozoic granites – Western Australian Volume, AGSO-Geoscience Australia, Canberra.

7 Implications for uranium mineral systems

S. F. Liu and S. Jaireth

7.1 OVERVIEW OF URANIUM MINERAL SYSTEMS AND IMPLICATIONS OF AEM DATA IN THE PATERSON AREA

There are 4 major known and potential uranium mineral systems in the Paterson area, including:

1. Unconformity-related uranium within the Neoproterozoic sediments and older basement, including:
 - The Yeneena Basin-Rudall Complex unconformity:
 - Coolbro Sandstone-Rudall Complex (known);
 - Taliwanya Formation-Rudall Complex (potential).
 - The Tarcunyah Formation-Archean unconformity (potential); and,
 - The Karara Formation-Rudall Complex unconformity (potential).
2. Stratabound uranium-copper-lead-zinc associated with the Broadhurst Formation-Coolbro Sandstone (Broadhurst-Coolbro) contact (known);
3. Sandstone-hosted uranium (potential); and,
4. Calcrete-hosted uranium (known).

Skirrow *et al.* (2009) classified uranium mineral systems in terms of the origins of ore-forming fluids ([Figure 7.1](#)): 1. magmatic-hydrothermal; 2. metamorphic fluids; and, 3. hydrosphere-derived (meteoric waters, lake waters, sea water and groundwaters). The four specific uranium mineral systems in the Paterson area, listed above, belong to the family of hydrosphere-derived basin- and surface-related uranium mineral systems of Skirrow *et al.* (2009).

The unconformity-related uranium within, the Neoproterozoic sediments and older basement rocks, and stratabound uranium-copper-lead-zinc associated with the Broadhurst-Coolbro contact, are parts of the Miles mineral system described in [Chapter 6](#). The Miles mineral system is a two-event model summarising mineralisation during the late Yeneena Basin development (840-830 Ma) and inversion of the Yeneena Basin (830-810 Ma) during the Miles Orogeny, which deformed the Yeneena Basin sediments and basement rocks by folding and faulting, discussed in [Chapters 3 and 6](#). During the Yeneena Basin development, normal faulting was associated with extension which drove downward fluid movement of basinal brines during diagenesis. During the inversion of the Yeneena Basin in the Miles Orogeny, normal faults, developed during basin formation, turned to thrusting associated with folding in a contractional regime which drove upward fluid movement ([Figure 6.13](#)).

The Miles mineral system has been discussed in detail in [Chapter 6](#), including: 1. geodynamic setting; 2. architecture (basin, structure and igneous architecture); 3. origin of ore fluids and metals; 4. fluid pathways and drivers; 5. depositional mechanisms; and, 6. post-depositional modifications. Datasets that could be used in potential assessment and exploration were also introduced.

In this chapter, we discuss the implications of AEM data for assessing the potential of the above listed four major types of uranium mineral systems in the Paterson area in the context of the essential components of these systems ([Table 7.1](#)). The components of relevant uranium mineral systems discussed in this chapter are short-listed from the extensive lists compiled in Skirrow *et al.* (2009), because a full assessment of all mappable criteria for the four major uranium mineral systems is beyond the scope and timeframe of the Paterson AEM project.

As will be discussed in detail in the following sections, regional AEM data is useful in mapping several key components of uranium mineral systems ([Table 7.1](#)):

- Unconformities ([Section 7.3.1](#));
- Reductants ([Section 7.3](#));

- Sedimentary packages with contrasting conductivities ([Section 7.4.1.1](#));
- Palaeovalleys ([Section 7.4.1.2](#)); and,
- Faults as fluid pathways and traps ([Section 7.3](#));

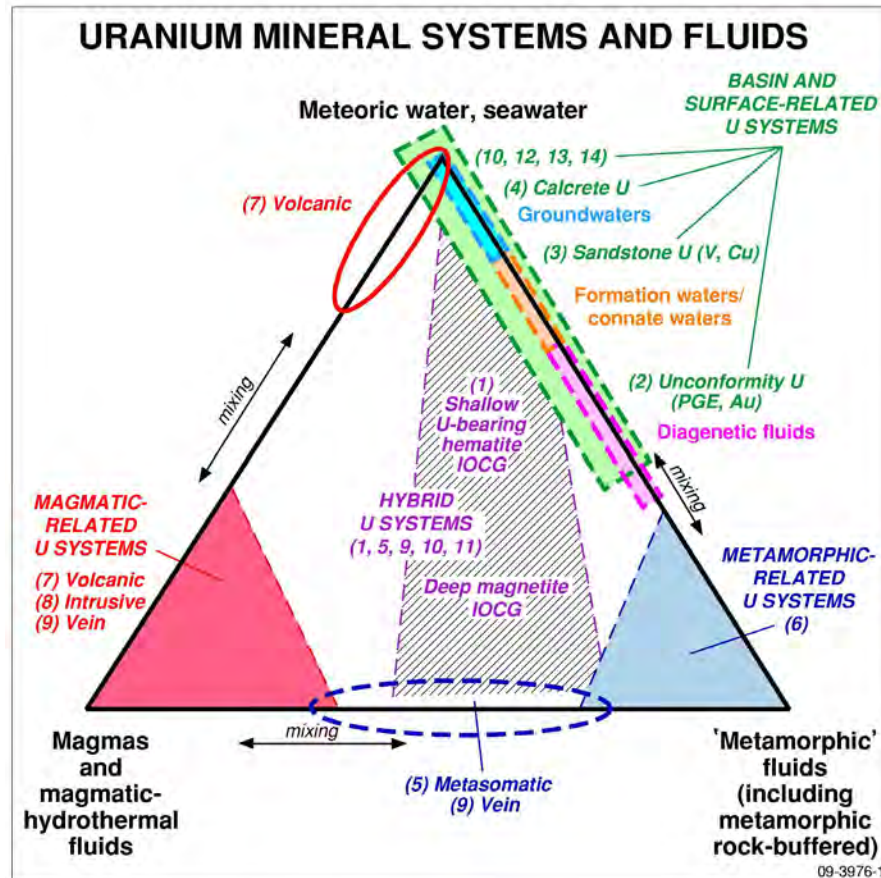


Figure 7.1: Scheme of three families of uranium mineralising systems, and three end-member fluid types. Numbered deposit types are from the IAEA Red Book, in order of economic importance in Australia. Source: Skirrow et al. (2009).

Due to the lack of data at this stage, no prospectivity maps are produced other than for calcrete-hosted uranium mineral systems. Instead, we have shown permissive areas and ranked them according to their potential and level of certainty using critical components of relevant systems. The method of assessment used is qualitative and the assessment documents the presence or absence of critical components of the uranium mineral systems in the permissive areas.

In the following sections, we will first discuss the concentration of uranium in rocks of the area and uranium anomalies and then discuss the implications of AEM data for exploration of uranium mineral systems in the area in the context of key available datasets.

7.2 CONCENTRATION OF URANIUM IN ROCKS AND URANIUM ANOMALIES IN THE PATERSON AREA

To assess potential of uranium mineral systems, it is important to know the availability of source rocks for uranium in the area of assessment. Geochemical analyses of rocks from the Paterson area

are scarce and these are mostly restricted to outcrop areas or to samples from drill holes. Analysed samples are mostly from the Rudall Complex and the Mt Crofton Granite Suite. Airborne radiometric data, however, provide a good regional picture of uranium abundances in the top 30 cm or so of outcrop rocks and regolith (Wilford *et al.*, 1997). In particular, the radiometric data show uranium anomalies in the area. Below is a summary of these two sources of data which provides background information of the sources of uranium for mineralisation in the Paterson area.

Table 7.1: Key assessment criteria for potential of uranium mineral systems and implications of AEM data in the Paterson area.

DIAGENETIC FLUID-RELATED URANIUM MINERAL SYSTEMS	SANDSTONE-HOSTED URANIUM MINERAL SYSTEM (ROLL FRONT, TABULAR AND PALAEOVALLY TYPES)	CALCRETE-HOSTED URANIUM MINERAL SYSTEM	
UNCONFORMITY-RELATED URANIUM MINERAL SYSTEM	STRATABOUND URANIUM-COPPER ASSOCIATED WITH BROADHURST-COOLBRO CONTACT		
CRITERIA MAPPED IN AEM			
Unconformity Reductants in rocks below the unconformity.	Reductants / conductive parts (carbonaceous materials and sulfides) of Broadhurst Formation.	Highly permeable coarse-grained sandstone package (e.g., Permian Paterson Formation) palaeovalley.	
OTHER CRITERIA			
Felsic igneous rocks as uranium sources. Thick sandstone package above the unconformity. Favourable fault systems. Alteration and mineralisation (from distribution of mapped gossans and interpretation from ASTER data).	Contact between Broadhurst Formation and Coolbro Sandstone. Fluid pathways. Redox gradients (particularly the presence of hematitic alteration in the Coolbro Sandstone), some of which may be mapped from magnetic data. Muscovite alteration and surface carbonate as interpreted from ASTER data.	Felsic igneous rocks as uranium sources. Presence of <i>in situ</i> organic materials or other reductants (sulfides, Fe ⁺² -bearing silicates and oxides) and/or mobile reductants (hydrocarbons and associated gases such as H ₂ S).	Mapped calcrete. Felsic igneous rocks as uranium sources. Mafic igneous rocks and/or ferruginous duricrust materials as vanadium sources. Ground water geochemistry: U and V concentrations.

7.2.1 Radiometric data

The regional distribution of uranium-rich materials is depicted in the airborne radiometric data ([Figure 7.2](#)). Uranium abundances of surface materials (bedrock and regolith) in the Paterson area are shown in [Figure 7.3](#); surface materials with relatively high uranium abundances are shown in red whereas blue areas correspond to surface materials with relatively low or near-zero values of uranium in this image ([Figure 7.3](#)).

In the Pilbara Craton bedrocks with high uranium abundances are granitic and felsic volcanic rocks

(Figure 7.3). In the area of Warroo Hill to Mt Gregory, the Gregory Granite Complex and the mixed sequence of felsic volcanic rocks and sedimentary rocks of the Fortescue Basin commonly show uranium contents of 7 ppm or more in the radiometric data. In the Rudall Complex, there are not only uranium anomalies in granitic gneisses (Figure 7.3), but also in some Neoproterozoic sediments and Cenozoic ferruginous duricrust materials in valleys. The radiometric data show that granitic gneisses in the Rudall Complex commonly contain uranium abundances of 4-10 ppm at surface.

At Kintyre and to the north, metasedimentary rocks of the Yandagooge Formation show uranium anomalies of 4-11 ppm while surrounding areas are mostly 1-1.5 ppm. To the west-southwest of Kintyre, granitic rocks of the Rudall Complex show uranium anomalies of 4-6 ppm.

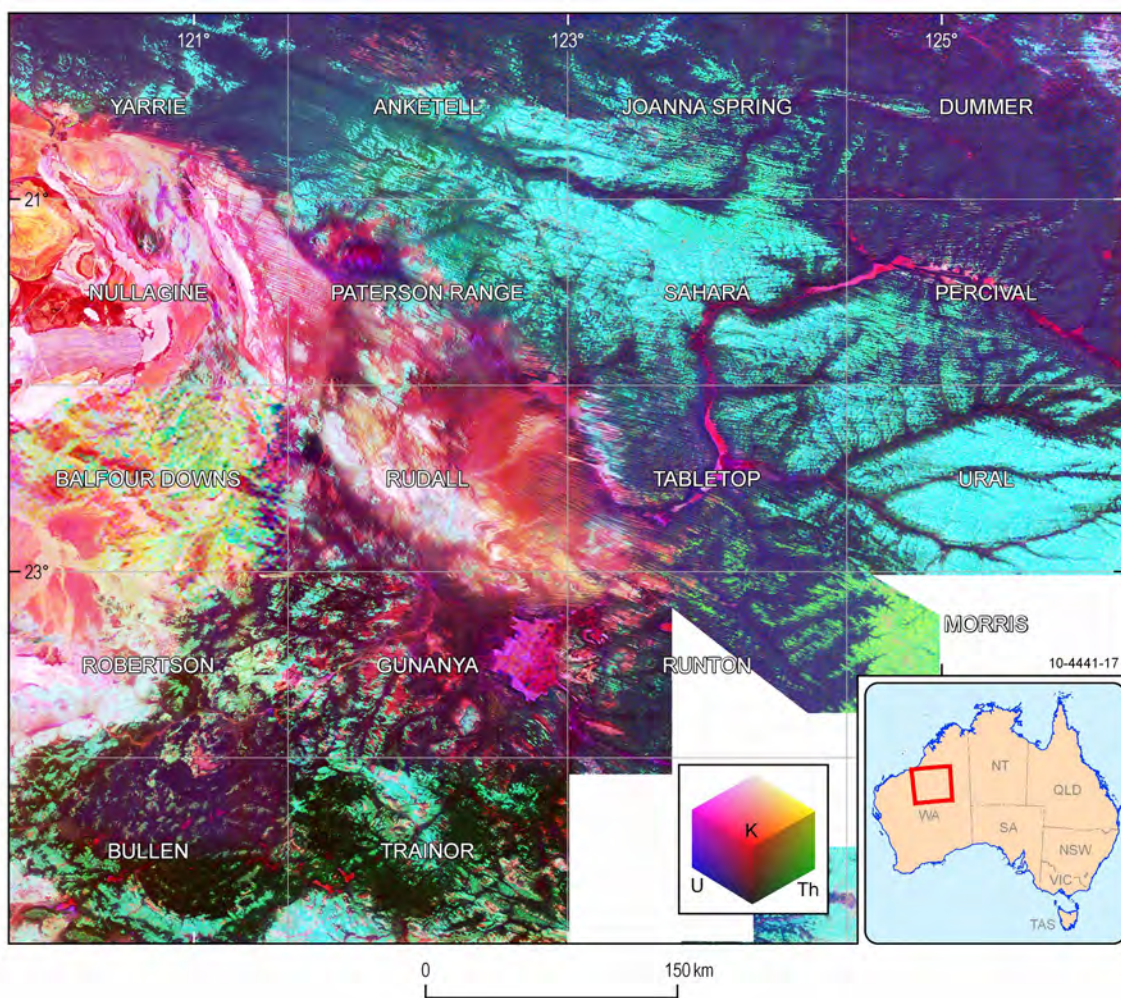


Figure 7.2: Ternary diagram of radiometric data from the Paterson region, after Minty et al. (2008), showing 1:250 000 map tiles.

Metasedimentary rocks of the Yandagooge Formation at Cassandra (location shown in Figure 6.2) show apparent uranium anomalies of 3.5-4.5 ppm at surface in the radiometric data, while the surrounding areas are mostly 1.5-2.5 ppm at surface.

Ferruginous duricrust materials in the drainage valleys east, south and north of Cassandra also show uranium anomalies of 3.5-4.5 ppm at surface. The drainage north of Cassandra feeds into the Rudall

River. This indicates possible mobilisation of uranium into the current drainage systems.

There is a uranium anomaly (4-8 ppm) corresponding to outcropping Neoproterozoic Broadhurst Formation in a topographic low area northeast of the Broadhurst Range (about 20 km ENE to NE of Kintyre). Similarly, about 30 km west of Kintyre, there are uranium anomalies of 3-5 ppm in partially regolith-covered Neoproterozoic Broadhurst Formation and undivided Yeneena Basin sediments. The anomaly here is some 10 km wide and 30 km long trending NNW (Figure 7.3). The uranium content of the surrounding area is mostly 2 ppm or less. Compared with the Broadhurst Formation in the valley northeast of Broadhurst Range, the lower uranium anomalies in the radiometric data here are probably due to weathering.

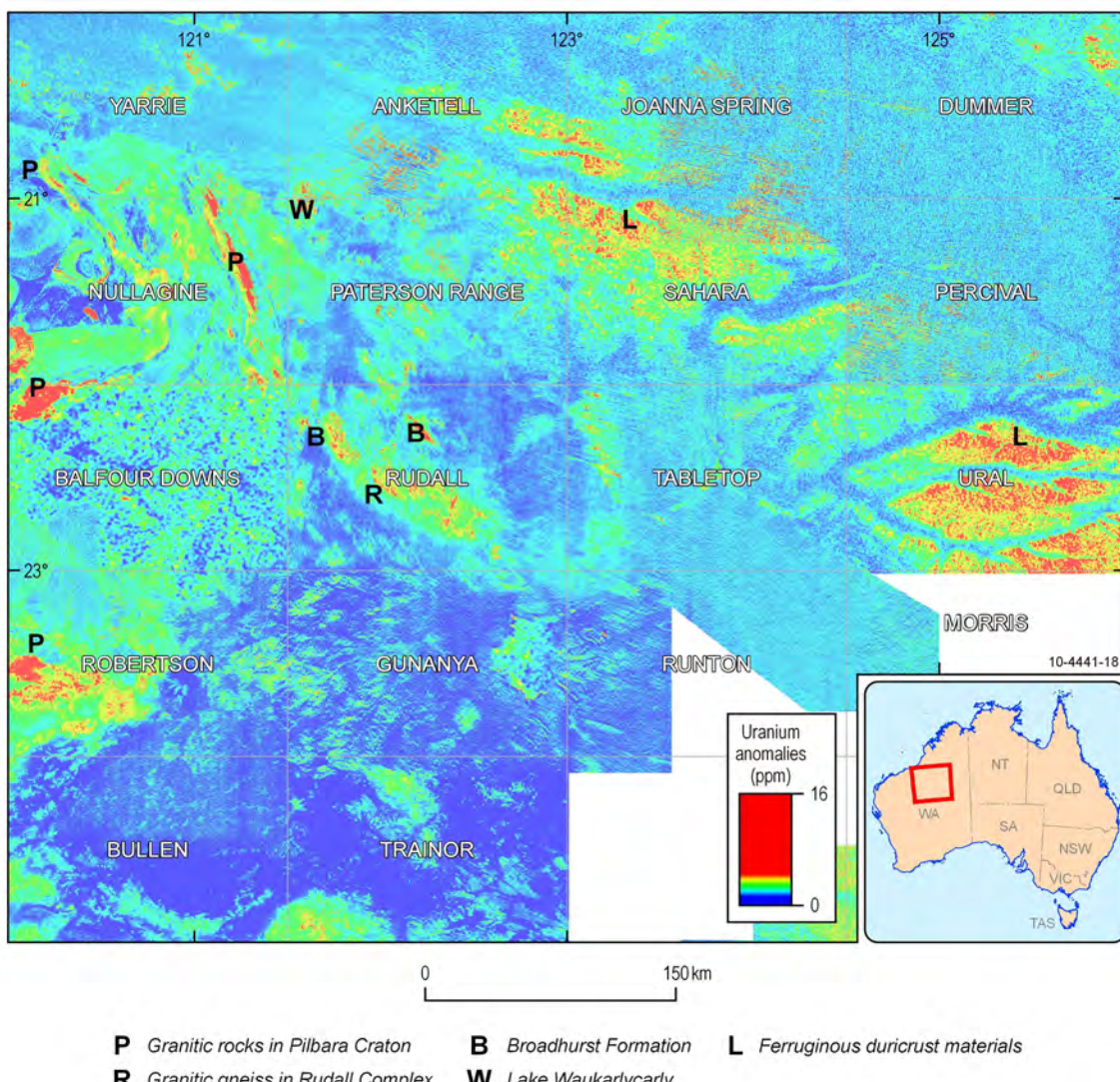


Figure 7.3: Uranium anomalies in radiometric data from the Paterson region, after Minty *et al.* (2008), showing 1:250 000 map tiles.

The large areas of ferruginous duricrust materials on the URAL and SAHARA 1:250 000 map sheets also show anomalous uranium abundances of 3.5-4 ppm, compared to surrounding sand plain areas of mostly 1.5 ppm or less.

7.2.2 Geochemical analyses

The Geological Survey of Western Australia published geochemical analyses as part of its 1:100 000 surface geology mapping of the Broadhurst and Connaughton 1:100 000 sheets. Whole rock analyses of fresh samples indicate that these rocks have up to 14 ppm uranium (Bagas and Smithies, 1998; [Figure 7.4](#)). Geoscience Australia's Ozchem database houses 78 geochemical analyses from the Mt Crofton Granite suite in the Telfer area and one analysis from the Gregory Range Suite. The sample from the Gregory Range Suite is a biotite monzogranite, which contains 6 ppm uranium.

Analysed samples from the Mt Crofton Granite Suite include monzogranite, syenogranite, granite and aplite. These rocks have uranium contents from 2 to 38 ppm and 90% of the samples are in the range of 4 to 26 ppm. More than 30 samples have more than 10 ppm uranium. These data suggest that the Mt Crofton Granite Suite is comparatively uranium-rich.

7.2.3 Uranium/thorium ratios

Uranium (U) and thorium (Th) are closely associated in minerals and rocks. The ratio of U/Th (ppm values) can be used to measure uranium enrichment or thorium depletion. However, uranium abundance is commonly in the order of several ppm in rocks while thorium is commonly in the order of several tens of ppm or greater ([Figures 7.3 & 7.5](#)). Thus the U/Th ratio of ppm values is commonly low. More than 98.7% of Western Australian samples in the GA Ozchem database have U/Th ratios less than 2 (90.5% less than 0.5 and 46.7% less than 0.2, [Table 7.2](#)). For better graphic presentations of uranium enrichment or thorium depletion, the ratio of U^2/Th (ppm values) is commonly used to show a larger range of the ratio and more sensitive display of uranium anomalies. 16.5% of Western Australia analyses have U^2/Th ratio greater than 2 and 2.9% greater than 10 ([Table 7.3](#)).

Table 7.2: U/Th ratios of analysed samples from Western Australia. Data are from Geoscience Australia's Ozchem database. Analyses with negative uranium or zero or negative thorium values are not used in the statistics.

U/TH RATIO	CUMULATIVE NO. OF SAMPLES	PERCENTAGE
>100	8559	100%
100	8553	99.9%
10	8527	99.6%
2	8449	98.7%
1	8310	97.1%
0.5	7749	90.5%
0.2	3997	46.7%
0.1	1682	19.7%
0	298	3.5%

For bedrocks, uranium enrichment is clearly shown over felsic igneous rocks in the Pilbara Craton and Rudall Complex, and over the Broadhurst Formation west and northeast of Kintyre in the uranium anomaly image of [Figure 7.3](#), and U^2/Th ratio (ppm values) image of [Figure 7.6](#). These rocks are good source rocks for potential uranium mineralisation in the area. The advantage of using U^2/Th ratios to enhance secondary uranium enrichment or thorium depletion in surface materials is clearly shown in [Figure 7.6](#). The apparent uranium anomalies over areas of ferruginous duricrust materials in the SAHARA and URAL 1:250 000 map sheet areas, as shown in [Figure 7.2](#), are reduced in the U^2/Th ratio image ([Figure 7.6](#)). In addition, the U^2/Th ratio image of [Figure 7.6](#) also shows U^2/Th ratio anomalies at Lake Auld and Lake Disappointment.

Table 7.3: U^2/Th ratios of analysed samples from Western Australia. Data are from Geoscience Australia's Ozchem database. Analyses with negative uranium or zero or negative thorium values are not used in the statistics *

U2/TH RATIO	CUMULATIVE NO OF SAMPLES	PERCENTAGE
>100	8559	100%
100	8481	99.1%
10	8308	97.1%
2	7175	83.5%
1	5784	67.6%
0.5	4029	47.1%
0.2	2045	23.9%
0.1	1181	13.8%
0	301	3.5%

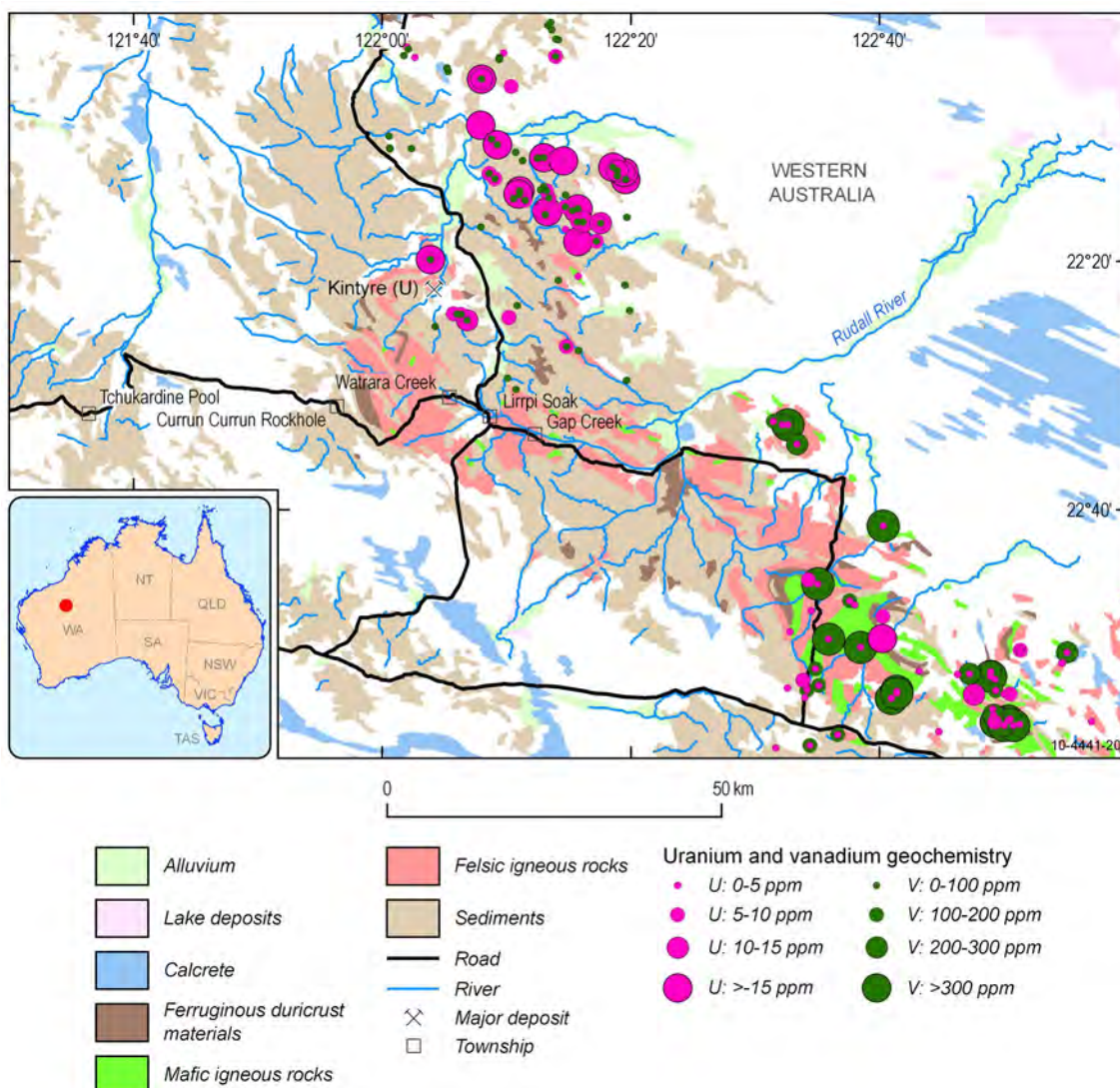


Figure 7.4: Uranium and vanadium abundances in the Rudall 1:250 000 map sheet area. Geochemical data from Bagas and Smithies (1998) and Hickman and Clarke (1994).

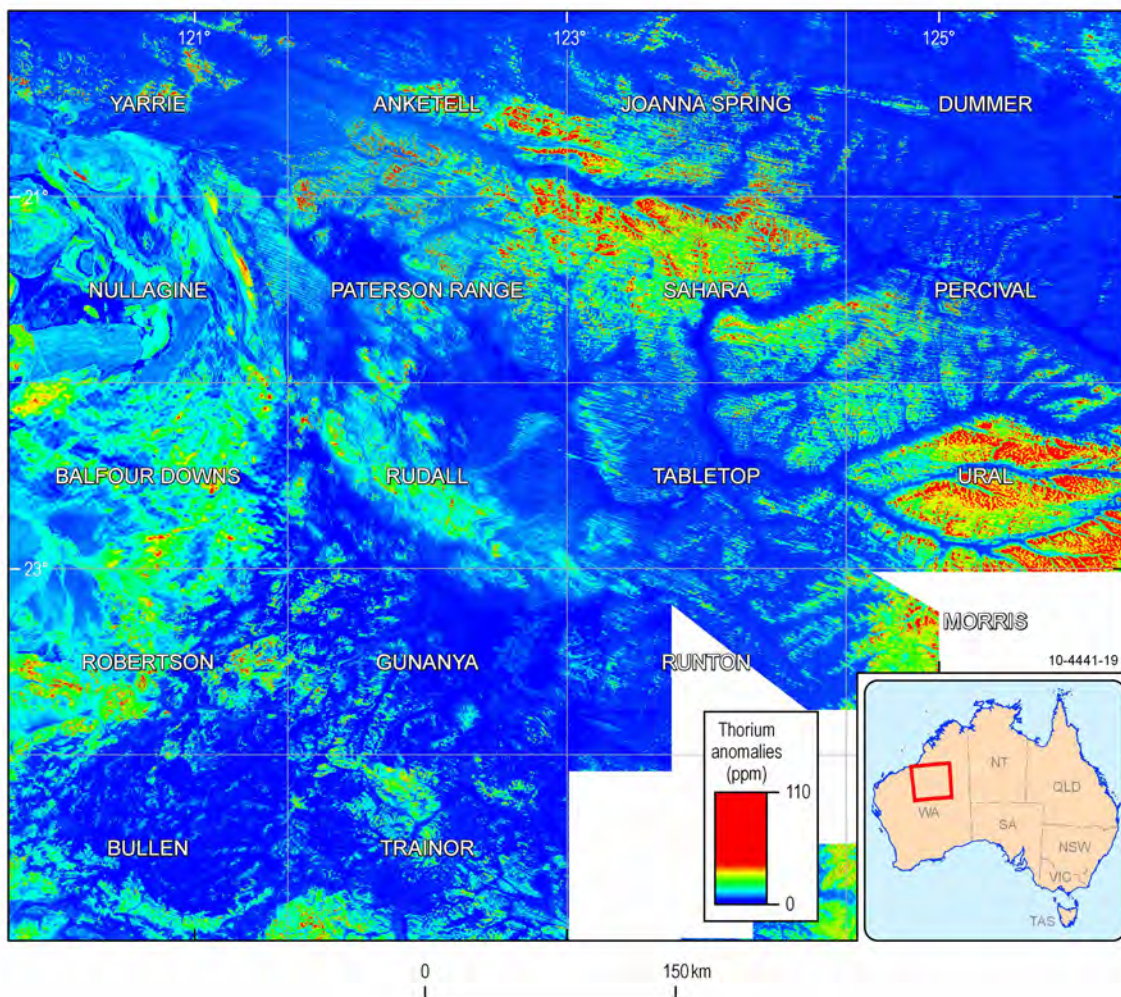


Figure 7.5: Thorium anomalies in radiometric data from the Paterson region, after Minty et al. (2008), showing 1:250 000 map tiles.

Secondary uranium enrichment or thorium depletion is further enhanced in normalised U^2/Th ratios (Figure 7.7). This treatment removes or reduces the more primitive U^2/Th ratio anomalies, e.g., the felsic igneous rocks in Pilbara Craton, Rudall Complex, and Broadhurst Formation. Even anomalies over the ferruginous duricrust materials in the SAHARA and URAL 1:250 000 map sheets are minimised. However, several prominent normalised U^2/Th ratio anomalies are revealed in the following areas:

- Lake Waukarlycarly;
- Tobin Lake;
- Lake Auld;
- Lake Disappointment; and,
- The drainage valleys southeast of Lake Disappointment.

In the Paterson area, the radiometric data show apparent thorium depletion in drainage systems whereas uranium enrichment is not evident (Figures 7.3 & 7.5). Therefore, the normalised U^2/Th ratios show thorium depletion rather than uranium enrichment in the drainage systems, for example, Lake Waukarlycarly, Lake Disappointment, Lake Auld, and Tobin Lake, in the Paterson region (Figure 7.7).

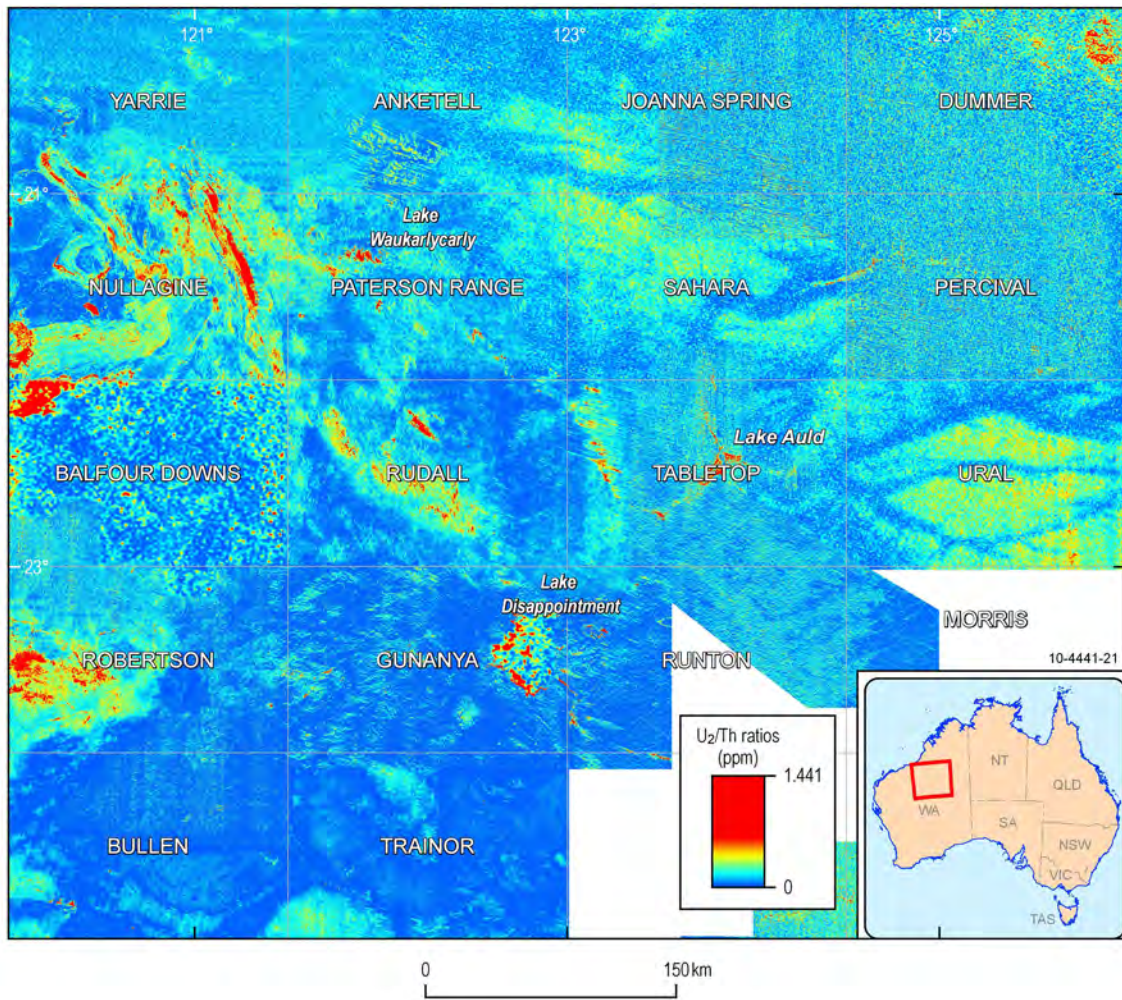


Figure 7.6: Image of U^2/Th ratio anomalies from the Paterson region (U^2/Th ratios of ppm values), after Minty et al. (2008), showing 1:250 000 map tiles.

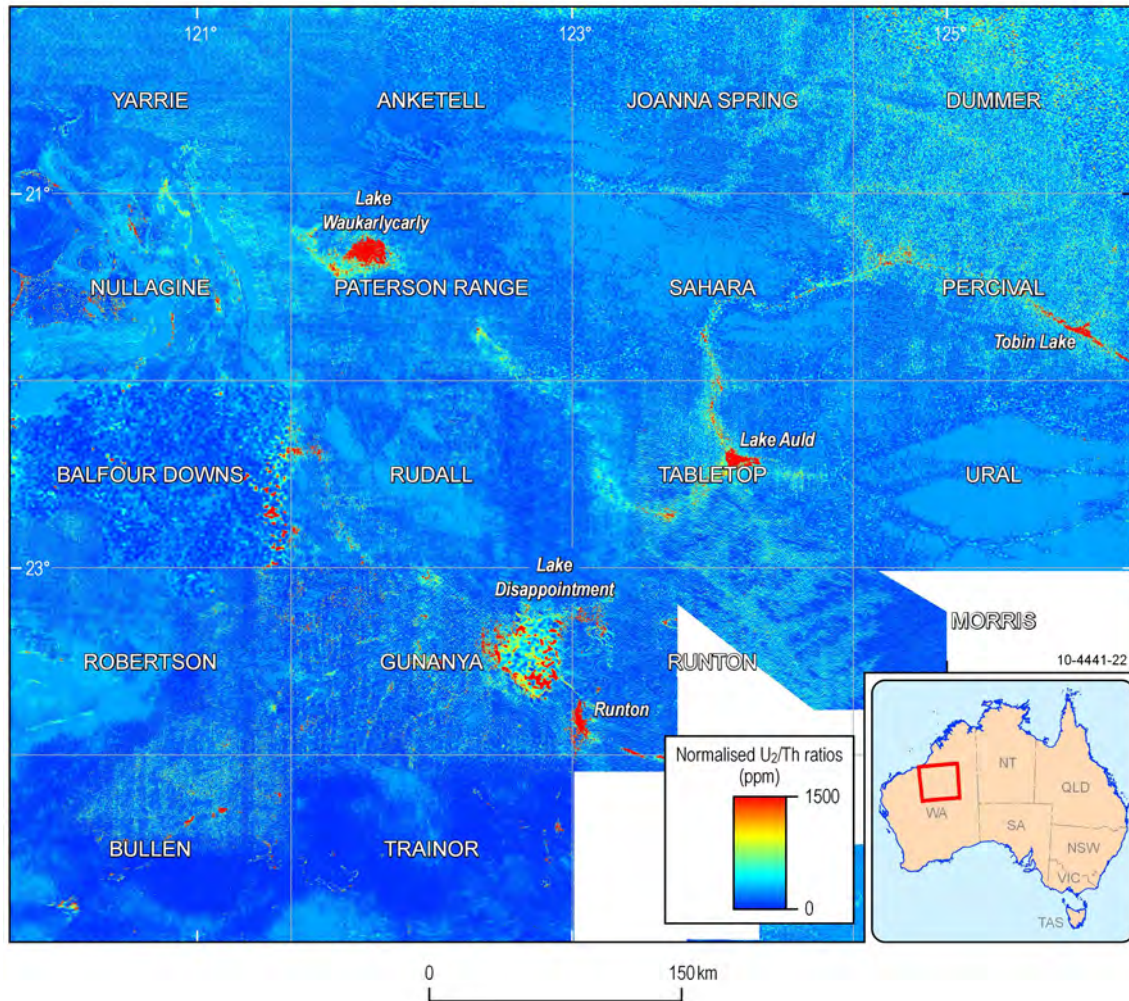


Figure 7.7: Normalised U^2/Th ratio anomalies from the Paterson region, after Minty et al. (2008), showing 1:250 000 map tiles. Instead of calculating the U^2/Th ratios from ppm values, ‘normalised’ U^2/Th ratios are calculated by scaling uranium and thorium values to 0–255 (standard 8-bit colour range) from optimised ternary ($KThU$) radiometric image data (Figure 7.2) first and then calculating the U^2/Th ratios. By doing so, “normal” samples seem to have U^2/Th ratios close to 1 or a small value while anomalies are enhanced. This is an advantage of using ‘normalised’ U^2/Th ratios to further assess uranium enrichment or thorium depletion.

7.3 DIAGENETIC FLUID-RELATED URANIUM MINERAL SYSTEMS

As discussed in detail in [Chapter 6](#) and summarised in [Section 7.1](#), the Miles mineral system includes two specific uranium mineral systems, namely: 1. unconformity-related uranium associated with the unconformities of Neoproterozoic over older basement rocks; and, 2. stratabound uranium-copper associated with the Broadhurst-Coolbro contact. These two systems are actually products of the same geological process in the same geodynamic setting, i.e., late Yeneena Basin development to inversion of the Yeneena Basin during the Miles Orogeny ([Chapter 6, Figures 6.13 & 7.8](#)). The source of fluids was also the same, being basinal brines formed during diagenesis, which may be modified to some extent during the Miles Orogeny.

The differences in these two types of mineralisation may include: (a) fluid pathways; and, (b) trap rocks, trap sites and associated alteration. It is beyond the scope of this study to examine these aspects in detail. However, we will discuss key components of these specific uranium mineral systems and discuss the implications of AEM data in the context of assessing the potential of these uranium mineral systems.

7.3.1 Unconformity-related uranium mineral systems

Unconformity-related uranium mineral systems are thought to include the following processes (Cuney and Kyser, 2008; [Figure 7.8](#)):

- Uranium and other associated metals are leached from uranium-rich rocks by oxidised diagenetic fluids. The uranium-bearing fluids are typically moderate temperature (ca. 150-200°C) and saline. Such temperature implies the prior existence of a thick, sedimentary cover sequence (at least 5-7 km based on a geothermal gradient of 30°C/km or thicker if the gradient is lower); and,
- Uranium is deposited when these oxidised fluids come into contact with reductants in the basin or in the basement rocks. Examples of possible reductants include carbonaceous, often graphitic, metasediments, Fe²⁺-rich rocks (such as chloritised metasediments or pyrite-bearing rocks) and hydrocarbons (predominantly for Phanerozoic systems). Zones of faulting and brecciation, particularly in the basement, are important for focusing the fluids and enhancing their interaction with reduced rock assemblages. There is also a general association of calcareous rocks with reduced rocks in the basement which indicate that changes in pH may have some bearing on deposition of uranium.

Key components and mappable criteria used to assess the potential of unconformity-related uranium mineral systems in the Paterson area in this study are summarised in [Table 7.4](#), following the ‘Five Questions’ approach of mineral systems analysis proposed by Barnicoat (2007).

In the following sections we assess the potential of unconformity-related uranium mineral systems associated with the following unconformities between Neoproterozoic sediments and older basement rocks, including:

- The Tarcunyah Group-Archean (Tarcunyah-Archean) unconformity;
- The Yeneena Basin-Rudall Complex (Yeneena-Rudall) unconformity:
 - Coolbro Sandstone-Rudall Complex (Coolbro-Rudall) unconformity;
 - Taliwanya Formation-Rudall Complex (Taliwanya-Rudall) unconformity; and
- The Karara Formation-Rudall Complex (Karara-Rudall) unconformity.

Implications of AEM data are discussed in this context.

These unconformities are shown in [Figure 7.9](#). The presence or absence of key components for unconformity-related uranium mineral systems associated with these unconformities and potentials for these uranium mineral systems are summarised in [Table 7.5](#).

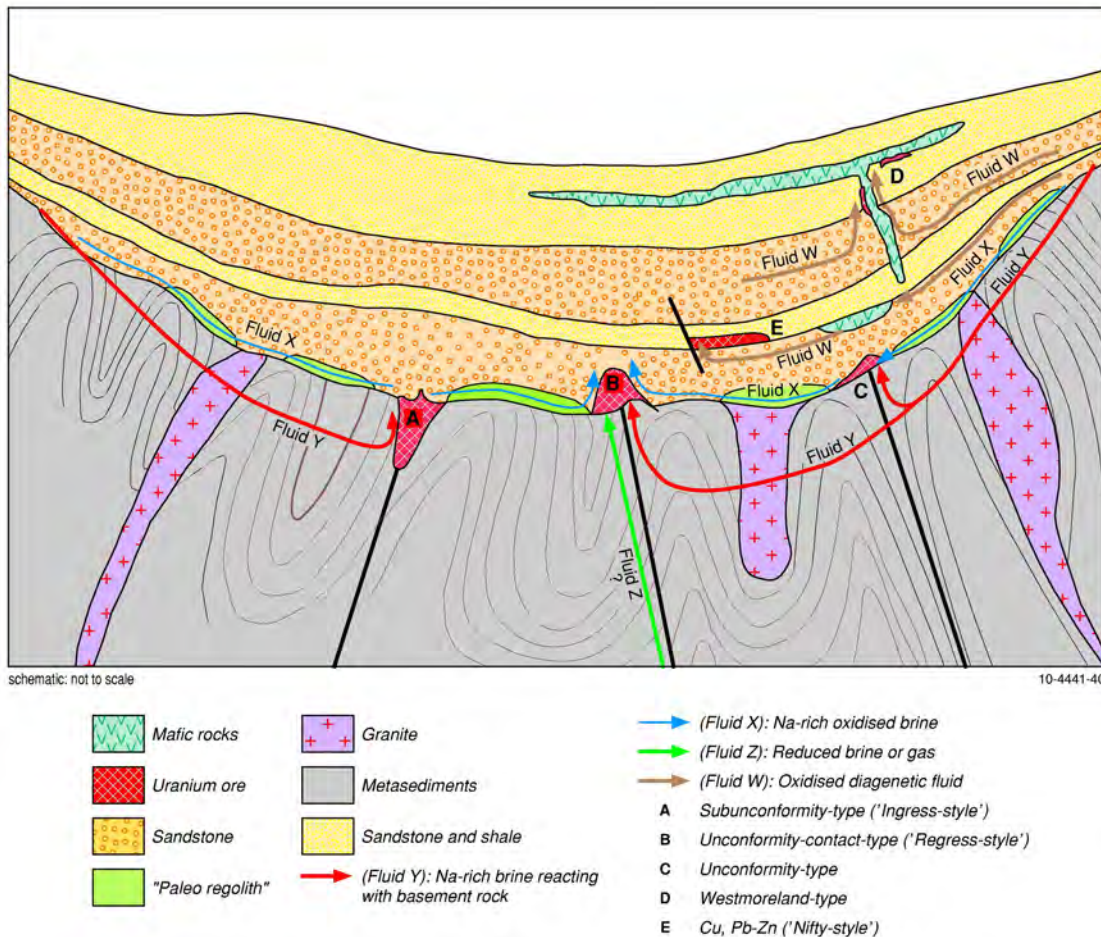


Figure 7.8: Conceptual model for diagenetic fluid-related uranium mineral systems, modified after Derome et al. (2005).

Table 7.4: Key mappable criteria for assessing potential of unconformity-related uranium mineral systems in the Paterson area, modified after Table A6 of Skirrow et al. (2009).*

QUESTION*	MAPPABLE CRITERIA	SOURCE DATA
Q2, Q4	Unconformities.	Surface and solid geology, AEM data.
Q3	Felsic igneous rocks as uranium sources.	Surface and solid geology, radiometric data, geochemistry data.
Q2, Q4	Thick highly permeable siliciclastic sandstone package (best fluvial, originally at least 5-7 km thick) above the unconformity.	Surface and solid geology.
Q5	Reductants as trap rocks below the unconformity.	Surface and solid geology, AEM data.
Q4	Faults as fluid pathways as well as structural traps.	Surface and solid geology.

*Questions are as follows (after Barnicoat, 2007):

- Q1: What is the geodynamic and P-T-t history of the system?
- Q2: What is the architecture of the system?
- Q3: What are the characteristics and sources (reservoirs) of water, metals, ligands and sulfur?
- Q4: What are the fluid flow drivers and pathways?
- Q5: What are the transport and depositional processes for metals, ligands and sulfur?
- Q6: How and where do later geological processes allow preservation of deposits?

The Tarcunyah-Archean unconformity is mapped in the solid geology between the following formations of the Tarcunyah Group and the Archean (Pilbara Craton and Fortescue Basin) ([Figure 7.9](#)):

- The Eel Creek Formation;
- The Waroongunyah Formation; and,
- The Googhenama Formation.

The Yeneena-Rudall unconformity is mapped in the solid geology in two areas ([Figure 7.9](#)):

- The Coolbro Sandstone over Rudall Complex in the Kintyre area and to the north; and,
- The Coolbro and Taliwanya formations over Rudall Complex in the McKay Range area.

In the area of Camel-Tabletop Fault Zone and McKay Fault east of McKay Range, the Karara Formation of the Tarcunyah Group is mapped as unconformably overlying the Rudall Complex ([Figure 7.9](#)).

7.3.1.1 Potential of unconformity-related uranium within the Tarcunyah-Archean unconformity

The Tarcunyah-Archean unconformity is mapped in surface geology maps or interpreted in solid geology maps, including GSWA's 1:100 000 and 1:250 000 geological mapping (Williams and Trendall, 1998a; 1998b; 1998c), GA's 1:1 000 000 Surface Geology of Western Australia (Stewart, 2008) and the 1:250 000 solid geology map for the Paterson area by Czarnota *et al.* (2009b). The unconformity is moderately to steeply east-dipping as indicated by bedding above the unconformity. In places the unconformity has been sheared. The stratigraphy of the Neoproterozoic Tarcunyah Group is summarised in [Table 7.6](#).

Table 7.6: Tarcunyah Group stratigraphy, after Grey *et al.* (2005) and Williams (2004).

Formation	
Tarcunyah Group	Nooloo Formation
	Wongarlong Formation
	Yandanunyah Formation
	Brownrigg Sandstone
	Waroongunyah Formation / Eel Creek Formation
	Googhenama Formation
	Choorun Formation
	Waters Formation
	Gunanya Sandstone / Karara Formation

The unconformity is clearly mapped by AEM data as a conductivity contrast. [Figure 7.10](#) shows selected AEM conductivity sections plotted over a pre-Permian solid geology map. The Archean below and to the west of the unconformity is generally resistive while the Tarcunyah Group, here including the Googhenama Formation, Waroongunyah Formation and Eel Creek Formation, is more conductive in most places. Thus many AEM conductivity sections show a sharp contrast between the Tarcunyah Group and the underlying Archean Pilbara Craton or Fortescue Group, although such a contrast in conductivity in these two packages of rocks may not be apparent across the unconformity in all conductivity sections. The geometry of AEM anomalies is also consistent with the unconformity dipping moderately to steeply towards the east as inferred and interpreted from surface and solid geology mapping.

East of the Gregory Range, the Tarcunyah-Archean unconformity is mapped or interpreted to be between the Googhenama Formation and the Archean Pilbara Craton (Williams and Trendall, 1998a). This unconformity can be traced further north to the area west of Hammerhead where the

Googhenama Formation unconformably overlies the Pilbara Craton or Fortescue Basin in different places (Figure 6.2; Williams and Trendall, 1998b; 1998c). The Googhenama Formation comprises up to 500 m of interbedded fine- to coarse-grained sandstone and granular, pebbly to boulder conglomerate unconformably overlying the Archean Pilbara Craton (Figures 7.9 and 7.10). The Googhenama Formation was deposited on a mature, undulating surface of weathered granitic rocks; basal conglomerates contain locally-derived granitic and gneissic clasts. The conglomerate beds occupy channels, incised either within the granitic basement or pene-contemporaneously within the Googhenama Formation. Single-pebble horizons, current striations and abundant cross-bedding indicate a fluvial environment and may imply deposition in a braided stream environment (Williams and Trendall, 1998a). Thus, the Googhenama Formation is considered a fertile package of rocks for unconformity-related uranium mineral systems.

The Googhenama Formation is the lowest unit of the Tarcunyah Group in the Gregory Range-Warroo Hill area. The total thickness of the Tarcunyah Group is more than six kilometres (Bagas *et al.*, 2000; Chapter 3).

On the solid geology maps, the Waroongunyah Formation is interpreted to unconformably overlie the Archean Fortescue Basin. The Eel Creek Formation is interpreted to unconformably overlie the Archean Pilbara Craton and Fortescue Basin (Figures 7.9 & 7.10). The Eel Creek Formation is shown as a correlative of the Waroongunyah Formation on YARRIE (Williams, 2004).

The Waroongunyah Formation is characteristically a mixture of thin-bedded, laminated, multicoloured dolomite and brown to grey, calcareous shale and siltstone. Thin beds of medium- to coarse-grained dolomitic sandstone, wacke and pebbly dolomite are found at irregular intervals throughout this succession (Williams, 2003). The Waroongunyah Formation is not a favourable package of rocks for unconformity-related uranium mineral systems because of its dolomitic lithology (low permeability) and lack of fluvial coarse-grained sandstone. The Eel Creek Formation consists of black, grey, blue and green mudstone, shale, siltstone and fine-grained, thin-bedded sandstone (Williams, 2003). This package of rocks may not be very favourable for unconformity-related uranium mineral systems in terms of lithology and low permeability, however, the mudstone and shale units may act as reductants themselves.

Uranium source rocks are readily available in the Gregory Range to Warroo Hill area and include the Archean granites of the Gregory Suite and felsic volcanic rocks of the Fortescue Basin.

7.3.1.1.1 Warroo Hill

In the Warroo Hill area the Googhenama Formation of the Tarcunyah Group unconformably overlies the Archean Fortescue Group and Pilbara Craton (Williams and Trendall, 1998b; 1998c). Here the Archean rocks define a north-northwest trending synform, plunging to the south-southeast with faults developed approximately parallel to the axial plane of the regional fold. An east-northeast trending fault displaced the Googhenama Formation with dextral movement.

Above the unconformity the Tarcunyah Group, consisting of the Googhenama Formation and the Waroongunyah Formation, is in faulted contact with the Broadhurst Formation of the Yeneena Group to the east.

Below the unconformity is the Hardey Formation of the Fortescue Group (Table 7.7). Three members of this formation are mapped on BRAESIDE and ISABELLA (Williams and Trendall, 1998b; 1998c). This formation is a mixed sequence of felsic and mafic lavas and sedimentary rocks.

Table 7.5: Key components of mineral systems and potential of unconformity-related uranium mineral systems.

	TARCUNYAH-ARCHEAN UNCONFORMITY		YENEENA-RUDALL UNCONFORMITY		KARARA-RUDALL UNCONFORMITY
COMPONENT	WARROO HILL	MT GREGORY	KINTYRE-RUDALL	MCKAY RANGE	TABLETOP-RUNTON
Uranium-rich source rocks	Felsic igneous rocks in Archean Pilbara Craton (Gregory Granite Complex) and Fortescue Basin (felsic volcanic rocks).	Felsic igneous rocks in Archean Pilbara Craton (Gregory Granite Complex).	Felsic igneous rocks in the Rudall Complex.	Felsic igneous rocks in the Rudall Complex.	Felsic igneous rocks in the Rudall Complex.
Unconformity	Googhenama Formation (Tarcunyah Group) over Archean Pilbara Craton and Fortescue Basin.	Googhenama Formation (Tarcunyah Group) over Archean Pilbara Craton (Gregory Granite Complex).	Coolbro Sandstone over Rudall Complex (Talbot Terrane).	Throssell Range Group (Taliwanya Formation, Pungkuli Formation, and Coolbro Sandstone) over Rudall Complex (Talbot & Connaughton Terranes).	Karara Formation (Tarcunyah Group) over Rudall Complex (Tabletop and Connaughton Terranes).
Sandstone package above the unconformity	Googhenama Formation: interbedded fine- to coarse-grained sandstone and granular, pebbly to boulder conglomerate, fluviaatile.	Googhenama Formation: interbedded fine- to coarse-grained sandstone and granular, pebbly to boulder conglomerate, fluviaatile.	Coolbro Sandstone: regionally extensive (up to 3-4 km thick) fluviaatile sandstone with minor shale interbeds.	Coolbro Sandstone: regionally extensive (up to 3-4 km thick) fluviaatile sandstone with minor shale interbeds Taliwanya Formation: arkosic sandstone and local basal conglomerate and coarse sandstone with rare heavy-mineral bands, fluviaatile.	Karara Formation: arkosic sandstone, interbedded with thin beds of feldspathic granule to pebble conglomerate at the base (fluviaatile to deltaic) and overlain by thinly bedded dolomite.
Reductants in rocks below the unconformity	Pelitic sediments (phyllite and slate, the presence of carbonaceous materials unknown, may contain Fe+2-bearing silicates). Mafic igneous rocks.	Mafic igneous rocks that intrude Gregory Granite Complex and along the unconformity.	In Rudall Complex: pelitic and graphitic units of the Yandagooge Formation and mafic and ultramafic rocks in the complex, rocks with Fe+2 bearing minerals such as chlorite, and iron sulfides.	In Rudall Complex: pelitic and graphitic units of the Yandagooge Formation and mafic and ultramafic rocks in the complex, rocks with Fe+2 bearing minerals such as chlorite, and iron sulfides.	In Rudall Complex: mafic and ultramafic rocks in the complex, rocks with Fe+2 bearing minerals such as chlorite, and iron sulfides.
Faults	Present. Unconformity partly sheared, later faults cut unconformity	Present. Unconformity partly sheared later faults cut unconformity.	Present. Several generations of faults formed in the basement and during Miles Orogeny.	Present Several generations of faults formed in the basement and during Miles Orogeny.	Present. Several generations of faults formed in the basement and during Miles Orogeny.
Reductants in cover sequence	Unknown.	Unknown.	In Coolbro Sandstone: shale or pelitic schist (the presence of carbonaceous materials unknown, may contain Fe+2-bearing silicates) calcareous shale.	In Pungkuli Formation: shale and pyritic shale. In Taliwanya Formation: minor shale.	Shale (the presence of carbonaceous materials unknown, may contain Fe+2-bearing silicates), and rare basalt or fine-grained doleritic sills.
Potential & certainty	Moderate to high potential with moderate certainty.	Moderate to high potential with moderate certainty.	High potential with high certainty.	High potential with moderate to high certainty.	Moderate potential with moderate certainty.

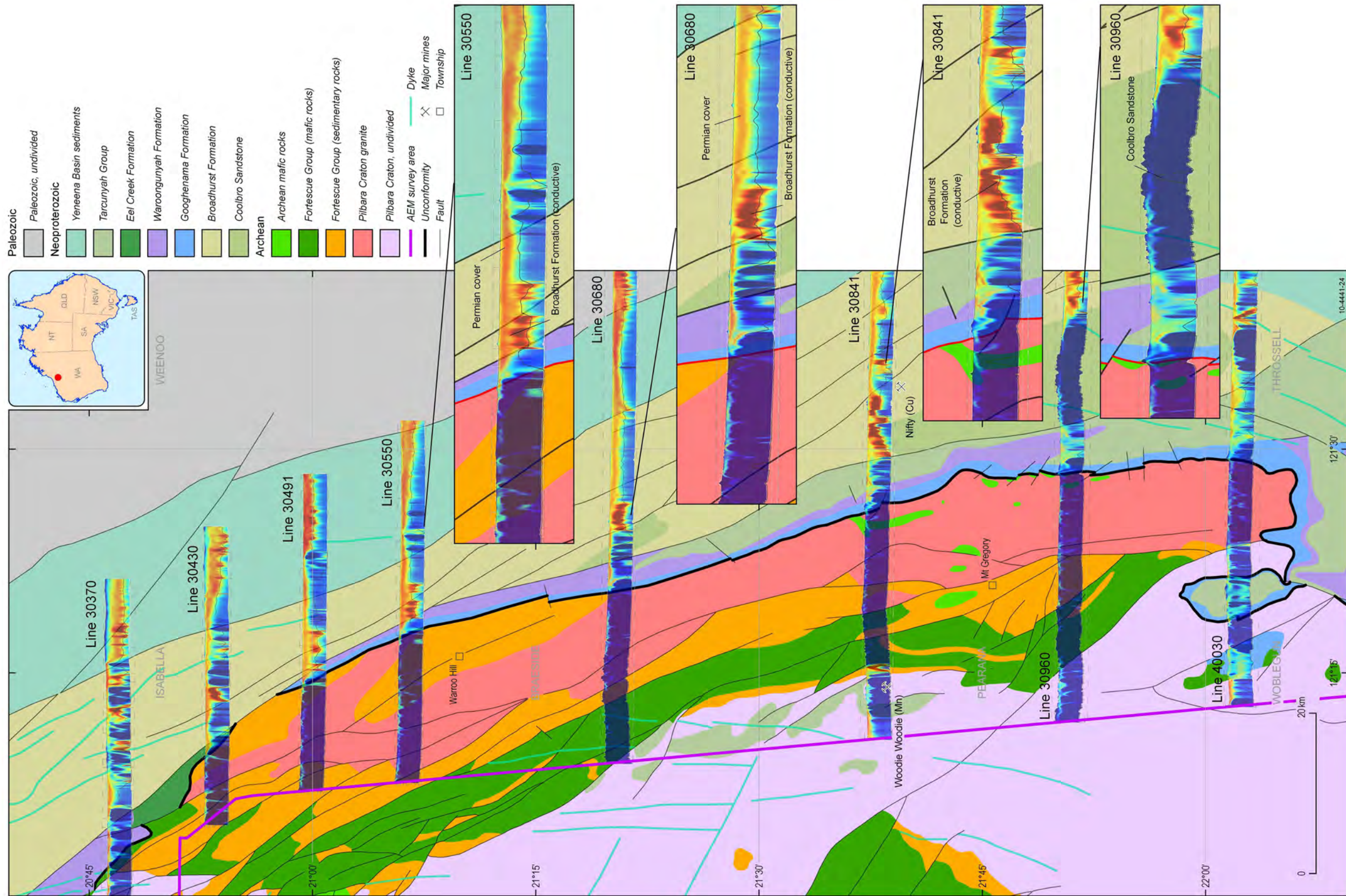


Figure 7.10: Conductivity sections over pre-Permian solid geology of the Warroo Hill-Mt Gregory area. Conductivity colour bar shown in Figure 4.8.

In addition to the uranium-rich granitic rocks of the Gregory Granitic Complex in the Pilbara Craton, the felsic igneous rocks of the formation may provide an additional source of uranium for mineralisation while the pelitic sedimentary rocks (e.g., phyllite and slate) and mafic igneous rocks of this formation and other Archean dolerite and gabbro in the area may act as reductants/trap rocks in the basement for unconformity-related uranium mineral systems.

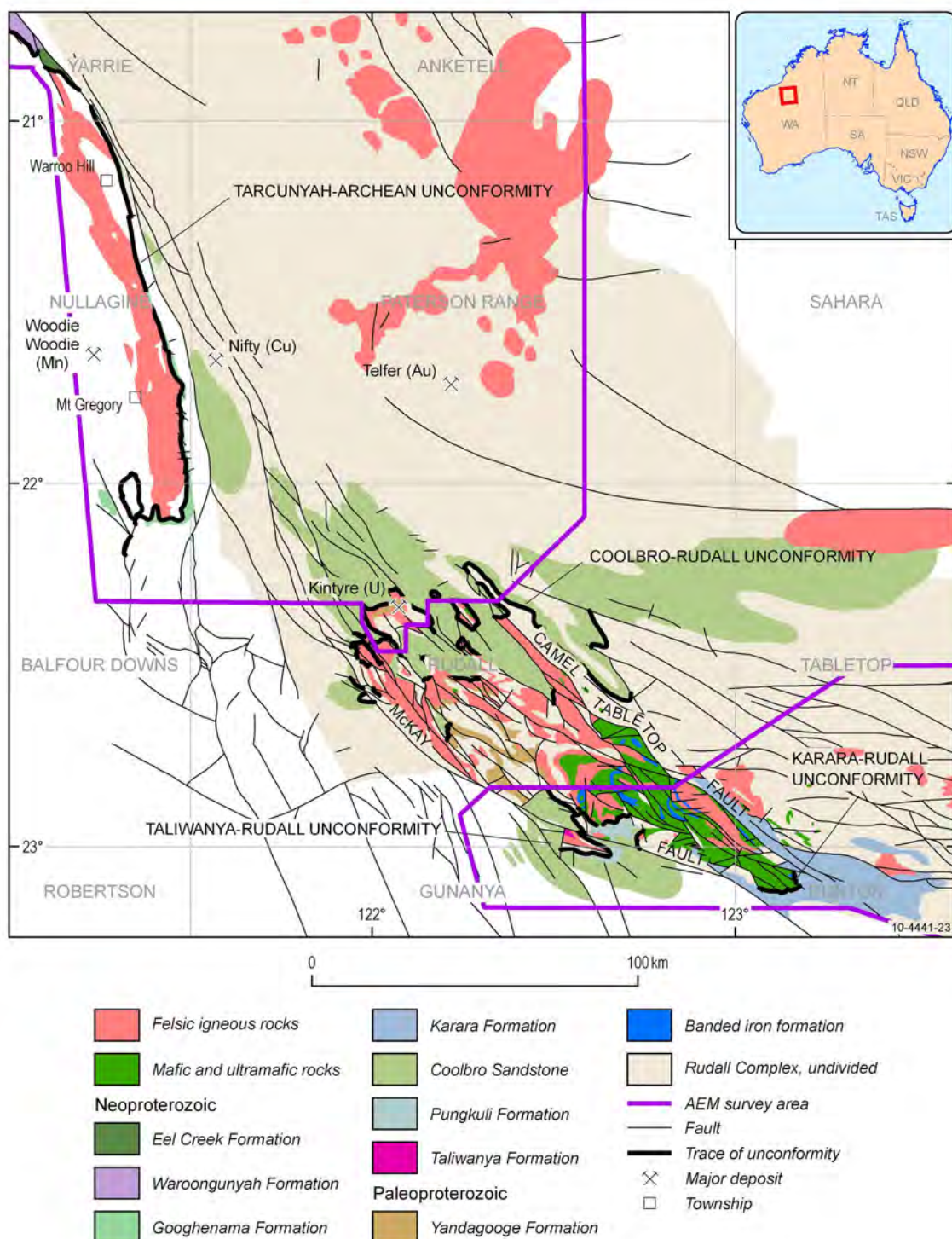


Figure 7.9: Neoproterozoic unconformities in the Paterson region.

There are copper and zinc prospects in the Hardey Formation in the Warroo Hill area on BRAESIDE (Warroo and Warroo North, [Figure 6.2](#)). The age of copper and zinc mineralisation and their link to uranium mineralisation associated with the Miles Orogeny is unknown. We draw attention to the potential for unconformity-related uranium mineral systems associated with the Tarcunyah (Googhenama Formation)-Archean unconformity in the area because key components for these systems are present. Uranium potential is considered to be moderate to high with moderate certainty ([Table 7.5](#)).

Table 7.7: Hardey Formation (Fortescue Group) stratigraphy, after Williams and Trendall (1996a).

MEMBER	LITHOLOGY	COMMENT
Tanguin Member	Mixed felsic and mafic lavas (rhyolite and basalt), and tuffaceous sedimentary rocks.	Contains reductants (Potential trap).
Warroo Hill Member	Metamorphosed fine- to coarse-grained clastic rock, tuff, and mafic rock: <ul style="list-style-type: none"> • Metasandstone, metaconglomerate, metasiltstone, and quartzite; • Metamorphosed pelitic sedimentary rock; quartz-mica schist, phyllite, and slate; • Metadolomite; and, • Metabasalt and metabasaltic andesite, local amygdalites. 	Contains reductants (potential trap).
Koongaling Volcanic Member	Porphyritic and fine-grained felsic lavas; dacite, rhyodacite, rhyolite; including quartz-feldspar-mica schist.	Potential source rock of uranium.

7.3.1.1.2 *Mt Gregory*

In the area east of Mt Gregory the Googhenama Formation of the Tarcunyah Group unconformably overlies the Gregory Granitic Complex of the Pilbara Craton ([Figures 7.9 & 7.10](#)). Mafic and ultramafic rocks are mapped in the complex, including metamorphosed dolerite and gabbro, amphibolites, metamorphosed ultramafic rocks and talc-chlorite-tremolite-serpentine assemblages on PEARANA (Williams and Trendall, 1996b). The mafic and ultramafic rocks are mapped along the unconformity and within the granitic complex.

The unconformity is faulted with dextral movements along northwest trending faults and sinistral movements along east-west trending faults, which suggest they were probably conjugate faults.

On PEARANA the Googhenama Formation is mapped as consisting of medium- to coarse-grained sandstone and pebble to boulder conglomerate. It is conformably overlain by the Waroongunyah Formation of shale, siltstone, sandstone and dolomite (Williams and Trendall, 1996b).

Here the mixed sandstone and conglomerate succession of the Googhenama Formation is up to 500 m thick. The Googhenama Formation crops out in a 50 km-long, almost continuous ridge on the eastern margin of PEARANA. The Formation was deposited on an undulating surface of weathered granitic and gneissic rocks and its basal conglomerates contain locally derived clasts. In general, the conglomerates are poorly sorted and polymictic in the lower part of the Googhenama Formation while they are well sorted and quartz pebble-dominated (oligomicetic) higher up. From north to south on PEARANA, the Googhenama Formation contains fewer conglomerate beds and smaller clasts. Cross-bedding indicates palaeo-flow directions southeastward and northeastward away from the Pilbara Craton. The Pilbara Craton and Bangemall Basin appear to have provided source materials for the Tarcunyah Group in this area (Williams and Trendall, 1996b).

The locally derived and weathered granitic or gneissic clasts are good sources of uranium in addition to their protoliths in the Gregory Granitic Complex of the Pilbara Craton. Permeability is expected to be relatively high in the coarse-grained sandstones and conglomerates, making them fertile uranium source rocks and mineralisation host rocks. Favourable reductants do not seem to be present in the Googhenama Formation itself. However, the shale units in the overlying Waroongunyah Formation and mafic and ultramafic rocks in the basement could act as reductants/trap rocks for unconformity-related uranium mineral systems. It is unknown if the shale units contains carbonaceous materials. They may contain Fe⁺²-bearing silicates.

Thus it is considered that these systems have likely operated in the area with moderate to high potential and moderate certainty ([Table 7.5](#)).

7.3.1.1.3 Further assessment of potential

To further assess the potential of unconformity-related uranium mineral systems associated with the Tarcunyah-Archaean unconformity in the Warroo Hill-Mt Gregory area, the following work is recommended:

- Map possible alteration along and near the unconformity from ASTER data, which may indicate potential sites of mineralisation;
- Map gradients from magnetic data, which may assist determining potential trap sites; and,
- Evaluate the diagenetic history of the Googhenama Formation to assess the possibility that it could have formed fertile fluids for uranium mineralisation.

7.3.1.2 Potential of unconformity-related uranium associated with the Yeneena-Rudall unconformity

The Neoproterozoic Yeneena Basin consists of the Throssell Range Group and the Lamil Group in the Paterson area. The lithologies of the Throssell Range Group's constituent formations are listed in [Table 7.8](#). The unconformity between the Throssell Range Group and Rudall Complex is mapped in two areas ([Figure 7.9](#)):

1. The unconformity between the Coolbro Sandstone and Rudall Complex is mapped in surface and solid geology maps in the central and northern parts of the Rudall 1:250 000 map sheet area, including at Kintyre. This unconformity has drawn much attention because of the uranium deposit at Kintyre; and,
2. The unconformity is mapped between three different formations of the Throssell Range Group (Taliwanya Formation, Pungkuli Formation and Coolbro Sandstone) and the Rudall Complex. It is mapped on surface and solid geology maps in the McKay Range area, on both sides of the McKay Fault.

In the following sections we will first review how the unconformity is depicted in surface and solid geological mapping and in the AEM data ([Sections 7.3.1.2.1 & 7.3.1.2.2](#)) and then discuss the potential of the unconformity-related uranium mineral systems in the Kintyre-Rudall and McKay Range areas in light of available key data sets (Sections 7.3.1.2.3 to 7.3.1.2.5). This will be followed by some recommendations for further assessment of potential in Section 7.3.1.2.6.

Table 7.8: Throssell Range Group stratigraphy, after Czarnota *et al.* (2009a).

FORMATION	LITHOLOGY	COMMENT
Isdell Formation	Deep water carbonate with a higher silt component in the upper parts, which are intruded by dolerite sills.	Not suitable as source of oxidised diagenetic fluids.
Broadhurst Formation	Thinly laminated sandstones, siltstones and black shales with discontinuous carbonate lenses that generally fine upwards.	Not suitable as source of oxidised diagenetic fluids, but a good chemical trap.
Coolbro Sandstone	Regionally extensive (up to 2.5 km thick) fluvialite sandstone with minor shale interbeds that fine upwards.	Suitable to generate oxidised diagenetic fluids.
Pungkuli Formation	Shale, minor sandstone, carbonate, and pyritic shale.	Potential chemical trap.
Taliwanya Formation	Locally developed, immature, coarse conglomerate unconformably overlying basement.	Potential to generate oxidised diagenetic fluids.

7.3.1.2.1 The Coolbro-Rudall unconformity

The Kintyre uranium deposit is hosted in the Yandagooge Formation in the Talbot Terrane of the Rudall Complex, just below the Coolbro-Rudall unconformity ([Figures 7.9 & 7.11](#)). The deposit is located on the hanging wall of a major NW-trending and NE-dipping thrust fault ([Figure 7.11](#)) and is close to the outcropping unconformity. The Coolbro-Rudall unconformity has been mapped in surface and solid geology maps (Hickman and Clarke, 1993; Bagas, 1999a; Czarnota *et al.*, 2009a).

At AMG 030315 on BROADHURST (Hickman and Clarke, 1993), about 2.7 km northwest of Kintyre, the Coolbro-Rudall unconformity is mapped in a small outcrop of about 500 m across between the Coolbro Sandstone and quartz-muscovite schist of Yandagooge Formation. Here the Coolbro Sandstone is mapped as dipping 70° to the east-northeast while the Yandagooge Formation dips at 60° to the north. The unconformity is probably folded and is on the hanging wall of a major northwest trending and northeast dipping thrust. West of Kintyre on the foot wall of the northwest trending thrust, the unconformity is concealed under Permian and Cenozoic sediments in a drainage valley.

At AMG 941299 on THROSELL (Williams *et al.*, 1996), about 10 km west of Kintyre, the Coolbro-Rudall unconformity is mapped in the hinge area of a mesoscopic scale, northwest-plunging anticline with thrusts developed approximately parallel to the axial plane of the fold. The unconformity is between the basal polymictic conglomerate of the Coolbro Sandstone and orthogneiss derived from porphyritic biotite granitic rocks of Rudall Complex. Foliations in the orthogneiss dip at 50-60° to the northeast and east.

At AMG 184926 on RUDALL (Hickman and Bagas, 1996), for a segment about 1 km, the Coolbro-Rudall unconformity is mapped between the Coolbro Sandstone (including its basal polymictic conglomerate unit) and the Yandagooge Formation. Here the Yandagooge Formation is mapped as dipping 80° to the northeast while the Coolbro Sandstone dips 80° to the west. Mineral lineation in the Coolbro Sandstone at the unconformity plunges 70° to the north.

The basal polymictic conglomerate of the Coolbro-Rudall unconformity is also mapped in a number of other locations including over granitic gneisses of the Rudall Complex on THROSELL, BROADHURST and RUDALL. In most places the position of the Coolbro-Rudall unconformity on solid geology maps is inferred from the presence of Coolbro Sandstone and Rudall Complex rocks on either side of the unconformity.

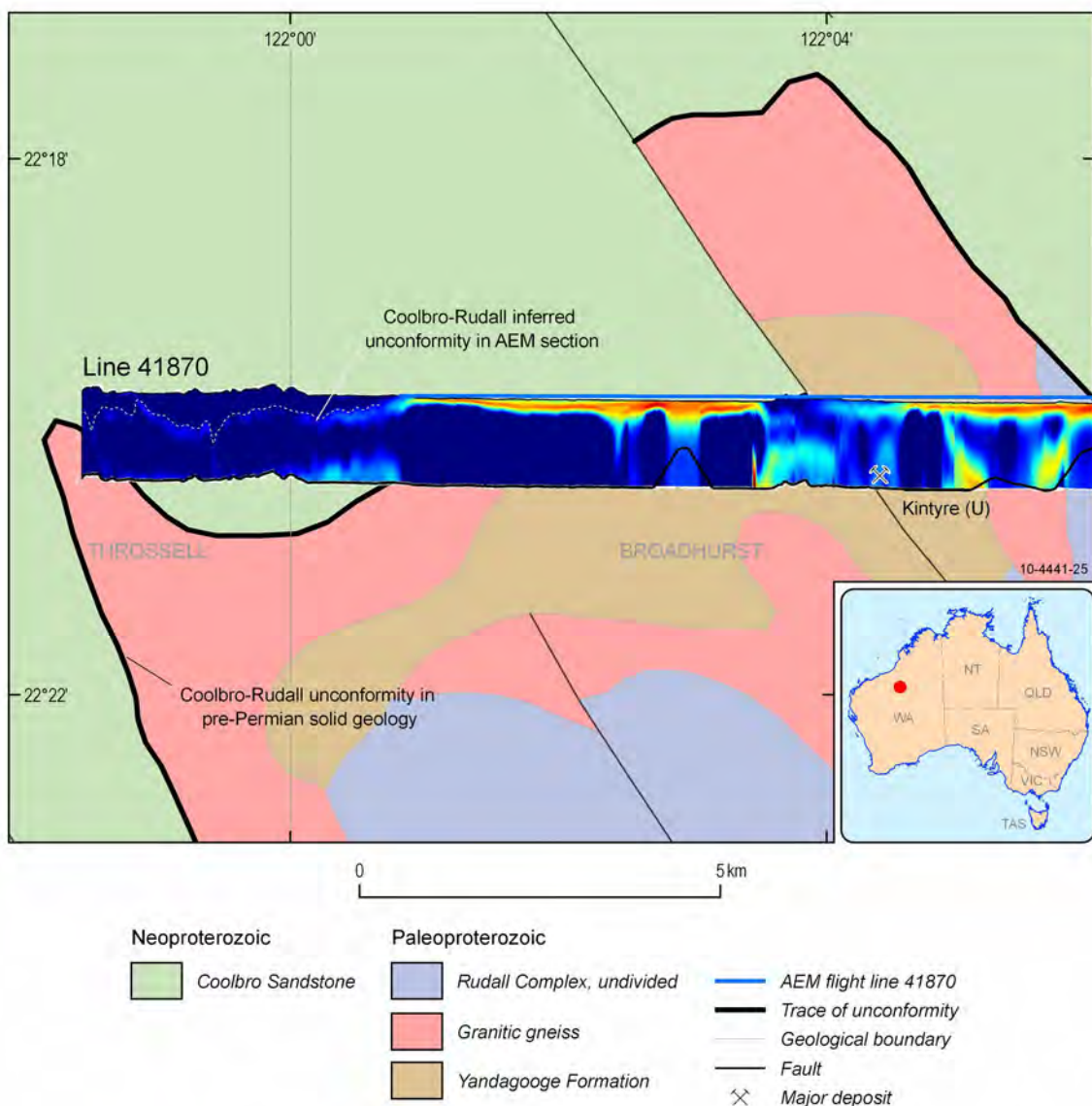


Figure 7.11: The Coolbro-Rudall unconformity depicted in a Geoscience Australia layered earth inversion (GA-LEI) AEM conductivity section for flight line 41870, west of Kintyre. The unconformity surface is traced with a dotted line on the section and 1:100 000 map sheet names and boundaries are shown. The GA-LEI AEM conductivity section of flight line 41870 is placed over pre-Permian solid geology. The GA-LEI conductivity section is 3 times vertically exaggerated. At the western end of the AEM conductivity section, the Coolbro-Rudall unconformity is shown in the section by continuous, sub-horizontal zigzag anomalies which separate the overlying Coolbro Sandstone from the underlying Rudall Complex. Both units have similar conductivities (generally resistive), although the Rudall Complex has small, weak conductors mixed throughout. The unconformity is a sub-horizontal undulating surface, dipping west ca. 200 m over 5 km. The zigzag shape of anomalies reflects the folded undulating unconformity surface. The elevated conductivity along the unconformity is probably due to palaeo-weathering of the Rudall Complex or later alteration at or below the unconformity surface. This GA-LEI AEM conductivity section is also described in Costelloe et al. (2010b), Chapter 4, Section 5.6 and Figure 5.25 of this Record.

Wherever the unconformity is mapped or inferred, it seems to have moderate to steep dips where it is trending northwest, which is the direction of major structural grain in the area. Most contacts in this direction are faulted. In addition, most Proterozoic rocks in the Paterson area are folded. This makes it difficult for AEM to detect the unconformity because of the structural complexity, high dip angle and depth of the unconformity. The unconformity is probably best mapped under cover by AEM data in the ridge areas of anticlines (in synclines the unconformity may be too deep for AEM to detect). One such area is west of Kintyre ([Figure 7.11](#); Costelloe *et al.*, 2010b). Here a segment of several kilometres of the Coolbro-Rudall unconformity between the Coolbro Sandstone and pelitic metasediments of the Yandagooge Formation and granitic gneiss of the Rudall Complex has been mapped in surface and solid geology maps. This segment of the unconformity lies at the hinge area of a regional anticlinorium which plunges to the northwest ([Figures 7.9 & 7.11](#)). From about AMG 003309 to AMG 971307 on the north side of the creek, bedding measurements recorded on BROADHURST show dips of 30° to 45° to the northeast. To the north, northwest trending thrusts dip moderately (55°) to steeply (80°) to the northeast.

The elevation of the interpreted unconformity falls away rapidly between line 40360 in the south and line 41860 in the north (Costelloe *et al.*, 2010b). The depth of the interpreted unconformity is consistent with the geological observations and interpretations of the area that the unconformity broadly dips to the northwest in the hinge area of the anticlinorium here. Further north, the unconformity may be deeper than the limit of detection of about 400 m for the AEM method deployed here.

To map the unconformity surface under cover from AEM data in other areas of the Paterson region, it is important to note the following points:

- Weathering and alteration may enhance conductivity along the unconformity, as seen in the example near Kintyre, but the conductivity difference between the weathered/ altered rocks along the unconformity and fresh rocks may be subtle, depending on the degree of weathering and alteration. In addition, the low contrast in conductivity between the Coolbro Sandstone and Rudall Complex may require special reprocessing of the AEM data including stretched colour look-up tables to display the processed AEM data to reveal subtle differences between the surrounding rocks and the unconformity.
- Proterozoic rocks in the Paterson Orogen experienced two regional deformation events that produced tight and inclined folds and thrust faults during the Miles Orogeny. The deformation events may have caused some contacts between Neoproterozoic sediments and the Rudall Complex to be faulted and dipping at moderate to high angles, mostly to the northeast. Such contacts may be difficult to distinguish from artefacts in the AEM data, which are often shown as moderate to steep-dipping features or "tails" in the vertically exaggerated conductivity sections.
- The depth of the unconformity in the area of investigation. The AEM method is more likely to detect and map the unconformity in the ridge area of anticlines of Neoproterozoic over Rudall Complex, such as in the area north of Kintyre. In the Paterson North survey area it is very likely that the depth of the unconformity increases towards the north and north-northwest away from the exposed Rudall Complex. In much of the survey area the Coolbro-Rudall unconformity may be close to or deeper than the optimum detection limit for the AEM method deployed (see DOI grid; [Figure 4.4](#)).

7.3.1.2.1.1 Potential of unconformity-related uranium in the Kintyre-Rudall area

A number of widespread reductants or trap rocks have been mapped in the Rudall Complex and Coolbro Sandstone in the Kintyre-Rudall area by GSWA's 1:100 000 surface geology mapping. [Figure 7.12](#) shows that the following reductants/trap rocks are mapped on BROADHURST (Hickman and Clarke, 1993) and RUDALL (Hickman and Bagas, 1996) in the Rudall Complex:

- Pyrite/graphite schist;
- Calc-silicate rocks with Fe⁺²-bearing minerals; and,
- Mafic and ultramafic rocks with Fe⁺²-bearing minerals.

In the Coolbro Sandstone the following reductants or trap rocks are noted:

- Shale or pelitic schist (the presence of carbonaceous materials unknown, may contain Fe⁺²-bearing silicates); and,
- Calcareous shale.

As seen from the distribution of reductants/trap rocks in the Rudall Complex and Coolbro Sandstone ([Figure 7.12](#)), and distribution of uranium occurrences ([Figure 6.2](#)), much of the Coolbro Sandstone and Rudall Complex near the Coolbro-Rudall unconformity and trap rocks are fertile grounds for unconformity-related uranium mineral systems in the Kintyre-Rudall area on BROADHURST, RUDALL, THROSSELL and POISONBUSH, thus potential is high for this type of uranium deposit with high certainty. Unconformity-related uranium deposits are expected below and above the Coolbro-Rudall unconformity, e.g., the Kintyre deposit.

7.3.1.2.2 The Taliwanya-Rudall unconformity

The Taliwanya-Rudall unconformity is mapped in 1:100 000 and 1:250 000 surface geology maps in the McKay Range area on both sides of the regional northwest-trending McKay Fault. South of the McKay Fault in the McKay Range area, the sandstone and conglomerate sequence of the Taliwanya Formation is mapped unconformably overlying the Rudall Complex. The Taliwanya Formation is overlain by the Pungkuli Formation, Coolbro Sandstone and Broadhurst Formation up-sequence. In parts, the Coolbro Sandstone and the Pungkuli Formation are also interpreted to unconformably overlie the Rudall Complex. The Taliwanya-Rudall unconformity defines a west-northwest trending anticline of about 5 km wide and 15 km long, plunging to the east-southeast ([Table 7.8](#), [Figure 7.13](#)).

As discussed above and in [Section 5.9](#), the Coolbro Sandstone and Rudall Complex are in general resistive. This seems to be the case for flight line 20280 in the Paterson South survey area ([Figure 7.13](#)). Much of the eastern two thirds of the GA-LEI conductivity section of Line 20280 is resistive (dark blue), although the Broadhurst Formation is clearly shown as conductive in this line and in line 20390. The Pungkuli Formation corresponds to thin moderate conductive anomalies north of the McKay Fault. Below the thin, horizontal conductive anomalies over the Pungkuli Formation are a number of thin and steep conductive anomalies in a dark blue background. These nearly vertical anomalies may correspond to carbonaceous beds and/or Fe-rich rocks in the Rudall Complex (graphitic shales, mafic rocks and banded iron formation). The McKay Fault is clearly depicted in lines 20540 and 20680.

In the southwest part of line 20390, the Coolbro Sandstone is shown as resistive, being dark blue in the conductivity section. Below it is a moderately conductive unit which may be the Pungkuli Formation or a conductive part of Rudall Complex such as the Yandagooge Formation.

7.3.1.2.2.1 Potential of unconformity-related uranium in the McKay Range area

South of the McKay Fault in the McKay Range area ([Figures 6.2 & 7.13](#)) the east-southeast plunging anticline is underlain by Rudall Complex, which consists of quartz-feldspar gneiss, orthogneiss derived from porphyritic biotite granitic rocks, quartzite, quartz-mica schist, metamorphosed argillaceous sedimentary rocks, banded iron formation, chert, pyrite-graphite schist and amphibolite (Bagas, 1997). The argillaceous rocks, banded iron formation, pyrite-graphite schist and amphibolite are potential reductants for unconformity-related uranium mineralisation.

Surface geology mapping in the McKay Range area at 1:100 000 scale was carried out by Bagas (1997) on GUNANYA and by Bagas and Smithies (1996) on CONNAUGHTON. Gunanya Sandstone mapped by Bagas (1997) and Bagas and Smithies (1996) in these areas was re-interpreted to be Coolbro Sandstone by Czarnota *et al.* (2009b) in their regional compilation of a 1:250 000 solid geology map for the Paterson area. No reductants were mapped in this unit here by either Bagas (1997) or Czarnota *et al.* (2009b).

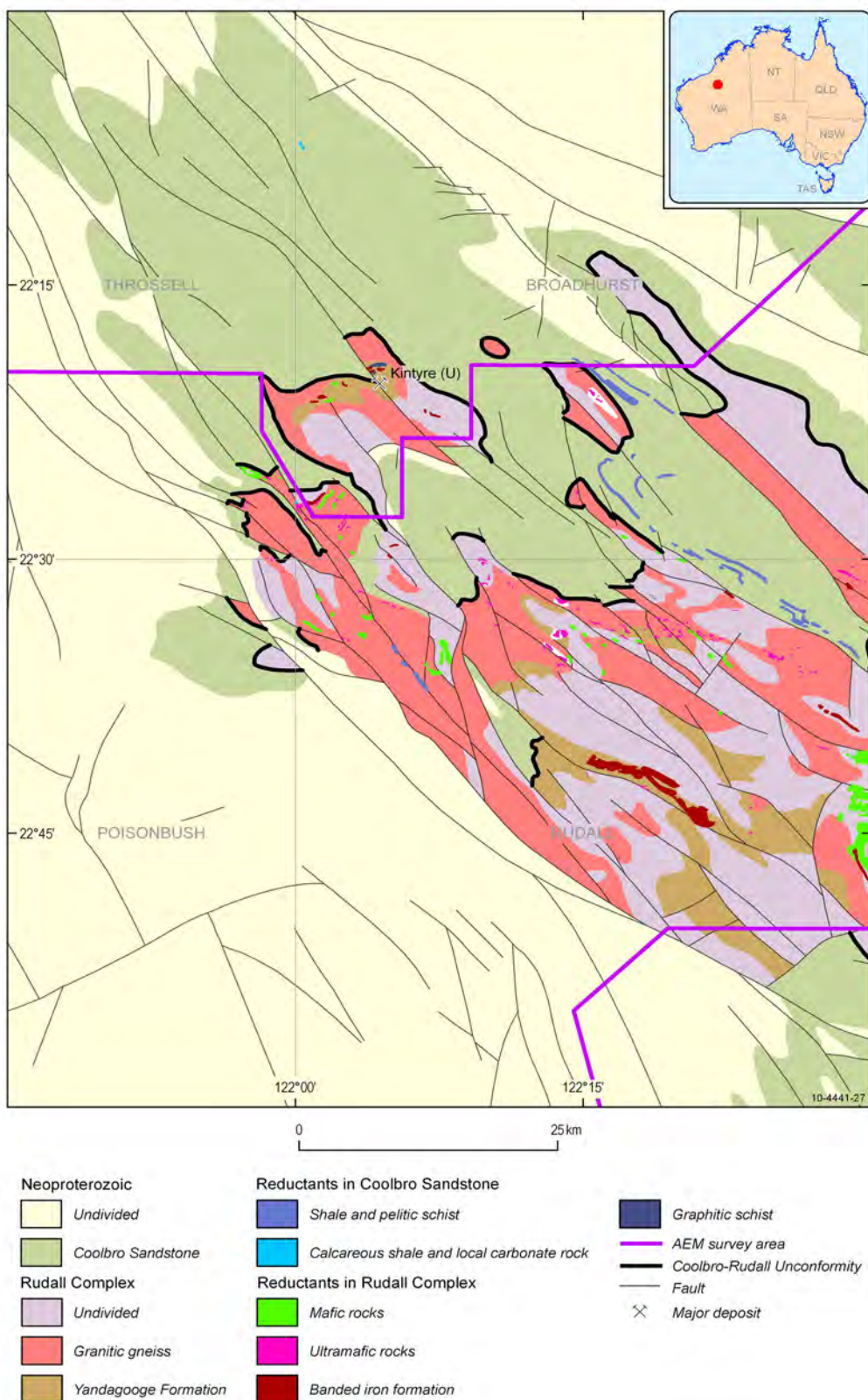


Figure 7.12: Potential trap rocks in the Rudall Complex and Coolbro Sandstone in the Kintyre-Rudall area.

The Taliwanya Formation is the basal formation of the Throssell Range Group in southern CONNAUGHTON and southeastern RUDALL, on both sides of the McKay Fault. It was formally defined by Bagas & Smithies (1998). The Formation is up to 170 m thick and is principally composed of polymictic conglomerate and arkosic sandstone with rare heavy mineral bands. The conglomerate is lenticular and interpreted as a channel-fill deposit. The Taliwanya Formation also contains thin interbeds of fine-grained lithic wacke, siltstone and shale, which become more abundant towards the conformable contact with the overlying Pungkuli Formation.

The Pungkuli Formation is mapped as reddish brown to grey shale, minor sandstone, carbonate and pyritic shale. The pyritic shale in the Pungkuli Formation could act as a potential reductant for uranium mineralisation. The Pungkuli Formation is about 900 m thick in the core of the McKay Anticline, but Cenozoic and Permian cover prevent an assessment of its thickness north of the McKay Range (Bagas and Smithies, 1998).

In summary, essential components for unconformity-related uranium mineral systems within the Taliwanya/Coolbro-Rudall unconformity are present in the McKay Range area:

- Uranium source rocks are readily available in the Rudall Complex (felsic igneous rocks);
- Fluvial sandstone and conglomerate sequences are present (Taliwanya Formation and Coolbro Sandstone);
- Favourable fault systems are present as fluid pathways; and,
- A range of reductants or trap rocks are present, including shale and pyritic shale mapped in the Pungkuli Formation, and mafic and ultramafic rocks in the Rudall Complex.

Thus the McKay Range area is considered to have moderate to high potential for unconformity-related uranium mineral systems with the Taliwanya/Coolbro-Rudall unconformity with moderate to high certainty ([Table 7.5](#)).

7.3.1.2. Further assessment of potential

Further assessment of potential for uranium minerals systems related to the Yeneena-Rudall unconformity requires more detailed mapping of trap rocks in the Rudall Complex and Coolbro Sandstone, indications of mineralisation from geological mapping, geophysical and remotely sensed data and analysis of favourable fault systems.

Other work to assist further assessment of potential could include:

- Detailed analysis of favourable fault systems as fluid pathways for mineralisation, such as the northwest thrust fault that hosts the Kintyre deposit;
- Indications of uranium deposition, which can be mapped regionally from radiometric data;
- Indications of alteration and mineralisation, which can be mapped from the distribution of mapped gossans and interpreted from remotely sensed data, e.g., ASTER data. Such mapping is important to define exploration targets below the unconformity, e.g., those hosted in the Yandagooge Formation of Rudall Complex; and,
- Three-dimensional geological modelling to depict the geometry of fold and fault systems.

7.3.1.3 Potential of unconformity-related uranium associated with the Karara-Rudall unconformity

On BLANCHE-CRONIN, the Tarcuryah Group is mapped to unconformably overlie the rocks of the Throssell Range Group and the Rudall Complex (Bagas, 1999b). Here the Tarcuryah Group includes the Karara Formation and unassigned units of shale, siltstone, sandstone and dolomite. The Karara Formation is restricted to a small area along the Camel-Tabletop Fault Zone and north of McKay Fault ([Figures 7.9 & 7.13](#)). It correlates with Googhenama Formation at the eastern margin of NULLAGINE; both are at the lowest part of Tarcuryah Group ([Table 7.6](#)).

The Karara Formation consists of medium- to coarse-grained, characteristically light pink to purple, arkosic sandstone, interbedded with thin beds of feldspathic granule to pebble conglomerate at the

base and overlain by thinly bedded dolomite. Conglomerate at the base of the Karara Formation is matrix-supported, crudely bedded and cross-bedded and contains well-sorted, rounded pebbles of vein quartz, sandstone from the Throssell Range Group and various rock types from the Rudall Complex. The conglomerate is about 350 m thick and grades upward into sandstone. The basal part of the conglomerate is interbedded with siltstone and shale and contains rare, sheared basalt or fine-grained doleritic sills. The matrix of the mafic rock is pervasively hydrothermally altered to a fibrous sericite-chlorite assemblage. The basal conglomerate is common within the Camel-Tabletop Fault Zone, indicating that the Zone may have been an active growth fault during the deposition of the Karara Formation under shallow water conditions (Bagas *et al.*, 2000).

The AEM dataset clearly shows a conductivity anomaly along the Camel-Tabletop Fault Zone ([Figure 7.13](#)). The higher conductivity along the fault zone may be due to saline ground water in it, but is most likely due to Karara Formation rocks caught within the fault zone. It is clear that there are sharp conductivity contrasts across some faults in the area interpreted to be Karara Formation (e.g., flight lines 20540, 20680 & 20820 in [Figure 7.13](#)). Parts of the Karara Formation seem to be moderately conductive (lines 20820 & 10280).

There are a number of copper, lead, zinc and gold prospects in the Karara Formation. Locations of these are shown in [Figure 6.2](#). East of No. 23 Well (e.g., AMG 207547 and AMG 287491) the Karara Formation is hydrothermally altered and mineralized with gold and base metals near fine-grained, sheared mafic rocks (Bagas, 1999b). As discussed in [Chapter 6](#), during the Miles Orogeny there was a close association of uranium and copper mineralisation and these occurrences may also indicate some potential for uranium mineralisation associated with the Karara Formation.

No reductants are mapped in the Karara Formation on Blanche-Cronin, but a variety of reductants are mapped in the Connaughton and Tabletop terranes of the Rudall Complex, including amphibolites and ultramafic rocks. It is considered that, in the area of mapped and interpreted Karara Formation, there is moderate potential for unconformity-related uranium mineral systems.

Future work to assess the potential of this type of uranium mineralisation may include:

- Mapping of alteration from ASTER data; and,
- Mapping of any significant trap rocks (reductants) in the Karara Formation.

7.3.2 Stratabound uranium-copper mineral systems associated with the Broadhurst-Coolbro contact

As discussed in [Chapter 6](#) and [Section 7.1](#), stratabound uranium-copper mineralisation (“Nifty-style”) associated with the Broadhurst-Coolbro contact in the Paterson area was formed in the same process of the Miles mineral system as for the unconformity-related uranium mineral systems during the late stage of Yeneena Basin development (840-830 Ma) and inversion of the Basin (830-810 Ma) during Miles Orogeny ([Figure 7.8](#)).

These stratabound uranium-copper deposits are stratigraphically and structurally controlled. The stratigraphic controls are best demonstrated by the uranium-copper prospects localised along the Coolbro-Broadhurst contact and by the presence of copper deposits within carbonate-rich intervals of the upper Broadhurst Formation. Structurally, copper deposits in the upper Broadhurst Formation are associated with D₄ folds. Uranium-copper deposits along the contact between the Coolbro Sandstone and Broadhurst Formation appear to be associated with the northeast-dipping faults and with a second set of faults with a northerly trend (see [Section 6.2.4](#)). Based on the available information, it is considered that some of these deposits are related to oxidised fluids generated by the diagenesis of sediments of the Coolbro Sandstone (see [Chapter 6](#) for discussions in detail). These diagenetic fluids flowed along the upper part of the Coolbro Sandstone. When reduced by reductants in the Broadhurst Formation at suitable structurally controlled trap sites, mineralisation occurred (for example “Nifty-style” at site E on [Figure 7.8](#)).

Important components for assessing the potential of stratiform uranium-copper mineral systems associated with the Broadhurst-Coolbro contact in the Paterson area are summarised in [Table 7.9](#).

Table 7.9: Key mappable criteria for assessing potential of stratabound uranium-copper associated with the Broadhurst-Coolbro contact in the Paterson area.

QUESTION*	MAPPABLE CRITERIA	SOURCE DATA
Q4	Contact between Broadhurst Formation and Coolbro Sandstone.	Solid geology map (Czarnota <i>et al.</i> 2009b; Figure 6.2).
Q5	Reduced parts of the Broadhurst Formation near the contact, i.e., conductive zones of the Formation.	AEM data (Figures 7.14 & 7.15).
Q4	Fluid pathways (faults).	Surface & Solid geology, magnetic data, AEM data.
Q5	Indications of mineralisation-related alteration and deposition of uranium, in particular hematitic alteration zones in the Coolbro Sandstone.	ASTER data.

*Questions are as follows (after Barnicoat 2007):

- Q1: What is the geodynamic and P-T-t history of the system?
- Q2: What is the architecture of the system?
- Q3: What are the characteristics and sources (reservoirs) of water, metals, ligands and sulphur?
- Q4: What are the fluid flow drives and pathways?
- Q5: What are the transport and depositional processes for metals, ligands and sulphur?
- Q6: How and where do later geological processes allow preservation of deposits?

The mapping of alteration and deposition of uranium is beyond the scope of this study. In the following sections we will discuss the major faults in the area ([Section 7.3.1](#)), some of which are new structures interpreted in this study, and the electrical conductivity of the Broadhurst Formation ([Section 7.3.2](#)). These address the questions of fluid pathways and reductants for the stratabound uranium-copper mineral systems associated with the Broadhurst-Coolbro contact in the context of mineral systems assessment.

7.3.2.1 Major faults

Using magnetic and gravity data, in conjunction with surface geology mapping data, we have interpreted several new major faults in the Paterson area ([Figure 6.2](#)). The Isdell Formation is interpreted to have been deposited largely in a trough bounded by the Trotman Hill Fault and the Warrabarty-Coolbro faults. The Coolbro Sandstone is interpreted to be in fault contact with the Isdell Formation along the Coolbro Fault. The Mt Eva and Camel-Tabletop Fault Zone and the Maroochydore Fault are interpreted to join the Warrabarty Fault and Coolbro Fault southeast of Goosewhacker. These are crustal-scale faults and have probably been long lived, pre-dating the deposition of the Yeneena Basin sequences. They might have been re-activated during basin inversion, during the Miles Orogeny and later during the Paterson Orogeny. They are expected to be fluid pathways during these times for the Miles mineral system. Folds and secondary faults are potential trap sites for mineralisation.

Known Broadhurst Formation-hosted copper-zinc-lead mineral occurrences are mainly in two areas. One is the Maroochydore and Broadhurst-Sunday Creek area, where there are several major faults, e.g., the Coolbro Fault, the Maroochydore Fault and Mt Eva and Camel-Tabletop Fault Zone. The second area is around Rainbow-Nifty-Finch in the vicinity of the Vines Fault and the McKay Fault.

We draw attention to the area around Moses Chair, to the south of it, and west of Lead Hills and Wanderer. Here folded and faulted sequences of Broadhurst Formation and Coolbro Sandstone are in close proximity to, and are probably on the hanging wall of, the McKay Fault. There is potential for similar mineralisation here.

7.3.2.2 Conductive Broadhurst Formation

Most, if not all, of the stratabound uranium-copper deposits and prospects are hosted in the lower part of the Broadhurst Formation, in close spatial association with conductive zones as determined from ground EM and AEM data (see [Chapter 6](#) and Czarnota *et al.*, 2009a; 2009b). Thus, mapping of the conductive parts of the Broadhurst Formation is very critical for exploration of the mineralisation associated with the Broadhurst Formation. Geoscience Australia's AEM dataset provides a powerful and efficient way to do so regionally.

Using exploration company-provided ground EM and AEM data, Czarnota *et al.* (2009a; 2009b) mapped a separate conductive unit of the Broadhurst Formation in their 1:250 000 Proterozoic solid geology map for the Paterson area. Much of their mapped conductive Broadhurst Formation is confirmed in the GA's new regional AEM data ([Figures 7.14 & 7.15](#)). However, there are discrepancies. New interpretation is required to map the conductive parts of the Broadhurst Formation consistently across the regional AEM survey area.

The Broadhurst Formation is a 1000-2000 m thick succession of carbonaceous shale, turbiditic sandstone-shale and minor sandstone, dolomite and limestone. It is most completely exposed in the Broadhurst Range between Sunday Creek and Coolbro Creek. Hickman and Clarke (1994) produced a generalised stratigraphic column for all but the upper-most part of the Formation (also see [Section 3.2.2.3](#)):

- Fault contact with overlying Isdell Formation;
- Carbonaceous shale and local sandstone and siltstone;
- Sulfidic units in shale, dolomite and limestone;
- Turbiditic argillaceous greywacke; local graded bedding and slump structures; and,
- Shale containing pyrite-pyrrhotite, local pebbly sandstone and local dolomite, at the base

Lateral facies variations were observed on BROADHURST. Outside the Broadhurst Range, outcrops of the Broadhurst Formation are generally small and isolated. The absence of distinctive marker beds does not allow recognition of stratigraphic levels (Hickman and Clarke, 1994). In places the Broadhurst-Coolbro boundary is transitional (Bagas, 2004b).

The Broadhurst Formation is variably sulfidic, with up to 10 vol. % pyrite and pyrrhotite present near the base of the unit. Pyrrhotite is abundant at the base, giving a distinctive aeromagnetic signature (Hickman and Clarke, 1993). At Maroochydore, dolomitic siltstone grades upward into highly carbonaceous and sulfidic shale, some of which comprises up to 80 vol. % frambooidal pyrite (Reed, 1996).

The Broadhurst Formation is also variably organic-rich. At Maroochydore, the analysis of a carbonaceous shale from the footwall succession contains a total organic content of 2.9 wt. %, but a mudstone sample yielded a total organic content of 0.5 wt. %. Two samples from the hanging wall succession contain a total organic content of 0.5-0.9 wt. % (Reed, 1996).

The carbonaceous materials and sulfides in the Broadhurst Formation are the sources of much of the high conductivity of this unit and are potential reductants for mineralisation. At Maroochydore, in the mineralised horizon and footwall carbonaceous shales, Reed (1996) reported conductivity values of 70 S/m, which is significantly higher than non-carbonaceous and pyrite-poor rocks, with conductivities in the range of 5 to 10 S/m. Reed (1996) used the conductivity contrast to map out host sequence and structure in the subsurface at Maroochydore.

The presence of high quantities of carbonaceous material, combined with the presence of significant carbonate-dominated intervals and local sulfide-rich zones, make the Broadhurst Formation highly reactive with hydrothermal fluids, particularly oxidised fluids, to produce uranium-copper-zinc-lead mineralisation associated with the formation. Geochemical modelling shows zonation of uranium-copper-zinc-lead mineralisation occurs when oxidised fluids encountered reductants, with uranium being the first mineral to precipitate (Bastrakov *et al.*, 2010; see [Chapter 6](#)).

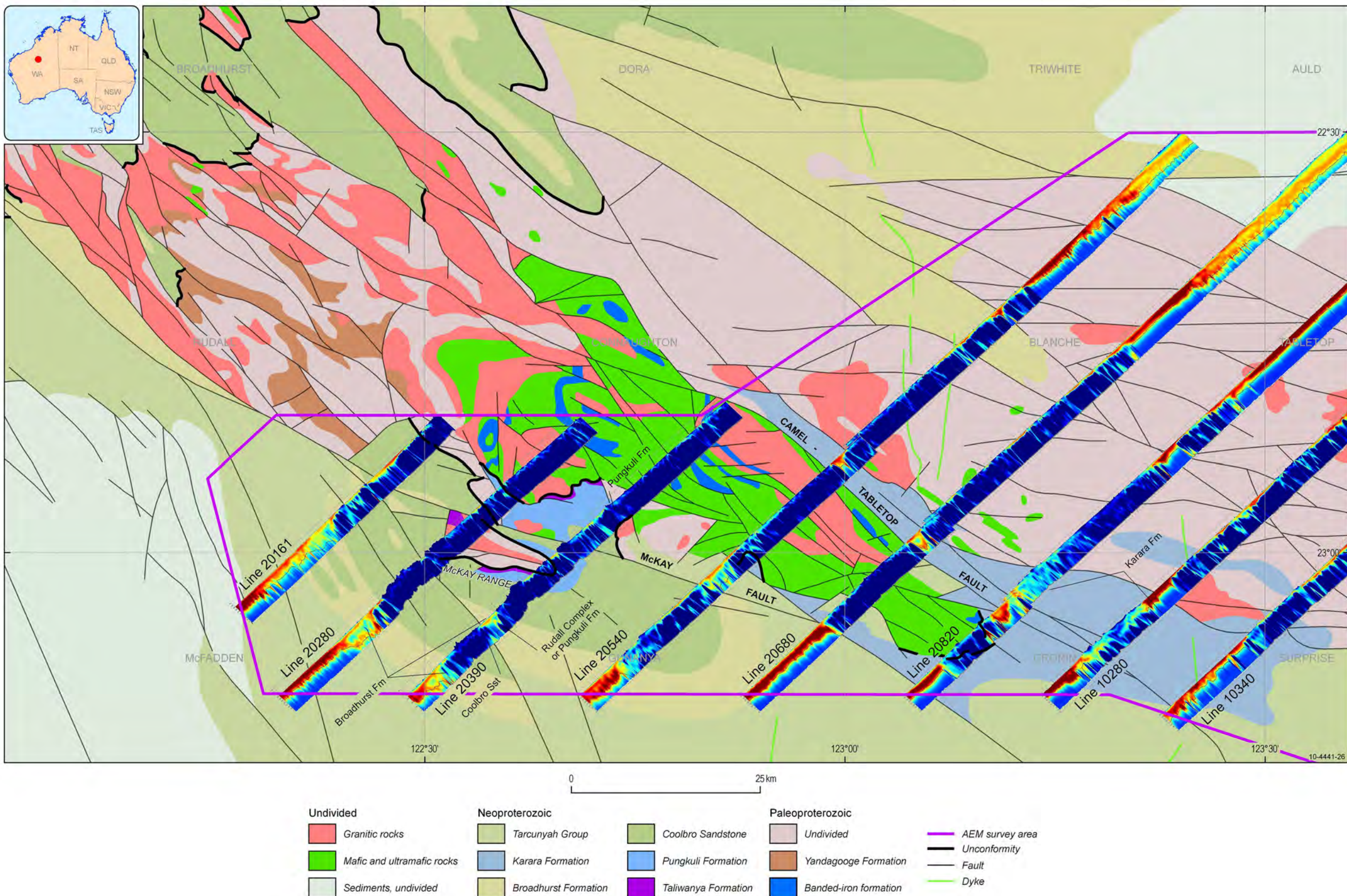


Figure 7.13: Conductivity sections over pre-Permian solid geology in the Paterson South survey area (1:100 000 map tiles shown). Conductivity colour bar shown in Figure 4.8.

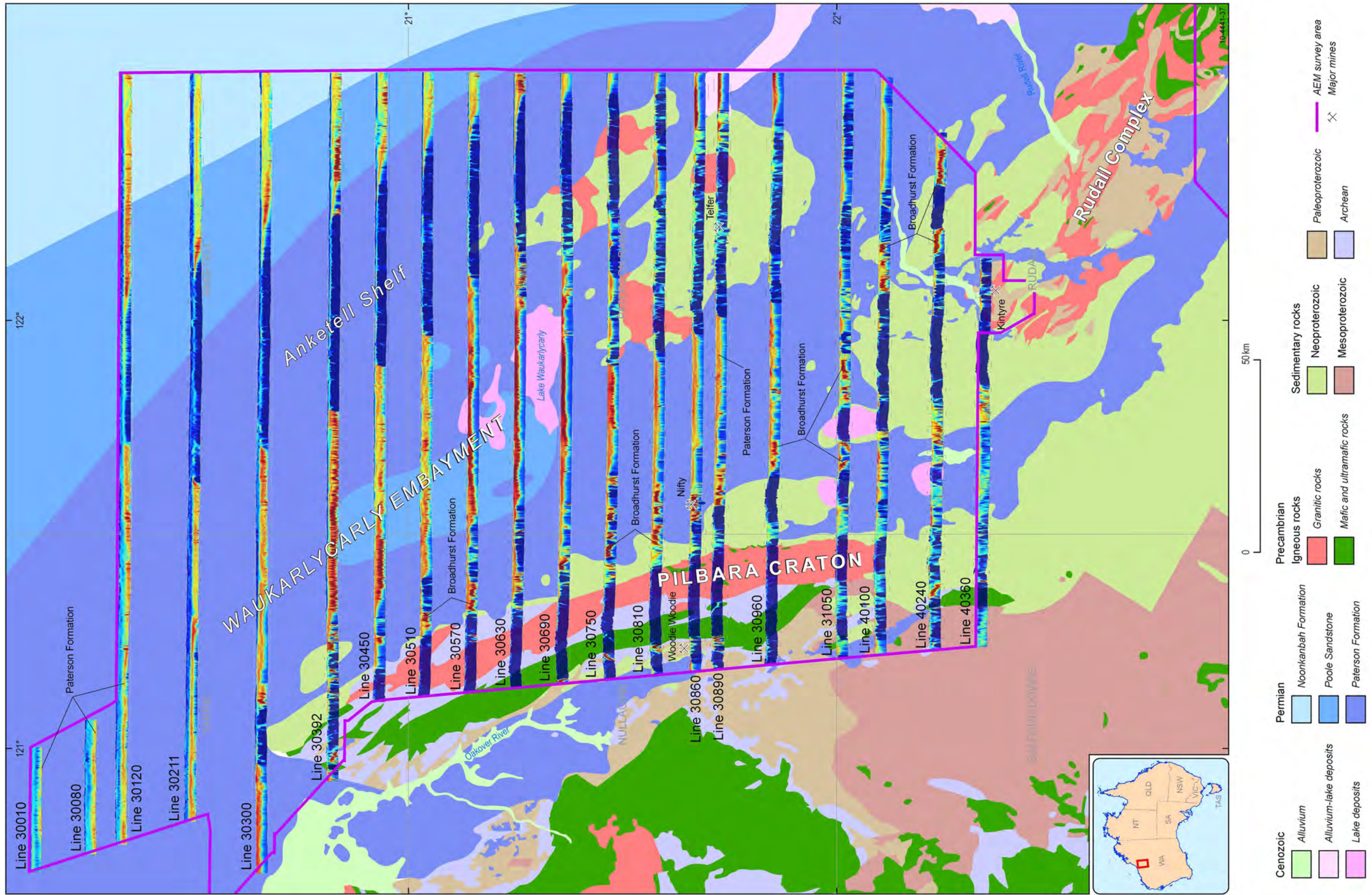


Figure 7.14: Selected AEM conductivity sections over pre-Permian solid geology in the Paterson area. Conductivity colour bar shown in Figure 4.8.

The close spatial association of uranium mineralisation with copper, lead and zinc mineralisation in the Proterozoic in the Paterson Orogen, including the Rudall Complex, is well illustrated in [Figure 6.2](#), which shows that eight of the nine uranium occurrences in the area are associated with copper, lead and zinc mineralisation. This association is useful in assessing the potential of uranium-copper mineral systems associated with the Broadhurst-Coolbro contact.

The highly conductive parts of Broadhurst Formation are readily mappable under Cenozoic and Permian cover in the regional AEM data and may be used to map fold structures under cover. Examples of these are shown in [Figures 4.10, 5.5, 5.7, 5.11, 5.34](#) and [7.14](#). Major conductive parts of the Broadhurst Formation are outlined in a GA-LEI 0–400 m conductance image in [Figure 5.5](#) and [5.11](#) and on a GA-LEI conductivity depth slice at 150 m on [Figure 7.15](#) (see discussions in [Chapter 5](#)).

7.3.2.3 Further assessment

Further assessment of potential for the stratabound uranium-base metal (copper, lead-zinc) mineral systems associated with the Broadhurst-Coolbro contact should aim to map potential trap sites, mineralisation associated alteration and indications of mineralisation. The following datasets will be useful in this assessment:

- Distribution of redox gradients (particularly the presence of hematitic alteration in the Coolbro Sandstone), some of which may be mapped from magnetic data;
- Distribution of muscovite alteration as interpreted from ASTER data;
- Distribution of surface carbonate as interpreted from ASTER data; and,
- Sites of analysed gossans, including those geochemical analyses from GSWA's 1:100 000 surface geology mapping.

7.4 SANDSTONE-HOSTED URANIUM MINERAL SYSTEMS

Sandstone-hosted uranium mineral systems include those in confined aquifers (also known as *roll-front* and *tabular* types) and those in palaeochannels (also known as *basal channel* type). Both these types of deposits are generally confined to sediments deposited in continental fluvial or marginal marine (mixed fluvial-marine) environments.

Sandstone-hosted uranium deposits within confined aquifers form where uranium-bearing oxidised groundwater moving through sandstone aquifers reacts with reducing materials ([Figure 7.16](#)). In a single fluid situation ([Figure 7.16A](#)), uranium carried in oxidised groundwater is reduced by *in situ* reductants (e.g., organic materials) in the sandstone unit. Groundwater moves faster in the central part of the aquifer than along contacts with overlying or underlying less permeable units (e.g., mudstone), thus roll-front ore bodies form. In a two-fluid situation ([Figure 7.16B](#)), uranium in oxidised groundwater is reduced by hydrocarbons and/or H₂S released from an underlying oil and/or gas field. Both roll-front and tabular ore bodies may form. The locations of ore zones and the sizes of mineral deposits depend on the abundance and reactivity of the reductant (Jaireth *et al.*, 2008).

Sandstone-hosted uranium deposits in palaeochannels are formed in processes similar to roll-front and tabular deposits, but are closely linked with the evolution of palaeodrainage systems in the area (Dahlkamp, 1993; Jaireth, 2010), for example at the Beverley deposit ([Figure 7.17](#)). The mineralisation is located in fluvial palaeochannels incised into older rocks, some of which often contain uranium-rich felsic rocks. The key components and mappable criteria used for assessing the potential of sandstone-hosted uranium systems in the Paterson area in this study are summarised in [Table 7.10](#).

In the following sections we will first summarise the AEM responses of Permian and younger sediments, and palaeochannels, before discussing the potential of sandstone-hosted uranium mineral systems in the Paterson area.

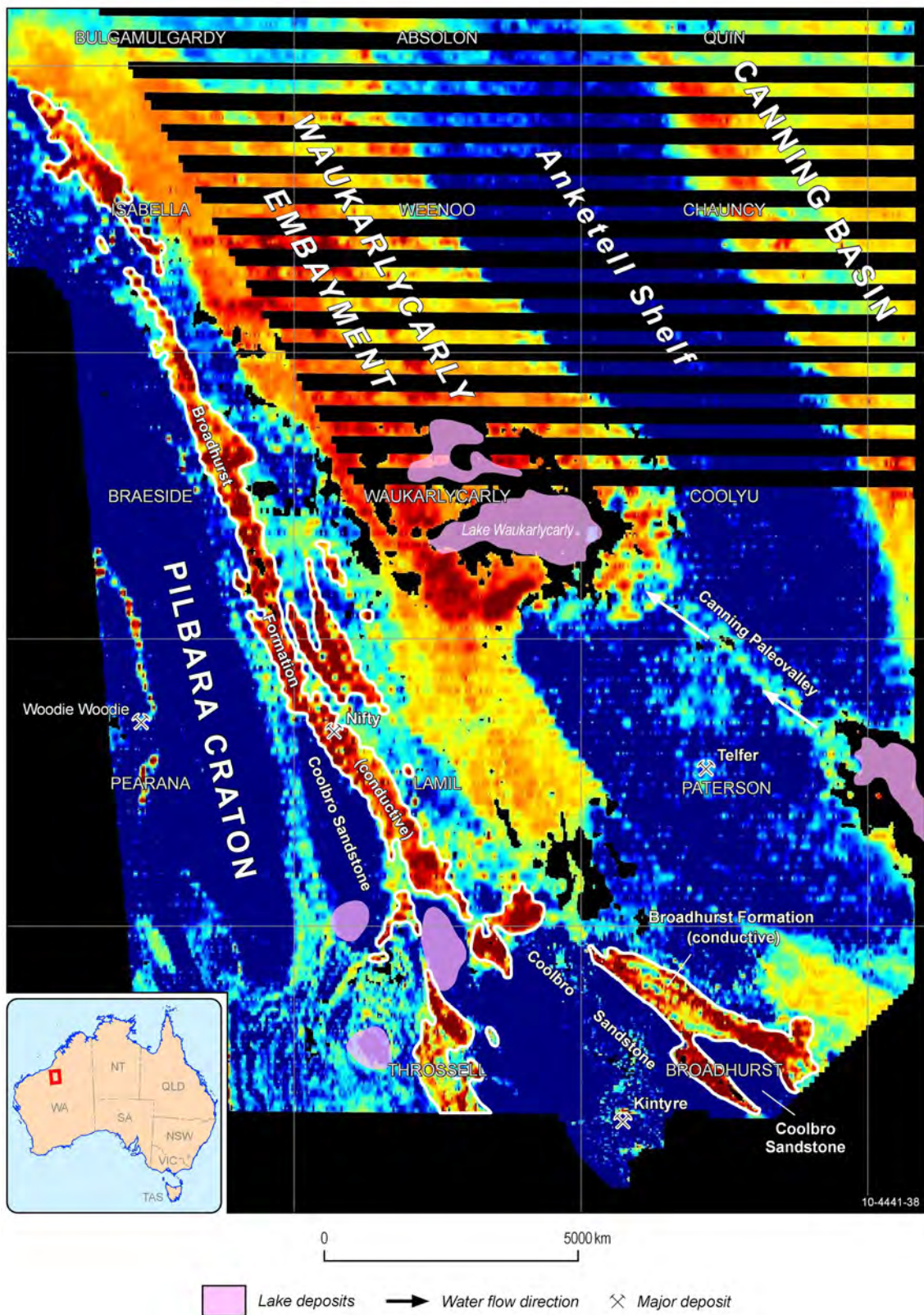


Figure 7.15: GA-LEI conductivity depth slice at 150 m for the Paterson North survey area. Lake polygons are displayed at 25% transparency and 1:100 000 map tiles are shown.

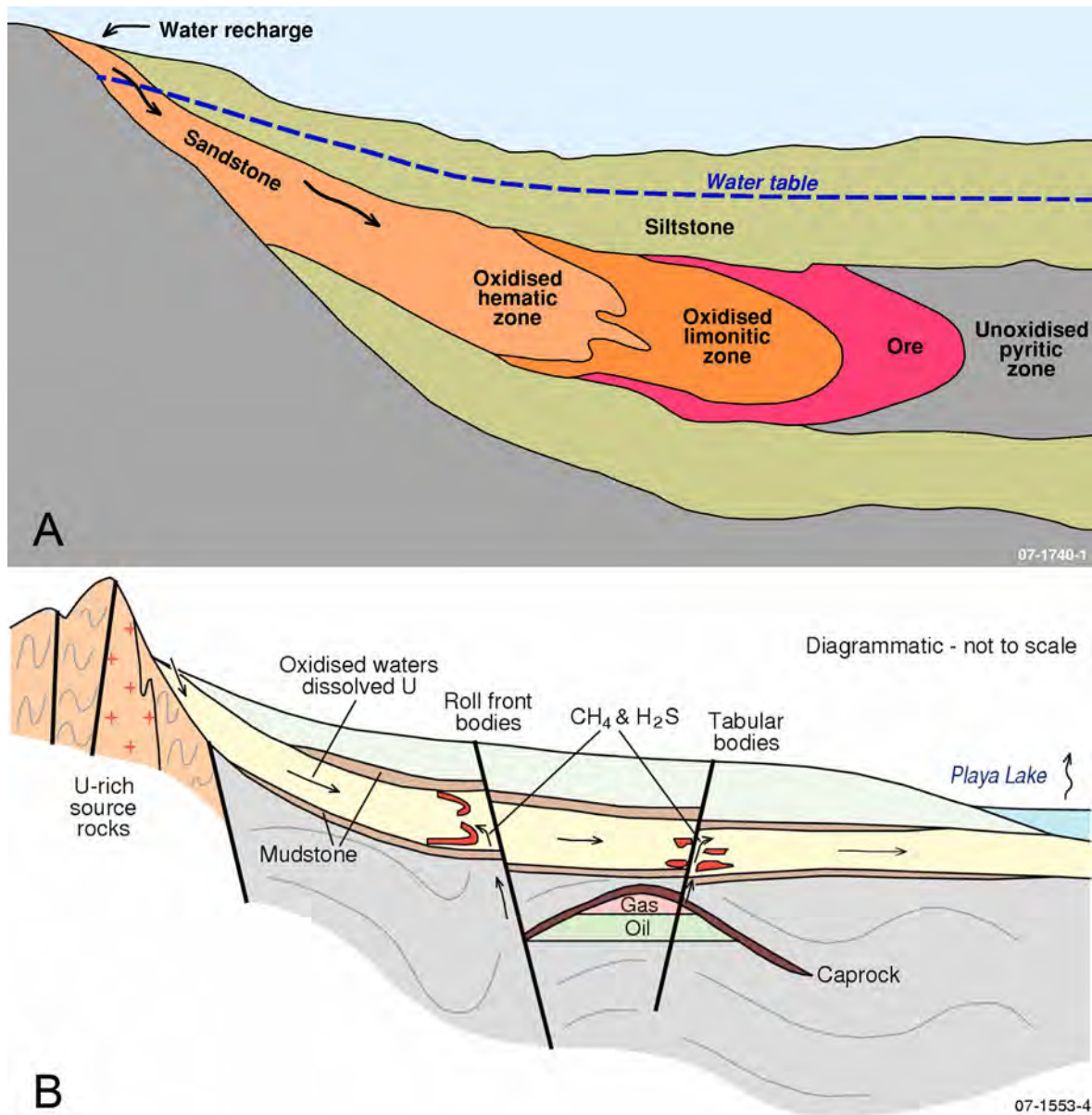


Figure 7.16: Conceptual models of sandstone-hosted uranium mineral systems, after Jaireth *et al.* (2008): A. single fluid model; B. two-fluid model.

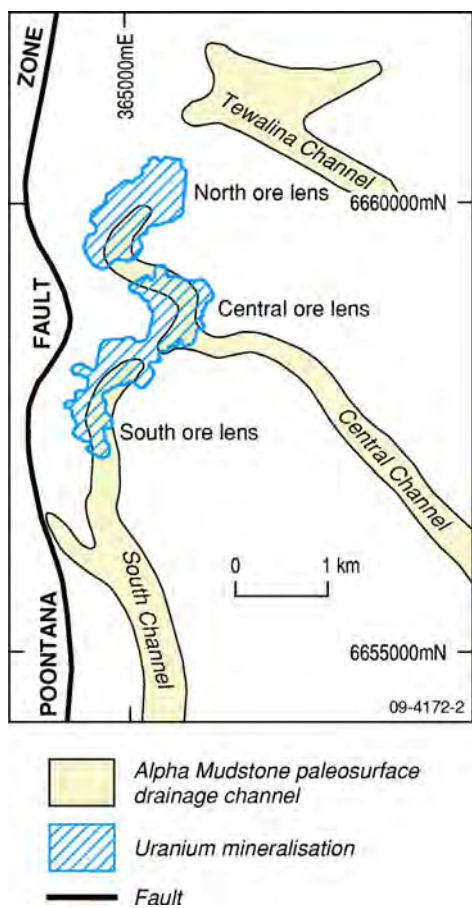


Figure 7.17: Palaeovalley-palaeochannel type sandstone-hosted uranium deposit at Beverley, South Australia, after Jaireth (2010).

7.4.1 AEM responses of Permian and younger sediments

The AEM data are very effective in mapping conductive geological units in shallow crust, including palaeovalleys or palaeochannels (see [Section 5.7](#)), which are filled by Permian and younger sediments. [Figure 7.14](#) shows selected conductivity sections over pre-Mesozoic solid geology. These provide background information for assessing potential of sandstone-hosted uranium mineral systems in the Paterson region.

7.4.1.1 Permian and Mesozoic sequences

The Permian solid geology and glacial flow directions are shown in [Figure 3.8](#), produced with information from the 1:250 000 surface geology mapping, The Bureau of Mineral Resources' Canning Basin 1:1 000 000 geology map (Towner *et al.*, 1980) and a drill hole database compiled by Roach (2009). Glacial flow directions are from the surface geology mapping. The Permian and Mesozoic stratigraphy is summarised in [Tables 3.8](#) and [3.9](#).

In the Paterson AEM survey areas much of the Permian succession consists of the Paterson Formation. It is well depicted in the AEM data throughout the survey areas. It is shown to include a conductive unit, although it is not known how much of the Paterson Formation is non-conductive. In the northwest corner of the Paterson North survey area, the Paterson Formation seems to have been little disturbed structurally ([Figure 7.14](#)). Here the conductivity anomaly associated with the Paterson Formation is buried at 200–300 m depth (flight lines 30010, 30080 and 30120). The cover sequence of this unit consists of Mesozoic and Quaternary materials and groundwater may be less saline, resulting in lower conductivity.

Table 7.10: Key mappable criteria for assessing sandstone-hosted uranium mineral systems, modified after Table A5 of Skirrow *et al.* (2009).

QUESTION*	MAPPABLE CRITERIA	SOURCE DATA
Q3	Felsic igneous rocks as uranium sources.	Surface geology maps, radiometric data, geochemistry data.
Q2, Q4	Highly permeable coarse-grained sandstone (often semi-consolidated) over- and underlain by impermeable shale/mudstone.	Surface and solid geology.
Q5	Presence of in situ organic materials or other reductants (sulfides, Fe ⁺² -bearing silicates and oxides) and/or mobile reductants (hydrocarbons and associated gases such as H ₂ S).	Surface and solid geology maps.
Q4, Q2	Palaeovalley.	Remotely sensed data and surface geology maps.

*Questions are as follows (after Barnicoat 2007):

- Q1: What is the geodynamic and P-T-t history of the system?
- Q2: What is the architecture of the system?
- Q3: What are the characteristics and sources (reservoirs) of water, metals, ligands and sulfur?
- Q4: What are the fluid flow drivers and pathways?
- Q5: What are the transport and depositional processes for metals, ligands and sulfur?
- Q6: How and where do later geological processes allow preservation of deposits?

Elsewhere, the conductivity anomaly of the Paterson Formation may be complicated by structures, groundwater salinity and conductive components in drainage systems above the Formation and conductive units below the Formation. In flight lines 30120 and 30210, in the northern part of Paterson North survey area, interpretation of the conductivity sections suggest that the Paterson Formation is affected by faults in the Waukarlycarly Embayment ([Figures 5.16](#) and [7.14](#)).

In the northeast of the Paterson North survey area, the AEM data clearly show that the Paterson Formation, Mesozoic and younger sediments on-lap Proterozoic sediments of the Anketell Shelf (Lamil Group) ([Figures 5.6](#), [5.14](#), [5.18-5.20](#), [5.22](#) and [7.14](#)). One such example is at the east end of line 30300 ([Figures 5.22](#) and [7.14](#)), where sequences of the Permian Noonkanbah Formation, Poole Sandstone and Paterson Formation are interpreted to unconformably overlie Neoproterozoic Yeneena Basin sediments. A thin layer (ca. 50 m) of Quaternary and Mesozoic sediments and regolith overlie the Permian sequences disconformably. West of the Waukarlycarly Embayment, in the Throssell Shelf area, the Paterson Formation is often seen as overlying conductive Neoproterozoic Broadhurst Formation, as such in line 30630.

Form lines of the top of the major resistor are interpreted in [Chapter 5](#) ([Figure 5.19](#)). These form lines are interpreted to approximate the sub-Permian surface in most parts of the area and also correlate with known palaeovalley systems (see [Section 5.7](#)).

7.4.1.2 Mapping palaeovalleys with AEM

The Paterson AEM dataset clearly shows several major palaeovalleys, including the Canning Palaeovalley and Disappointment Palaeovalley (see [Chapter 5](#)). The Canning Palaeovalley, north and east of Telfer, connects groundwater flow from Lake Dora to Lake Waukarlycarly. [Figure 7.15](#) is a conductivity depth slice of the Paterson North survey area at 150 m. It clearly shows resistive areas of the Pilbara Craton, Coolbro Sandstone and the Anketell Shelf. Linear, moderate to high conductivity anomalies (reddish-orange) mostly correspond to conductive parts of the Broadhurst Formation. The Waukarlycarly Embayment and Canning Basin correspond to broad moderate anomalies in the AEM data.

The Canning Palaeovalley north and east of Telfer is well depicted in [Figure 7.15](#). This palaeovalley may be filled with Eocene to Oligo-Miocene (Magee, 2009) sediments incised into Permian sediments ([Figures 3.8 & 5.30](#)), although there is no drill hole data in the palaeochannel to verify this assertion. As Permian sediments are thin in the area, it is likely that the palaeochannel has also incised the Proterozoic basement.

The Disappointment Palaeovalley is largely concealed under Cenozoic sands and sand dunes, but it is clearly depicted in the AEM data ([Figures 5.31 & 7.18](#)). It connects water flow from Lake Disappointment to Lake Winifred ([Figure 7.18](#)). The northern part of this palaeovalley, near Lake Winifred, appears to enter Permian sediments in the Permian solid geology map ([Figure 3.7](#)), but it is also likely that this palaeovalley is filled with Eocene to Oligo-Miocene sediments (Magee, 2009) and that it also incises into Proterozoic rocks.

7.4.2 Potential for sandstone-hosted uranium mineral systems

Most significant sandstone-hosted uranium deposits in the world are hosted in Devonian or younger sediments (Dahlkamp, 1993). The lack of abundant plant-derived organic material in older sediments limits the possibility of sandstone-hosted uranium deposits in them. Hence, in the Paterson area the potential of sandstone-hosted uranium mineral systems is mainly within Permian and younger sediments and palaeochannels.

Mesozoic sediments crop out or are interpreted to be present north of the Percival Palaeovalley on PATERSON RANGE and YARRIE, east of Lake Dora and Lake Disappointment, and in the Disappointment Palaeovalley ([Figures 5.31 and 7.18](#)). However, uranium-rich pre-Permian felsic igneous rocks, including those in the Pilbara Craton, Rudall Complex and the Mt Crofton Granite Suite in the Telfer area, lie on the southwest side of the Percival Palaeovalley from the eastern part of YARRIE to Lake Winifred, west of the Disappointment Palaeovalley, or northwest of Lake Disappointment ([Figure 3.8](#)). Uranium from these rocks is not interpreted to be available for sandstone-hosted uranium deposits in the preserved Mesozoic sediments from YARRIE to Lake Winifred and east of the Disappointment Palaeovalley. Thus, the potential of sandstone-hosted uranium mineral systems is low in these rocks.

In the following sections we will examine the potential of sandstone-hosted uranium mineral systems associated with the Permian Paterson Formation, Cenozoic sediments and a number of palaeovalleys in the Paterson area in light of the key components listed in [Table 7.10](#) for sandstone-hosted uranium mineral systems.

7.4.2.1 Paterson Formation and palaeovalleys

Much of the Permian sediment close to uranium-rich felsic igneous rocks (< 100 km) in the Paterson area is the Paterson Formation ([Section 3.2.4.1, Figure 3.7](#)), which is a glacial-fluvial sequence of sandstones and conglomerates suitable for hosting sandstone-hosted uranium deposits in confined aquifers.

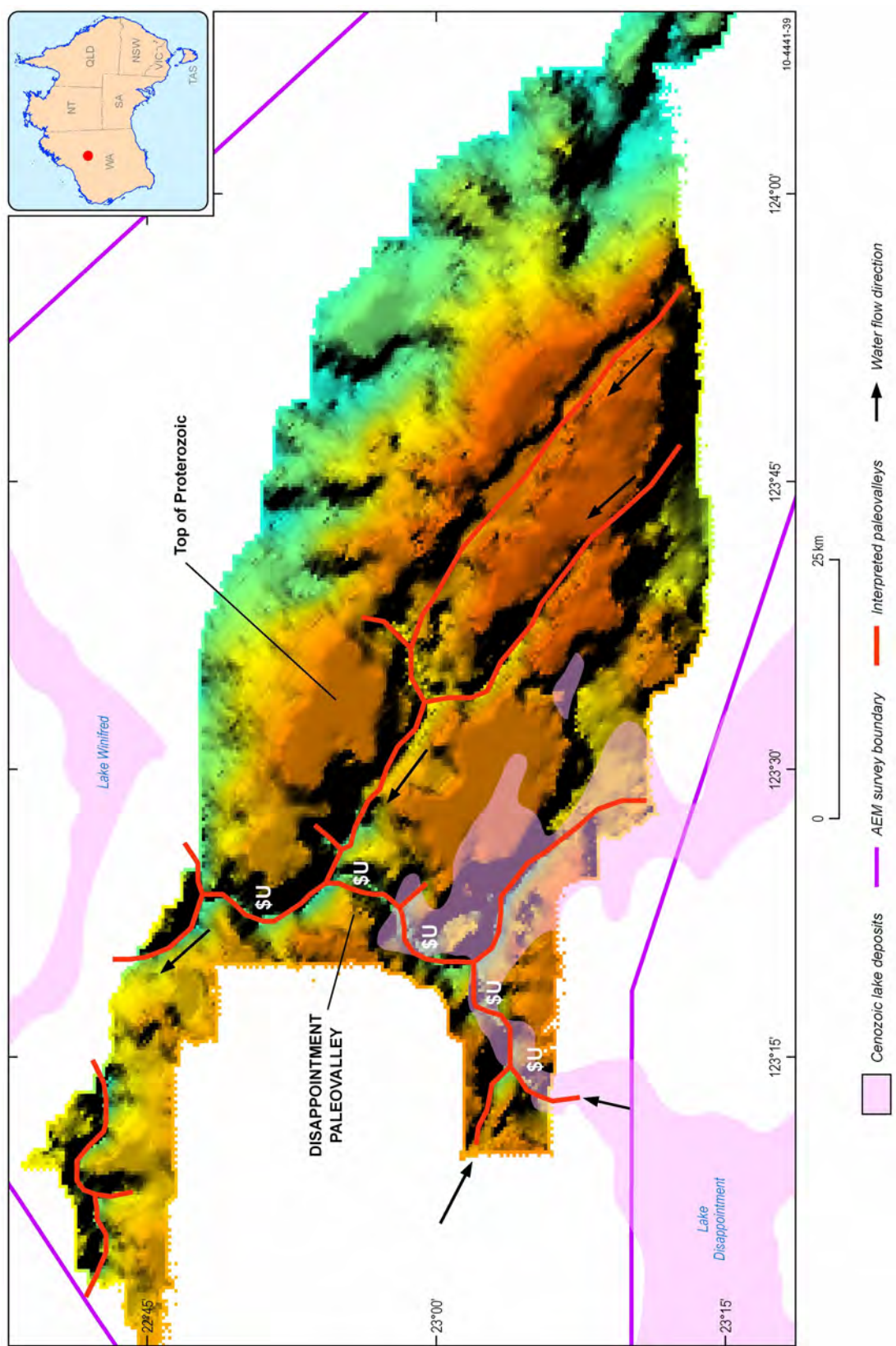


Figure 7.18: Inferred top surface of Proterozoic in 3D from AEM data in the Paterson South survey area.

Some of the Permian sedimentary rocks have been eroded since sedimentation and there has been differential uplift and erosion of different parts of the Permian sequences across the survey area. However, within the recognisable fault blocks the positions of Permian palaeovalleys seem to have remained about the same relative to immediate surroundings. This means that the exact geometry of basins and embayments at Permian time are difficult to reconstruct, but preserved remnants of Permian sedimentary rocks indicate the positions of palaeo-embayments at Permian time, e.g., the Paterson Formation ([Figure 3.7](#)), including:

- The Oakover River valley;
- The area between Nifty, Telfer and Kintyre;
- The area north-northwest of Telfer; and,
- The Waukarlycarly Embayment on a larger scale.

Archean and Proterozoic felsic igneous rocks, as uranium sources to these embayments, are present in the Pilbara Craton, Rudall Complex and in the Telfer area (Mt Crofton Granite Suite). Some faults are present in the Permian sediments (Paterson Formation, [Figure 3.8](#)). In the northern portion of PATERSON RANGE, well-bedded sandstone is folded into zones of disharmonic, tight, concentric folds which are commonly cut by thrusts and steeply dipping faults. These structures may be the results of deformation caused by the movement of glaciers, or slumping of sediments made unstable by the melting of ice (Chin *et al.*, 1982). Several regional scale faults are interpreted from the AEM data in the Waukarlycarly Embayment, probably as growth faults along basin boundaries ([Figure 3.8](#)). Faults in the Permian are potential fluid pathways for mineralisation.

There are no known *in situ* organic materials or other reductants in the Permian Paterson Formation. Published 1:100 000 and 1:250 000 geological maps and their explanatory notes do not show or mention such materials. Nevertheless, there is potential for mobile reductants, including hydrocarbons and H₂S, in the area. There has been exploration for hydrocarbons in the Canning Basin and Waukarlycarly Embayment. Paleozoic sediments in these basins may have reached the hydrocarbon window and thus may provide a source of mobile hydrocarbons and associated reductants. To assess this model there is a need to map structures that could have channelled hydrocarbons and/or to map seepage sites, which is beyond the scope of the present study.

Several major palaeovalleys, filled with Permian or younger sediments, have been mapped in the surface geology mapping or have been interpreted from the new AEM data in the Paterson region ([Figures 3.7, 5.15, 5.18, 5.21, 5.27-33, 7.15, & 7.18](#)):

- The Disappointment Palaeovalley ([Figures 5.31 and 7.18](#));
- Oakover Valley ('A' on [Figure 3.18](#));
- South of Telfer ('D' on [Figure 3.8](#)); and,
- Canning Palaeovalley ('E' on [Figure 3.8, Figure 5.18 and 5.30](#)).

In the following sections we will discuss the potential of sandstone-hosted uranium systems in these palaeovalleys in light of the above the key components listed in [Table 7.10](#).

7.4.2.2 Disappointment Palaeovalley

The Disappointment Palaeovalley links groundwater flow from Lake Disappointment to Lake Winifred and is buried by Cenozoic sands and sand dunes, but it is clearly depicted in the AEM data ([Section 5.7, Figures 5.31 and 7.18](#)). This palaeovalley is interpreted to be up to 150 m deep, based on conductivity anomaly contours ([Section 5.7](#)). It has several bends that may concentrate organic-rich sediments in point bars and is fed by several tributaries. Uranium may be readily available from the weathering of felsic igneous rocks in the Rudall Complex. Oxidised fluid containing uranium may flow into the palaeovalley from Lake Disappointment, tributaries running from the Rudall Complex into the palaeovalley or via the Camel-Tabletop Fault Zone, which is clearly depicted in the AEM data and may have acted as a fluid pathway.

The northern part of the Disappointment Palaeovalley cuts into the Permian Paterson Formation as mapped in surface geology mapping and the Czarnota *et al.* (2009b) solid geology interpretation. There is a possibility that the Paterson Formation may extend much further south along the Disappointment Palaeovalley (if it is a Permian palaeovalley) and into the Lake Disappointment area.

The Disappointment Palaeovalley itself is probably filled with Cenozoic (Eocene to Oligo-Miocene) sediments (Magee, 2009). It is not known if the palaeovalley has incised the Proterozoic basement. Either way, this palaeovalley is a fertile ground for palaeochannel type sandstone-hosted uranium deposits because key components for the system are likely to be present:

- Sources of uranium in felsic igneous rocks of the Rudall Complex;
- A palaeovalley with a number of bends; and,
- Plant-derived organic materials.

It is considered that the Disappointment Palaeovalley has moderate to high potential with moderate certainty.

7.4.2.3 Oakover Valley

The Oakover Valley trends north-northwest from BALFOUR DOWNS through NULLAGINE to YARRIE ('A' on [Figure 3.8](#)). It is around 30 km wide at its widest point on YARRIE. Here Permian Paterson Formation disconformably overlies Mesoproterozoic, Paleoproterozoic and Archean rocks. The Paterson Formation is overlain by the Paleogene-Neogene Oakover Formation and colluvial sand, silt and gravel or pebbles, which are partly consolidated ([Table 7.11](#)). The Oakover River drainage systems are filled with alluvial deposits, which incise older sediments, Permian in places.

In the upper stream area of the Oakover Valley, some Permian sediments (Paterson Formation) have apparently been eroded, e.g., on the southeastern corner of NULLAGINE and northeastern corner of BALFOUR DOWNS ([Figure 3.7](#)).

Organic materials are likely to be present in Cenozoic colluvial and Quaternary alluvial deposits, although the amount of organic materials is unknown. Thus it is considered that the areas of Quaternary alluvial deposits have moderate to high potential for palaeovalley/palaeochannel type sandstone-hosted uranium deposits with moderate certainty. Because it is not known if organic materials were present in the glacial Permian sediments in the Oakover Valley, potential may be moderate for palaeovalley/palaeochannel type sandstone-hosted uranium deposits in the Permian palaeovalleys/palaeochannels but certainty is low.

7.4.2.4 Palaeovalleys on RUDALL

There are two Permian sediment-filled palaeovalleys on RUDALL ('B' and 'C' on [Figure 3.8](#)). At the current level of erosion, both Permian palaeovalleys seem to originate from the central-south part of RUDALL. Field geological mapping suggests glacial flow to the north or northwest in these palaeovalleys (Bagas *et al.*, 2000). Much of the Permian sediment in the palaeovalley in the central part appears to have been eroded; only remnants of Permian close to the unconformity with Rudall Complex are now exposed at the bottom of the valley.

In the palaeovalley on the west and south part of RUDALL ('B' on [Figure 3.8](#)) there are some small and scattered outcrops of Permian Paterson Formation. The Permian sequence in the valley is likely to be thin, probably mostly in the order of several meters or up to 10 or 20 meters.

Table 7.11: Stratigraphy in the Oakover Valley area, compiled from published 1:100 000 and 1:250 000 geological mapping.

	Quaternary	Alluvium	Alluvial sand, clay, and gravel in active drainage areas.
Cenozoic	Paleogene - Neogene	Colluvium	Colluvial sand, silt and gravel or pebble, partly consolidated.
		Oakover Formation	Variably silicified limestone, silty limestone, calcareous sandstone, siltstone and marl.
Permian		Paterson Formation	Conglomerate (including diamictite), sandstone and siltstone (largely glaciogenic).
Mesoproterozoic	Bangemall Supergroup/ Manganese Group	Woblegun Formation	Interbedded shale, siltstone, sandstone, and conglomerate, local dolostone and stromatolitic dolostone.
Paleoproterozoic	Hamersley Group	Pinjian Chert Breccia	Chert breccia and poorly bedded chert.
		Carawine Dolomite	Massive to well-bedded, recrystallised dolostone, and stromatolitic dolostone; minor chert.
Archean	Fortescue Group	Jeerinah Formation	Siliciclastic sedimentary rocks; local volcanic rocks, and dolerite sills.
		Maddina Formation	Massive amygdaloidal, or vesicular basalt and basaltic andesite; local komatiitic basalt, dacite, and rhyolite.
		Tumbiana Formation	Basaltic volcanic rocks and carbonate rocks.

On RUDALL the basal tillite of the Paterson Formation consists of well-rounded pebbles to boulders, set in a clay matrix, with boulders locally exceeding 5 m in diameter. The pebbles and boulders include quartzite, orthogneiss and paragneiss from a diverse source region including the local Rudall Complex. The tillite is overlain by interbedded, cross-bedded, medium- to coarse-grained sandstone, siltstone and mudstone (Bagas and Smithies, 1998; Bagas *et al.*, 2000). These sands and silts are suitable hosts for palaeovalley-type sandstone uranium deposits.

Uranium source rocks of felsic igneous rocks are readily available in the Rudall Complex near Kintyre, incised by these two palaeovalleys. For sandstone-hosted uranium deposits in these valleys, potential may be moderate but certainty is low because of the lack of knowledge regarding the presence, abundance and nature of reductants (organic materials) in these two palaeovalleys.

7.4.2.5 Canning Palaeovalley

The Canning Palaeovalley ([Figure 5.30](#), ‘E’ on [Figures 3.7 & 7.15](#)) links groundwater flow from Lake Dora to Lake Waukarlycarly ([Chapter 5](#)). Permian sediments of the Paterson Formation have been mapped along the palaeovalley (Chin *et al.*, 1982), but there are no exploration drilling data in the Palaeovalley (Roach, 2009). Surface geological mapping reveals the presence of aeolian sand, calcrete and calcareous silt and sand derived from calcrete along the palaeovalley. It is likely that the Canning Palaeovalley incised the Proterozoic basement here and is filled with Eocene to Oligo-Miocene sediments (Magee, 2009).

Organic materials such as plant fragments and carbonised wood should be present in the Canning Palaeovalley and in the fan area at the north end of the valley where water flowed into Lake Waukarlycarly and water flow speed reduced. Uranium source rocks are readily available in the Mt Crofton Granite suite in the Telfer area and from felsic igneous rocks in the Rudall Complex further up stream.

Thus it is considered that there is moderate to high potential for palaeovalley/palaeochannel type sandstone-hosted uranium deposits in the Canning Palaeovalley and in the fan area at the north end

of the Palaeovalley and entry to Lake Waukarlycarly, with moderate certainty.

7.5 CALCRETE-HOSTED URANIUM MINERAL SYSTEMS

Calcrete-hosted uranium mineral systems are discussed in [Section 6.3](#). Essential criteria used to assess the potential of calcrete-hosted uranium systems (valley- and playa-type) in this section for the Paterson area are summarised in [Table 7.12](#).

Table 7.12: Key mappable criteria for assessing calcrete-hosted uranium mineral systems.

QUESTION*	MAPPABLE CRITERIA	SOURCE DATA
Q3	Felsic igneous rocks as uranium sources.	Surface and solid geology maps, radiometric data, geochemistry data.
Q3	Mafic igneous rocks and/or ferruginous duricrust materials as vanadium sources.	Surface and solid geology maps, geochemistry data.
Q4, Q2	Palaeovalleys: large ground water flow system and flow directions.	Surface geology maps, remotely sensed data.
Q4, Q2	Palaeovalleys with calcrete.	Surface geology maps, remotely sensed data.

*Questions are as follows (after Barnicoat 2007):

- Q1: What is the geodynamic and P-T-t history of the system?
- Q2: What is the architecture of the system?
- Q3: What are the characteristics and sources (reservoirs) of water, metals, ligands and sulfur?
- Q4: What are the fluid flow drivers and pathways?
- Q5: What are the transport and depositional processes for metals, ligands and sulfur?
- Q6: How and where do later geological processes allow preservation of deposits?

Source rocks for uranium have been discussed in [Section 7.2.1](#). They include Archean to Mesoproterozoic felsic igneous rocks of the Pilbara Craton, Rudall Complex and Neoproterozoic Mt Crofton Granite Suite in the Telfer area ([Figure 6.1](#)). Ferruginous regolith materials on URAL and SAHARA, JOANNA SPRING, ANKETELL and PATERSON RANGE also have medium to high abundances of uranium (3.5 to 4 ppm, [Figure 7.3](#)), although its leachability may be lower from ferruginous duricrust materials than from granitic rocks. Ferruginous duricrust is also commonly enriched in vanadium and can therefore be a good source of vanadium to create carnotite.

Major modern drainage and palaeodrainage systems, including several lakes and alluvial systems, are shown in [Figure 7.20](#). Flow directions of surface and ground water are determined from topographic maps, a digital elevation model and groundwater mapping and are depicted in [Figure 7.21](#). Palaeovalleys are well depicted in the AEM dataset (see [Chapter 5](#), [Figures 5.29, 5.30, 5.31, 5.32, 7.15 and 7.18](#)). [Figure 5.30](#) shows the Canning Palaeovalley over the Anketell Shelf from Lake Dora to Lake Waukarlycarly. [Figure 7.22](#) shows calcrete over a palaeovalley which connects water flows from Lake Disappointment towards Lake Winifred and Lake Blanche.

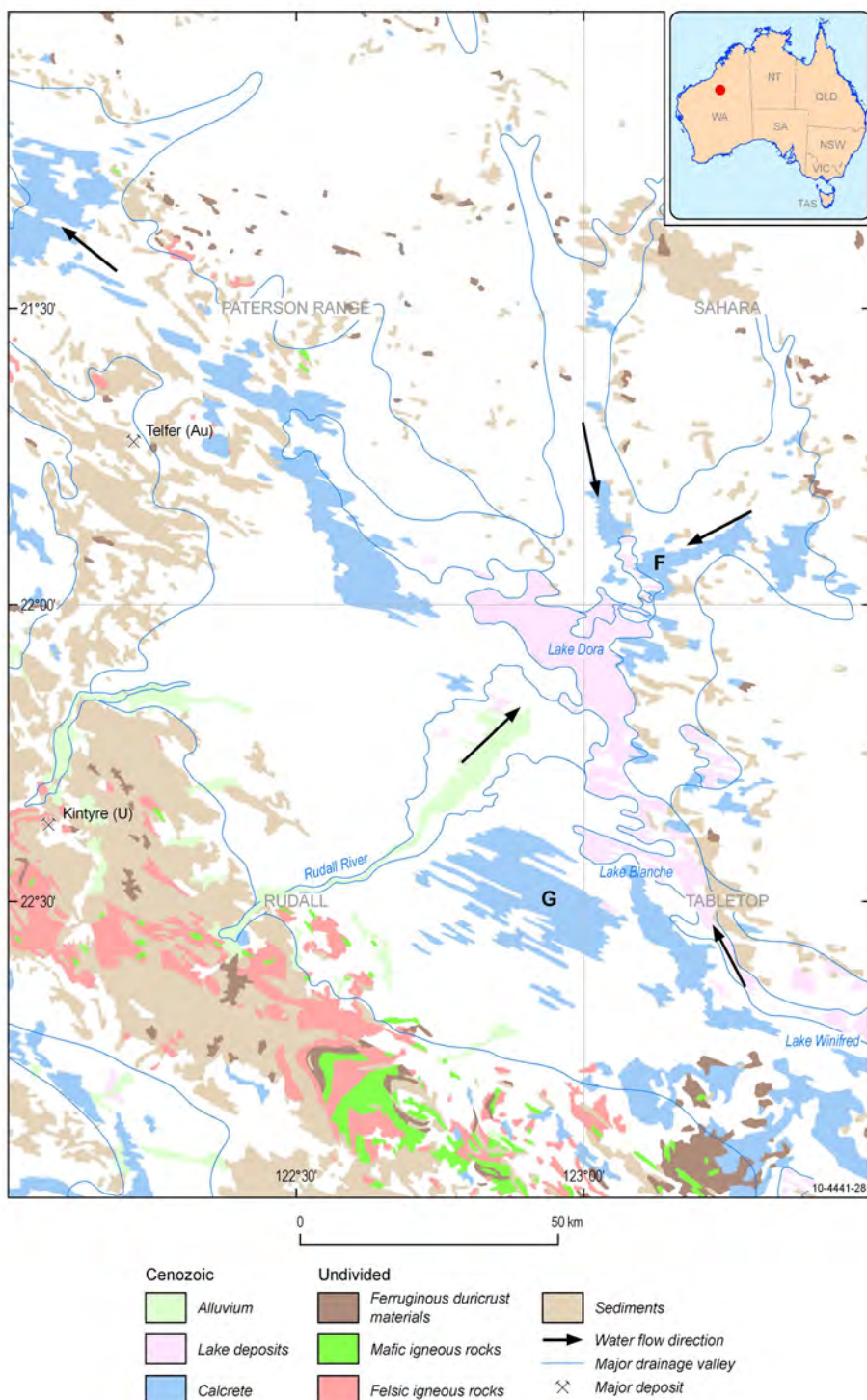


Figure 7.19: The Rudall River-Lake Dora area, showing 1:250 000 map tile names and boundaries.

7.5.1 Prospectivity for calcrete-hosted uranium mineral systems

Mapped key components of calcrete-hosted uranium systems in the Paterson area are shown in [Figure 7.21](#):

- Major current drainage and palaeodrainage systems;
- Calcrete mapped in the 1:1 000 000 Surface Geology of Western Australia (Stewart, 2008) map;
- Source rocks for uranium (pre-Permian felsic igneous rocks and Cenozoic ferruginous duricrust materials); and,
- Source rocks for vanadium (pre-Permian mafic and ultramafic igneous rocks, banded iron formation and Cenozoic ferruginous duricrust materials).

We present a prospectivity map ([Figure 7.23](#)) that shows the potential and certainty of calcrete-hosted uranium systems in the Paterson region. The Paterson region is divided into several prospective areas for discussions of calcrete-hosted uranium mineral systems on the basis of drainage systems including recharge and discharge areas, source areas for uranium and vanadium and water flow directions in drainage systems, ([Figure 7.23](#), [Table 7.13](#)):

- Lake Waukarlycarly ([Figure 7.24](#));
- Lake Disappointment west ([Figure 7.25](#));
- Lake Disappointment southeast ([Figure 7.26](#));
- Lake Winifred ([Figure 7.22](#));
- Lake Auld-Percival Lakes-Tobin Lake ([Figure 7.27](#)); and,
- Lake Dora and Lake Blanche ([Figure 7.19](#)).

Key features for calcrete-hosted uranium mineral systems for these areas are summarised in [Table 7.13](#). Potential assessments of these areas are discussed below.

7.5.2 Lake Waukarlycarly

Surface water flows into Lake Waukarlycarly mainly from the valley around Nifty, Kintyre and Telfer in the south and groundwater flows from Lake Dora in the southeast ([Figure 7.24](#)). To a lesser extent Lake Waukarlycarly also collects surface water from smaller and shorter drainages in the north and northeast. The main discharge area is around the southern edge of the Lake. Here there is a large and continuous area of calcrete that is mapped for about 20 km by 60 km.

Uranium is readily available from felsic igneous rocks in the Pilbara Craton, Rudall Complex and Mt Crofton Granite Suite. Geochemical analyses of granitic samples from Rudall Complex contain uranium up to 14 ppm (Bagas and Smithies, 1998). The uranium anomalies are clearly shown in [Figure 7.3](#). Vanadium is readily available from mafic and ultramafic rocks in the Pilbara Craton and Rudall Complex and perhaps from mafic to intermediate rocks of the Mt Crofton Granite Suite. In the Rudall Complex vanadium abundances are commonly more than 200 ppm in mafic and ultramafic rocks (Bagas and Smithies, 1998; [Figure 7.5](#)).

Small areas of scattered uranium anomalies in the Lake Waukarlycarly area are apparent in the radiometric data ([Figure 7.3](#)).

Based on available information, the mapped calcrete area along the southern edge of Lake Waukarlycarly area is considered to have moderate to high potential for calcrete-type uranium mineralisation for both valley- and playa-type ([Figure 7.23](#)). Exploration in the 1970s has identified uranium mineralisation in this area (Muggeridge, 1980) and the presence of the Lamil Hills prospect indicates the presence of a fertile calcrete-hosted uranium system in the area ([Section 6.3](#)).

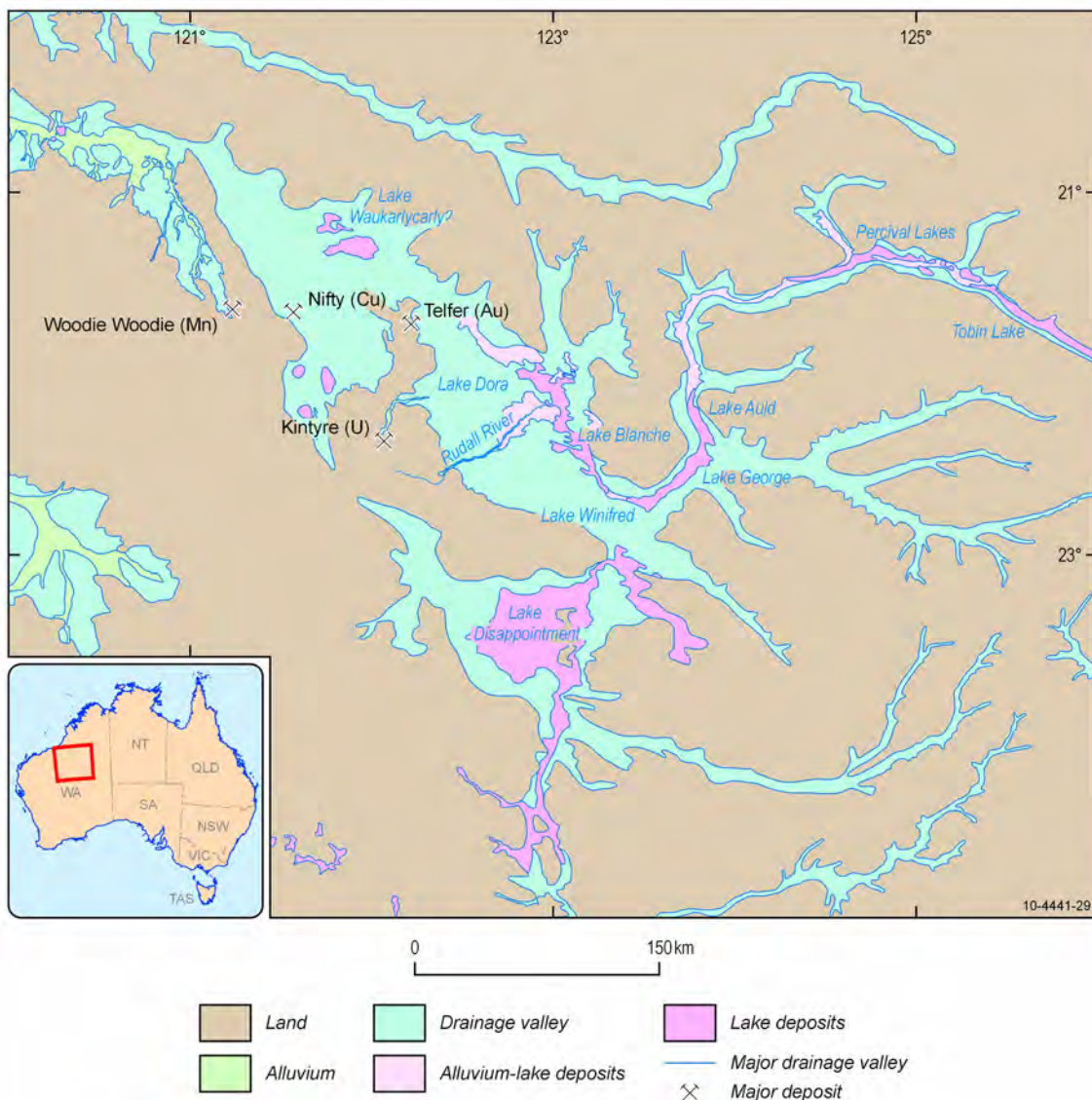


Figure 7.20: Major current drainage and palaeo-drainage systems in the Paterson area.

7.5.3 Lake Disappointment west

On the west side of Lake Disappointment, surface water flows into the Lake from several drainage systems (Figure 7.25). The drainage system from the northwest (I on Figures 7.23 & 7.25) is an alluvial system collecting surface water from the Rudall Complex on the northwest side of the Lake, where source rocks of uranium and vanadium are readily available. A calcrete-hosted uranium system may exist here.

Table 7.13: Potential of calcrete-hosted uranium systems in the Paterson region (see Figure 7.23).

CRITERIA	LAKE WAUKARLYCARLY	LAKE WINIFRED	LAKE DISAPPOINTMENT W	LAKE DISAPPOINTMENT SE	LAKE AULD	TOBIN LAKE- PERCIVAL LAKES-LAKE AULD
Ground water flow system	Valley around Nifty – Kintyre – Telfer and from Lake Dora (Figure 7.24).	Lake Disappointment – Lake Winifred (Figure 7.22).	Network of drainages from north and west (Figure 7.25).	Two branches of drainages join at the southeast corner of Lake Disappointment (Figure 7.26).	West-flowing drainage from Ural (Figure 7.27).	West-flowing drainage (Figure 7.27).
Ground water flow system size	Large.	Large.	Moderate to small for any single drainage system.	Large.	Large.	Large.
Calcrete	Mapped around the Lake; southern part continuous 20 km x 60 km, northern part patchy.	Large area of continuous calcrete.	Mapped in valley and delta areas west and southwest of lake, up to 10 km x 30 km, continuous.	Large area of continuous calcrete (16 km x 35 km) mapped at junction of the two major drainage systems. Elsewhere small areas & patchy along drainages.	Large area of continuous calcrete outcrop (6 km x 25 km) in delta area of the west-flowing drainage from URAL.	Small patchy areas along the drainage.
Source of U	Present. Felsic igneous rocks well exposed in Pilbara Craton west of the Lake. Felsic igneous rocks in the Telfer area. Felsic igneous rocks also exposed Rudall Complex.	Present. Felsic igneous rocks exposed in Rudall Complex.	Present in some areas. Felsic igneous rocks exposed in Rudall Complex north of lake, little exposed felsic igneous rocks west and south of lake.	Present. Ferruginous materials on Morris ca. 300km east of delta calcrete area on Runton. Unknown elsewhere.	Present. Ferruginous materials on URAL	Present. Ferruginous materials in the area.
Source of V	Present. Mafic igneous rocks exposed in Pilbara Craton and Rudall Complex.	Present. Mafic igneous rocks exposed in Rudall Complex	Present. Mafic igneous rocks exposed in Rudall Complex, and Officer Basin.	Perhaps from mafic igneous rocks exposed on TRAINOR and STANLEY. Unknown elsewhere.	Unknown. Ferruginous materials (ferricrete).	Unknown. Ferruginous materials (ferricrete).
Indication of uranium enrichment	Yes, as indicated by uranium anomalies in radiometric data around the lake area and Lamil Hill prospect.	-	-	-	-	
Potential for calcrete-type uranium system	High in the rim of calcrete south of lake for valley- and playa-type (A). Moderate to high for (B, C, D)	Moderate-high potential for valley-type in palaeovalley near Lake Winifred (H).	Moderate for valley-type in the valley immediately southwest of Rudall Complex (I), low – moderate for valley- and delta-type elsewhere (J, K, L, M, N).	Moderate for valley-type at junction of the two drainage systems & in valley at border of Runton and Madley (P), low-moderate for (Q, R, S).	Moderate for delta type at Lake Auld (U), moderate for valley type (T), low for (V, W)	Moderate for valley type in Percival Lakes - Tobin Lake (X, Y, Z).
Certainty	Moderate – high for (A), moderate for (B), (C) and (D)	Moderate to low (H).	Moderate for (I), low to moderate for (J, K, L, M, N).	Moderate for (P), low-moderate for (Q, R, S).	Moderate for (U, T), low for (V, W).	Moderate (X, Y, Z).

For the drainage systems J-K-L west of Lake Disappointment (Figures 7.22 & 7.25), surface water is collected from the edge of the Pilbara Craton on BALFOUR DOWNS, ROBERTSON and GUNANYA. A network of calcrete is mapped in these areas. Calcrete outcrops are cut by the modern drainage system, which indicates migration of drainage systems. Source rocks for uranium do not seem to be readily available. It is thus considered that this calcrete area has low potential for uranium mineralisation (J-K-L, Figures 7.23 & 7.25).

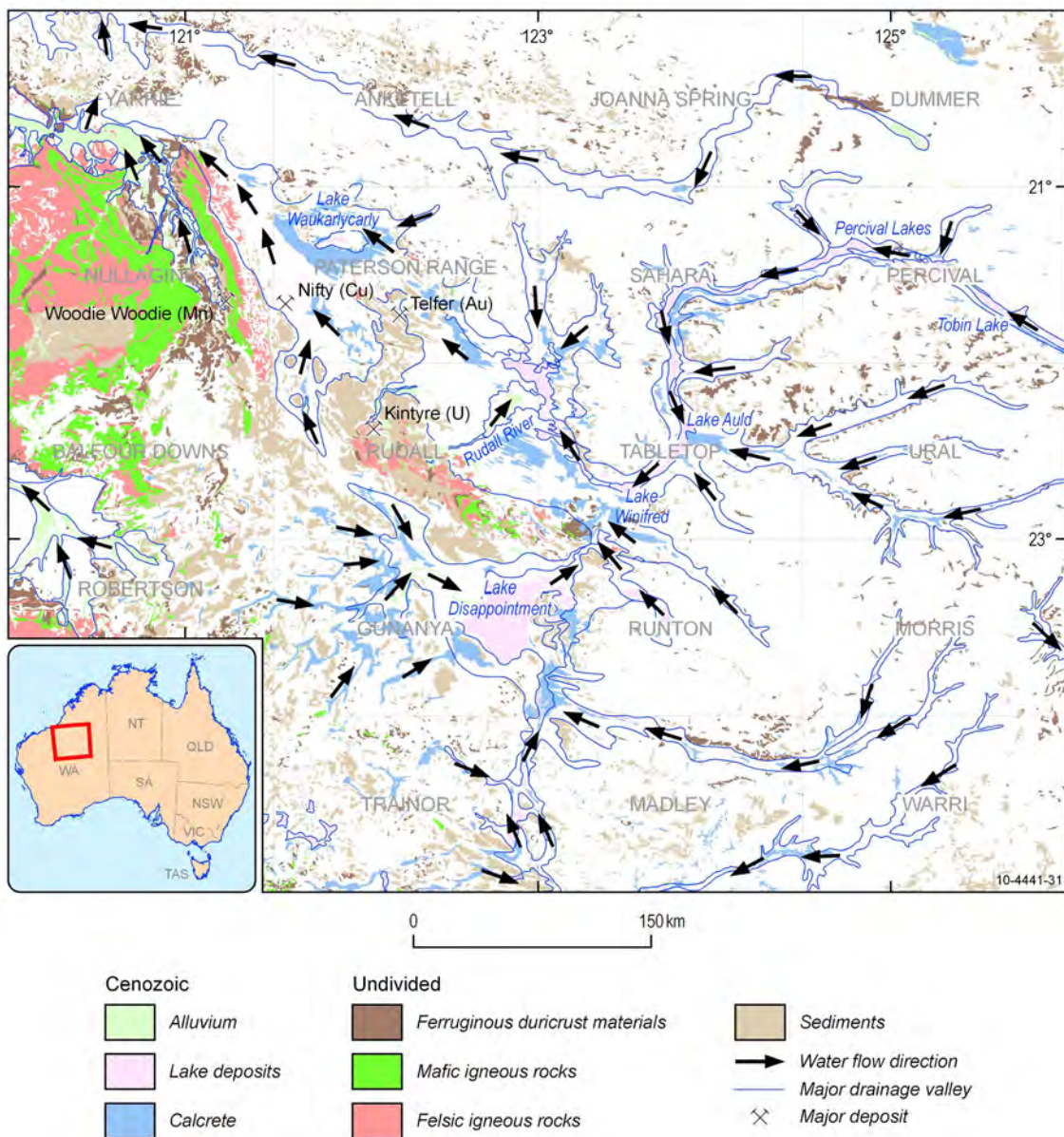


Figure 7.21: Distribution of key components of calcrete-hosted uranium systems in the Paterson area. Diagram shows: major drainage systems; calcrete mapped in the 1:1 000 000 Surface Geology of Western Australia map (Stewart, 2008); source rocks of uranium (pre-Permian felsic igneous rocks, Cenozoic ferruginous duricrust materials); and, source rocks of vanadium (pre-Permian mafic and ultramafic igneous rocks, banded iron formation and Cenozoic ferruginous duricrust materials).

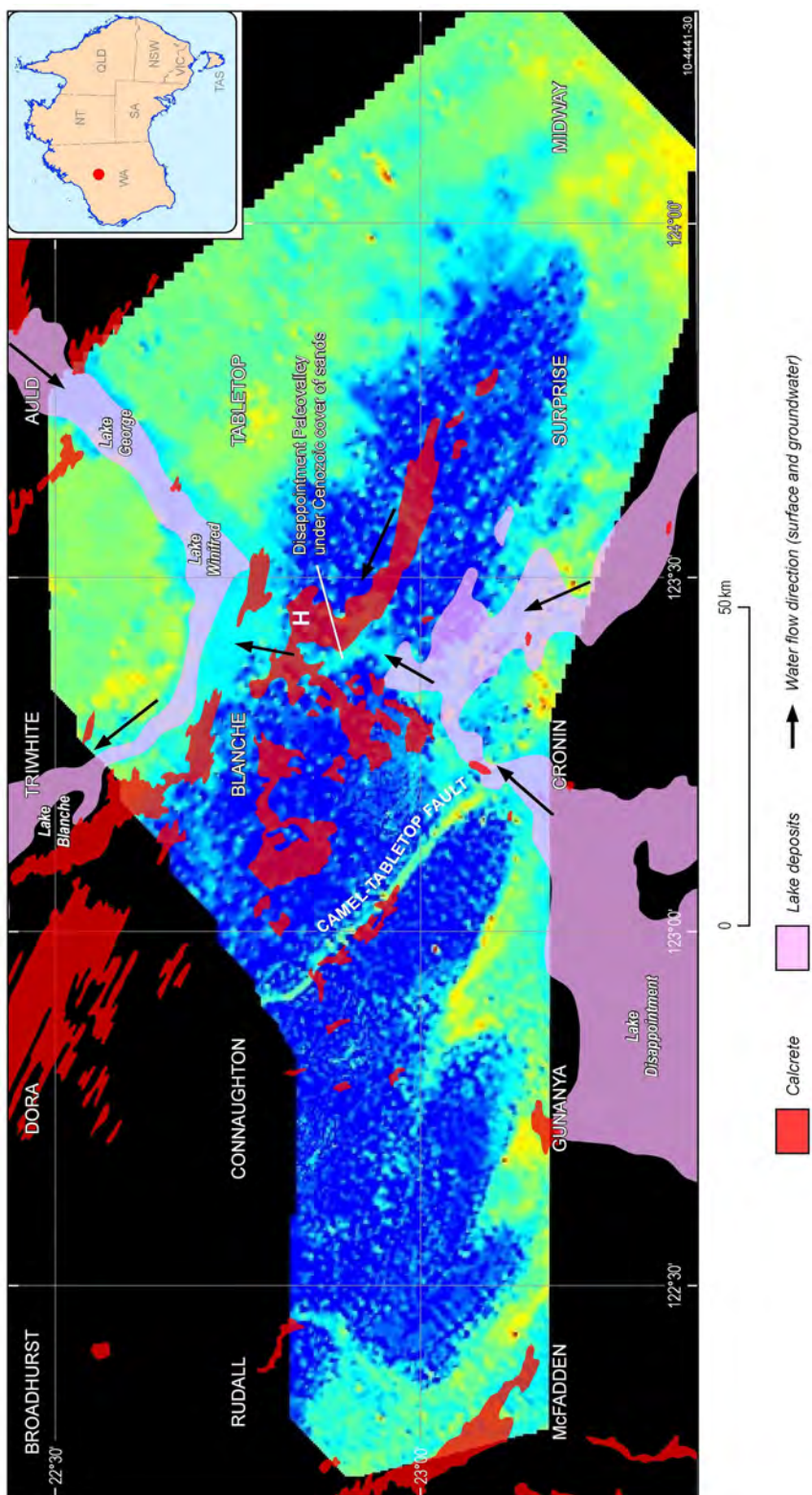


Figure 7.22: Calcrete and lakes over GA-LEI 200-250 m conductivity depth slice of the Paterson South survey area. Map shows 1:100 000 map tiles shown in grey lines and text. Calcrete and current lake polygons are displayed at 25% transparency. Note colour change in overlayed areas. Conductivity colour bar shown in Figure 4.8.

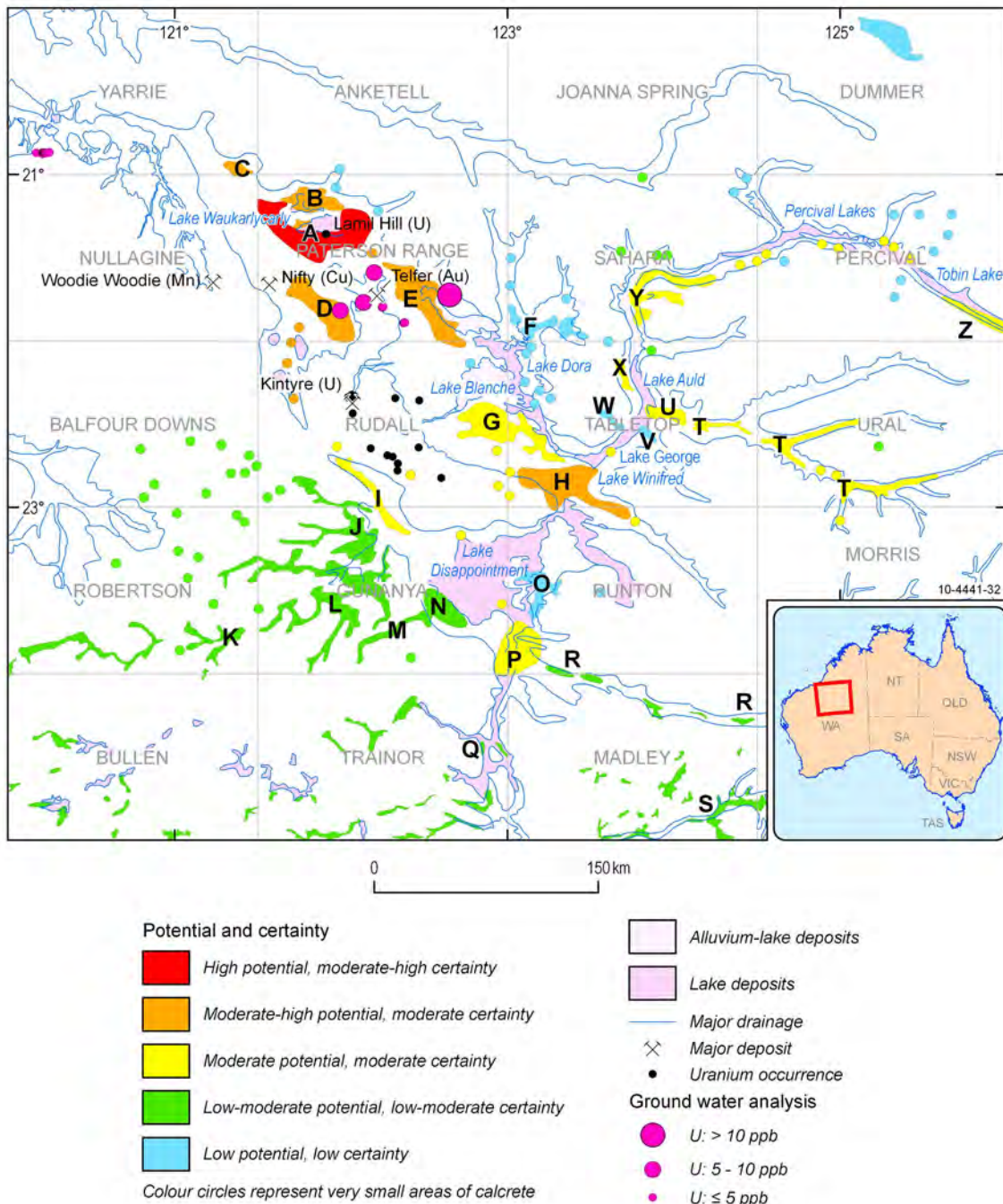


Figure 7.23: Prospectivity map for calcrete-hosted uranium mineral systems in the Paterson area. Potential is high in the calcrete-rim area south of Lake Waukarlycarly (A). Potential is moderate to high for in the area north and northwest of Lake Waukarlycarly (B & C), in the valley between Kintyre & Woodie Woodie-Nifty (D), east of Telfer (E) and south of Lake Winifred (H). Elsewhere potential is low to low-moderate.

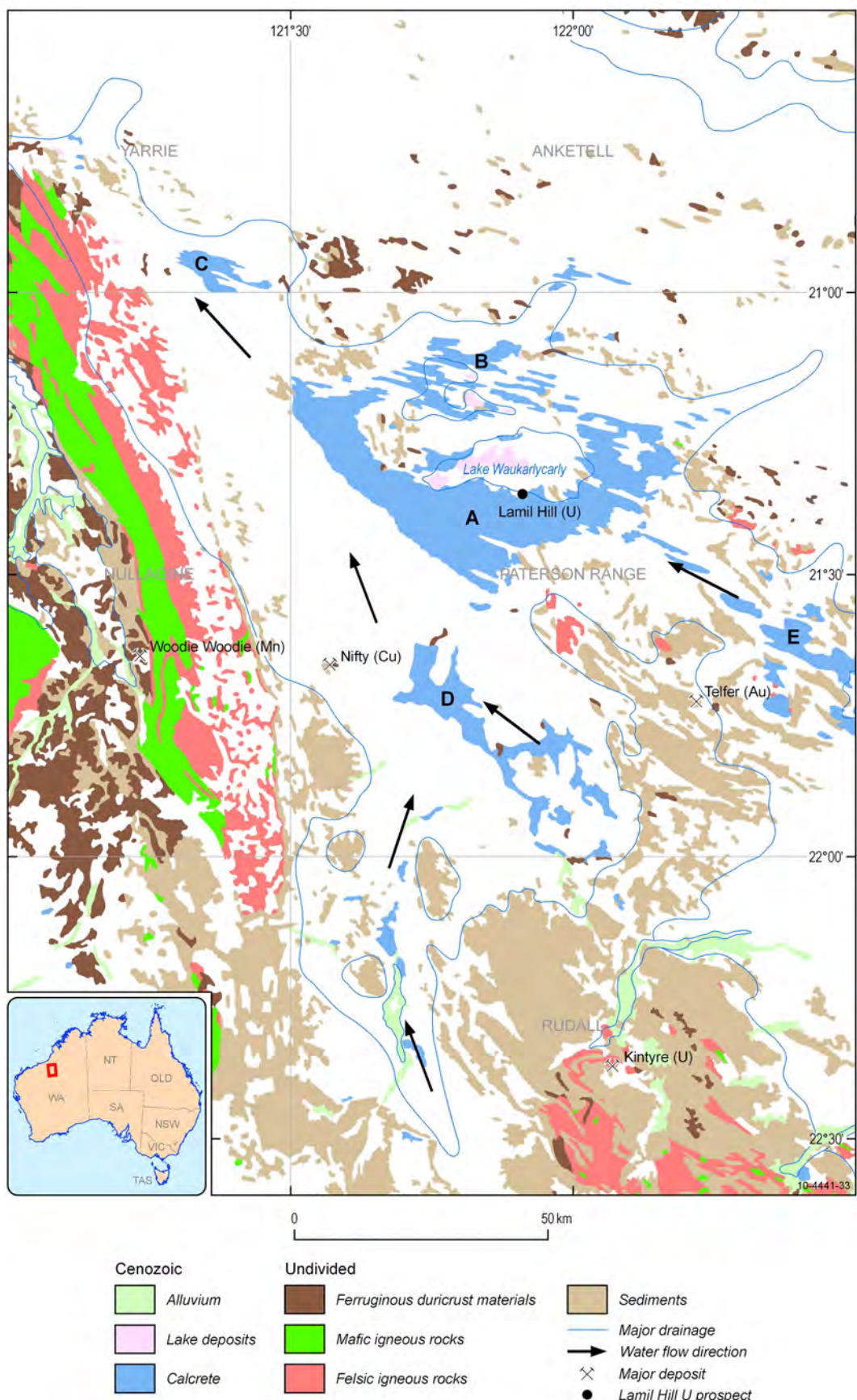


Figure 7.24: The Lake Waukarlycarly area. 1:250 000 map tile names and boundaries are shown.

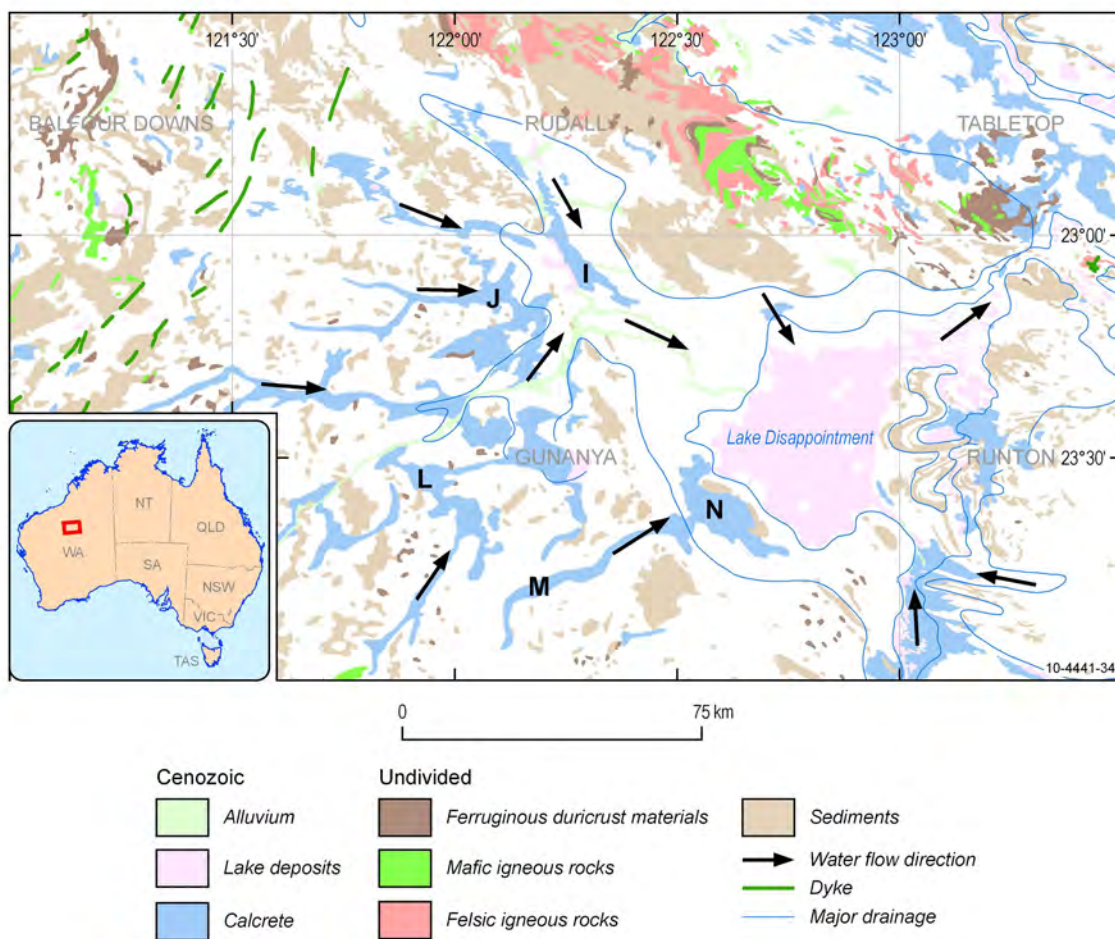


Figure 7.25: Lake Disappointment West area. 1:250 000 map tile names and boundaries are shown.

The drainage system from the southwest of the lake (M-N) is smaller and shorter (Figures 7.23 & 7.25). It is confined to the southern part of GUNANYA. At the southwest bank of Lake Disappointment a delta area of calcrete, in the order of 10 km by 30 km, occurs. Sources of uranium does not seem to be readily available in the recharge area of this small and short drainage system, although vanadium may be sourced from the northern part of TRAINOR. Available data suggest low potential for uranium mineralisation in the mapped calcrete at the southwest bank of Lake Disappointment (M-N, Figures 7.23 & 7.25).

7.5.4 Lake Disappointment southeast

The southeast corner of Lake Disappointment collects surface water from two branches of drainage systems (Figure 7.26). One runs from MORRIS through WARRI and MADLEY into the Lake at the southwest corner of RUNTON. The other runs from WARRI through MADLEY, joins drainages on the southern part of TRAINOR before flowing into the Lake. The recharge areas of these drainages are largely sediments and regolith.

The lack of radiometric data on much of MADLEY and WARRI (Figure 7.3) leads to uncertainty for the supply of uranium, although vanadium may be sourced from the weathering of some mafic rocks on TRAINOR for mineralisation in the drainage junction area at the southwestern corner of RUNTON. A source of vanadium for uranium mineralisation in the drainage valley at the RUNTON-MADLEY border is unknown.

Therefore, it is considered that the potential for calcrete-type uranium mineralisation is uncertain, perhaps low to moderate (P, Q, R, S), although potential may be higher in the junction area of the two branches of drainage systems at the corner of GUNANYA, RUNTON, TRAINOR and MADLEY (Figures 7.22 & 7.26).

7.5.5 Lake Winifred

South of Lake Winifred a large area of mapped calcrete occurs (Figures 7.21, 7.22 & 7.23). Here three drainage systems emerge, one flowing northeast from Lake Disappointment and two others flowing northwest from RUNTON. The AEM dataset clearly shows a palaeovalley drainage system linking Lake Disappointment and Lake Winifred (Figure 7.18). Source rocks of uranium and vanadium are readily available in the Rudall Complex for transport through the drainage system of Lake Disappointment to Lake Winifred, where a calcrete-hosted uranium mineral system is predicted to exist (Figure 7.18, H on Figures 7.22 and 7.23), more likely in the bends of the palaeovalley and near the entry into Lake Winifred (Figure 7.18).

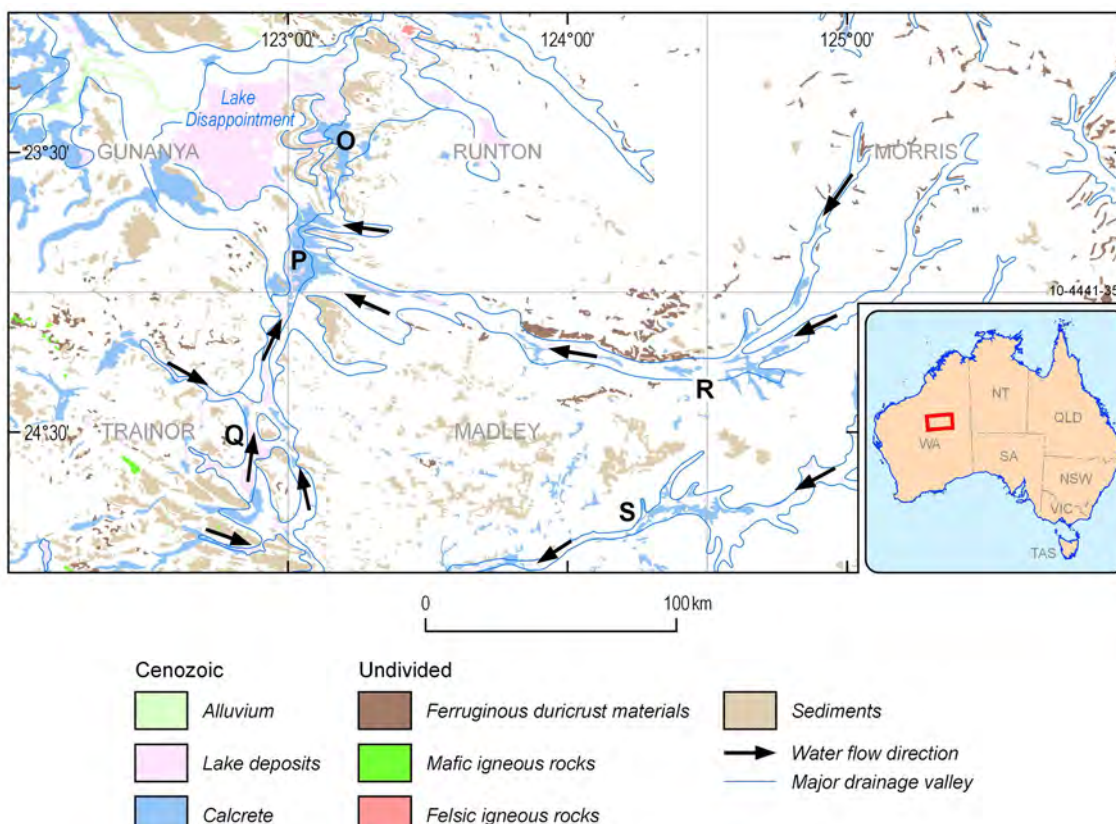


Figure 7.26: Lake Disappointment Southeast area. 1:250 000 map tile names and boundaries are shown.

7.5.6 Lake Auld and Percival Lakes-Tobin Lake

Drainage systems on URAL merge towards Lake Auld on TABLETOP (Figure 7.27). Calcrete is mapped in scattered areas in these drainages, with the largest mapped calcrete outcrop in the delta area in the drainage from URAL into Lake Auld. There calcrete crops out in a continuous area of 6 km by 25 km. Uranium seems to be available in the ferruginous duricrust materials of the area as indicated by the uranium anomalies on URAL and perhaps MORRIS to the south and WILSON to the east (Figure 7.3), although leachability of uranium from ferruginous duricrust materials may be

lower than from granitic rocks. The source for vanadium is uncertain. Therefore it is considered there is low to moderate potential for delta type calcrete-hosted uranium deposit in Lake Auld and valley-type elsewhere in the drainage system (Figure 7.23).

Similarly for the drainage system from Tobin Lake-Percival Lakes towards Lake Auld and Lake George, potential for valley-type calcrete uranium deposit is low to moderate (Figure 7.23).

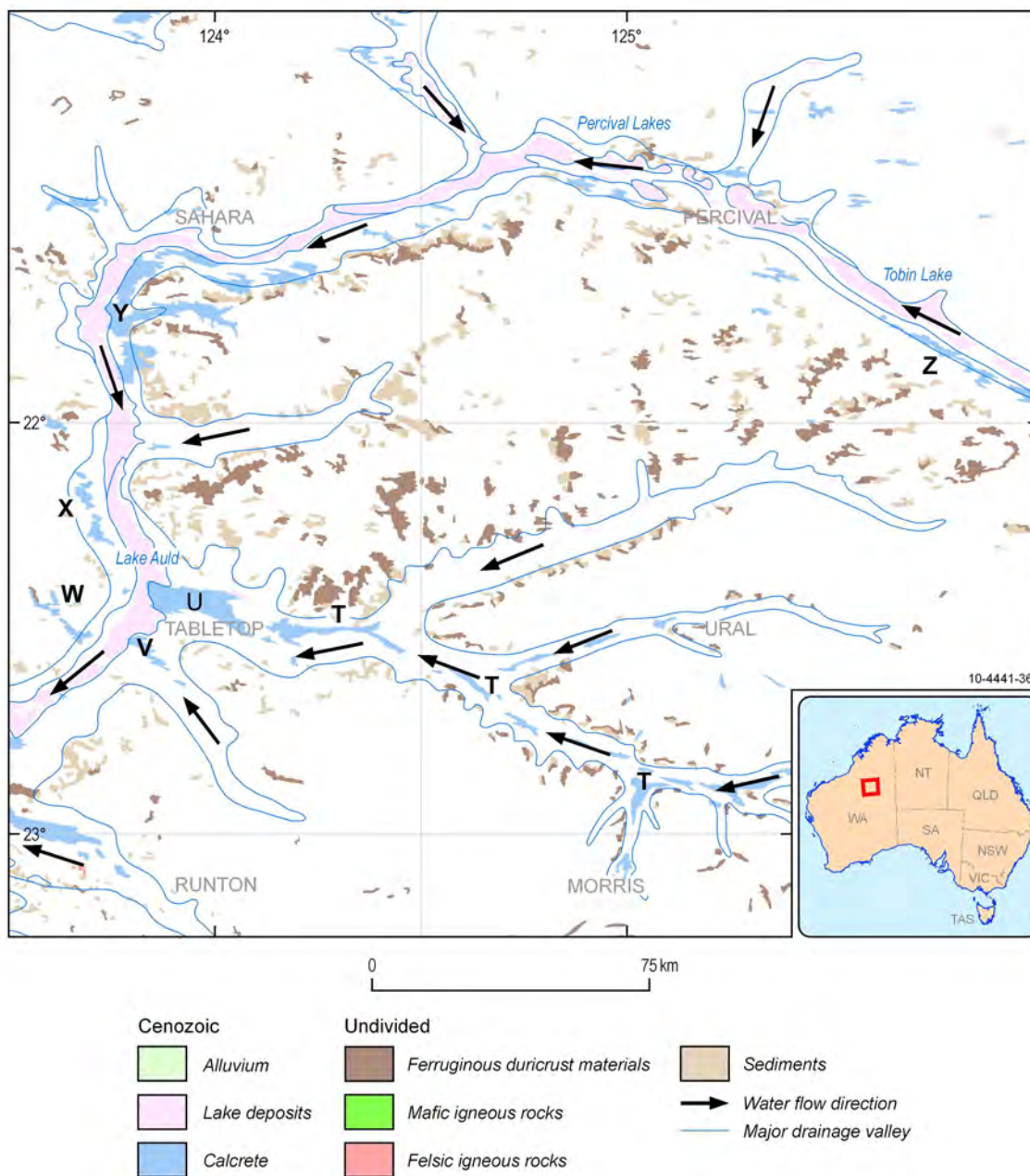


Figure 7.27: Percival Lakes – Lake Auld area. 1:250 000 map tile names and boundaries are shown.

7.5.7 Lake Dora and Lake Blanche

Uranium is apparently enriched in regolith materials in the Rudall Complex as seen in the uranium anomaly over ferruginous duricrust materials at Cassandra. Granitic gneisses in the complex are rich in uranium and mafic and ultramafic rocks rich in vanadium (Bagas and Smithies, 1998; [Figure 7.3](#)). In the process of weathering a large amount of uranium must have been transported from the complex towards Lake Dora ([Figure 7.19](#)), then towards Lake Waukarlycarly.

Large areas of calcrete are mapped in the area east of Rudall River and south of Lake Blanche, between Telfer and Lake Dora. There is likely to be moderate potential for calcrete-hosted uranium mineral systems here ('G' on [Figure 7.23](#)). North and east of Lake Dora, however, potential for this type of uranium deposit is low because of the lack of source rocks for uranium and vanadium.

7.6 CONCLUSIONS

Regional AEM is a useful geophysical tool for mapping the shallow crust. Airborne electromagnetic data provide valuable insights into identifying and mapping: 1. buried palaeotopography including palaeovalleys and altered and/or weathered unconformity surfaces; and, 2. depths to conductive geological units (and related faults) that may be less evident in other regional datasets

Known uranium deposits and prospects in the Paterson area are related to the Coolbro-Rudall unconformity and to the playa calcretes, including a calcrete-hosted uranium prospect at Lamil Hill south of Lake Waukarlycarly. We consider that there is potential for uranium in several new plays or areas, including:

1. Unconformity-related uranium associated with the unconformities of:
 - A. Tarcunyah-Archean (e.g., east of Warroo Hill and Mt Gregory);
 - B. Taliwanya-Rudall (e.g., McKay Range); and,
 - C. Karara-Rudall.
2. Stratabound uranium-copper associated with the Broadhurst-Coolbro contact ('Nifty-style');
3. Sandstone-hosted uranium associated with Permian Paterson Formation, and Permian and Cenozoic palaeovalleys (e.g., Canning and Disappointment Palaeovalleys); and,
4. Calcrete-hosted uranium (e.g., Lake Waukarlycarly, east and west of Telfer, and south of Lake Winifred).

Points 1 and 2 above are parts of the Miles mineral system during the late stage of Yeneena Basin development and inversion of the Yeneena Basin during Miles Orogeny.

For these uranium mineral systems in the Paterson area, AEM is useful in detecting unconformities (e.g., Coolbro-Rudall, Tarcunyah-Archean), mapping reductants in basement rocks (graphitic schists of the Yandagooge Formation, mafic and ultramafic rocks of the Rudall Complex) and sedimentary rocks above unconformities (conductive parts of the Broadhurst Formation), conductive sandstone packages (e.g., the Permian Paterson Formation) and palaeovalleys (e.g., the Canning and Disappointment palaeovalleys).

Care should be exercised in designing and processing AEM surveys to detect and depict unconformities by considering the possible subtle conductivity contrast between rock packages above and below the unconformities, alteration along and weathering of unconformity surfaces and the depth and structural complexity of folded sequences including unconformities.

Further work to assess potential of uranium mineral systems associated with Neoproterozoic unconformities and stratabound uranium-copper of the Miles mineral system should include:

1. Detailed and systematic mapping of reductants in the Rudall Complex, Broadhurst Formation and Coolbro Sandstone;
2. Evaluation of the diagenetic history of the Googhenama Formation to assess the possibility of diagenetic fluids;
3. Mapping of alteration and indications of deposition of uranium from the distribution of mapped gossans and interpretation of remotely sensed data (e.g., ASTER); and,
4. Analysis of favourable fault systems.

To further determine the potential and certainty of sandstone-hosted uranium mineral systems associated with the Permian Paterson Formation, and Permian and Cenozoic palaeovalleys, work is required to detect and map out of the presence of any possible *in situ* and/or mobile reductants in or at base of the Paterson Formation. Similarly, the abundance and nature of plant-derived reductants need to be studied to further determine potential and certainty of palaeovalley-type sandstone-hosted uranium mineral systems associated with Permian and Cenozoic palaeovalleys.

7.7 REFERENCES

- Bagas, L., 1997. Gunanya, WA Sheet 3451. 1:100 000 Geological Series, Western Australia Geological Survey. 1st edition.
- Bagas, L., 1999a. Rudall, WA Sheet SF51-10. 1:250 000 Geological Series, Western Australia Geological Survey Perth. 2nd edition.
- Bagas, L., 1999b. Geology of the Blanche-Cronin 1:100 000 sheet (part sheets 3551 and 3552), 1:100 000 Geological Series - Explanatory Notes. Geological Survey of Western Australia, Perth. 16 p.
- Bagas, L., 2004b. The Neoproterozoic Throssell Range and Lamil Groups, northwest of Paterson Orogen, Western Australia. Western Australia Geological Survey. 18 p.
- Bagas, L. and Smithies, R. H., 1996. Connaughton, WA Sheet 3452. 1:100 000 Geological Series, Western Australia Geological Survey. 1st edition.
- Bagas, L. and Smithies, R. H., 1998. Geology of the Connaughton 1:100 000 sheet, 1:100 000 Geological Series Explanatory Notes. Western Australia Geological Survey, Perth. 38 p.
- Bagas, L., Williams, I. R. and Hickman, A. H., 2000. Rudall, Western Australia (2nd Edition). 1:250,000 Geological Series - Explanatory Notes. Western Australia Geological Survey. 50 p.
- Barnicoat, A. C., 2007. Mineral systems and exploration science: Linking fundamental controls on ore deposition with the exploration process. In: *Digging Deeper: Proceedings of the Ninth Biennial SGA meeting, Dublin*. Society for Geology Applied to Mineral Deposits, 1407-1411 pp.
- Bastrakov, E. N., Jaireth, S. and Mernagh, T. P., 2010. *Solubility of uranium in hydrothermal fluids at 25°-300°: Implications for the formation of uranium deposits*. Geoscience Australia, Canberra. **Record**, 86 p.
- Chin, R. J., Hickman, A. H. and Towner, R. R., 1982. Paterson Range, Western Australia. 1:250 000 Geological Series - Explanatory Notes. Geological Survey of Western Australia, Perth. 29 p.
- Costelloe, M. T., Roach, I. C. and Hutchinson, D. K., 2010b. Paterson AEM survey directly detects major unconformity near Kintyre, WA. *Preview April 2010(145)*, 40-41.
- Cuney, M. and Kyser, K., 2008. Recent and not-so-recent developments in uranium deposits and implications for exploration. *Mineralogical Association of Canada Short Course Series Volume 39*. 257 p.
- Czarnota, K., Gerner, E., Maidment, D. W., Meixner, A. J. and Bagas, L., 2009a. *Paterson Area*

- 1:250 000 Scale Solid Geology Interpretation and Depth to Basement Model.* Geoscience Australia, Canberra. Record 2009/16, 37 p.
- Czarnota, K., Gerner, E., Maidment, D. W., Meixner, A. J. and Bagas, L., 2009b. *Proterozoic Solid Geology of the Paterson Province, 1:250 000 scale map.* Geoscience Australia.
- Dahlkamp, F. J., 1993. *Uranium Ore Deposits.* Springer-Verlag. 460 p.
- Derome, D., Cathelineau, M., Cuney, M., Fabre, C. and Lhomme, T., 2005. Mixing of Sodic and Calcic Brines and Uranium Deposition at McArthur River, Saskatchewan, Canada: A Raman and Laser-Induced Breakdown Spectroscopic Study of Fluid Inclusions. *Economic Geology* **100**, 1529-1545.
- Grey, K., Hocking, R. M., Stevens, M. K., Bagas, L., Carlsen, G. M., Irimies, F., Pirajno, F., Haines, P. W. and Apak, S. N., 2005. Lithostratigraphic nomenclature of the Officer Basin and correlative parts of the Paterson Orogen Western Australia. Department of Industry and Resources, Geological Survey of Western Australia, Perth. 89 p.
- Hickman, A. H. and Bagas, L., 1996. Rudall, W.A. Sheet3352. 1:100 000 Geological Series, Western Australia Geological Survey.
- Hickman, A. H. and Clarke, G. L., 1993. Broadhurst, W.A. Sheet 3353. 1:100 000 Geological Series, Western Australian Geological Survey.
- Hickman, A. H. and Clarke, G. L., 1994. Geology of the Broadhurst 1:100 000 sheet, Western Australia. Western Australia Geological Survey, Perth. 40 p.
- Jaireth, S., Clarke, J. and Cross, A., 2010. Exploring for sandstone-hosted uranium deposits in paleovalleys and paleochannels. *AUSGEO News* **97**, 21-25.
- Jaireth, S., McKay, A. and Lambert, I., 2008. Association of large sandstone uranium deposits with hydrocarbons. *AUSGEO News* **89**, 8-12.
- Magee, J., 2009. *Palaeovalley Groundwater Resources in Arid and Semi-Arid Australia.* Geoscience Australia, Canberra. Record 2009/03, 224 p.
- Minty, B. R. S., Franklin, R., Milligan, P. R., Richardson, L. M. and Wilford, J., 2008. Radiometric Map of Australia (1st edition), scale 1:5 000 000., Geoscience Australia, Canberra.
- Muggeridge, G. D., 1980. Final report on exploration compiled within temporary reserve 7012H Lamil Hills, Paterson Range, Western Australia. CRA Exploration.
- Reed, A., 1996. The structural, stratigraphic and temporal setting of the Maroochydore copper prospect, Paterson orogen, Western Australia. Unpublished Ph. D. thesis, Perth, Australia, University of Western Australia, 289 p.
- Roach, I. C., 2009. A drill hole database for the Paterson airborne electromagnetic (AEM) survey, Western Australia. Geoscience Australia, Canberra. Record 2009/31, 16 p.
- Skirrow, R. G., Jaireth, S., Huston, D. L., Bastrakov, E. N., Schofield, A., van der Wielen, S. E. and Barnicoat, A. C., 2009. Uranium mineral systems: processes, exploration criteria and a new deposit framework. Geoscience Australia, Canberra. Record 2009/20, 44 p.
- Stewart, A. J., 2008. Surface Geology of Australia 1:1 000 000 scale, Western Australia. Geoscience Australia, Canberra. http://www.ga.gov.au/minerals/research/national/nat_maps/nat_geol_maps.jsp.
- Towner, R. R., Gibson, D. L., Young, G. A. and P., M., 1980. Geology of the Canning Basin, Western Australia (1:1 000 000 surface geology map and 1:3 000 000 simplified geology and structure). Bureau of Mineral Resources, Geology and Geophysics, Canberra.
- Wilford, J. R., Bierwirth, P. N. and Craig, M. A., 1997. Application of airborne gamma-ray spectrometry in soil/regolith mapping and applied geomorphology. *AGSO Journal of Australian Geology and Geophysics* **17(2)**, 201-216.
- Williams, I. R., 2003. Yarrie, Western Australia. 1:250 000 Geological Series - Explanatory Notes. Geological Survey of Western Australia, Perth. 84 p.
- Williams, I. R., 2004. Yarrie, W.A. Sheet 51-1. 1:250 000 Geological Series., Western Australian Geological Survey. 3rd edition.

- Williams, I. R., Bagas, L. and Smithies, R. H., 1996. Throssell, W.A. Sheet 3252. 1:100 000 Geological Series, Western Australian Geological Survey.
- Williams, I. R. and Trendall, A. F., 1996a. Braeside, W.A. Sheet 3155. 1:100 000 Geological Series, Western Australia Geological Survey.
- Williams, I. R. and Trendall, A. F., 1996b. Pearana, W.A. Sheet 3154. 1:100 000 Geological Series, Western Australia Geological Survey.
- Williams, I. R. and Trendall, A. F., 1998a. Geology of the Pearana 1:100 000 sheet, 1:100 000 Geological Series Explanatory Notes. Western Australia Geological Survey, Perth. 33 p.
- Williams, I. R. and Trendall, A. F., 1998b. Geology of the Braeside 1:100 000 sheet, 1:100 000 Geological Series Explanatory Notes. Western Australia Geological Survey, Perth. 39 p.
- Williams, I. R. and Trendall, A. F., 1998c. Geology of the Isabella 1:100 000 sheet, 1:100 000 Geological Series Explanatory Notes. Western Australia Geological Survey, Perth. 24 p.

8 Summary and conclusions

I. C. Roach, D. K. Hutchinson, A. J. Whitaker, M. T. Costelloe, D. Huston, S. F. Liu and S. Jaireth

The Paterson airborne electromagnetic (AEM) survey is the first AEM survey of its kind conducted in Australia. From the outset the survey was designed to promote energy (uranium) and other minerals (particularly gold, copper, lead, zinc and manganese) exploration in a highly prospective, under-explored region. The survey was not designed to focus on specific targets, but to characterise a large region in which energy and world-class mineral targets occur, in the hope of encouraging further discoveries. The survey design changed during the planning process to become much more regional; initially, the survey was focussed on a very narrow region covering the Gregory and Throssell ranges and a small area of the Rudall Complex, but was enlarged considerably with the addition of flight lines spaced 6 km apart to the final flight plan, as presented in this Record.

The AEM data collected during the survey has met or exceeded all expectations, not only from a technical standpoint for its excellent repeatability, low noise and high detection limits, but also from a scientific perspective for the amount of new regional and detailed geological information which is possible to interpret from the data. This summary highlights some of the new perspectives which have come about as a result of the AEM survey and subsequent research. We also highlight the positives, the negatives, and the areas that need follow-up work, which were encountered during the acquisition, processing and interpretation phases of the survey.

8.1 IMPLICATIONS FOR URANIUM MINERAL SYSTEMS

The AEM data have proven valuable for identifying and mapping environments where potential uranium deposits may occur. These include: unconformity-related systems (e.g., Kintyre and prospects in the Sunday Creek-Maroochydore area); buried potential palaeovalley-palaeochannel sandstone-related systems in the Canning and Disappointment palaeovalleys, near the Gregory Range and within the Canning Basin; potential roll-front uranium systems in Permian sediments; and, saline water around salt lakes and valley calcrete occurrences where redox interfaces could occur.

A number of unconformities have been recognised within the AEM data set including the Coolbro Sandstone-Rudall Complex unconformity, which is important for its relationship to unconformity-style uranium mineralisation at Kintyre. This unconformity is visible as a saw-toothed, weak conductivity contrast between the overlying resistive Coolbro Sandstone and the underlying resistive Rudall Complex, which may reflect the presence of a weakly-conductive weathering profile on the palaeo-weathering surface and/or alteration of this contact. Unconformities between other Proterozoic rocks and between Proterozoic and Archean rocks are also recognised within the AEM data set and these too may have potential for further unconformity-style uranium or uranium-copper mineralisation. The unconformity-related, uranium-dominated deposits (e.g., Kintyre) are associated with northwest-striking faults and have a lithological association with the magnetic and moderately-to highly-conductive Yandagooge Formation, particularly iron-rich or carbonaceous successions. The AEM data also maps the carbonaceous and pyritic facies of the Broadhurst Formation which may be prospective for uranium and uranium-copper mineralisation at interfaces with the Coolbro Sandstone, especially near faults that may have acted to focus basinal fluids. Examples of unconformity systems interpreted from AEM and geological data are illustrated using examples from the AEM data set and GIS data in [Section 5.6](#) and [Chapter 7](#) of this Record.

Younger unconformities are recognised within the AEM data, such as those within the Canning Basin, for example, between Permian and Mesozoic successions, and between the Mesozoic successions, for example, the Anketell Sandstone and the Frezier Sandstone. These, like the

unconformity between the Permian Canning Basin succession and the underlying Neoproterozoic rocks (see [Section 5.5](#)), are not prospective for unconformity-style uranium deposits *per se*, but may indicate where sandstone-style deposits could potentially occur in overlying Permian (but probably not Mesozoic) sediments. These mineral systems rely on uranium dissolved from uranium-bearing host rocks entering groundwater aquifers and interacting with a reductant to create a uranium deposit, including:

- Sandstone-style palaeochannel roll-front or tabular uranium deposits similar to those in the Frome Embayment of South Australia (e.g., Beverley, Four Mile, Goulds Dam and Honeymoon) involving a solid reductant like carbon from plant remains relatively proximal to the source;
- Kazakhstan-style uranium deposits involving uranium in groundwater interacting with a liquid or gaseous hydrocarbon as a reductant, which may have leaked along a fault line from hydrocarbon traps deeper within a sedimentary basin, relatively distal from the source; and,
- Calcrete-type deposits accumulated around salt lakes and within valley calcretes that may host uranium at redox interfaces (e.g., Yeelirrie, Lake Way and Centipede). Palaeovalleys and aquifers channel surface and subsurface water flow towards redox interfaces at salt lakes. Bends may accumulate organic carbon material in point bars which could fix uranium.

We have been able to recognise conductive Permian and Mesozoic units within the Canning Basin and younger palaeovalley systems which could potentially host sandstone-style uranium deposits, as well as a number of fault systems which could potentially transfer hydrocarbons from deeper within the Canning Basin, especially in the Waukarlycarly Embayment, to act as reductants. These are described in [Sections 5.5](#) and [5.7](#) and [Chapter 7](#) of this Record.

Further work is required to assess the potential of uranium mineral systems associated with Neoproterozoic unconformities and stratabound uranium-copper of the Miles mineral system (see [Section 8.2](#)). This requires:

1. Detailed and systematic mapping of reductants in the Rudall Complex, Broadhurst Formation, Coolbro Sandstone and Canning Basin;
2. Evaluation of the diagenetic history of the Googhenama Formation to assess the possibility of diagenetic fluids acting as a uranium transport medium;
3. Mapping of alteration and indication of deposition of uranium from the distribution of mapped gossans and interpretation of remotely sensed data (e.g., ASTER satellite imagery);
4. Analysis of favourable fault systems for uranium- and hydrocarbon transport; and,
5. Recognition of the potential for iron oxide-copper-gold(-uranium) (IOCG) mineral systems in the Paterson region.

Further work is also required to detect and map the presence of any possible *in situ* and/or mobile reductants in, or at the base of, the Paterson Formation and within the Mesozoic sediments of the Canning Basin along hydraulic gradients from suitable uranium source rocks. This includes determining the abundance and nature of both plant- and hydrocarbon-derived reductants to further determine the potential and certainty of palaeovalley-type sandstone-hosted uranium mineral systems associated with Permian and Cenozoic palaeovalleys. The AEM data do not appear to directly detect redox fronts, which may represent potential sandstone-style uranium deposits. The data do highlight changes in ground water salinity around salt lakes and playas which could also correspond to redox fronts within valley calcrete systems, or which may delimit the maximum extents of sedimentation in which redox fronts are likely to occur.

Lastly, we caution that care should be exercised during AEM system selection when designing AEM surveys to detect unconformities so that detection levels and data processing methodologies are suitable to highlight subtle conductivity contrasts between materials above and below the unconformities. Unconformities imaged in this survey demonstrate that conductivity contrasts may be subtle, unconformities may have complex geometries and could be deeply buried. Furthermore,

while the AEM data do not appear to directly map mineralisation at Kintyre, they may map alteration of the Yandagooge Formation, which appears resistive at Kintyre but is conductive in other areas. Care needs to be taken with interpretation to search for obvious discrepancies such as this which may have real geological explanations.

8.2 IMPLICATIONS FOR OTHER MINERAL SYSTEMS

Geological and geochronological data suggest that two broad mineral systems have affected the Paterson region:

1. An 840-810 Ma system termed the Miles mineral system; and,
2. A 655-630 Ma system termed the O'Callaghans mineral system.

The Miles mineral system is interpreted to have operated during the Miles Orogeny and was associated with the inversion of the Yeneena Basin. Three broad deposit groups are inferred to have formed in this system:

1. Uranium-dominant (with anomalous copper) deposits localised within Paleo- to Mesoproterozoic basement just below the basal unconformity with the Coolbro Sandstone;
2. Uranium-copper deposits localised along the contact between the Coolbro Sandstone and the Broadhurst Formation; and,
3. Copper-dominant (with anomalous uranium) deposits in the upper part of the Broadhurst Formation.

The unconformity-related deposits also contain variable amounts of lead, zinc, silver, gold, platinum group elements, bismuth, molybdenum and antimony.

The deposits along the contact between the Coolbro Sandstone and Broadhurst Formation (e.g., Sunday Creek) are commonly associated with carbonaceous intervals, with uranium localised stratigraphically below copper. These deposits, although being stratabound, are commonly associated with anticlinal closures and/or faults.

Copper-dominant deposits appear to have, at least in part, replaced carbonate-rich units within the upper, conductive part of the carbonaceous shale-siltstone-dominated Broadhurst Formation. These deposits are commonly associated with northwest-striking faults and/or northwest-striking synclines. These deposits appear to be associated with uranium-enriched zones along their margins.

The Miles mineral system is interpreted to have involved low- to moderate-temperature fluids that flowed along an aquifer in the Coolbro Sandstone into structures which formed during, or were reactivated by, the Miles Orogeny, including thrust faults and synclines. The fluid flow pathway in the Coolbro Sandstone appears to be mappable using ASTER satellite imagery. There were possibly two stages to the mineral system. During the early stage (ca. 840 Ma), the fluids flowed downwards into the underlying basement, where they reacted with reduced carbon-rich or iron-rich rocks or with fluids in equilibrium with such rocks. Reduction of the uraniferous fluids during these reactions caused uranium deposition. During the later stage (ca. 810 Ma), the fluids flowed upwards into the reduced carbon-rich Broadhurst Formation along faults, depositing uranium and copper upon reaction with fluids in equilibrium with these rocks. These reactions took place near the contact with the Broadhurst Formation or in carbonate-rich intervals in the upper part of this unit. In all cases, reduction of the ore fluids was the cause of ore deposition. Other reduced rocks, such as mafic volcanics or intrusions, may also localise mineralisation. Isotopic evidence suggests that copper in these systems was derived from mafic rocks which intruded the Yeneena Basin at ca. 835 Ma.

The O'Callaghans mineral system is interpreted to have accompanied intrusion of the O'Callaghans Supersuite and formed epigenetic gold-copper deposits and skarn tungsten-copper-zinc-lead deposits. Gold-copper deposits are hosted by siliciclastic (e.g., Telfer) and intrusive mafic rocks

(e.g., Magnum) in the upper part of the Yeneena Basin and include both concordant and cross-cutting ore bodies. In both cases, the ore metals are hosted largely by veins and/or breccias.

The ore fluids which formed the gold-copper deposits were moderately saline, moderate-temperature fluids which have been interpreted as either evolved, magmatic-hydrothermal fluids or evolved basinal brines. In either case, granites of the O'Callaghans Supersuite most likely drove fluid flow. Many of these gold-copper deposits are localised within domes, some of which may be related to blind northwest-striking thrusts which formed, or were reactivated, during the formation of the O'Callaghans mineral system. These structures were most likely the fluid conduits. Ore deposition was most likely caused by a combination of chemical gradients (e.g., increase in the content of organic matter and/or carbonate, or reactions with mafic rocks) and rheology (e.g., rheological contrasts or easily fractured, brittle rocks).

The known tungsten-copper-zinc-lead deposits are hosted by carbonate rocks of the Puntapunta Formation (e.g., O'Callaghans); other carbonate-rich units (e.g., the Isdell Formation or the upper part of Broadhurst Formation) may also have potential as hosts. The mineralised zones are hosted by exoskarn along the margins of the O'Callaghans Supersuite granite.

No data are available for the fluids which formed the tungsten-copper-zinc-lead deposits, although they are most likely magmatic-hydrothermal. Skarn formation and metal deposition was probably caused by interaction of these magmatic-hydrothermal fluids with carbonate rocks.

The AEM data are useful for mapping boundaries between regional rock types with contrasting conductivities, or mapping highly conductive target units, while not appearing to map ore deposits directly. A number of formations within the Proterozoic rocks of the survey area can be recognised as having a conductivity contrast with surrounding materials, particularly those containing carbon and/or pyrite. These include parts of the Broadhurst Formation, parts of the Yandagooge Formation and parts of the Telfer Member. Subtle conductivity anomalies are also recognised in the Woodie Woodie area, interpreted as conductive Jeerinah Formation. We recommend that further work be taken to reprocess the AEM data and draw out the subtleties in these areas to determine whether the AEM system is detecting mineralisation or simply the host rocks of the mineralisation.

The unconformity interface between Canning Basin sediments and the underlying Proterozoic rocks is also recognised within the AEM data set; this has been mapped over a considerable area (see [Section 5.5](#) of this Record). This unconformity separates the Paleozoic Canning Basin from the Proterozoic Yeneena Basin and Rudall Complex. The ability to recognise and map this unconformity reduces exploration risk in the region by giving much better depth to target information for explorers.

The AEM data require detailed interpretation to determine possible relationships between conductivity anomalies and parts of the Miles and O'Callaghans mineral systems. We recommend that more thorough investigations are undertaken within these new mineral systems to determine these relationships in the Paterson area. We also recommend that further work be undertaken to improve isotopic dating of the mineral systems and regional geology to improve our understanding of the lithostratigraphy of the Paterson area.

8.3 IMPLICATIONS FOR REGIONAL GEOLOGY

The AEM data demonstrably improve our knowledge of regional 3D geology, especially geology under cover. The AEM method senses a different geophysical property—electrical conductivity—and reliably penetrates up to 400 m into the Earth, depending on local conditions affecting the calculated depth of investigation (DOI; see [Chapter 4](#)). Unlike magnetic and gravity methods, the AEM method can image subtle conductivity contrasts in sedimentary basins and, where conditions

are suitable, can provide meaningful information about both basin cover and crystalline or metamorphic basement rocks where these are juxtaposed.

Some of the regional geological relationships observed within the AEM data set include:

- High conductivity (ca. >250-1000 mS/m): salt lakes; saline ground water; areas of valley calcrete (probably due to associated saline lake sediments or groundwater); areas of Cenozoic Oakover Formation; carbonaceous and pyritic facies of the Neoproterozoic Broadhurst Formation; graphitic Paleoproterozoic Yandagooge Formation; and, parts of the Archean Jeerinah Formation;
- Moderate to high conductivity (ca. 100-1000 mS/m): parts of the Permian Paterson Formation, Poole Sandstone, Noonkanbah Formation and Triwhite Sandstone; Cenozoic fill in palaeovalley systems including the Canning and Disappointment palaeovalleys; parts of the Neoproterozoic Tarcunyah Group; parts of the Neoproterozoic Telfer Member; parts of the Archean Jeerinah Formation; and, parts of the Archean Pinjian Chert Member;
- Low to moderate conductivity (ca. 50-100 mS/m): parts of the Mesozoic sediments in the Canning Basin; the Wallal Palaeovalley; parts of the Neoproterozoic Tarcunyah Group; parts of the Neoproterozoic Malu and Wilki formations; and, regolith on top of basement including recent alluvium; and,
- Resistive (< ca. 50 mS/m): fresh bedrock, including the Archean Gregory Range Suite; most of the Archean Fortescue Group; the Archean Carawine Dolomite; the Paleo- to Mesoproterozoic Rudall Complex; the Neoproterozoic Coolbro Sandstone; granites of the Neoproterozoic O'Callaghans Supersuite; and, ferruginous duricrust and aeolian sediments.

The presence of faults was often deduced where there was a change in conductivity pattern across a lineament (such as the truncation of conductive bedding trends) and less commonly as linear, relatively-resistive corridors (especially near Kintyre). Faults were not seen as linear conductive corridors.

The AEM data were most informative of the presence of highly conductive bedrocks, particularly those containing carbon, pyrite and graphite. The data could be processed to show contact relationships between weakly to moderately conductive materials and underlying highly conductive rocks (for instance, Permian sediments overlying the Broadhurst Formation) or resistive rocks (for instance, Permian-Mesozoic sediment overlying Malu or Wilki Formation). With adequate geological control from drill hole lithological logs, the boundaries between rock units could be picked to within 20-30 m vertically from the Geoscience Australia layered earth inversion (GA-LEI) AEM conductivity sections. The data could not, however, be used to show the relationship between an overlying strong conductor and underlying weak conductor or resistor, because the AEM signal was trapped in the upper conductive layer.

The AEM data showed dipping strata where the conductivity contrast between materials is ideal and dip angles are relatively low, for instance in the Canning Basin area, where up to four separate conductive layers are visible in GA-LEI AEM conductivity sections. The data also could be used to interpret weathering features, particularly in the conductive facies of the Broadhurst Formation, which has a ca. 50 m thick zone of gradually increasing conductivity from weathered to fresh rock downwards from the contact with overlying Permian units, and the resistive Coolbro Sandstone, which has a thin zone (10-20 m thick) of increased conductivity ca. 10-20 m below the land surface, which is interpreted as conductive weathering products.

We found that we could not readily distinguish or map boundaries between resistive granite and surrounding resistive sediments. Contact aureoles were also resistive and did not provide a conductivity contrast in the Paterson region.

8.4 UTILITY OF REGIONAL AEM FOR MINERAL EXPLORATION

The Paterson AEM data set offers a new regional geological perspective by providing continuous, verifiable depth to target information for resistive or conductive basement, provided that the ground conditions are correct according to the DOI map (see [Chapter 4](#)), that there is adequate drill hole control and that the relationships between conductors discussed in [Section 8.3](#) are observed. The AEM data have the ability to provide new information regarding the distribution of major geological units (for instance, the Rudall Complex and parts of the Yeneena Basin) and also palaeotopographic features (e.g., the Anketell Shelf, the Throssell Shelf and the buried portions of the Rudall Complex under the Canning Basin). Thus, the data assist in reducing exploration risk by improving knowledge and targeting by characterising the type and extent of previously unknown regional geology under cover.

The DOI grid shown in [Figure 4.4](#) is the first example of a graphical AEM “Go map” that depicts the reliable depth of AEM signal penetration over a wide area. This can be used to plan future regional and tenement-scale AEM or ground EM surveys, further reducing the risk for geophysical exploration of the Paterson region.

The AEM data set illustrates the utility of relatively wide-spaced flight lines (1 and 2 km spacing) to provide along-line local detail and also between-line regional geological information to allow interpretation of 3D geology within a survey area. The survey also highlights the value of obtaining good geological control from a number of close-spaced flight lines over areas of interest to allow inferences to be extrapolated to the regional AEM data. The AEM data can, and did in this case, map discrete conductors in resistive rocks and allowed these conductors to be traced for many kilometres between flight lines. The conductive rocks are laterally continuous with known carbonaceous or sulfide-rich rocks and may be relevant to mineralisation, according to the mineral systems models proposed in [Chapter 6](#), [Chapter 7](#) and [Sections 8.1](#) and [8.2](#). Certainly, some of the conductivity anomalies are spatially correlated with known mineral deposits.

The GA-LEI interpretation products (conductivity sections, conductance grid, elevation slice grids and depth slice grids) provide a set of data-rich images for interpreting gross conductivity anomalies but also subtle conductivity contrasts, allowing greater geological interpretability. We have improved the utility of these images by providing them as georeferenced raster files. These can be imported rapidly into any GIS or image processing software to provide real-world coordinates for features within the data set. The gridded data sets each provide useful information in a different format. The conductance grid shows the summed conductivity over the total range of the data inversion, without necessarily solving for depth. This is a more “honest” approach to the AEM data as it does not contain the depth assumptions used in the depth- and elevation-sliced data (See [Section 4.4](#) and [Appendix 4](#)). The conductivity depth slices depict interpreted conductivity in slices below the ground surface, which is useful for interpreting depth to target information. The conductivity elevation slices depict the interpreted conductivity in slices based on height above datum, which is useful for interpreting the AEM data in 3D.

A number of lessons have been learned during the acquisition, processing and interpretation of the Paterson AEM survey:

- In hindsight it would have been preferable to fly more lines at 2 km line spacing rather than 6 km line spacing. Data flown at 6 km flight line spacing provide detail along-line and deliver useful regional information between lines but can not be gridded to provide useful interpolations with reasonable grid cell sizes;
- Regional geology was almost equally well described by 2 km flight line spacings as it was with 1 km flight line spacings. However, important local detail was obtained from 200 m and 1 km flight line spacings. Survey planning should include some areas of close-spaced infill to allow extrapolation of detailed geological information to the regional survey lines as

this survey did;

- Field work in support of verifying the data inversion should be expanded to collect more information regarding properties which affect the AEM response, as well as information regarding mineral systems. These data would include rock properties (electrical conductivity, magnetic susceptibility, density, porosity and permeability), drill hole lithological and induction conductivity logging and surface and ground water analysis. Simultaneously, samples should be collected for geochemical analysis in support of mineral systems analysis;
- AEM data inversions could be improved to include line-by-line inversions (rather than the sample-by-sample inversions presented in this Record); this would reduce vertical noise artefacts and provide smoother detail for horizontal and near-horizontal conductors. A greater number of enhanced products could be created, including inversions using 30 layers over 200 or 150 m (but also including the 400 m as presented in this Record) to assist in interpreting the near-surface data at a more detailed scale (1:10 000 or 1:25 000). This would assist in assessing existing, and identifying new, mineral system models, structural architecture, faults, fluid pathways and prospective horizons to enhance the chances of mineral discovery and reduce the risks involved with exploration;
- We do not have clear estimates of conductivity uncertainty (i.e., no confidence intervals) for the AEM data because of the paucity of real conductivity values from drill hole logging within the survey area. Only a limited number of drill holes were conductivity-logged within the survey area and, while these data have been useful in the validation process, the number of drill holes is too few to accurately set confidence intervals on the inversion data. Ideally, surveys should be verified by a drilling campaign during acquisition, where drill holes are strategically placed underneath flight lines. Uncertainty estimates could also be improved using Data Misfit and PDI calculations together to give a "model confidence" measure during the processing phase; and,
- It is important to compile data from existing drill hole logging before commencing a survey. Drill hole data could suggest areas where detailed infill lines should be flown and also areas where additional complementary drill holes could be drilled to aid interpretation of the AEM data.

8.5 IMPLICATIONS FOR GROUNDWATER

The AEM data are shown to have great utility for detecting saline surface and ground waters in detail along-line and, in general, within the regional gridded data. These waters are detected by looking for the presence of conductivity anomalies which conform to known palaeotopographic features which could represent palaeovalley or palaeochannel systems (such as the Canning, Disappointment and Wallal palaeovalleys). Similarly, such conductivity features could represent aquifers within sedimentary basins (such as Permian and Mesozoic strata in the Canning Basin) or fractured rock systems (such as those in the Yeneena Basin or Rudall Complex). Equally, resistivity anomalies coinciding with palaeotopographic features can be used to highlight areas which may host fresh ground waters, such as the Wallal Palaeovalley and some of the Permian palaeovalley features around the Kintyre area.

Again, interpretations of conductivity and resistivity anomalies need to be followed by detailed field work, which was beyond the scope of this survey.

8.6 THE FUTURE

There is scope for collecting more regional AEM data within Australia to map the fundamental geophysical property of electrical conductivity. We have shown here that, within the caveats set by

the DOI image and our understanding of the electrical properties of regional geological units, regional AEM surveying can provide an additional layer of data of similar utility to regional magnetic, gravity and radiometric data.

9 Acknowledgements

The acquisition, processing and interpretation of the Paterson AEM survey would not have been possible without the support of the following people and organisations:

- Reviewers (in alphabetical order):
 - Leon Bagas (GSWA), Andy Barnicoat, Ross Brodie, Mike Craig, Pauline English, David Huston, Russell Korsch, Brian Minty, Murray Richardson, Anthony Schofield, Roger Skirrow, Ned Stolz, Simon van der Wielen, Nick Williams and Lisa Worrall.
- Geoscience Australia Onshore Energy and Minerals Division GIS staff (in alphabetical order):
 - Lindsay Highet, Andrew Retter, Gerard Stewart and Henry Walshaw.
- Fugro Airborne Surveys Pty. Ltd.;
- Aditya Birla Minerals – Birla Nifty Operations for field support as well as land access, access to open bore holes, lithological logs;
- Consolidated Minerals – Woodie Woodie Operations for access to confidential data;
- Newcrest Mining Limited – Telfer Operations for access to open bore holes and lithological logs;
- Subscription companies for their support of the AEM project by funding additional infill lines, supplying historical data and providing geological support:
 - Rio Tinto;
 - Cauldron Energy;
 - Cameco;
 - Mega Uranium; and,
 - Western Areas.
- The Western Desert Lands Aboriginal Corporation (WDLAC) for granting access to the traditional lands of the Martu people;
- The Geological Survey of Western Australia;
- The Geophysics Group, Onshore Energy and Minerals Division, Geoscience Australia; and,
- Adrian Fisher for his early work in helping set up the survey.

Appendix 1 Fugro Airborne Surveys flight duration considerations

The following is a reproduction of a document prepared by Fugro Airborne Surveys Pty. Ltd. and describes the flight duration characteristics of the CASA aircraft used in the Paterson AEM survey.

FUGRO AIRBORNE SURVEYS PTY LTD



U3, 435 Scarborough Beach Road
Osborne Park, 6017
PO Box 1847
Osborne Park, 6916
Western Australia

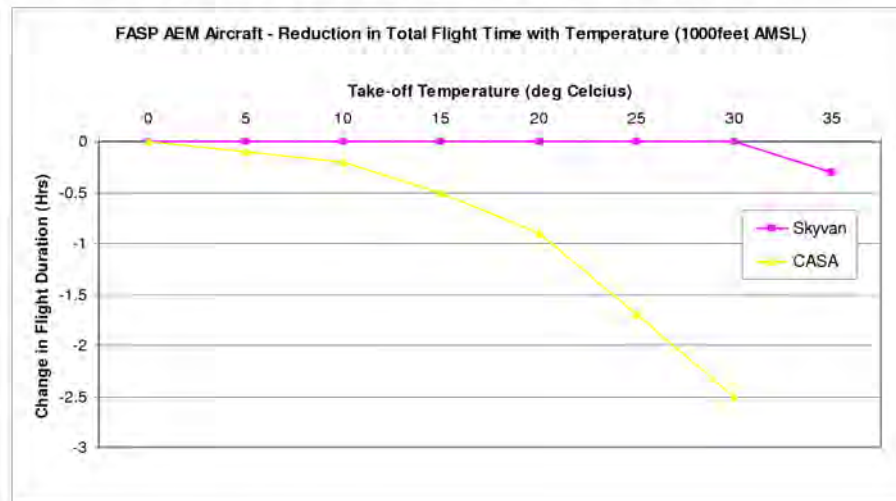
Telephone: +61 8 9273 6400
Facsimile: +61 8 9273 6466

FASP AEM Aircraft Flight Duration – Paterson (WA) and Pine Creek (NT) AEM Surveys

Assuming a fixed aircraft configuration and performance on an airstrip of sufficient length, flight endurance (total time in-flight including all legally required fuel reserves) will be primarily a function of the airfield elevation above mean sea level and the ambient take-off temperature.

With regard to flight duration (the time available for survey excluding fuel reserves) and the number of achievable flights per day, this is determined by the maximum flight endurance for the prevailing site conditions, meteorological (temperature, turbulence, rain, haze, lightening, etc) and geophysical (stereics and geomagnetic activity) conditions and other operational considerations such as ferry distance from the base of operations. There may also be other site specific factors identified during a standard job risk assessment that may have an influence including such things as the availability and proximity of suitable alternate airfields and any local legislative, weather or airfield requirement to carry additional fuel reserves over and above the minimum legal and company regulations for a survey flight operating under visual flight rules.

The following graph depicts the relationship between the take-off temperature and flight endurance at a nominal 1000 feet above mean sea level which represents the conditions encountered for the Paterson and Pine Creek AEM surveys with the Skyvan and CASA.



Fugro Airborne Surveys Pty Ltd ABN: 33 009 238 395
A member of the Fugro group of companies with offices around the world



FUGRO AIRBORNE SURVEYS PTY LTD



This table should be considered as a guide only because the final determination of flight endurance is made by the Pilot in Command based on prevailing site conditions, weight and balance calculations and aircraft performance as determined from the available aircraft performance charts.

Due to the fact that the airfields used on the Paterson and Pine Creek AEM surveys were less than 1000 feet above mean sea level, there was only a minor effect on take-off weight and flight endurance. The main consideration for flight endurance was temperature which was variable throughout the duration of each job depending upon the time of year.

In general for the Paterson and Pine Creek surveys, the primary causes of reduced flight duration, aborted flights and the inability to complete more than one flight per day on most occasions can be summarised as follows:

Wind / Turbulence

The affect of wind and turbulence on the aircraft and towed bird are variable depending on the terrain. Sections of both Pine Creek and Paterson areas had ridgelines / sand dunes that resulted in much higher turbulence causing coil knocks at relatively low wind speeds. The actual wind speed at which the effect becomes significant on the quality of the AEM data is also variable but in general for these survey areas it was determined that around 10 to 15 knots was the maximum before a flight would not be viable and the aircraft would remain grounded. During the flight, the operator would monitor the data for the effect of wind and turbulence appearing as spikes caused by coil knocks and if this continued for an extended period the flight would be aborted. Coil knocks are one of the most common causes for early termination of a flight, and the reason second flights are uncommon with wind speeds generally increasing throughout the morning and only subsiding late afternoon by which time it was too late to complete a viable flight. Strong and gusty winds were particularly problematic on the Paterson survey.

Sferics

Sferics was another very common cause for the early termination of flights and, particularly for the Pine Creek survey, a major source of scrubbed data, reflights and the inability to survey. During the flight a sferics monitor allowed the operator to monitor the activity and magnitude of sferics and at a predetermined maximum value (based on previous analysis of the data at the same levels) a flight would be ended early. On days where sferics activity was known to be high, it was usual to take readings on the ground with the receiver on each of the survey headings to measure the effect. This procedure was used repeatedly on the Pine Creek survey to determine if sferics levels were low enough for survey.

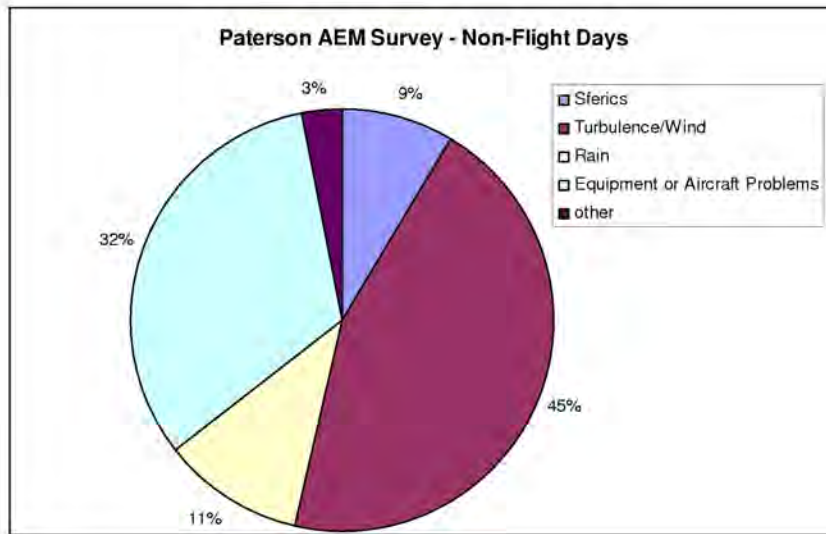
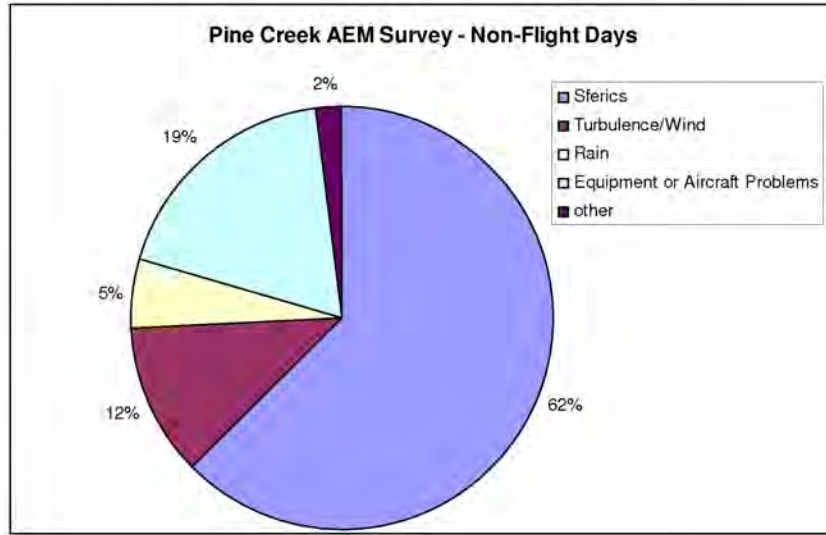
Lightening

During the Pine Creek survey, due to the onset of the wet season, a significant amount of lightening activity was observed. This activity was generally more prevalent during late afternoon and evening but on occasions resulted in the inability to survey at all. This was one of the reason very few second flights were conducted during this survey in the first field season of acquisition. Standard internet lightening tracking sites were used to aid planning and prediction of lightening activity.



FUGRO AIRBORNE SURVEYS PTY LTD

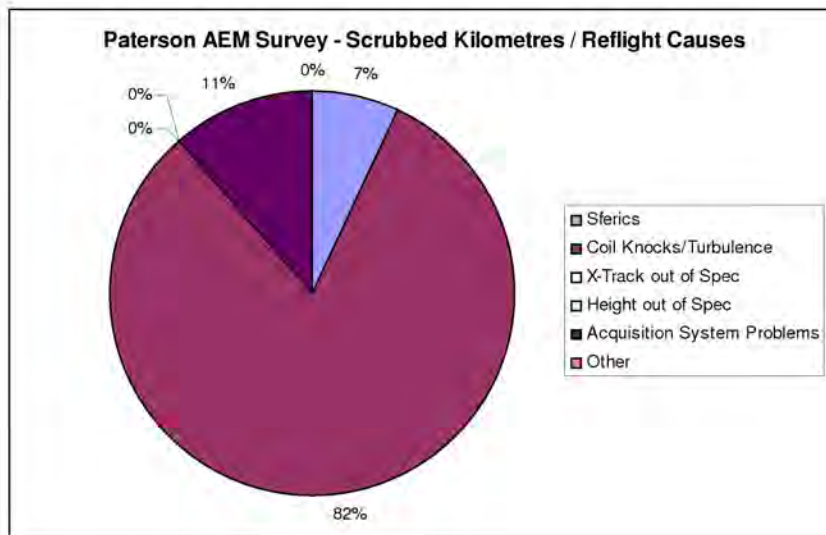
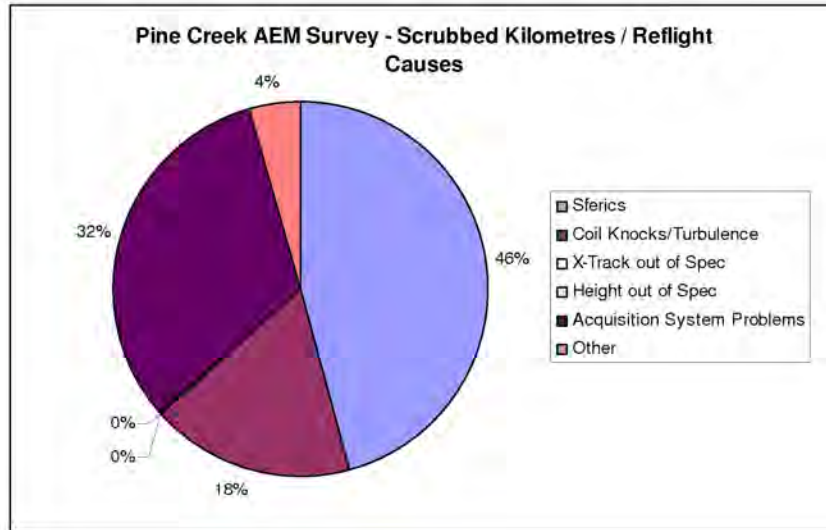
A breakdown of the causes for lost flying days as a percentage of total survey days on the Paterson and Pine Creek surveys (exclusive of scheduled items such as pilot days off, scheduled aircraft maintenance and mob/demob) is summarised as follows:





FUGRO AIRBORNE SURVEYS PTY LTD

A breakdown of the causes for **scrubbed kilometres** as a percentage of total survey kilometres on the Paterson and Pine Creek surveys is summarised as follows:



FUGRO AIRBORNE SURVEYS PTY LTD



Additional Considerations for Aircraft Performance

Modifications made to our survey aircraft have resulted in a degradation of their original performance characteristics due to the fitment of external geophysical acquisition equipment (loop cables and attachment structures, magnetometer stinger, and towed bird). As a result, the operation of these aircraft is subject to performance restrictions to ensure they can conform to certain regulations and be able to meet the performance requirements stipulated by those regulations and/or requirements. These limitations are in the form of take-off weight restrictions and graphed performance capabilities implemented by approved Supplemental Type Certificates, Engineering Orders and Civil Aviation Safety Authority requirements.

Essentially these requirements ensure that if the aircraft suffered an engine failure on take-off or an emergency situation such as engine fire, the crew under optimum conditions would be able to continue flight and safely land the aircraft as soon as possible at the most suitable location.

The performance capabilities and limitations are presented to the pilot as a flight manual supplement. These supplements include descriptions of operating limitations, and a number of graphed performance charts from which the limiting maximum take-off weight for the ambient conditions can be ascertained.

The main limiting charts are (but are not the only limiting charts):

Accelerate Stop Charts: this chart establishes a maximum take-off weight of the aircraft to be found given ambient temperature, aerodrome elevation and runway length and runway surface. It is a weight for the distance available that allows the aircraft to be accelerated to an emergency decision speed termed V_1 , suffer an emergency and be able to bring the aircraft to a stop on the remaining runway.

Take-Off Distance Charts: for the given runway length factored by 115% and conditions, a maximum weight can be established that allows the aircraft to accelerate and take-off and climb to a height of 35 feet above the available runway.

Take-Off Climb Limits: this maximum take-off weight limit occurs when the available climb gradient of the aircraft with one engine inoperative is equal to any of the minimum climb gradients required by the regulations.

Take-Off Climb One Engine Inoperative: this demands the aircraft be able to maintain a climb at a steady rate of one hundred feet per minute at 1000 feet above the aerodrome elevation under ambient conditions, and;

En-route Climb One Engine Inoperative: a steady rate of climb of at least 50 feet per minute at 1000 feet above an obstacle under ambient conditions.

Appendix 2 Additional climate data

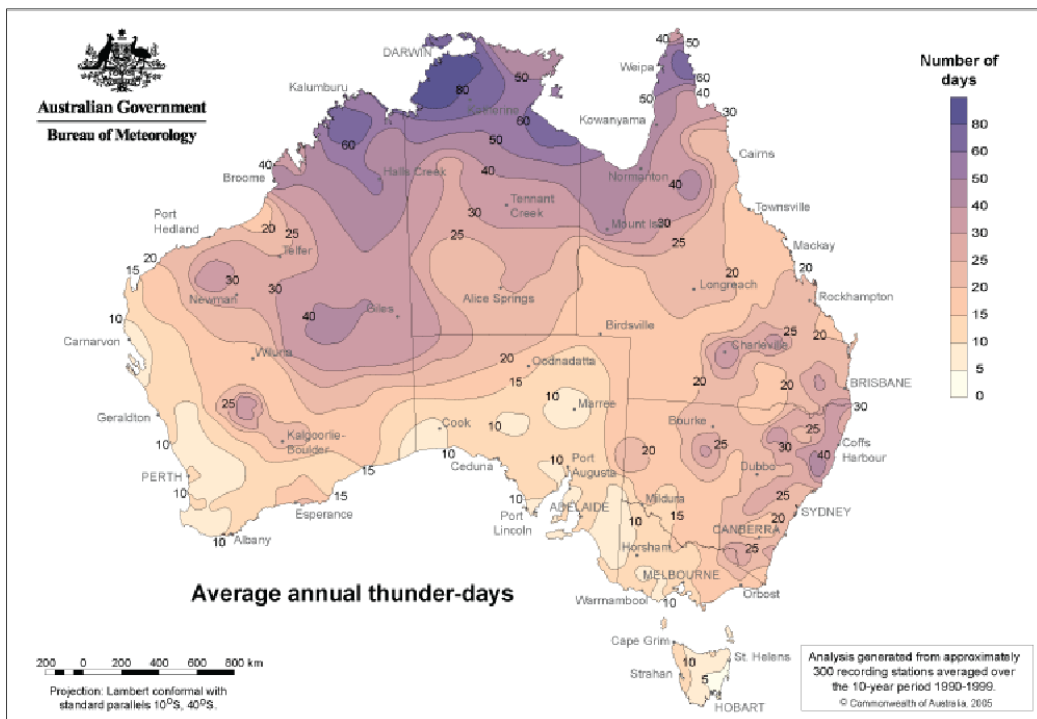


Figure A1.1: Average annual thunder days for Australia. From BOM (2009).

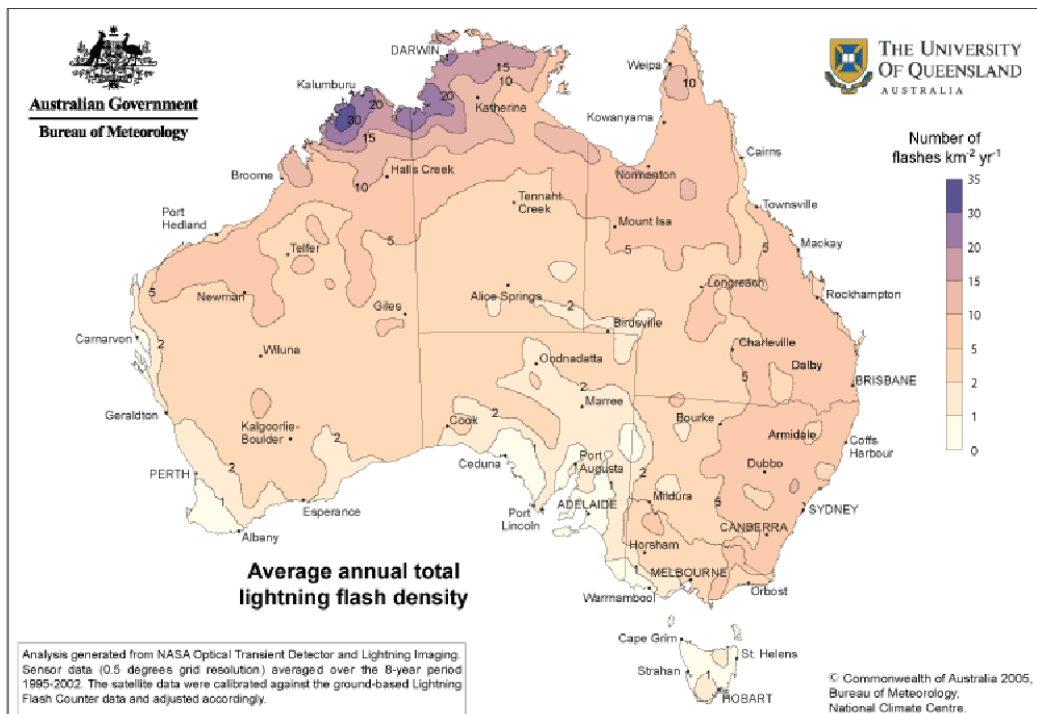


Figure A1.2: Average annual total lightning flash density for Australia. From BOM (2009).

Appendix 3 Inversion data

A3.1 GA PHASE 2 DATA RELEASE PRODUCTS TABLE

NAME	FORMAT	DESCRIPTION	COMMENTS
linedata			
master.inversion.dat	ASCII	ascii data file containing master inversion output (reference model = 0.004 S/m)	1 file containing 681 lines of data
master.inversion.hdr			
secondary.inversion.dat	ASCII	ascii data file containing inversion output used to calculate pdi (reference model = 0.04 S/m)	1 file containing 681 lines of data
secondary.inversion.hdr	hdr	associated header information in text format	1 txt file containing 125 lines of data
eintervals_10m.dat	ASCII	ascii data file containing inversion output sliced into 10 m elevation intervals	1 file containing 681 lines of data
eintervals_10m.hdr	hdr	associated header information in text format	1 txt file containing 82 lines of data
sections			
GA_LEI_georeferenced_jpeg	.jpeg and associated .jgw	georeferenced line sections of conductivity	Linenumber.jpg Linenumber.jgw
GA_LEI_multiplots	.pdf	line sections of conductivity, compared with AEM system geometry and data misfit.	Linenumber.pdf
grids			
Depth Slices	.ers	conductivity grids in slices of depth below surface	15 .ers files
Elevation slices	.ers	conductivity grids in slices of elevation above sea level (10 m and 50 m slices)	90 .ers files
Conductance	.ers	total conductance grids for 0-200m and 0-400m depth	2 .ers files
AEM Go Map conductance_jpeg	.ers .jpeg and associated .jgw	depth of investigation grid georeferenced grids conductance	1 .ers file 2 .jpg files
depth_slice_jpeg	.jpeg and associated .jgw	georeferenced grids depth slices	15 .jpg files
elevation_slice_jpeg	.jpeg and associated .jgw	georeferenced grids elevation slices	90 .jpg files
AEM_Go_Map_jpeg	.jpeg and associated .jgw	georeferenced grid AEM Go Map	1 .jpg file

A3.1 GA PHASE 2 DATA RELEASE PRODUCTS (CONTINUED)

NAME	FORMAT	DESCRIPTION	COMMENTS
report			
Paterson_Phase-2_report.pdf	.pdf	Explanatory notes	1 file
shapefiles			
Flight Lines		Three Paterson survey shape files and associated files	
Survey Boundary	.shp		19 files
National Park			

A3.2 GA-LEI INVERSION OF TEMPEST™ DATA

A 3.2.1 Introduction

The GA-LEI inversion program is capable of inverting data from most airborne time-domain AEM systems. It has the capability of inverting for layer conductivities, layer thicknesses and system geometry parameters, or some subset of these. There are options to use a multi-layer smooth-model formulation (Constable *et al.*, 1987) or a few-layer blocky-model formulation (Sattell, 1998). For the sake of simplicity, only the aspects of the algorithm that are relevant to the inversion of TEMPEST™ data using a multi-layer smooth-model are described here.

TEMPEST™ data consist of a collection (tens of thousands to millions) of point located multi-channel samples acquired at 0.2 s (approximately 12 m) intervals along survey flight lines. The algorithm independently inverts each sample. The data inputs to the inversion of each sample are the observed total (primary plus secondary) field X-component and Z-component data. Auxiliary information input into the algorithm are the measured and assumed elements of the system geometry, the thicknesses of the layers and prior information on the unmeasured elements of the system geometry and ground conductivity. The unknowns solved for in the inversion (outputs) are the electrical conductivity of the layers and the unmeasured elements of the system geometry.

Since each sample is inverted independently, the user may elect to invert all samples or some subset of them. The inversion of each sample results in an estimate of a one dimensional (1D) conductivity structure associated with that sample. Each estimated 1D conductivity structure, although theoretically laterally constant and extending infinitely in all directions, is only supported by the data within the system footprint which is approximately a square of side length 470 m centred about the sample point (Reid and Vrbancich, 2004). So, by progressively inverting all the samples and stitching together the resultant 1D conductivity structures, a depiction of the overall laterally variable 3D conductivity structure is built up.

A 3.2.2 Formulation

Figure A3.1 shows the overall framework under which the inversion of a single airborne sample is carried out. The elements of the figure are progressively described in the following sections.

A3.2.2.1 Coordinate system

Since each sample is inverted separately the coordinate system is different for the inversion of each sample. A right handed xyz Cartesian coordinate system is used. The origin of the coordinate system is on the Earth's surface directly below the centre of the transmitter loop. The x-axis is in the direction of flight of the aircraft at that sample location, the y-axis is in the direction of the left wing and the z-axis is directed vertically upwards.

A3.2.2.2 System geometry

The centre of the transmitter loop is located at $(0, 0, TX_h)$. Roll of the transmitter loop (TX_r) is defined as anti-clockwise rotation, about an axis through $(0, 0, TX_h)$ and parallel to the x-axis, so that a positive roll will bring the left wing up. Pitch of the transmitter loop (TX_p) is defined as anti-clockwise rotation, about an axis through $(0, 0, TX_h)$ and parallel to the y-axis, so that positive pitch will bring the aircraft's nose down. Yaw of the transmitter loop (TX_y) is defined as anti-clockwise rotation, about an axis through $(0, 0, TX_h)$ and parallel to the z-axis, so that a positive yaw would turn the aircraft left. However since the x-axis is defined to be in the direction of flight at each sample, the transmitter loop yaw is always zero by definition. The order of operations for calculating the vector orientations is to apply the pitch, roll then yaw rotations respectively.

The position of the receiver coils relative to the transmitter loop is defined by the transmitter to receiver horizontal inline separation (D_x), the transmitter to receiver horizontal transverse separation (D_y), and the transmitter to receiver vertical separation (D_z). The receiver coils are thus located at $(D_x, D_y, RX_h = TX_h + D_z)$. The receiver coils are always behind and below the aircraft ($D_x < 0, D_z < 0$).

The receiver coils' roll (RX_r), pitch (RX_p) and yaw (RX_y) have the same rotational convention as for the transmitter loop except that they are rotations about the point (D_x , D_y , D_z). The receiver coils are always assumed to be located on the y-axis ($D_y = 0$) and to have zero yaw ($RX_y = 0$). Although this is not in reality the case, the position and orientation is not measured and there is not enough information available to solve for these since Y-component data is not available.

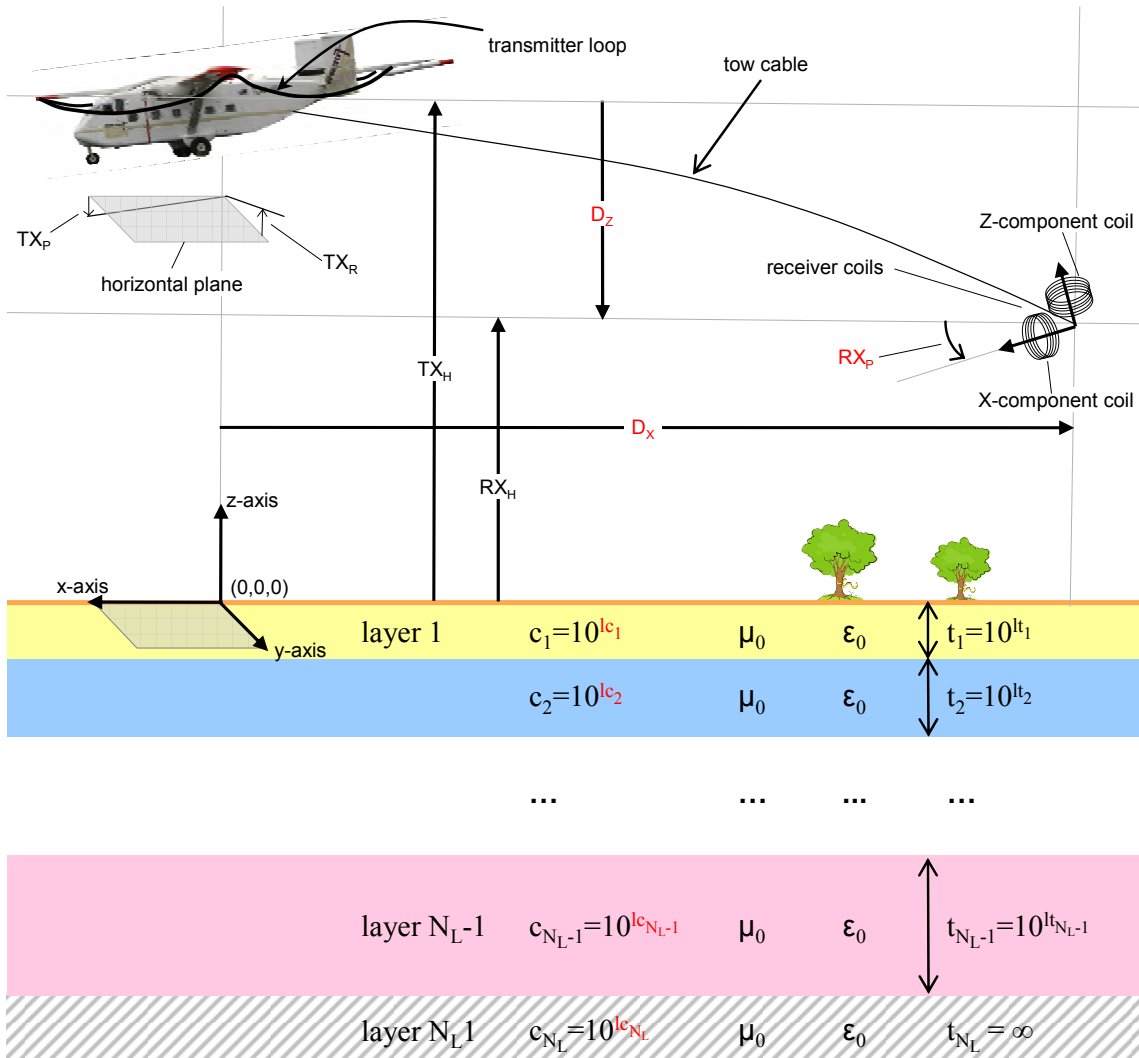


Figure A3.1: Schematic representation of the framework for GA-LEI inversion of TEMPESTTM AEM data. Red elements are the unknowns to be solved for.

Note that transmitter loop pitch data supplied by Fugro Airborne Surveys in processed TEMPESTTM data uses the convention where a positive transmitter pitch is nose up, and accordingly the supplied pitch is reversed in sign before being used in the inversion algorithm.

A3.2.2.3 Layered earth

The layered earth model is independent at each inverted sample location. The layered earth consists of N_L horizontal layers stacked on top of each other in layer cake fashion. The k^{th} layer has constant thickness t_k and the bottom layer is a halfspace that has infinite thickness ($t_{N_L} = \infty$), extending to infinite depth. The electrical conductivity of the k^{th} layer is c_k and it is constant throughout the layer. The magnetic permeability of all layers is assumed to be equal to the magnetic permeability of free

space μ_0 . The dielectric permittivity of all layers is assumed to be equal to the permittivity of free space ϵ_0 .

A3.2.2.4 Data

Part of the TEMPEST data processing sequence involves partitioning the total (secondary plus primary) field response that is actually observed into estimates of the unknown primary and secondary field components. Then an estimate of the transmitter to receiver horizontal in-line and vertical separations D_x and D_z are made from the partitioned primary field component. The procedure uses the measured transmitter pitch (TX_p) and roll (TX_r) and assumes the receiver coils are flying straight, level and directly behind the aircraft ($D_y=0$, $RX_r=0$, $RX_p=0$, and $RX_y=0$). It is the estimated secondary field data, the measured elements of the system geometry (TX_h , TX_p , TX_r , and TX_y) and the associated estimates of the unmeasured elements of the system geometry (D_x and D_z) that are delivered to clients. Implicit in the delivered dataset are the assumed elements of the system geometry ($D_y=0$, $RX_r=0$, $RX_p=0$, and $RX_y=0$). However the estimated primary field data are not delivered to clients.

Since the GA-LEI algorithm makes its own estimate of system geometry as part of the inversion procedure it works with total field data. The input data are the total (primary plus secondary) field X-component and Z-component data. Therefore the total field data are first reconstructed. This is a simple matter of recomputing the primary field from magnetic dipole formulae (Wait, 1982) using the delivered (measured, estimated and assumed) elements of the system geometry then adding them to the delivered secondary field data. Note that the height, pitch, roll and geometry corrected data that are usually delivered as part of TEMPEST datasets are not used because the GA-LEI algorithm makes its own estimate of system geometry as part of the inversion procedure.

The reconstructed X-component and Z-component total field data for the k^{th} window are $X_k = X^P + X^S_k$ and $Z_k = Z^P + Z^S_k$ respectively. Here the super scripts P and S represent primary and secondary field components. Since the TEMPEST™ system has $N_w = 15$ windows, the observed data vector of length $N_D = 2 \times N_w = 30$ used in the inversion is,

$$\mathbf{d}^{obs} = [X_1 \ X_2 \cdots X_{N_w} \ Z_1 \ Z_2 \cdots Z_{N_w}]^T \quad (1)$$

where T represents the matrix and vector transpose operator.

Errors on the data are calculated outside of the program and input along with the data. Errors are assumed to be uncorrelated and Gaussian distributed. They are estimated as standard deviations of the Gaussian error distribution for each window and receiver component. Typically errors are calculated from the parameters of an additive plus multiplicative noise model (Green and Lane, 2003). Parameters of the noise model are determined from analysis of high altitude and repeat line data. If X_k^{err} and Z_k^{err} , represent the estimated standard deviation of the error in the k^{th} window of the X- component and Z-component data respectively then the data error vector of length $N_D=30$ is,

$$\mathbf{d}^{err} = [X_1^{err} \ X_2^{err} \cdots X_{N_w}^{err} \ Z_1^{err} \ Z_2^{err} \cdots Z_{N_w}^{err}]^T. \quad (2)$$

A3.2.2.5 Model parameterisation

The unknown model parameter vector (\mathbf{m}) to be solved for in the inversion comprises earth model parameters and system geometry model parameters.

For the inversion of the TEMPEST dataset described here we choose to use a multi-layer smooth-model formulation (Constable *et al.*, 1987) rather than a few-layer blocky-model formulation (Sattell, 1998). Therefore we solve for the N_L conductivities of the layers but not the thicknesses. The layer thicknesses are inputs into the algorithm and are kept fixed throughout. To maintain

positivity of the layer conductivities we actually invert for the base ten logarithms of the conductivities of each layer.

We solve for $N_G=3$ system geometry parameters: the transmitter to receiver horizontal in-line separation (D_x), the transmitter to receiver vertical separation (D_z), and the pitch of the receiver coil assembly (RX_p).

The unknown model parameter vector of length $N_p=N_G + N_L$ to be solved for is the concatenated vector of log base ten layer conductivities $\mathbf{lc} = [\log c_1 \ \log c_2 \ \dots \log c_{N_L}]^T$ and the geometry parameters $\mathbf{g} = [D_x \ D_z \ RX_p]^T$, such that,

$$\mathbf{m} = [\mathbf{lc} \ | \ \mathbf{g}] = [\log c_1 \ \log c_2 \ \dots \log c_{N_L} \ D_x \ D_z \ RX_p]^T \quad (3)$$

A3.2.2.6 Forward model and derivatives

The forward model is the non-linear multi-valued function,

$$\mathbf{f}(\mathbf{m}) = [f_1(\mathbf{m}, \mathbf{p}) \ f_2(\mathbf{m}, \mathbf{p}) \dots f_{ND}(\mathbf{m}, \mathbf{p})], \quad (4)$$

which for a given a set of model parameters (\mathbf{m}) calculates the theoretical total field data equivalent to that which would be produced for an ideal system, after the measurement and transformation by the data processing steps (Lane *et al.*, 2000). Here each $f_k(\mathbf{m}, \mathbf{p})$ is a function, not only of the layer conductivities and system geometry parameters in the inversion model vector \mathbf{m} , but also of several other fixed parameters \mathbf{p} (layer thicknesses; transmitter height, pitch and roll; receiver roll and yaw, transmitter to receiver horizontal transverse separation; system waveform and window positions etc.).

The implementation of (4) is based upon the formulation of Wait (1982) in which he develops the frequency-domain expressions for the magnetic fields due to vertical and horizontal magnetic dipole sources above a horizontally layered medium. The formulation does not account for the contribution due to displacement currents. We also assume that effects of dielectric permittivity and magnetic susceptibility are negligible compared to electrical conduction, and set each layer's dielectric permittivity and magnetic permeability to that of free space ($\epsilon_k=\epsilon_0$, $\mu_k=\mu_0$).

The full transient (0.04 s) equivalent square current waveform, to which TEMPEST™ data are processed, was linearly sampled at 75,000 Hz (3000 samples) and transformed to the frequency domain via fast Fourier transform (FFT). Using Wait's (1982) expressions the secondary B-field was calculated for ~20 discrete frequencies between 25 Hz and 37,500 Hz (6 logarithmically equi-spaced frequencies per decade). The inphase and quadrature parts of each component were then individually splined to obtain linearly spaced values at the same frequencies as the nodes of the FFT transformed current waveform. Complex multiplication of splined B-field with the FFT transformed current waveform, followed by inverse FFT, yielded the B field transient response.

The transient was then windowed (boxcar) into the 15 windows by averaging those samples that fell within each window. The primary field, which is constant over all 15 windows, was then computed from Wait's expressions and added to yield the total field window response in the x -axis and z -axis directions. Finally these were rotated to be aligned with the X-component receiver coil's axis and Z-component receiver coil's axis according to the receiver pitch model parameter (RX_p) to yield $\mathbf{f}(\mathbf{m})$.

The inversion also requires the partial derivatives of $\mathbf{f}(\mathbf{m})$ with respect to the model parameters (see Equation 19). These were all calculated analytically. For computation of Wait's coefficient R_0 , we took advantage of the propagation matrix method (Farquharson *et al.*, 2004) because it is efficient for computation of the partial derivatives with respect to the multiple layer conductivities.

A3.2.2.7 Reference model

The algorithm uses the concept of a reference model (Farquharson and Oldenburg, 1993) to incorporate prior information from downhole conductivity logs or lithologic/stratigraphic logging in order to improve inversion stability and to reduce the trade-off between parameters that are not well resolved independently. Since prior information is not available everywhere within the survey area, and the inversions are carried out in independent sample by sample fashion, it is not plausible to place hard reference model constraints on the model parameters. Instead the reference model provides a soft or probabilistic constraint only. If, from prior information, it is concluded that the likely distribution of the model parameter m_k is a Gaussian distribution with mean m_k^{ref} and standard deviation m_k^{unc} , then we would define the reference model vector as,

$$\mathbf{m}^{ref} = [lc_1^{ref} \ lc_2^{ref} \cdots lc_{N_L}^{ref} \ D_x^{ref} \ D_z^{ref} \ RX_p^{ref}]^T \quad (5)$$

and the reference model uncertainty vector as,

$$\mathbf{m}^{unc} = [lc_1^{unc} \ lc_2^{unc} \cdots lc_{N_L}^{unc} \ D_x^{unc} \ D_z^{unc} \ RX_p^{unc}]^T \quad (6)$$

The reference model mean values and uncertainties are inputs to the inversion algorithm and they may be different from sample to sample. The uncertainty values assigned to the reference model control the amount of constraint that the reference model places on the inversion results. A large uncertainty value for a particular parameter implies that the assigned reference model mean value is not well known and thus is allowed to vary a long way from the mean. On the other hand a low uncertainty implies the parameter is well known.

A3.2.3 Objective function

The inversion scheme minimises a composite objective function of the form,

$$\Phi = \Phi_d + \lambda (\alpha_c \Phi_c + \alpha_g \Phi_g + \alpha_v \Phi_v) \quad (7)$$

where Φ_d is a data misfit term, Φ_c is a layer conductivity reference model misfit term, Φ_g is a system geometry reference model misfit term, and Φ_v is a vertical roughness of conductivity term. The relative weighting of the data misfit Φ_d and the collective model regularisation term,

$$\Phi_m = \alpha_c \Phi_c + \alpha_g \Phi_g + \alpha_v \Phi_v \quad (8)$$

is controlled by the value of regularisation factor λ . The three model regularisation factors α_c , α_g and α_v control the relative weighting within the model regularisation term Φ_m . The algorithm requires that the α values be set by the user on an application-by-application basis and they remain fixed throughout the inversion. However the λ is automatically determined within the algorithm by the method described in [Section A3.2.4.2](#).

A3.2.3.1 Data misfit

The data misfit Φ_d is a measure of the misfit, between the data (\mathbf{d}^{obs}) and the forward model of the model parameters ($\mathbf{f}(\mathbf{m})$), normalised by the expected error and the number of data. It is defined as,

$$\begin{aligned}\Phi_d &= \frac{1}{N_D} \sum_{k=1}^{N_D} \left(\frac{d_k^{obs} - \mathbf{f}(\mathbf{m})}{d_k^{err}} \right)^2 \\ &= [\mathbf{d}^{obs} - \mathbf{f}(\mathbf{m})]^T \mathbf{W}_d [\mathbf{d}^{obs} - \mathbf{f}(\mathbf{m})]\end{aligned}\quad (9)$$

The diagonal $N_D \times N_D$ matrix \mathbf{W}_d is,

$$\mathbf{W}_d = \frac{1}{N_D} \begin{bmatrix} \frac{1}{(d_1^{err})^2} & & & \\ & \frac{1}{(d_2^{err})^2} & & \\ & & \ddots & \\ & & & \frac{1}{(d_{N_D}^{err})^2} \end{bmatrix} \quad (10)$$

A3.2.3.2 Conductivity reference model misfit

The conductivity reference model misfit term Φ_c is a measure of the misfit, between the logarithmic conductivity model parameters (\mathbf{lc}) and the corresponding layer reference model values (\mathbf{lc}^{ref}) normalised by the layer thicknesses and reference model uncertainty. It is defined as,

$$\begin{aligned}\Phi_c &= \sum_{k=1}^{N_L} \frac{t_k}{T/N_L} \left(\frac{lc_k^{ref} - lc_k}{lc_k^{unc}} \right)^2 \\ &= [\mathbf{m}^{ref} - \mathbf{m}]^T \mathbf{W}_c [\mathbf{m}^{ref} - \mathbf{m}]\end{aligned}\quad (11)$$

where $T = \sum_{k=1}^{N_L} t_k$, and the diagonal $Np \times Np$ matrix \mathbf{W}_c is,

$$\mathbf{W}_c = \frac{N_L}{T} \begin{bmatrix} \frac{t_1}{(lc_1^{unc})^2} & & & & \\ & \frac{t_2}{(lc_2^{unc})^2} & & & \\ & & \ddots & & \\ & & & \frac{t_{N_L-1}}{(lc_{N_L-1}^{unc})^2} & \\ & & & & \frac{t_{N_L}}{(lc_{N_L}^{unc})^2} \\ & & & & 0 \\ & & & & 0 \\ & & & & 0 \end{bmatrix}. \quad (12)$$

Since the bottom layer is infinitely thick, for the purposes of this term we set $t_{N_L} = [t_{N_L-1}]^2/t_{N_L-2}$.

A3.2.3.3 System geometry reference model misfit

The system geometry reference model misfit term Φ_g is a measure of the misfit, between the system geometry model parameters (\mathbf{g}) and the corresponding system geometry reference model values (\mathbf{g}^{ref}) normalised by the number of unknown system geometry parameters ($N_G=3$) and their uncertainty. It is defined as,

$$\begin{aligned}\Phi_g &= \frac{1}{N_G} \sum_{k=1}^{N_G} \left(\frac{\mathbf{g}_k^{ref} - \mathbf{g}_k}{\mathbf{g}_k^{unc}} \right)^2 \\ &= [\mathbf{m}^{ref} - \mathbf{m}]^T \mathbf{W}_g [\mathbf{m}^{ref} - \mathbf{m}]\end{aligned}\quad (13)$$

The diagonal $N_p \times N_p$ matrix \mathbf{W}_g is,

$$\mathbf{W}_g = \frac{1}{N_G} \begin{bmatrix} 0 & & & & \\ & 0 & & & \\ & & \dots & & \\ & & & 0 & \\ & & & & \frac{1}{(D_x^{unc})^2} \\ & & & & & 1 \\ & & & & & & \frac{1}{(D_y^{unc})^2} \\ & & & & & & & \frac{1}{(RX_p^{unc})^2} \end{bmatrix}. \quad (14)$$

A3.2.3.4 Vertical roughness of conductivity

The vertical roughness of conductivity term Φ_v is a measure of the roughness of the conductivity profile. It sums the squared second derivative of the logarithm of the vertical conductivity profile, approximated by finite difference over adjacent layer triplets, taking into account the distance between layer centres. The result is normalised by the number of triplets (N_L-2) and is defined as,

$$\begin{aligned}\Phi_v &= \frac{1}{N_L-2} \sum_{k=2}^{N_L-1} \left(\frac{(lc_{k-1} - lc_k)}{1/2(t_{k-1} + t_k)} - \frac{(lc_k - lc_{k+1})}{1/2(t_k + t_{k+1})} \right)^2 \\ &= \mathbf{m}^T \mathbf{L}_v^T \mathbf{L}_v \mathbf{m}\end{aligned}\quad (15)$$

where the $N_L-2 \times N_p$ matrix \mathbf{L}_v is,

$$\mathbf{L}_v = \frac{1}{N_L - 2} \begin{bmatrix} \frac{1}{(t_1 + t_2)} \left(\frac{-1}{(t_1 + t_2)} + \frac{-1}{(t_2 + t_3)} \right) & \frac{1}{(t_2 + t_3)} \\ \frac{1}{(t_2 + t_3)} & \left(\frac{-1}{(t_2 + t_3)} + \frac{-1}{(t_3 + t_4)} \right) & \frac{1}{(t_3 + t_4)} \\ & \dots & \dots & \dots \\ & & & 0 \\ & & & 0 \\ & & & 0 \end{bmatrix} \quad (16)$$

Again for the purposes of this term we set $t_{N_L} = [t_{N_L-1}]^2 / t_{N_L-2}$.

A3.2.4 Minimisation scheme

A3.2.4.1 Linearisation

To minimise the objective function Φ , a linearised gradient based iterative minimisation scheme is used. Collection of the matrix notation misfit terms, Equations 9, 11, 13, and 15 that make up Φ , allows us to write,

$$\begin{aligned} \Phi(\mathbf{m}) = & [\mathbf{d}^{obs} - \mathbf{f}(\mathbf{m})]^T \mathbf{W}_d [\mathbf{d}^{obs} - \mathbf{f}(\mathbf{m})] \\ & + \lambda \alpha_c [\mathbf{m}^{ref} - \mathbf{m}]^T \mathbf{W}_c [\mathbf{m}^{ref} - \mathbf{m}] \\ & + \lambda \alpha_g [\mathbf{m}^{ref} - \mathbf{m}]^T \mathbf{W}_g [\mathbf{m}^{ref} - \mathbf{m}] \\ & + \lambda \alpha_v \mathbf{m}^T \mathbf{L}_v^T \mathbf{L}_v \mathbf{m} \end{aligned} \quad (17)$$

The inversion begins by setting the initial estimate of the model parameters to the reference model ($\mathbf{m}_0 = \mathbf{m}^{ref}$). During the n^{th} iteration the current estimate of the model parameters \mathbf{m}_n is perturbed by the parameter change vector,

$$\Delta \mathbf{m}_n = \mathbf{m}_{n+1} - \mathbf{m}_n. \quad (18)$$

The forward model at the new set of model parameters \mathbf{m}_{n+1} is approximated by a Taylor series expansion about \mathbf{m}_n , which, after excluding high order terms reduces to,

$$\mathbf{f}(\mathbf{m}_{n+1}) \approx \mathbf{f}(\mathbf{m}_n) + \mathbf{J}_n (\mathbf{m}_{n+1} - \mathbf{m}_n) \quad (19)$$

where $\mathbf{J}_n = \partial\mathbf{f}(\mathbf{m})/\partial\mathbf{m}$ is the Jacobian matrix whose $i^{\text{th}}, j^{\text{th}}$ element is the partial derivative of the i^{th} datum with respect to the j^{th} model parameter evaluated at \mathbf{m}_n in model space. Making use of Equation 19 and substituting $\mathbf{m} = \mathbf{m}_{n+1}$, allows Equation 17 to be rewritten as,

$$\begin{aligned}\Phi(\mathbf{m}_{n+1}) = & \left[\mathbf{d}^{obs} - \mathbf{f}(\mathbf{m}_n) - \mathbf{J}_n(\mathbf{m}_{n+1} - \mathbf{m}_n) \right]^T \mathbf{W}_d \left[\mathbf{d}^{obs} - \mathbf{f}(\mathbf{m}_n) - \mathbf{J}_n(\mathbf{m}_{n+1} - \mathbf{m}_n) \right] \\ & + \lambda \alpha_c \left[\mathbf{m}^{ref} - \mathbf{m}_{n+1} \right]^T \mathbf{W}_c \left[\mathbf{m}^{ref} - \mathbf{m}_{n+1} \right] \\ & + \lambda \alpha_g \left[\mathbf{m}^{ref} - \mathbf{m}_{n+1} \right]^T \mathbf{W}_g \left[\mathbf{m}^{ref} - \mathbf{m}_{n+1} \right] \\ & + \lambda \alpha_v \mathbf{m}_{n+1}^T \mathbf{L}_v^T \mathbf{L}_v \mathbf{m}_{n+1}\end{aligned}\quad (20)$$

Since the value of Φ will be minimised when $\partial\Phi/\partial\mathbf{m}_{n+1} = 0$, we differentiate Equation 20 with respect to \mathbf{m}_{n+1} and set the result to zero and get,

$$\begin{aligned}0 = & -2\mathbf{J}_n^T \mathbf{W}_d \left[\mathbf{d}^{obs} - \mathbf{f}(\mathbf{m}_n) - \mathbf{J}_n(\mathbf{m}_{n+1} - \mathbf{m}_n) \right] \\ & + \lambda \left[-2\alpha_c \mathbf{W}_c \left[\mathbf{m}^{ref} - \mathbf{m}_{n+1} \right] - 2\alpha_g \mathbf{W}_g \left[\mathbf{m}^{ref} - \mathbf{m}_{n+1} \right] + 2\alpha_v \mathbf{L}_v^T \mathbf{L}_v \mathbf{m}_{n+1} \right]\end{aligned}\quad (21)$$

Collecting terms in the unknown vector \mathbf{m}_{n+1} on the left hand side yields,

$$\begin{aligned}\left[\mathbf{J}_n^T \mathbf{W}_d \mathbf{J}_n + \lambda (\alpha_c \mathbf{W}_c + \alpha_g \mathbf{W}_g + \alpha_v \mathbf{L}_v^T \mathbf{L}_v) \right] \mathbf{m}_{n+1} = \dots \\ \mathbf{J}_n^T \mathbf{W}_d \left[\mathbf{d}^{obs} - \mathbf{f}(\mathbf{m}_n) + \mathbf{J}_n \mathbf{m}_n \right] + \lambda [\alpha_c \mathbf{W}_c + \alpha_g \mathbf{W}_g] \mathbf{m}^{ref}\end{aligned}\quad (22)$$

Since Equation 22 is in the familiar form of a system of linear equations ($\mathbf{A} \mathbf{m}_{n+1} = \mathbf{b}$) we are able to solve for \mathbf{m}_{n+1} using a variety of linear algebra methods. We use Cholesky decomposition.

A3.2.4.2 Choice of the value of λ

An initial value of λ is chosen such that the data and model objective functions will have approximately equal weight. This is automatically realised by computing the ratio of the data and model objective functions, from the reference model perturbed by 1%, and computing the ratio of the data and model misfits,

$$\lambda_{start} = \frac{\Phi_d(\mathbf{f}(1.01 \times \mathbf{m}_0))}{\Phi_m(1.01 \times \mathbf{m}_0)}.\quad (23)$$

Then at each iteration the inversion employs a 1D line search where, in solving for \mathbf{m}_{n+1} in Equation 22 different values of λ are trialled, until a value of λ_n is found such that,

$$\Phi_d(\mathbf{f}(\mathbf{m}_{n+1})) \approx \Phi_d^{t \arg et} = 0.7 \times \Phi_d(\mathbf{f}(\mathbf{m}_n)),\quad (24)$$

thus reducing Φ_d to 0.7 of its previous value.

A3.2.4.3 Convergence criterion

The iterations continue until the inversion terminates when one of the following conditions is encountered:

- Φ_d reaches a user defined minimum value $\Phi_d^{\min} = 1$;
- Φ_d has been reduced by less than 1% in two consecutive iterations;
- Φ_d can no longer be reduced; or
- The number of iterations reaches a maximum of 100 iterations.

A3.3 CONDUCTIVITY DATA HEADER INFORMATION

1	uniqueid	48	conductivity:27	95	x_window_predicted:14
2	survey	49	conductivity:28	96	x_window_predicted:15
3	date	50	conductivity:29	97	z_primary_predicted
4	flight	51	conductivity:30	98	z_window_predicted:1
5	line	52	thickness:1	99	z_window_predicted:2
6	fid	53	thickness:2	100	z_window_predicted:3
7	easting	54	thickness:3	101	z_window_predicted:4
8	northing	55	thickness:4	102	z_window_predicted:5
9	elevation	56	thickness:5	103	z_window_predicted:6
10	altimeter	57	thickness:6	104	z_window_predicted:7
11	tx_height	58	thickness:7	105	z_window_predicted:8
12	tx_roll	59	thickness:8	106	z_window_predicted:9
13	tx_pitch	60	thickness:9	107	z_window_predicted:10
14	tx_yaw	61	thickness:10	108	z_window_predicted:11
15	txrx_dx	62	thickness:11	109	z_window_predicted:12
16	txrx_dy	63	thickness:12	110	z_window_predicted:13
17	txrx_dz	64	thickness:13	111	z_window_predicted:14
18	rx_roll	65	thickness:14	112	z_window_predicted:15
19	rx_pitch	66	thickness:15	113	PhiD
20	rx_yaw	67	thickness:16	114	PhiM
21	nlayers	68	thickness:17	115	PhiC
22	conductivity:1	69	thickness:18	116	PhiT
23	conductivity:2	70	thickness:19	117	PhiG
24	conductivity:3	71	thickness:20	118	PhiS
25	conductivity:4	72	thickness:21	119	Lambda
26	conductivity:5	73	thickness:22	120	AlphaC
27	conductivity:6	74	thickness:23	121	AlphaT
28	conductivity:7	75	thickness:24	122	AlphaG
29	conductivity:8	76	thickness:25	123	AlphaS
30	conductivity:9	77	thickness:26	124	Iterations
31	conductivity:10	78	thickness:27	125	Carriage return
32	conductivity:11	79	thickness:28		
33	conductivity:12	80	thickness:29		
34	conductivity:13	81	x_primary_predicted		
35	conductivity:14	82	x_window_predicted:1		
36	conductivity:15	83	x_window_predicted:2		
37	conductivity:16	84	x_window_predicted:3		
38	conductivity:17	85	x_window_predicted:4		
39	conductivity:18	86	x_window_predicted:5		
40	conductivity:19	87	x_window_predicted:6		
41	conductivity:20	88	x_window_predicted:7		
42	conductivity:21	89	x_window_predicted:8		
43	conductivity:22	90	x_window_predicted:9		
44	conductivity:23	91	x_window_predicted:10		
45	conductivity:24	92	x_window_predicted:11		
46	conductivity:25	93	x_window_predicted:12		
47	conductivity:26	94	x_window_predicted:13		

A3.4 TECHNICAL SPECIFICATIONS OF MAP PROJECTIONS

Projection Name:	Map Grid of Australia, Zone 51
Units:	Metres
Datum:	Geocentric Datum of Australia 1994 (GDA94)
Epoch:	1994.0
Ellipsoid:	GRS80
Semi-major axis (a):	6 378 160.0 metres
Inverse flattening (1/f):	298.25
Central meridian	123°00'00''
False Easting:	500 000 metres
False Northing:	10 000 000 metres

A3.5 INDUCTION CONDUCTIVITY LOGGING

The following is Summarised from the GA internal report "*Logistics report for down-hole conductivity logging in the Paterson AEM Survey area, Western Australia, September 2008*" (Sorensen, 2008).

A3.5.1 Method

Induction conductivity logging tools measure the electrical conductivity of the material surrounding the borehole and provide a detailed indication of changes in conductivity with depth. Induction conductivity logging tools permit measurements of the electrical conductivity of the ground outside PVC cased boreholes generally without being sensitive to the presence of usually more conductive borehole fluid within the casing. Induction conductivity logging tools are capable of making reliable scientific measurements, however, their method of use has not been standardised. The following sections outline the method that was used in this data acquisition (Sorensen and Lane, 2007b).

The induction conductivity logging tool works in a similar way to ground or airborne electromagnetic systems. A small transmitter coil in the probe creates a primary magnetic field which gives rise to an electrical field in the materials surrounding the borehole. This electrical field creates eddy currents within the material, the strength of which depends on the conductivity of the material. These eddy currents then create a magnetic field which is measured with a receiver coil within the probe. [Figure A3.1](#) shows the principles of operation.

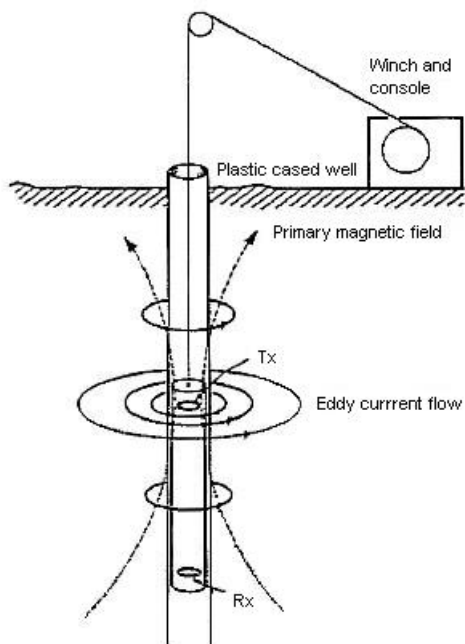


Figure A3.2: The principle of operation of inductive conductivity borehole logging tool, from McNeill et al. (1990).

The geophysical logging equipment used on the fieldtrip was rented from Auslog Pty. Ltd. of Brisbane, Queensland. The following equipment was used:

- Induction conductivity probe (HI327F serial no S500);
- 500 m cable winch;
- Logging matrix console; and,

- Laptop computer with Wellvision™ logging software.

The location and elevation of each borehole was established using a Garmin GPSMAP 60CSx hand-held GPS receiver. The standing water level was measured using a tape measure or a water level indicator when available. The height of the casing was measured using a tape measure.

Before lowering the conductivity probe, the condition of each hole was tested by running a dummy probe down and up the hole. If the dummy probe did not descend to the completion depth of the hole, the subsequent run with the conductivity induction tool was only carried out to the depth reached by the dummy probe.

Before calibration and data acquisition the temperature of the conductivity tool was stabilised. This was achieved by leaving the tool in the borehole at ca. 30m depth for 10-15 min.

Three calibration rings were provided with the induction conductivity logging tool: 100; 300; and, 500 mS/m. Calibration was always carried out before and after logging each borehole.

After temperature stabilisation of the instrument, calibration was carried out using the three calibration rings. The same procedures were adopted for each known calibration value; the probe was moved away from any metal and held in the air. To ensure that the probe was in a similar position while each calibration was performed, the probe was rested on the shoulder of one of the field party members as recommended by Auslog Pty Ltd. This procedure was then repeated for the other two calibration points.

Upon the completion of the tool calibration the temperature was again stabilised at 30 m depth for approximately 10 min. Prior to measuring the tool was positioned at a zero level, defined as the point at which the ‘neck’ of the probe (the point at which the end of the cable connector meets the probe) was level with the surface of the ground. While measuring, the logging speed was kept between 3-7 m/min, but was mainly between 5 and 7m/min. The details of the measuring procedures used for each bore were recorded on field logging sheets provided later in this appendix.

All holes were logged at least twice; once as the tool descended, and a second time as the tool ascended. On the completion of the upwards run, the two conductivity logs were overlain to ensure that repeatability was obtained. In a number of cases a minor discrepancy between the two logs existed, and additional runs with the tool were performed until the logs were consistent. In all cases consistency was observed after 1-2 additional logs were measured.

After each hole was logged the probe was recalibrated using the same procedures that were used in the pre-logging calibration. This was done to ensure a calibration of the probe was in the same state as when actually measuring in the borehole. It was then possible to compare pre- and post-logging calibrations and decide on which one was the most appropriate one to apply to the data in the processing step. In most of the cases the post-logging calibration seemed to be the most suitable as the conductivity tool was calibrated in a state as close as possible to borehole conditions.

A3.5.2 Results

After logging the 19 boreholes, the first logged hole (THRP161B) was re-logged. This was to ensure repeatability of the instrument over the 10 days it was used. Comparison of the repeat log and the original log ([Figure A3.2](#)) shows very little variation between the logs, indicating good repeatability.

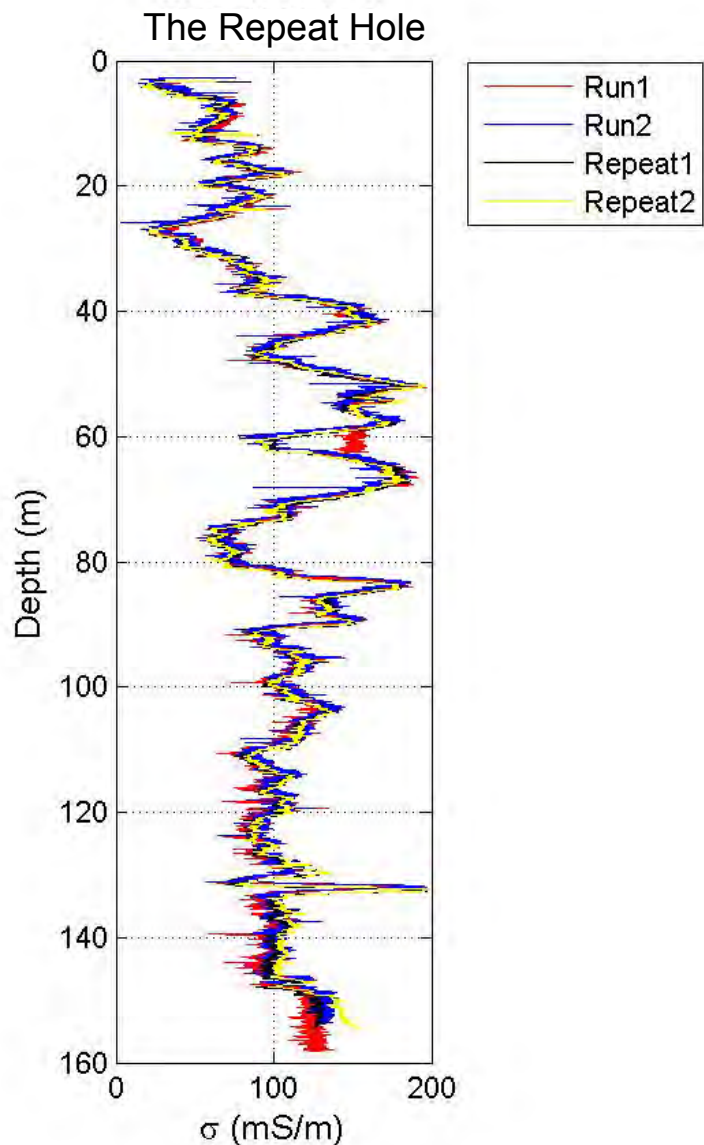


Figure A3.3: Comparison of logs from the repeat hole, from the beginning and end of field trip. Run1 and Run2 were acquired at the beginning of the trip, and Repeat1 and Repeat2 were acquired at the end of the field trip.

Figure A3.3 shows a sample of the 14 non confidential conductivity logs. Multiple runs at each hole are displayed. These plots show conductivity with depth, filtered with a median filter and then by moving average filter (both with filter width of between 5 and 31 points). The raw conductivity logs are not included in this report. The remainder of the logs are provided in Hutchinson *et al.* (2010)

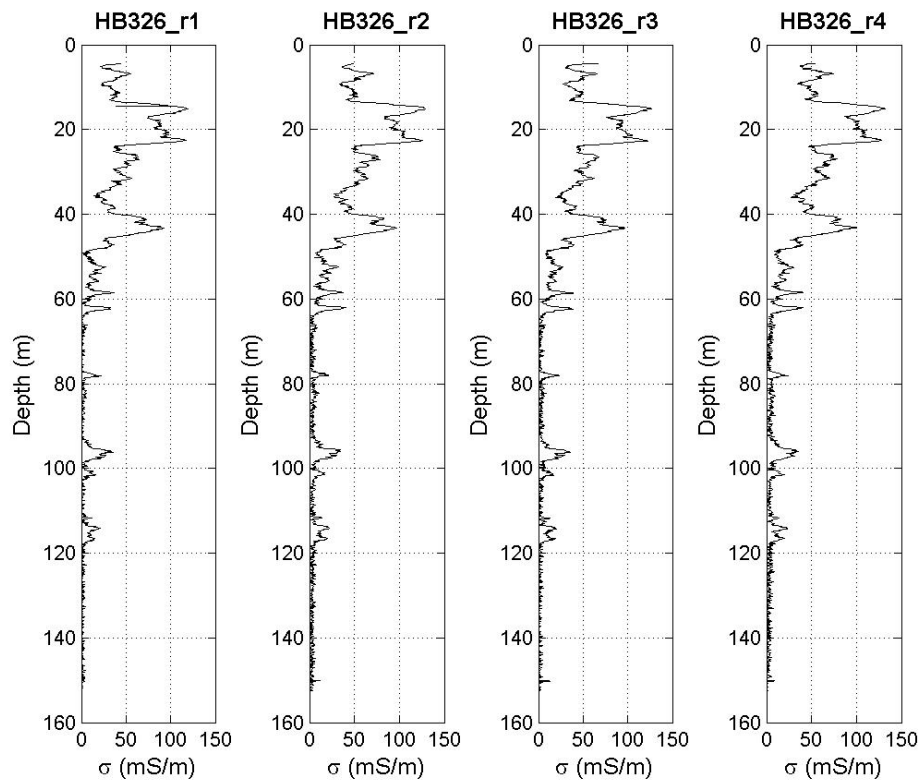


Figure A3.4: An example of repeat conductivity logs for hole HB326.

A3.5.3 Field sheets

Field sheets were filled in for each of the conductivity logs acquired during the 2008 field trip to the Paterson Region; an example is provided below (Table A3.1).

Table A3.1: Example of field sheets acquired for conductivity logs.

		Method (e.g. tape, GPS etc.)
Location/Site name	08DKRCD011	
Easting	51 K 0348403	GPS
Northing	7657601	GPS
Map Datum	WGS84	GPS
Projection		
Surface elevation	811ft	GPS
Height of casing		
Water level	3.72m	
Depth of hole	428m	
Drill method	RC + DD	
Casing info	Type	Size
	PVC	40mm
Depth interval		
428m		

Probe information

Type of probe	Name	Serial number
Conductivity	A085	S500

Log information (08DKRCD011)

Type of log	Induction Conductivity			
Name of operator(s)	Camilla Sorensen (Geoscience Australia)			
Run #	1	2	3	4
Date	30/08/2008	30/08/2008		
Time	9.45	11		
Logging speed (m/min)	6 m/min	7 m/min		
Temperature stabilised?	Probe left at 30m for 10min	Yes		
Repeatability?	Yes reasonably			
Irregularities	None	None		
Weather info	Hot	Hot		
Units of measurement	mS/m	mS/m		

A3.6 COMPARISON BETWEEN BORE HOLE CONDUCTIVITY LOGS AND GA LEI

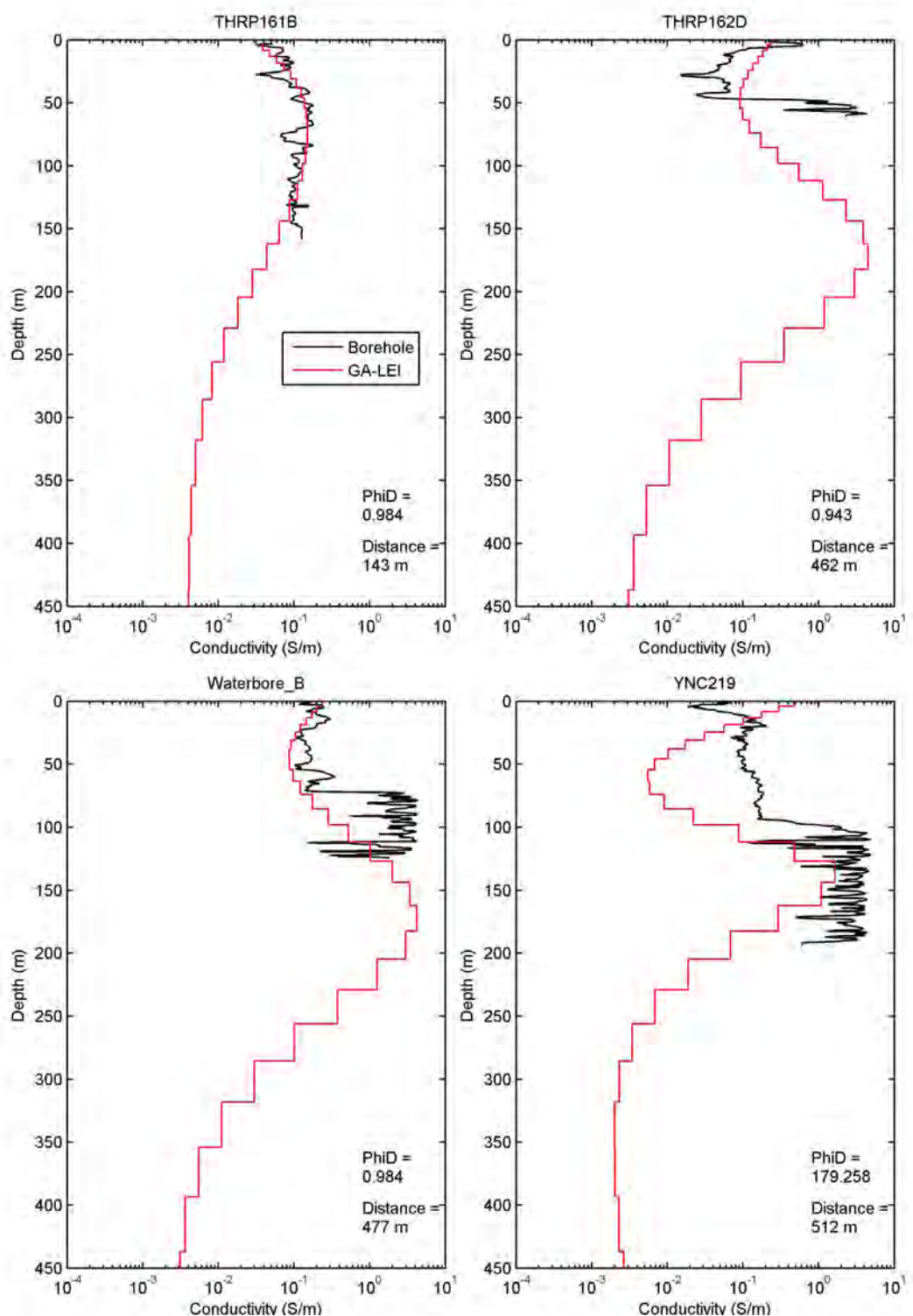


Figure A3.5: Conductivity logs compared to GA-LEI results.

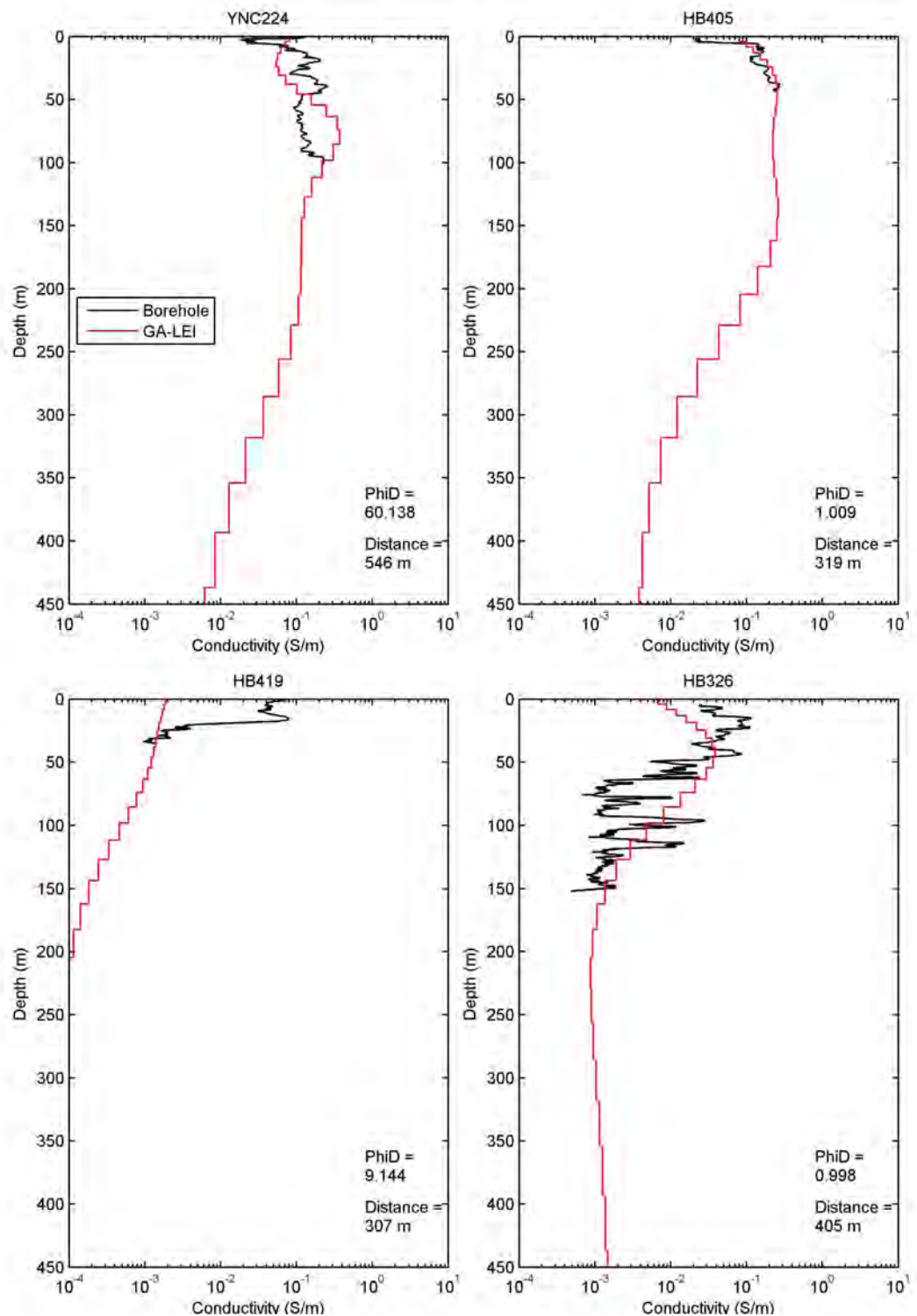


Figure A3.5: Conductivity logs compared to GA-LEI results (continued).

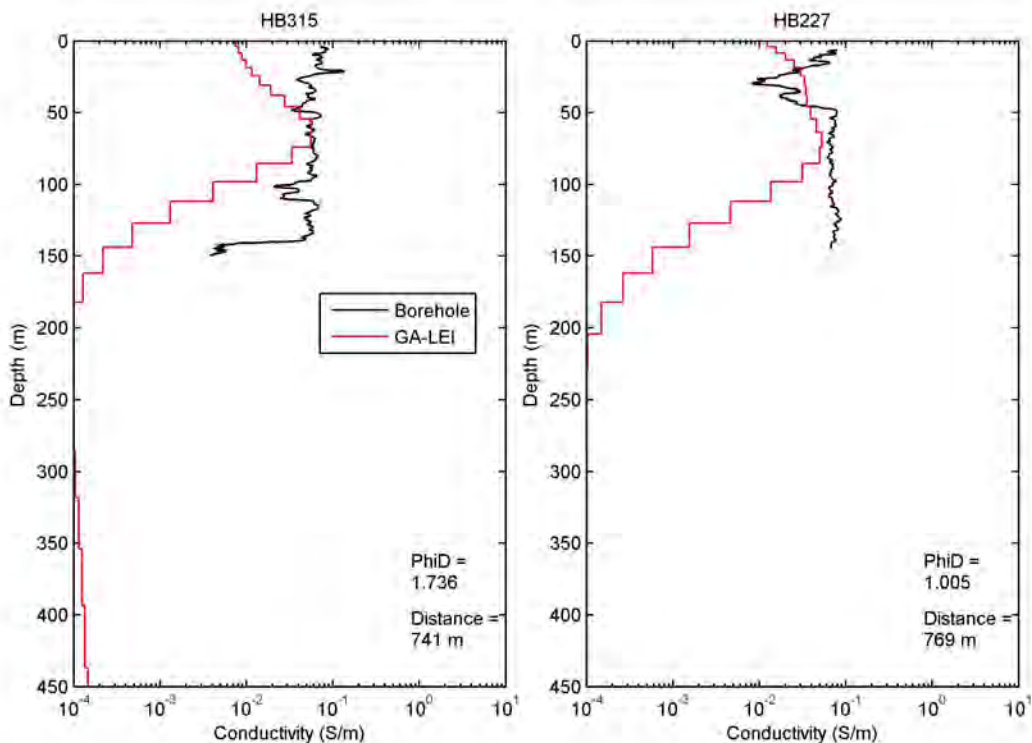


Figure A3.5: Conductivity logs compared to GA-LEI results (continued).

A3.7 INDUCTION CONDUCTIVITY LOGGING

- Constable, S., Parker, R. and Constable, C., 1987. Occam's inversion; a practical algorithm for generating smooth models from electromagnetic sounding data. *Geophysics* **52**, 289-300.
- Farquharson, C. G. and Oldenburg, D. W., 1993. Inversion of time domain electromagnetic data for a horizontally layered earth. *Geophysical Journal International* **114**, 433-442.
- Farquharson, C. G., Oldenburg, D. W. and Routh, P. S., 2004. Simultaneous 1D inversion of loop-loop electromagnetic data for magnetic susceptibility and electrical conductivity. *Geophysics* **68**, 1857-1869.
- Green, A. and Lane, R., 2003. Estimating Noise Levels in AEM Data. *ASEG 16th Geophysical Conference and Exhibition*, Adelaide, Australian Society of Exploration Geophysicists, February 2003.
- Hutchinson, D. K., Costelloe, M. T., Roach, I. C. and Sorensen, C., 2010. Paterson TEMPEST AEM Survey, Western Australia, 2010 Final Inversion Data and Conductivity Models. Geoscience Australia, Canberra. **Unpublished report**. Online: https://www.ga.gov.au/products/servlet/controller?event=GEOCAT_DETAILS&catno=70297.
- Lane, R., Green, A., Golding, C., Owers, M., Pik, P., Plunkett, C., Sattel, D. and Thorn, B., 2000. An example of 3D conductivity mapping using the TEMPEST airborne electromagnetic system. *Exploration Geophysics* **31**(2), 162-172.
- McNeill, J. D., Bosnar, M. and Snelgrove, F. B., 1990. Resolution of an electromagnetic borehole conductivity logger for geotechnical and ground water applications. Geonics Limited, Mississauga, Ontario. **Technical Note TN-25**, 29 p. Online: <http://www.geonics.com/pdfs/technicalnotes/tn25.pdf>.
- Reid, J. E. and Vrbancich, J., 2004. A comparison of the inductive-limit footprints of airborne electromagnetic configurations. *Geophysics* **69**, 1229-1239.

- Sattell, D., 1998. Conductivity information in three dimensions. *Exploration Geophysics* **29**, 157-132.
- Sorensen, C., 2008. Logistics report for down-hole conductivity logging in the Paterson AEM Survey area, Western Australia, September 2008. Geoscience Australia. **Unpublished report**.
- Sorensen, C. and Lane, R., 2007b. Guidelines for conductivity borehole logging procedures. Geoscience Australia. **Unpublished report**.
- Wait, J. R., 1982. Geo-electromagnetism. Academic Press Inc, New York.

